Neuroimaging of Fetal Cell Therapy in Parkinson's Disease

Nicholas Piyachati Lao-Kaim

August 2020

IMPERIAL COLLEGE LONDON

DIVISION OF NEUROLOGY

DEPARTMENT OF BRAIN SCIENCES

Thesis submitted in fulfilment of the requirements for the degree of Doctor of Philosophy

For mum, dad and Anna

"It is not the critic who counts; not the man who points out how the strong man stumbles, or where the doer of deeds could have done them better. The credit belongs to the man who is actually in the arena, whose face is marred by dust and sweat and blood; who strives valiantly; who errs, who comes short again and again, because there is no effort without error and shortcoming; but who does actually strive to do the deeds; who knows great enthusiasms, the great devotions; who spends himself in a worthy cause; who at the best knows in the end the triumph of high achievement, and who at the worst, if he fails, at least fails while daring greatly, so that his place shall never be with those cold and timid souls who neither know victory nor defeat."

- Theodore Roosevelt, *"The Man in the Arena", Citizenship in a Republic (1910)*

Abstract

Parkinson's disease is the second most common neurodegenerative disease characterised by the elevated formation of α-synuclein-immunopositive intraneuronal proteinaceous inclusions (Lewy pathology) and the progressive loss of neuromelanin-laden dopaminergic cells of the substantia nigra pars compacta, resulting in the loss of striatal dopaminergic terminals and emergence of cardinal motor features including bradykinesia, rigidity, tremor and postural instability. Dopaminomimetic agents provide effective symptomatic relief in the early stages of illness, yet due to the inherently progressive nature of the disease and the induction of debilitating side effects their efficacy is eventually lost. Cellular restorative strategies involving intrastriatal transplantation of human fetal ventral mesencephalic (hfVM) tissue gained traction from the early 1990's, when several multi-disciplinary teams reported drastic motoric improvements concomitant with graft-derived dopaminergic re-innervation. However, outcomes of double-blind randomised controlled trials and the presentation of novel dyskinetic movements persisting in the "off-state" called for substantial revision of cell delivery strategies. The current thesis utilises positron emission tomography to examine the effects of hfVM implantation under the Transeuro protocol on dopaminergic ([^{18}F]FDOPA, [^{11}C]PE2I) and serotonergic ([^{11}C]DASB) systems in patients with Parkinson's disease and elucidate the neural underpinnings of its clinical impact. The main findings are; 1) implanted hfVM tissue led to increases in putamenal dopamine synthesis and storage capacity, dopamine and serotonin transporter density as compared to non-transplanted patients; 2) modification to surgical procedures provided inhomogenous and inconsistent re-innervation; 3) hfVM transplantation was associated with clinical improvements in measures of bradykinesia, rigidity and tremor; 4) graft-related changes in posterior putamenal dopamine and serotonin transporter density predicted symptomatic relief of bradykinesia and tremor; 5) heterogeneity of posterior putamenal re-innervation may impact upon potential clinical benefit; 6) graft-induced dyskinesia was associated with greater post-operative increases in dopamine transporter expression in the anterior putamen; 7) there was no evidence that graft-induced dyskinesia was related to serotonergic hyperinnervation. The novel findings presented in this thesis have major implications for cell-based restorative strategies beyond the hfVM era and will likely foster informed

[re]consideration of many aspects of therapeutic delivery and trial design. For its ability to provide mechanistic insight *in vivo*, neuroimaging may continue to play a central role in the optimisation of future interventions.

Declaration of Originality

I declare that the written and intellectual content of this thesis is the product of my own work and was completed in the Department of Brain Sciences (2016-2020) under the supervision of Prof. Paola Piccini. All the assistance received in preparing this thesis and sources have been acknowledged.

Copyright Declaration

The copyright of this thesis rests with the author. Unless otherwise indicated, its contents are licensed under a Creative Commons Attribution-Non Commercial 4.0 International Licence (CC BY-NC). Under this licence, you may copy and redistribute the material in any medium or format. You may also create and distribute modified versions of the work. This is on the condition that: you credit the author and do not use it, or any derivative works, for a commercial purpose. When reusing or sharing this work, ensure you make the licence terms clear to others by naming the licence and linking to the licence text. Where a work has been adapted, you should indicate that the work has been changed and describe those changes. Please seek permission from the copyright holder for uses of this work that are not included in this licence or permitted under UK Copyright Law.

Acknowledgments

First and foremost, I must thank Prof. Paola Piccini, for giving me the opportunity to work, study and complete this thesis under her supervision. I'm not sure how I managed to get through the door after a more than incompetent interview, but I knew where the substantia nigra was and I think that was the ticket. In any case, I am eternally grateful.

I would like to thank Hyacinth Henry, for her outstanding ability to keep everything flowing like clockwork, for seemingly being able to understand all my nonsense and for actually solving most of my problems, quite easily I must add.

I owe my deepest thanks to Dr. Antonio Martín-Bastida, for his incredible knowledge in neurology and for teaching me almost everything I now know on the clinical assessment (Froment's sign included) and clinicopathologic mechanisms of Parkinson's disease. I will never forget his close support in the final days prior to the submission of this thesis, when even from all the way over in Spain and during his well-needed holidays from clinical COVID-19 duties he still requested and proof-read many of these chapters.

I would like to thank Dr. Andreas-Antonios Roussakis, for his second-to-none expertise in research ethics and governance, neurological assistance and knowledge, highly fascinating conversations on travel and language, and for always keeping my best interests in mind.

I would like to thank Dr. Zhou Zeng, for all her support in the final month prior to the submission of this thesis. Our discussions helped massively and her insistence on coming in to the office so that I would not be alone surely prevented me from going insane. Without her, I would still be in the middle of an EndNote nightmare.

I'd like to thank Dr. Marta Gennaro, who out of everyone I've ever worked with had a degree of empathy (could be sympathy) like no other and with whom I could confide openly during the last couple years of my thesis. I also need to thank you for surrendering your mum's lasagne recipe, which was made very frequently, and in very large quantities.

I am very grateful to all the patients who took part in this study, in spite of all the difficulties and hardships that they face, and to Parkinson's UK, for sponsoring my PhD studentship.

I owe my thanks to Dr. Graham Searle, who really got me started on understanding the depths of PET analysis and was (still is, I think) always within shouting distance if I ever needed a friendly helping hand resurrecting his brainchild, MIAKAT™.

I would like to thank my closest friend and best of men James "l'equitation l'equitation" Botton, who understands the way my mind works unlike almost anyone else and so always seems to know exactly what to say, how to say it and when, and by that token when not to say anything at all. I've not been a terribly good friend lately, but despite my prolonged radio silence you've still found ways to remind me of your support and brotherly love.

I would also like to thank Mark and Claire who have both been so supportive over the past few years and whose opinions I very much respect. It was really invaluable and very settling to be able to bounce my thoughts past you and on many occasions, hear the echoes come right back at me, with perhaps a little added dash of wisdom. I especially appreciated the occasional whisky snap (most definitely on big rocks) here and there, because although it reminded me of what I was missing, it also showed me what I have to look forward to!

I am so grateful to you, Lady Wook, for supporting and believing in me throughout this whole entire saga, for cooking for me, tidying after me, making me laugh, for sticking to me like a gremlin and making sure I didn't hurt myself, for loving (putting up with) me in spite of my incessant moaning and incurable irritability and for pushing every other important thing onto the back-burner all so that I could complete this work. Thank you is just not enough; I simply would not have been able to do any of this without you behind me.

Finally, I would like to thank my mum and dad who have both always been there for me, supported and trusted me unconditionally, in their very different ways, in all the decisions I have ever made in my life. I know very well that I can be very difficult if not impossible to communicate with at times; the patience you've had for me, especially over the last few years, has been nothing short of a miracle. Your persistent shows of love and affection, like insisting on driving all the way to London just to bring me pick-your-own strawberries and home-cooked meals, although I tell you it's annoying, is in fact something special that has kept me going when it all seemed utterly pointless and striving to make you both the proudest of all parents. This thesis is as much yours as it is mine.

Publications

Publication of data relating to the Transeuro trial remained under embargo at the time of writing. Thus, no articles have as yet been published concerning the clinical and neuroimaging outcomes of transplantation as detailed in the chapters that follow. Manuscripts in preparation are therefore listed below, alongside all peer-reviewed articles covering unrelated subject matter that have been accepted for publication during the course of this PhD.

Barker RA, TRANSEURO Consortium. Designing stem-cell-based dopamine cell replacement trials for Parkinson's disease. *Nat Med* 2019; 25: 1045-1053.

Hannaway N, **Lao-Kaim NP**, Martín-Bastida A, Roussakis AA, Howard J, Wall MB, *et al*. Longitudinal changes in functional imaging responses to movements in Parkinson's disease patients. *Parkinsonism Relat Disord, manuscript in press*.

Lao-Kaim NP, Martín-Bastida A, Roussakis AA, Searle GE, Paul G, Widner H, *et al*. Effects of hfVM-derived dopaminergic and serotonergic putamenal re-innervation on the motor symptoms of Parkinson's disease at 18-months post-surgery. *Manuscript in preparation*.

Lao-Kaim NP, Martín-Bastida A, Roussakis AA, Searle GE, Paul G, Widner H, *et al*. Examination of local re-innervation and dopamine/serotonin ratio in the generation of post-operative graft-induced dyskinesia in Parkinson's disease. *Manuscript in preparation*.

Lao-Kaim NP, Martín-Bastida A, Roussakis AA, Searle GE, Paul G, Widner H, *et al*. Positron emission tomography imaging of the short-term longitudinal effects of intraputamenal hfVM transplantation on dopaminergic and serotonergic function in Parkinson's disease. *Manuscript in preparation*.

Lao-Kaim NP, Piccini P, Tai YF. Restorative strategies in movement disorders: the contribution of imaging. *Curr Neurol Neurosci Rep* 2017; 17(12): 98.

Lee J-Y, **Lao-Kaim NP**, Pasquini J, Deuschl G, Pavese N, Piccini P. Pallidal dopaminergic denervation and rest tremor in early Parkinson's disease: PPMI cohort analysis. *Parkinsonism Relat Disord* 2018; 51: 101-104.

Li W*, **Lao-Kaim NP***, Roussakis AA, Martín-Bastida A, Valle-Guzman N, Paul G, *et al*. ^{11}C-PE2I and ^{18}F-Dopa for assessing progression rate in Parkinson's: A longitudinal study. *Mov Disord* 2018; 33(1): 117-127.

Li W, **Lao-Kaim NP**, Roussakis AA, Martín-Bastida A, Valle-Guzman N, Paul G, *et al*. Longitudinal functional connectivity changes related to dopaminergic decline in Parkinson's disease. *NeuroImage Clin* 2020; 28: 102409.

Martín-Bastida A, **Lao-Kaim NP**, Loane C, Politis M, Roussakis AA, Valle-Guzman N, *et al*. Motor associations of iron accumulation in deep grey matter nuclei in Parkinson's disease: a cross-sectional study of iron related magnetic resonance imaging susceptibility. *Eur J Neurol* 2017; 24(2): 357-365.

Martín-Bastida A*, **Lao-Kaim NP***, Roussakis AA, Li W, Xing Y, Schwarz ST, *et al*. Relationship between neuromelanin and dopamine terminals within the Parkinson's nigrostriatal system. *Brain* 2019; 142: 2023-2036.

Martín-Bastida A, **Lao-Kaim NP**, Xing Y, Loane C, Roussakis AA, Schwarz ST, *et al*. Longitudinal motor associations of iron accumulation in Parkinson's disease: a study with high-pass filtered phase imaging. *Manuscript in preparation*.

Mohamed MA, Zeng Z, Gennaro M, Myers JFM, Calsolaro V, Femminella GD, *et al*. Astrogliosis in Aging and Parkinson's disease Dementia: a new clinical study with ^{11}C-BU99008 PET/CT. *Manuscript in submission*.

Porter E, Roussakis AA, **Lao-Kaim NP**, Piccini P. Multimodal dopamine transporter (DAT) imaging and magnetic resonance imaging (MRI) to characterise early Parkinson's disease. *Parkinsonism Relat Disord* 2020; 79: 26-33.

Roussakis AA, Gennaro M, Gordon MF, Reilmann R, Borowsky B, Rynkowski G, *et al*. A PET-CT study on microglia activation state in Huntington's patients treated with laquinimod. *Manuscript in submission*.

Roussakis AA, Gennaro M, **Lao-Kaim NP**, Towey D, Piccini P. Dopamine transporter density in *de novo* Parkinson's disease does not relate to the development of levodopa-induced dyskinesia. *J Neuroinflamm Neurodegener Dis* 2019; 3(1).

Roussakis AA, **Lao-Kaim NP**, Piccini P. Brain imaging and impulse control disorders in Parkinson's disease. *Curr Neurol Neurosci Rep* 2019; 19: 67.

Roussakis AA, Towey D, Gennaro M, **Lao-Kaim NP**, Piccini P. Parkinson's Disease Dyskinesias Possibly Relate to Greater Dopamine Transporter Losses in the Putamen Over Time. *J Neurol Exp Neurosci* 2019; 5(S1): S6-S11.

Roussakis AA, Zeng Z, **Lao-Kaim NP**, Martín-Bastida A, Piccini P, TRANSEURO Consortium. Parkinson's disease laterality: a ^{11}C-PE2I PET imaging study. *J Neurol* 2021; 268: 582-589.

Zeng Z, Roussakis AA, **Lao-Kaim NP**, Piccini P. Astrocytes in Parkinson's disease: from preclinical assays to in vivo imaging and therapeutic probes. *Neurobiol Aging* 2020; 95: 264-270.

(* - Joint first authorship)

Conference Presentations

Gennaro M, Roussakis AA, **Lao-Kaim NP**, Searle G, Kalk N, Lingford-Hughes A, Gunn R, Piccini P. Modified pipeline for ^{11}C-PBR28 PET data for the quantification of striatal TSPO-specific binding: application to Huntington's disease. *European Conference for Clinical Neuroimaging, Brussels, Belgium, May 2019. (2ND PLACE ECCN AWARD).*

Lao-Kaim, NP (2019). Positron emission tomography findings relating to the effect of intraputaminal fetal ventral mesencephalic cell transplant. *5th GFORCE-PD Annual Meeting, Cambridge, UK, Apr 2019*.

Lao-Kaim NP, Martín-Bastida A, Roussakis AA, Searle G, Paul G, Widner H, Foltynie T, Barker RA, Piccini P, TRANSEURO Consortium. Positron emission tomography imaging of the short-term longitudinal effects of intraputamenal hfVM transplantation on dopaminergic and serotonergic function in Parkinson's disease. *Network for European CNS Transplantation and Restoration, Online Event, Nov 2020.*

Li W, **Lao-Kaim NP**, Roussakis AA, Martín-Bastida A, Loane C, Valle-Guzman N, Kefalopoulou Z, Politis M, Foltynie T, Barker RA, Piccini P. Comparison of DAT and DOPA PET tracer for assessing severity and progression in patients with Parkinson's disease. *Movement Disorders Society, Berlin, Germany, Jun 2016*.

Martín-Bastida A, **Lao-Kaim NP**, Roussakis AA, Politis M, Li W, Valle-Guzman N, Kefalopoulou Z, Paul G, Widner H, Foltynie T, Barker RA, Piccini P. Imaging nigrostriatal circuitry with ^{11}C-PE2I PET and Neuromelanin-sensitive MR in Parkinson's disease. *European Academy of Neurology, Copenhagen, Denmark, Jun 2016*.

Martín-Bastida A, **Lao-Kaim NP**, Roussakis AA, Politis M, Li W, Valle-Guzman N, Kefalopoulou Z, Paul G, Widner H, Foltynie T, Barker RA, Piccini P. Multimodal imaging assessment of nigrostriatal pathway in Parkinson's disease using ^{11}C-PE2I PET and Neuromelanin-sensitive MR. *Movement Disorders Society, Berlin, Germany, Jun 2016. (SELECTED TOP ABSTRACT).*

Martín-Bastida A, **Lao-Kaim NP**, Xing Y, Loane C, Roussakis AA, Schwarz ST, Li X, Valle-Guzman N, Mahlknecht P, Paul G, Widner H, Foltynie T, Barker RA, Auer DP, Piccini P. Assessing longitudinal iron deposition in deep grey matter nuclei with high-pass filtered phase magnetic resonance imaging in Parkinson's disease. *European Academy of Neurology, Amsterdam, Netherlands, Jun 2017*.

Martín-Bastida A, **Lao-Kaim NP**, Xing Y, Loane C, Roussakis AA, Schwarz ST, Li X, Valle-Guzman N, Mahlknecht P, Paul G, Widner H, Foltynie T, Barker RA, Auer DP, Piccini P. High-pass filtered phase magnetic resonance imaging to detect longitudinal motor associations of iron accumulation in Parkinson's disease. *Movement Disorders Society, Vancouver, Canada, Jun 2017*.

Piccini P, **Lao-Kaim NP**. A 2021 Update on Imaging. *Virtual GFORCE-PD Meeting, Online Event, Mar 2021.*

Roussakis AA, **Lao-Kaim NP**, Martín-Bastida A, Valle-Guzman N, Kefalopoulou Z, Paul-Visse G, Widner H, Politis M, Foltynie T, Barker RA, Piccini P. Increased serotonin-to-dopamine transporter ratios in Parkinson's disease dyskinesias: a longitudinal study. *European Academy of Neurology, Copenhagen, Denmark, May 2016*.

Roussakis AA, **Lao-Kaim NP**, Martín-Bastida A, Valle-Guzman N, Kefalopoulou Z, Paul-Visse G, Widner H, Politis M, Foltynie T, Barker RA, Piccini P. Levodopa-induced dyskinesia in Parkinson's: a longitudinal PET study. *Association of British Neurologists, Brighton, UK, May 2016*.

Table of Contents

Abstract 4

Declaration of Originality 6

Copyright Declaration 7

Acknowledgments 8

Publications 10

Conference Presentations 13

Table of Contents 15

List of Figures 20

List of Tables 23

Abbreviations 24

Chapter 1. Parkinson's Disease 31

1.1. Epidemiology & aetiology 31

1.2. Clinical signs and symptoms 33

1.3. Pathology & pathophysiology 38

1.4. Nigrostriatal dysfunction and dopamine depletion 49

1.5. Pathophysiological and clinical implications of nigrostriatal dopamine depletion 57

1.6. Current treatments for Parkinson's disease 69

1.7. Fetal Cell Therapy in Parkinson's disease 79

1.7.1. Imaging findings in open-label trials 81

1.7.1.1. Dopamine synthesis and storage capacity 81

1.7.1.2. D_2 receptor density and dopamine release 84

1.7.1.3. Dopamine transporter expression 85

1.7.1.4. Non-dopaminergic imaging findings 89

1.7.2. NIH-funded randomised controlled trials 92
1.7.3. Imaging for the efficacy of hfVM transplants 94
1.7.3.1. Patient selection 94
1.7.3.2. Graft survival and viability 95
1.7.3.3. Graft-induced dyskinesias 96
1.7.3.3.1. Dopamine hyperinnervation 97
1.7.3.3.2. Patchy innervation 99
1.7.3.3.3. Serotonergic hypothesis 101
1.8. The current thesis: The Transeuro trial 105
Chapter 2. Transeuro Protocol, Materials and Methods 107
2.1. Observational arm 109
2.1.1. Subject recruitment 109
2.1.2. Motor assessments 110
2.1.3. Cognitive assessment 111
2.2. Magnetic resonance imaging arm 114
2.2.1. Subject recruitment 114
2.3. Transplant arm 115
2.3.1. Subject recruitment 116
2.3.2. [^{18}F]FDOPA exclusion & randomisation 116
2.3.3. Human fetal ventral mesencephalic cell transplant 117
2.3.4. Positron emission tomography 119
2.3.4.1. Basic Principles 119
2.3.4.2. [^{18}F]FDOPA 124
2.3.4.3. [^{11}C]PE2I 126
2.3.4.4. [^{11}C]DASB 127
2.3.5. Drug withdrawal 129

2.3.6. Transplant patient dropouts and exclusions 129
2.4. Ethical approvals 131
2.5. Neuroimaging protocol 132
2.5.1. Image acquisition 132
2.5.2. Structural magnetic resonance imaging 132
2.5.3. Positron emission tomography 132
2.5.4. Image processing 133
Chapter 3. Effects of Intraputamenal hfVM Transplants on Dopaminergic and Serotonergic Function in Parkinson's Disease 140
3.1. Statistical analysis 142
3.1.1. Region of interest analysis 142
3.1.1.1. Within-group analysis 142
3.1.1.2. Between-group analysis 143
3.1.1.3. Regression analysis 143
3.1.2. Putamenal coverage analysis 144
3.1.2.1. Group voxelwise analysis 144
3.1.2.2. Sub-regional analysis 145
3.2. Results 147
3.2.1. Subject demographics 147
3.2.2. Graft survival and growth: [^{18}F]FDOPA 147
3.2.2.1. Regional within-group ANCOVA 147
3.2.2.2. Regional between-group mixed ANCOVA 151
3.2.2.3. Longitudinal voxelwise analysis 153
3.2.2.4. Putamenal coverage 157
3.2.3. Graft DAT expression: [^{11}C]PE2I 160
3.2.3.1. Regional within-group ANCOVA 160

3.2.3.2. Regional between-groups mixed ANCOVA 162
3.2.3.3. Longitudinal voxelwise analysis 164
3.2.3.4. Putamenal coverage 168
3.2.4. The relationship between AADC activity and DAT expression 171
3.2.5. Graft SERT Expression: [11C]DASB 175
3.2.5.1. Regional within-group ANCOVA 175
3.2.5.2. Regional between-group mixed ANCOVA 177
3.2.5.3. Longitudinal voxelwise analysis 179
3.2.5.4. Putamenal coverage 183
3.3. Discussion 186
Chapter 4. Effects of Intraputamenal hfVM Transplants on the Motor Symptoms of Parkinson's Disease 194
4.1. Statistical analysis 196
4.1.1. Linear mixed effects models 196
4.1.2. Multiple Regression 197
4.2. Results 200
4.2.1. Progression of the cardinal motor symptoms in transplanted patients 200
4.2.2. Effect of dopaminergic and serotonergic re-innervation on the cardinal motor symptoms of transplanted patients 211
4.3. Discussion 218
Chapter 5. Graft-induced Dyskinesia and the Relationship with Dopaminergic and Serotonergic Re-innervation 227
5.1. Statistical analysis 230
5.2. Results 231
5.2.1. Clinical and demographic analysis 231
5.2.2. Analysis of absolute PET values and imbalance indices 231

5.2.3. Serotonergic to dopaminergic ratio analysis 231
5.2.4. Case Report: Patient 18 236
5.3. Discussion 241
Chapter 6. General Discussion: Summary of Findings 250
Chapter 7. Limitations and Future Directions 254
Bibliography 257
Appendix 314

List of Figures

Figure 1.1: Lewy bodies and Lewy neurites in Parkinson's disease. 40

Figure 1.2: Six neuropathological stages in Parkinson's disease 43

Figure 1.3: Schematic of the organisation of striato-nigro-striatal projections 51

Figure 1.4: The main functional subdivisions of the cortico-basal ganglia-thalamo-cortical circuits 58

Figure 1.5: Cortico-basal ganglia-thalamo-cortical circuitry 61

Figure 1.6: Mechanisms of action for currently available medications in the treatment of Parkinson's disease. 70

Figure 1.7: Proposed model for serotonergic neuron involvement in L-dopa-induced dyskinesias. 73

Figure 1.8: [^{18}F]FDOPA examinations of graft survival and growth. 83

Figure 1.9: Inconsistent findings for the ability of grafted neurons to express the dopamine transporter 87

Figure 1.10: Effects of hfVM transplantation on cortical activity. 91

Figure 1.11: Restoration of dopamine storage and synthesis capacity, basal and drug-induced dopamine release by hfVM transplantation. 99

Figure 1.12: Patchy innervation may explain the emergence of graft-induced dyskinesia 101

Figure 1.13: Serotonergic hyperinnervation in the grafted striatum of two patients from the Lund open-label trial. 103

Figure 2.1: Patient flow diagram for the Transeuro trial. 108

Figure 2.2: Surgical technique for transplantation of hfVM tissue. 118

Figure 2.3: Positron emission tomography and coincidence detection. 120

Figure 2.4: Storage of count data as projections and sinograms. 123

Figure 2.5: Illustration of image reconstruction by back-projection. 124

Figure 2.6: Metabolic pathway of [^{18}F]FDOPA. 125

Figure 2.7: Skeletal structural formula for [^{11}C]PE2I. 126

Figure 2.8: Skeletal structural formula for [^{11}C]DASB. 128

Figure 2.9: Image pre-processing and analysis pipeline for [^{18}F]FDOPA, [^{11}C]PE2I and [^{11}C]DASB PET 139

Figure 3.1: 3D rendering of the striatal mask 146

Figure 3.2: Within-group ANCOVA for [^{18}F]FDOPA. 150

Figure 3.3: Between-group ANCOVA for [^{18}F]FDOPA. 152

Figure 3.4: Voxelwise analysis of post-transplant changes in [^{18}F]FDOPA. 153

Figure 3.5: Post-operative [^{18}F]FDOPA changes for patients 007, 008, 014 and 018. 155

Figure 3.6: Post-operative [^{18}F]FDOPA changes for patients 023, 026, 027 and 029. 156

Figure 3.7: Antero-posterior putamenal profiles for [^{18}F]FDOPA. 158

Figure 3.8: Within-group ANCOVA for [^{11}C]PE2I. 161

Figure 3.9: Between-group ANCOVA for [^{11}C]PE2I. 163

Figure 3.10: Voxelwise analysis of post-transplant changes in [^{11}C]PE2I 164

Figure 3.11: Post-operative [^{11}C]PE2I changes for patients 007, 008, 014 and 018 166

Figure 3.12: Post-operative [^{11}C]PE2I changes for patients 023, 026, 027 and 029 167

Figure 3.13: Antero-posterior putamenal profiles for [^{11}C]PE2I 169

Figure 3.14: Relationship between cell survival and dopamine transporter expression 174

Figure 3.15: Within-group ANCOVA for [^{11}C]DASB 176

Figure 3.16: Between-group ANCOVA for [^{11}C]DASB 178

Figure 3.17: Voxelwise analysis of post-transplant changes in [^{11}C]DASB 179

Figure 3.18: Post-operative [^{11}C]DASB changes for patients 007, 008, 014 and 018 181

Figure 3.19: Post-operative [^{11}C]DASB changes for patients 023, 026, 027 and 029 182

Figure 3.20: Antero-posterior putamenal profiles for [^{11}C]DASB 184

Figure 4.1: Mixed model plots showing progression of clinical symptoms following transplant. 209

Figure 4.2: Mixed model plots showing progression of objective measures of clinical severity following transplant. 210

Figure 4.3: Plots illustrating multiple regression results for the prediction of post-operative clinical change by dopaminergic and serotonergic PET measures. 216

Figure 5.1: Regional differences in dopaminergic measures between patients with and without graft-induced dyskinesia 234

Figure 5.2: Regional differences in dopaminergic to serotonergic ratio between patients with and without graft-induced dyskinesia. 235

Figure 5.3: UPDRS-III motor and AIMS dyskinesia rating scores for patient 18 238

Figure 5.4: Longitudinal dopaminergic and serotonergic changes in patient 18. 239

List of Tables

Table 2.1: Table listing the number of patients recruited from specialist movement disorders clinics at each institution under the Transeuro project.....107

Table 2.2: UPDRS-III and symptom sub-scores. 112

Table 2.3: Injected dose and injected mass for each tracer, group and time-point. 133

Table 3.1: Subject demographics at baseline and follow-up time-points for the transplant and control groups.....149

Table 3.2: Results of the voxelwise paired t-test comparing pre-transplant to post-transplant [^{18}F]FDOPA 154

Table 3.3: Putamenal volume showing post-operative increases in [^{18}F]FDOPA. 159

Table 3.4: Results of the voxelwise paired t-test comparing pre-transplant to post-transplant [^{11}C]PE2I 165

Table 3.5: Putamenal volume showing post-operative increases in [^{11}C]PE2I 170

Table 3.6: Relationship between cell survival and dopamine transporter expression.....172

Table 3.7: Results of the voxelwise paired t-test comparing pre-transplant to post-transplant [^{11}C]DASB.....180

Table 3.8: Putamenal volume showing post-operative increases in [^{11}C]DASB.....185

Table 4.1: Progression of clinical symptoms following transplant. 203

Table 4.2: Progression of objective measures of clinical severity following transplant. 207

Table 4.3: Relationship between changes in dopaminergic and serotonergic imaging measures and clinical progression following transplant.....213

Table 5.1: Pre-transplant demographic and clinical measures for the GID+ and GID- groups. 232

Abbreviations

5-HT: Serotonin

5-HT_{1A}: Serotonin 1A receptor

5-HT_{1B}: Serotonin 1B receptor

5-HT_{2C}: Serotonin 2C receptor

6-OHDA: 6-hydroxydopamine

8-OH-DPAT: 5-HT_{1A} agonist ((±)-8-hydroxy-2-dipropylaminotetralin hydrobromide)

AADC: Aromatic Amino acid Decarboxylase

AC: Attenuation-Corrected

ACE-R: Addenbrooke's Cognitive Examination – Revised

AC-PC: Anterior Commissure-Posterior Commissure

ADAM: 2-((2-((dimethylamino)methyl)phenyl)thio)-5-iodophenylamine

ADD image: Signal-averaged image

AFM: 2-[2-(dimethylaminomethyl)phenylthio]-5-fluoromethylphenylamine

AIC: Akaike Information Criterion

AIMS: Abnormal Involuntary Movement Scale

ANCOVA: Analysis of Covariance

ARSAC: Administration of Radioactive Substances Advisory Committee

AV-133: 9-fluoropropyl-(+)-dihydrotetrabenazine

β-CFT: 2β-carbomethoxy-3β-(4-fluoro)tropane

β-CIT: 2β-carbomethoxy-3β-(4-iodophenyl)tropane

BG: Basal Ganglia

BOLD: Blood-Oxygen-Level-Dependent

BP_{ND}: Non-displaceable Binding Potential

BU99008: 2-(4,5-Dihydro-1H-imidazol-2-yl)-1-methyl-1H-indole

cAMP: Cyclic Adenosine Monophosphate

CDRS: Clinical Dyskinesia Rating Scale

CI: Confidence Interval

CNS: Central Nervous System

COMTI: Catechol-*O*-Methyltransferase Inhibitor

CT: Computed Tomography

DA: Dopamine

DAPA: dihydroxyphenylalanine

DARTEL: Diffeomorphic Anatomical Registration Through Exponentiated Lie algebra

DASB: 3-amino-4-(2-dimethylaminomethylphenylsulfanyl)-benzonitrile

DAT: Dopamine Transporter

DBS: Deep Brain Stimulation

DDCI: Dopamine Decarboxylase Inhibitor

df: degrees of freedom

DLPFC: Dorsolateral Prefrontal Cortex

DNA: Deoxyribonucleic Acid

DSM-IV: Diagnostic and Statistical Manual of Mental Disorders IV

DTBZ: Dihydrotetrabenazine

DV: Dependent Variable

DYS+/-: with/without Dyskinesia

ESS: Extra Sum-of-Squares

FDG: Fluorodeoxyglucose

FDOPA: Fluorodopa

FE-PE2I: (E)-*N*-(3-iodoprop-2-enyl)-2β-carbofluoroethoxy-3β-(4′-methyl-phenyl)nortropane

fMRI: Functional Magnetic Resonance Imaging

FE-CBT: fluoroethyl-methyl-2β-carboxymethoxy-3β-4-bromophenyl-tropane

FE-CIT: *N*-ω-fluoroethyl-2β-carbomethoxy-3β-(4-iodophenyl)nortropane

FMRIB: Oxford Centre for Functional MRI of the Brain

FP-CIT: *N*-ω-fluoropropyl-2β-carbomethoxy-3β-(4-iodophenyl)nortropane

FSL: FMRIB Software Library

FU: Follow-Up

FWE: Family-Wise Error

FWHM: Full Width at Half Maximum

GABA: Gamma-Aminobutyric Acid

GID: Graft-Induced Dyskinesia

GID+/-: with/without Graft-Induced Dyskinesia

GPe: Globus Pallidus pars Externa

GPi: Globus Pallidus pars Interna

GRAPPA: Generalized Autocalibrating Partial Parallel Acquisition

H&Y: Hoehn & Yahr scale

hfVM: Human Fetal Ventral Mesencephalon

HLA: Human Leukocyte Antigen

IBF: 5-iodo-7-*N*-[(1-ethyl-2-pyrrolidinyl)methyl]carboxamido-2,3-dihydrobenzofuran

IBZM: Iodobenzamide

IC: Internal Capsule

ICC: Intra-class Correlation Coefficient

IPT: *N*-(3-iodopropen-2-yl)-2β-carbomethoxy-3β-(chlorophenyl)tropane

K_i: Uptake rate constant

L-dopa: Levodopa

LE: Lower Extremity

LEDD: Levodopa-Equivalent Daily Dosage

LEGA: Likelihood Estimation Graphical Analysis

LID: Levodopa-Induced Dyskinesia

LOR: Line of Response

LP: Lewy Pathology

MADAM: *N*-dimethyl-2-(2-amino-4-fluoromethylhenylthio)benzylamine

MAOBI: Monoamine Oxidase type B Inhibitor

McN5652: 1,2,3,5,6,10b-Hexahydro-6-(4-(methylthio)-phenyl)pyrrolo-(2, 1-a)-isoquinoline

MIAKAT: Molecular Imaging and Kinetic Analysis Toolbox

MMSE: Mini-Mental State Examination

MNI: Montreal Neurological Institute

MPRAGE: Magnetization-Prepared RApid Gradient Echo

MPTP: 1-methyl-4-phenyl-1,2,3,6-tetrahydropyridine

MRI: Magnetic Resonance Imaging

MSN: Medium Spiny Neuron

nAC: non-Attenuation-Corrected

NACP: Precursor protein of the Non-Amyloid-β Component

NET: Norepinephrine Transporter

NHS: National Health Service

NIH: National Institutes of Health

NMDA: *N*-methyl-D-aspartate

NMSP: *N*-methylspiperone

NNC112: 8-chloro-7-hydroxy-3-methyl-5-(7-benzofuranyl)-2,3,4,5-tetrahydro-IH-3-benzazepine

NRES: National Research Ethics Service

OMD: 3-O-methyldopa

OMPFC: Orbitomedial Prefrontal Cortex

PD: Parkinson's Disease

PE: Phase Encode

PE2I: *N*-(3-iodopro-2*E*-enyl)-2β-carbomethoxy-3β-(4'-methylphenyl)nortropane

PET: Positron Emission Tomography

PIGD: Postural-Instability & Gait Difficulty

PHNO: 4-propyl-9-hydroxynaphthoxazine

PK11195: *N*-methyl-*N*-(1-methylpropyl)-3-isoquinoline-carboxamide

PPMI: Parkinson's Progression Markers Initiative

QQ: Quantile-Quantile

RBD: Rapid-eye-movement sleep Behaviour Disorder

REM: Rapid Eye Movement

RMSE: Root Mean Square Error

ROI: Region of Interest

SCH23390: (R)-(+)-7-chloro-8-hydroxy-3-methyl-1-phenyl-2,3,4,5-tetrahydro-1H-3-benzazepine

SD: Standard Deviation

SE_B: Standard error of the coefficient

SERT: Serotonin Transporter

SMA: Supplementary Motor Area

SN: Substantia Nigra

SNc: Substantia Nigra pars Compacta

SNr: Substantia Nigra pars Reticulata

SPECT: Single-Photon Emission Computed Tomography

SPM: Statistical Parametric Mapping

SRTM: Simplified Reference Tissue Model

SSRI: Selective Serotonin Reuptake Inhibitor

STN: Subthalamic Nucleus

TBZOH: Dihydrotetrabenazine

TD: Tremor-Dominant

TH: Tyrosine Hydroxylase

TRODAT-1: [2-[[2-[[[3-(4-chlorophenyl)-8-methyl-8-azabicyclo]3.2.1]oct-2-yl]methyl](2-mercaptoethyl)amino]ethyl]amino]ethanethiolato(3-)-*N*2,*N*20,*S*2,*S*20]oxo-[1*R*-(exo-exo)]

TrypOH: Tryptophan Hydroxylase

UE: Upper Extremity

UPDRS: Unified Parkinson's Disease Rating Scale

UPDRS-III: motor component of UPDRS

VA: Ventroanterior

VL: Ventrolateral

VMAT2: Vesicular Monoamine Transporter 2

VTA: Ventral Tegmental Area

Chapter 1. Parkinson's Disease

1.1. Epidemiology & aetiology

Parkinson's disease (PD) is the second most common neurodegenerative disease after Alzheimer's disease (Fratiglioni and Qiu, 2009). While affecting approximately 0.3% of the entire population (Tanner and Goldman, 1996; Pringsheim *et al.*, 2014) the prevalence of PD appears to increase exponentially with age; across population-based studies and door-to-door surveys, estimates range between 0.2-0.5% at 60 years of age, rising to 0.8-4.4% among persons aged 80 and over (Tanner and Goldman, 1996; de Lau and Breteler, 2006). The number of cases is consistently in favour of males at a ratio of ~1.4 (Parkinson's Disease Collaborators, 2018) and has been found to be lower amongst Asian and Black ethnicities (Tanner and Goldman, 1996; Van Den Eeden *et al.*, 2003; Wright Willis *et al.*, 2010).

Standardised incidence rates are estimated at between 8-18 cases per 100,000 person-years but as with prevalence experience a sharp increase from under 100 per 100,000 person-years for persons aged 60 to approximately 350, and in some populations up to 700, per 100,000 person years by the age of 80 (de Lau and Breteler, 2006). In general, onset rarely occurs before 50 years of age (de Lau and Breteler, 2006), however, early and juvenile onset PD are now recognised and may comprise up to 10% of cases (Ferguson *et al.*, 2016). The mortality ratio is 1.5 times higher in PD patients compared to the age-matched healthy population, with life expectancy from onset until death ranging between 6.9 to 14.3 years (Macleod *et al.*, 2014). This is significantly higher in early-onset PD at the expense of increased years of life lost (Ferguson *et al.*, 2016).

A recent study has confirmed a stark rise in prevalence from 2.5 to 6.1 million cases worldwide between 1990 and 2016 (Parkinson's Disease Collaborators, 2018). Further increases to 8.7-9.3 million are forecast by 2030 (Dorsey *et al.*, 2007). Although this could be explained by a general rise in the elderly populous it is not the sole contributory factor. Improved study quality, greater awareness of diagnosis and other forms of Parkinsonism (Adler *et al.*, 2014; Rizzo *et al.*, 2016), increased life expectancy (Wanneveich *et al.*, 2018), declining smoking rates (Rossi *et al.*, 2018) and geographical location and/or socio-demographic index, largely corresponding to environmental toxicant exposure due to rapid

industrialisation and proximity to pesticides and heavy metals (Kieburtz and Wunderle, 2013; Pezzoli and Cereda, 2013; Pringsheim *et al.*, 2014), have also been proposed (Dorsey *et al.*, 2007; Parkinson's Disease Collaborators, 2018). Taking these additional factors into account, projections suggest that global burden could potentially exceed 17 million by 2040 (Dorsey and Bloem, 2018; Dorsey *et al.*, 2018; Parkinson's Disease Collaborators, 2018; Rossi *et al.*, 2018; Wanneveich *et al.*, 2018). In addition to this rise in prevalence, evidence has recently emerged suggesting that incidence rates may also be increasing, particularly in males (Savica *et al.*, 2016).

1.2. Clinical signs and symptoms

Parkinson's disease was first medically described by surgeon James Parkinson in 1817. In his seminal work entitled "*An Essay on the Shaking Palsy*", the observation of six separate cases led to his defining the disease as one of:

> "*Involuntary tremulous motion, with lessened muscular power, in parts not in action and even when supported; with a propensity to bend the trunk forwards, and to pass from a walking to a running pace: the senses and intellects being un-injured*"
>
> - James Parkinson, 1817 (Parkinson, 2002)

He also observed that symptoms would present asymmetrically and that individuals often exhibited speech impairment, fatigue, hypersomnolence, sialorrhea, dysphagia, micrographia and incontinence. Parkinson originally termed the disease "shaking palsy" or "paralysis agitans", but it would later be renamed Parkinson's disease by the French neurologist Jean-Martin Charcot who critically recognised that such patients suffer from a slowness of movement that emerges long before muscular rigidity predominates, that does not relate to a general weakening and which does not necessarily co-occur with resting tremor:

> "*…you can easily recognize how difficult it is for them to do things even though rigidity or tremor is not the limiting feature. Instead, even a cursory exam demonstrates that their problem relates more to slowness in execution of movement rather than to real weakness. In spite of tremor, a patient is still able to do most things, but he performs them with remarkable slowness. Between the thought and the action there is a considerable time lapse. One would think neural activity can only be effected after remarkable effort"*
>
> - Jean-Martin Charcot, 1872 (Factor and Weiner, 2008)

Indeed, these observations form the backbone of the current clinical view of Parkinson's disease, as a progressive movement disorder that is principally characterised by a symptom triad of bradykinesia, rigidity and resting tremor, with an additional fourth symptom of postural instability that emerges only in advanced disease (Hoehn and Yahr, 1967; Gibb and

Lees, 1988; Hughes *et al.*, 1992; Postuma *et al.*, 2015a). Diagnosis is based on clinical examination, as formalised by the UK Parkinson's Disease Society Brain Bank and Movement Disorder Society. Both stipulate that bradykinesia, defined as the slowness of voluntary movement with progressive decrement in amplitude and speed over repetitive action, stands as an essential feature (Gibb and Lees, 1988; Hughes *et al.*, 1992; Postuma *et al.*, 2015a). At least one of the other two cardinal symptoms must also be present; tremor in the order of 4-6Hz at rest that is suppressed by action and/or rigidity, defined as the velocity-independent resistance to passive movement (Postuma *et al.*, 2015a). Unilateral onset and persistent symptomatic asymmetry, significant beneficial response to dopaminergic therapy, progressive worsening of symptoms and the development of levodopa-induced dyskinesia and on-off phenomenon after prolonged pharmacological intervention are used as supporting diagnostic features. Broadly, patients can be categorised as either a tremor-dominant (TD) or postural-instability & gait difficulties (PIGD) subtype, the former generally showing a younger onset but slower progression with good medication response and prognosis while the latter has a significantly higher propensity for balance impairment and falls, presents as a more bradykinetic/rigid phenotype, has higher likelihood for cognitive impairment, is generally older onset and progresses faster with poorer prognosis (Thenganatt and Jankovic, 2014). The heterogeneity in disease presentation and progression however makes classification challenging and contentious, with alternative categories such as akinetic-rigid-dominant proposed (Marras and Lang, 2013; Kotagal, 2016) while a number of patients are deemed as either mixed or indeterminate and many switch from TD to PIGD over time (Lee *et al.*, 2019a).

Patients often report subtle motor manifestations 5-10 years prior to initial neurological exam (Gaenslen *et al.*, 2011; Postuma *et al.*, 2012b; Darweesh *et al.*, 2017; Fereshtehnejad *et al.*, 2019), most commonly being that of dysgraphia (McLennan *et al.*, 1972; Rosenblum *et al.*, 2013; Letanneux *et al.*, 2014; Fereshtehnejad *et al.*, 2019), hypophonia (Gaenslen *et al.*, 2011; Postuma *et al.*, 2012b; Hlavnicka *et al.*, 2017; Fereshtehnejad *et al.*, 2019), sialorrhea (Gaenslen *et al.*, 2011; Fereshtehnejad *et al.*, 2019), reduced arm swing (Gaenslen *et al.*, 2011), balance (Gaenslen *et al.*, 2011; Schrag *et al.*, 2015; Fereshtehnejad *et al.*, 2019) and hypomimia (Postuma *et al.*, 2012b; Fereshtehnejad *et al.*, 2019; Simonet *et al.*, 2019) which is often

misattributed to changes in mood or attitude towards others (Gunnery *et al.*, 2016). Charcot himself commented on blankness of expression, stating that:

> *"... the muscles of the face are motionless, there is even a remarkable fixity of look, and the features present a permanent expression, of mournfulness, sometimes of stolidness or stupidity*".
>
> - Jean-Martin Charcot, 1872 (Factor and Weiner, 2008)

Non-motor symptoms such as hyposmia, dysautonomia, sleep and psychiatric disturbance are also acknowledged as supporting features of PD (Gibb and Lees, 1988; Hughes *et al.*, 1992; Jankovic, 2008; Berg *et al.*, 2015; Postuma *et al.*, 2015a) and can have a significant if not equal impact on a patients' overall quality of life (Gallagher *et al.*, 2010; Antonini *et al.*, 2012). Many first appear, with varying chronicity across individuals, within the prodromal phase (Gaenslen *et al.*, 2011; Fereshtehnejad *et al.*, 2019). Most notably, rapid eye movement sleep behaviour disorder (RBD), characterised by loss of REM sleep atonia, is consistently found to strongly predict neurodegenerative disease (Iranzo *et al.*, 2014; Berg *et al.*, 2015; Postuma *et al.*, 2015b; Postuma *et al.*, 2015c), with idiopathic RBD cases showing a 50-fold higher risk for PD (Postuma and Berg, 2016) and about half phenoconverting over an average of 14 years (Schenck *et al.*, 2013). By comparison, subtle motor signs constitute a 10-fold higher risk for phenoconversion (Postuma and Berg, 2016). Sensitivity is low however, and only 46% of individuals with established PD satisfy criteria for RBD (Sixel-Döring *et al.*, 2011). In contrast, hyposmia is highly prevalent in both the prodromal phase (Ross *et al.*, 2008; Ponsen *et al.*, 2009; Gaenslen *et al.*, 2011; Postuma *et al.*, 2012a; Siderowf *et al.*, 2012; Berg *et al.*, 2015) and in the post-diagnostic phase, affecting 96.7% of established PD cases (Haehner *et al.*, 2009), but is much less specific and presents in many other conditions (Hawkes, 2003; Postuma *et al.*, 2012a). A recent study using mixed models to estimate the lead times for prodromal symptoms found that both RBD and hyposmia could appear over 20 years prior to the formal diagnosis of PD and over 10 years prior to the appearance of motor prodromes (Fereshtehnejad *et al.*, 2019). Reduced bowel movements are also frequently reported and there is ample evidence indicating that those with constipation are more than twice as likely to acquire motor-PD within 10-17 years following initial complaint (Abbott *et al.*, 2001; Gaenslen *et al.*, 2011; Noyce *et al.*, 2012; Schrag *et al.*, 2015; Adams-Carr *et al.*, 2016; Postuma

and Berg, 2016; Fereshtehnejad *et al.*, 2019). Clinically significant comorbid depression occurs in some 35% of PD patients (Reijnders *et al.*, 2008) while a similar percentage suffer from at least one anxiety disorder (Dissanayaka *et al.*, 2010; Leentjens *et al.*, 2011). Both are slightly more common in individuals who later go on to develop motor-PD and are believed to become prominent particularly in the final years preceding diagnosis, albeit with comparatively low relative risk, sensitivity and specificity (Alonso *et al.*, 2009; Noyce *et al.*, 2012; Postuma *et al.*, 2012a; Shen *et al.*, 2013; Gustafsson *et al.*, 2015; Schrag *et al.*, 2015; Darweesh *et al.*, 2017; Fereshtehnejad *et al.*, 2019).

Under UK Brain Bank guidelines, pooled diagnostic accuracy has been calculated at 82.7% (Hughes *et al.*, 1992; Rizzo *et al.*, 2016), while in the clinic can be as low as 53% in drug-responsive patients within the first 5 years of disease (Adler *et al.*, 2014) and can be amended in around one third of early cases at follow-up assessment (Caslake *et al.*, 2008). Misdiagnosis is attributable mostly to progressive supranuclear palsy, multiple system atrophy or essential tremor, with which Parkinson's disease shares many symptoms especially early on in the disease course (Rizzo *et al.*, 2016).

As the disease progresses postural reflexes become more affected resulting in more severe gait difficulties and impaired balance. Figures vary widely, but a significant number of patients will also experience festinating gait, described as the occurrence of rapid small steps to maintain centre of gravity when the body involuntarily leans forward, and/or recurrent freezing episodes, that is the sudden and transient inability to move (Giladi *et al.*, 2001; Bloem *et al.*, 2004; Hely *et al.*, 2005; Macht *et al.*, 2007; Hely *et al.*, 2008; Jankovic, 2008). These factors, as well as the overall worsening of symptoms, result in a higher frequency of falls and subsequent loss of independence and reduced quality of life by incapacitation (Giladi *et al.*, 2001; Bloem *et al.*, 2004; Hely *et al.*, 2008; Allen *et al.*, 2013; Hiorth *et al.*, 2014; Kader *et al.*, 2016). PD patients are more than twice as likely to sustain any type of fracture (Melton *et al.*, 2006) and the risk of injury-related mortality is increased by 51% as compared to the age-matched healthy population (Allyson Jones *et al.*, 2012). Significant imbalance on its own carries a three-fold increase in mortality risk if observed within 15 years of diagnosis (Hely *et al.*, 2005). Furthermore, fear of falling can lead to a feeling of vulnerability and an avoidance of various physical and functional activities and tasks, self-imposed withdrawal

from societal participation and ultimately a more sedentary lifestyle (Rahman *et al.*, 2011; Kader *et al.*, 2016; Jonasson *et al.*, 2018), which in itself could perpetuate the risk of falling through lack of muscle strengthening and conditioning (Bloem *et al.*, 2004; Shen *et al.*, 2016).

Between one third to a half of patients will also sustain one or a combination of deformities of the joints or axial skeleton, most commonly including striatal limb, antecollis, Pisa syndrome, camptocormia or scoliosis (Ashour and Jankovic, 2006; Jankovic, 2008; Doherty *et al.*, 2011; Pandey and Kumar, 2016; Tinazzi *et al.*, 2019), characterised by extreme abnormal flexion and differentiated by the body region affected and the plane along which the flexion occurs. These deformities are linked to greater disease severity and longer disease duration (Ashour and Jankovic, 2006; Pandey and Kumar, 2016; Tinazzi *et al.*, 2019) as well as to higher frequency of falls and mild-moderate back pain in 46% of those with a postural affliction (Tinazzi *et al.*, 2019) and contribute to significant disability and interference with activities of daily living.

Other troubling symptoms typically experienced with greater severity and frequency in the later stages of disease include dysphagia with increased choking, dysarthria, urinary incontinence, constipation, symptomatic orthostatic hypotension, respiratory disturbances that increase risk for respiratory tract infections such as pneumonia, hypersomnolence, RBD and other sleep disturbances, psychosis and depression, all of which significantly affect a patients' functional ability and overall quality of life (Fernandez and Lapane, 2002; Hely *et al.*, 2005; Jankovic, 2008). Finally, evidence shows that the incidence of dementia subsequent to the diagnosis of PD is up to five times higher than in those without disease (de Lau *et al.*, 2005) and up to 75% of individuals will show evidence of cognitive decline within 20 years of diagnosis at an average onset of 10 years disease duration (Buter *et al.*, 2008; Hely *et al.*, 2008). Cognitive impairment and the onset of dementia are strongly associated with recurrent falls, admission to nursing homes and increased mortality (Levy *et al.*, 2002; de Lau *et al.*, 2005; Melton *et al.*, 2006; Latt *et al.*, 2009; Allen *et al.*, 2013; Macleod *et al.*, 2014).

1.3. Pathology & pathophysiology

The neuropathological and diagnostic hallmarks of Parkinson's disease consist of the elevated formation of eosinophilic proteinaceous inclusions in neuronal perikarya and cellular processes termed Lewy bodies and Lewy neurites and the progressive loss of pigmented neurons in the substantia nigra pars compacta (Gibb and Lees, 1988, 1991; Gibb *et al.*, 1991; Hughes *et al.*, 1992; Forno, 1996; Spillantini *et al.*, 1997; Braak *et al.*, 1999; Damier *et al.*, 1999b; Dickson, 2012).

First described by Fritz Jacob Heinrich Lewy in 1912 (Engelhardt and Gomes, 2017), Lewy bodies can be distinguished broadly into two morphological subtypes. The "classical" brainstem-type Lewy body upon standard hematoxylin-eosin staining typically appears as a spherical intracytoplasmic inclusion of 5-30μm diameter with a compact eosinophilic core, concentric lamellar bands and pale-staining peripheral halo that under electron microscopy reveals a dense granular centre surrounded by an ordered outer layer of irradiating filaments measuring 5-20nm in diameter (Gibb and Lees, 1988; Forno, 1996; Spillantini *et al.*, 1997; Spillantini *et al.*, 1998; Olanow *et al.*, 2004) (Figure 1.1). Cortical-type Lewy bodies are also eosinophilic but are rather more irregular and are generally smaller, with a fibrillary structure lacking a well-defined core and peripheral halo (Mahul-Mellier *et al.*, 2020). Intraneuritic inclusions (Lewy neurites), observed most frequently within the axon, can have various morphological guises, appearing as anywhere from coarse and elongated varicose, club-shaped or branching forms causing ballooning of the nerve cell to filiform or spindle-like aggregates less than the diameter of the axon but extending up to 700nm in length, often forming bundles that can be traced for up to 4mm (Spillantini *et al.*, 1997; Spillantini *et al.*, 1998; Braak *et al.*, 1999; Goedert *et al.*, 2013; Mahul-Mellier *et al.*, 2020). Recent evidence supports the view that those fibrillar aggregates initially formed in the nerve cell processes as Lewy neurites are transported over time to the perinuclear region where they eventually accumulate and rearrange into highly organised Lewy body-like structures (Braak *et al.*, 2003b; Kanazawa *et al.*, 2008; Mahul-Mellier *et al.*, 2020). Precursory depositions termed pale bodies, so-called due to their weak eosinophilicity, are also known to initiate aggregation in the soma of pigmented brainstem neurons (Wakabayashi *et al.*, 1998).

The discovery in 1997 of a high penetrance point mutation within exon 4 (G209A) of the α-synuclein gene (*SNCA*) in several independent Greek and Italian kindreds with autosomal-dominant, early-onset Parkinson's disease represented the first significant evidence implicating this protein in disease pathogenesis (Polymeropoulos *et al.*, 1997). Later the same year, immunohistochemical analysis revealed that most Lewy pathology in the substantia nigra, hippocampal formation and cingulate cortex of patients with autopsy-confirmed Parkinson's disease and dementia with Lewy bodies were strongly immunoreactive for α-synuclein and ubiquitin, the former being identified as the more extensive and predominant constituent (Spillantini *et al.*, 1997; Spillantini *et al.*, 1998). Double-labelled tissue sections showed that classic-type Lewy bodies exhibit intense α-synuclein immunoreactivity of the peripheral rim while anti-ubiquitin antibodies accumulate at the core and with considerable intermediate co-localisation, though morphology and degree of ubiquitin staining can vary substantially (Spillantini *et al.*, 1997; Baba *et al.*, 1998; Mezey *et al.*, 1998; Spillantini *et al.*, 1998; Gómez-Tortosa *et al.*, 2000; Sakamoto *et al.*, 2002).

α-synuclein is a small soluble acidic protein of 140 amino acid residues that is highly concentrated in pre-synaptic terminals and ubiquitously expressed throughout the brain (Maroteaux *et al.*, 1988). Structurally, it is composed of a positively charged N-terminus, a hydrophobic non-amyloid-β component and a highly negatively charged acidic C-terminus. The central hydrophobic region is critical for its ability to self-assemble and form amyloid-like fibrils with a cross-β-sheet structure and Greek key topology (Serpell *et al.*, 2000; Tuttle *et al.*, 2016), with deletion of the offending 12-residue stretch abrogating the capacity for α-synuclein to polymerize (Giasson *et al.*, 2001).

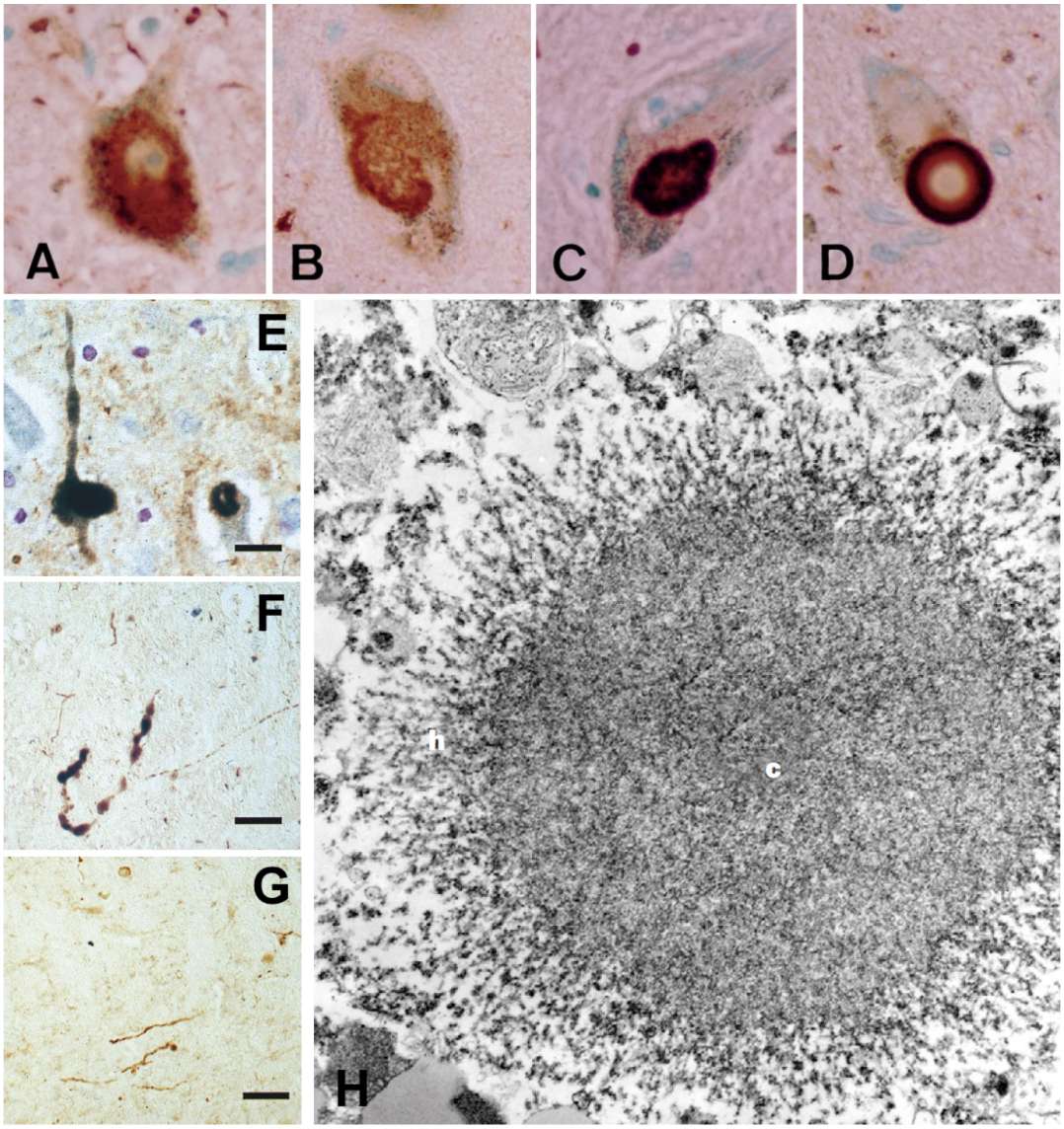


Figure 1.1: Lewy bodies and Lewy neurites in Parkinson's disease. A-D | Different maturation stages of the Lewy body differentiated by anti-NACP immunostaining (antibodies NACP-1 and NACP-2); A | Diffuse cytoplasmic staining of a morphologically normal-looking neuron (x600), B | irregularly shaped staining of a poorly pigmented neuron (x600), C | discrete staining corresponding to the pale body (x600), D | typical Lewy body (x740). E-F | Club-shaped (E, bar = 18μm) and varicose (F, bar = 90μm) Lewy neurites double-stained for α-synuclein (antibody PER1) and ubiquitin (antibody 1510). G | Filamentous Lewy neurites single-stained for α-synuclein (antibody PER1) (bar = 100μm). H | Electron micrograph of a Lewy body demonstrating a granular core [c] and outer halo composed of radiating filaments [h]. Images reproduced from; A-D | (Wakabayashi et al., 1998), E-G | (Spillantini et al., 1998), H | (Olanow et al., 2004).

While monomeric α-synuclein is considered intrinsically disordered, its structure bestows highly dynamic conformational qualities whose regulation is dependent on the local cellular milieu (Ahn *et al.*, 2002; Stephens *et al.*, 2019). The amino acid sequence found within the N-

terminal domain, consisting of a series of seven 11-residue imperfect repeats of the highly conserved hexamer motif KTKEGV, confers a propensity for α-synuclein to adopt amphipathic broken α-helical structures upon binding to anionic phospholipid membranes (Davidson *et al.*, 1998; Perrin *et al.*, 2000; George, 2002; Chandra *et al.*, 2003; Bodner *et al.*, 2009; Middleton and Rhoades, 2010; Fusco *et al.*, 2014; Pirc and Ulrih, 2015), with different conformations assumed depending on the composition and characteristics (e.g. membrane curvature) of its interactive partner (Bodner *et al.*, 2009; Middleton and Rhoades, 2010; Lashuel *et al.*, 2013). This affinity for a wide variety of lipid assemblies underlies many of its proposed physiological functions including regulation of neurotransmitter release, synaptic plasticity, control of synaptic membrane processes and biogenesis, cellular trafficking, maintenance of vesicle pool homeostasis and modulation of neuronal survival (Davidson *et al.*, 1998; Burré *et al.*, 2010; Scott and Roy, 2012; Burre *et al.*, 2014; Wang *et al.*, 2014; Hunn *et al.*, 2015; Emamzadeh, 2016; Shahmoradian *et al.*, 2019).

Structural perturbations to α-synuclein such as those resulting from the six known *SNCA* missense mutations on the N-terminal domain (p.Ala30Pro (Krüger *et al.*, 1998), p.Ala53Glu (Pasanen *et al.*, 2014), p.Ala53Thr (Polymeropoulos *et al.*, 1997), p.Glu46Lys (Zarranz *et al.*, 2004), p.Gly51Asp (Lesage *et al.*, 2013), p.His50Gln (Appel-Cresswell *et al.*, 2013; Flagmeier *et al.*, 2016)), post-translational modifications (e.g. phosphorylation at serine-129) (Burre *et al.*, 2018; Chen *et al.*, 2019), α-synuclein overexpression (as is the case with *SNCA* multiplication carriers (Singleton *et al.*, 2003) or when degradation machinery are impaired) and pathogenic conditions within the cellular environment (e.g. pH, salt or iron concentration) significantly disrupt various lipid-protein, protein-protein and intramolecular interactions (Buell *et al.*, 2014; Wang *et al.*, 2014; Fusco *et al.*, 2016; Bengoa-Vergniory *et al.*, 2017; Dettmer *et al.*, 2017; Ranjan and Kumar, 2017; Burre *et al.*, 2018; Lima *et al.*, 2019; Meade *et al.*, 2019; Shahmoradian *et al.*, 2019; Stephens *et al.*, 2019; Zhang *et al.*, 2019), with deleterious effects likely relating to both loss and gain of function mechanisms (Alegre-Abarrategui *et al.*, 2019). Such disease conditions promote protein misfolding and affect the propensity for α-synuclein to form intermediate oligomeric species that further transition to amyloid-like fibrillary state (Caughey and Lansbury, 2003; Winner *et al.*, 2011; Kalia *et al.*, 2013; Buell *et al.*, 2014; Lee *et al.*, 2014; Wang *et al.*, 2014; Chu and Kordower, 2015; Roberts *et al.*, 2015;

Flagmeier *et al.*, 2016; Bengoa-Vergniory *et al.*, 2017; Skamris *et al.*, 2019; Mahul-Mellier *et al.*, 2020).

The distribution of Lewy pathology (LP) in the PD brain follows a stereotypic topographical pattern. Early indications that an unconventional "prion-like" mechanism may underlie disease progression were documented by Braak and colleagues, whose seminal immunohistopathologic findings that LP deposition appeared to follow a non-random rostrocaudal succession across distinct but interconnected regions of the PD brain led to their proposal that the disease advances in six neuropathological stages (Braak *et al.*, 2003a; Braak *et al.*, 2003b) (Figure 1.2). The same group theorised the initiation of the disease cascade and sequential temporospatial disease pattern to be the work of an unknown external pathogen, such as a neurotropic virus, that first gains bodily access via nasal and/or enteric entry points, before spreading along projection neurons by axonal transport and trans-synaptic transmission to the initial induction sites of the CNS and across susceptible portions of the connectome thereafter, promoting α-synuclein misfolding and aggregation along its path (Hawkes *et al.*, 2007). However, for a small percentage of individuals no Lewy pathology was found in these primary transit structures i.e. the dorsal motor nucleus (7%) and amygdala (10%), despite all cases showing inclusions in the SN. These latter findings stand in opposition to such a proposal of a clinicopathologic staging system and obligatory trigger site(s) within the CNS, instead highlighting a topographic heterogeneity of disease affliction between PD patients (Kalaitzakis *et al.*, 2008).

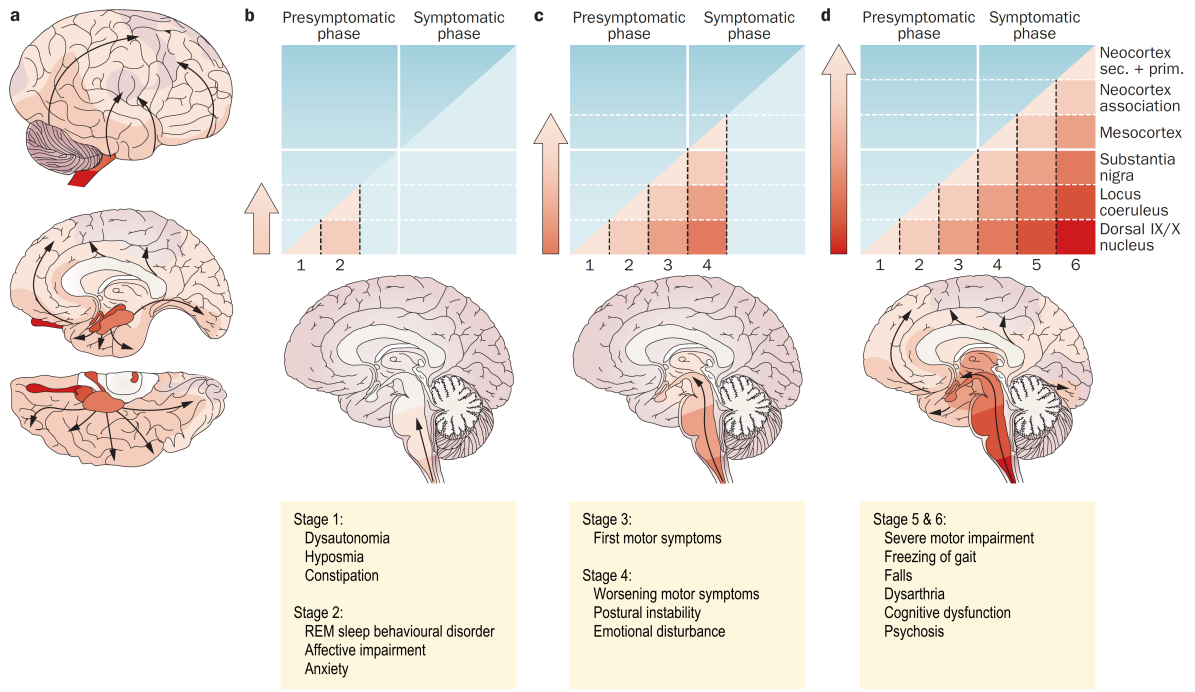


Figure 1.2: Six neuropathological stages in Parkinson's disease and associated clinical presentation (b-d), following a rostrocaudal pattern of progression (a). Deeper red shading represents greater severity of pathology. According to the observations of Braak and colleagues (Braak et al., 2003a; Braak et al., 2003b), the earliest stages of disease are characterised by α-synuclein-immunopositive inclusions almost exclusively in the dorsal motor nucleus of the glossopharyngeal and vagal nerves and/or intermediate reticular zone of the medulla oblongata and in the olfactory bulb and anterior olfactory structures. Stage 2 is defined by the involvement of the pontine tegmentum, with α-synuclein immunoreactivity detected in the caudal raphe, gigantocellular nucleus of the reticular formation and locus coeruleus, as well as nonthalamic nuclei that project diffusely to the cerebral cortex including nucleus tuberomamillaris, nucleus basalis of Meynert, interstitial nucleus of the diagonal band and medial septal nucleus. Stages 1 and 2 are associated with the prodromal phase of disease. The clinical phase, in which the cardinal Parkinson's motor symptoms first emerge, begins at stage 3 when Lewy pathology reaches the midbrain, including the substantia nigra pars compacta, tegmental pedunculopontine nucleus and the upper raphe group, and the central subnucleus of the amygdala. Stage 4 marks the spread of Lewy pathology to the temporal mesocortex and limbic regions including additional subnuclei of the amygdala, cingulate cortex, entorhinal cortex and hippocampal formation and is associated with a worsening of motor symptoms, postural instability and emotional disturbance. Finally in advanced disease (stages 5 & 6), pathological lesions develop in projection neurons of the deep layers of the neocortex, first in prefrontal and high-order sensory association areas and thereafter spreading to first order sensory association areas, premotor areas and primary sensory and motor fields. In these stages motor impairment is severe with increased freezing of gait, frequency of falls, dysarthria and choking and many patients experience cognitive dysfunction, psychosis and viscerosensory/visceromotor dysregulation. Figure adapted from (Goedert et al., 2013).

Post-mortem examination of patients who had previously undergone intraputamenal transplantation of human fetal ventral mesencephalic tissue offered evidence fuelling an

alternative hypothesis, that the prion-like disease process may in fact be driven by misfolded α-synuclein itself (Brundin *et al.*, 2008; Lerner and Bagic, 2008; Kordower and Brundin, 2009; Olanow and Prusiner, 2009). Out of 17 patients who have come to autopsy and in whom LP was investigated, 10 developed pathological inclusions in melanised grafted neurons with similar morphology to those natively found in the SNc, staining positive for serine-129 phosphorylated α-synuclein, ubiquitin and thioflavin-S, marking β-sheet formation (Kordower *et al.*, 1995; Kordower *et al.*, 1996; Freed *et al.*, 2001; Kordower *et al.*, 2008a; Kordower *et al.*, 2008b; Li *et al.*, 2008; Mendez *et al.*, 2008; Li *et al.*, 2010; Schrag *et al.*, 2010; Kurowska *et al.*, 2011; Ahn *et al.*, 2012; Hallett *et al.*, 2014; Li *et al.*, 2016; Kordower *et al.*, 2017). The frequency and density of Lewy pathology deposition in grafted neurons appears to increase with age. Across studies, all LP positive grafts were more than 10 years old whereas 5 of the 6 grafts without pathology were aged between 7 months and 9 years. In one interesting case where right/left surgical procedures were performed 12-years and 16-years prior to death, the younger graft displayed LP in only 1.9% of melanised neurons while this increased to 5% in the older graft (Li *et al.*, 2008). Furthermore, soluble non-aggregated α-synuclein was detected in 40% of 12-year-old TH-immunoreactive cells whereas this doubled to 80% in the 16-year-old TH+ cells (Li *et al.*, 2008). In another case series, accumulation of cytoplasmic α-synuclein became evident in grafts 4 years of age, while additional aggregated masses were detected only in the 2 patients with 14-year-old grafts (Kordower *et al.*, 2008a; Kordower *et al.*, 2008b). α-synuclein immunoreactivity is not normally seen in developmentally young neurons, and in healthy individuals over 20 years of age α-synuclein is seen to be in a soluble non-aggregated form, as indicated by proteinase K protocol (Chu and Kordower, 2007). Thus ectopic placement of embryonic neurons within a PD microenvironment could permit the movement of misfolded α-synuclein from diseased host neurons to their new young and healthy grafted neighbours (Brundin *et al.*, 2008; Lerner and Bagic, 2008; Kordower and Brundin, 2009; Olanow and Prusiner, 2009). Moreover, it is now known that oligomeric and fibrillar α-synuclein conformers are capable of propagating from cell to cell across anatomically connected regions via exocytosis/endocytosis, direct diffusion, exosomes or tunnelling nanotubes (Emmanouilidou *et al.*, 2010; Volpicelli-Daley *et al.*, 2011; Ma *et al.*, 2019), where they can subsequently induce the conversion of normal cytosolic endogenous α-synuclein into pathological conformations

by a permissive templating process (Danzer *et al.*, 2007; Brundin *et al.*, 2008; Kordower *et al.*, 2008a; Li *et al.*, 2008; Desplats *et al.*, 2009; Hansen *et al.*, 2011; Volpicelli-Daley *et al.*, 2011; Luk *et al.*, 2012; Masuda-Suzukake *et al.*, 2013; Visanji *et al.*, 2013; Lee *et al.*, 2014; Masuda-Suzukake *et al.*, 2014; Recasens and Dehay, 2014; Chu and Kordower, 2015; Peelaerts *et al.*, 2015; Tarutani *et al.*, 2016; Leak *et al.*, 2019).

It is important to note that although the presence of α-synuclein and ubiquitin-rich Lewy bodies and neurites in the brain offers a convenient means by which disease progression can be objectively schematised, the relationship between Lewy pathology, cellular dysfunction and death is unclear (Dickson *et al.*, 2008; Kalaitzakis *et al.*, 2008; Jellinger, 2009; Parkkinen *et al.*, 2011; Berg *et al.*, 2014; Dijkstra *et al.*, 2014; Schulz-Schaeffer, 2015; Surmeier *et al.*, 2017a). About 25% of elderly individuals who show no clinical signs of Parkinsonism are found to display midbrain Lewy pathology at autopsy (Fearnley and Lees, 1991; Markesbery *et al.*, 2009), while some symptomatic PD patients do not show any Lewy pathology at all (Poulopoulos *et al.*, 2012; Doherty *et al.*, 2013; Kalia *et al.*, 2015). In studies of incidental cases, significant cellular dysfunction and neurodegeneration in the substantia nigra has been shown to precede the formation of Lewy pathology (Milber *et al.*, 2012; Dijkstra *et al.*, 2014). Additionally, LP-containing nigral neurons appear morphologically healthier than their non-LP-containing counterparts (Gertz *et al.*, 1994) and are in comparison less likely to undergo apoptotic cell death (Tompkins and Hill, 1997). Some lines of thought propose that Lewy bodies could be so-called "innocent bystanders" of disease and that their formation reflects a cellular effort to sequester misfolded α-synuclein and other mutated, damaged or unwanted proteins and organelles for autophagic degradation and clearance as part of an aggresomal or other cytoprotective process (Olanow *et al.*, 2004; Tanaka *et al.*, 2004; Wakabayashi *et al.*, 2007; Parkkinen *et al.*, 2008; Wakabayashi *et al.*, 2013; Mahul-Mellier *et al.*, 2020). Indeed, at least 90 molecules have been identified within Lewy bodies, including components of the ubiquitin-proteasome system, p62 and heat-shock proteins (Leverenz *et al.*, 2007; Wakabayashi *et al.*, 2013). Moreover, mounting evidence suggests that prefibrillar oligomeric α-synuclein species confer significantly greater toxicity than mature fibrils and have considerable negative impact upon essential cellular processes including membrane, proteasomal, mitochondrial and endoplasmic reticulum function, inflammation, autophagy, Ca^{2+} homeostasis and synaptic transmission (Caughey and Lansbury, 2003; Danzer *et al.*,

2007; Winner *et al.*, 2011; Kalia *et al.*, 2013; Buell *et al.*, 2014; Lee *et al.*, 2014; Wang *et al.*, 2014; Chu and Kordower, 2015; Roberts *et al.*, 2015; Flagmeier *et al.*, 2016; Bengoa-Vergniory *et al.*, 2017; Skamris *et al.*, 2019; Mahul-Mellier *et al.*, 2020). Thus, Lewy pathology may be a proxy for neurodegeneration with intermediate oligomeric conformations instead acting as the critical drivers for pathogenesis (Bengoa-Vergniory *et al.*, 2017).

While the current consensus nevertheless appears to accept that toxic α-synuclein species can spread by a prion-like mechanism, it has been argued that neuronal fate is also determined by a particular set of regional or cell-autonomous factors (Brundin and Melki, 2017; Surmeier *et al.*, 2017a). Indeed, Braak noted that disproportionately long and thin projection neurons that are poorly myelinated or unmyelinated, resulting in a comparatively high energy expenditure, are especially vulnerable and that these characteristics are the basis of a non-random and stereotypic pathological pattern (Braak *et al.*, 2004). One region that meets these risk factors and which is of particular clinicopathologic relevance is the substantia nigra pars compacta. Neurodegeneration in this region occurs in all PD patients and is amongst the highest of all midbrain nuclei (Giguere *et al.*, 2018), with several studies estimating that approximately 30% of neuromelanin-containing neurons are lost by the time of clinical diagnosis (Fearnley and Lees, 1991; Ma *et al.*, 1997; Greffard *et al.*, 2006; Kordower *et al.*, 2013). The fact that SNc neurons synthesize dopamine confers even greater risk; excess cytosolic dopamine, and more specifically reactive quinones and semiquinones that are produced during neuromelanin biosynthesis, have been associated with neurotoxicity (Sulzer *et al.*, 2000; Sulzer and Zecca, 2000; Mosharov *et al.*, 2009; Hare and Double, 2016; Herrera *et al.*, 2017; Zucca *et al.*, 2017; Segura-Aguilar, 2019) and especially in the presence of α-synuclein (Mosharov *et al.*, 2009), while vesicular packing of cytosolic dopamine by VMAT2 reduces cell loss and dysfunction (Lohr *et al.*, 2014). Dopamine shares an intricate relationship with iron, which has been placed as an essential mediator of dopamine metabolism and the generation of neurotoxic intermediates and end products (Hare and Double, 2016). In its ferric form (Fe^{3+}), iron is credited with catalysing the oxidation of dopamine to dopamine-*o*-quinone in the initial step of the neuromelanin synthesis pathway (Sulzer and Zecca, 2000; Zecca *et al.*, 2008; Hare and Double, 2016; Zucca *et al.*, 2017). Iron is present in naturally high concentrations in the basal ganglia nuclei (Dexter *et al.*, 1991) and is consistently found in post-mortem and *in vivo* magnetic resonance imaging studies to be

further elevated in the substantia nigra of patients with Parkinson's disease, with its accumulation positively correlated to various measures of disease severity (Sofic *et al.*, 1988; Dexter *et al.*, 1991; Ulla *et al.*, 2013; Wieler *et al.*, 2015; Wang *et al.*, 2016; Martin-Bastida *et al.*, 2017). It is also well known that free ferrous iron (Fe^{2+}) acts as a catalyst in a reaction with hydrogen peroxide (Fenton reaction), producing highly toxic reactive oxygen species (hydroxyl radicals) and ferric iron that further lead to oxidative-stress-related damage to cellular components including proteins, lipids and DNA (Dexter *et al.*, 1991). Furthermore, redox-active iron interacts with α-synuclein and depending on the O_2 environment promotes its oligomerisation into a PD-relevant assembly (Abeyawardhane *et al.*, 2018). Pigmented neurons of the SNc may be particularly vulnerable in this regard because neuromelanin, which normally acts as a neuroprotective iron chelator, can itself become neurotoxic when oversaturated and iron becomes bound to low-affinity sites in a redox-active state. Dying neurons release insoluble neuromelanin granules into the extracellular milieu where they remain for long periods of time inducing chronic inflammation and production of reactive oxygen species via microglial activation, as well as by the slow release of ferric iron and other toxins that were previously adsorbed and stabilised in the neuromelanin structure (Faucheux *et al.*, 2003; Zecca *et al.*, 2003; Block *et al.*, 2007; Zecca *et al.*, 2008; Zucca *et al.*, 2017).

Other regions that share similar attributes, such as the VTA situated adjacent to the SNc, are however relatively spared from developing pathological inclusions and neuronal loss. Thus some more recent hypotheses based on comparative studies suggest that Ca^{2+}-related physiology, such as a particular reliance on Ca^{2+} for tonic pacemaking activity that can lead to sustained mitochondrial oxidant stress and reduced concentrations of the Ca^{2+} buffering protein calbindin D_{28k}, which has been associated with suppressing Lewy body formation, might account for the differential susceptibility (German *et al.*, 1992; Damier *et al.*, 1999b; Follett *et al.*, 2013; Rcom-H'cheo-Gauthier *et al.*, 2016; Surmeier *et al.*, 2017b; Alegre-Abarrategui *et al.*, 2019). Interestingly, an early study demonstrated that even within sub-regions of the SNc, the most extreme and prominent loss of neurons occurred in the calbindin-poor nigrosomes, while the calbindin-rich nigral matrix was comparatively protected (Damier *et al.*, 1999b). Others note that complex axonal arborisation and an extremely high number of axon terminals contribute to an elevated bioenergetic demand to

sustain physiological neurotransmission, which increases the rate of mitochondrial oxidative phosphorylation and production of reactive oxygen species. Accordingly, it has been demonstrated that reducing the energy demand by decreasing the arborisation size reduces oxidative stress and neuronal vulnerability to neurotoxic substances (Pacelli *et al.*, 2015).

Thus certain structural and physiological characteristics may not only render neurons more susceptible to α-synuclein pathology and its prion-like propagation but also to the effects of aging, as well as toxins and genetic mutations that are associated with the disease. Although their relative roles within a unified pathogenic mechanism are incompletely understood it is probable that cellular dysfunction and death is the consequence of a complex interplay between these aforementioned factors (Sulzer, 2007; Mosharov *et al.*, 2009; Hare and Double, 2016; Surmeier *et al.*, 2017a; Alegre-Abarrategui *et al.*, 2019).

1.4. Nigrostriatal dysfunction and dopamine depletion

The trajectory of neurodegeneration in the SNc proceeds at a negative exponential rate, decreasing by 45-50% in the first decade of affliction (adjusted by age), such that by the time the first motor symptoms manifest approximately 30% of neuromelanin-laden neurons in this region have already been lost (Fearnley and Lees, 1991; Ma *et al.*, 1997; Greffard *et al.*, 2006; Kordower *et al.*, 2013). This rate of decline is almost 10 times greater than that which could be accounted for by normal aging, wherein a linear fallout of 4.3-6% per decade is observed (Fearnley and Lees, 1991; Gibb and Lees, 1991; Cabello *et al.*, 2002; Rudow *et al.*, 2008). In descriptive anatomy, neuronal tracing and staining studies define two cellular tiers within the SNc; a calbindin-rich dorsal tier that encompasses the ventral tegmental area (VTA) and a ventral tier which is largely calbindin-negative, comprised of a densocellular group and the cell columns and whose dendrites extend ventrolaterally deep into the SN pars reticulata (SNr) (Lynd-Balta and Haber, 1994; Damier *et al.*, 1999a; Haber *et al.*, 2000). Neuronal loss across the nuclear subdivisions follows a caudorostral pattern strongly favouring destruction of the lateral part of the ventral tier (Rinne *et al.*, 1989; Fearnley and Lees, 1991; Halliday *et al.*, 1996; Damier *et al.*, 1999b; Parkkinen *et al.*, 2011; Milber *et al.*, 2012; Kordower *et al.*, 2013). At symptom onset, cell death in the ventrolateral region alone reaches 64% (Fearnley and Lees, 1991) while ventromedial and dorsal parts are still only modestly affected in early-stage disease (Fearnley and Lees, 1991; Kordower *et al.*, 2013). This pattern is maintained throughout moderate-late stage disease; across patients with 1-38 years of illness, an average 91% of melanised neurons in the ventrolateral SNc were estimated to have been lost, followed by the medial part of the ventral tier (71%) and lastly the dorsal tier (56%) (Fearnley and Lees, 1991). This spatial gradient largely corresponds to findings derived using calbindin D_{28k}-based segmentation that demonstrates a strict sequential order of involvement of the five calbindin-poor nigrosomal pockets, starting with N1 which topographically overlaps with the ventrolateral area and where dopamine neurons are virtually non-existent (average 98% loss), then moving rostrally through N2 → N4 → N3 → N5 (Damier *et al.*, 1999b). In the calbindin-positive neuropil (nigral matrix) within which the nigrosomes are embedded, dopamine cells are affected to a much lesser extent but still similarly conform to a caudorostral progression (Damier *et al.*, 1999b). Similar results have been obtained *in vivo* using iron-sensitive magnetic resonance imaging sequences, where the

classic "swallowtail" sign that normally appears on transverse nigral sections due to differences in iron content between the nigrosomes and nigral matrix disappears in the early stages of Parkinson's disease as N1 undergoes cellular degeneration (Blazejewska *et al.*, 2013; Schwarz *et al.*, 2014; Schwarz *et al.*, 2018). This consistently observed pattern stands in contrast to that which is seen in healthy ageing, wherein a gradient is observed but which preferentially affects the dorsal tier (-6.9% per decade) and to a lesser extent the medial (-5.4% per decade) and lateral (-2.1% per decade) parts of the ventral tier (Fearnley and Lees, 1991).

Dopaminergic neurons of both the ventral and dorsal SNc tiers are an integral part of basal ganglia circuitry, sending efferent projections chiefly to the striatum and cortex and receiving afferents derived mainly from the striatum and pedunculopontine nucleus. According to anterograde and retrograde tracing studies in animals, the general topography of nigrostriatal fibers aligns to a mediolateral configuration; the medial SNc and VTA harbour connections with the medial striatum and the lateral SNc and VTA with the lateral striatum. However, along the dorsal-ventral axis the nigrostriatal pathway exhibits an inverse topographic arrangement. Efferents arising in the dorsal tier of the SNc terminate in the ventromedial striatum including the head of the caudate and anterior putamen, while neurons projecting to the dorsal caudate nucleus and dorsal putamen of the sensorimotor striatum originate almost exclusively from the ventral tier of the SNc. Striatonigral fibers show similar dorsoventral topography, albeit with differential weighting in the proportion of neurons dedicated to each regional target. That is, whilst a large portion of the SNc, including the dorsal tier and densocellular group, is innervated by afferent connections originating from the ventral striatum, and efferent projections arising in the SNc predominantly terminate in the dorsolateral striatum, reciprocity in both instances is relatively minimal (Carpenter and Peter, 1972; Szabo, 1980; Lynd-Balta and Haber, 1994; Haber *et al.*, 2000; Haber, 2014) (Figure 1.3).

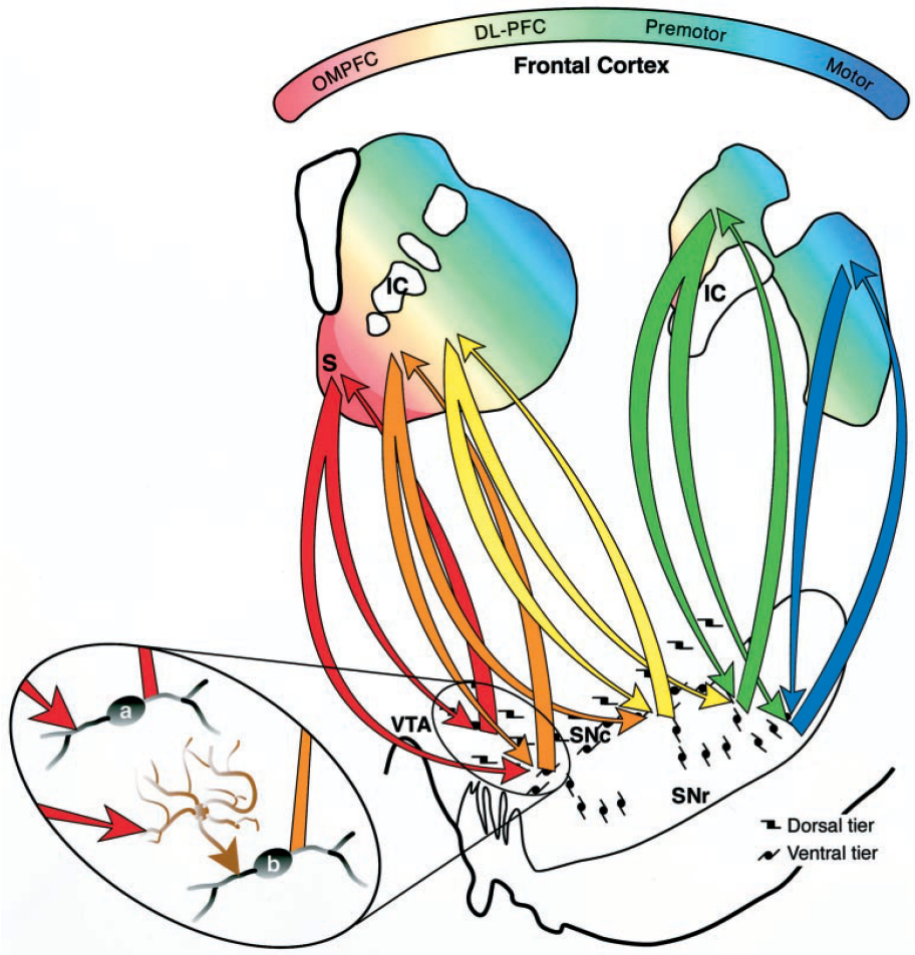


Figure 1.3: Schematic of the organisation of striato-nigro-striatal projections conforming to a mediolateral and inverse dorsoventral topography. The colour gradient within the striatal nuclei illustrates the general arrangement of limbic (red), associative (green) and motor (blue) corticostriatal inputs. Midbrain projections from the shell of the ventromedial striatum [S], distinguished from the rest of the striatum by its calbindin-negative staining and comparatively limited input from the cortex, midbrain and thalamus, target the ventral tegmental area and ventromedial SNc (red arrows). Midbrain projections from the VTA to the shell form a "closed," reciprocal loop (red arrow). An ascending striato-nigro-striatal spiral begins via feed-forward projections from the medial SN to the core of the ventromedial striatum (orange arrow) and continues dorsolaterally through sequential open-loop pathways (yellow, green and blue arrows), allowing ventral striatal regions to influence the more dorsal striatal regions. a | The reciprocal component (red arrows) of each limb of the striato-nigro-striatal projection terminates directly on a dopamine cell, resulting in inhibition. b | The feed-forward component (orange arrow) terminates indirectly on a dopamine cell via a GABAergic interneuron (brown cell), resulting in disinhibition. IC = internal capsule; DL-PFC = dorsolateral prefrontal cortex; OMPFC = orbito-medial prefrontal cortex; S = shell of the ventromedial striatum; SNc = substantia nigra pars compacta; SNr = substantia nigra pars reticulata; VTA = ventral tegmental area. Figure extracted from (Haber et al., 2000).

In contrast to the destruction of melanised cells within the SNc, the depletion of

dopaminergic markers at the striatal terminal appears to be much more profound (Hornykiewicz, 1998). Post-mortem investigations report that the Parkinson's disease striatum exhibits severe dopaminergic denervation of between 50-80% at the point of motor symptom onset, as indicated using biochemical measurement of dopamine and homovanillic acid concentrations (Bernheimer *et al.*, 1973; Nyberg *et al.*, 1983; Kish *et al.*, 1988), [^{3}H]TBZOH binding to the vesicular monoamine transporter type 2 (VMAT2) (Scherman *et al.*, 1989) and tyrosine hydroxylase immunoreactivity (Beach *et al.*, 2008; Kordower *et al.*, 2013). For comparison, the natural age-related decline in dopaminergic function in the putamen and caudate has been estimated at 5-8% per decade (Scherman *et al.*, 1989; Marek *et al.*, 2001; Nurmi *et al.*, 2001; Bohnen *et al.*, 2006; Ishibashi *et al.*, 2009; Shingai *et al.*, 2014). A comprehensive post-mortem investigation conducted by Kordower *et al.* (2013) found that from the earliest time points the number of neuromelanin-containing neurons remaining in the SNc significantly outweighed the number of tyrosine hydroxylase and dopamine transporter immunoreactive neurons detected in the nigrostriatal system (Kordower *et al.*, 2013). A similar mismatch has been demonstrated within sub-regions of the SNc in incidental Lewy body disease cases (Milber *et al.*, 2012). This imbalance continues throughout the first two decades of illness and converges over time. By 4-5 years post-diagnosis, axons innervating the dorsal putamen that continued to express tyrosine hydroxylase were virtually absent and those that were detected displayed degenerative morphologies. At the same time point, up to ~50% of dopaminergic nigral cell bodies remained viable (Kordower *et al.*, 2013). That the loss of nigral cell bodies lags behind the loss of dopaminergic phenotype is in line with the "dying back" hypothesis, that axonal degeneration may occur initially before proceeding retrograde towards the perikarya, potentially due to a preceding and more prominent degree of α-synuclein aggregation in the presynaptic terminal over the cell body (Hornykiewicz, 1998; Cheng *et al.*, 2010; Chu *et al.*, 2012; Burke and O'Malley, 2013; Schulz-Schaeffer, 2015; Calo *et al.*, 2016; Grosch *et al.*, 2016; Tagliaferro and Burke, 2016). This is consistent with *in vivo* imaging studies using diffusion-weighted imaging, in which the microstructural integrity measured along the nigrostriatal tract, as delineated by probabilistic tractography, was compromised at the distal end of the axon whilst remaining relatively intact at the proximal end (Andica *et al.*, 2018) and nuclear imaging studies in which the decrease of dopamine transporter density and vesicular

monoamine transporter, as measured using [^{11}C]β-CIT-FE, [^{18}F]FE-PE2I, [^{18}F]FP-CIT, [^{18}F]DTBZ and [^{18}F]AV-133 positron emission tomography (PET) in early and *de novo* PD with respect to healthy control values, is shown to be far greater in the striatum than the substantia nigra by an order of magnitude between 1.5-2.2, inflated to 1.7-2.8 if the putamen is considered separately (Okamura *et al.*, 2010; Hsiao *et al.*, 2014; Caminiti *et al.*, 2017; Fazio *et al.*, 2018; Lee *et al.*, 2019b).

Nuclear imaging modalities such as PET and single-photon emission computed tomography (SPECT), in conjunction with radioligands that target several molecules involved in the handling of dopamine, have provided additional insight into the dopaminergic state at symptomatic threshold in the living Parkinson's disease brain. Studies using tracers quantifying the dopamine transporter and vesicular monoamine transporter have yielded similar decrements to those found at autopsy (Guttman *et al.*, 1997; Lee *et al.*, 2000; Bohnen *et al.*, 2006; de la Fuente-Fernandez *et al.*, 2011; Nandhagopal *et al.*, 2011). However, estimates derived using [^{18}F]FDOPA tend to be more conservative, with a functional loss ranging between 20-40% (Morrish *et al.*, 1996; Morrish *et al.*, 1998; Nurmi *et al.*, 2001; Hilker *et al.*, 2005a; Gallagher *et al.*, 2011b; Nandhagopal *et al.*, 2011). [^{18}F]FDOPA is a fluorinated analogue of the endogenous dopamine precursor L-dopa that is decarboxylated by the aromatic amino acid decarboxylase (AADC) enzyme within the same metabolic pathway and stored in presynaptic vesicles as [^{18}F]-labelled dopamine, thereby providing a measure of presynaptic dopamine synthesis and storage capacity (Kuwabara *et al.*, 1993; Heiss and Hilker, 2004). By employing a longitudinal multitracer PET protocol, Nandhagopal *et al.* (2011) demonstrated that in comparison to dopamine transporter density and VMAT2 binding, which had dropped to ~40% of normative values at symptom onset, the activity of AADC in the same patients exhibited a significantly smaller reduction to ~60% of normal (Nandhagopal *et al.*, 2011). It has been hypothesised that this disparity reflects a disease-related compensatory mechanism whereby fractional dopamine biosynthesis in remaining presynaptic terminals is up-regulated while reuptake of dopamine after its release into the synaptic cleft is simultaneously down-regulated (Tedroff *et al.*, 1999; Lee *et al.*, 2000; Ribeiro *et al.*, 2002; Adams *et al.*, 2005; Bruck *et al.*, 2006; Moore *et al.*, 2008; Nandhagopal *et al.*, 2011; Pavese *et al.*, 2011). Similar up-regulatory plasticity has been observed at the post-synaptic membrane, with several studies using [^{123}I]IBF (Ichise *et al.*, 1999; Kim *et al.*, 2002) and

[^{123}I]IBZM (Seppi *et al.*, 2004; Plotkin *et al.*, 2005; Verstappen *et al.*, 2007; Jakobson Mo *et al.*, 2013) SPECT, [^{11}C]raclopride (Rinne *et al.*, 1990; Brooks *et al.*, 1992; Sawle *et al.*, 1993; Antonini *et al.*, 1994; Antonini *et al.*, 1995; Rinne *et al.*, 1995; Antonini *et al.*, 1997; Turjanski *et al.*, 1997; Dentresangle *et al.*, 1999; Kaasinen *et al.*, 2000; de la Fuente-Fernández *et al.*, 2001; Ghaemi *et al.*, 2002; Piccini *et al.*, 2003; Boileau *et al.*, 2009; Van Laere *et al.*, 2010), [^{11}C]NMSP (Kaasinen *et al.*, 2000) and [^{11}C]-(+)-PHNO PET (Boileau *et al.*, 2009; Payer *et al.*, 2016) demonstrating that striatal D_2 and D_3 receptor availability is either normal or heightened, in some cases by up to 44% (Rinne *et al.*, 1995), in *de novo* and early-stage PD as compared to controls, likely as a consequence of presynaptic deficiency and lowered synaptic dopamine levels (Sawle *et al.*, 1993). In contrast, striatal D_1 receptor density quantified using [^{11}C]SCH23390 (Rinne *et al.*, 1990; Shinotoh *et al.*, 1993; Turjanski *et al.*, 1997; Ouchi *et al.*, 1999) and [^{11}C]NNC112 PET (Cropley *et al.*, 2008) remains unchanged in early disease.

Across the striatum, denervation predominantly affects the putamen with relative indemnity of the caudate nucleus, is more prominent in the hemisphere contralateral to the body side on which motor symptoms are more severe and also exhibits a characteristic gradient mirroring that which is seen in the SNc, that is, beginning in the posterior-dorsal aspect before invading the anterior-ventral domain (Bernheimer *et al.*, 1973; Nyberg *et al.*, 1983; Kish *et al.*, 1988; Scherman *et al.*, 1989; Brooks *et al.*, 1990; Sawle *et al.*, 1993; Morrish *et al.*, 1996; Dentresangle *et al.*, 1999; Ichise *et al.*, 1999; Rinne *et al.*, 1999; Tedroff *et al.*, 1999; Lee *et al.*, 2000; Nurmi *et al.*, 2001; Ghaemi *et al.*, 2002; Nurmi *et al.*, 2003; Lee *et al.*, 2004; Adams *et al.*, 2005; Bohnen *et al.*, 2006; Bruck *et al.*, 2006; Huang *et al.*, 2007; Wang *et al.*, 2007; Martin *et al.*, 2008; Moore *et al.*, 2008; Bruck *et al.*, 2009; Nandhagopal *et al.*, 2009; Cheng *et al.*, 2010; Okamura *et al.*, 2010; Gallagher *et al.*, 2011b; Pavese *et al.*, 2011; Oh *et al.*, 2012; Hsiao *et al.*, 2014; Lin *et al.*, 2014; Han *et al.*, 2016; Sung *et al.*, 2017; Li *et al.*, 2018). An early [^{18}F]FDOPA PET imaging study implementing a grid-like segmentation within the anatomical boundaries of the putamen and caudate head comprehensively elucidated this pattern; in the striatum contralateral to the asymptomatic body side in unilateral PD patients, the caudal putamen showed a dorsal-to-ventral graduation of dopamine hypometabolism of 52-87% of normal, compared with the rostral putamen (52-95%) and caudate (71-99%). Furthermore this pattern was maintained in two separate groups of increasing disease severity (Morrish *et al.*, 1996). More recently, using [^{18}F]-FP-CIT PET, Han *et al.* (2016)

demonstrated dopamine transporter density to have dropped most prominently in the posterodorsal putamen to 23% of normal values by 4.5 years post-diagnosis, followed by the posteroventral putamen (34%), anterior putamen (47%), posterior caudate (68%), anterior caudate (63%) and ventral striatum (67%) (Han *et al.*, 2016).

The rate of striatal dopaminergic dysfunction also differs in accordance with this rostrocaudal gradient as well as depending on the duration of illness and the dopaminergic marker under investigation. Serial acquisition of [^{18}F]FDOPA (Nurmi *et al.*, 2001; Bruck *et al.*, 2006), [^{123}I]FP-CIT (Colloby *et al.*, 2005), [^{18}F]FP-CIT (Sung *et al.*, 2017) and [^{18}F]CFT (Nurmi *et al.*, 2003) in early-moderate PD yields estimates of between 1-14.5% decline annually with respect to baseline values, depending on clinical asymmetry and striatal division, such that within a fixed interval the posterior-dorsal region of the putamen degenerates faster than the anterior-ventral putamen, ventral striatum and caudate, and the striatal nuclei contralateral to the more severe body side show greater rates of decline than those in the ipsilateral hemisphere. Other study designs including those that compare rates between discrete disease severity groups (Staffen *et al.*, 2000; Sung *et al.*, 2017), between successive session intervals (Pirker *et al.*, 2003; Bruck *et al.*, 2009; Gallagher *et al.*, 2011b) or employ regression procedures on either single measurement or longitudinal datasets (Scherman *et al.*, 1989; Lee *et al.*, 2004; Schwarz *et al.*, 2004; Hilker *et al.*, 2005a; Nandhagopal *et al.*, 2009; Nandhagopal *et al.*, 2011; Hsiao *et al.*, 2014; Sung *et al.*, 2017) assert that DA nerve terminal dysfunction decelerates with time and conforms to a negative exponential curve. Using nonlinear mixed effects models to account for irregular measurement intervals and differences in the duration of illness between subjects at the time of scanning, Nandhagopal *et al.* found that while an anterior-posterior gradient is present at the onset of motor symptoms and is maintained throughout the disease course, the decay constant is similar across regions (Nandhagopal *et al.*, 2009). These findings imply that the observed PD-related gradient may be explained in part by the variability in the time of disease initiation across striatal divisions, but that once it has started non-specific mechanisms underlying disease progression affect each of the sub-regions to a similar degree. In a later study by the same group in which the longitudinal trajectories between dopaminergic markers were compared, it was found that AADC activity decreases significantly more rapidly than both VMAT2 and DAT within the first 15 years of clinical PD, thereafter proceeding at similar rates, a

relationship that is thought to reflect de-compensation in the face of more severe and progressive neuronal loss (Nandhagopal *et al.*, 2011). Indeed, earlier work implementing ratio analyses in a group of PD patients of 4.8 years disease duration demonstrated a significant elevation in the AADC:VMAT2 ratio with respect to healthy controls but only in the caudate and rostral portions of the putamen, while the VMAT2:DAT ratio was significantly depressed in the intermediate and caudal putamen (Lee *et al.*, 2000). In another study, a PD group with slightly lower duration of illness (3.2 years) displayed increased AADC:DAT ratios across striatal divisions but that was most prominently inflated in the intermediate and dorsal putamen, reaching approximately 160% and 198% respectively relative to controls (Tedroff *et al.*, 1999). The imbalance between dopaminergic markers also changes as a function of disease severity; across the whole striatum, AADC:VMAT2 ratios were significantly altered only at H&Y1 while changes in VMAT2:DAT were evident only at H&Y2/3 (Lee *et al.*, 2000). Collectively these data suggest that striatal dopaminergic dysfunction in PD, in both the absolute and relative sense, can be described by a complex interplay between multiple dopaminergic markers reflecting the combination of both progressive neurodegeneration and compensatory-de-compensatory mechanisms that are spatiotemporally dynamic, its state at any one time strongly depending on both the duration or severity of illness and the positioning along the rostrocaudal axis.

1.5. Pathophysiological and clinical implications of nigrostriatal dopamine depletion

The basal ganglia consists of a collection of interconnected subcortical nuclei including the substantia nigra pars compacta and striatum (putamen and caudate), as well as the substantia nigra pars reticulata, subthalamic nucleus and the globus pallidus pars interna and pars externa. Together with the thalamus and cortex, they form a series of highly organised parallel neural circuits (Alexander *et al.*, 1986; Alexander and Crutcher, 1990) that sub-serve a variety of motor and non-motor functions, including but not limited to motor skill learning (Hikosaka *et al.*, 2002; Doyon *et al.*, 2009; Jin and Costa, 2015), associative learning (Pasupathy and Miller, 2005), formation of habits (Yin and Knowlton, 2006), interval-timing (Buhusi and Meck, 2005), decision-making (Cox and Witten, 2019), behavioural inhibition (Jahanshahi *et al.*, 2015), emotional control (Marchand, 2010), social loss aversion (Delgado *et al.*, 2008) and planning and cognitive flexibility (Vaghi *et al.*, 2017). Five such circuits were originally proposed in accordance with the function of the cortical projection region engaged, namely the motor, oculomotor, dorsolateral prefrontal, lateral orbitofrontal and anterior cingulate circuits (Alexander *et al.*, 1986), yet this is not exhaustive and almost all cortical areas project to the striatum, forming a multitude of loops that can be broadly divided into sensorimotor, associative and limbic domains (Parent and Hazrati, 1995) (Figure 1.4). With respect to the motor circuit, the main entry point to the basal ganglia is through the dorsolateral striatum, which receives excitatory glutamatergic afferents from the somatosensory, premotor and motor cortices and the centromedian and parafascicular areas of the thalamus. The main output nuclei of the basal ganglia are the GPi and the SNr, which send inhibitory GABAergic axons to the ventral anterior and ventrolateral thalamic sub-regions (VA/VL), thereafter projecting glutamatergic efferents back to the cortex (Albin *et al.*, 1989; Alexander and Crutcher, 1990; DeLong, 1990).

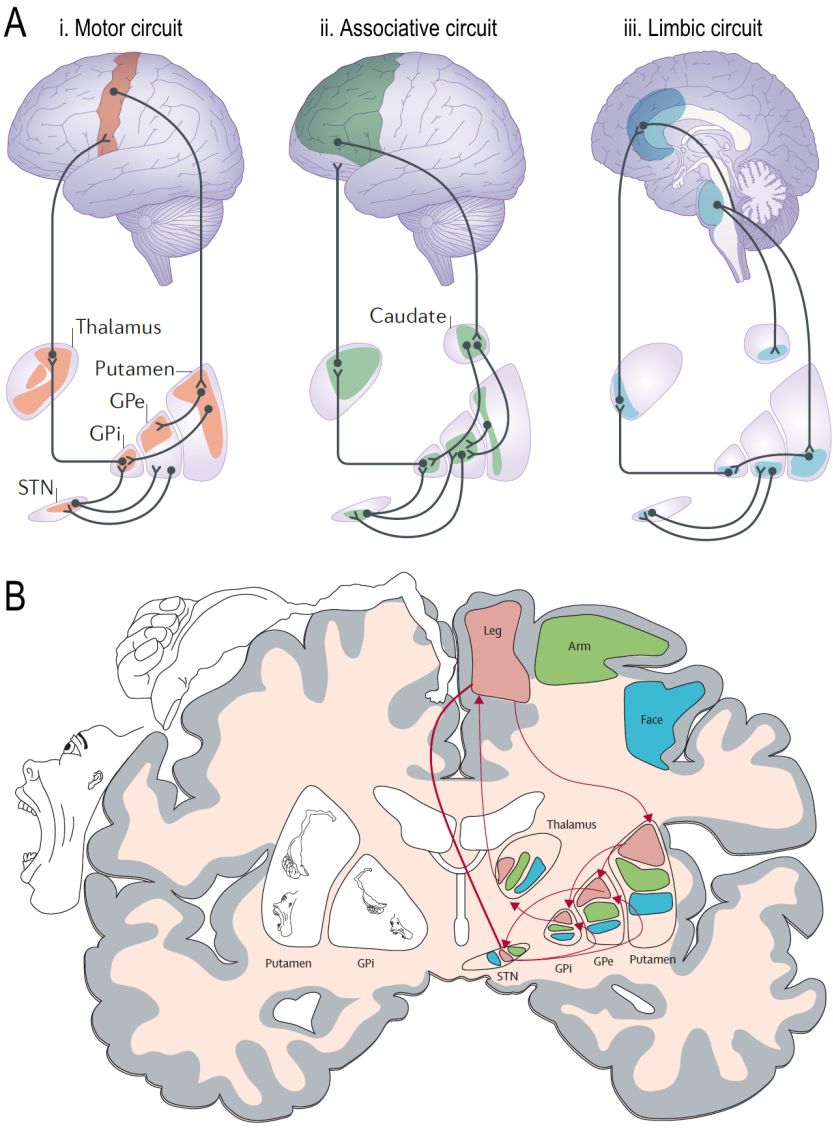


Figure 1.4: The main functional subdivisions of the cortico-basal ganglia-thalamo-cortical circuits. A | Simplified schematic of the main functional subdivisions of the cortico-basal ganglia-thalamo-cortical circuits, comprising (i) sensorimotor, (ii) associative and (iii) limbic territories. The striatum and subthalamic nucleus constitute the main input regions of the basal ganglia while the internal segment of the globus pallidus and the substantia nigra pars reticulata are the main output stations. As with the cortex, the basal ganglia and thalamus are functionally compartmentalised, such that the cortico-basal ganglia-thalamo-cortical loops largely retain topographical segregation throughout the entire processing stream (Alexander et al., 1986; Alexander and Crutcher, 1990; Obeso et al., 2008). However, partial overlap between functional territories and the existence of open loop or unidirectional feed-forward architectures is understood to permit the integration of information between channels and enable adaptive behaviour (Joel and Weiner, 1994; Haber, 2003; Aoki et al., 2019). B | Evidence suggests that the motor circuit, indicated by red arrows, is somatotopically organised throughout the entire loop in a manner that mimics the representation of the cortical homunculus (Obeso et al., 2008); lower limbs are represented dorsally and medially, the face is represented ventrally and laterally and the upper limbs are represented in between. GPe = globus pallidus pars externa; GPi = globus pallidus pars interna; STN = subthalamic nucleus. Figures extracted from; A | (Jahanshahi et al., 2015), B | (Rodriguez-Oroz et al., 2009).

Approximately 98% of the striatum is composed of inhibitory GABAergic medium spiny neurons (MSN), which can be described by a high spine density, negative resting potential and low firing rates (Kreitzer and Malenka, 2008). These MSNs can be further discriminated into two distinct populations of similar quantity, based principally on their gene expression and projection targets (Gerfen *et al.*, 1990; Deng *et al.*, 2006; Kreitzer and Malenka, 2008; Gerfen and Surmeier, 2011). MSNs of the striatonigral "direct pathway" extend axons from the striatum directly to the GPi and SNr and preferentially (>90%) express D_1-like DA receptors as well as neuropeptides substance P and dynorphin. Meanwhile, MSNs of the striatopallidal polysynaptic "indirect pathway" predominantly express D_2-like DA receptors (>90%) and the neurotransmitter enkephalin, influencing the basal ganglia output nuclei polysynaptically via projections relayed through GABAergic connections of the GPe and glutamatergic neurons of the STN (Gerfen and Surmeier, 2011; Tritsch and Sabatini, 2012). The classical model posits that these two separate pathways control the initiation of movement through their functionally antagonistic effects on basal ganglia motor output. Thus, excitation of the direct pathway MSNs reduces basal ganglia output and dis-inhibits the thalamus, ultimately increasing excitation of the cortex and promoting movement. In contrast, excitation of the indirect pathway MSNs reduces the inhibitory effect of the GPe on the STN, subsequently increasing basal ganglia output and decreasing thalamic excitation onto the cortex, thereby suppressing movement (Albin *et al.*, 1989; Alexander and Crutcher, 1990; DeLong, 1990; Kravitz *et al.*, 2010).

The principal source of dopaminergic input to the basal ganglia originates from the SNc, which projects via the nigrostriatal tract to the striatum wherein dopaminergic signalling is integrated with cortical and thalamic glutamatergic inputs (Surmeier *et al.*, 2007). Dopamine exerts a powerful neuromodulatory effect on the cortico-basal ganglia-thalamo-cortical loop that is critically dependent on the G-protein-coupled DA receptor subtype to which it becomes bound. Broadly speaking, binding of DA to D_1-like $G_{s/olf}$-coupled DA receptors on striatonigral MSNs increases the likelihood of neuronal firing while binding to D_2-like $G_{i/o}$-coupled DA receptors on striatopallidal MSNs depresses activation likelihood. These opposing effects are understood to result from the differential impact on adenylyl cyclase-mediated synthesis of the intracellular second messenger cyclic adenosine monophosphate (cAMP) and consequently on the gating and trafficking of voltage-dependent and ligand-

gated ion channels embedded in the dendritic membrane, altering the way the MSNs respond to glutamatergic signals (Surmeier *et al.*, 2007). Accordingly, dopaminergic signalling serves to promote movement by shifting the balance of activity between the direct and indirect pathways in favour of a net suppression of the GPi and SNr. However, the classic model posits that under circumstances of dopamine deficiency the direct pathway becomes hypoactive while the indirect pathway becomes hyperactive, resulting in excessive basal ganglia output, inhibition of excitatory thalamocortical efferents and consequentially the suppression of movement (Figure 1.5). While this and other models assume that information processing is encoded by changes in neuronal firing rates resulting directly from neurodegeneration, a substantial body of evidence suggests that the aberrant firing patterns and synchrony of the surviving neurons may underlie the key clinical manifestations of disease (Obeso *et al.*, 2008; McGregor and Nelson, 2019).

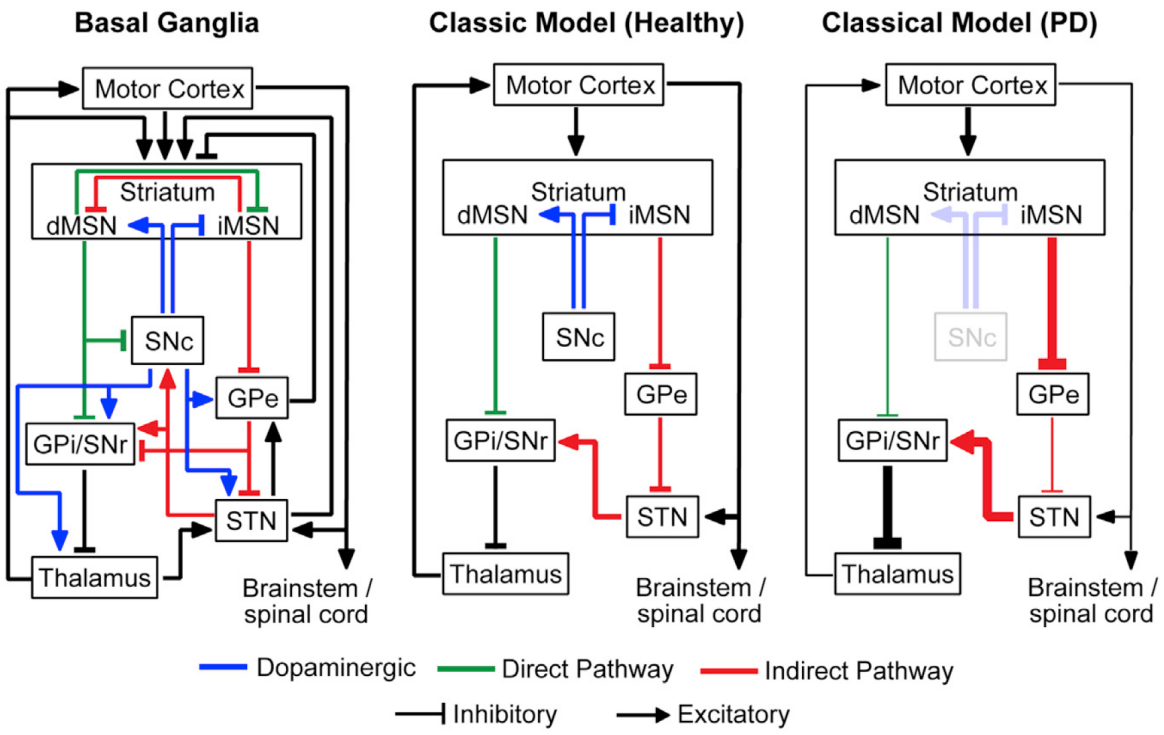


Figure 1.5: Cortico-basal ganglia-thalamo-cortical circuitry (left) and the simplified classical model in the healthy state (centre), highlighting the role of dopamine in the direct and indirect modulation of basal ganglia output. In the Parkinsonian dopamine deficient state (right) the excitation of direct pathway MSNs is diminished, consequentially reducing GABAergic inhibitory action on the SNr and GPi. Conversely, dopamine depletion of the indirect pathway MSNs lowers the suppression of inhibitory GABAergic signalling to the GPe, which in turn dampens GABAergic inhibition of the STN leading to excessive glutamatergic excitation of the GPi and SNr. Thus, the classic model hypothesises that in Parkinson's disease the output nuclei of the basal ganglia become overactive as a result of compromised dopaminergic modulation, causing excessive inhibition of excitatory thalamocortical efferents and consequentially motor suppression. dMSN = direct pathway medium spiny neurons; GPe = globus pallidus pars externa; GPi = globus pallidus pars interna; iMSN = indirect pathway medium spiny neurons; PD = Parkinson's disease; SNc = substantia nigra pars compacta; SNr = substantia nigra pars reticulata; STN = subthalamic nucleus. Figure extracted from (McGregor and Nelson, 2019).

A number of nuclear imaging studies have confirmed a significant inverse relationship between the severity of Parkinsonian motor symptoms and striatal presynaptic dopaminergic function, using [^{18}F]FDOPA for quantification of AADC activity (Brooks *et al.*, 1990; Ishikawa *et al.*, 1996; Morrish *et al.*, 1996; Vingerhoets *et al.*, 1997; Morrish *et al.*, 1998; Broussolle *et al.*, 1999; Dentresangle *et al.*, 1999; Rakshi *et al.*, 1999; Lee *et al.*, 2000; Pal *et al.*, 2001; Dhawan *et al.*, 2002; Ribeiro *et al.*, 2002; Eshuis *et al.*, 2006; Nandhagopal *et al.*, 2009; Gallagher *et al.*, 2011b; Li *et al.*, 2018), [^{11}C]- or [^{18}F]-labelled DTBZ (Lee *et al.*, 2000; Bohnen *et al.*, 2006; Martin *et al.*, 2008; Bohnen *et al.*, 2009; Nandhagopal *et al.*, 2009; Hsiao *et al.*, 2014)

and [^{18}F]-AV-133 (Okamura *et al.*, 2010) to image VMAT2 and a wide variety of SPECT and PET compounds selective for the dopamine transporter, including [^{123}I]β-CIT (Seibyl *et al.*, 1995; Ishikawa *et al.*, 1996; Ichise *et al.*, 1999; Staffen *et al.*, 2000; Marek *et al.*, 2001; Pirker, 2003), its N-fluoroalkyl analogues [^{123}I]- or [^{18}F]-labelled FP-CIT (Benamer *et al.*, 2000; Spiegel *et al.*, 2005; Eshuis *et al.*, 2006; Ottaviani *et al.*, 2006; Isaias *et al.*, 2007; Spiegel *et al.*, 2007; Verstappen *et al.*, 2007; Wang *et al.*, 2007; Rossi *et al.*, 2010; Oh *et al.*, 2012; Jakobson Mo *et al.*, 2013; Hong *et al.*, 2014; Simuni *et al.*, 2018) and [^{11}C]FE-CIT (Caminiti *et al.*, 2017), and other cocaine derivatives such as [^{99m}Tc]TRODAT-1 (Patel *et al.*, 2019), [^{11}C]- or [^{18}F]-labelled β-CFT (Rinne *et al.*, 1999; Bohnen *et al.*, 2007), [^{76}Br]FE-CBT (Ribeiro *et al.*, 2002), [^{123}I]PE2I (Prunier *et al.*, 2003), [^{11}C]PE2I (Li *et al.*, 2018; Martin-Bastida *et al.*, 2019), [^{18}F]FE-PE2I (Fazio *et al.*, 2015), as well as the non-tropane *d-threo*-[^{11}C]methylphenidate (Lee *et al.*, 2000). In contrast, no relationship with motor severity has been found with striatal post-synaptic availability of the D_1-receptor, estimated using [^{11}C]SCH23390 PET (Shinotoh *et al.*, 1993; Turjanski *et al.*, 1997), or the D_2-receptor, estimated using [^{11}C]raclopride PET (Brooks *et al.*, 1992; Turjanski *et al.*, 1997; Dentresangle *et al.*, 1999), [^{123}I]IBF (Ichise *et al.*, 1999) and [^{123}I]IBZM (Verstappen *et al.*, 2007; Jakobson Mo *et al.*, 2013) SPECT, with the exception that D_2-receptor asymmetry closely corresponds with clinical asymmetry (Rinne *et al.*, 1995), while there is also some evidence for a negative relationship with D_3-receptor density quantified using [^{11}C]-(+)-PHNO PET (Boileau *et al.*, 2009). Dual time-point [^{11}C]raclopride studies show that presynaptic dopamine release / synaptic dopamine levels, as evidenced by the reduction in D_2 receptor availability following pharmacological [exogenous levodopa or methamphetamine] challenge, is negatively correlated with baseline motor severity (Tedroff *et al.*, 1996) and positively with the degree of drug-induced motor improvement (Piccini *et al.*, 2003; Pavese *et al.*, 2006). The evaluation of separable PD symptoms by partitioning standardised motor assessment procedures, such as the commonly used Unified Parkinson's Disease Rating Scale (UPDRS), into constituent sub-scores has consistently revealed this relationship to be driven primarily by bradykinesia and to a marginally lesser extent, rigidity and postural instability / gait disturbance (Seibyl *et al.*, 1995; Vingerhoets *et al.*, 1997; Rinne *et al.*, 1999; Benamer *et al.*, 2000; Pal *et al.*, 2001; Pirker, 2003; Pavese *et al.*, 2006; Isaias *et al.*, 2007; Spiegel *et al.*, 2007; Martin *et al.*, 2008; Okamura *et al.*, 2010; Rossi *et al.*, 2010; Helmich *et al.*, 2011; Maillet *et al.*, 2016; Li *et al.*, 2018; Martin-Bastida *et al.*, 2019). These

findings are reproducible under objective, non-operator-biased testing conditions using timed tests for hypokinesia of the upper limbs, such as the Purdue pegboard, grooved pegboard and alternating tap tests (Vingerhoets *et al.*, 1997; Pal *et al.*, 2001; Ribeiro *et al.*, 2002; Bohnen *et al.*, 2007; Verstappen *et al.*, 2007; Nandhagopal *et al.*, 2009). In contrast, almost all imaging studies examining tremor fail to find a significant negative association with striatal dopaminergic function (Seibyl *et al.*, 1995; Vingerhoets *et al.*, 1997; Rinne *et al.*, 1999; Benamer *et al.*, 2000; Pirker, 2003; Ottaviani *et al.*, 2006; Isaias *et al.*, 2007; Spiegel *et al.*, 2007; Martin *et al.*, 2008; Rossi *et al.*, 2010; Helmich *et al.*, 2011; Maillet *et al.*, 2016; Lee *et al.*, 2018; Li *et al.*, 2018; Martin-Bastida *et al.*, 2019). An early paper by Vingerhoets *et al.* (1997) using stepwise multiple regression demonstrated that striatal AADC activity was most strongly explained by bradykinesia sub-scores of the Modified Columbia Rating Scale and that the coefficient increased slightly upon addition of the axial sub-scale. When included, Purdue pegboard scores superseded researcher-rated bradykinesia as the strongest predictor of striatal dopaminergic deficit. Neither rigidity nor tremor improved the relationship further, however in isolation rigidity showed a moderate and significant correlation with [^{18}F]FDOPA, while the association with tremor was weak (Vingerhoets *et al.*, 1997).

Somewhat surprisingly, the majority of longitudinal designs that evaluate the correlation between changes in dopaminergic biomarker and clinical measures over a fixed scanning interval report this association to be weak, attaining trend level significance at best (Antonini *et al.*, 1997; Morrish *et al.*, 1998; Marek *et al.*, 2001; Nurmi *et al.*, 2001; Pirker *et al.*, 2002; Nurmi *et al.*, 2003; Pirker, 2003; Colloby *et al.*, 2005; Bruck *et al.*, 2006; Bruck *et al.*, 2009; Nandhagopal *et al.*, 2009; Jakobson Mo *et al.*, 2013; Simuni *et al.*, 2018). However, in a recent multitracer study from our lab in which mild-moderate stage PD patients were scanned at two time points over a mean of 19 months, we found that changes in bradykinesia-rigidity sub-scores of the UPDRS-III over the study period were significantly correlated with changes in putamenal [^{11}C]PE2I BP_{ND} only, and not with changes in [^{18}F]FDOPA K_i (Li *et al.*, 2018). Furthermore, while striatal [^{18}F]FDOPA K_i and [^{11}C]PE2I BP_{ND} were both inversely associated with total motor and bradykinesia-rigidity severity at baseline, [^{11}C]PE2I BP_{ND} was found to be a significantly stronger predictor and was present over a wider spatial extent (Li *et al.*, 2018). These data imply that motor progression, specifically the worsening of hypokinesia, is more closely related to striatal DAT decline than to AADC activity. This

might constitute evidence supporting compensatory up-regulation of the latter, which could conceivably result in a more complex higher order polynomial relationship than down-regulation of the former. Yet alterations in DAT density and overall motor severity, as well as bradykinesia severity (Nurmi *et al.*, 2003), incurred over repeat visits are not correlated when DAT is quantified using [^{123}I]β-CIT (Marek *et al.*, 2001; Pirker *et al.*, 2002; Pirker, 2003) or [^{18}F]CFT (Nurmi *et al.*, 2003), and other multiligand studies, while not performing direct comparisons, have found that the association of symptom severity with [^{18}F]FDOPA is either equivalently strong to those found with DAT measurements derived using [^{123}I]FP-CIT (Ishikawa *et al.*, 1996; Eshuis *et al.*, 2006), or weaker, as is the case with [^{76}Br]FE-CBT (Ribeiro *et al.*, 2002). Given the superior DAT-to-SERT selectivity of PE2I over other commonly used DAT radionuclides (Neumeyer *et al.*, 1994; Aloyo *et al.*, 1995; Abi-Dargham *et al.*, 1996; Emond *et al.*, 1997) and the ubiquitous distribution of AADC across monoaminergic neuronal populations, most of which are capable of taking up and metabolising [^{18}F]FDOPA (Brown *et al.*, 1999; Rakshi *et al.*, 1999; Moore *et al.*, 2003; Moore *et al.*, 2008; Pavese *et al.*, 2011; Pavese *et al.*, 2012) we suggested that the disparate findings may stem from differential non-dopaminergic contributions to the overall tracer signal and provide further evidence in support of a dopaminergic basis for the emergence and progression of hypokinesia (Li *et al.*, 2018).

The pathophysiological basis of tremor is less clear, though despite the lack of linear correlation, there are grounds for the involvement of dopaminergic decline. Many research groups who divide patients into sub-types based on their clinical presentation at disease onset or at study baseline find that tremor-dominant patients show greater preservation of dopaminergic function in the putamen and caudate than their akinetic-rigid or mixed symptom counterparts (Spiegel *et al.*, 2007; Rossi *et al.*, 2010; Eggers *et al.*, 2011; Helmich *et al.*, 2011; Schillaci *et al.*, 2011; Qamhawi *et al.*, 2015; Lee *et al.*, 2018) and exhibit a slower annual rate of dopaminergic decline (Hilker *et al.*, 2005b). However, while Eggers *et al.* (2011) initially confirmed these findings, when akinetic-rigid patients were systematically paired with patients from a smaller group of 23 tremor-dominant patients on age, disease duration, H&Y, overall UPDRS and LEDD the degree of striatal dopaminergic denervation became statistically equivalent (Eggers *et al.*, 2011). In another study of drug-naïve patients matched by hypokinetic severity, those with additional tremor exhibited even greater DAT loss

within the caudate, while no difference was seen in the putamen (Isaias *et al.*, 2007). Additionally, by visual inspection of [^{123}I]FP-CIT SPECT images, experienced clinicians blinded to patient identity were able to discern between akinetic-rigid and tremor-dominant subtypes based on the formation of "egg" or "eagle-wing" uptake patterns (Eggers *et al.*, 2011). These *in vivo* data validate neuropathological findings that tremor-dominant patients exhibit more modest dopaminergic cell loss within the lateral as compared to the medial SNc (which projects to the anterior putamen and caudate nucleus), plus degeneration of the A8 retrorubral field located dorsocaudal to the SNc (which projects to the dorsolateral striatum, ventromedial thalamus and pallidum) that is usually preserved in the akinetic-rigid subtype (Paulus and Jellinger, 1991; Helmich *et al.*, 2012; Jellinger, 2012). Taken together these results suggest that dopaminergic denervation may be a prerequisite condition for the appearance of tremor, but that it is probably generated by alternative neural circuitry.

An important multimodal study conducted by Helmich *et al.* (2011) using [^{123}I]FP-CIT SPECT and resting-state functional magnetic resonance imaging with concurrent electromyographic readings of the most affected upper limb found that tremor amplitude co-fluctuated with the BOLD response in the contralateral motor cortex, ventral intermediate nucleus of the thalamus and ipsilateral cerebellum. Whereas the basal ganglia were unresponsive to variations in tremor amplitude, increased activity in the GPi, GPe and putamen was transiently evoked at the onset of tremor episodes. Seed-based functional connectivity analysis revealed that tremor-dominant patients had enhanced coupling between the GPi and motor cortex and between the putamen and motor cortex as compared to non-tremor patients, and stronger functional coupling between these regions was related to greater tremor amplitude. Crucially, in the same patients, it was found that GPi but not striatal [^{123}I]FP-CIT binding correlated with resting tremor, while the opposite was true for bradykinesia (Helmich *et al.*, 2011), and in a previous post-mortem investigation it has been demonstrated that tremor is uniquely related to homovanillic acid concentrations in the pallidum (Bernheimer *et al.*, 1973). Thus, a specific pattern of basal ganglia dysfunction, potentially sub-served by preferential destruction of the retrorubral dopaminergic projections to the GPi, may trigger activity within the cerebello-thalamo-cortical circuit via their convergence point in the primary motor cortex, with the latter loop producing and

modulating tremor intensity (Helmich *et al.*, 2011; Helmich *et al.*, 2012; Dirkx *et al.*, 2016). The role of pallidal dopaminergic denervation in this so-called 'dimmer-switch' model (Helmich *et al.*, 2012) has been supported by recent dynamic causal modelling findings that dopamine-replacement medication attenuates tremor-onset related activity in the pallidum and potentiates self-inhibition of the thalamic ventral intermediate nucleus, the magnitude of which significantly predicts the clinical responsiveness of tremor, but not bradykinesia or rigidity, between the on- and off-medication states (Dirkx *et al.*, 2017).

However, some tremor-dominant patients are clinically and functionally unresponsive to dopamine therapy (Dirkx *et al.*, 2017). One study using high-performance liquid chromatography at post-mortem indicated that tremor-dominant patients had near normal levels of DA in the ventral portions of the internal pallidum and a 40% decrease in the dorsal portions, whereas akinetic-rigid patients showed a more substantial loss of 55-80% across the nucleus (Rajput *et al.*, 2008). *In vivo*, Isaias *et al.* (2012) demonstrated no difference in pallidal DAT binding between patients classified as having bilateral, unilateral or no tremor (Isaias *et al.*, 2011). A more recent [^{123}I]FP-CIT SPECT study analysing 382 drug-naïve early-stage patients from the Parkinson's Progression Marker Initiative cohort found that tremor-dominant patients had either higher or equal DAT binding than non-tremor patients in the least and most affected GPi respectively. Moreover, the authors failed to find a correlation between dopaminergic denervation of this region with tremor amplitude, constancy or overall severity in neither the tremor-dominant group nor the entire cohort, when least and most affected sides were considered either separately or together (Lee *et al.*, 2018). These findings do not necessarily refute the 'dimmer-switch' model but raise the possibility of non-dopaminergic mechanisms in the generation of tremor.

Indeed, the basal ganglia nuclei, including the GPi, are substantially innervated by serotonergic afferents originating predominantly from the dorsal raphe nucleus (Ginovart *et al.*, 2001; Ichise *et al.*, 2003; Kish *et al.*, 2005; Miguelez *et al.*, 2014), which begins to accumulate Lewy pathology in the prodromal and early clinical phases of illness (Braak *et al.*, 2003b; Braak and Del Tredici, 2016). Although affected to a lesser magnitude than the dopaminergic system (Kish *et al.*, 2008; Maillet *et al.*, 2016), serotonergic axonal neurodegeneration in Parkinson's disease is widespread and has repeatedly been demonstrated *in vivo* using

SERT-specific PET ligands [^{11}C]DASB and [^{11}C]-(+)-McN5652 to involve multiple areas of the brainstem, striatum, limbic and frontal cortices (Kerenyi *et al.*, 2003; Guttman *et al.*, 2007; Albin *et al.*, 2008; Loane *et al.*, 2013; Maillet *et al.*, 2016; Pagano *et al.*, 2017; Wilson *et al.*, 2019). In early disease the global serotonergic state appears relatively preserved (Strecker *et al.*, 2011; Fazio *et al.*, 2020), only affecting the caudate, hypothalamus, thalamus and anterior cingulate at the earliest post-diagnostic phase, but then followed by the putamen, insula, posterior cingulate and prefrontal cortex within 5-10 years of illness and finally the raphe nuclei, ventral striatum and amygdala in the years thereafter (Politis *et al.*, 2010a), although denervation appears to be much more rapid across genetic variants, such as for individuals with the A53T *SNCA* mutation (Wilson *et al.*, 2019). In some studies, [^{18}F]FDOPA uptake in the raphe, which is taken to reflect AADC activity within the serotonergic neurons of this region (Brown *et al.*, 1999; Moore *et al.*, 2003; Pavese *et al.*, 2012), is found to be elevated as compared to normal in the early stages of illness, potentially as a compensatory response to diffuse pathology, before yielding as the disease progresses (Rakshi *et al.*, 1999; Moore *et al.*, 2008; Pavese *et al.*, 2011). Similar results have been obtained for raphe VMAT2 density as indicated by [^{18}F]AV-133 PET, albeit seemingly maintained into advanced illness (Hsiao *et al.*, 2014). A trend for this early up-regulatory effect has also recently been observed for the serotonin transporter using [^{11}C]DASB PET in the brainstem, striatum and hypothalamus of pre-symptomatic LRRK2 mutation carriers, which is then lost upon motor onset (Wile *et al.*, 2017). Another study found a small increase in mesencephalic [^{123}I]ADAM binding in *de novo* PD as compared to normal, though only 9 patients were included and the results were non-significant (Beucke *et al.*, 2011). In a longitudinal setting, raphe serotonin transporter density was calculated to decrease by 16.6% between 2.5 and 4.5 years post-diagnosis, but with considerable heterogeneity across individuals (Pasquini *et al.*, 2019a). Within roughly the same time frame, recent multivariate network analysis of [^{11}C]MADAM PET scans demonstrated a longitudinal reduction in global network efficiency and increased network segregation, driven mainly by the loss of association between the raphe nuclei and its subcortical and cortical projection areas (Fazio *et al.*, 2020).

In the raphe complex, 5-HT$_{1A}$ receptor density as measured using [^{11}C]WAY 100635 PET was significantly related to overall tremor severity but not to bradykinesia or rigidity (Doder *et al.*, 2003). Similarly, serotonin transporter density in the raphe, as well as of the putamen and

caudate, was related to the degree of action-postural tremor in tremor-dominant patients, while this group concurrently exhibited significantly lower SERT levels in the raphestriatal system, the thalamus and Brodmann areas 4 and 10 in comparison to the akinetic-rigid subtype (Loane *et al.*, 2013). Due to its monoaminergic binding characteristics, [^{123}I]FP-CIT SPECT scans collected as part of the PPMI study have been used in two papers from the same research group to simultaneously quantify serotonergic and dopaminergic transporter availability in the raphe and striatum respectively. Tremulous patients showed higher DAT density in the putamen but lower SERT density in the raphe as compared to akinetic-rigid patients, and binding levels in the latter significantly predicted tremor constancy and overall severity. Over the entire cohort of 345 PD patients, SERT binding in the raphe significantly predicted tremor constancy and overall severity as well as tremor amplitude (Qamhawi *et al.*, 2015). Interestingly, in a second study analysing the 2-year follow-up scans acquired in a subset of 173 of these patients, this relationship was not evident. In contrast, tremor constancy, amplitude and overall severity were strongly predicted by the raphe:putamen [^{123}I]FP-CIT binding ratio at 2 year follow-up, and to a slightly lesser extent at baseline, illustrating a role for both neurotransmitter systems in generating tremor (Pasquini *et al.*, 2018).

1.6. Current treatments for Parkinson's disease

Whilst Parkinson's disease is now understood to encompass widespread pathology from its onset, the principal clinically relevant feature remains the loss of dopamine in the striatum. As such, Parkinsonian motor symptoms can be treated successfully in the early stages of disease by dopamine replacement regimes. The mode in which dopamine replacement is initiated is highly dependent on several factors including age of onset, duration/severity of illness, symptom profile and personal preference, however, by far the most effective pharmacological treatment has been with oral levodopa preparations (Fox *et al.*, 2011; Connolly and Lang, 2014; Fox *et al.*, 2018) which are converted to dopamine by aromatic amino acid decarboxylase within dopamine and serotonin neurons following absorption and transit across the blood-brain-barrier. The addition of carbidopa or benserazide blocks metabolism of levodopa by AADC in the periphery, thereby increasing availability in the brain at significantly lower doses and negating the occurrence of peripheral side effects (Muller, 2015) (Figure 1.6). Of the cardinal motor symptoms bradykinesia and rigidity are most responsive to levodopa preparations, a more modest and variable benefit is seen for tremor, while axial symptoms including speech and balance are comparatively unaided (Sethi, 2008).

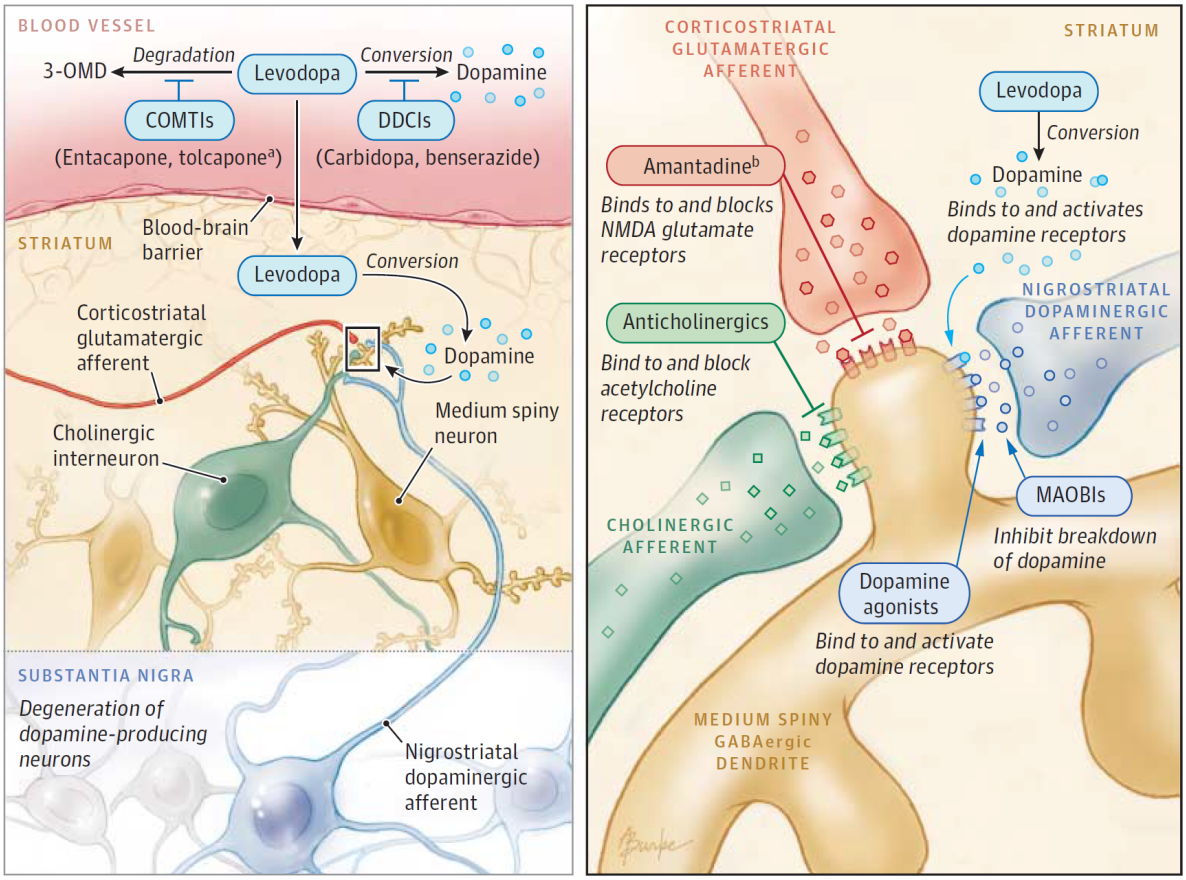


Figure 1.6: Mechanisms of action for currently available medications in the treatment of Parkinson's disease. L-dopa is the most effective pharmacological agent and is transported across the blood-brain barrier where it is converted centrally to dopamine by the AADC enzyme. Co-administration with dopamine decarboxylase inhibitors (e.g. carbidopa, benserazide) block its metabolism in the periphery, while catechol-O-methyltransferase inhibitors (e.g. entacapone, tolcapone, opicapone) attenuates its degradation to 3-O-methyldopa. The monoamine oxidase type B enzyme can be inhibited through irreversible binding (e.g. selegiline, rasagiline) thus reducing the breakdown of dopamine and other monoamine neurotransmitters. Dopamine agonists (e.g. ropinirole, rotigotine, pramipexole) exert anti-Parkinsonian effect by directly targeting and activating the dopamine receptors. Amantadine is a non-competitive antagonist of the N-methyl-D-aspartate glutamate receptor that moderates the excitatory glutamatergic cortico-striatal input to the GABAergic medium spiny neurons, while also augmenting dopamine release and delaying its re-uptake. 3-OMD = 3-O-methyldopa; AADC = aromatic amino acid decarboxylase; COMTI = catechol-O-methyltransferase inhibitor; DDCI = dopamine decarboxylase inhibitor; MAOBI = monoamine oxidase type B inhibitor; NMDA = N-methyl-D-aspartate. Figure extracted from (Connolly and Lang, 2014).

The clinical efficacy of levodopa is evident throughout the disease course; however levodopa does not confer neuroprotection from the natural trajectory of nigrostriatal denervation (Parkinson Study Group, 2000, 2002; Rakshi *et al.*, 2002; Whone *et al.*, 2003; Fahn *et al.*, 2004; Simuni *et al.*, 2018; Verschuur *et al.*, 2019) and conversely may serve to promote it,

with several double-blind randomised controlled trials using [^{123}I]β-CIT SPECT (Parkinson Study Group, 2000, 2002; Fahn *et al.*, 2004) and [^{18}F]FDOPA PET (Rakshi *et al.*, 2002; Whone *et al.*, 2003) demonstrating significantly greater, and potentially dose-dependent (Fahn *et al.*, 2004), decline of striatal DAT density and AADC activity in patients taking levodopa to those who were not. Consequentially motor severity continues to decrease steadily over time (Rinne *et al.*, 1998; Parkinson Study Group, 2000; Rascol *et al.*, 2000; Parkinson Study Group, 2002; Whone *et al.*, 2003; Fahn *et al.*, 2004; Holloway *et al.*, 2004; Oertel *et al.*, 2006; PD MED Collaborative Group, 2014; Simuni *et al.*, 2018; Barker and Transeuro Consortium, 2019; Verschuur *et al.*, 2019) requiring ever increasing daily doses to achieve adequate symptomatic relief (Nyholm *et al.*, 2010; PD MED Collaborative Group, 2014). Furthermore, after several years of stable response to levodopa therapy, patients inevitably develop a number of drug-induced complications, namely "wearing off", "delayed-on", "partial-on", "no-on" and "on-off" motor fluctuations and "peak-dose", "diphasic" or "square-wave" dyskinesias presenting as choreic, ballistic, myoclonic or dystonic involuntary movements (Magrinelli *et al.*, 2016), that can significantly impact upon daily activities and quality of life (Chapuis *et al.*, 2005; Hechtner *et al.*, 2014). In recent prospective studies, the cumulative incidence of motor fluctuations and dyskinesias has been estimated at between 43-54% and 15-28% at 5 years post-diagnosis and 100% and 56% at 10 years respectively (Bjornestad *et al.*, 2016; Scott *et al.*, 2016; Kim *et al.*, 2020), although some studies have reported higher incidence and earlier onset (Ahlskog and Muenter, 2001; Eusebi *et al.*, 2018). Cumulative levodopa use, the total levodopa dosage and the severity of illness have been named amongst the strongest risk factors for both motor fluctuations and dyskinesias (Fahn *et al.*, 2004; Olanow *et al.*, 2013; Cilia *et al.*, 2014; Hong *et al.*, 2014; Bjornestad *et al.*, 2016; Scott *et al.*, 2016; Eusebi *et al.*, 2018; Kim *et al.*, 2020), although the relationship with levodopa chronicity has long been debated (Cilia *et al.*, 2014; Bjornestad *et al.*, 2016; Verschuur *et al.*, 2019; Kim *et al.*, 2020).

The underlying pathophysiology of motor complications are not completely understood but major factors are thought to include fluctuating plasma and synaptic dopamine levels resulting from intermittent administration of short-acting agents, erratic absorption in the gastrointestinal tract and the incapacity of the surviving dopaminergic neuronal population to store and buffer swings in exogenous levodopa, leading to non-physiologic pulsatile

stimulation of the post-synaptic dopamine receptors and altered firing patterns of the basal ganglia output neurons (Obeso *et al.*, 2000; Olanow *et al.*, 2006; Jenner, 2008; Bastide *et al.*, 2015; Picconi *et al.*, 2018). This is in keeping with *in vivo* reports in human subjects using [^{11}C]raclopride PET prior to and following levodopa challenge to evaluate presynaptic dopamine release. In one report, patients who later developed motor fluctuations 1-2.5 years following the study exhibited significantly different patterns of levodopa-induced dopamine release than those whose response remained stable. Specifically, striatal dopamine levels in future fluctuators spiked 1 hour following levodopa dosing, but then reduced to below baseline levels after 4 hours. Conversely, stable responders showed a comparatively moderate increase in synaptic dopamine levels after 1 hour which further increased between time-points (de la Fuente-Fernández *et al.*, 2001). A similar interaction was found in a later study by the same group comparing patients without motor complications to those with established dyskinesias (de la Fuente-Fernandez *et al.*, 2004). The magnitude of this early levodopa-induced reduction in [^{11}C]raclopride binding potential is associated with the duration (de la Fuente-Fernandez *et al.*, 2004) and severity (Tedroff *et al.*, 1996) of illness and is positively correlated with the severity of dyskinesias (Pavese *et al.*, 2006; Politis *et al.*, 2014). In addition, two studies evaluating the risk of developing motor complications identified abnormal presynaptic dopamine transporter density as an important predictor alongside levodopa exposure and clinical measures of disease severity (Hong *et al.*, 2014; Eusebi *et al.*, 2018).

The notion that non-physiologic dopamine signalling underlies motor complications is compounded by work demonstrating a possible relationship with the serotonergic neuronal population. Serotonergic neurons are capable of taking up and converting L-dopa, storing and releasing dopamine in an activity–dependent manner but critically, the absence of necessary D_2-autoreceptor-mediated feedback and dopamine transporters on their presynaptic terminals may ultimately lead to dysregulated release and excessive swings in extracellular dopamine levels (Maeda *et al.*, 2005; Carlsson *et al.*, 2007; Carta *et al.*, 2007; Carta *et al.*, 2010) (Figure 1.7). Indeed, administration of levodopa in tandem with the 5-HT_{1A} receptor agonist buspirone, which inhibits serotonergic signalling activity, attenuated the excessive reduction in striatal [^{11}C]raclopride PET binding in patients with dyskinesia, while in stable responders there was no effect of buspirone pre-treatment on striatal synaptic

dopamine levels. The magnitude of the buspirone effect on [^{11}C]raclopride binding was greater for dyskinetic patients with a higher degree of serotonergic innervation, as quantified using [^{11}C]DASB PET. Moreover, the extent to which buspirone dampened presynaptic dopamine release was more pronounced in patients with milder dyskinesia, potentially due to inadequate buspirone dosage in more severe cases, and in this subgroup was correlated with the degree of clinical improvement (Politis *et al.*, 2014). The same study also identified a correlation between dyskinesia severity following levodopa challenge without buspirone and putamenal serotonin transporter density, albeit only reported for the mild-moderate and not the moderate-severe dyskinesia subgroup (Politis *et al.*, 2014), while others have found this relationship within the pallidum, which also appears to show elevated serotonin transporter density in patients with dyskinesia as compared to those without (Smith *et al.*, 2015). More recently, dyskinetic patients were found to exhibit a significantly elevated proportion of serotonergic to dopaminergic neurons in the putamen in favour of the former (Lee *et al.*, 2015; Roussakis *et al.*, 2016), though this [^{11}C]DASB-to-[^{123}I]FP-CIT ratio was not correlated with dyskinesia severity (Roussakis *et al.*, 2016).

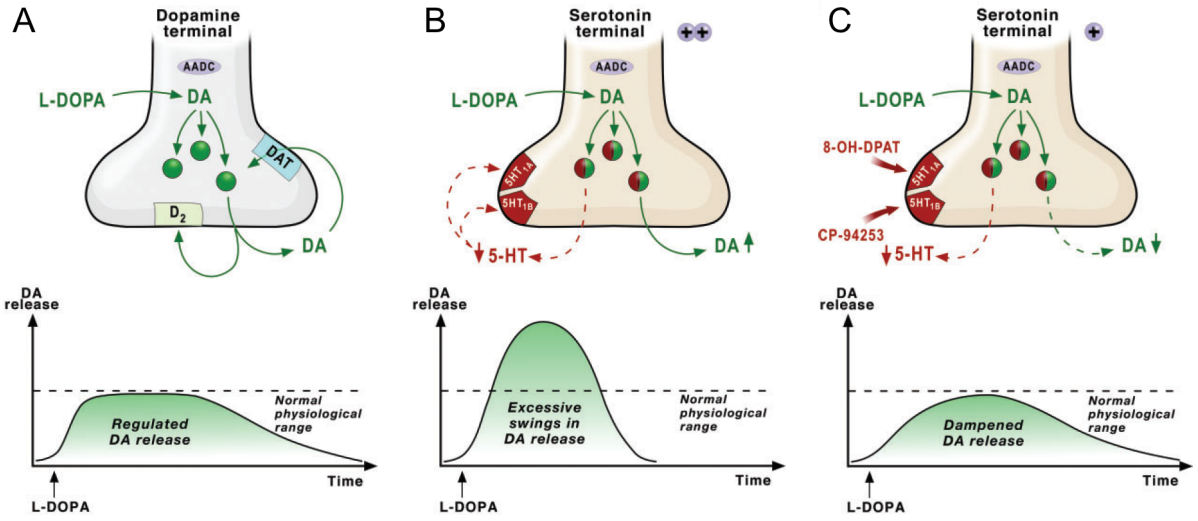


Figure 1.7: Proposed model for serotonergic neuron involvement in L-dopa-induced dyskinesias. A | In the early stages of Parkinson's disease, exogenously delivered L-dopa is taken up, converted, stored and released by the substantial number of surviving dopaminergic neurons. The presence of the dopamine transporter and D_2 autoreceptor on the presynaptic terminal enables auto-regulatory feedback and the maintenance of consistent levels of synaptic dopamine and its physiological release. B | As the disease progresses the further reductions in dopaminergic population result in excess extracellular L-dopa, which can be taken up, converted and stored within the presynaptic vesicles of serotonin neurons. The lack of dopamine-specific auto-regulatory machinery and the depletion of endogenous serotonin cause dysregulated non-physiologic release, excessive swings in synaptic dopamine and pulsatile stimulation

patterns of post-synaptic receptors. C | 5-HT$_{1A}$ and 5-HT$_{1B}$ receptor agonists are hypothesised to reduce dyskinetic movements by moderating serotonergic activity and dampening uncontrolled dopamine release. 5-HT = serotonin; 8-OH-DPAT = 5-HT$_{1A}$ agonist (±)-8-hydroxy-2-dipropylaminotetralin hydrobromide; AADC = aromatic amino acid decarboxylase; CP-94253 = 5-HT$_{1B}$ agonist; DA = dopamine; DAT = dopamine transporter; L-dopa = levodopa. Figure adapted from (Carta et al., 2007).

As such, strategies for a more continuous delivery of dopamine to the striatum have been explored (Figure 1.6). Long-acting dopamine agonists such as oral ropinirole, pramipexole and transdermal rotigotine are used as monotherapy in common practice to delay the initiation of levodopa, which has been shown in several randomised clinical trials to prolong the onset of motor fluctuations and dyskinesias (Rinne *et al.*, 1998; Parkinson Study Group, 2000; Rascol *et al.*, 2000; Lees *et al.*, 2001; Whone *et al.*, 2003; Holloway *et al.*, 2004; Oertel *et al.*, 2006; Parkinson Study Group CALM Cohort Investigators, 2009; Chondrogiorgi *et al.*, 2014; PD MED Collaborative Group, 2014), with no rapid catch-up effect when levodopa therapy is eventually started (Rascol *et al.*, 2006; Hauser *et al.*, 2007). However, dopamine agonists are not as efficacious as levodopa, they have only limited effect in extending the honeymoon period and can sometimes induce dyskinesia (Rinne *et al.*, 1998; Parkinson Study Group, 2000; Rascol *et al.*, 2000; Lees *et al.*, 2001; Whone *et al.*, 2003; Holloway *et al.*, 2004; Oertel *et al.*, 2006; Rascol *et al.*, 2006; Parkinson Study Group CALM Cohort Investigators, 2009; Chondrogiorgi *et al.*, 2014), and almost all patients will eventually require supplementation with levodopa (PD MED Collaborative Group, 2014; Simuni *et al.*, 2018). Moreover, dopamine agonists are associated with equally distressing side effects including impulse control disorders (Wu *et al.*, 2009; Weintraub and Nirenberg, 2013; Voon *et al.*, 2017) and psychosis (Ecker *et al.*, 2009). Usage as adjunct therapy in advanced disease to smooth the peak-trough variation in plasma/synaptic dopamine concentration is effective in reducing off-time and increasing on-time without troublesome dyskinesia (Lieberman *et al.*, 1998; Mizuno *et al.*, 2007; Poewe *et al.*, 2007; Mizuno *et al.*, 2014; Nomoto *et al.*, 2014). Similar outcomes have been reported with administration of extended release levodopa formulations (Hauser *et al.*, 2013; Stocchi *et al.*, 2014) and monoamine oxidase B inhibitors (MAOBI) such as rasagiline and selegiline in late-stage (Parkinson Study Group, 2005; Rascol *et al.*, 2005), while as monotherapy the latter shows lower efficacy than dopamine agonists and more modest capacity to delay levodopa (Olanow *et al.*, 2009b; PD MED Collaborative Group, 2014). Catechol-*O*-methyltransferase inhibitors (COMTI), such as

entacapone, tolcapone and opicapone, designed to extend the plasma elimination half-life of levodopa (Muller, 2015), while helping to control motor complications in advanced disease (Rascol *et al.*, 2005; Ferreira *et al.*, 2016; Lees *et al.*, 2017) are not as effective as extended release levodopa formulations (Stocchi *et al.*, 2014) and may even accelerate their onset (Stocchi *et al.*, 2010). A 2010 Cochrane meta-analysis of 44 clinical trials evaluating dopamine agonists, MAOBIs and COMTIs as adjuvant therapies to levodopa in patients who had developed motor complications concluded that in comparison to placebo, patients reported reduced off-time, reduced levodopa requirement and improvement to UPDRS motor and activities of daily living scores, however, this was at the expense of increased incidence of drug-induced dyskinesia and other side effects including constipation, dizziness, hallucinations, dry mouth, hypotension, insomnia, nausea, vomiting and somnolence. Indirect comparisons between the three drug classes revealed that dopamine agonists conferred the greatest reduction in off-time compared to MAOBIs and COMTIs, but this also was associated with increased risk of dyskinesias (Stowe *et al.*, 2010). Amantadine, a non-competitive antagonist of the *N*-methyl-D-aspartate (NMDA) receptor that acts to moderate the excitatory glutamatergic cortico-striatal input to the GABAergic medium spiny neurons in the striatum (Picconi *et al.*, 2018) has also been shown in a recent meta-analysis to reduce the severity dyskinesia as compared to placebo, as well as mildly improving motor symptoms, with higher doses providing greater anti-dyskinetic effects but with increased adverse events (Kong *et al.*, 2017). Some trials also report modest improvement in motor fluctuations and off-time by NMDA antagonism (Verhagen Metman *et al.*, 1998; Pahwa *et al.*, 2015; Oertel *et al.*, 2017) but evidence for this is inconsistent (Sawada *et al.*, 2010; Ory-Magne *et al.*, 2014).

Thus in the early to moderate stages of Parkinson's disease treatment by orally administered drugs is frequently adjusted to suit the patients' needs and is regarded as both a short- and long-term risk-benefit exercise. However, with time and increasing daily drug requirements, motor complications eventually become refractory to optimised medical therapy and intolerable to many patients. At this point more invasive interventions are indicated, including advanced methods for continuous dopaminergic drug delivery and deep brain stimulation (DBS) predominantly of the subthalamic nucleus and internal globus pallidus (Fox *et al.*, 2011; Connolly and Lang, 2014; Fox *et al.*, 2018). A recent double-blind

randomised controlled trial has confirmed the efficacy of continuous subcutaneous infusion of the non-selective dopamine agonist apomorphine using ambulatory pumps in treating persistent motor fluctuations. Specifically, the treatment group gained up to 2 hours of on-time per day without dyskinesia as compared to saline, equivalent to ~40% of baseline off-time, and were able to reduce levodopa equivalent daily dosage (Katzenschlager *et al.*, 2018). This latter benefit may in part underlie the findings of reduced dyskinesia duration and frequency in earlier open-label trials (Jenner and Katzenschlager, 2016). Retrospective data has also suggested that it may be useful for the treatment of impulse control disorders, potentially by allowing reductions in oral dopamine agonist intake (Barbosa *et al.*, 2017). However, this therapy is also associated with heightened incidence of adverse events that uniquely include formation of skin nodules and erythema at the infusion site, as well as dyskinesia and other peripheral side effects commonly incited by dopamine agonists (Katzenschlager *et al.*, 2018).

Comparable primary outcomes have been reported in patients receiving percutaneous levodopa-carbidopa infusion, administered within the jejunum through a surgically placed gastrojejunostomy tube connected transabdominally to an external pump. As compared to patients infusing placebo intestinal gel and taking standard immediate release oral levodopa-carbidopa, the investigational group reported 2-fold and 3-fold improvements in daily off-time and on-time without dyskinesia respectively after 12 weeks (Olanow *et al.*, 2014), translating to a within-group benefit of 50-60% for both measures with respect to baseline, similar to that which has been found at 54 weeks (Fernandez *et al.*, 2015) and 24 months (Antonini *et al.*, 2017) in larger open-label trials. In contrast to findings relating to immediate release oral preparations (de la Fuente-Fernández *et al.*, 2001; de la Fuente-Fernandez *et al.*, 2004), serial [^{11}C]raclopride PET has shown that reductions in striatal binding potential remained stable and without significant swings between 1, 4, 7 and 10 hours after jejunal infusion was switched on (Politis *et al.*, 2017), mirroring earlier pharmacokinetic findings pertaining to steadier plasma levodopa concentrations (Stocchi *et al.*, 2005). However, up to 89% of individuals experience device-related complications including breakage, leakage, dislocation, malfunction, occlusion, infection and abdominal pain, and up to 17% are deemed serious (Olanow *et al.*, 2014; Fernandez *et al.*, 2015; Antonini *et al.*, 2017), highlighting that its implementation carries high risk and maintenance requires

specialised multidisciplinary management.

Deep brain stimulation involves application of an electrical current to specified regions of the brain, usually the subthalamic nucleus or globus pallidus pars interna, via implantation of electrodes connected to a battery-powered internal pulse generator (Harnack and Kupsch, 2010). The mechanisms associated with DBS are still under investigation and are thought to exert multifactorial, local and network-wide effects. In general, it is thought to modulate the aberrant intrinsic oscillatory and burst firing patterns within the transplanted nucleus by replacement with one that is high-frequency and regularized, preventing its propagation throughout the subcortico-cortical loops and reducing the expression of disease-related metabolic spatial covariance patterns (Santaniello *et al.*, 2015; Herrington *et al.*, 2016). In the off-medication state, DBS 1 year following surgery can alleviate overall motor severity by ~50-60%, comparable to that which is seen following acute levodopa challenge (Fasano *et al.*, 2010; St George *et al.*, 2010; Castrioto *et al.*, 2011; Zibetti *et al.*, 2011; Aviles-Olmos *et al.*, 2014), having greater benefits in more advanced patients (Kleiner-Fisman *et al.*, 2006; Deuschl *et al.*, 2019; Schuepbach *et al.*, 2019) and in those with better pre-surgical levodopa response (Kleiner-Fisman *et al.*, 2006). In the on-medication state, neurostimulation-related improvements at the same time point are at best modest, returning to baseline levels by 5 years post-surgery and further worsening thereafter (Fasano *et al.*, 2010; St George *et al.*, 2010; Castrioto *et al.*, 2011; Zibetti *et al.*, 2011; Aviles-Olmos *et al.*, 2014). The relative lack of efficacy in the on- as compared to off-medication states permits a significant reduction in drug requirement by more than half without sacrificing therapeutic benefit (Fasano *et al.*, 2010; Castrioto *et al.*, 2011; Zibetti *et al.*, 2011; Aviles-Olmos *et al.*, 2014). Clinical severity also progresses over time in the off-medication state though ~20-40% improvement over baseline is still retained one decade following surgery. Interestingly, early improvements in quality of life (Kleiner-Fisman *et al.*, 2006; Williams *et al.*, 2010; Schuepbach *et al.*, 2013) seem to be transient and do not parallel symptomatic relief (Aviles-Olmos *et al.*, 2014). Longitudinal motoric decline is primarily driven by initial and accruing resistance of axial symptoms, most notably speech (Wertheimer *et al.*, 2014), postural instability and gait disturbance as well as bradykinesia to stimulation, while tremor and rigidity exhibit sustained long-term benefit (Fasano *et al.*, 2010; St George *et al.*, 2010; Castrioto *et al.*, 2011; Zibetti *et al.*, 2011; Aviles-Olmos *et al.*, 2014). Both motor fluctuations and dyskinesias are also substantially

ameliorated by DBS in the long-term, which may in part reflect concomitant reductions in medication intake (Castrioto *et al.*, 2011; Zibetti *et al.*, 2011; Aviles-Olmos *et al.*, 2014), but may also be a consequence of DBS in attenuating the early exaggerated spikes in dopamine release induced by acute provision of exogenous levodopa, as observed using [^{11}C]raclopride PET (Nimura *et al.*, 2005). Other studies using [^{11}C]raclopride PET without levodopa-challenge have not found any difference in synaptic dopamine levels between DBS-on and DBS-off states, meaning that DBS does not exert disease modulating effects by increasing striatal DA transmission (Hilker *et al.*, 2003; Strafella *et al.*, 2003; Thobois *et al.*, 2003). In fact, DBS does not arrest progressive dopaminergic loss. Striatal [^{18}F]FDOPA PET (Hilker *et al.*, 2005a) and [^{123}I]FP-CIT SPECT (Lokkegaard *et al.*, 2007) uptake continues to decline at rates of 9-13% and 7.7% per annum respectively, similar to that which is observed in individuals without DBS. High-performance liquid chromatography measurements of dopamine, homovanillic acid and dopamine turnover (Pal *et al.*, 2018), as well as nigral depigmentation scores related to neuronal loss (Pal *et al.*, 2017), showed no difference between DBS and non-DBS post-mortem samples. Moreover, DBS patients exhibited greater accumulation of α-synuclein within the substantia nigra, olfactory bulb and locus coeruleus, as well as higher Lewy body brain load, as compared to non-DBS patients (Pal *et al.*, 2017). DBS is associated with up to 4-fold increased risk for serious adverse events (Weaver *et al.*, 2009) and approximately 20% of patients will experience at least one that is DBS-related (Williams *et al.*, 2010), including intracranial haemorrhage, infarct, infection/erosion commonly at the implant sites, device malfunction/complications, post-operative confusion, oculomotor dysfunction, dysarthria and cognitive disturbance, potentially requiring removal of the hardware (Kleiner-Fisman *et al.*, 2006; Groiss *et al.*, 2009; Follett *et al.*, 2010; Williams *et al.*, 2010). Moreover, the possibility of battery and electrode replacement constitute reasons for additional surgical procedures, exposing patients to even greater risk over time.

1.7. Fetal Cell Therapy in Parkinson's disease

Despite the initial reductions of motor symptoms and improvements to quality of life gained through the introduction of levodopa, adjunct and more invasive therapies at various stages throughout the PD therapeutic strategy, none of these interventions have proven capable of exerting neuroprotective or neurorestorative effects on the progressively degenerating dopaminergic neuronal population. As such they all gradually lose efficacy, prompting increasing drug requirements to effect symptomatic relief but that must be weighed against the severity of motor fluctuations and dyskinesias associated with L-dopa dosage, earning it the epithet of a double-edged sword.

Towards a more complete and restorative approach, it has been thought that introducing new healthy dopaminergic neurons in replacement of those that have been lost through the degenerative process would in principle not only alleviate Parkinsonian symptoms but do so with greater permanence and in a manner that physiologically resembles the endogenous neural system, additionally obviating the need for exogenous dopamine provision. Amongst these cellular strategies, implantation of allogeneic dopaminergic neuroblasts derived from the human fetal ventral mesencephalon (hfVM) into the site of greatest denervation, the striatum, remains the most efficacious to date, showing favourable graft survival and capacity to restore dopamine and motor function over non-authentic dopamine-producing cellular alternatives such as autologous adrenal medullary tissue (Olanow *et al.*, 1990; Goetz *et al.*, 1991; López-Lozano *et al.*, 1991), autologous carotid body tissue (Minguez-Castellanos *et al.*, 2007) and allogeneic retinal pigmented epithelial cells (Gross *et al.*, 2011). Beginning in the late 1980's, a series of open-label clinical trials and long-term follow-up studies conducted across multiple sites worldwide, including Halifax, Canada (Mendez *et al.*, 2000; Mendez *et al.*, 2002; Mendez *et al.*, 2005; Mendez *et al.*, 2008); Lund, Sweden (Lindvall *et al.*, 1990; Hoffer *et al.*, 1992; Lindvall *et al.*, 1992; Sawle *et al.*, 1992; Widner *et al.*, 1992; Lindvall *et al.*, 1994; Wenning *et al.*, 1997; Hagell *et al.*, 1999; Piccini *et al.*, 1999; Brundin *et al.*, 2000; Hagell *et al.*, 2000; Piccini *et al.*, 2000; Hagell *et al.*, 2002; Piccini *et al.*, 2005; Pogarell *et al.*, 2006; Li *et al.*, 2008; Li *et al.*, 2010; Politis *et al.*, 2010b; Schrag *et al.*, 2010; Kurowska *et al.*, 2011; Politis *et al.*, 2011; Politis *et al.*, 2012; Kefalopoulou *et al.*, 2014; Li *et al.*, 2016); Paris, France (Peschanski *et al.*, 1994; Remy *et al.*, 1995; Defer *et al.*, 1996; Cochen *et al.*, 2003); China

(Folkerth and Durso, 1996); La Habana, Cuba (Molina *et al.*, 1992a; Molina *et al.*, 1992b); Mexico (Madrazo *et al.*, 1991); Madrid, Spain (López-Lozano *et al.*, 1997); Birmingham, UK (Kudoh *et al.*, 1999); and California (Ahn *et al.*, 2012), Los Angeles (Kopyov *et al.*, 1996; Kopyov *et al.*, 1997; Blüml *et al.*, 1999; Jacques *et al.*, 1999; Ross *et al.*, 1999), Denver (Freed *et al.*, 1992), New Haven (Spencer *et al.*, 1992), and Tampa (Freeman *et al.*, 1995; Kordower *et al.*, 1995; Kordower *et al.*, 1996; Kordower *et al.*, 1997; Kordower *et al.*, 1998; Hauser *et al.*, 1999; Kordower *et al.*, 2008a; Kordower *et al.*, 2008b; Cisbani *et al.*, 2017) in the United States, provided evidence that intrastriatal hfVM allotransplantation has the potential to exert meaningful symptomatic improvement in the practically-defined off-state by ~30% from baseline within 1-2 years and beginning as early as 3 months following surgery, as indicated using standardised UPDRS motor assessments (see Appendix). Motor performance in the off-state in some instances became similar to that in the on-state (Lindvall *et al.*, 1990; Lindvall *et al.*, 1992; Molina *et al.*, 1992b; Remy *et al.*, 1995; Kefalopoulou *et al.*, 2014) and for some patients in whom unilateral transplantation was conducted on the hemisphere of greatest denervation, the most afflicted contralateral body side became symptomatically equivalent if not milder than the ipsilateral body side (Lindvall *et al.*, 1990; Hoffer *et al.*, 1992; Lindvall *et al.*, 1992; Lindvall *et al.*, 1994; Peschanski *et al.*, 1994; Wenning *et al.*, 1997).

Interestingly, not all symptoms may be affected equally; data from the Madrid trial suggests that significant alleviation commences and peaks earlier for rigidity and hypomimia, followed by postural stability, dysarthria, bradykinesia, gait disturbance and finally tremor (López-Lozano *et al.*, 1997). Although not formally tested, this study also indicated the greatest response to transplant for rigidity, a milder response of bradykinesia and a highly variable response of tremor throughout a 5-year follow-up (López-Lozano *et al.*, 1997). Surprisingly, no other open-label study has systematically evaluated each of the cardinal motor signs in the off-state in the same cohort. However, across multiple sites a number of authors have reported dramatic reductions in clinician-rated rigidity (Lindvall *et al.*, 1990; Madrazo *et al.*, 1991; Lindvall *et al.*, 1992; Widner *et al.*, 1992; Lindvall *et al.*, 1994; Wenning *et al.*, 1997; Brundin *et al.*, 2000), bradykinesia as rated by clinicians (Madrazo *et al.*, 1991; Freed *et al.*, 1992) as well as objectively tested using electromyographic recordings (Lindvall *et al.*, 1990; Lindvall *et al.*, 1992; Lindvall *et al.*, 1994; Wenning *et al.*, 1997) and timed motor assessments (including pronation-supination, finger dexterity, hand-arm movement and/or

foot tapping) (Lindvall *et al.*, 1990; Hoffer *et al.*, 1992; Lindvall *et al.*, 1992; Widner *et al.*, 1992; Lindvall *et al.*, 1994; Peschanski *et al.*, 1994; Remy *et al.*, 1995; Defer *et al.*, 1996; Kopyov *et al.*, 1996; Kopyov *et al.*, 1997; Wenning *et al.*, 1997; Hagell *et al.*, 1999; Hauser *et al.*, 1999; Kudoh *et al.*, 1999; Brundin *et al.*, 2000; Mendez *et al.*, 2002; Mendez *et al.*, 2005) and postural stability and gait disturbance, also evaluated both clinically (Madrazo *et al.*, 1991; Freed *et al.*, 1992; Hoffer *et al.*, 1992; Folkerth and Durso, 1996) and by using timed tests (Widner *et al.*, 1992) including sit-stand-walk performance (Kopyov *et al.*, 1996; Kopyov *et al.*, 1997; Kudoh *et al.*, 1999).

Across open-label trials, activities of daily living, time spent in the off-state, time spent in the on-state with and without dyskinesia, the overall severity of dyskinesias, frequency of off episodes, freezing and falling also show improvement within 2 years. Decreases of ~25% have been recorded for the daily requirement of L-dopa during the same period, with some individuals able to withdraw from medication altogether (see Appendix). Importantly, these transplant-mediated clinical effects are seen to be sustained in patients followed up beyond 3 years post-operatively (Defer *et al.*, 1996; López-Lozano *et al.*, 1997; Piccini *et al.*, 1999; Hagell *et al.*, 2002; Pogarell *et al.*, 2006). For three individuals from the Lund series, motor severity at 13-16 years following the procedure remained significantly lower (-70%) than a group of non-transplanted moderate-stage PD patients, despite the former having lived with the disease for 20 years longer (Politis *et al.*, 2012). This degree to which hfVM transplants may slow clinical progression is not usually achievable by any other known therapy.

1.7.1. Imaging findings in open-label trials

1.7.1.1. Dopamine synthesis and storage capacity

Positron emission tomography (PET), utilised predominantly in conjunction with radionuclides targeting dopaminergic markers, has been an important tool for objectively assessing post-operative graft function *in vivo*. [^{18}F]FDOPA has been used with particular frequency for its ability to provide measurements of presynaptic dopamine synthesis and storage capacity (Kuwabara *et al.*, 1993; Heiss and Hilker, 2004) and in this regard is interpreted as a marker of graft survival and viability within the host environment. Early open-label trials have reported elevations of [^{18}F]FDOPA uptake in transplanted putamina to within the range of normative values as early as 8 months post-transplant, with mean

increases of ~55% up to 12 months and further rising to ~65% between 1-3 years post-surgery, while some patients acquired substantial increases of up to 200% with respect to baseline values (Freed *et al.*, 1992; Sawle *et al.*, 1992; Widner *et al.*, 1992; Lindvall *et al.*, 1994; Remy *et al.*, 1995; Wenning *et al.*, 1997; Hagell *et al.*, 1999; Hauser *et al.*, 1999; Brundin *et al.*, 2000; Mendez *et al.*, 2000; Mendez *et al.*, 2002; Mendez *et al.*, 2005; Mendez *et al.*, 2008; Politis *et al.*, 2010b; Politis *et al.*, 2011) (see Appendix). In four patients from the Lund series whom had undergone long-term follow-up over 7-14 years the increased [^{18}F]FDOPA uptake in the transplanted putamen was not only sustained but exhibited further increases from the early post-operative period (Piccini *et al.*, 1999; Politis *et al.*, 2010b; Politis *et al.*, 2011). Alongside these regenerative effects, continued loss of native dopaminergic neurons has been seen in the substantia nigra and median raphe by 12 months but with no further decrease at 24 months in these or any other brain region (Piccini *et al.*, 2005) (Figure 1.8). For unilaterally transplanted individuals, the non-grafted striatum generally followed the expected degenerative course, although some studies have found modest increases in AADC activity in non-grafted striatal nuclei (Lindvall *et al.*, 1990; Freed *et al.*, 1992; Hoffer *et al.*, 1992; Sawle *et al.*, 1992; Spencer *et al.*, 1992; Lindvall *et al.*, 1994; Peschanski *et al.*, 1994; Remy *et al.*, 1995; Wenning *et al.*, 1997; Mendez *et al.*, 2000), raising the possibility that transplant-related neurorestorative effects may not be restricted to the target nucleus alone. Indeed, it is worth noting that whereas non-transplanted PD patients exhibit widespread [^{18}F]FDOPA decrements across limbic, frontal, subcortical and brainstem regions, in three of the long-term follow-up Lund patients, extrastriatal [^{18}F]FDOPA uptake was significantly lower than healthy control values only in the amygdala (Politis *et al.*, 2012). [^{18}F]FDOPA uptake following surgery was related to daily off-time, on time and contralateral finger dexterity in one study (Remy *et al.*, 1995). However, given that these correlations would be expected in non-transplanted individuals it is perhaps more telling in terms of therapeutic efficacy that in a sub-group of the Tampa open-label cohort, pre- to post-operative changes in putamenal [^{18}F]FDOPA uptake were strongly correlated with improvements in total UPDRS scores, as well as the amount of time spent in the off-state and on-state with and without dyskinesia (Hauser *et al.*, 1999). This would indicate that clinical recovery is dependent on the expression of AADC within grafted cells and their functional capacity for dopamine synthesis and storage.

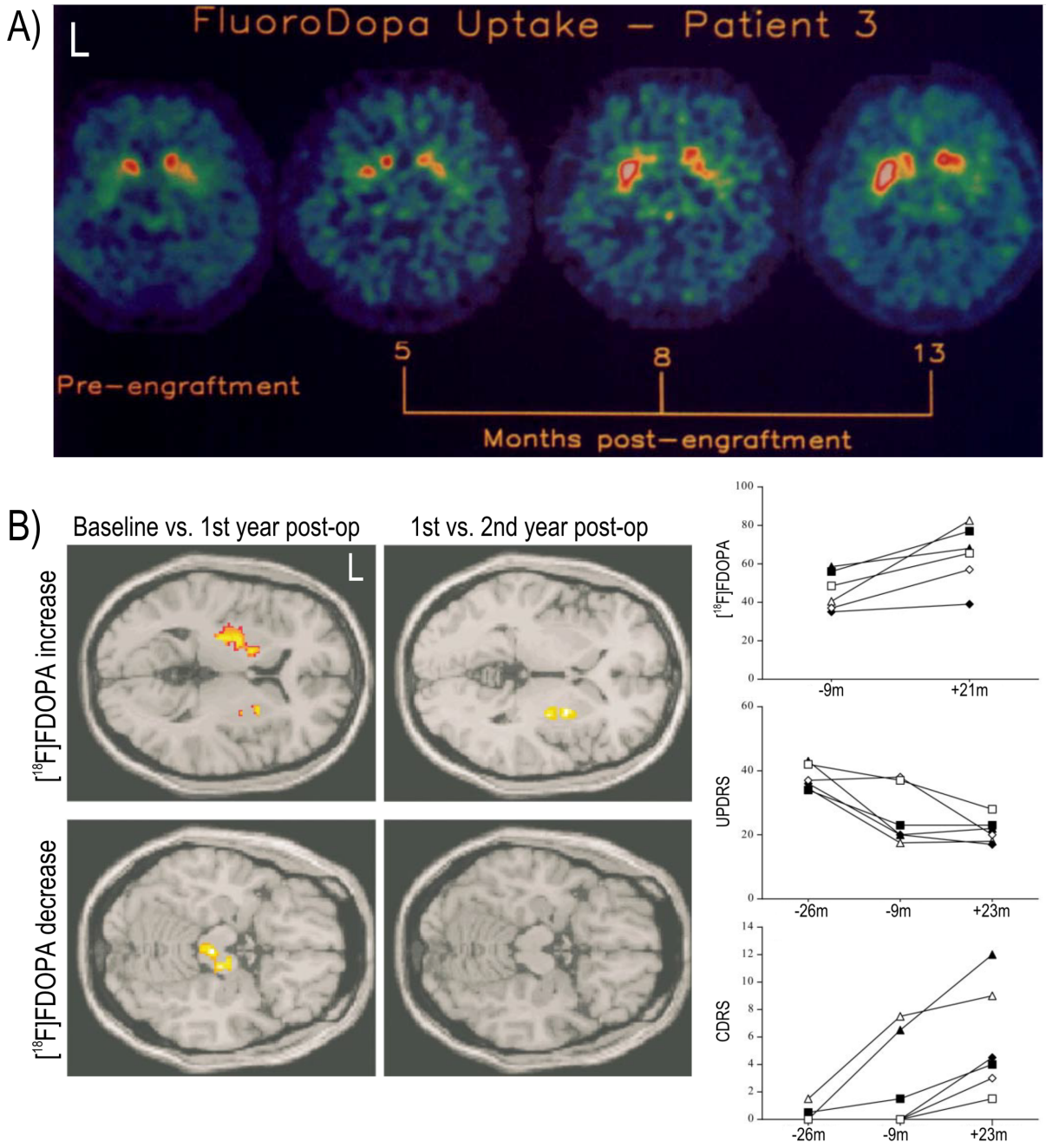


Figure 1.8: [18F]FDOPA examinations of graft survival and growth. A | Whole-brain ratio analysis with occipital reference for patient 3 of the Lund open-label trial who received unilateral transplantation into three sites of the left putamen. Sequential scans reveal progressive increases in dopamine storage capacity in the transplanted putamen over the course of 13 months. B | Voxel-wise analysis of six patients from the Lund series who received bilateral intrastriatal deposits (left). As compared to baseline, patients exhibited bilateral increases in [18F]FDOPA uptake after one year, and a further increase in the right putamen by the second year. [18F]FDOPA values continued to decrease in the right substantia nigra and median raphe at one year as compared to baseline. The effects of withdrawal of immunosuppression are also shown in the plots to the right. There was a further increase in dopamine synthesis and storage capacity at 21 months following as compared to 9 months prior to withdrawal. Across a similar interval, there was no change in UPDRS motor severity scores while there was a significant increase in CDRS-rated "off-state" graft-induced dyskinesia symptoms. CDRS = clinical dyskinesia rating scale; UPDRS =

unified Parkinson's disease rating scale. Figures extracted from; A | (Sawle et al., 1992), B | (Piccini et al., 2005).

Corroborative evidence supporting the interpretation of [^{18}F]FDOPA as a measure of graft survival has come from several post-mortem studies in which patients had died of unrelated causes relatively soon after their last PET scan (Kordower *et al.*, 1995; Kordower *et al.*, 1998; Mendez *et al.*, 2005). In one case from the Halifax cohort, putamenal transplant was successful in the right hemisphere but for the left hemisphere the procedure was halted after a bleed in the cannula after the first deposit. At 3 years this patient showed overall clinical improvement which was more marked in the left body side, and while the right putamen exhibited 222% increase in [^{18}F]FDOPA uptake, the left degenerated by 45%. At 52 months, immunohistochemical analysis showed no surviving tyrosine-hydroxylase positive cells within the left putamenal tracks, but over 200, 000 in the right putamen (Mendez *et al.*, 2005). In another case from the Tampa study who gained significant global improvements at 15 months following bilateral implants in the posterior putamen, [^{18}F]FDOPA PET at 12 months revealed significant increases of 82% in the bilateral putamen in addition to a significant 39% increase in the right caudate nucleus, with no longitudinal change in the left caudate. In keeping with this, post-mortem investigation at 18 months showed that grafts placed in the medial portion of the right putamen gave rise to fibres that crossed the internal capsule and innervated the right caudate while no such fibres were observed in the left hemisphere (Kordower *et al.*, 1995). No evidence had been found for induced sprouting of host fibres, hence changes in [^{18}F]FDOPA uptake likely resulted from graft-derived fiber outgrowth (Kordower *et al.*, 1995; Kordower *et al.*, 1998).

1.7.1.2. D_2 receptor density and dopamine release

Using the D_2 receptor antagonist [^{11}C]raclopride in a unilaterally transplanted patient at 10 years following surgery who experienced excellent clinical benefit, it has been found that the basal density of available D_2 receptors were no different from normal controls in the grafted putamen but remained up-regulated in the non-grafted putamen and bilateral caudate, suggesting that transplant-related reinnervation restores tonic dopamine release and D_2 receptor occupancy to normal levels (Figure 1.11). Acute administration of methamphetamine in the same patient induced large reductions in [^{11}C]raclopride binding

in the grafted putamen, almost a 5-fold decrease as compared to the non-transplanted putamen, and near equivalent to that seen in healthy individuals (Piccini *et al.*, 1999). This normalisation in methamphetamine-induced dopamine release has been observed in several cases from the 5th to the 10th post-operative year (Piccini *et al.*, 1999; Politis *et al.*, 2010b; Politis *et al.*, 2011; Politis *et al.*, 2012). In contrast, in one cohort of 8 patients, dopamine release was only partially restored by the hfVM grafts by about 25% as compared to non-transplanted patients, and still remained at approximately 20% of healthy control values (Piccini *et al.*, 2005). It is however unclear at what time-point these patients were studied following the procedure, and the large calculated group variance may reflect the fact that patients with poor clinical outcomes were included in the analysis. The percentage decrease in [^{11}C]raclopride binding in this study was strongly correlated to putamenal [^{18}F]FDOPA uptake, such that higher dopamine synthesis and storage capacity equated to greater dopamine release in the grafted putamen. Yet the authors also report a trend that for a similar level of [^{18}F]FDOPA uptake, dopamine release was more pronounced in non-grafted as compared to grafted patients (Piccini *et al.*, 2005), potentially implying that although evident to a certain degree (and to a large degree in select cases), the functional capability for grafted neurons to release endogenous dopamine and restore post-synaptic D_2 receptor occupancy may be limited.

1.7.1.3. Dopamine transporter expression

Studies examining the ability of grafted neurons to express the dopamine transporter (DAT), a transmembrane protein that facilitates reuptake of extracellular DA back into the presynaptic terminal, have also shown some inconsistency. Despite a significant 30% increase of [^{18}F]FDOPA uptake in a sub-group of 6 patients from the Paris cohort, Cochen *et al.* (2003) found that DAT binding, as measured with [^{76}Br]FE-CBT PET, in the same grafted putamen showed only a minor and non-significant increase of 8% from baseline (Cochen *et al.*, 2003) (Figure 1.9). Using [^{11}C]nomifensine PET, Hoffer *et al.* (1992) found in two Lund case studies who had received transplantation in the striatum contralateral to the most severely affected limbs, that DAT density at 5-6 months was either similar between the left and right or asymmetric in favour of greater binding in the previously more affected side. In patient 2 who was scanned again at 12 months, the initial gains in DAT density were not sustained and oppositely reverted to a more rapid rate of decline than the non-operated side

over the interval (Hoffer *et al.*, 1992). In contrast, continual elevation of [^{123}I]IPT and [^{123}I]FP-CIT binding has been observed up to 14 years post-graft, though not necessarily uniformly across target regions, with one patient achieving and sustaining "normal" levels at the latest time-point in the clinically least affected striatum but reversal back to baseline levels following transient increase over the first 3 years in the more affected striatum (Pogarell *et al.*, 2006; Politis *et al.*, 2011), potentially reflecting differences between the sides in terms of the preparation and overall quality of the hfVM tissue used and/or how the inherent lateralisation of disease severity may have differential impact upon implanted cells (Pogarell *et al.*, 2006).

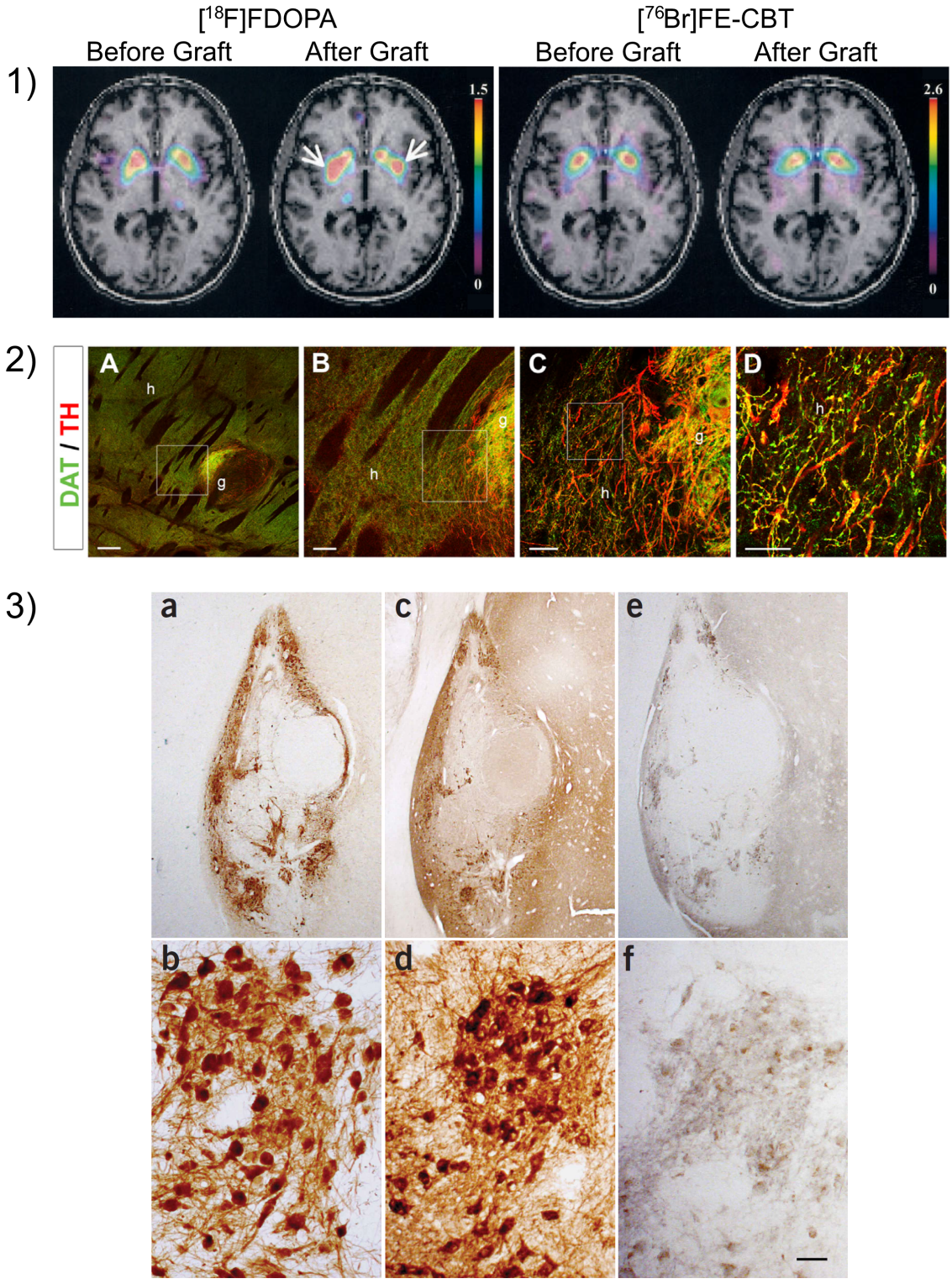


Figure 1.9: Inconsistent findings for the ability of grafted neurons to express the dopamine transporter. 1 | [18F]FDOPA and [76Br]FE-CBT PET scans showing AADC activity and DAT density respectively in a single patient from the Paris open-label trial, before and 6-24 months (not specified) after bilateral intraputamenal hfVM transplantation. Significant increases in AADC activity can be seen in the right putamen and to a lesser extent in the left putamen, while DAT density showed minimal post-operative change. 2 | Double immunostaining for DAT (green) and TH (red) in one subject from the Lund open-

label trial 4 years following transplant. Successively higher magnification illustrated from left to right with boxed areas representing the area shown in the subsequent panel. DAT immunostaining shows robust punctate localisation along morphologically healthy TH-immunoreactive fibers. g = graft; h = host; Bars, 400μm (A), 100μm (B), 50μm (C), 20μm (D). 3 | Low (a, c, e) and high (b, d, f) power photomicrographs of a transplant in the post-commissural putamen of an individual from the Tampa randomised controlled trial at 14 years post-surgery, stained for TH (a, b), VMAT2 (c, d) and DAT (e, f), illustrating that while the graft is viable it lacks DAT expression. Bar, 520μm (a, c, e), 80μm (b, d, f). DAT = dopamine transporter; TH = tyrosine hydroxylase. Figures extracted from; 1 | (Cochen et al., 2003), 2 | (Hallett et al., 2014), 3 | (Kordower et al., 2008a).

Interestingly, [^{123}I]IPT, [^{123}I]FP-CIT (Pogarell *et al.*, 2006; Politis *et al.*, 2011) and [^{11}C]nomifensine (Hoffer *et al.*, 1992) binding ratios did not appear to be confluent with those obtained using [^{18}F]FDOPA, which in some instances was seen to increase while DAT density dropped (Hoffer *et al.*, 1992; Politis *et al.*, 2011). Moreover, no correlation was found between changes in [^{76}Br]FE-CBT binding and [^{18}F]FDOPA uptake between scanning sessions (Cochen *et al.*, 2003) suggesting that the capability for grafted neurons to synthesize DA is not related to their expression of DAT and potential for re-innervating the host striatum. These *in vivo* findings echo those found at post-mortem, whereby in four patients with 12-22 year old grafts very light to no DAT-immunostaining was seen in a large proportion of surviving grafted neurons (Kordower *et al.*, 2008a; Kordower *et al.*, 2008b; Kurowska *et al.*, 2011), whereas in another six patients who came to autopsy 18 months to 14 years following surgery, DAT was expressed by tyrosine hydroxylase immunoreactive neurons and extensively innervated the transplanted nuclei (Kordower *et al.*, 1996; Hallett *et al.*, 2014) (Figure 1.9). The integrity of the dopaminergic cell terminals may however be an important factor to the eventual clinical outcome. In the Paris study, over the same period in which motor severity showed no significant improvement, AADC activity significantly increased but DAT density did not (Cochen *et al.*, 2003). The decline in [^{11}C]nomifensine binding from 5 to 12 months post-surgery in patient 2 of the Lund series largely paralleled the period in which walking ability switched from gradual improvement to gradual worsening and electroencephalographic recordings of motor readiness potential amplitude in the primary motor cortex during contralateral hand movements went from slightly increased from baseline (no change in the corresponding non-operated side) to indistinguishable, while [^{18}F]FDOPA in the grafted putamen increased by 27% over the same interval (Hoffer *et al.*, 1992). Lastly, Pogarell *et al.* (2006) found continual rises in striatal

[^{123}I]IPT binding aligned with progressive clinical improvement in one patient up to 8 years post-surgery, while a slight decrease in DAT density from 3 to 8 years was evident in a patient whose clinical benefit suffered a slight loss of gain over the same period (Pogarell *et al.*, 2006). That said, the relationship between DAT expression in individuals receiving hfVM transplants and measures of clinical outcome has not yet been formally addressed.

1.7.1.4. Non-dopaminergic imaging findings

Non-dopaminergic imaging techniques have also been employed and have provided further supplementary information on graft survival and function. Using proton magnetic resonance spectroscopy, Ross *et al.* (1999) found that the concentration of *N*-acetylaspartate within the putamenal graft sites, a metabolite marker of neuronal viability and maturity which was confirmed to be present only in trace amounts in fetal tissue assayed *in vitro*, was no different from putamenal samples derived from non-transplanted adults *in vivo* and only marginally shy of pre-operative levels at approximately 12 months following surgery. Even for grafts displaying the lowest concentrations of *N*-acetylaspartate, values were many times greater than those quantified *in vitro*, thus indicating the maturation of grafted cells into adult-type neurons (Ross *et al.*, 1999). In addition, other metabolites such as myo-inositol, a key compound relevant for cellular signal transduction and osmoregulation (Fisher *et al.*, 2002) and choline, a precursor of the neurotransmitter acetylcholine and marker of cell membrane composition (Michel *et al.*, 2006), were identified and even found to be elevated with respect to non-grafted individuals, which may either reflect neuronal development towards a neurochemical signature resembling that observed in adults, or conversely increased cellular membrane turnover, demyelination and glial activation consistent with degeneration (Faghihi *et al.*, 2017).

Functional magnetic resonance imaging has revealed blood-oxygenation-level-dependent changes that correlate with intermittent wrist-forearm lever movements in small clusters of the contralateral putamen, illustrating stimulus-driven neuronal activation within the graft sites and functional integration of the foreign tissue 2.5-3 years after surgery, beyond the time frame within which graft-related increases in dopamine synthesis are expected to plateau. Curiously, the movement-related activity was consistently detected only on one side of the brain, despite both patients undergoing bilateral intraputamenal procedures

(Blüml *et al.*, 1999). The capacity of the re-innervated striatum to affect downstream regions of the motor network has also been probed in a small group of four patients using $H_2{}^{15}O$ PET as a surrogate measure of regional cerebral blood flow. Relative to when patients were at rest inside the scanner, paced joystick movements of the left hand in one of four freely chosen directions invoked greater activation in the bilateral rostral supplementary motor area and the right dorsolateral prefrontal cortex at 18.3 months following surgery as compared to pre-operative scans, regions known to be involved in the preparation and selection of voluntary movement. Despite a significant increase in [^{18}F]FDOPA being detected at 6.5 months (+77%), with no further elevation at 18.3 months, no significant changes in regional cerebral blood flow were identified at this earlier stage, demonstrating that functional restoration of the wider cortico-basal ganglia-thalamo-cortical network is comparatively delayed (Piccini *et al.*, 2000) (Figure 1.10). Moreover, while disease severity as measured using the UPDRS motor subscale decreased slightly (-25%) at the first post-graft time-point, the clinical improvement only became significant at the 2nd time-point (-50%), in concert with the cortical response. Taken together, this illustrates that hfVM implants exert biological effects beyond the transplanted nucleus and that functional remediation depends not only on striatal reinnervation but network-wide host-graft integration (Piccini *et al.*, 2000).

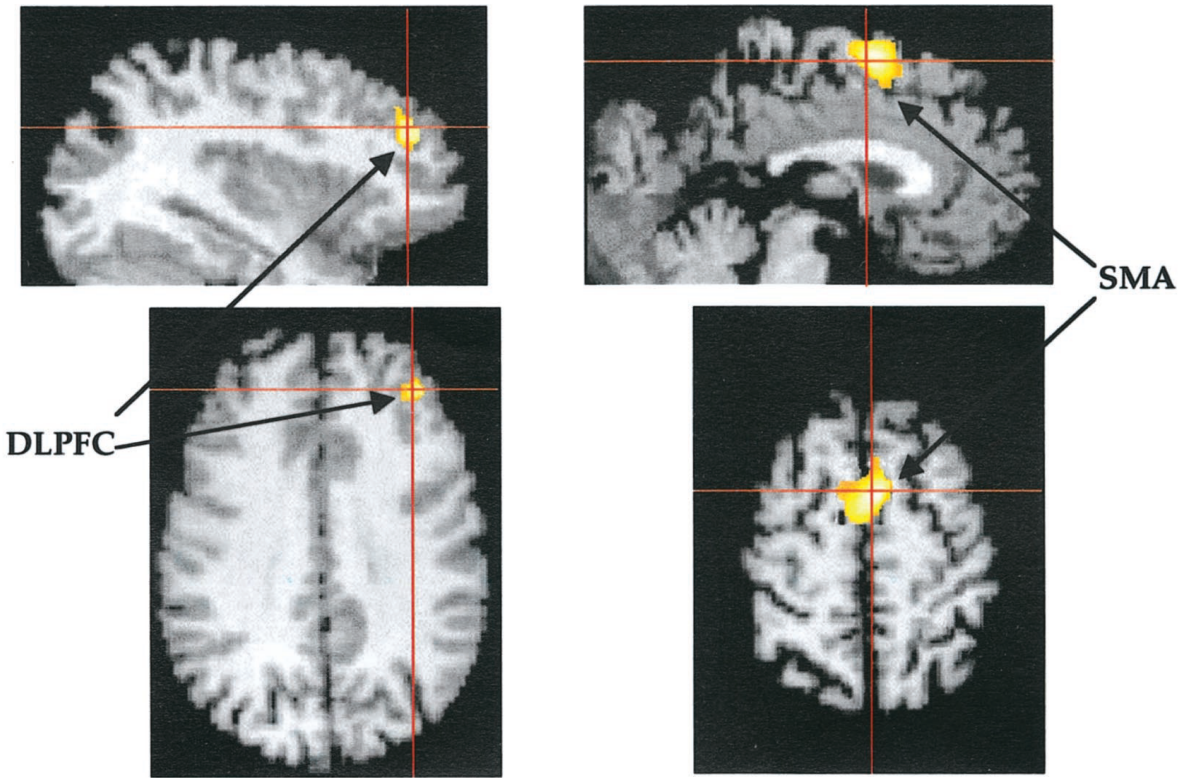


Figure 1.10: Effects of hfVM transplantation on cortical activity. Voxel-wise analysis showing increased movement-related $H_2{}^{15}O$ PET derived regional cerebral bloodflow in the right dorsolateral prefrontal cortex (DLPFC) and rostral supplementary motor area (SMA) in four Parkinson's disease patients who had received bilateral intrastriatal transplantation of hfVM tissue 18.3 months prior. These increases were not detected at 6.5 months despite significant elevation of striatal [^{18}F]FDOPA K_i, demonstrating delayed recovery of cortical function. Figure extracted from (Piccini et al., 2000).

More recently, single-unit recordings in a patient transplanted 10 years prior who experienced substantial reductions in UPDRS motor scores of more than 50% within 4 years and sustained [^{18}F]FDOPA levels at 9 years post-surgery have demonstrated long-term electrophysiological alterations in neurons of the globus pallidus interna (GPi). Examination of the patient after medication withdrawal revealed a significant reduction in resting discharge rates in comparison to non-transplanted individuals in the off-state, albeit still remaining slightly but statistically higher than those observed in one patient tested in the on-state. In contrast, gamma oscillatory activity (>35Hz), which is normally promoted by provision of L-dopa, was not corrected by hfVM transplant and remained at a lower frequency range (2-30Hz). Voluntary hand movements were however associated with marked phasic inhibition of GPi neuronal firing by 63% relative to baseline which was not seen in non-transplanted participants in either on- or off-states. Because no changes were

recorded in the external pallidal segment at rest, the authors conclude that modulation of excessive pallidal outflow, downstream effects on thalamocortical circuitry and ultimately symptomatic relief most likely originate from an increased graft-derived dopaminergic effect on D_1-type striatal GABAergic medium spiny neurons within the direct basal ganglia pathway (Richardson *et al.*, 2011).

1.7.2. NIH-funded randomised controlled trials

Although the potential benefits of intrastriatal hfVM transplantation are clearly evident, it is also apparent that a substantial number of patients undergoing the procedure derived little to no or only transient clinical benefit, and those who did demonstrated variable degrees of alleviation across separable motor symptoms. The open-label literature is extremely challenging to compare, given a vast array of inter-trial differences including but not limited to the methods for embryonic dissection, number of donors used, gestational fetal age, surgical procedures, number of trajectories and deposits on withdrawal, implantation target nuclei being either caudate, putamen, substantia nigra or a combination, age and disease severity of patients included, length of follow-up and primary outcome measures (assessment instruments, left/right/bilateral or on-/off-state reporting), which in some instances were different even between individuals within the same study (see Appendix). It is also the case that individual patients have been included in several different studies, in some instances without specific acknowledgment, and although insightful, long-term case reports may be biased in favour of patients with optimal and sustained symptomatic relief, as these patients are simply the most likely to be amenable to further evaluation. There was also a concern that merely undertaking a serious invasive therapeutic intervention for the treatment of Parkinsonian symptoms may in itself invoke the expected motoric changes. Indeed, the placebo effect in Parkinson's patients has been well documented (Goetz *et al.*, 2008b; Lidstone *et al.*, 2010).

In light of this, two large NIH-funded, double-blind, randomised sham-surgery-controlled designs were initiated and reported in the early 2000's (Freed *et al.*, 2001; Olanow *et al.*, 2003). The first, conducted between centres in New York and Denver, involved 40 advanced Parkinson's disease patients randomly assigned in a double-blind manner to receive either bilateral intraputamenal hfVM implants, with tissue strands derived from a total of four

embryos aged 7-8 weeks post-conception and delivered via two needle trajectories per side, or an identical surgical procedure in which twist-drill holes were made in the skull but the dura mater was not penetrated (Freed *et al.*, 2001). One transplanted patient was subsequently lost to follow-up due to death from unrelated causes. At 12 months the study failed to meet its primary endpoint and reported no effect of transplant on subjective global severity ratings, even after patients were allowed to retrospectively re-score themselves using pre-operatively recorded videos. There were also no differences in standardised ratings of disease severity, as measured using the total UPDRS in the off-state, or daily L-dopa requirement, despite a significant 40% increase in putamenal [^{18}F]FDOPA uptake. However, when groups were divided by age at the time of surgery, younger patients did exhibit a 28% decrease in off-state disease severity and a 30% increase in ability to carry out daily living activities which was proven to be a significant improvement over young sham controls, while the older subgroups remained comparable. Interestingly, there was no difference between old and young transplanted individuals on post-operative [^{18}F]FDOPA-assessed graft viability and only in the younger group did the change in UPDRS motor severity, particularly bradykinesia, correlate with the change in [^{18}F]FDOPA uptake (Freed *et al.*, 2001; Nakamura *et al.*, 2001).

A later trial conducted in Tampa (FL, USA) recruited 34 moderate-advanced patients to a multi-dose, placebo-controlled double-blind trial with a 24 month follow-up (Olanow *et al.*, 2003). Patients randomised to the transplant group were subjected to bilateral implantation of solid pieces of hfVM tissue dissected from either one or four embryos aged 6-9 weeks post-conception into each post-commissural putamen, delivered via 8 needle trajectories per side. The placebo group were treated identically but received only partial burr holes that did not fully penetrate the skull. The primary outcome measure, that was the change in motor sub-score of the UPDRS in the off-state, was not significantly different across the three groups at the final time-point, although there was a trend towards a difference between the placebo and four-donor groups in which +9.4 and -0.72 points were recorded over time respectively and which in contrast to the previous study appeared to be driven by tremor. No benefit was seen in terms of activities of daily living, L-dopa equivalent daily dosage or time spent in the off- and on-states with or without drug-induced dyskinesia. Yet when patients were divided according to disease severity at baseline, milder patients showed a

significant treatment effect whereby the placebo and one-donor groups experienced a 47% and 25% decline in motor function whilst the four-donor group showed a modest 7% improvement. Post-hoc analysis revealed that the magnitude of these longitudinal changes was significantly different only between the four-donor and placebo groups. For the patients with severe disease at the time of surgery, no such results were detected. In contrast, [^{18}F]FDOPA analysis over the same time period revealed significant bilateral increases in both the one- and four-donor groups as compared to placebo irrespective of disease severity, with a trend towards greater elevation in the left putamen of the four-donor over the one-donor group (Olanow *et al.*, 2003).

It is worth noting here that the sham-surgery groups in both randomised trials either continued to deteriorate or remained unchanged in terms of motor severity and/or [^{18}F]FDOPA uptake (Freed *et al.*, 2001; Olanow *et al.*, 2003), opposing suggestions of a significant placebo effect in prior open-label trials.

1.7.3. Imaging for the efficacy of hfVM transplants

1.7.3.1. Patient selection

Results from the Tampa and Denver/New York trials conflict in some ways, not only in the symptoms reportedly improved by hfVM transplants, but also with regards to optimal patient characteristics. Age and disease severity are not necessarily mutually exclusive, yet Olanow *et al.* (2003) failed to confirm an effect of younger age on transplant efficacy (Olanow *et al.*, 2003), which was a key finding in the earlier randomised controlled trial (Freed *et al.*, 2001). Conversely, extended analysis of the Denver/New York cohort, including follow-up data from the unblinded phase as well as 14 patients originally randomised to sham-surgery who subsequently received the intervention open-label, found no influence of baseline disease duration or severity on the change in total UPDRS scores, instead confirming an interaction between time and age on transplant outcome (Ma *et al.*, 2010). However, voxelwise analysis of baseline scans revealed that higher pre-operative [^{18}F]FDOPA signal in the ventrorostral putamen correlated with greater improvements in motor scores at 1 and 2 years follow-up (Ma *et al.*, 2010). Similar findings were found in a previous retrospective study, in which patients with the poorest global outcomes were associated with more advanced neurodegeneration that extended into the ventral striatum (Piccini *et al.*, 2005).

Thus host age and/or disease severity could to some degree modulate the extent to which, or length of time taken, for the implants to become functional (Ma *et al.*, 2011). Interestingly, the Denver/New York follow-up study did not find the same time by age interaction when considering [^{18}F]FDOPA uptake (Ma *et al.*, 2010), which might suggest that the impact of patient characteristics on graft-derived clinical benefit may depend on factors beyond graft survival alone, including phenotypic expression of the dopamine transporter and/or the ability for grafted neurons to effect downstream regions of the basal ganglia-thalamo-cortical network.

1.7.3.2. Graft survival and viability

The magnitude of the [^{18}F]FDOPA increase in both of these studies, although significant, was less pronounced (20-40%) than those reported previously (Freed *et al.*, 2001; Olanow *et al.*, 2003), raising the possibility of a critical threshold of graft survival, below which symptomatic improvement may be negligible. The reasons for this are still not completely understood but may be due to the absence of (Freed *et al.*, 2001) or minor and very short-course (Olanow *et al.*, 2003) immunosuppression. Indeed, it is known that hfVM tissue is capable of eliciting alloimmune responses through upregulated expression of major histocompatibility complex molecules in the presence of pro-inflammatory cytokines, induced in this case by surgical trauma (McLaren *et al.*, 2001; Laguna Goya *et al.*, 2011). Autopsy examinations in seven of these patients who died 7-53 months following surgery showed a comparatively modest number of tyrosine-hydroxylase immunoreactive cells within the graft sites, and while exhibiting organotypic seamless reinnervation and extensive fiber outgrowth, immunostaining using antibody markers for activated microglia (CD45), lymphocytes (CD3) and the HLA class II antigen also revealed the presence of neuroinflammatory processes (Freed *et al.*, 2001; Olanow *et al.*, 2003). In contrast, Piccini *et al.* (2005) found that completely withdrawing immunosuppression approximately 29 months post-surgery did not compromise graft survival and moreover, [^{18}F]FDOPA PET at 21 months post-withdrawal showed further increases in AADC activity as compared to scans acquired prior to the tapering process (Piccini *et al.*, 2005) (Figure 1.8). No evidence of ongoing immune or neuroinflammatory response was seen in one of these patients whose withdrawal was complete by 64 months and who has since come to autopsy 24 years post-surgery (Li *et al.*, 2016). Thus an extended period of immunosuppression may be necessary

to prevent the rejection of hfVM tissue; at least until the host immune system develops a tolerance against allogeneic antigens.

Other reasons may be related to the preparation and/or the amount of viable tissue implanted (i.e. the number of donor foetuses), which in addition to Olanow *et al.* (2003) has also been demonstrated in open-label trials (Kopyov *et al.*, 1997; Cochen *et al.*, 2003) to be of critical importance to both clinical benefit as well as dopaminergic remediation. Lastly, the length of time for fetal cells to mature and affect extrastriatal dopaminergic circuitry may extend beyond the follow-up periods employed. Indeed, in a sub-group of 15 patients from the Denver/New York trial followed up for 4 years post-surgery unblinded, results resembled the original findings at 1 year, but motor severity was significantly decreased at 2 and 4 years, albeit with a slight loss of accrued benefit at the latter time point. Moreover, these improvements were concomitant with continually rising [^{18}F]FDOPA values that still remained below a 46% increase from baseline (Ma *et al.*, 2010). The original Denver/New York transplant cohort re-called for evaluation at 36 months also displayed significant improvements in UPDRS scores at this time point that were not present at 1 year, although no imaging measures were reported (Freed *et al.*, 2001).

1.7.3.3. Graft-induced dyskinesias

In addition to the inadequate clinical improvement in these randomised controlled trials were reports of patients exhibiting atypical dyskinetic movements in the "off-state". These phenomena were noted in 5/33 and 13/23 patients in the Denver/New York and Tampa studies respectively, emerging as early as 5 months after grafting, persisting despite reduction or complete withdrawal of dopaminergic medication and which in some cases were refractory to amantadine and severe enough to necessitate additional surgical intervention (Greene *et al.*, 1999; Freed *et al.*, 2001; Hagell *et al.*, 2002; Ma *et al.*, 2002; Olanow *et al.*, 2003; Pogarell *et al.*, 2006; Olanow *et al.*, 2009a; Richardson *et al.*, 2011; Kefalopoulou *et al.*, 2014). These movements, initially termed "runaway" dyskinesia (Ma *et al.*, 2002) and later dubbed graft-induced dyskinesia (GID) (Hagell and Cenci, 2005), were in fact noted in some patients from the open-label trials (Defer *et al.*, 1996; Jacques *et al.*, 1999) but were largely overlooked as a serious side effect of transplantation, perhaps due to a lack of tools for their specific assessment, especially in milder cases. On retrospective blinded video-

based re-evaluation, 14 patients from the original Lund series were reported to have either developed or shown increased graft-induced dyskinesia which reached maximal severity at approximately 40 months post-surgery (Hagell *et al.*, 2002). Their presentation appears to vary somewhat, but they have been described as resembling diphasic drug-induced dyskinesias, with a combination of choreiform, dystonic and repetitive movements that while sporadically distributed preferentially affect the lower extremities (Hagell and Cenci, 2005). They rarely resemble dyskinesias induced by L-dopa dosing even within the same individual. Their appearance may be positively associated with the degree of post-operative improvement in cardinal motor symptom severity (Ma *et al.*, 2002; Olanow *et al.*, 2009a), however this has not been a consistent finding (Hagell *et al.*, 2002; Olanow *et al.*, 2009a) and while some have drawn a link between peak post-operative GID and drug-induced dyskinesia severity (Hagell *et al.*, 2002), others find no correlation between the two (Olanow *et al.*, 2009a), supporting the notion that these side effects are driven by differing mechanisms. Conversely, the time spent in the on-state with dyskinesia prior to surgery (Olanow *et al.*, 2009a), and not pre-operative dyskinesia severity (Hagell *et al.*, 2002; Olanow *et al.*, 2009a), has been linked to post-surgical GID development. Lower baseline cardinal motor symptom severity (Ma *et al.*, 2002) and putamenal [^{18}F]FDOPA uptake (Hagell *et al.*, 2002) may also be predictive of GID development, however these results have also met opposition (Olanow *et al.*, 2009a).

1.7.3.3.1. Dopamine hyperinnervation

One initial hypothesis was that continued fiber outgrowth from the graft sites could be responsible for excessive dopamine signalling (Freed *et al.*, 2001). Indeed, a surplus of dopamine might exact over-activity within the direct basal ganglia pathway, resulting in aberrant over-inhibition of GPi outflow. Single-unit recording experiments in a patient who at 10 years experienced medically refractory GID revealed this over-inhibition to be topographically non-specific, arising in GPi neurons that were spatially distant and unlikely to all exert control over the hand-related movements that were being performed. By contrast, less than 15% of neurons in non-transplanted individuals in both off- and on-medicated states showed significant hand-movement-related inhibition and in those that did the decrease in discharge rates were far less pronounced than those seen in the transplanted patient. In addition, GPi neurons in the grafted patient exhibited increases in irregular

discharge patterns at rest akin to the cellular electrophysiological properties observed in non-transplanted patients following intake of L-dopa (Richardson *et al.*, 2011). However, the post-operative change in putamenal dopamine synthesis and storage capacity as assessed using [^{18}F]FDOPA does not correlate with GID severity (Hagell *et al.*, 2002; Olanow *et al.*, 2003; Olanow *et al.*, 2009a) and while one study found increases to be up to three times greater in patients with as compared to without GID (Ma *et al.*, 2002), others found these groups to be comparable at the same 24-month time-point (Olanow *et al.*, 2003; Olanow *et al.*, 2009a).

The potential role of excessive dopamine release has also been addressed using [^{11}C]raclopride upon intravenous methamphetamine challenge. In the grafted putamen of patients who had eventually developed GID, Piccini *et al.* (2005) detected a mean 9.55% decrease in binding potential following drug-induced dopamine release as compared to following saline placebo, marginally higher than non-transplanted individuals (6.84%) but far less than in healthy controls (25.2%) (Piccini *et al.*, 2003; Piccini *et al.*, 2005). There was no association between GID severity and the degree of drug-induced [^{11}C]raclopride displacement, nor basal D_2-receptor density in either the anterior, posterior or whole putamen (Piccini *et al.*, 2005). Moreover, in one well-studied patient who within the first 11 years following surgery reported on blinded video evaluation only very mild non-troublesome GID on the body side contralateral to their unilateral graft and for whom further worsening was not observed up until their death at 24 years (Li *et al.*, 2016), dual [^{11}C]raclopride PET at one decade indicated a methamphetamine-induced binding reduction of 26.6% in the transplanted putamen as compared to saline, similar if not slightly higher than healthy controls (Piccini *et al.*, 1999) (Figure 1.11). Taken together, these imaging data demonstrate that GID is unlikely to be associated with excessive dopamine synthesis or release from presynaptic terminals of grafted DA neurons.

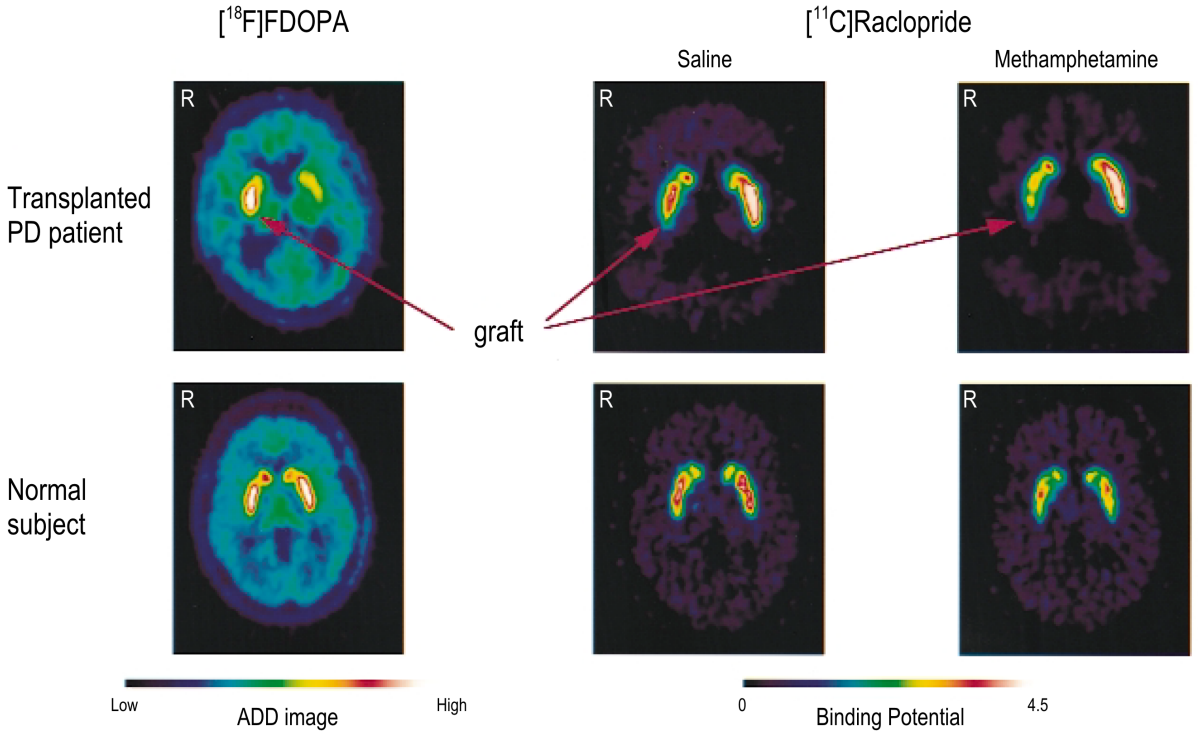


Figure 1.11: Restoration of dopamine storage and synthesis capacity, basal and drug-induced dopamine release by hfVM transplantation. ADD images of [18F]FDOPA and parametric images of [11C]raclopride before and after methamphetamine challenge in a single patient from the Lund open-label trial 10 years after right-sided intraputamenal transplantation. The bottom row presents data acquired from a normal subject for comparison. Basal D_2 receptor availability is normalised in the grafted putamen whereas it remains high in the non-engrafted side. The binding reduction following methamphetamine is similar to that seen in normal subjects for the right putamen while no difference was observed for the left. ADD = signal-averaged image; PD = Parkinson's disease. Figure extracted from (Piccini et al., 1999).

1.7.3.3.2. Patchy innervation

The site of cell deposition and patchy/uneven reinnervation has also been hypothesised as a possible factor for the emergence of GID (Freed *et al.*, 2001; Olanow *et al.*, 2003; Hagell and Cenci, 2005; Carlsson *et al.*, 2006; Olanow *et al.*, 2009a). Using voxel-wise analysis, Ma *et al.* (2002) identified significantly higher post-operative [18F]FDOPA uptake within the left posterodorsal and left anteroventral putamen in patients who within 2 years of surgery developed GID as compared to those who did not. However, the authors importantly acknowledge that these results may be confounded by the superior treatment response observed in the GID group. Thus, when compared to the non-GID patients who derived the greatest symptomatic benefit, only the anteroventral cluster remained significantly elevated (Ma *et al.*, 2002), supporting earlier suggestions that putamenal grafting should be weighted towards the posterodorsal aspect where denervation is greatest (Freed *et al.*, 2001) (Figure

1.12). In another study, patients who displayed significant [^{18}F]FDOPA increases in grafted regions of the striatum were scored according to a composite Likert-scale metric which takes into account the relative contributions of favourable benefits to unfavourable side-effects such as GID. Patients deemed to have the best global ordered outcome scores were found to exhibit preserved [^{18}F]FDOPA uptake in the non-transplanted ventral striatum throughout the study period. In contrast, those with moderate global ordered outcomes showed significant loss of AADC activity in this area within the first two years of follow-up, while in patients who responded poorest this was already the case prior to surgery (Piccini *et al.*, 2005). The results drawn from these cohorts appear contradictory with particular regard to ventral striatal [^{18}F]FDOPA uptake, while the use of a combined metric in the latter study makes it difficult to draw conclusions pertaining specifically to GID, limiting comparability with the former. However, they collectively highlight a possible role for imbalanced and/or incomplete re-establishment of dopaminergic function across the putamenal axis in the generation of GID, which might conceivably result from spontaneous local hotspots of graft survival, inhomogenous tissue delivery, regionally selective grafting and/or continued neurodegeneration of host neurons in non-grafted regions.

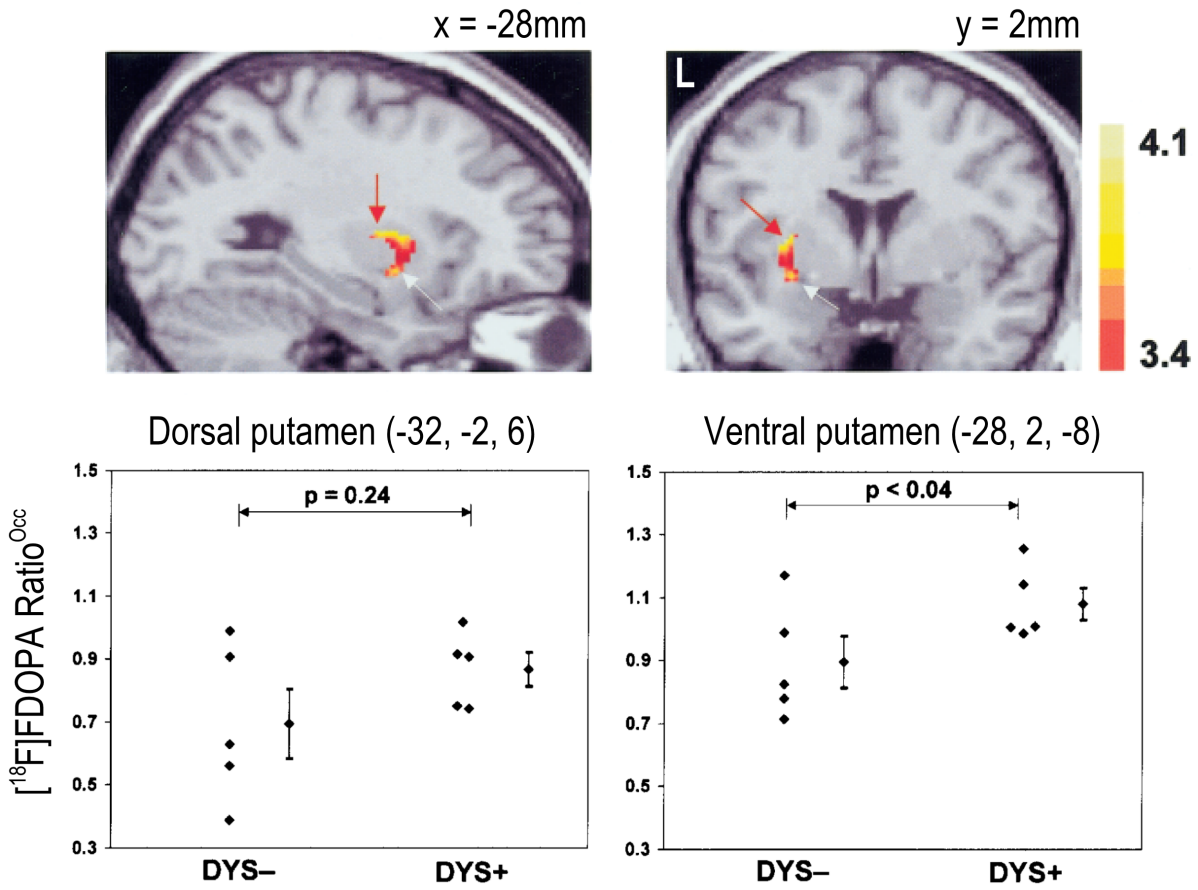


Figure 1.12: Patchy innervation may explain the emergence of graft-induced dyskinesia. Voxel-wise statistical parametric analysis of [¹⁸F]FDOPA ratio^{Occ} images demonstrating greater uptake in the left rostral and dorsal regions of the putamen in bilaterally implanted patients from the Denver/New York randomised controlled trial who developed graft-induced dyskinesia within two years of surgery (n = 5) as compared to those who did not (n = 12) (top). The lower scatter plots illustrate that patients with graft-induced dyskinesia exhibited greater dopaminergic re-innervation in the ventral putamen as compared to a subset of non-dyskinetic patients who derived the greatest symptomatic benefit from transplantation, while there was no difference in the dorsal cluster. DYS+ = transplanted patients with graft-induced dyskinesia; DYS- = transplanted patients without graft-induced dyskinesia. Figure extracted from (Ma et al., 2002).

1.7.3.3.3. Serotonergic hypothesis

More recently, attention has shifted towards the composition of the grafted hfVM tissue, which contains only about 10% newborn dopamine neurons and a varied proportion of other cell types not considered relevant in PD neurodegeneration (Isacson *et al.*, 2003). Of particular interest is the implantation and subsequent growth of serotonergic neurons (Mendez *et al.*, 2008), which develop caudal to, but in close proximity and sometimes intermixed with, dopaminergic neurons (Marklund *et al.*, 2014). Serotonergic neurons are known to be capable of converting L-dopa, storing and releasing dopamine in an activity–

dependent but dysregulated manner and have been implicated in the generation of involuntary and uncontrollable movements caused by acute L-dopa dosing i.e. drug-induced dyskinesia (Maeda *et al.*, 2005; Carlsson *et al.*, 2007; Carta *et al.*, 2007; Carta *et al.*, 2010; Politis *et al.*, 2014; Lee *et al.*, 2015; Smith *et al.*, 2015; Roussakis *et al.*, 2016). This intriguing hypothesis was tested *in vivo* in three long-term case studies from the Lund series who all derived excellent and sustained clinical benefits from bilateral implants for up to 16 years, with complete withdrawal of dopaminergic medication and concomitant normalisation of putamenal dopamine synthesis / storage capacity ([^{18}F]FDOPA) and release (methamphetamine-induced [^{11}C]raclopride binding change), but in whom severe GID also developed (Politis *et al.*, 2010b; Politis *et al.*, 2011). Using [^{11}C]DASB, which binds selectively to the serotonin transporter (SERT), a membrane protein located on the serotonergic presynaptic axon terminal that regulates neurotransmission by facilitating reuptake of serotonin from the synaptic cleft, it was found that these patients exhibited supranormal levels of putamenal SERT expression, quantified at a 46-172% and 106-285% increase over the mean binding values for healthy controls and non-transplanted advanced PD patients respectively (Politis *et al.*, 2010b; Politis *et al.*, 2011). In all 3 cases, pharmacological activation of the inhibitory 5-HT autoreceptors, which act to suppress serotonergic neurotransmission, by administration of the 5-HT$_{1A}$ agonist buspirone, substantially attenuated GID severity by ~60% between 90-240 minutes after the initial dose, while UPDRS motor sub-scores remained unchanged (Figure 1.13). Although supporting serotonergic involvement, these data do not sufficiently explain why differing levels of hyperinnervation were seen in two patients (46% vs. 77%) who reportedly experienced comparable GID severity as indicated by off-state AIMS scores (AIMS = ~12) (Politis *et al.*, 2010b; Politis *et al.*, 2011). In accordance with current models, dopamine neurotransmission should not entail serotonergic involvement if the density of dopaminergic neurons in the local environment is at the level required to handle the given concentration. Thus, when considering the putamenal ratio between [^{11}C]DASB binding potential and [^{18}F]FDOPA influx, both patients exhibited similar elevations of 140% and 146%, as compared to those seen in a group of 12 healthy controls. For the remaining patient whose GID was much more severe (AIMS = ~20), this ratio was further elevated to 230% (Politis *et al.*, 2010b; Politis *et al.*, 2011).

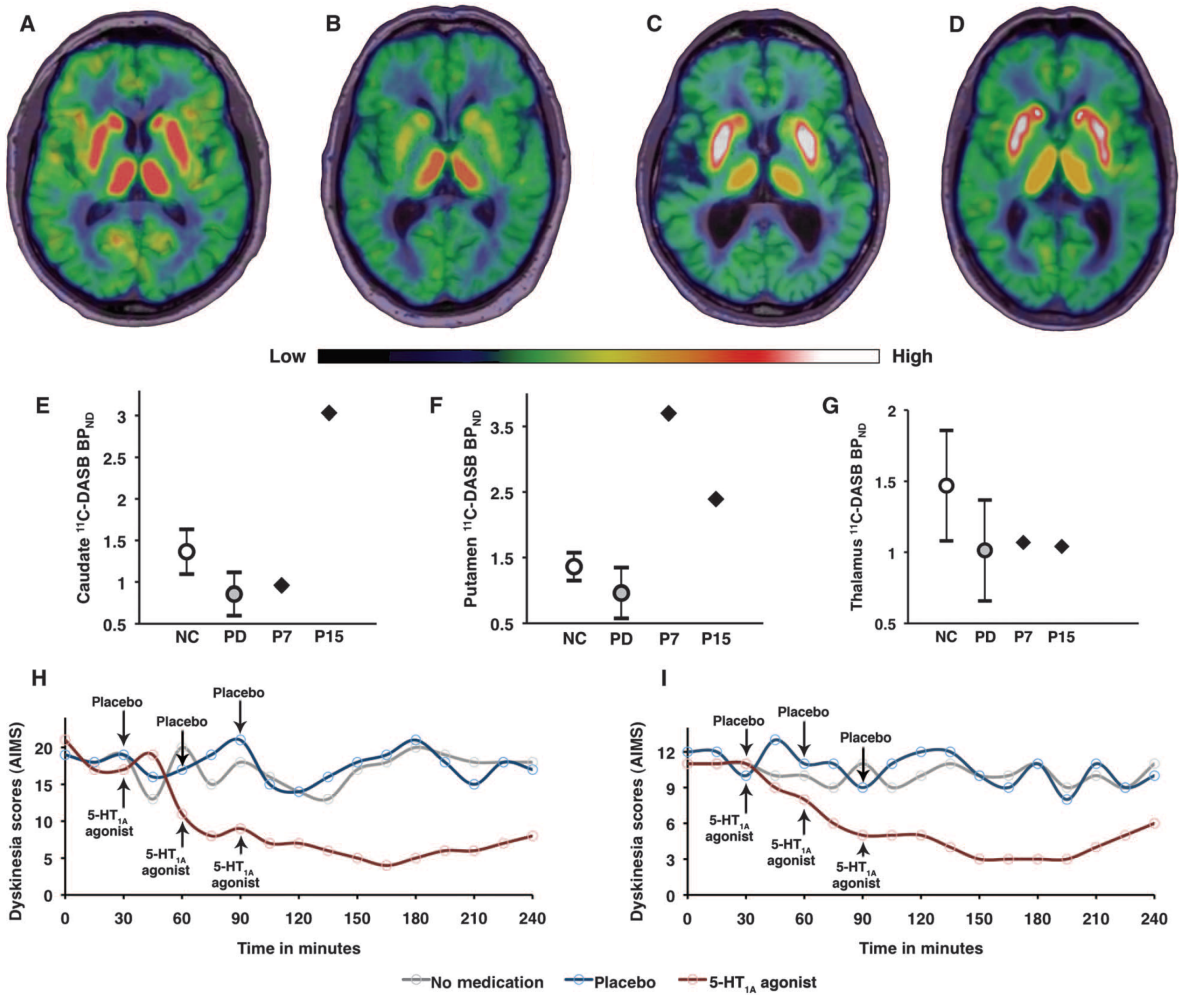


Figure 1.13: Serotonergic hyperinnervation in the grafted striatum of two patients from the Lund open-label trial. A-D | Summed [11C]DASB PET images overlaid onto structural magnetic resonance images, viewed axially at the level of the dorsal basal ganglia. E-G | Plots illustrating substantial elevations in [11C]DASB BP_{ND} for each transplant patient in the caudate and putamen with respect to mean values for a group of healthy volunteers (n = 12) and a group of age- and gender-matched non-transplanted advanced PD patients (n = 12). H-I | AIMS dyskinesia scores for each transplanted patient after a double-blind acute challenge with 3 repeated 5mg doses of the 5-HT1A agonist (buspirone) or 3 repeated doses of placebo given orally at 30-minute intervals. 5-HT = serotonin; AIMS = abnormal involuntary movement scale; BP_{ND} = non-displaceable binding potential; NC = normal control; PD = Parkinson's disease. Figure extracted from (Politis et al., 2010b).

Whilst compelling, there were no baseline [11C]DASB scans against which to compare and quantify the degree to which the hfVM grafts contributed to serotonergic hyperinnervation, either separately or with relation to measures of dopaminergic function. There were also no transplanted patients who did not develop GID recruited to the study and it is possible that these individuals might have displayed comparable imaging values post-operatively. Moreover, it is likely that GID in these cases emerged long before [11C]DASB PET was

undertaken. In one patient, GID was experienced from 13 years prior, for which he underwent bilateral DBS due to its severity 7 years later (Politis *et al.*, 2011). For the other two patients, it is not reported when their GID began (Politis *et al.*, 2010b), but their inclusion in a prior group analysis where the mean time to maximal severity was 40 months (Hagell *et al.*, 2002) suggests that it was probably much earlier, leaving an extensive period of time within which multiple plastic alterations may have occurred in both hfVM and host neurons. In addition, in one post-mortem case examined 16 years after grafting for whom DBS was necessary to treat Parkinsonian and GID symptoms, very few serotonergic neurons were seen within the graft (Kordower *et al.*, 2017), whereas in five other 3-14 year cases who did not develop GID, ample surviving serotonin neurons were detected (Mendez *et al.*, 2008). Nevertheless, the degree of dopamine mishandling through aberrant modification of serotonergic to dopaminergic innervation is mechanistically plausible.

1.8. The current thesis: The Transeuro trial

Given the certainty of continued PD progression and the development of motor complications in patients treated with L-dopa therapy, cell-based interventions still remain a highly promising reparative approach. On the basis of post-hoc analyses and the insights gained from the previous open-label and double-blind cohorts, a new multi-centre clinical trial was conceived whose principal goal was to evaluate whether the consistency and efficacy of hfVM transplantation could be improved by careful optimisation of major technical aspects believed to have resulted in their heterogeneous outcomes, with the aim that this would translate into longer-lasting clinical benefit with minimal side effects, including GID. This includes adjustments to the selection of patients, favouring those who are younger and at a milder stage of disease both in terms of clinical severity and dopaminergic denervation; the immunosuppressive regime, in order to reduce the risk of detrimental neuroinflammatory responses at the graft site which may compromise cell survival or function; the mode of engraftment, to ensure a more homogenous delivery of hfVM cells across the entire putamenal axis; and tissue collection, dissection and preparation procedures, to improve upon the number of viable cells and the composition of the final suspension with respect to the presence of serotonergic progenitors.

Understanding the neural alterations responsible for the changes in symptomatic expression in patients undergoing hfVM transplant is crucial in order to realise the full potential of cell-based strategies going forward. Immunohistochemical evaluations at autopsy have been insightful in this regard, but have mostly been conducted many years after the end of formal follow-up periods and with large variations from the time of surgery and as such are somewhat limited with respect to clinical correlates. Moreover, the scope of objective *in vivo* information retrieved from previous trials is severely limited, primarily constituting [^{18}F]FDOPA PET with relatively few small sample studies using alternative imaging techniques at varying times post-graft, as discussed above. As such, a comprehensive battery of neuroimaging assessments was also designed to examine aspects of dopamine and serotonin innervation prior to grafting, as well as how these measures change as a result of surgery. These include [^{11}C]PE2I and [^{11}C]DASB PET for the assessment of dopamine and serotonin transporter expression respectively, as well as [^{18}F]FDOPA PET to assess AADC

activity. The current thesis reports the novel multimodal imaging outcomes of hfVM cell therapy in Parkinson's disease patients under the Transeuro protocol, including those concerning the relationship between these *in vivo* biomarkers and changes to motor severity and emergence of GID.

The aims of the current thesis were as follows:

1. To examine the effects of intraputamenal hfVM transplants in patients with Parkinson's disease, administered under the Transeuro open-label clinical trial, at 18 months post-surgery with regards to:
    a. Grafted cell dopamine synthesis and storage capacity, using [^{18}F]FDOPA PET
    b. The ability for grafted cells to express the dopamine transporter, using [^{11}C]PE2I PET
    c. The presence of serotonergic cells within the graft, using [^{11}C]DASB PET
    d. The ability for cell transplantation to homogenously re-innervate the target nucleus
2. To examine the relationship between changes in [^{18}F]FDOPA, [^{11}C]PE2I and [^{11}C]DASB PET measures
3. To examine the effects of intraputamenal hfVM transplant on the severity of the cardinal motor symptoms of Parkinson's disease and their relation with graft composition
4. To examine the relationship between dopaminergic and serotonergic innervation and the emergence of GID

Chapter 2. Transeuro Protocol, Materials and Methods

The Transeuro trial adopted a nested/hierarchical format, in which interested participants entered subsequent sub-studies with additional assessments and/or procedures, providing they met the additional relevant inclusion/exclusion criteria at each stage. A general overview of the trial design is provided in Figure 2.1 and the number of subjects recruited from participating European centres in Table 2.1.

Table 2.1: Table listing the number of patients recruited from specialist movement disorders clinics at each institution under the Transeuro project.

Centre	Observational	MRI	Transplant & PET
Addenbrooke's Hospital, Cambridge University Hospitals NHS Foundation Trust, Cambridge	48	13	9
Charing Cross Hospital, Imperial College Healthcare NHS Trust, London	18	7	4
National Hospital for Neurology and Neurosurgery, University College London Hospitals NHS Foundation Trust	27	17	11
Skånes universitetssjukhus, Lund, Sweden	30	11	11
University Hospital of Wales, Cardiff & Vale NHS Trust, Cardiff	10	1	1

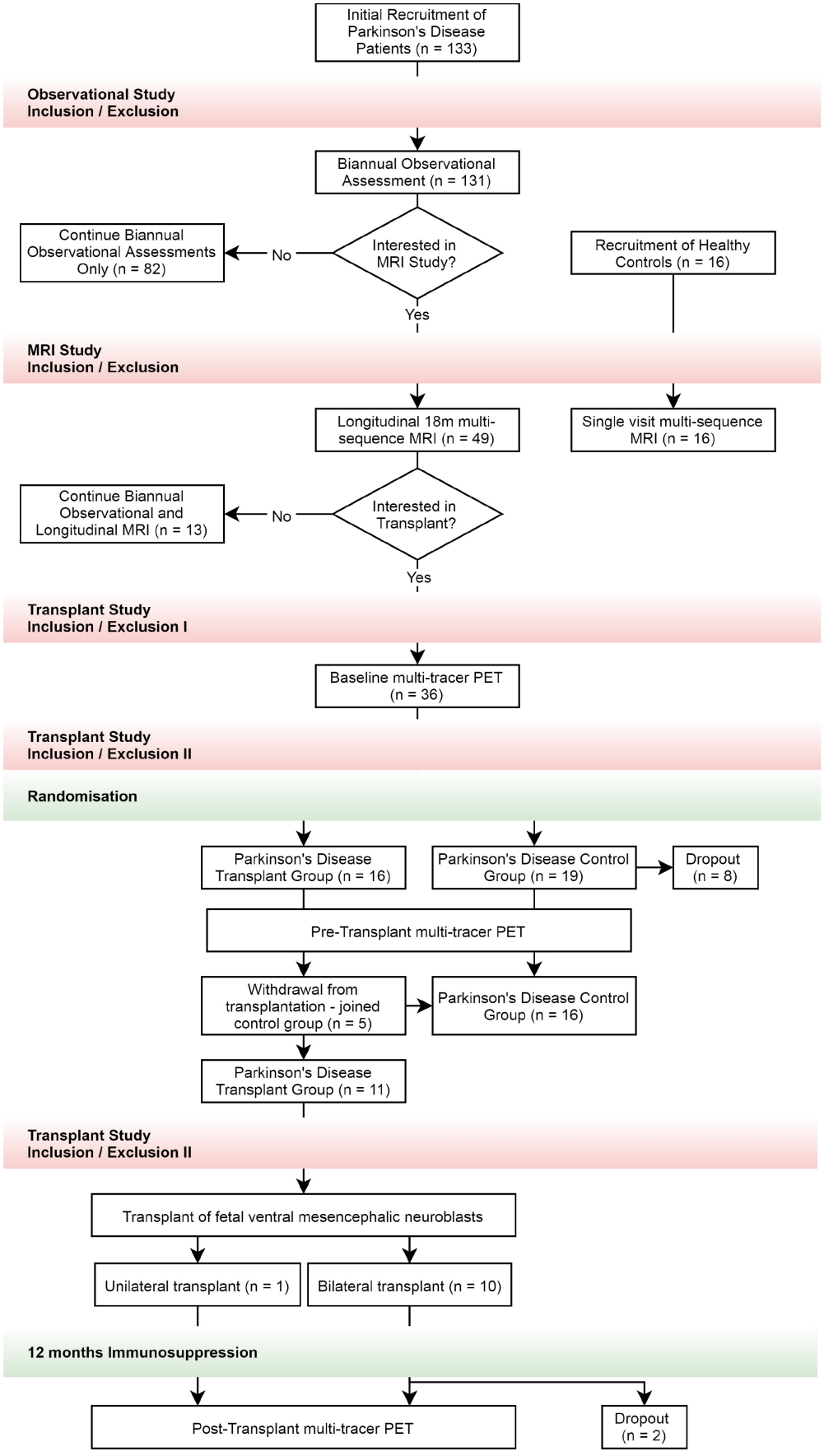


Figure 2.1: Patient flow diagram for the Transeuro trial.

2.1. Observational arm

The Transeuro observational study entitled "*An observational study to assess longitudinal changes in clinical abnormalities in patients with Parkinson's Disease*" encompassed the administration of an extensive battery of motor, cognitive and neuropsychological tests on a biannual basis, with the purpose of monitoring how symptom progression occurs over time in early-stage Parkinson's disease patients. It also allowed for the close monitoring of the natural progression of Parkinson's disease patients who would otherwise be suitable for hfVM transplants in case they displayed atypical symptomatic patterns over time.

2.1.1. Subject recruitment

A total of 131 non-demented mild-to-moderate stage Parkinson's disease patients were recruited from specialist movement disorder clinics in the UK and Sweden under the FP7 EU funded Transeuro research project (http://www.transeuro.org.uk/) (Figure 2.1). Diagnosis of Parkinson's disease was performed by movement disorder specialists in accordance with the Parkinson's UK Brain Bank Criteria (Hughes *et al.*, 1992). Exclusion criteria were as follows:

- Atypical or secondary parkinsonism
- Duration of illness ≥ 13 years
- Age ≤ 30 years or ≥ 65 years
- Hoehn & Yahr Score ≥ 2 in the practically-defined on-medication state
- Abnormal Involuntary Movement Scale (AIMS) score ≥ 2 in any body part
- Mini-Mental State Examination (MMSE) score of less than 24 or evidence for dementia using DSM-IV criteria
- Unable to do normal copying of interlocking pentagons and/or semantic fluency score for naming animals of less than 20 over 90 seconds as these have been associated with earlier onset dementia in PD
- Ongoing major medical or psychiatric disorder including depression and psychosis
- On any medicinal therapy other than levodopa, dopamine agonists, monoamine oxidase type B (MAOB) inhibitors, anticholinergics or amantadine
- Concomitant neuroleptic and/or cholinesterase inhibitor treatment
- Previous neurosurgery, cell therapy or organ transplantation

- Other concomitant significant neurological disorder or major CNS injury/insult in the past

2.1.2. Motor assessments

The Movement Disorders Society Unified Parkinson's Disease Rating Scale Part-III (UPDRS-III) (Goetz *et al.*, 2008a), Hoehn and Yahr Scale (Hoehn and Yahr, 1967) and the Abnormal Involuntary Movement Scale (AIMS) (Guy, 1976) were used to evaluate and calculate motor disability in the practically-defined off-medicated state. Scales were administered by two experienced raters in the same video-recorded session, with one rater acting as the primary assessor. For the UPDRS-III and AIMS, each item was administered and observed once, apart from rigidity items 3.3a-e of the UPDRS-III, which involved examination by both raters sequentially. Marking of the motor scales was done concurrently but independently during the session. As it is not possible to retrospectively review rigidity items of the UPDRS-III, rigidity scores were compared between raters immediately following the first administration and a joint re-examination of the patient and discussion took place until both raters were satisfied. For all other UPDRS-III items, in the case of discordant ratings, video recordings were reviewed and discussed by both raters until agreement.

UPDRS-III items were subsequently divided into bradykinesia (items 4-8 and 14), rigidity (item 3), tremor (items 15-18) and axial (items 1-2 and 9-13) subscores, and further subdivided for each body side (right/left) where appropriate (Table 2.2). Clinical laterality (most/least affected Parkinsonian side) was established based on clinical history recorded by the neurology unit at which patients were diagnosed. Clinical asymmetry was also evaluated at research appointments throughout the study and was derived by comparing the sums of the lateralisation items for the whole UPDRS-III (Total UPDRS-III [Right] vs. Total UPDRS-III [Left]) in the practically-defined off-medicated state.

Motor tasks for objectively examining motor severity were also carried out:

- For the 9-hole Peg Board test, patients were presented with a 12 x 12cm wooden block with 9 holes spaced 3cm apart in a 3 x 3 grid. Patients were instructed to place a set of 3cm long dowels into each and every one of the holes as quickly as they

could with one hand. Each hand was tested twice. The outcome measure was the time taken to place all the dowels in all the holes.

- For the Tap Test, patients were presented with a 2-button box with buttons spaced 5cm apart. Using one hand, patients were instructed to press each of the buttons in an alternating sequence for 30 seconds. The outcome measure was the number of button presses achieved within the allotted time. Button presses were not counted unless the button was fully depressed. Each hand was tested twice.

2.1.3. Cognitive assessment

The Addenbrooke's Cognitive Examination – Revised (ACE-R) (Mioshi *et al.*, 2006) was used to provide an overall assessment of cognitive function and impairment. The ACE-R consists of 19 items broadly testing 5 different cognitive domains: attention & orientation, memory, fluency, language and visuospatial ability, and has shown good sensitivity for detecting mild cognitive impairment in Parkinson's disease as well as Parkinson's disease dementia (McColgan *et al.*, 2012; Rocha *et al.*, 2014). The maximum score is 100 and a mini-mental state exam score can be derived. The ACE-R was administered orally by a trained researcher.

Table 2.2: UPDRS-III and symptom sub-scores. Table listing individual UPDRS-III items and method by which bradykinesia, rigidity, tremor, axial and lateralised (right/left side) subscores were calculated. Calculation of motor subscores was through the summation of individual UPDRS-III items as indicated by checked/unshaded cells.

	Total UPDRS-III			Bradykinesia			Rigidity			Tremor			Axial
	Bilateral	Left	Right	Bilateral	Left	Right	Bilateral	Left	Right	Bilateral	Left	Right	
3.1 Speech	✓	✓	✓										✓
3.2 Facial Expression	✓	✓	✓										✓
3.3a Rigidity – Neck	✓	✓	✓				✓	✓	✓				
3.3b Rigidity – rUE	✓		✓				✓		✓				
3.3c Rigidity – lUE	✓	✓					✓	✓					
3.3d Rigidity – rLE	✓		✓				✓		✓				
3.3e Rigidity – lLE	✓	✓					✓	✓					
3.4a Finger Tapping – Right Hand	✓		✓	✓		✓							
3.4b Finger Tapping – Left Hand	✓	✓		✓	✓								
3.5a Hand Movements – Right Hand	✓		✓	✓		✓							
3.5b Hand Movements – Left Hand	✓	✓		✓	✓								
3.6a Pronation-Supination – Right Hand	✓		✓	✓		✓							
3.6b Pronation-Supination – Left Hand	✓	✓		✓	✓								
3.7a Toe Tapping – Right Foot	✓		✓	✓		✓							
3.7b Toe Tapping – Left Foot	✓	✓		✓	✓								
3.8a Leg Agility – Right Leg	✓		✓	✓		✓							
3.8b Leg Agility – Left Leg	✓	✓		✓	✓								
3.9 Arising from Chair	✓	✓	✓										✓
3.10 Gait	✓	✓	✓										✓
3.11 Freezing of Gait	✓	✓	✓										✓
3.12 Postural Stability	✓	✓	✓										✓
3.13 Posture	✓	✓	✓										✓

3.14 Global Spontaneity of Movement	✓	✓	✓	✓	✓	✓							
3.15a Postural Tremor – Right Hand	✓		✓							✓		✓	
3.15b Postural Tremor – Left Hand	✓	✓								✓	✓		
3.16a Kinetic Tremor – Right Hand	✓		✓							✓		✓	
3.16b Kinetic Tremor – Left Hand	✓	✓								✓	✓		
3.17a Rest Tremor Amplitude – rUE	✓		✓							✓		✓	
3.17b Rest Tremor Amplitude – lUE	✓	✓								✓	✓		
3.17c Rest Tremor Amplitude – rLE	✓		✓							✓		✓	
3.17d Rest Tremor Amplitude – lLE	✓	✓								✓	✓		
3.17e Rest Tremor Amplitude – Lip/Jaw	✓	✓	✓							✓	✓	✓	
3.18 Constancy of Rest Tremor	✓	✓	✓							✓	✓	✓	

l = left; r = right
LE = lower extremity; UE = upper extremity
Range of scales [Max]:
Axial: [28]
Bradykinesia: [44]
Bradykinesia (Left/Right): [24]
Rigidity: [20]
Rigidity (Left/Right): [12]
Tremor: [40]
Tremor (Left/Right): [24]
UPDRS-III: [132]
UPDRS-III (Left/Right): [88]

2.2. Magnetic resonance imaging arm

The Transeuro magnetic resonance imaging study entitled "*An imaging study to assess structural and functional connectivity in a longitudinal study of patients with Parkinson's disease*" involved the application of a range of magnetic resonance imaging sequences designed to examine how structural connections and motor-related cortical and subcortical function are altered over the course of early Parkinson's disease, as well as how these measures may change as a result of hfVM cell therapy. This multi-sequence MRI study was conducted every 18 months for up to 3 visits.

2.2.1. Subject recruitment

Of the patients enrolled onto the observational study, 49 were recruited to take part in the magnetic resonance imaging arm. Additional exclusion criteria were:

- Any contraindication to MRI, including:
    - Metallic foreign bodies
    - Intracranial aneurysm clips
    - Defibrillators
    - Cardiac pacemakers
    - Cochlear implants
    - Neurostimulators
    - MR-incompatible metallic implants
    - Metallic tattoos
    - Pregnancy
- Patients who are left-handed

As part of this study only right-handed patients were selected as previous literature using functional magnetic resonance imaging (fMRI) has suggested that the functional organization of motor areas differs between left-handed and right-handed individuals (Solodkin *et al.*, 2001).

2.3. Transplant arm

The Transeuro transplant study entitled "*An Open Label Study to Assess the Safety and Efficacy of Neural Allo-Transplantation with Fetal Ventral Mesencephalic Tissue in Patient's with Parkinson's disease*" is an open-label randomised controlled trial designed to evaluate the efficacy of and molecular changes associated with intraputamenal transplantation of human fetal ventral mesencephalic (hfVM) neuroblasts in patients with Parkinson's disease using positron emission tomography. As of amendment no. 6 (11.11.14), patients completed the positron emission tomography scans at 3 time points, twice prior to transplantation, at baseline and 18 months, and once at 18 months post-transplantation.

The decision to perform follow-up scans at 18 months following surgery was based on previous hfVM transplant trial results indicating that significant clinical benefits are evident between 3-12 months post-graft (Lindvall *et al.*, 1992; Widner *et al.*, 1992; Peschanski *et al.*, 1994; Freeman *et al.*, 1995; Lopez-Lozano *et al.*, 1997; Wenning *et al.*, 1997; Hauser *et al.*, 1999; Freed *et al.*, 2001) and that the associated increase in [^{18}F]FDOPA uptake, pertaining to dopamine synthesis and storage capacity, occurs primarily within this period, with only minor changes beyond this point (Hagell *et al.*, 1999; Brundin *et al.*, 2000; Olanow *et al.*, 2003; Ma *et al.*, 2010). Patients who developed GID tended to do so between 5-24m post-graft (Greene *et al.*, 1999; Freed *et al.*, 2001; Ma *et al.*, 2002; Olanow *et al.*, 2003), though Olanow *et al.* (2009) indicated in an analysis comprising 34 transplanted patients that mean time to onset was on average 5.1 ±3.3 months post-graft (Olanow *et al.*, 2009a). Furthermore, Piccini *et al.* (2000) have shown, using $H_2{}^{15}O$ PET, a delay in the restoration of cortical function (rostral supplementary motor area and dorsolateral prefrontal cortex) with significant increases at 18.3 but not 6.5 months (Piccini *et al.*, 2000). Thus, 18 months is a suitable period of time for allowing the grafted cells to mature and innervate the peristriatal area, to produce changes in the host cortical networks and to allow for symptomatic response including the possibility of side-effects in transplanted individuals. It also ensures no overlap with the immunosuppressive regime, enforced for 12 months, which may have some effects on clinical presentation and a possible influence on imaging outputs.

2.3.1. Subject recruitment

Of the 49 patients enrolled on the MRI study, 36 patients were recruited to take part in the transplant trial. Additional exclusion criteria for entry into this trial were:

- Clinically insignificant response to levodopa and/or apomorphine challenge (in patients not currently taking dopaminergic medication)
- Patients on anticoagulants
- Contraindication to surgery under general anaesthesia
- Contraindication to immunosuppressive therapy

2.3.2. [^{18}F]FDOPA exclusion & randomisation

After all eligible patients enrolled on the transplant study underwent positron emission tomography at baseline, a further two exclusion criteria were enforced:

- [^{18}F]FDOPA PET patterns consistent with atypical or secondary Parkinsonism
- Significant decline of [^{18}F]FDOPA signal in the ventral striatum

[^{18}F]FDOPA based exclusion was performed visually by an experienced movement disorder clinician and consisted of evaluation of the rostrocaudal gradient of denervation as well as the prominence of asymmetric [^{18}F]FDOPA uptake in the ventral striatum as compared to the posterior and anterior putamen. One patient was excluded based on [^{18}F]FDOPA PET patterns that were not consistent with idiopathic Parkinson's disease.

Remaining patients were then randomly assigned in an unblinded fashion to either the transplant group (n = 16) or the control group (n = 19). 8 patients from the control group subsequently withdrew from the study. Patients in the control group remained on best pharmacological and physical supportive therapy for Parkinson's disease as determined by their own consultant neurologists.

Patients were then scanned again at 18 months, with 5 patients subsequently withdrawing consent for the transplantation procedure. At this stage, [^{18}F]FDOPA-based exclusion criteria did not result in any dropouts (Figure 2.1).

2.3.3. Human fetal ventral mesencephalic cell transplant

For the transplant group, bilateral image-guided surgery was performed in two sequential unilateral stages while under general anaesthesia. The hfVM tissue was derived from 3-5 embryos at 6-8 weeks post-conception per putamen, which were procured through established tissue collection procedures from surgical and medical termination of pregnancies. Embryos were dissected with careful attention to avoiding serotonergic neurons from the developing brainstem, stored for no more than 4 days in Hibernate E and lazaroids and used to prepare a crude cell suspension, which enables more homogenous tissue content between deposits. Tissue preparation procedures were conducted within a certified good manufacturing practice facility or a clean room. More than 80% viability of the cell suspensions was required on the day of surgery.

Needle trajectories were calculated based on the size of each individual putamen with avoidance of the sulci and ventricles after fitting patients with a Leksell stereotactic headframe. A series of 5 trajectories were made through a 14mm burr hole placed at the level of the coronal suture; 3 targeting the post-commissural putamen and 2 targeting the pre-commissural putamen (Figure 2.2). The Rehncrona-Legradi transplantation instrument (Lindvall *et al.*, 1992) or a modified version (Barker and Transeuro Consortium, 2019) was used to deliver 8 single 2.5µl deposits of crude cell suspension, each over 15-20 seconds, along the length of each putamenal tract beginning at the farthest site. Retraction of the cannula to the next planned deposit location along the trajectory was made after a 2 minute waiting time and slow withdrawal of the cannula was made 8 minutes following the last deposit. A total of 100µl was deposited within each putamen.

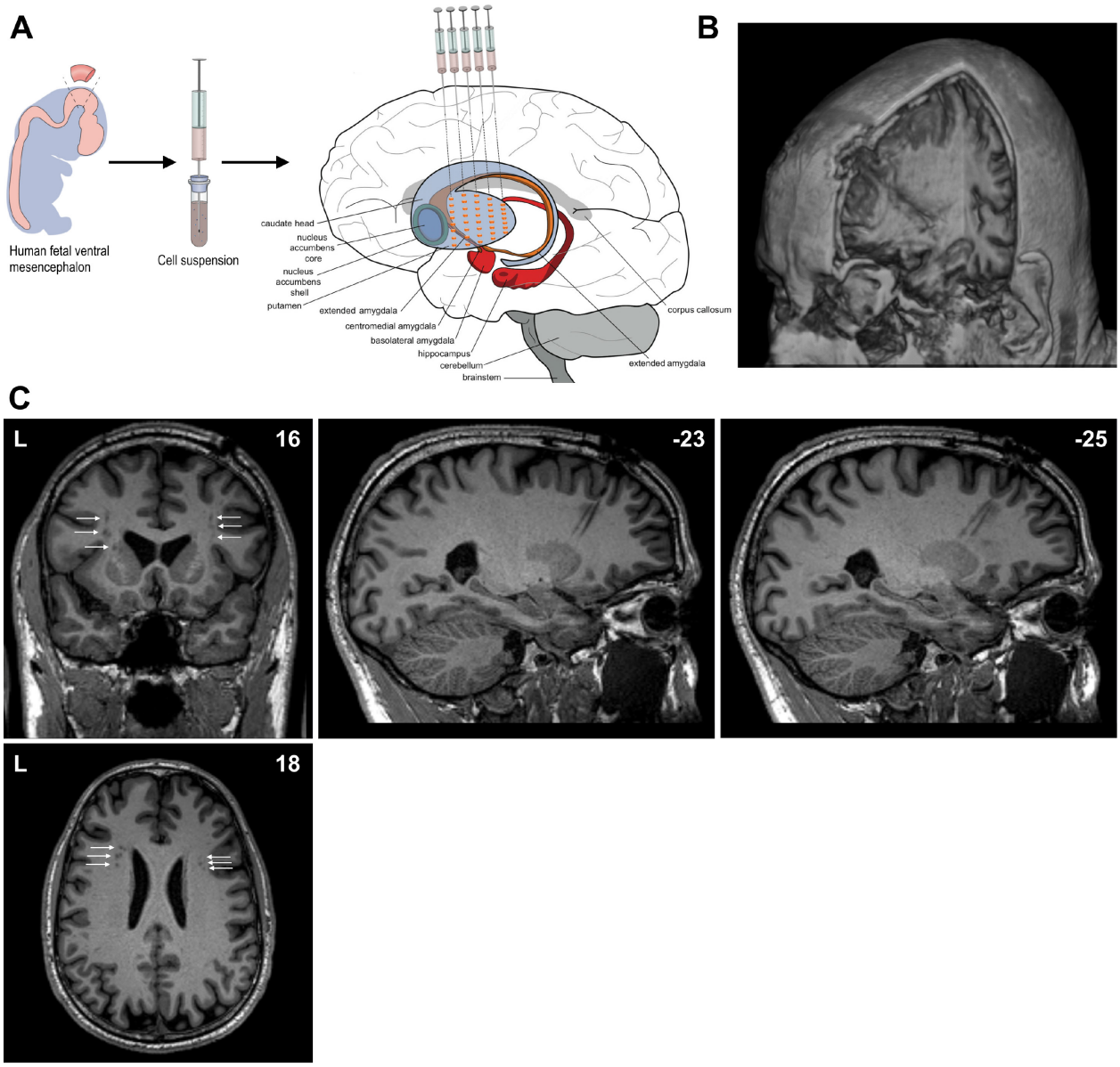


Figure 2.2: Surgical technique for transplantation of hfVM tissue. A | Schematic illustrating surgical technique for implantation of human fetal ventral mesencephalic cells. Crude cell suspensions for each putamen were prepared from 3-5 hfVM dissections (aged between 6-8 weeks post-conception) and delivered via five trajectories along the anterior-posterior putamenal axis using the Rehncrona-Legradi instrument, with eight deposits made on withdrawal. Co-ordinates were ascertained by pre-operative magnetic resonance imaging while the patient was fitted with a Leksell stereotactic headframe. B | Three-dimensional rendering of the T1-weighted structural magnetic resonance image for one transplanted patient demonstrating the full length of a single trajectory through the 14mm burr hole at the level of the coronal suture to the anterior putamen. C | Coronal, sagittal and axial views of the T1-weighted structural magnetic resonance image of another transplanted patient demonstrating multiple trajectories through the cortical white matter towards pre-planned targets along the anterior to posterior putamenal axis. Fetal and brain figures adapted from (Parmar et al., 2020) and (Loonen and Ivanova, 2015).

Immunosuppressive treatment to prevent the rejection of allogeneic tissue began the day before surgery and consisted of a combination of cyclosporine (2mg/kg twice per day [giving serum levels between 100-200ng/ml]), azathioprine (2mg/kg once per day) and prednisolone (40mg once per day), the latter being tapered down to 5mg once per day by 12 weeks. 1g intravenous methyl prednisolone was also given at the time of surgery. Oral medications were continued for at least one year post-surgery and maintained at daily doses in accordance with blood concentrations of cyclosporine and other haematological and biochemical measures. Co-trimoxazole 80/400mg, three times per week, was also given as prophylaxis for the duration of immunosuppression. Patients were closely monitored by expert clinicians for 12 months following surgery to identify any adverse events/reactions and to modify post-operative drug regimens as necessary.

2.3.4. Positron emission tomography

2.3.4.1. Basic Principles

Positron emission tomography is an imaging technique in which biochemical and physiological processes may be studied *in vivo* by injection or inhalation of naturally occurring tracer molecules labelled with positron-emitting radioactive nuclides into the subject of interest. These proton-rich radioactive isotopes, such as ^{11}C, ^{13}N, ^{15}O, ^{18}F,and ^{123}I, undergo beta-positive decay in which a proton in the unstable positively-charged nucleus converts to a neutron, emitting a positron and a neutrino and resulting in nuclear transmutation by lowering the atomic number of the parent nuclide. The positron, the anti-matter counterpart of the electron, travels a short distance (~1mm) depending on the isotope and energy of the emitted particle before encountering and annihilating with an electron from the surrounding matter. The annihilation event produces two 511keV photons that travel in almost perfect anti-parallel fashion (Figure 2.3), in order to conserve momentum (Verel *et al.*, 2005; Cherry and Dahlbom, 2006; Turkheimer *et al.*, 2014).

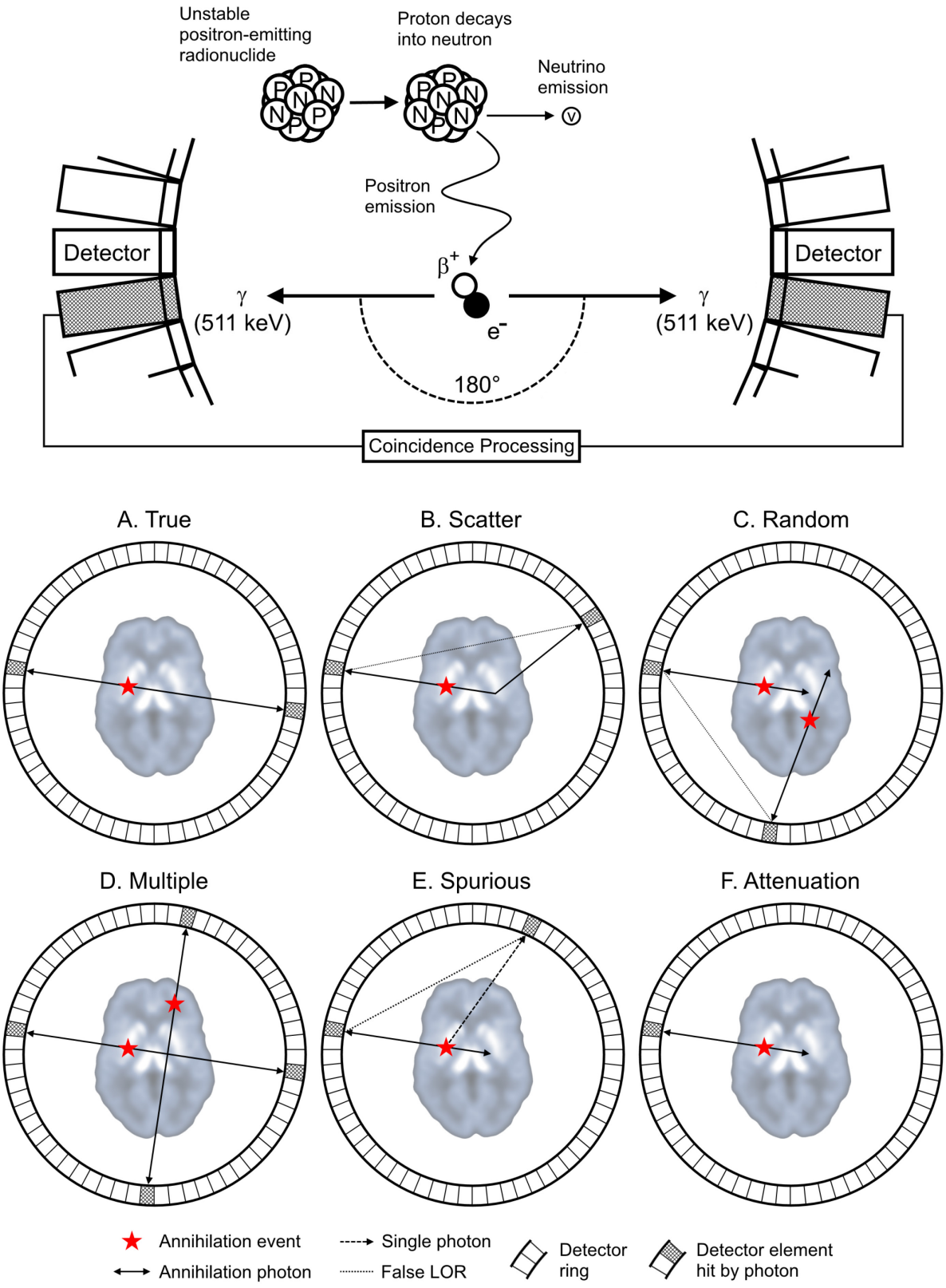


Figure 2.3: Positron emission tomography and coincidence detection. Top | Schematic illustrating positron emission from an unstable positively-charged radionuclide, annihilation with an electron after travelling a short distance, which converts mass into two 511 keV photons that travel in almost perfectly opposing directions, and coincident detection of gamma rays by the scintillation crystals and photo-detectors of the surrounding detector ring. Bottom | Schematic illustrations of coincident detection

problems; A. True events occur when two detected photons originate from the same annihilation event without changing direction or losing energy. B. Scatter events occur when one or both photons lose energy and are deflected from their original path upon interaction with electrons in the surrounding matter, known as Compton scatter, resulting in erroneous LOR assignment to the coincident pair. C. Random events refer to a situation in which two single photons arising from unrelated annihilation events are detected within the coincident time window, leading to false pair measurement. D. Multiple events occur when at least three photons emitted from two or more annihilation events are detected simultaneously, causing ambiguity in discerning which photons constitute a true pair. E. Spurious true coincidence can arise when annihilation photons are registered together with single gamma particles emitted from the same decay event that fall within the pre-specified energy window of the detection system. F. Attenuation refers to the loss of true coincidences by photoelectric absorption of the emitted annihilation photons or by Compton processes, including deflection outside of the detector ring and sub-threshold energy following partial transfer to interacting electrons. Shaded elements represent those which have detected annihilation photons. P = proton, N = neutron, v = neutrino, e^- = electron, β^+ = positron, γ = gamma ray, keV = kiloelectronvolt. Figure modified from (Verel et al., 2005).

Annihilation photons are registered using a PET camera; multiple rings of detectors consisting of scintillation materials (e.g. bismuth germanate or cerium-doped lutetium oxyorthosilicate) that emit visible light upon interaction with incident high-energy gamma rays, coupled with photo-detectors (e.g. photomultiplier tubes) that detect scintillation events and generate electrical timing signals of measurable magnitude that are fed downstream to coincidence circuitry. If two photons with energy falling between 350-650keV are detected within a short pre-specified time-window of approximately 5-15ns they are assumed to be "coincident" and arising from the same annihilation event (Verel *et al.*, 2005; Cherry and Dahlbom, 2006). Because photons resulting from a single annihilation are emitted simultaneously and at a near 180° angle, coincident pairs are assigned a line of response (LOR) running directly between the two relevant detectors, representing the area within the field of view along which the positron emitting radiotracer may be located. The exploitation of coincidence events to provide positional information in this way is often referred to as electronic collimation. The spatial resolution attainable by PET imaging is however limited by two main sources of localisation error. The first arises from the distance a positron travels from its source prior to annihilation and which is associated with its energy upon emission from the parent nuclide, termed *positron range*. The second relates to the net momentum of the positron and electron at the point of annihilation, which to some degree (±0.25°) perturbs the angle of gamma ray emission, an effect termed *non-collinearity* (Cherry and Dahlbom, 2006).

In addition to "true" coincidences, that is, when two detected photons originate from the same annihilation event without changing direction or losing energy, a number of other event types that do not carry valid spatial information are accepted by the coincidence detection system. These include *scatter*, *random*, *multiple* and *spurious* events and must be accounted for in order to maintain accurate estimations of the activity distribution (Figure 2.3). Such degrading events are also considered to exacerbate the issue of scanner dead-time (Cherry and Dahlbom, 2006); the inability of the system to register every discrete event due to a finite response rate and recovery period of each of its components. Dead-time is primarily influenced by the time spent integrating charge from the photo-detectors arising from scintillation flashes in the detector crystals, which is in turn related to the scintillation decay time constant of the crystal material. If a photon deposits energy within a crystal detector during the signal integration period triggered by a previous acquisition (*pulse pile-up*), the total charge may exceed the upper energy discrimination level and both events subsequently discounted. Alternatively if the total charge remains within range then the two events may be treated as one with inaccurate energy and positioning. The net result is a non-linear loss of true count rates as a function of specific activity concentration, referred to as *dead-time loss*, and demands correction in order to obtain valid quantitative images, most commonly by utilising decaying source measurements to fit idealized (*paralysable* and *non-paralysable*) dead- time models (Meikle and Badawi, 2005; Cherry and Dahlbom, 2006; Usman and Patil, 2018). Furthermore, the vast majority (50-75%) of annihilation photons are either absorbed by intervening tissue along the LOR due to photoelectric effects, or deflected outside of the detector field upon interaction with electrons in the surrounding matter, known as Compton scatter. For the latter process, the partial energy transfer to the recoiling electron may also render the gamma particle sub-threshold with respect to the energy detection window. The loss of true coincidences in this way is termed *attenuation* and can be readily corrected for by derivation of attenuation correction factors through the acquisition of separate transmission scans using gamma sources or X-rays (computerised tomography) prior to tracer injection (Cherry and Dahlbom, 2006; Turkheimer *et al.*, 2014).

Following physical corrections, the total number of counts recorded by a pair of detectors becomes proportional to the total radioactivity along the LOR running between them. These data are organised and stored as parallel sets of line integrals at specified angles, known as

projections, or as stacks of many projections at a number of different angles, known as sinograms (Figure 2.4). Reconstruction into cross-sectional images can then be achieved, of which there are two main methodological classes. *Back-projection* involves the re-distribution of LOR data back to their original paths; each element of an image matrix that the path intersects is assigned a value corresponding to the number of counts measured by that pair of detectors, weighted by the distance the path has traversed through that element. This process is repeated for all valid detector pairs. Counts associated with each back-projection are summed to yield a reconstructed image which is then filtered to remove blurring caused by the placement of counts in areas devoid of radioactivity i.e. oversampling (Figure 2.5). *Iterative* methods involve an initial guess as to the activity distribution and subsequently the generation of projection data (e.g. by *forward projection*) that would describe this guessed image. These estimated projections are then compared to the acquired data and the initial guess is adjusted in accordance with some defined optimisation procedure, such that over a number of iterations the estimate will eventually resemble the true distribution (Cherry and Dahlbom, 2006; Turkheimer *et al.*, 2014).

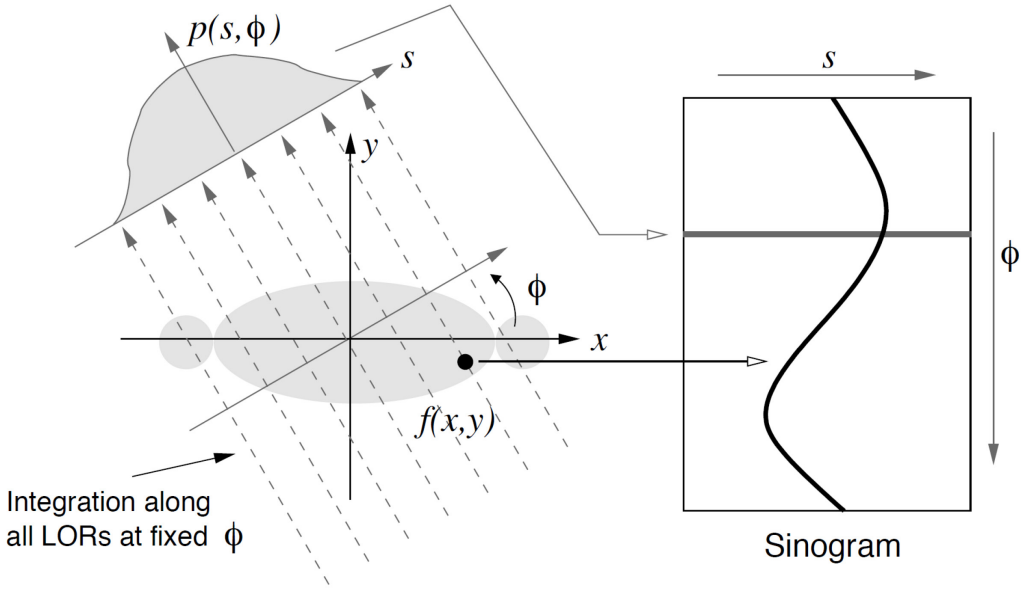


Figure 2.4: Storage of count data as projections and sinograms. Parallel sets of line integral data at fixed angles are known as projections, p(s, ϕ), where s is the distance of the LOR to the centre and ϕ is the projection angle. The collection of all projections for all angles (0 ≤ ϕ < 2π) is termed a sinogram, where a single point in f(x, y) traces a sinusoid in the sinogram. LOR = line of response. Figure extracted from (Alessio and Kinahan, 2006).

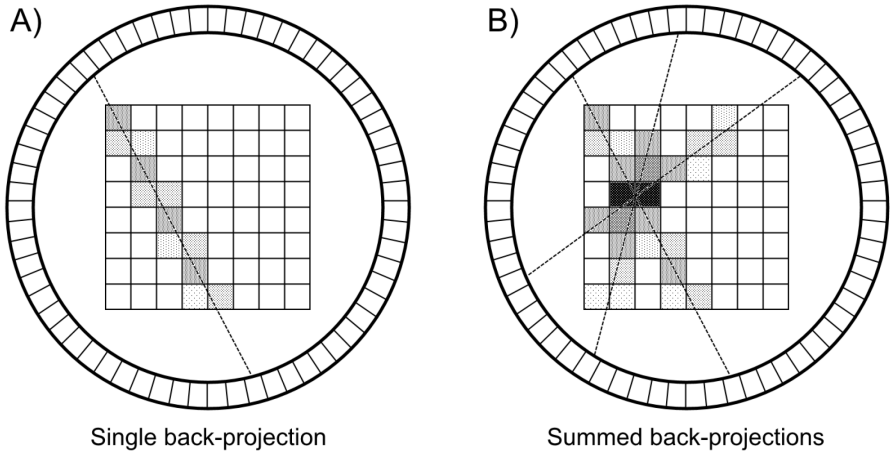


Figure 2.5: Illustration of image reconstruction by back-projection. A | A single back-projection assigns a value to each pixel of an image matrix based on the number of counts detected along that LOR, weighted by the pathlength of the line through the pixel. B | Summation of three back-projections from separate detector pairs showing formation of an image and the necessity of additional filtering to account for oversampling in areas outside the object. The depth of pixel shading represents the value magnitude.

2.3.4.2. [^{18}F]FDOPA

[^{18}F]FDOPA (L-3,4-Dihydroxy-6-[^{18}F]fluorophenylalanine) is a fluorinated analogue of the natural dopamine precursor L-dopa. Given its chemical similarity, [^{18}F]FDOPA undergoes all of the same transport processes and metabolic steps as L-dopa, including but not limited to its transport into the presynaptic terminal, decarboxylation by the aromatic amino acid decarboxylase (AADC) enzyme into [^{18}F]dopamine and subsequent storage in presynaptic vesicles by the vesicular monoamine transporter (Figure 2.6). As such, [^{18}F]FDOPA provides measurements that reflect the activity of AADC, dopamine synthesis and dopamine storage capacity (Firnau *et al.*, 1987; Kuwabara *et al.*, 1993; Heiss and Hilker, 2004).

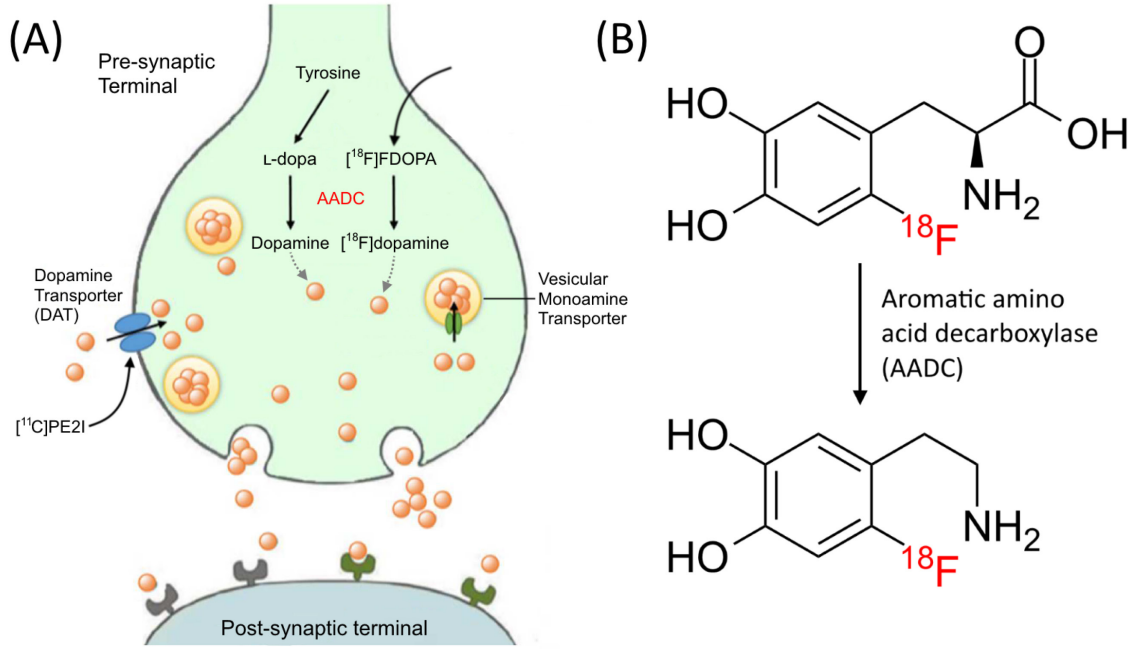


Figure 2.6: Metabolic pathway of [18F]FDOPA. A | Schematic representation of a dopaminergic synaptic terminal, illustrating the pathway of [18F]FDOPA in the presynaptic bouton as a false substrate for aromatic amino acid decarboxylase and its non-reversible catalysis to [18F]dopamine. The presynaptic dopamine transporter, the site for which [11C]PE2I has high affinity, is also labelled. B | Skeletal structural formulae for the conversion of [18F]FDOPA to [18F]-labelled dopamine. Figure A adapted from (Beaurain et al., 2019).

Post-mortem data on the density of tyrosine hydroxylase containing cells in the substantia nigra and of dopamine levels in the striatum were found to be positively correlated with striatal [18F]FDOPA uptake rate constants extracted from scans taken pre-mortem, in a mixed neurological sample consisting of Parkinson's disease, Alzheimer's disease, amyotrophic lateral sclerosis and progressive supranuclear palsy (Snow *et al.*, 1993). *In vivo* in Parkinson's disease, putamenal [18F]FDOPA derived measures have been consistently found to be inversely related to advancing illness, both in the duration of disease as well as in standardised motor assessments such as the UPDRS-III motor sub-score (Brooks *et al.*, 1990; Ishikawa *et al.*, 1996; Otsuka *et al.*, 1996; Vingerhoets *et al.*, 1997; Broussolle *et al.*, 1999; Rakshi *et al.*, 1999; Ghaemi *et al.*, 2002; Ribeiro *et al.*, 2002; Eshuis *et al.*, 2006; Nandhagopal *et al.*, 2009; Gallagher *et al.*, 2011a; Gallagher *et al.*, 2011b; Li *et al.*, 2018). In previous transplantation and other clinical trials in Parkinson's disease, [18F]FDOPA has been the gold standard nuclear imaging radioligand for monitoring dopaminergic function as a result of

therapy (see Introduction). Thus, [^{18}F]FDOPA is used in the current study to provide *in vivo* measures of graft survival and function.

2.3.4.3. [^{11}C]PE2I

[^{11}C]PE2I ([^{11}C]N-(3-iodopro-2*E*-enyl)-2β-carbomethoxy-3β-(4'-methylphenyl)nortropane) binds with high selectivity to the dopamine transporter (DAT) (Emond *et al.*, 1997; Gunther *et al.*, 1997; Guilloteau *et al.*, 1998; Hall *et al.*, 1999; Halldin *et al.*, 2003; Jucaite *et al.*, 2006; Seki *et al.*, 2010; Ziebell *et al.*, 2010; Sasaki *et al.*, 2012; Ziebell *et al.*, 2012; Appel *et al.*, 2015), a transmembrane protein that facilitates the reuptake of DA from the synaptic cleft back into the presynaptic terminal and thus an essential component in the regulation of dopamine (Figure 2.6) (Figure 2.7).

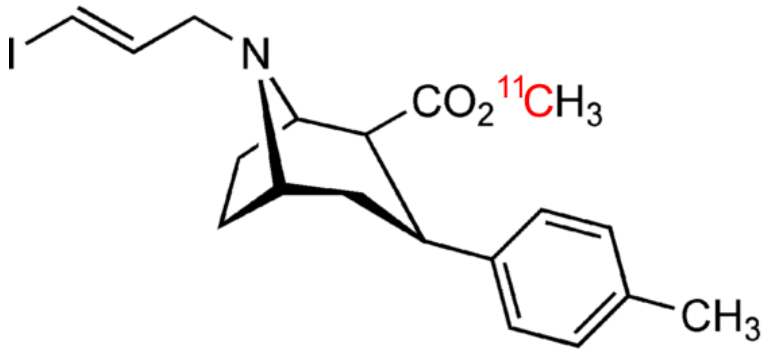


Figure 2.7: Skeletal structural formula for [^{11}C]PE2I.

Experimental work in macaques with MPTP-induced nigrostriatal degeneration shows a close positive relationship between striatal DAT density, striatal DA concentration and nigrostriatal cell loss (Bezard *et al.*, 2001). In human PD patients, significant decreases in striatal DAT density have been demonstrated *in vivo* using single photon emission computerised tomography (SPECT) with [^{123}I]βCIT and later generation fluoroalkyl analogues [^{123}I]FP-CIT and [^{123}I]FE-CIT, with reductions negatively correlating to symptom severity (Seibyl *et al.*, 1995; Booij *et al.*, 1997; Benamer *et al.*, 2000; Antonini *et al.*, 2001). However, these ligands also have affinity for other monoamine transporters including the serotonin transporter (Neumeyer *et al.*, 1994; Abi-Dargham *et al.*, 1996), which is known to be present in large concentrations in the striatum (Ginovart *et al.*, 2001; Ichise *et al.*, 2003; Kish *et al.*, 2008). Indeed, autoradiographic and *in vivo* data have shown that in serotonin-predominant regions such as the thalamus, binding of these radioligands was virtually

abolished following the administration of the selective serotonin reuptake inhibitor (SSRI) citalopram (Gunther *et al.*, 1997), which also reduced putamen and caudate labelling by up to 45% (Gunther *et al.*, 1997; Ziebell *et al.*, 2010). In contrast, PE2I has approximately 29.4x greater selectivity for DAT over SERT (Emond *et al.*, 1997; Guilloteau *et al.*, 1998), far exceeding that of βCIT (1.68x), FP-CIT (2.78x) and FE-CIT (3.6x) (Neumeyer *et al.*, 1994; Abi-Dargham *et al.*, 1996). PE2I binding in SERT-rich cortical regions is negligible and in the striatum is not diminished by SSRI-induced SERT blockade (Hall *et al.*, 1999; Halldin *et al.*, 2003). Labelled with carbon-11, PE2I has been revealed as a potential tool for differential diagnosis, being as sensitive to pathophysiological changes in Parkinsonian disorders as both [^{123}I]FP-CIT SPECT and [^{18}F]FDG PET combined (Appel *et al.*, 2015). Its utility for monitoring the efficacy of restorative interventions in Parkinson's disease has recently been highlighted, showing greater sensitivity for detecting dopaminergic neurodegeneration-related changes in UPDRS-III-defined motor severity, particularly bradykinesia, than AADC imaging using [^{18}F]FDOPA (Li *et al.*, 2018).

In vivo and post-mortem studies of the dopamine transporter in hfVM grafted patients have been inconsistent, with some finding substantial DAT expression (Kordower *et al.*, 1996; Pogarell *et al.*, 2006; Politis *et al.*, 2011; Hallett *et al.*, 2014) while others demonstrate low DAT levels in spite of dopamine neuron survival (Hoffer *et al.*, 1992; Cochen *et al.*, 2003; Kordower *et al.*, 2008a; Kordower *et al.*, 2008b; Kurowska *et al.*, 2011), suggested to be indicative of their down-regulation as is characteristic of native neurons in un-grafted PD patients (Tedroff *et al.*, 1999; Lee *et al.*, 2000; Ribeiro *et al.*, 2002; Adams *et al.*, 2005; Bruck *et al.*, 2006; Moore *et al.*, 2008; Nandhagopal *et al.*, 2011; Pavese *et al.*, 2011). As such, [^{11}C]PE2I will be used to evaluate whether transplanted cells retain their dopaminergic phenotype and whether this contributes to symptomatic relief.

2.3.4.4. [^{11}C]DASB

[^{11}C]DASB ([^{11}C]-3-amino-4-(2-dimethylaminomethylphenylsulfanyl)-benzonitrile) binds selectively to the serotonin transporter (SERT), an integral plasma membrane protein that facilitates the reuptake of serotonin from the synaptic cleft back into the presynaptic neuron (Figure 2.8). [^{11}C]DASB is a highly selective radionuclide, showing nanomolar affinity for cloned human SERT that is between 1200-1300 fold greater than for DAT and

norepinephrine transporters (NET) in *in vitro* binding assays (Wilson *et al.*, 2000) and with negligible affinity for a broad range of receptors, enzymes and ion-channels (Wilson *et al.*, 2002). Autoradiographic data demonstrate diminished binding in SERT knockout mice and 50% reductions in heterozygote SERT mice (Li *et al.*, 2004). In rats, pre-treatment with an SSRI ((+)-McN5652) significantly reduced [^{11}C]DASB specific binding values in multiple brain regions similarly to that produced by pre-treatment with cold ligand, with no effects on specific binding by selective DAT (GBR12909) and NET (desipramine) inhibitors (Wilson *et al.*, 2000), and its sensitivity to changes in SERT levels is demonstrable by its dose-dependency to different amounts of pre-injected fluoxetine (Wilson *et al.*, 2002). Comparative studies in baboons have demonstrated favourable specific-to-nonspecific binding and faster kinetics for [^{11}C]DASB when evaluated against [^{11}C]-(+)-McN5652 and other potent diphenyl sulphide derivatives [^{11}C]ADAM, [^{11}C]DAPA, and [^{11}C]AFM, enabling greater detectability of SERT levels especially in low density regions at shorter scan times (Huang *et al.*, 2002; Szabo *et al.*, 2002).

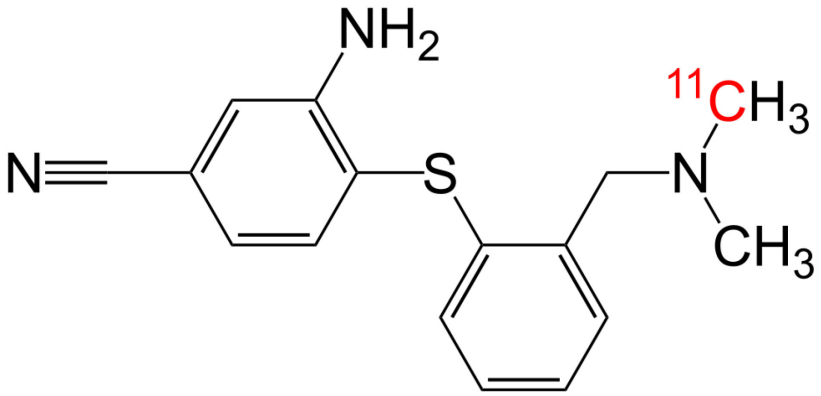


Figure 2.8: Skeletal structural formula for [^{11}C]DASB.

In vivo, the regional distribution of [^{11}C]DASB binding values conforms to known regional SERT density across the human brain, with greatest levels of radioactivity in the hypothalamus and midbrain, slightly less in the thalamus, amygdala and striatal nuclei, intermediate in remaining limbic regions, low-moderate in the neocortices and finally lowest in the cerebellum (Houle *et al.*, 2000; Ginovart *et al.*, 2001; Frankle *et al.*, 2004). Continuous 4-week treatment or acute high-dose pre-scan administration of oral SSRIs results in an estimated 80% reduction in [^{11}C]DASB binding potential across all regions (Houle *et al.*, 2000; Meyer *et al.*, 2004). Moreover, *in vivo* regional [^{11}C]DASB binding values significantly

correlate with post-mortem measures of SERT density using [^{3}H]paroxetine (Ginovart *et al.*, 2001).

In vivo and post-mortem investigations of the survival and growth of serotonergic neurons in hfVM grafts have so far been largely limited to case studies at hugely variable intervals following surgery, and the inconsistency between analysis methods with regards to their involvement in the generation of GID is apparent (Mendez *et al.*, 2008; Politis *et al.*, 2010b; Politis *et al.*, 2011; Kordower *et al.*, 2017). Moreover, the potential involvement of serotonergic re-innervation in the alleviation of cardinal motor symptomatology for which serotonergic neurodegeneration is thought to play a role, most notably tremor (Doder *et al.*, 2003; Loane *et al.*, 2013; Qamhawi *et al.*, 2015; Pasquini *et al.*, 2018), has not yet been investigated in hfVM transplanted PD patients. As such, [^{11}C]DASB will be used to evaluate whether transplanted nuclei exhibit increases in serotonergic innervation and whether this is related to clinical benefit and the emergence of GID.

2.3.5. Drug withdrawal

Patients were instructed to withdraw from all standard anti-Parkinson's disease medications at least 24 hours prior to motor and imaging assessments. For prolonged release medications, the withdrawal period was extended to 48 hours. This included levodopa, dopamine agonists, catechol-*O*-methyltransferase inhibitors, monoamine oxidase B inhibitors and amantadine. Caffeine in any form was not permitted within 12 hours prior to scans. Levodopa equivalent daily dosage (LEDD) for each participant was calculated (Tomlinson *et al.*, 2010).

2.3.6. Transplant patient dropouts and exclusions

Three patients who were randomised to the transplant group and received hfVM grafts were removed from analyses for the following reasons:

Patient 1 – This patient only performed the [^{11}C]DASB scan at the post-transplant time-point as there was a significant issue with the quality of the production of dopaminergic tracers. The patient was invited back after procedures were quality control tested but declined due to reported anxiety.

Patient 17 – This patient withdrew from [^{18}F]FDOPA PET at the post-transplant time-point after ~20 minutes of acquisition time, due to reported discomfort in the scanner bore. [^{18}F]FDOPA images were successfully obtained in a re-scheduled run the following day, however the patient declined any further PET imaging with either [^{11}C]PE2I or [^{11}C]DASB.

Patient 32 – The surgical procedure was only performed on the right putamen, following which, the patient opted to withdraw from the second surgery. In addition, this patient only completed the [^{18}F]FDOPA scan at the post-transplant time-point.

Only transplant patients who underwent bilateral surgical intervention and who completed the multimodal imaging protocol at pre-transplant and post-transplant time-points were included in the analyses, in order to improve accuracy pertaining to the effects of complete intraputamenal transplant, to limit the complexity of statistical models given the relatively small sample size and to facilitate comparability between the results for each tracer.

2.4. Ethical approvals

Ethical approval for observational and multimodal imaging protocols was obtained from the appropriate Research Ethics Committees for Transeuro in the UK (NRES: 10/H0304/77, 10/H0805/73 & 12/EE/0096) and Sweden (EPN2013/758, IK2013/685). Approval was granted by ARSAC for radiation exposure relating to the positron emission tomography scans (RPC 630/3764/28563). Participants were informed of the aims of the study, the treatment and possible hazards to which they will be exposed, that their data will be kept strictly confidential and that they are able to withdraw from the study at any time without giving reason and without it prejudicing their subsequent clinical care. Participant informed consent was obtained in writing in accordance with the Declaration of Helsinki.

2.5. Neuroimaging protocol

2.5.1. Image acquisition

All scans were conducted at Invicro LLC (Hammersmith Hospital, London).

2.5.2. Structural magnetic resonance imaging

MRI scans were acquired for all Parkinson's disease patients on a 3T Siemens Magnetom Trio system with 32-channel head coil and consisted of a high-resolution volumetric T1-weighted magnetization-prepared rapid gradient echo sequence (MPRAGE: repetition time = 2300ms; echo time = 2.98ms; flip angle = 9; time to inversion = 900ms; GRAPPA acceleration factor PE = 2; field of view = 240*256mm; matrix size = 240*256). One whole brain volume was acquired consisting of 160 contiguous slices of 1mm thickness and lasting 301 seconds. Patients were instructed to remain as still as possible for the duration of the scan.

2.5.3. Positron emission tomography

Parkinson's disease patients underwent [^{18}F]FDOPA (L-3,4-Dihydroxy-6-[^{18}F]fluorophenylalanine), [^{11}C]PE2I (*N*-(3-iodoprop-2*E*-enyl)-2β-carbo[^{11}C]methoxy-3β-(4-methylphenyl)nortropane) and [^{11}C]DASB ([^{11}C]*N*,*N*-Dimethyl-2-(2-amino-4-cyanophenylthio)benzylamine) PET on a Siemens Biograph TruePoint HI-REZ 6 PET/CT system. For the [^{18}F]FDOPA scan, 150mg oral dose of carbidopa was administered 1 hour prior to injection to reduce peripheral metabolism. Patients were positioned supine such that the transaxial plane was parallel to the AC-PC plane. Memory foam padding was used to minimise movement and maximise patient comfort, while video monitoring was used to aid repositioning should any gross movements occur. Radioligand volumes were prepared to 10ml using saline solution and administered intravenously as single bolus injections followed immediately by 10ml saline flush (Table 2.3). Administration was at a rate of 1 ml/s.

Table 2.3: Injected dose and injected mass for each tracer, group and time-point.

		Transplant Group (n = 8)			Control Group (n[a])	
Tracer	Injected Dose/Mass	Baseline	Pre-Transplant	Post-Transplant	Baseline	18m FU
[^{18}F]FDOPA	Injected Dose (MBq)	178.58± 3.49	176.56± 4.14	165.63± 14.47	162.63± 27.57	172.13± 19.36
	Injected Mass (μg)	1020.13± 246.62	1325.69± 420.89	1166.28± 554.14	1115.02± 313.05	1231.49± 402.62
[^{11}C]PE2I	Injected Dose (MBq)	298.83± 66.08	315.45± 64.52	317.44± 25.39	326.64± 15.36	332.49± 10.09
	Injected Mass (μg)	4.29± 2.50	3.62± 0.71	3.65± 1.44	4.23± 2.17	4.35± 2.43
[^{11}C]DASB	Injected Dose (MBq)	391.86± 57.99	428.77± 9.81	376.85± 82.24	427.33± 13.42	315.45± 64.52
	Injected Mass (μg)	2.45± 1.24	2.74± 1.50	2.22± 1.23	2.44± 1.78	3.62± 0.71

[a] 16 patients were scanned with [^{18}F]FDOPA and [^{11}C]PE2I and 14 patients were scanned with [^{11}C]DASB
FU = follow-up

Dynamic emission data were acquired continuously while patients were at rest for 90 minutes post-injection. Data were binned into a dynamic series of 26 temporal frames (8x15s, 3x60s, 5x120s, 5x300s, 5x600s) and reconstructed with corrections for decay, scatter and attenuation using a filtered back-projection algorithm (direct inversion Fourier transform) with a matrix size of 128x128, zoom of 2.6 and 2mm isotropic pixel size and smoothed using a 3D 5mm full-width at half-maximum (FWHM) trans-axial Gaussian image filter. A low-dose CT transmission scan (0.36mSv) was acquired for attenuation and scatter correction.

2.5.4. Image processing

Pre-processing and kinetic modelling for [^{18}F]FDOPA, [^{11}C]PE2I and [^{11}C]DASB PET scans was conducted using MIAKAT™ release version 4.3.13 (Molecular Imaging and Kinetic Analysis Toolbox, Invicro LLC, London, UK) (Gunn *et al.*, 2016) (Figure 2.9). MIAKAT™ provides an integrated analytical framework for the analysis of PET acquisitions, utilising both FSL (FMRIB Image Analysis Group, Oxford, UK) (Jenkinson *et al.*, 2012) and SPM (Statistical Parametric Mapping, Wellcome Trust Centre for Neuroimaging, London, UK)

functions in combination with in-house pre-processing and kinetic modelling procedures, and is implemented within MATLAB® R2016B (Mathworks, Natick, MA, USA).

First, MPRAGE images were segmented and rigid-body registered to the Montreal Neurological Institute (MNI) template (Mazziotta *et al.*, 1995). MPRAGE images in 'pseudo-MNI' space ($MPRAGE_{REG}$) for all visits of each patient were then entered into serial longitudinal registration, which incorporates rigid-body registration, diffeomorphic modelling and intensity inhomogeneity correction to create a within-subject mid-point average structural image and associated deformation fields (Ashburner and Ridgway, 2012). The mid-point average for each patient was used for manual subcortical region of interest delineation in Analyze12.0, in accordance with the anatomical-landmark-based methods derived from work on the *in vivo* distribution of D_3 receptors using [^{11}C](+)-PHNO (Tziortzi *et al.*, 2011). Specifically, the border between the ventral striatum, putamen and caudate was defined by first placing three markers on the sagittal plane; a single-voxel thick horizontal line on the mid-sagittal slice (i.e. nearest the inter-hemispheric gap), placed such that it was immediately ventral to the splenium of the corpus callosum, and two whole-slice markers placed on the most lateral aspects of the caudate nuclei. On the coronal plane, diagonal lines were drawn connecting the inter-hemispheric marker with the points where the lateral markers crossed the most ventral boundary of the striatal grey matter. The striatal grey matter ventromedial to these diagonal boundaries and anterior to the anterior commissure was defined as the ventral striatum. Striatal grey matter dorsomedial to these diagonal boundaries was defined as the caudate nucleus, and dorsolateral grey matter was defined as the putamen. The putamen was also sub-divided into posterior and anterior divisions by placement of a coronal whole-slice marker through the anterior commissure. ROI maps were then brought from the mid-point average back to $MPRAGE_{REG}$ space for each visit using the inverse deformation fields estimated by the serial longitudinal registration. Flow fields mapping the transformation from MNI template to $MPRAGE_{REG}$ were estimated using Diffeomorphic Anatomical Registration Through Exponentiated Lie algebra (DARTEL) (Ashburner, 2007) and applied to an MNI-based regional atlas (CIC Atlas v1.2 (Tziortzi *et al.*, 2011)) to define the cerebellum. Grey matter segmentation maps were used to isolate cerebellar grey matter.

Motion correction was conducted on the dynamic PET data to correct for intra-scan head movement using frame-to-frame rigid registration (mutual information cost function), with the 16th frame corresponding to 780-900 seconds post-injection as a reference, chosen due to high signal-to-noise ratio. Realignment for all dynamic series performed well and no image artefacts due to substantial head movement were observed.

A two-pass procedure was adopted to bring the realigned dynamic frames into $MPRAGE_{REG}$ space at each visit. First, attenuation-corrected and non-attenuation-corrected realigned frames corresponding to 10-90 minutes for [^{18}F]FDOPA and 0-10 minutes for [^{11}C]PE2I and [^{11}C]DASB were summed to obtain signal-averaged (ADD) images and co-registered to the $MPRAGE_{REG}$ (smoothed using an 8mm full-width at half maximum Gaussian kernel) using normalized mutual information as a cost function. Registered ADD images were then visually evaluated for quality of alignment against the $MPRAGE_{REG}$. The registered ADD images resulting from the estimation that produced the best alignment were subsequently retained and designated as the targets to which the remaining ADD images were re-co-registered in a PET-to-PET second pass, again using normalised mutual information as a cost function. This procedure was adopted because the quality of cross-modal co-registration was highly variable across scans and subjects, with intra-modal co-registration offering substantial and consistent improvement in the alignment of images. In general, the attenuation-corrected [^{11}C]PE2I 0-10 minute ADD images performed best in the co-registration to the $MPRAGE_{REG}$ in the first pass, while in the second pass, substantial improvement was obtained for [^{11}C]DASB when co-registering non-attenuation-corrected 0-10 minute ADD images to the non-attenuation-corrected [^{11}C]PE2I 0-10 minute ADD images, and for [^{18}F]FDOPA when co-registering non-attenuation-corrected 10-90 minute ADD images to the non-attenuation-corrected [^{11}C]PE2I 0-10 minute ADD images after smoothing the latter with an 8mm FWHM Gaussian kernel. Parameters estimated from frame-to-frame realignment and the two-pass co-registration procedures were applied to the corresponding dynamic PET data in one step to minimise interpolation error.

PET image processing was evaluated at each step before region of interest maps were applied to the realigned and registered dynamic PET frames ($MPRAGE_{REG}$ space) to generate

regional time-activity curves (TACs) for all regions of interest for each side separately, as well as bilaterally.

Multiple-time graphical analysis for irreversible binding (Patlak plot) (Patlak and Blasberg, 1985) was used to quantify the uptake rate constant (K_i) for [^{18}F]FDOPA, which represents the net influx and irreversible trapping of the tracer and its metabolites in tissue. Cerebellar grey matter was used as a reference region as the activity of the aromatic L-amino acid decarboxylase (AADC) enzyme in this region has been found to be low or negligible (Lloyd and Hornykiewicz, 1972; Lloyd *et al.*, 1975; Mackay *et al.*, 1978; Rahman *et al.*, 1981) and is therefore assumed to have no irreversible compartment. Reliable parameter estimation using Patlak graphical analysis requires that tracer concentrations in the reversible compartments and plasma reach equilibrium. A linear start time (t^*) of 30 minutes post-injection was therefore used, after which the Patlak plot became linear with the slope representing the net influx constant (K_i).

Multiple-time graphical analysis for reversible binding (Logan plot) (Logan *et al.*, 1996) was used to quantify the non-displaceable binding potential (BP_{ND}) for [^{11}C]PE2I, representing the ratio of specifically bound radioligand to that of free and non-specific (non-displaceable) radioligand at equilibrium (Innis *et al.*, 2007). Several studies have validated the use of Logan plot for analysis of radiolabelled PE2I data (Pinborg *et al.*, 2002; DeLorenzo *et al.*, 2009; Odano *et al.*, 2012; Odano *et al.*, 2017), with one report demonstrating superior performance over non-invasive likelihood estimation in graphical analysis (LEGA) and the simplified reference tissue model (SRTM) methods on measures of test-retest reliability and amount of variance explained due to inter-subject over intra-subject variability (intra-class correlation coefficient) (DeLorenzo *et al.*, 2009). Cerebellar grey matter was used as a reference as previous studies in humans have demonstrated negligible tracer uptake in this region (Hall *et al.*, 1999; Halldin *et al.*, 2003; Jucaite *et al.*, 2006). While it has been shown that [^{11}C]PE2I kinetics in the cerebellum and other regions low in dopamine transporters are best described using a two-tissue compartmental model (due to the presence of a parallel compartment, radiometabolites or specific binding), this does not preclude derivation of reliable and reproducible parameter estimates by bloodless approaches that assume one-tissue compartment kinetics in the reference region, albeit resulting in the underestimation of BP_{ND}

by approximately half of that which can be determined using plasma input (Jucaite *et al.*, 2006; Hirvonen *et al.*, 2008; DeLorenzo *et al.*, 2009; Odano *et al.*, 2012). The slope of the plot corresponding to $BP_{ND} + 1$ was estimated after an equilibration time of $t^* = 30$ minutes, after which the intercept effectively remained constant.

[^{11}C]DASB kinetics can be described by a one-tissue compartmental model, thereby permitting the use of simplified quantitative methods for the estimation of BP_{ND} (Ginovart *et al.*, 2001; Frankle *et al.*, 2006), representing the ratio of specifically bound radioligand to that of free and non-specific (non-displaceable) radioligand at equilibrium (Innis *et al.*, 2007). To this end, the basis function implementation of the simplified reference tissue model was used (Lammertsma and Hume, 1996; Gunn *et al.*, 1997), including constraint of the reference tissue clearance parameter (k'_2) to a first-pass global estimate (SRTM2) (Wu and Carson, 2002). Fixing k'_2 has yielded substantial noise reductions for tracers whose kinetics can be described by a one-tissue compartmental model (Wu and Carson, 2002) and significantly mitigated noise-induced bias and variability for quantification of [^{11}C]DASB BP_{ND} when compared to its three-parameter counterpart (SRTM) (Ichise *et al.*, 2003; Endres *et al.*, 2011). The basis function implementation was preferred as it is more stable in high noise situations and when specific binding comprises only a small fraction of the signal (Frankle *et al.*, 2006). Cerebellar grey matter was used as a reference region, as post-mortem semi-quantitative Western blot analysis has shown only trace concentrations of the serotonin transporter in this region (Kish *et al.*, 2005). It should be noted however, that this region is not completely devoid of serotonin transporters. [^{11}C]DASB imaging using arterial/plasma input functions demonstrates that although the cerebellum, and more specifically, cerebellar grey matter, shows the lowest change in distribution volume following acute treatment with selective serotonin reuptake inhibitors (SSRI) (Parsey *et al.*, 2006), occupancy was still calculated at between 29-39%, depending on the cerebellar sub-region, pharmacological agent and model (Parsey *et al.*, 2006; Turkheimer *et al.*, 2012), leading to an overall regionally-dependent underestimation of BP_{ND} derived from reference tissue models of up to 15% (Ginovart *et al.*, 2001; Frankle *et al.*, 2006; Turkheimer *et al.*, 2012). Some authors have proposed methods involving correction factors to adjust for this bias (Gunn *et al.*, 2011; Turkheimer *et al.*, 2012), however in the absence of specific SSRI occupancy data for this disease group such

corrections may introduce additional error. Thus, we consider the SRTM2 with parameter constraint a reasonable choice in the current study.

Parametric images were also generated by fitting the models to each voxel of the realigned and registered dynamic PET series in $MPRAGE_{REG}$ space. To enable comparisons at the group level, DARTEL (Ashburner, 2007) was performed entering grey and white matter segments of the mid-point average image for each patient, generating flow fields mapping subject-specific to study-specific templates through an iterative procedure in which input images are repeatedly registered to their own group average. Composite deformations comprised of the flow fields mapping $MPRAGE_{REG}$ → mid-point average and mid-point average → study-specific template were then generated and applied to the parametric images using the deformations utility in SPM12 while preserving concentrations to ensure voxel values were not modulated for volumetric changes.

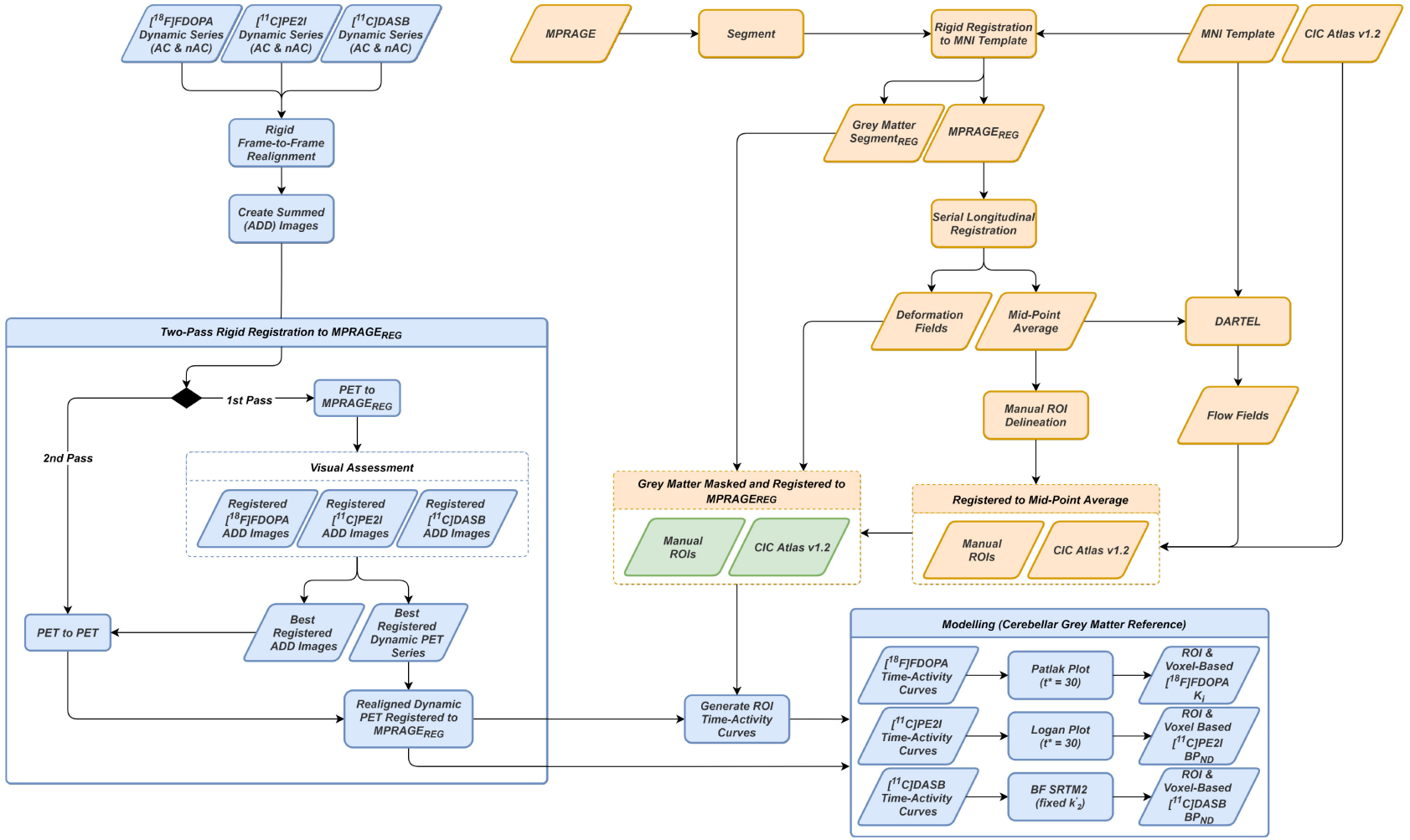


Figure 2.9: Image pre-processing and analysis pipeline for [18F]FDOPA, [11C]PE2I and [11C]DASB PET. AC = attenuation-corrected; ADD = signal-averaged image; BF = basis function; BP_{ND} = non-displaceable binding potential; DARTEL = diffeomorphic anatomical registration using exponentiated Lie algebra; K_i = influx constant; MNI = Montreal Neurological Institute; MPRAGE = magnetization-prepared rapid gradient echo; nAC = non-attenuation-corrected; PET = positron emission tomography; REG = rigid-registered to MNI template; ROI = region of interest; SRTM = simplified reference tissue model.

Chapter 3. Effects of Intraputamenal hfVM Transplants on Dopaminergic and Serotonergic Function in Parkinson's Disease

In this chapter, the effects of hfVM tissue grafting into the bilateral putamen of 8 patients with Parkinson's disease on dopamine synthesis and storage capacity ([^{18}F]FDOPA), dopamine transporter density ([^{11}C]PE2I) and serotonin transporter density ([^{11}C]DASB) will be examined and compared to a group of 16 patients who did not undergo transplantation but who remain on best currently available drug therapy. The effects within the putamen will also be compared against the longitudinal changes within the caudate, as a within-subject striatal control region. Voxelwise and sub-regional putamenal analysis will be undertaken in order to ascertain whether grafting under the Transeuro protocol results in consistent homogenous delivery and re-innervation across the transplanted nucleus. Lastly, the relationship between changes in [^{18}F]FDOPA and [^{11}C]PE2I will be examined in order to evaluate whether PD-related compensatory changes affect the grafted cells after placement within the diseased host environment.

The aims of the current chapter are:

- To compare the longitudinal changes in dopaminergic and serotonergic imaging measures in transplanted patients against non-transplanted patients
- To compare the longitudinal changes in dopaminergic and serotonergic imaging measures in the putamen against the caudate in transplanted patients
- To evaluate the spatial distribution of transplant-related alterations across the striatum
- To examine whether the expression of the dopamine transporter is related to the survival of grafted dopaminergic cells

The hypotheses of the current chapter are:

- hfVM transplants will result in an increase in putamenal dopaminergic and serotonergic imaging markers at 18 months post-surgery while non-transplanted individuals and nuclei will continue to deteriorate over time
- The putamen in transplanted patients will exhibit homogeneous re-innervation covering the entire nucleus
- The change in [^{18}F]FDOPA at 18 months post-surgery will be predictive of the change in [^{11}C]PE2I measures over the same interval and this relationship will be different from that observed in non-transplanted patients

3.1. Statistical analysis

3.1.1. Region of interest analysis

Region of interest-based statistical analyses were performed using R version 3.6.2 (R Core Team, 2019) and packages "afex" (Singmann *et al.*, 2017), "emmeans" (Lenth, 2018), "Hmisc" (Harrell Jr, 2017), "ggplot2" (Wickham, 2016), "ggpubr" (Kassambara, 2019), "moments" (Komsta and Novomestky, 2015), "car" (Fox and Weisberg, 2019), "caret" (Kuhn, 2020), "lm.beta" (Behrendt, 2014), "psych" (Revelle, 2019), "MASS" (Venables and Ripley, 2002), "dplyr" (Wickham *et al.*, 2020) and "tidyr" (Wickham and Henry, 2020).

3.1.1.1. Within-group analysis

3-way repeated measures analyses of covariance were carried out including all bilaterally transplanted patients who completed the multi-PET protocol at all three time-points (n = 8), in order to examine whether differences in mean striatal [^{18}F]FDOPA K_i, [^{11}C]PE2I BP_{ND} and [^{11}C]DASB BP_{ND} values depended on *visit* (baseline, pre-transplant, post-transplant), striatal *region* (putamen, caudate) and *brain side* (right, left). The caudate was included as an internal control region that is also known to exhibit substantial dopaminergic neurodegeneration over time in Parkinson's disease. Left and right brain side was included to ascertain whether the response to transplant was affected by the order in which they occurred, the right putamen having received hfVM tissue first in all patients (interval between surgical procedures = 3.88 ±2.49 months). Mean-centred disease duration and age at baseline were included as continuous covariates as they have been shown to be related to dopaminergic function and more specifically to [^{18}F]FDOPA K_i. In the case of a significant 3-way interaction, partial interactions between *region* and *visit* were investigated at each level of *brain side*. Post-hoc Tukey-adjusted pairwise comparisons of the estimated marginal means were conducted to evaluate pairwise differences where appropriate.

Normal distribution of residuals was evaluated by visual assessment of density and QQ plots and by Shapiro-Wilk test, sphericity using Mauchly's test with Greenhouse-Geisser-corrected values reported where appropriate, homogeneity of regression slopes by evaluating interactions between the covariates and independent variables and correlated covariates using Pearson's product moment.

3.1.1.2. Between-group analysis

3-way mixed analyses of covariance with repeated measures were carried out in order to examine whether differences in mean putamenal [^{18}F]FDOPA K_i, [^{11}C]PE2I BP_{ND} and [^{11}C]DASB BP_{ND} values depended on *group* (transplant, control) and *visit*, where the latter included either pre-transplant and post-transplant time-points for the transplant group (n=8), or baseline and 18-months follow-up time-points for the control group, for which data were available for 16 patients for [^{18}F]FDOPA K_i and [^{11}C]PE2I BP_{ND} and 14 patients for [^{11}C]DASB BP_{ND}. *Parkinsonian brain side* (most affected, least affected), where the most affected brain side was defined as contralateral to the body side on which Parkinsonian symptoms are most severe, as indicated by clinical history and UPDRS-III scores, was also included as an independent factor. Greater symptomatic response to transplant has previously been linked to a preservation of ventral striatal dopaminergic function (Piccini *et al.*, 2005), while other studies have demonstrated more pronounced [^{18}F]FDOPA changes in the side with lower pre-operative values (Brundin *et al.*, 2000). Thus it may be that reparative efficacy depends on the pre-operative putamenal state. Mean-centred disease duration and age at baseline were included as continuous covariates as they have been shown to be related to dopaminergic function and more specifically to [^{18}F]FDOPA K_i. In the case of a significant 3-way interaction, partial interactions between *group* and *visit* were investigated at each level of *Parkinsonian brain side*. Post-hoc Tukey-adjusted pairwise comparisons of the estimated marginal means were conducted to evaluate pairwise differences where appropriate.

Testing for the violation of ANCOVA assumptions were as above, with the addition of homogeneity of variance, assessed using Levene's test with data transformations applied as appropriate, and independence between covariate and independent variables, assessed using independent *t*-tests.

3.1.1.3. Regression analysis

Hierarchical multiple linear regression was conducted in order to examine whether changes in putamenal [^{11}C]PE2I BP_{ND} values over time (Δ[^{11}C]PE2I BP_{ND}) could be predicted by changes in putamenal [^{18}F]FDOPA K_i over the same period (Δ[^{18}F]FDOPA K_i) and whether this was moderated by receipt of intraputamenal transplantation. Previous work has

suggested that the compensatory molecular changes occurring in the putamen in Parkinson's disease also differ across the most and least affected sides (Lee *et al.*, 2000; Nandhagopal *et al.*, 2009), thus the effect of *Parkinsonian brain side* was also examined.

In the base additive model, *group* was included as a categorical predictor, where Δ[^{18}F]FDOPA K_i and Δ[^{11}C]PE2I BP_{ND} for patients who received transplantation (transplant group, n = 8) were defined as [*post-transplant - pre-transplant*]. The transplant group was compared to Parkinson's disease patients who did not receive transplantation during the course of the study (control group, n = 16), where delta values were taken between consecutive scanning time-points [*18-month follow-up - baseline*]. *Parkinsonian brain side* (most/least affected) was also included as a categorical predictor in the base model. In the second model, an additional term was included for the interaction between Δ[^{18}F]FDOPA K_i and *group*. In the third model, an additional three interaction terms were included, in order to test whether the interaction between Δ[^{18}F]FDOPA K_i and *group* depended on *Parkinsonian brain side*.

The extra sum of squares F-test was used to evaluate whether the addition of predictors at each step of the hierarchical multiple regression made a significant improvement to the model fit at the expense of loss of degrees of freedom.

Normal distribution of the residuals was assessed graphically using normal QQ plots, density plots and Shapiro-Wilk test, heteroscedasticity by plotting residuals against fitted values and Breusch-Pagan test, multicollinearity by variance inflation factors, independence of observations by the Durbin-Watson statistic and outliers and highly influential data points were detected by normal QQ plots as well as Mahalanobis distance using the "car"(Fox and Weisberg, 2019) and "psych" packages (Revelle, 2019).

3.1.2. Putamenal coverage analysis

3.1.2.1. Group voxelwise analysis

Voxelwise analysis at the group level was conducted to examine how transplant-related alterations were distributed across the striatum. For each tracer, parametric images at the pre-transplant and post-transplant time-points for the transplant group, normalised to the DARTEL-generated study-specific template, were entered into a paired t-test in spm12. An

explicit mask was used to restrict voxelwise statistics to the striatum (putamen, caudate and ventral striatum). This was created by applying the mid-point average → study-specific template DARTEL flow fields (Ashburner and Ridgway, 2012) to each of the striatal ROI maps, averaging them and binarizing the output. Voxelwise statistical maps were thresholded at $P_{FWE} < 0.05$, unless otherwise stated.

3.1.2.2. Sub-regional analysis

Estimates of putamenal coverage with relation to the transplant were also derived for each transplanted patient. Difference images for each tracer, hereby denoted with Δ, were generated by voxelwise subtraction of pre-transplant from post-transplant parametric images, after application of the flow fields mapping each of the images from $MPRAGE_{REG}$ space to the mid-point average. The putamenal mask generated for the study-specific template above was then manually segmented into five equally spaced divisions, matching the number of trajectories through which hfVM cells were deposited, along the anterior-posterior axis on the axial plane (Figure 3.1). Each sub-putamenal division consisted of eight coronal slices. This parcellated putamenal ROI map was then projected back to the mid-point average for each patient using the reverse flow fields previously generated. Coverage was defined as the volume of each putamenal sub-division that exhibited positive values within these difference images and expressed as a percentage of their total volume. Non-parametric Friedman's test was used to examine whether there was a difference in the percentage of positive volume between putamenal sub-divisions and followed by post-hoc Dunn-Bonferroni tests in the event that the null hypothesis was rejected. Spearman's rho and Euclidean distance were used to evaluate the similarity between patients in the spatial distribution of hfVM-induced increases in putamenal imaging measures. Euclidean distance was double-scaled to within a range of 0-1 by use of the following equation:

$$d_2 = \frac{\sqrt{\sum_{i=1}^{r} \left(\frac{(p_{1i} - p_{2i})^2}{md_i} \right)}}{\sqrt{r}}$$

, where d_2 is the double-scaled Euclidean distance, r is the number of regions, p is the patient and md_i is the squared absolute maximum (100) to minimum (0) value difference per region i of r regions.

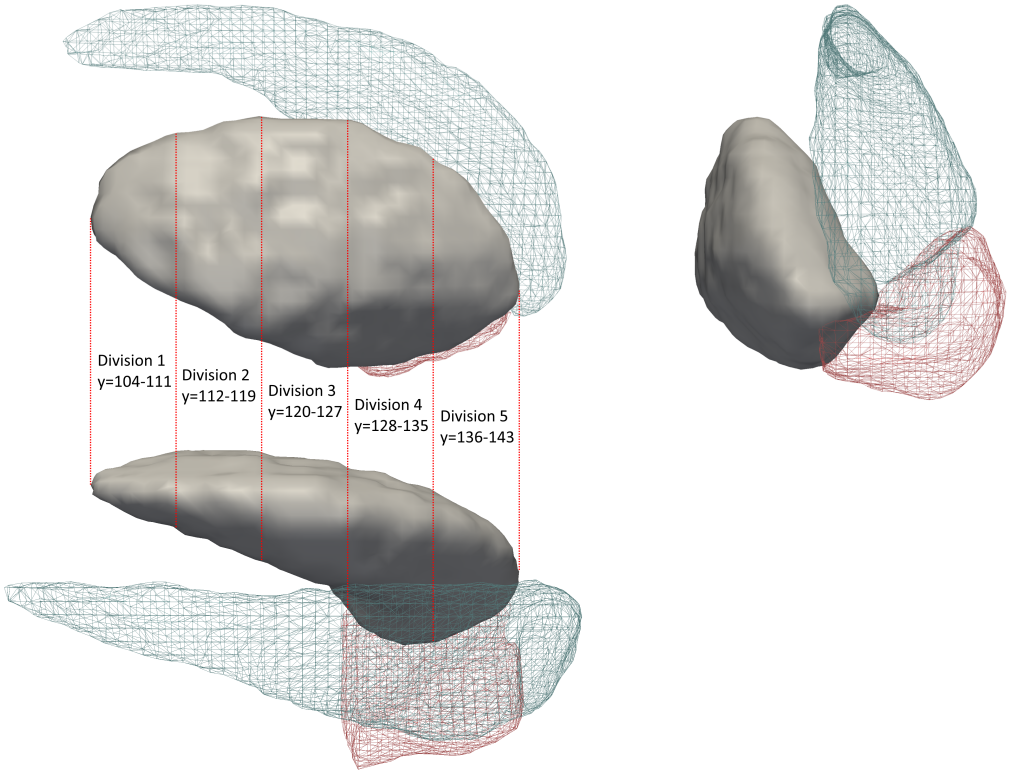


Figure 3.1: 3D rendering of the striatal mask, including the putamen (solid grey), caudate (blue mesh) and ventral striatum (red mesh), generated by normalising manual delineations performed in MPRAGE$_{REG}$ *space for each subject, in accordance with anatomical guidelines previously described (Tziortzi et al., 2011), to the DARTEL-generated study-specific template and subsequently averaging them. Putamenal sub-regions were created along the anterior-posterior axis by manual division on the axial plane into five equal partitions of eight slices each.*

3.2. Results

3.2.1. Subject demographics

Subject characteristics at baseline and follow-up time-points are displayed in Table 3.1. There were no significant differences for any variable when comparing transplant and control groups at baseline. However, in comparison to the control group at baseline, the transplant group at the pre-transplant time-point showed higher "off-state" UPDRS-III total ($t(8.23) = 2.49$, $p = 0.037$), UPDRS-III tremor ($t(22) = 2.24$, $p = 0.036$) scores and greater disease duration ($t(22) = 2.83$, $p = 0.01$). Note that for the purposes of this chapter, comparisons were only conducted between pre-operative time-points. The examination of clinical effects of transplant (i.e. post-operative time-points) will be the subject of Chapter 4.

3.2.2. Graft survival and growth: [^{18}F]FDOPA

3.2.2.1. Regional within-group ANCOVA

A 3-way repeated measures analysis of covariance was carried out including all bilaterally transplanted patients who completed 3 [^{18}F]FDOPA scans ($n = 8$), in order to examine whether differences in mean striatal [^{18}F]FDOPA K_i values depended on *visit* (baseline, pre-transplant, post-transplant), striatal *region* (putamen, caudate) and *brain side* (right, left).

Results revealed a significant *region* by *visit* interaction ($F(2, 10) = 5.47$, $p = 0.025$), indicating that differences in [^{18}F]FDOPA K_i over time were dependent on *region* (Figure 3.2). Post-hoc Tukey-adjusted pairwise comparisons of the estimated marginal means revealed a significant decrease in caudate [^{18}F]FDOPA K_i at post-transplant as compared to baseline ($\Delta Mean_{EM}$ = -0.00107, *95% CI* [-0.00212, -0.00002], $p = 0.046$), while no significant differences were shown in the putamen over the same period ($\Delta Mean_{EM}$ = -0.00013, *95% CI* [-0.00118, 0.00092], $p = 0.994$). Pairwise differences were also observed between regions, whereby the putamen showed significantly lower [^{18}F]FDOPA K_i as compared to the caudate at pre-transplant ($\Delta Mean_{EM}$ = -0.00106, *95% CI* [-0.00202, -0.0001], $p = 0.028$), and a trend towards significance at baseline ($\Delta Mean_{EM}$ = -0.00089, *95% CI* [-0.00186, 0.00006], $p = 0.069$), while no difference was seen at post-transplant ($\Delta Mean_{EM}$ = 0.00004, *95% CI* [-0.00092, 0.00099], $p = 0.999$).

There was no effect of *brain side* on the interaction between *region* and *visit* ($F(2, 10) = 0.21$, $p = 0.814$). Additionally, there were no significant interactions between *visit* and *brain side* ($F(2, 10) = 0.38$, $p = 0.691$) or *region* and *brain side* ($F(1, 5) = 0.32$, $p = 0.593$).

Table 3.1: Subject demographics at baseline and follow-up time-points for the transplant and control groups.

	Parkinson's Disease Transplant (n = 8)			Parkinson's Disease Control (n = 16)	
	Baseline	Pre-Transplant [c]	Post-Transplant [d]	Baseline	Follow-up [e]
Gender (m:f)	6:2	6:2	6:2	13:3	13:3
Age (years)	53.82±8.50	55.29±8.37	58.02±7.73	55.90±4.72	57.53±4.71
Disease duration (years) [b]	6.07±2.32	7.53±2.29	10.26±2.16	5.15±1.75	6.78±1.79
"Off-state" UPDRS-III:					
Total [b]	33.63±12.56	38.88±13.01	33.63±13.32	27.57±5.32	32.71±7.24
Bradykinesia	15.00±7.62	16.38±5.42	16.38±6.78	12.93±4.23	15.07±4.16
Rigidity	6.50±3.34	7.50±4.11	6.00±3.16	5.43±2.53	6.79±2.69
Tremor [b]	8.13±4.70	9.38±4.00	6.75±5.65	5.29±5.31	6.93±5.28
Axial	4.00±2.27	5.63±4.47	4.50±3.38	3.93±1.86	3.93±1.64
"Off-state" Peg Board	30.72±19.78	34.25±29.83	30.94±15.22	25.09±5.08	26.46±4.92
"Off-state" Tap Test	72.72±27.63	68.06±18.71	67.69±23.60	75.07±29.14	76.68±28.58
"Off-state" H&Y	1.88±0.35	2.13±0.35	2.00±0.00	2.00±0.00	2.00±0.00
"On-State" AIMS	0.75±2.12	1.75±2.92	5.00±6.89	0.13±0.50	1.25±2.32
"Off-State" AIMS	0.00±0.00	0.00±0.00	2.38±3.70	0.00±0.00	0.00±0.00
LEDD	814.44± 345.90	909.25± 355.65	1029.25± 324.15	658.02± 367.57	839.34± 379.24
ACE-R	97.38±2.33	98.63±0.92	97.75±1.67	98.81±1.68	97.81±2.64

ACE-R = Addenbrooke's cognitive exam revised; AIMS = abnormal involuntary movement scale; H&Y = Hoehn & Yahr scale; LEDD = levodopa-equivalent daily dosage; UPDRS-III = unified Parkinson's disease rating scale part-III

[a]Denotes significant difference between Transplant and Control groups at Baseline

[b]Denotes significant difference between the Transplant group at Pre-Transplant and Control group at Baseline

[c]Pre-transplant assessment was conducted at a mean of 17.54 ±1.91m from baseline

[d]Post-transplant assessment was conducted at a mean of 50.34 ±11.88m from baseline

[e]Follow-up was conducted at a mean of 19.58 ±3.79m from baseline

H&Y was assessed using non-parametric Mann-Whitney U test

Gender was assessed using Fisher's Exact test

All other tests between groups were conducted using independent t-tests

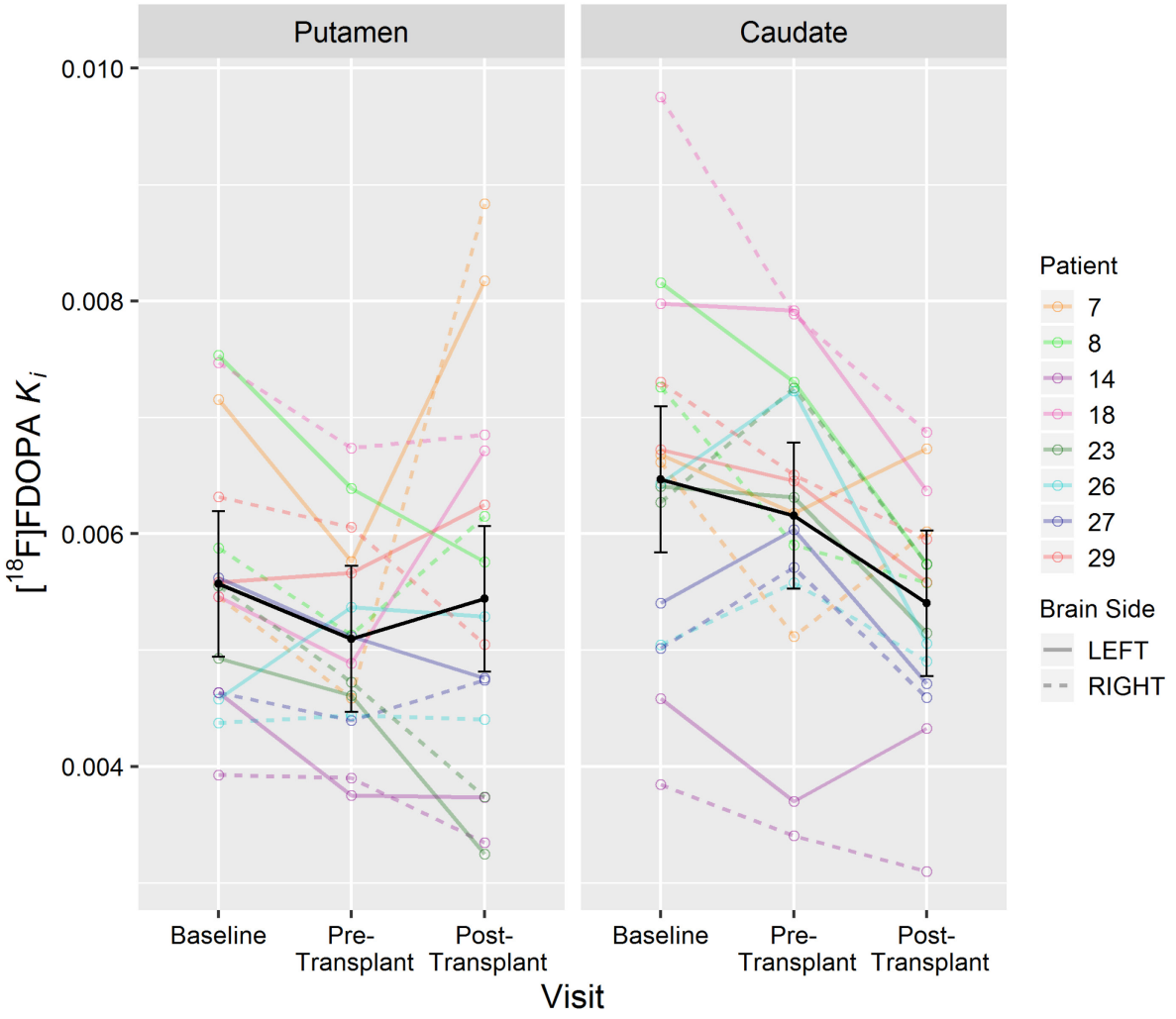


Figure 3.2: Within-group ANCOVA for [18F]FDOPA. Change in mean [18F]FDOPA K_i over time in striatal nuclei of Parkinson's disease patients who have received intraputamenal transplants of fetal ventral mesencephalic tissue (n = 8). Strip plots illustrate a 2-way interaction between region (putamen, caudate) and visit (baseline, pre-transplant, post-transplant) when data were collapsed across brain side (right, left) and adjusting for mean-centred age and disease duration at baseline. Patients included in this analysis are displayed in separate colours and with differentiation between left and right brain sides (solid and dashed lines respectively). Solid black lines and error bars represent estimated marginal means and individual 95% confidence intervals respectively.

3.2.2.2. Regional between-group mixed ANCOVA

A 3-way mixed analysis of covariance with repeated measures was carried out including all bilaterally transplanted patients (n = 8) and control patients (n = 16) who completed 2 [^{18}F]FDOPA scans, in order to examine whether differences in mean putamenal [^{18}F]FDOPA K_i values depended on *group* (transplant, control), *visit* (pre-transplant/baseline and post-transplant/18-month follow-up for transplant/control groups respectively) and *Parkinsonian brain side* (most affected, least affected).

The assumption of independence between the covariate and independent variables was violated for disease duration at baseline. Analyses are therefore reported after dropping disease duration from the model.

Results revealed a trend towards a significant *group* by *visit* interaction (F(1, 21) = 3.76, p = 0.066). This suggests that differences in [^{18}F]FDOPA K_i over time may be dependent on *group* (Figure 3.3). Post-hoc Tukey-adjusted pairwise comparisons of the estimated marginal means revealed that this borderline significant trend was driven by significantly higher mean putamenal [^{18}F]FDOPA K_i in the transplant group at the post-transplant visit as compared to the control group at 18-month follow-up ($\Delta Mean_{EM}$ = 0.00113, *95% CI* [0.00007, 0.00219], p = 0.034).

There was no effect of *Parkinsonian brain side* on the interaction between *group* and *visit* (F(1, 21) = 2.06, p = 0.166). There was however a significant interaction between *visit* and *Parkinsonian brain side* (F(1, 21) = 6.99, p = 0.015), which was driven by significantly higher [^{18}F]FDOPA K_i in the clinically least affected putamen as compared to the clinically most affected putamen at the baseline/pre-transplant visit ($\Delta Mean_{EM}$ = 0.00078, *95% CI* [0.00039, 0.00116], p < 0.001), while no difference was observed between the sides at the 18-month follow-up/post-transplant time-point ($\Delta Mean_{EM}$ = 0.00025, *95% CI* [-0.00013, 0.00063], p = 266).

Inclusion of mean-centred disease duration did not alter the results of the 3-way ANCOVA.

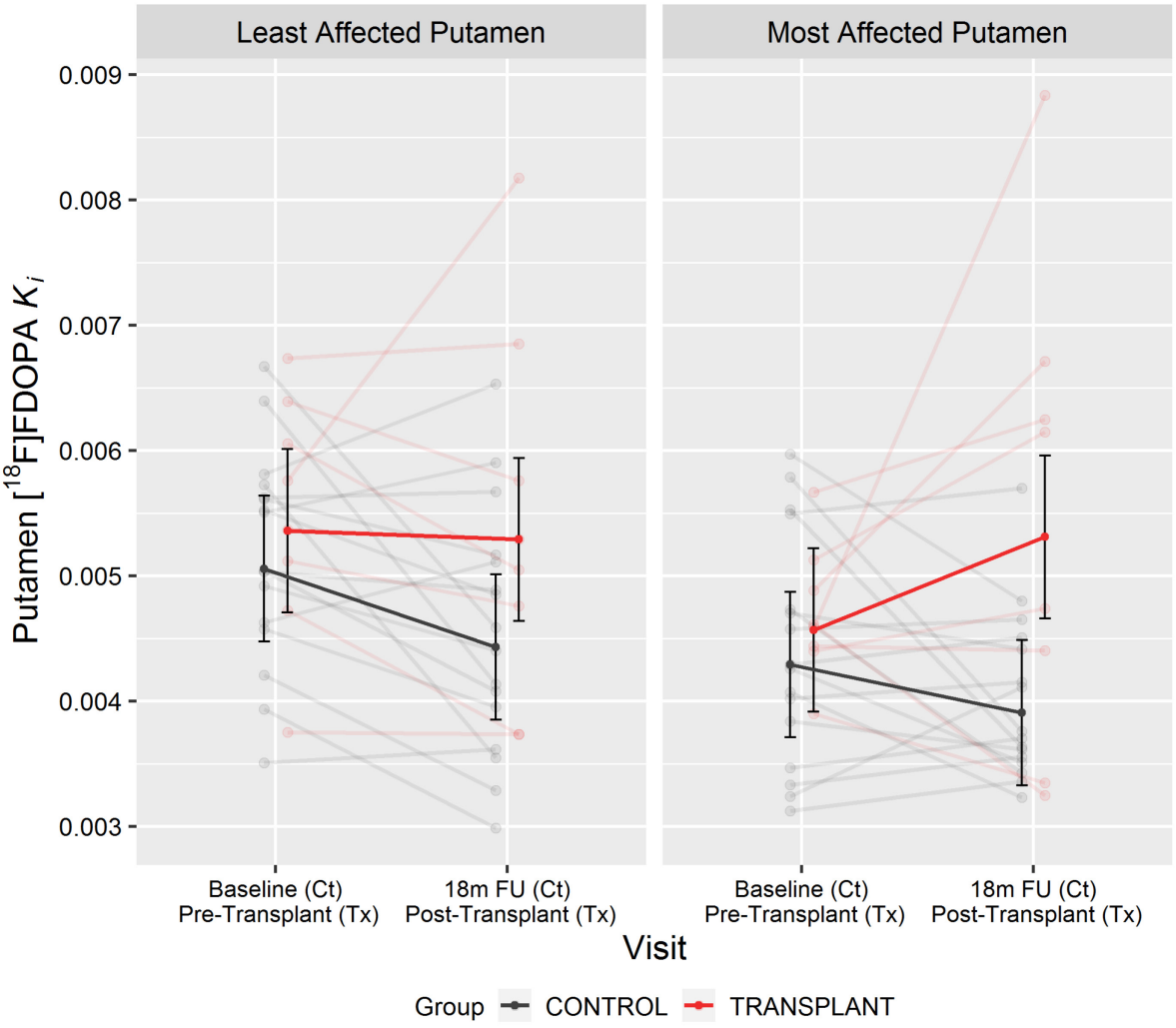


Figure 3.3: Between-group ANCOVA for [¹⁸F]FDOPA. Change in mean [¹⁸F]FDOPA K_i over time in the putamen of Parkinson's disease patients who have received intraputamenal transplants of fetal ventral mesencephalic tissue (Tx, n = 8) and Parkinson's disease patients who have not received transplant (Ct, n = 16). Strip plots illustrate results of a 3-way interaction analysis between group (transplant, control), visit (pre-transplant/baseline & post-transplant/18-month follow-up for transplant/control groups respectively) and Parkinsonian brain side (most affected, least affected), adjusting for mean-centred age at baseline, in which there was a borderline significant trend for a 2-way interaction between group and visit. Solid black and red lines and associated error bars represent estimated marginal means and individual 95% confidence intervals for the control and transplant groups respectively. FU = follow-up.

3.2.2.3. Longitudinal voxelwise analysis

Voxelwise analysis was conducted using images collected at pre-transplant and post-transplant time points for the transplant group only, to identify sub-regions of the striatum showing a significant change in [^{18}F]FDOPA K_i. No significant clusters survived after family-wise error correction at $P_{FWE} < 0.05$, or at an uncorrected peak threshold of $P < 0.001$. After relaxing the threshold to uncorrected $P < 0.05$, clusters showing an increase at post-transplant were identified in the left and right putamen bordering on the left and right caudate. Conversely, decreases were seen in the left and right caudate, as well as in the right putamen and nucleus accumbens (Figure 3.4, Table 3.2).

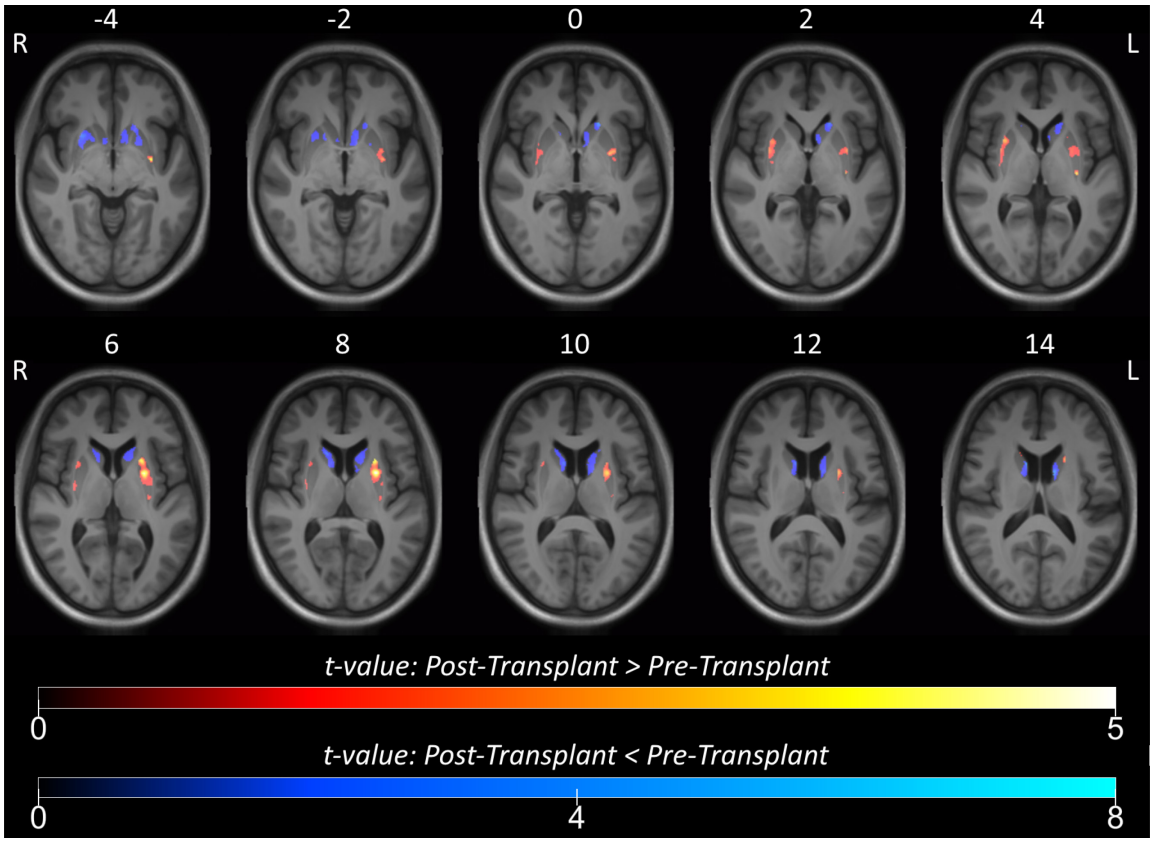


Figure 3.4: Voxelwise analysis of post-transplant changes in [^{18}F]FDOPA. Statistical parametric maps showing results of the voxelwise paired t-test comparing pre-transplant to post-transplant [^{18}F]FDOPA K_i parametric images for bilaterally transplanted Parkinson's disease patients (n = 8). Voxelwise statistics were restricted to the striatum and are overlaid onto the study-specific template generated using DARTEL after thresholding at uncorrected p < 0.05.

Table 3.2: Results of the voxelwise paired t-test comparing pre-transplant to post-transplant [^{18}F]FDOPA K_i parametric images for bilaterally transplanted Parkinson's disease patients (n = 8). MNI co-ordinates refer to the peak voxel within each cluster after thresholding at uncorrected $p < 0.05$ and their anatomical location is reported with reference to the Harvard-Oxford subcortical structural atlas.

Contrast	Region	MNI Co-ordinates	k	t-value
Post-Transplant > Pre-Transplant	Left Putamen	-24 2 5	1049	5.86
	Left Putamen	-29 -18 0	65	3.96
	Right Putamen	30 7 1	457	3.12
	Left Caudate	-19 13 12	45	3.02
	Right Caudate	18 17 14	7	2.86
	Left Putamen	-27 -13 10	1	1.93
Post-Transplant < Pre-Transplant	Left Caudate	-11 2 15	2011	8.16
	Right Putamen / Amygdala / Cerebral Cortex	24 3 -12	503	6.7
	Right Caudate	12 9 12	702	5.36
	Left Caudate	-16 -12 22	120	3.16
	Right Nucleus Accumbens	7 9 -8	149	2.9
	Right Putamen / Caudate	15 13 -3	7	2.23

The whole-brain spatial extent of the change in striatal [^{18}F]FDOPA K_i over time was also visualised by creating parametric delta images (i.e. subtracting pre-transplant from post-transplant) in MPRAGE$_{REG}$ space for each individual patient who underwent transplant (Figure 3.5) (Figure 3.6).

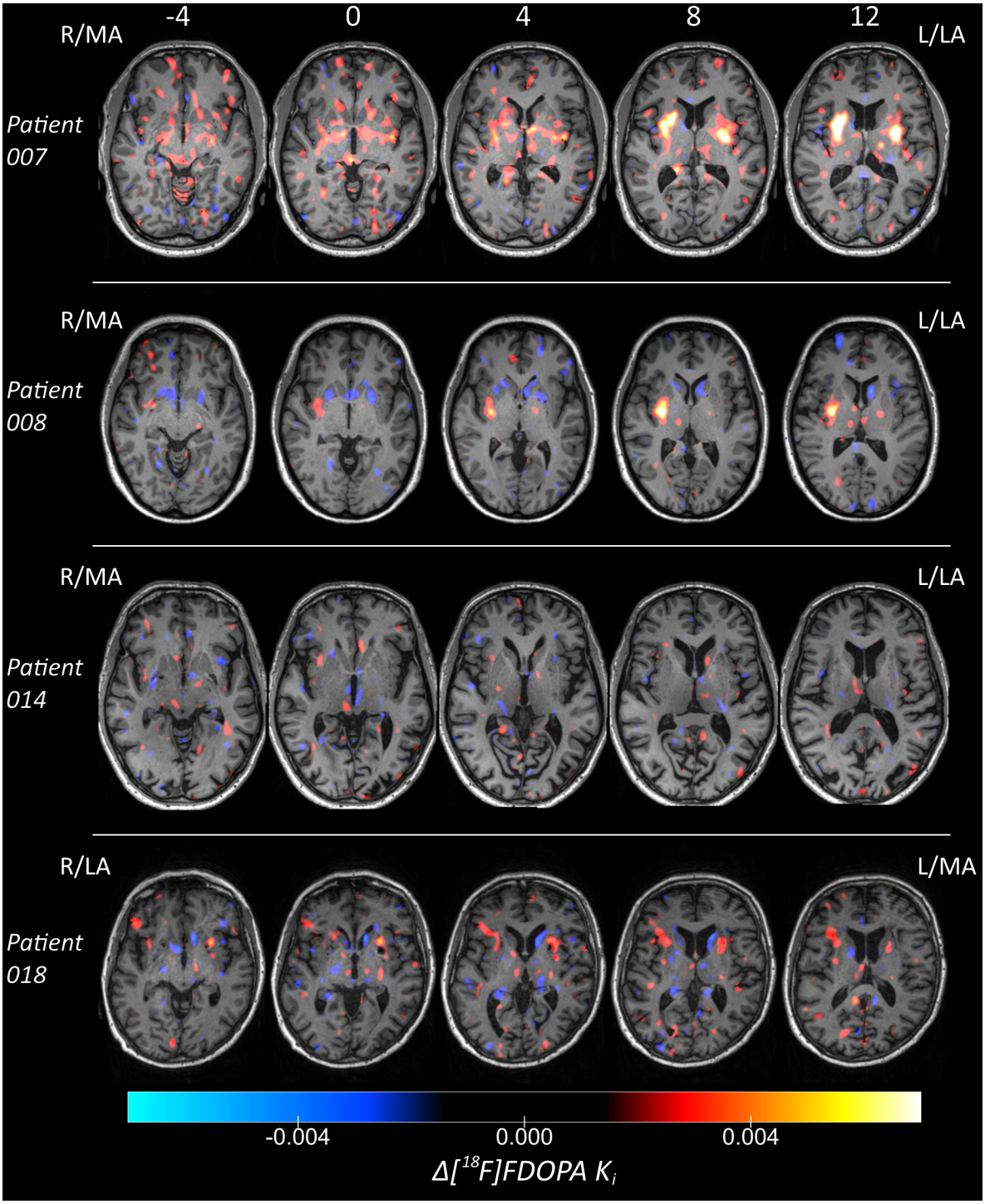


Figure 3.5: Post-operative [18F]FDOPA changes for patients 007, 008, 014 and 018. [18F]FDOPA K_i difference (Δ) images were derived by subtracting pre-transplant parametric images from post-transplant parametric images, overlaid onto post-transplant MPRAGE$_{REG}$ scans and displayed at 5 axial levels of the striatum. LA = least affected; MA = most affected.

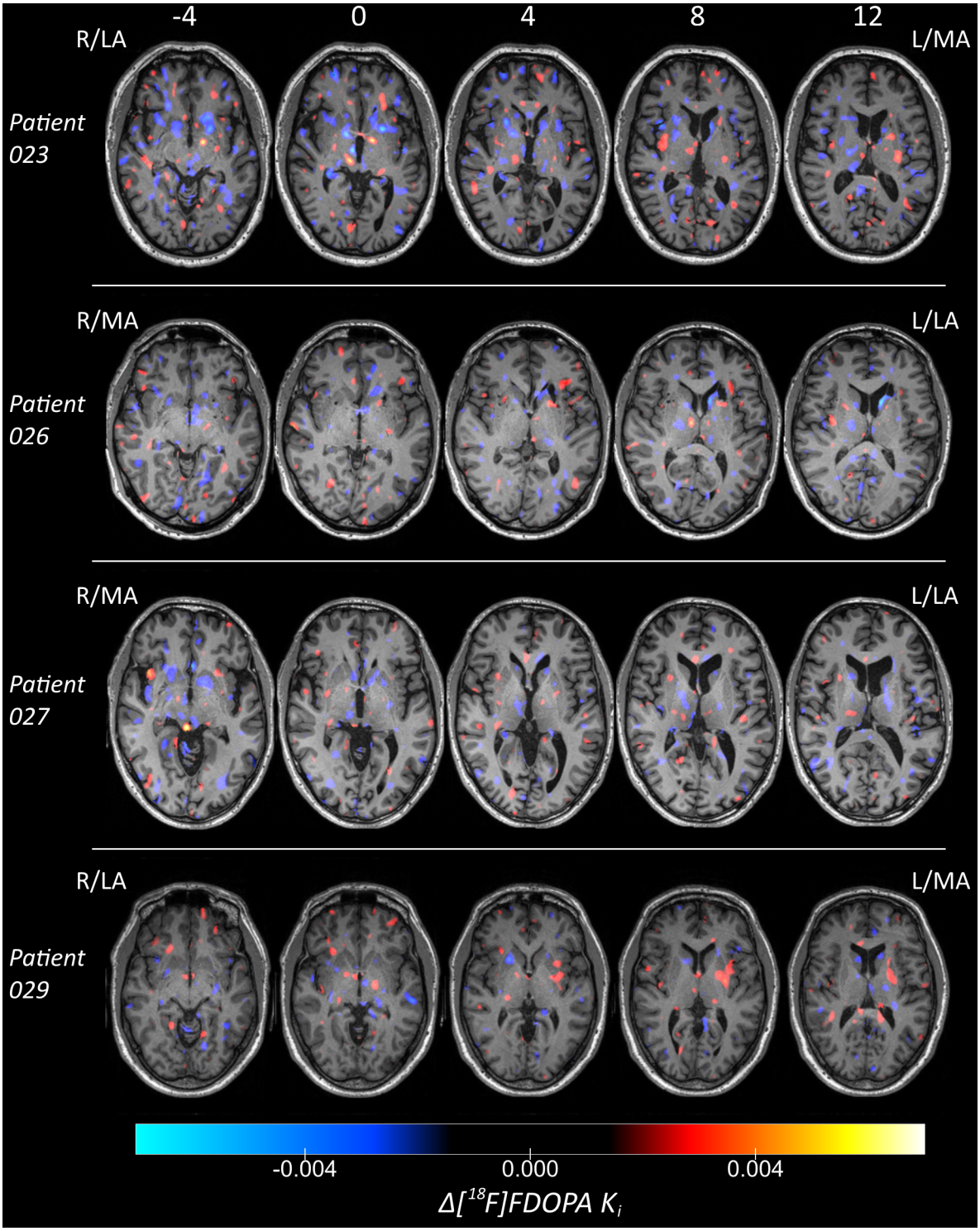


Figure 3.6: Post-operative [18F]FDOPA changes for patients 023, 026, 027 and 029. [18F]FDOPA K_i difference (Δ) images were derived by subtracting pre-transplant parametric images from post-transplant parametric images, overlaid onto post-transplant MPRAGE$_{REG}$ scans and displayed at 5 axial levels of the striatum. LA = least affected; MA = most affected.

3.2.2.4. Putamenal coverage

Data showing volume (mm^3) coverage of increased [^{18}F]FDOPA uptake for the whole putamen as well as its anterior-posterior divisions is shown in Table 3.3. On average, the volume of the whole putamen that showed a positive change at post-transplant was 59.45 ±20.61% in the left and 50.20 ±23.79% in the right.

Non-parametric Friedman's test showed that there was no statistical difference between putamenal divisions when all divisions for both sides were included ($\chi^2(9) = 12.79$, $p = 0.172$) or when the left and right putamen were examined separately (Left: $\chi^2(4) = 6.4$, $p = 0.171$; Right: $\chi^2(4) = 6.62$, $p = 0.158$) (Figure 3.7). However, plots suggest that the anterior-posterior coverage profiles were inconsistent across transplanted individuals. Spearman's rho correlations support this observation, showing a range of both positive and negative coefficients between patient profiles with only one positive correlation between patients 007 and 008 surpassing the threshold for significance (Benjamini-Hochberg corrected). In contrast, Euclidean distance measures suggest this pair to be dissimilar, while the most similar pairing was between patients 014 and 023. There was however a general dissimilarity across each of the putamenal coverage profiles.

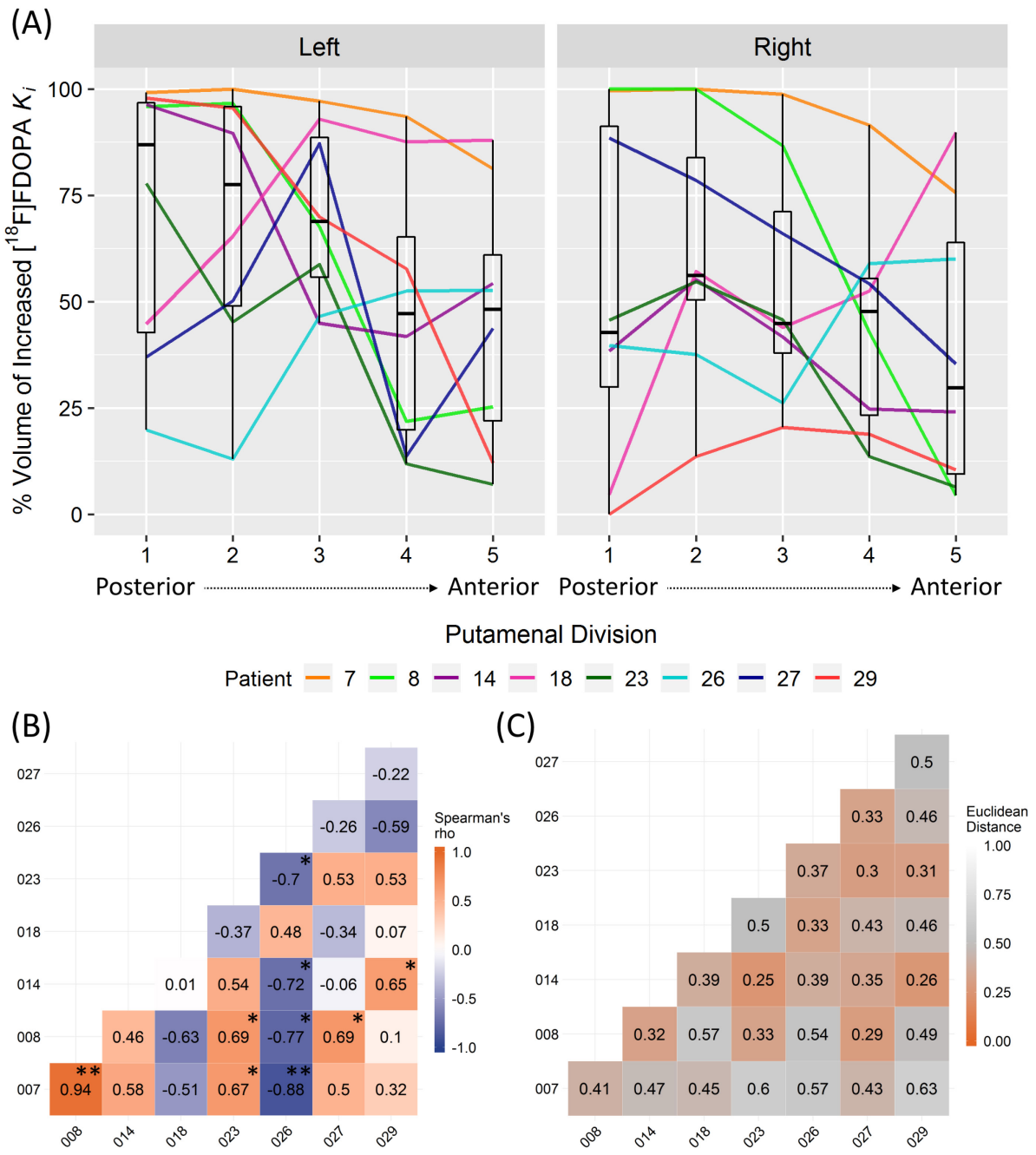


*Figure 3.7: Antero-posterior putamenal profiles for [¹⁸F]FDOPA. A | Antero-posterior spatial profiles generated for each participant showing the volume of each putamenal sub-region that exhibited a positive change in [¹⁸F]FDOPA K_i between pre-transplant and post-transplant time-points. Box and whisker plots represent the median and interquartile range. B | Spearman's rho correlation matrix showing correlations of antero-posterior spatial profiles (across both left and right putamen) between individual transplant patients. C | Double-scaled Euclidean distance matrix showing the similarity of antero-posterior spatial profiles (across both left and right putamen) between individual transplant patients. *p < 0.05, **Significant after Benjamini-Hochberg false discovery rate correction at threshold p < 0.05.*

Table 3.3: Putamenal volume showing post-operative increases in [^{18}F]FDOPA. Table showing the total volume (mm^3) and volume exhibiting positive voxel values in Δ[^{18}F]FDOPA K_i images for each putamenal sub-division along the antero-posterior axis for the left and right sides.

		Left Putamenal Division							Right Putamenal Division					
Patient	Volume (mm^3)	1	2	3	4	5	Whole		1	2	3	4	5	Whole
7	Positive	239	818	1373	1522	389	4341		246	741	1422	1477	366	4252
	Total	241	818	1413	1628	479	4579		247	741	1440	1614	484	4526
8	Positive	209	727	963	368	119	2386		218	762	1255	705	21	2961
	Total	218	752	1424	1683	471	4548		218	762	1448	1645	480	4553
14	Positive	238	766	644	729	306	2683		101	502	574	397	136	1710
	Total	247	855	1433	1744	564	4843		263	910	1375	1601	565	4714
18	Positive	84	435	1193	1204	411	3327		10	391	539	739	432	2111
	Total	188	665	1284	1375	467	3979		217	684	1227	1408	481	4017
23	Positive	175	341	734	176	33	1459		93	390	605	200	30	1318
	Total	225	754	1250	1481	467	4177		204	713	1324	1477	468	4186
26	Positive	44	92	643	884	293	1956		89	308	382	974	345	2098
	Total	222	711	1383	1684	556	4556		224	820	1458	1654	575	4731
27	Positive	99	430	1350	259	262	2400		230	623	1085	1035	203	3176
	Total	268	857	1549	1897	600	5171		260	794	1645	1908	574	5181
29	Positive	180	689	920	853	54	2696		0	94	281	276	50	701
	Total	184	721	1316	1477	448	4146		193	690	1374	1468	477	4202

3.2.3. Graft DAT expression: [^{11}C]PE2I

3.2.3.1. Regional within-group ANCOVA

A 3-way repeated measures analysis of covariance was carried out including all bilaterally transplanted patients who completed 3 [^{11}C]PE2I scans (n = 8), in order to examine whether differences in mean striatal [^{11}C]PE2I BP_{ND} values depended on *visit* (baseline, pre-transplant, post-transplant), striatal *region* (putamen, caudate) and *brain side* (right, left).

Results revealed a significant *region* by *visit* interaction (F(2, 10) = 30.26, p < 0.001), indicating that differences in [^{11}C]PE2I BP_{ND} over time were dependent on *region* (Figure 3.8). Post-hoc Tukey-adjusted pairwise comparisons of the estimated marginal means revealed a significant decrease in caudate [^{11}C]PE2I BP_{ND} from baseline to pre-transplant ($\Delta Mean_{EM}$ = -0.259, *95% CI* [-0.491, -0.027], p = 0.024) and from pre-transplant to post-transplant ($\Delta Mean_{EM}$ = -0.541, *95% CI* [-0.772, -0.309], p < 0.001), while in the putamen, there was no difference between baseline and post-transplant ($\Delta Mean_{EM}$ = 0.021, *95% CI* [-0.211, 0.252], p = 0.998) but a trend towards a significant increase between pre-transplant and post-transplant ($\Delta Mean_{EM}$ = 0.217, *95% CI* [-0.015, 0.448], p = 0.074). There were additional significant pairwise differences between regions, in which [^{11}C]PE2I BP_{ND} was lower in the putamen as compared to the caudate at baseline ($\Delta Mean_{EM}$ = -0.762, *95% CI* [-1.239, -0.284], p = 0.004) and pre-transplant visits ($\Delta Mean_{EM}$ = -0.699, *95% CI* [-1.176, -0.221], p = 0.006), but not at post-transplant ($\Delta Mean_{EM}$ = 0.059, *95% CI* [-0.419, 0.536], p = 0.99).

There was no effect of *brain side* on the interaction between *region* and *visit* (F(1.05, 5.25) = 1.44, p = 0.285 [Greenhouse-Geisser corrected]). Additionally, there were no significant interactions between *visit* and *brain side* (F(1.05, 5.26) = 0.45, p = 0.539 [Greenhouse-Geisser corrected]) or *region* and *brain side* (F(1, 5) = 0.21, p = 0.668).

Assessment of QQ plots and histograms suggested that residuals were mildly platykurtic and mildly positively skewed, with Shapiro-Wilk test confirming departure from the normal distribution (p = 0.024). Tests were therefore repeated after applying a log transform to the data, which enabled conformation to a normal distribution. There was no difference in the results between the non-transformed data and log transformed data. The non-transformed results are presented to facilitate ease of interpretation.

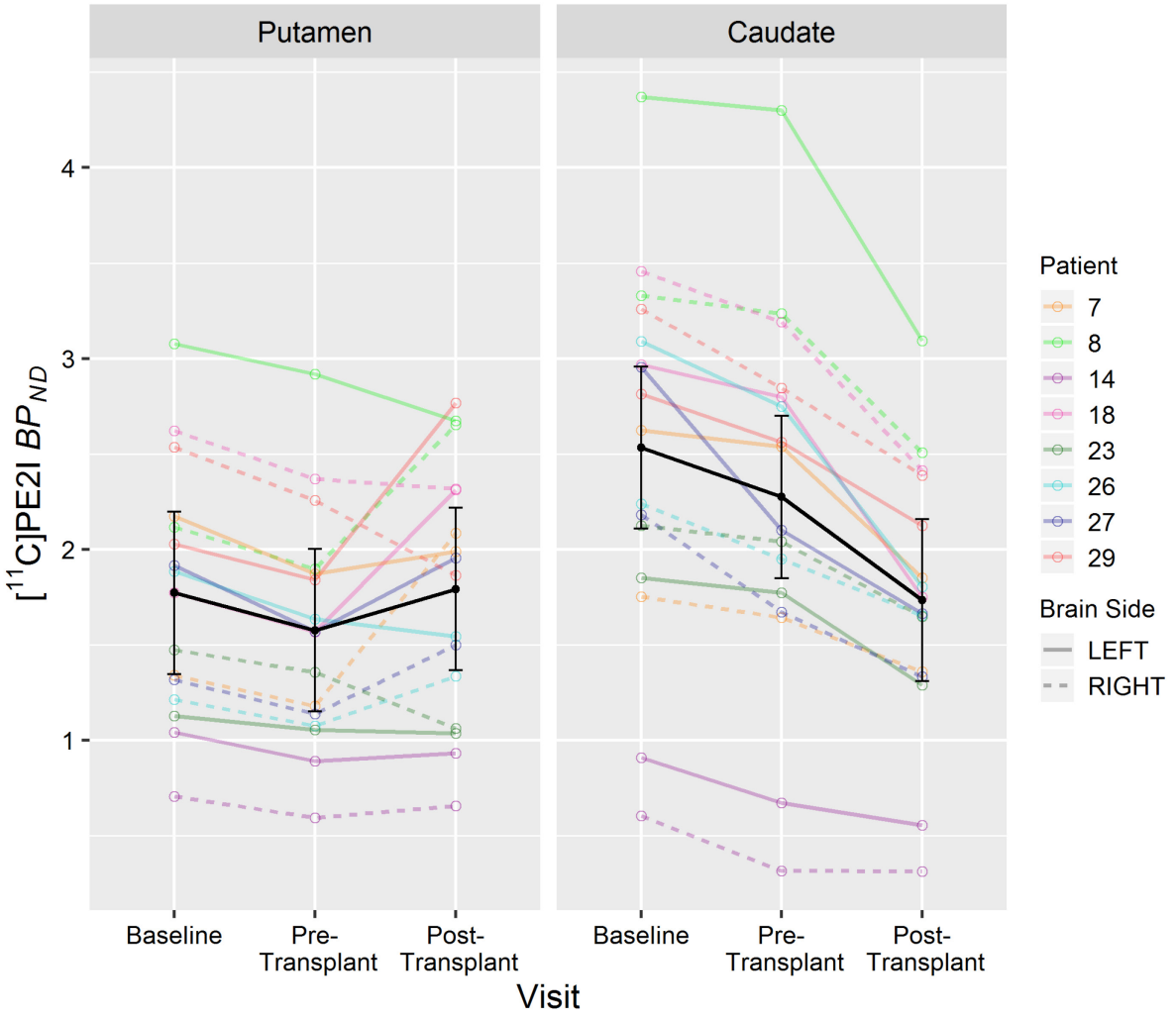


Figure 3.8: Within-group ANCOVA for [11C]PE2I. Change in mean [11C]PE2I BP_{ND} over time in striatal nuclei of Parkinson's disease patients who have received intraputamenal transplants of fetal ventral mesencephalic tissue (n = 8). Strip plots illustrate a 2-way interaction between region (putamen, caudate) and visit (baseline, pre-transplant, post-transplant) when data were collapsed across brain side (right, left) and adjusting for mean-centred age and disease duration at baseline. Patients included in this analysis are displayed in separate colours and with differentiation between left and right brain sides (solid and dashed lines respectively). Solid black lines and error bars represent estimated marginal means and individual 95% confidence intervals respectively.

3.2.3.2. Regional between-groups mixed ANCOVA

A 3-way mixed analysis of covariance with repeated measures was carried out including all bilaterally transplanted patients (n = 8) and control patients (n = 16) who completed 2 [^{11}C]PE2I scans, in order to examine whether differences in mean putamenal [^{11}C]PE2I BP_{ND} values depended on *group* (transplant, control), *visit* (pre-transplant/baseline and post-transplant/18-month follow-up for transplant/control groups respectively) and *Parkinsonian brain side* (most affected, least affected).

The assumption of homogeneity of regression slopes for disease duration at baseline was violated, as was the assumption of independence between the covariate and independent variables. Analyses are therefore reported after dropping disease duration from the model.

Results revealed a significant *group* by *visit* by *Parkinsonian brain side* interaction (F(1, 21) = 12.82, p = 0.002), indicating that differences in [^{11}C]PE2I BP_{ND} over time were dependent on both *group* and *Parkinsonian brain side* (Figure 3.9). Partial interactions between *group* and *visit* at each level of *Parkinsonian brain side* were investigated, showing a significant *group* by *visit* interaction in the most affected side (F(1, 21) = 42.60, p < 0.001), while no interaction was observed in the least affected side (F(1, 21) = 3.21, p = 0.088). Post-hoc Tukey-adjusted pairwise comparisons of the estimated marginal means at the level of the most affected side revealed a decrease in putamenal [^{11}C]PE2I BP_{ND} at 18-month follow-up as compared to baseline for the control group ($\Delta Mean_{EM}$ = -0.168, *95% CI* [-0.321, -0.014], p = 0.030), while a significant increase from pre- to post-transplant was observed for the transplant group ($\Delta Mean_{EM}$ = 0.493, *95% CI* [0.275, 0.709], p < 0.001). Additionally, while no difference between the groups was observed at baseline/pre-transplant ($\Delta Mean_{EM}$ = 0.060, *95% CI* [-0.399, 0.519], p = 0.965), the transplant group showed significantly higher [^{11}C]PE2I BP_{ND} at post-transplant than the control group at 18-month follow-up ($\Delta Mean_{EM}$ = 0.720, *95% CI* [0.261, 1.179], p = 0.002). Inclusion of mean-centred disease duration did not alter the results of the 3-way and partial 2-way ANCOVA analyses.

For this model, Levene's test indicated departure from homogenous variances, and assessment of QQ plots and histograms suggested that the residuals were mildly platykurtic, with Shapiro-Wilk confirming departure from the normal distribution (p = 0.025). Tests were therefore repeated after applying an inverse transform to the data, which

enabled homogenous variances and conformation to normal distribution. There were no differences in the results between the non-transformed data and inverse transformed data. The non-transformed results are presented to facilitate ease of interpretation.

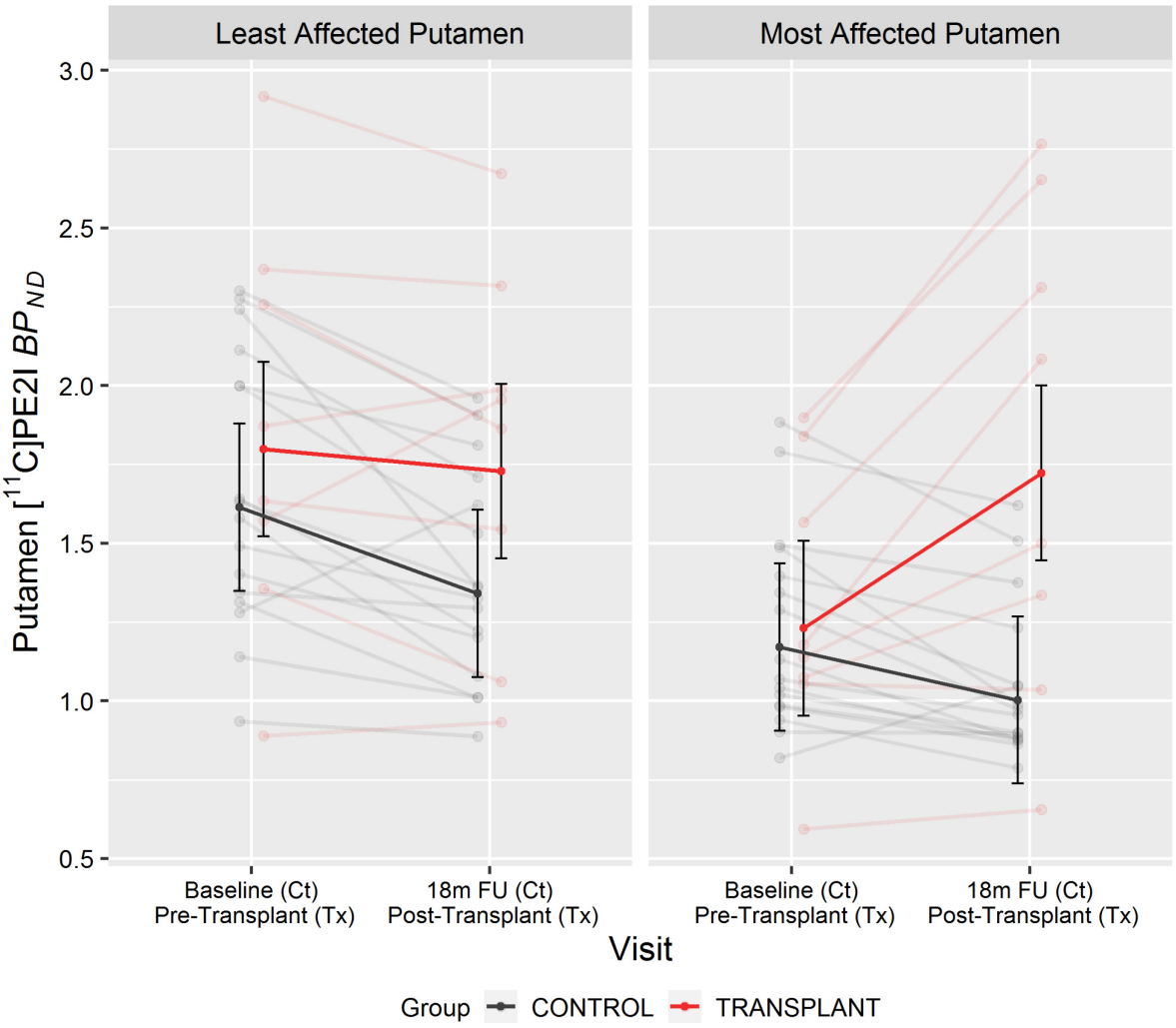


Figure 3.9: Between-group ANCOVA for [11C]PE2I. Change in mean [11C]PE2I BP_{ND} over time in the putamen of Parkinson's disease patients who have received intraputamenal transplants of fetal ventral mesencephalic tissue (Tx, n = 8) and Parkinson's disease patients who have not received transplant (Ct, n = 16). Strip plots illustrating a 3-way interaction between group (transplant, control), visit (pre-transplant/baseline & post-transplant/18-month follow-up for transplant/control groups respectively) and Parkinsonian brain side (most affected, least affected) and adjusting for mean-centred age at baseline. Solid black and red lines and associated error bars represent estimated marginal means and individual 95% confidence intervals for the control and transplant groups respectively. FU = follow-up.

3.2.3.3. Longitudinal voxelwise analysis

Voxelwise analysis was conducted using images collected at pre-transplant and post-transplant time points for the transplant group only, to identify sub-regions of the striatum showing a significant change in [^{11}C]PE2I BP_{ND}. No significant clusters survived after family-wise error correction at $P_{FWE} < 0.05$, or at an uncorrected peak threshold of $P < 0.001$. After relaxing the threshold to uncorrected $P < 0.05$, clusters showing an increase at post-transplant were identified in the left and right putamen. Clusters showing a decrease at post-transplant were seen in the left nucleus accumbens, extending into the left caudate, and in the right caudate, extending into the right nucleus accumbens (Figure 3.10, Table 3.4).

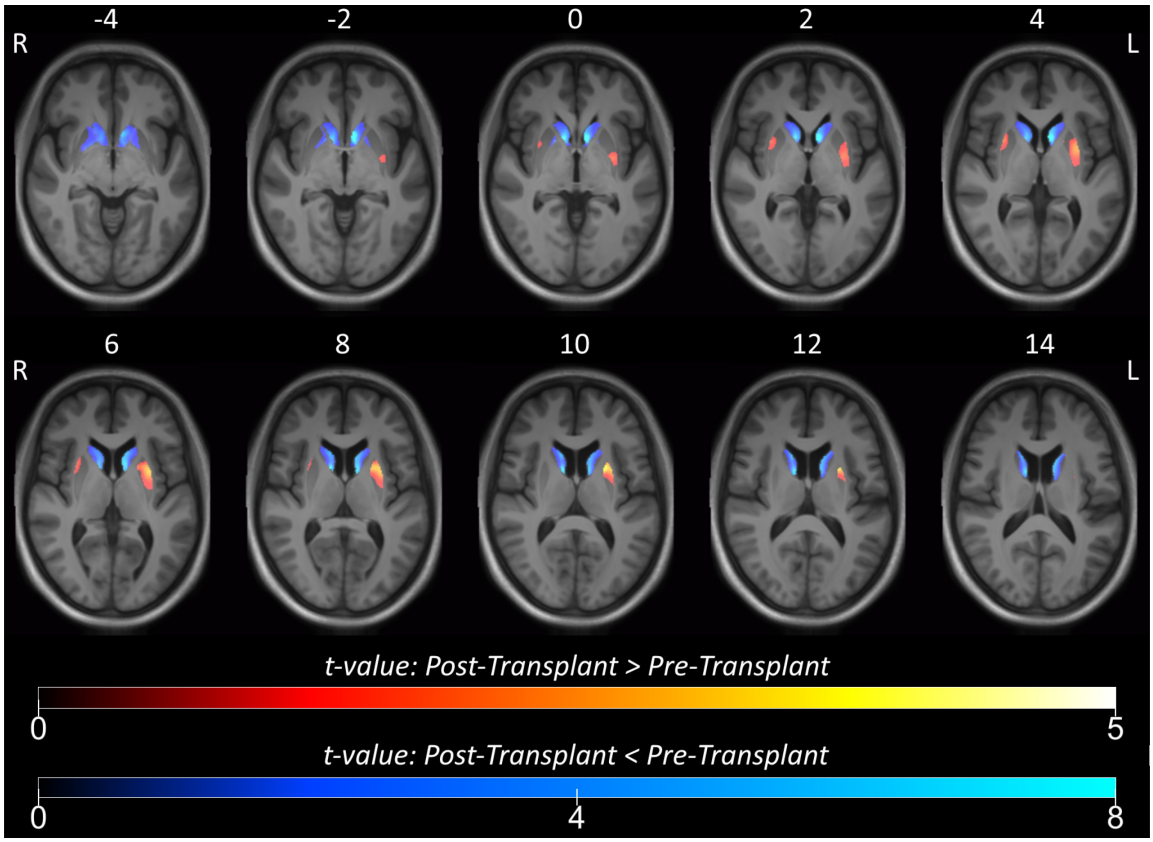


Figure 3.10: Voxelwise analysis of post-transplant changes in [^{11}C]PE2I. Statistical parametric maps showing results of the voxelwise paired t-test comparing pre-transplant to post-transplant [^{11}C]PE2I BP_{ND} parametric images for bilaterally transplanted Parkinson's disease patients (n = 8). Voxelwise statistics were restricted to the striatum and are overlaid onto the study-specific template generated using DARTEL after thresholding at uncorrected p < 0.05.

Table 3.4: Results of the voxelwise paired t-test comparing pre-transplant to post-transplant [^{11}C]PE2I BP_{ND} parametric images for bilaterally transplanted Parkinson's disease patients (n = 8). MNI co-ordinates refer to the peak voxel within each cluster after thresholding at uncorrected $p < 0.05$ and their anatomical location is reported with reference to the Harvard-Oxford subcortical structural atlas.

Contrast	Region	MNI Co-ordinates	k	t-value
Post-Transplant > Pre-Transplant	Left Putamen	-21 6 8	1504	4.38
	Right Putamen	31 9 2	272	2.78
Post-Transplant < Pre-Transplant	Left Nucleus Accumbens	-5 13 -6	4005	12.52
	Right Caudate	11 10 -3	4174	8.81

The whole-brain spatial extent of the change in striatal [^{11}C]PE2I BP_{ND} over time was also visualised by creating parametric delta images (i.e. subtracting pre-transplant from post-transplant) in $MPRAGE_{REG}$ space for each individual patient who underwent transplant (Figure 3.11) (Figure 3.12).

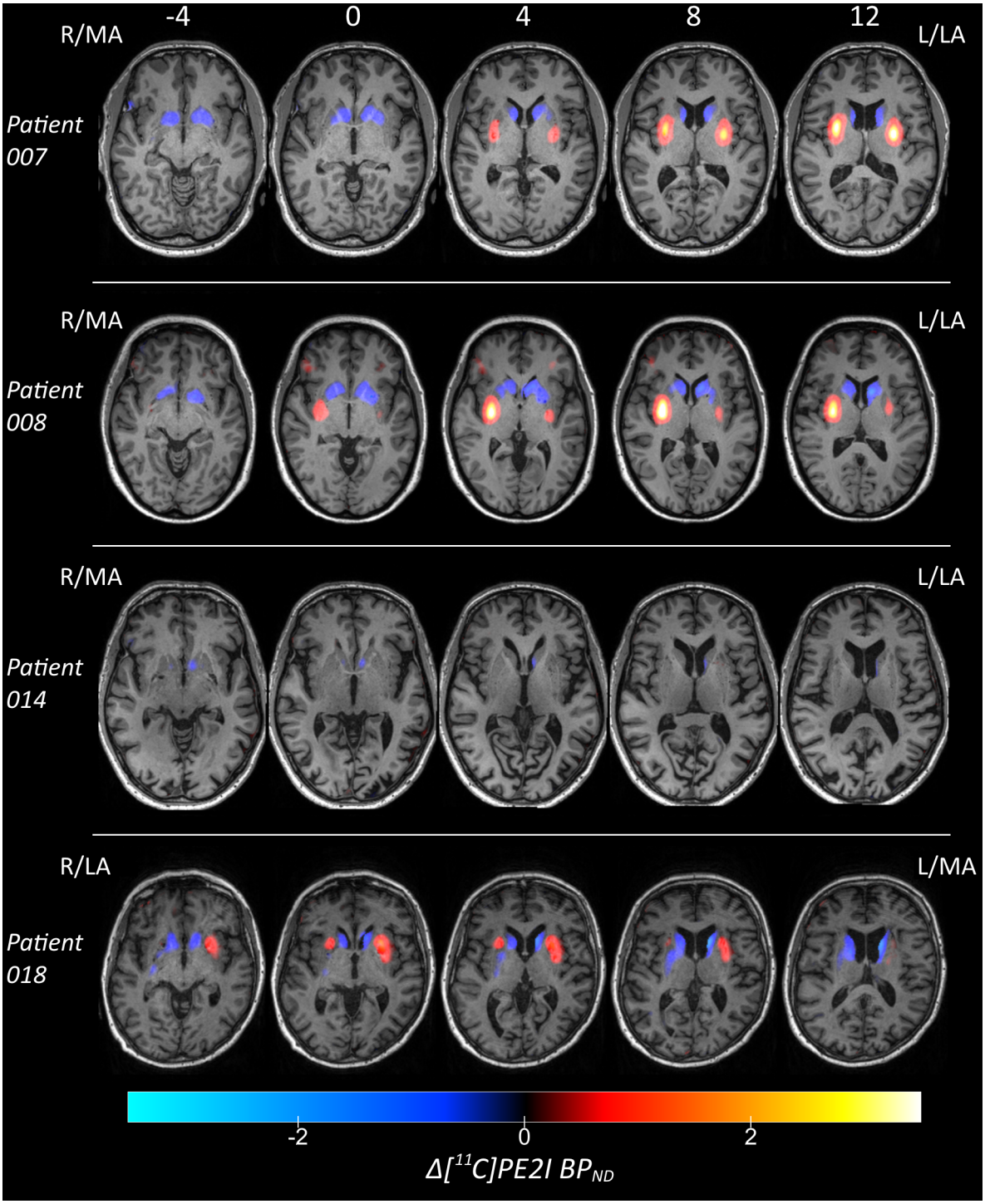


Figure 3.11: Post-operative [11C]PE2I changes for patients 007, 008, 014 and 018. [11C]PE2I BP_{ND} difference (Δ) images were derived by subtracting pre-transplant parametric images from post-transplant parametric images, overlaid onto post-transplant $MPRAGE_{REG}$ scans and displayed at 5 axial levels of the striatum. LA = least affected; MA = most affected.

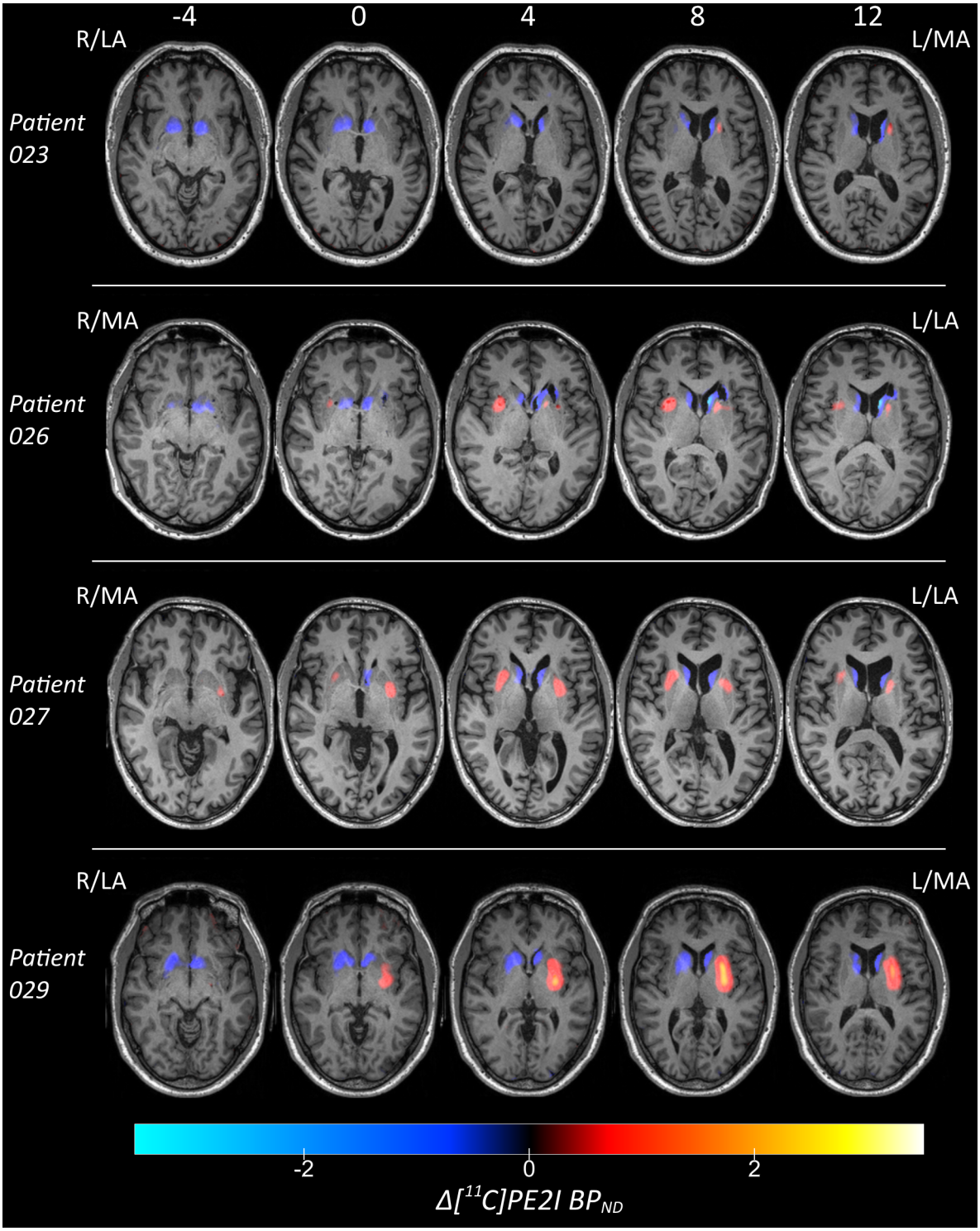


Figure 3.12: Post-operative [11C]PE2I changes for patients 023, 026, 027 and 029. [11C]PE2I BP_{ND} difference (Δ) images were derived by subtracting pre-transplant parametric images from post-transplant parametric images, overlaid onto post-transplant $MPRAGE_{REG}$ scans and displayed at 5 axial levels of the striatum. LA = least affected; MA = most affected.

3.2.3.4. Putamenal coverage

Data showing volume (mm^3) coverage of increased [^{11}C]PE2I binding for the whole putamen as well as its anterior-posterior divisions is shown in Table 3.5. On average, the volume of the whole putamen that showed a positive change at post-transplant was 63.46 ±24.33% in the left and 53.83 ±32.51% in the right.

Non-parametric Friedman's test showed that there was no statistical difference between putamenal divisions when all divisions for both sides were included ($\chi^2(9) = 7.53$, $p = 0.582$) or when the left and right putamen were examined separately (Left: $\chi^2(4) = 7.2$, $p = 0.126$; Right: $\chi^2(4) = 1.69$, $p = 0.791$) (Figure 3.13). However, plots suggest that the anterior-posterior coverage profiles were inconsistent across transplanted individuals. Spearman's rho correlations support this observation, showing a range of both positive and negative coefficients between patient profiles with only Patients 007 and 008 surpassing the threshold for a significant positive correlation (Benjamini-Hochberg corrected). Euclidean distance measures are also in line with this, showing low dissimilarity between patients 007 and 008 and relatively higher dissimilarity between all other patient pairs.

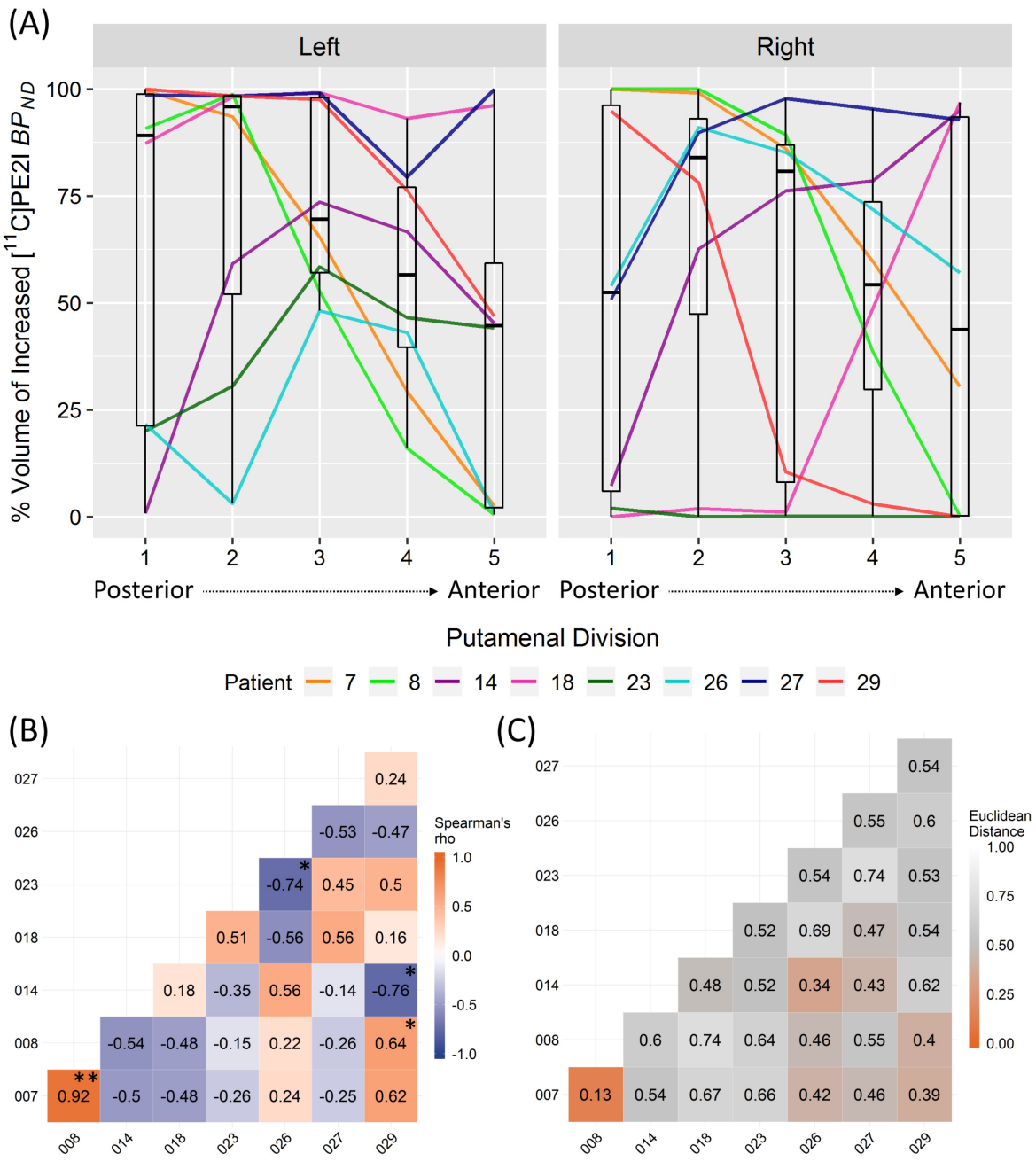


*Figure 3.13: Antero-posterior putamenal profiles for [¹¹C]PE2I. A | Antero-posterior spatial profiles generated for each participant showing the volume of each putamenal sub-region that exhibited a positive change in [¹¹C]PE2I BP_{ND} between pre-transplant and post-transplant time-points. Box and whisker plots represent the median and interquartile range. B | Spearman's rho correlation matrix showing correlations of antero-posterior spatial profiles (across both left and right putamen) between individual transplant patients. C | Double-scaled Euclidean distance matrix showing the similarity of antero-posterior spatial profiles (across both left and right putamen) between individual transplant patients. *p < 0.05, **Significant after Benjamini-Hochberg false discovery rate correction at threshold p < 0.05.*

Table 3.5: Putamenal volume showing post-operative increases in [^{11}C]PE2I. Table showing the total volume (mm^3) and volume exhibiting positive voxel values in Δ[^{11}C]PE2I BP_{ND} images for each putamenal sub-division along the antero-posterior axis for the left and right sides.

		Left Putamenal Division							Right Putamenal Division					
Patient	Volume (mm^3)	1	2	3	4	5	Whole		1	2	3	4	5	Whole
7	Positive	240	765	924	476	12	2417		247	734	1239	963	147	3330
	Total	241	818	1413	1628	479	4579		247	741	1440	1614	484	4526
8	Positive	198	743	750	270	2	1963		218	762	1293	634	1	2908
	Total	218	752	1424	1683	471	4548		218	762	1448	1645	480	4553
14	Positive	2	506	1054	1161	255	2978		19	569	1048	1256	537	3429
	Total	247	855	1433	1744	564	4843		263	910	1375	1601	565	4714
18	Positive	164	653	1273	1280	449	3819		0	13	13	686	466	1178
	Total	188	665	1284	1375	467	3979		217	684	1227	1408	481	4017
23	Positive	45	230	731	689	206	1901		4	0	2	1	0	7
	Total	225	754	1250	1481	467	4177		204	713	1324	1477	468	4186
26	Positive	48	22	666	725	5	1466		121	746	1241	1189	328	3625
	Total	222	711	1383	1684	556	4556		224	820	1458	1654	575	4731
27	Positive	264	843	1535	1506	600	4748		132	713	1608	1819	533	4805
	Total	268	857	1549	1897	600	5171		260	794	1645	1908	574	5181
29	Positive	184	709	1284	1126	210	3513		183	539	143	44	0	909
	Total	184	721	1316	1477	448	4146		193	690	1374	1468	477	4202

3.2.4. The relationship between AADC activity and DAT expression

One patient from the transplant group was identified as an outlier by means of normal QQ plots and Mahalanobis distance and was therefore removed from further analysis.

The base additive model was significant, with *group* and *Parkinsonian brain side* making significant explanatory contributions to the prediction of Δ[^{11}C]PE2I BP_{ND}, while a trend toward significance was detected for Δ[^{18}F]FDOPA K_i. The addition of an Δ[^{18}F]FDOPA K_i by *group* interaction term resulted in a significant improvement to the model fit (ESS = 0.858, $F(1, 41) = 17.421$, $p < 0.001$), with all terms except Δ[^{18}F]FDOPA K_i significant in contributing to an overall explained variance of 62% (Figure 3.14). The addition of 2nd and 3rd order interaction terms involving *Parkinsonian brain side* resulted in no significant improvement to the second model (ESS = 0.106, $F(3, 38) = 0.703$, $p = 0.556$) (Table 3.6). The regression equation for model 2 was:

$$\Delta[^{11}C]PE2I\ BP_{ND} = -0.31 - 10.885x_1 + 0.431x_2 + 0.164x_3 + 359.14x_1x_2 + \epsilon$$

, where x_1 is Δ[^{18}F]FDOPA K_i, x_2 is *group* identity with a dummy code of 0 for control and 1 for transplant groups and x_3 is *Parkinsonian brain side* with the least and most affected sides dummy coded as 0 and 1 respectively.

All assumptions for multiple linear regression were met apart from the distribution of residuals which was moderately leptokurtic and non-normal (Shapiro-Wilk, $p < 0.001$). We therefore conducted identical analysis after transforming Δ[^{11}C]PE2I BP_{ND} using a Lambert $W\ x\ F$ function estimated using the "LambertW" package (Goerg, 2016). The significance of parameter estimates were identical to the previous analysis therefore results pertaining to the untransformed values are reported. There was no significant improvement to any of the models by addition of mean-centred age, gender, disease duration or inter-scan interval.

Table 3.6: Relationship between cell survival and dopamine transporter expression. Hierarchical multiple linear regression analysis including the dependent variable Δ[11C]PE2I BP_{ND} and predictor variables Δ[18F]FDOPA K_i, group (transplant, control) and Parkinsonian brain side (least affected, most affected).

	Model Fit						Estimated Coefficients				
	F(3, 42)	p	R^2	$R^2_{Adjusted}$	RMSE	AIC	B	SE_B	β	t(42)	p
Additive Model	11.70	<0.001	0.455	0.416	0.250	13.022					
Intercept							-0.281	0.068	0.000	4.110	<0.001
Δ[18F]FDOPA K_i							85.710	46.357	0.221	1.849	0.072
Group							0.361	0.086	0.490	4.185	<0.001
Side							0.203	0.079	0.299	2.567	0.014
	F(4, 41)	p	R^2	$R^2_{Adjusted}$	RMSE	AIC	B	SE_B	β	t(41)	p
Model 2	16.56	<0.001	0.618	0.580	0.209	-1.267					
Intercept							-0.310	0.058	0.000	5.319	<0.001
Δ[18F]FDOPA K_i							-10.885	45.613	-0.028	0.239	0.813
Group							0.431	0.075	0.586	5.751	<0.001
Side							0.164	0.068	0.242	2.421	0.020
Δ[18F]FDOPA K_i * Group							359.140	86.045	0.482	4.174	<0.001
	F(7, 38)	p	R^2	$R^2_{Adjusted}$	RMSE	AIC	B	SE_B	β	t(38)	p
Model 3	9.557	<0.001	0.638	0.571	0.204	2.249					
Intercept							-0.284	0.068	0.000	4.155	<0.001
Δ[18F]FDOPA K_i							-15.542	62.582	-0.040	0.248	0.805
Group							0.332	0.137	0.451	2.420	0.020
Side							0.115	0.092	0.169	1.240	0.223
Δ[18F]FDOPA K_i * Group							349.412	207.394	0.469	1.685	0.100
Δ[18F]FDOPA K_i * Side							20.305	92.844	0.039	0.219	0.828
Group * Side							0.200	0.175	0.212	1.148	0.258

Δ[^{18}F]FDOPA K_i * Group * Side							-51.814	235.416	-0.059	0.220	0.827

AIC = Akaike information criterion

B = unstandardized regression coefficient

β = standardized coefficient

R^2 = coefficient of determination

$R^2_{Adjusted}$ = coefficient of determination adjusted for number of predictors

RMSE = root mean square error

SE_B = standard error of the coefficient

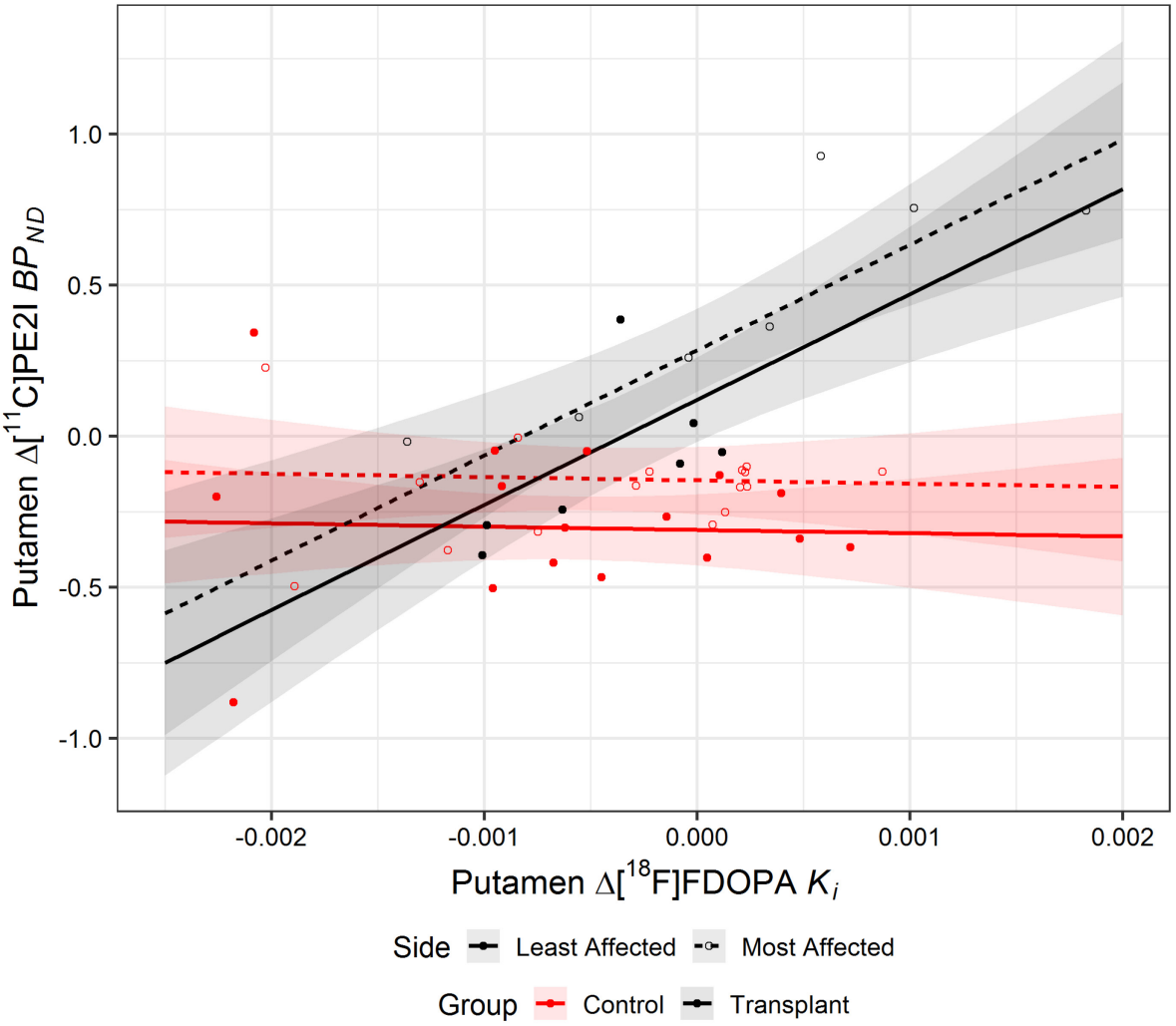


*Figure 3.14: Relationship between cell survival and dopamine transporter expression. Scatterplot showing results of the multiple linear regression analysis, illustrating that Δ[¹¹C]PE2I BP_{ND} can be predicted by Δ[¹⁸F]FDOPA K_i, group (transplant, control), Parkinsonian brain side (least affected, most affected) and the Δ[¹⁸F]FDOPA K_i * group interaction with 62% variance explained. Filled and hollow circles represent raw data for the least and most affected sides respectively for the transplant (black) and control (red) groups. Solid and dashed lines represent predicted values from the model for the least and most affected sides respectively. Shading represents 95% confidence intervals about the lines of best fit.*

3.2.5. Graft SERT Expression: [^{11}C]DASB

3.2.5.1. Regional within-group ANCOVA

A 3-way repeated measures analysis of covariance was carried out including all bilaterally transplanted patients who completed 3 [^{11}C]DASB scans (n = 8), in order to examine whether differences in mean striatal [^{11}C]DASB BP_{ND} values depended on *visit* (baseline, pre-transplant, post-transplant), striatal *region* (putamen, caudate) and *brain side* (right, left).

Assessment of QQ plots and histograms suggested that residuals were moderately leptokurtic, with Shapiro-Wilk test confirming departure from normality ($p < 0.001$). Data were therefore transformed using the Box-Cox procedure ($\lambda = 0.23$), which substantially reduced kurtosis and enabled conformation to a normal distribution.

Results revealed a significant *region* by *visit* interaction ($F(1.10, 5.49) = 25.77$, $p = 0.003$ [Greenhouse-Geisser corrected]), indicating that differences in [^{11}C]DASB BP_{ND} over time were dependent on *region* (Figure 3.15). Post-hoc Tukey-adjusted pairwise comparisons of the estimated marginal means revealed significantly greater [^{11}C]DASB BP_{ND} in the putamen as compared to the caudate at baseline ($\Delta Mean_{EM} = 0.729$, *95% CI* [0.398, 1.061], $p < 0.001$), pre-transplant ($\Delta Mean_{EM} = 0.757$, *95% CI* [0.426, 1.088], $p < 0.001$) and post-transplant ($\Delta Mean_{EM} = 1.469$, *95% CI* [1.138, 1.800], $p < 0.001$) visits. There were also significant pairwise differences over time whereby caudate [^{11}C]DASB BP_{ND} was significantly decreased at the post-transplant visit as compared to baseline ($\Delta Mean_{EM} = -0.544$, *95% CI* [-0.956, -0.132], $p = 0.008$) and pre-transplant ($\Delta Mean_{EM} = 0.509$, *95% CI* [-0.921, -0.097], $p = 0.013$), while in the putamen there was no change at post-transplant as compared to baseline ($\Delta Mean_{EM} = 0.195$, *95% CI* [-0.217, 0.607], $p = 0.583$) or pre-transplant ($\Delta Mean_{EM} = 0.203$, *95% CI* [-0.209, 0.615], $p = 0.548$).

There was no effect of *brain side* on the interaction between *region* and *visit* ($F(1.06, 5.32) = 0.15$, $p = 0.723$ [Greenhouse-Geisser corrected]). Additionally, there were no significant interactions between *visit* and *brain side* ($F(1.06, 5.32) = 0.63$, $p = 0.466$ [Greenhouse-Geisser corrected]) or *region* and *brain side* ($F(1, 5) = 0.001$, $p = 0.973$).

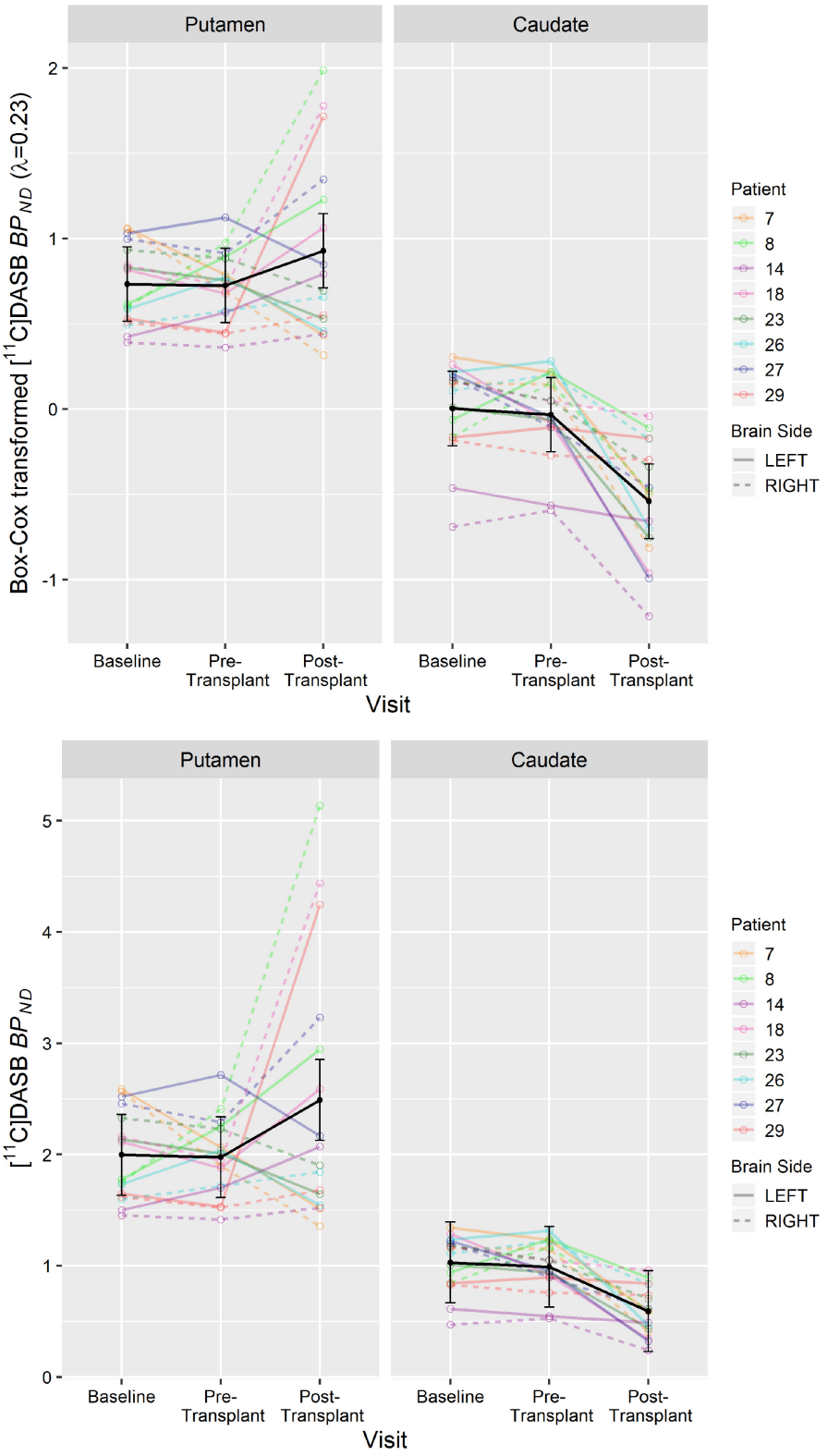


Figure 3.15: Within-group ANCOVA for [11C]DASB. Change in mean Box-Cox transformed (λ = 0.23) [11C]DASB BP_{ND} over time in striatal nuclei of Parkinson's disease patients who have received intraputamenal transplants of fetal ventral mesencephalic tissue (n = 8) (top plot). Strip plots illustrate a 2-way interaction between region (putamen, caudate) and visit (baseline, pre-transplant, post-transplant) when data were collapsed across brain side (right, left) and adjusting for mean-centred age and disease

duration at baseline. Non-transformed data are also displayed (bottom plot). Patients included in this analysis are displayed in separate colours and with differentiation between left and right brain sides (solid and dashed lines respectively). Solid black lines and error bars represent estimated marginal means and individual 95% confidence intervals respectively.

3.2.5.2. Regional between-group mixed ANCOVA

A 3-way mixed analysis of covariance with repeated measures was carried out including all bilaterally transplanted patients (n = 8) and control patients (n = 14) who completed 2 [^{11}C]DASB scans, in order to examine whether differences in mean putamenal [^{11}C]DASB BP_{ND} values depended on *group* (transplant, control), *visit* (pre-transplant/baseline and post-transplant/18-month follow-up for transplant/control groups respectively) and *Parkinsonian brain side* (most affected, least affected).

Results revealed a significant *group* by *visit* interaction (F(1, 18) = 5.47, p = 0.031), indicating that differences in [^{11}C]DASB BP_{ND} over time were dependent on *group* (Figure 3.16). Post-hoc Tukey-adjusted pairwise comparisons of the estimated marginal means revealed that this interaction was driven by a significant increase in [^{11}C]DASB BP_{ND} at post-transplant as compared to pre-transplant for the transplant group ($\Delta Mean_{EM}$ = 0.666, *95% CI* [0.001, 1.331], p = 0.049), with no significant change in the control group over the same period ($\Delta Mean_{EM}$ = -0.0993, *95% CI* [-0.583, 0.385], p = 0.897). In addition, while mean [^{11}C]DASB BP_{ND} was not different between groups at baseline/pre-transplant ($\Delta Mean_{EM}$ = 0.055, *95% CI* [-0.686, 0.796], p = 0.991), it was found to be significantly greater in the transplant group at post-transplant as compared to the control group at 18-month follow-up ($\Delta Mean_{EM}$ = 0.821, *95% CI* [0.079, 1.562], p = 0.027).

There was no effect of *Parkinsonian brain side* on the interaction between *group* and *visit* (F(1, 18) = 3.30, p = 0.086). Additionally, there were no significant interactions between *visit* and *Parkinsonian brain side* (F(1, 18) = 2.69, p = 0.119) or *group* and *Parkinsonian brain side* (F(1, 18) = 0.51, p = 0.484).

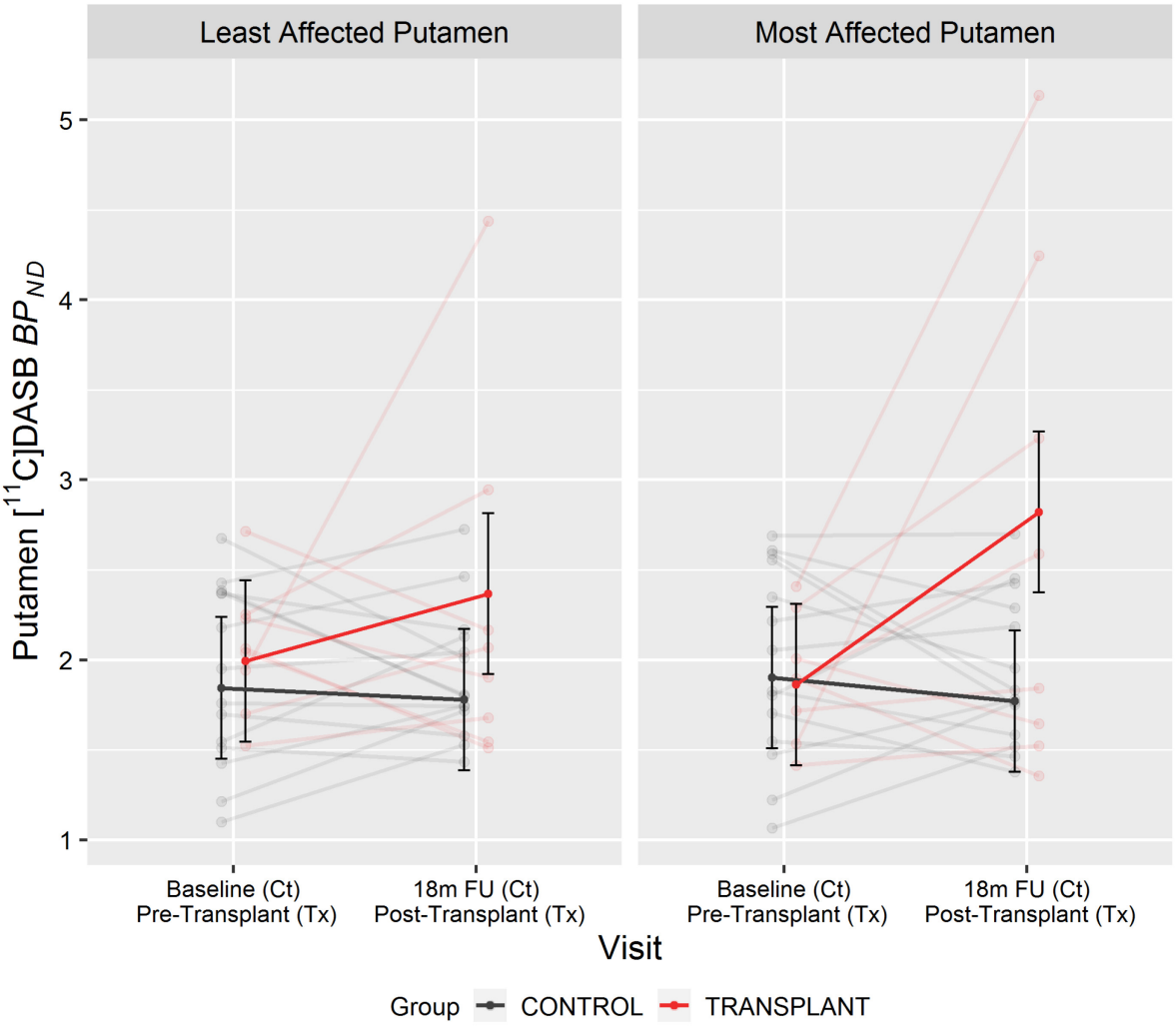


Figure 3.16: Between-group ANCOVA for [11C]DASB. Change in mean [11C]DASB BP_{ND} over time in the putamen of Parkinson's disease patients who have received intraputamenal transplants of fetal ventral mesencephalic tissue (Tx, n = 8) and Parkinson's disease patients who have not received transplant (Ct, n = 14). Strip plots illustrate results of a 3-way interaction analysis between group (transplant, control), visit (pre-transplant/baseline & post-transplant/18-month follow-up for transplant/control groups respectively) and Parkinsonian brain side (most affected, least affected), adjusting for mean-centred age and disease duration at baseline. ANCOVA revealed a significant 2-way interaction between group and visit after data were collapsed across Parkinsonian brain side. Solid black and red lines and associated error bars represent estimated marginal means and individual 95% confidence intervals for the control and transplant groups respectively. FU = follow-up.

3.2.5.3. Longitudinal voxelwise analysis

Voxelwise analysis was conducted using images collected at pre-transplant and post-transplant time points for the transplant group only, to identify sub-regions of the striatum showing a significant change in [^{11}C]DASB BP_{ND}. No significant clusters survived after family-wise error correction at $P_{FWE} < 0.05$, or at an uncorrected peak threshold of $P < 0.001$. After relaxing the threshold to uncorrected $P < 0.05$, clusters exhibiting increased [^{11}C]DASB BP_{ND} at post-transplant were identified in the left and right putamen. Clusters showing a decrease at post-transplant were seen in the left and right caudate and in the right putamen bordering on the right nucleus accumbens (Figure 3.17, Table 3.7).

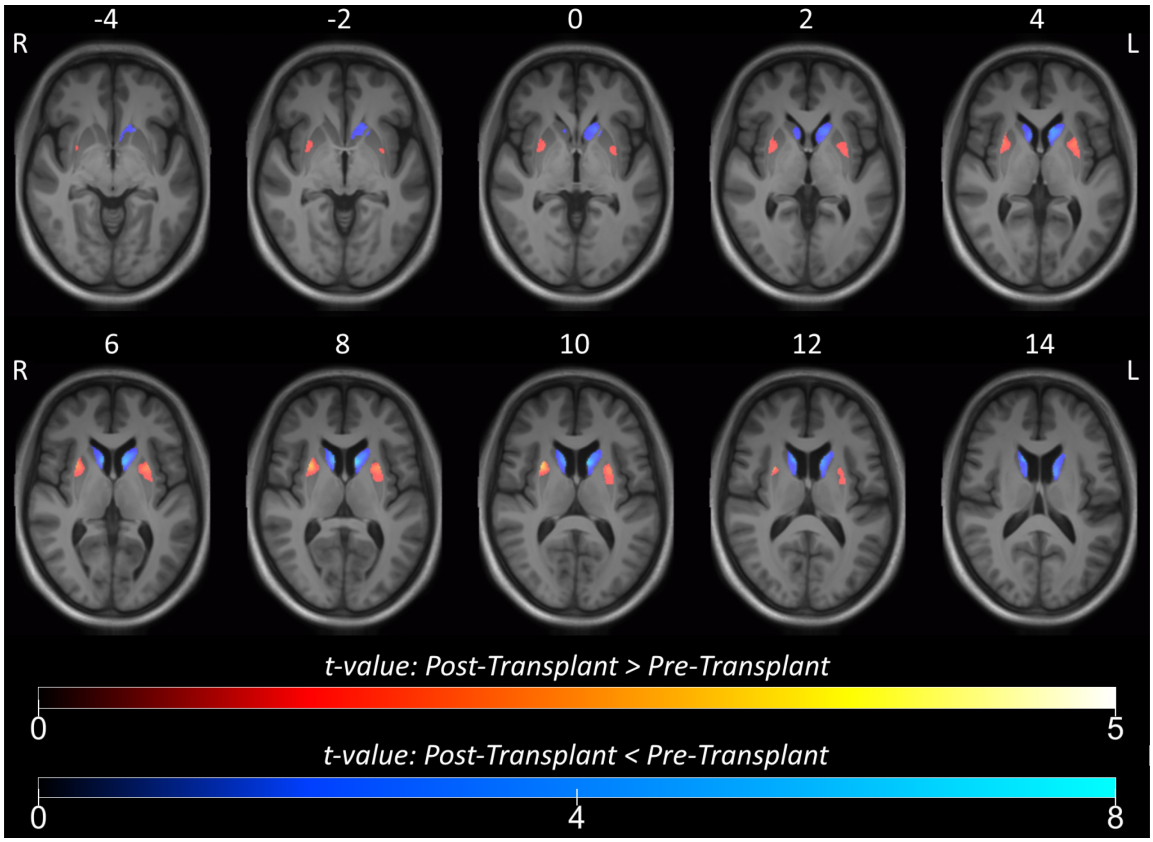


Figure 3.17: Voxelwise analysis of post-transplant changes in [^{11}C]DASB. Statistical parametric maps showing results of the voxelwise paired t-test comparing pre-transplant to post-transplant [^{11}C]DASB BP_{ND} parametric images for bilaterally transplanted Parkinson's disease patients (n = 8). Voxelwise statistics were restricted to the striatum and are overlaid onto the study-specific template generated using DARTEL after thresholding at uncorrected p < 0.05.

Table 3.7: Results of the voxelwise paired t-test comparing pre-transplant to post-transplant [^{11}C]DASB BP_{ND} parametric images for bilaterally transplanted Parkinson's disease patients (n = 8). MNI co-ordinates refer to the peak voxel within each cluster after thresholding at uncorrected $p < 0.05$ and their anatomical location is reported with reference to the Harvard-Oxford subcortical structural atlas.

Contrast	Region	MNI Co-ordinates	k	t-value
Post-Transplant > Pre-Transplant	Right Putamen	29 8 7	915	3.36
	Left Putamen	-27 7 5	1123	2.81
Post-Transplant < Pre-Transplant	Left Caudate	-7 11 7	3085	7.25
	Right Caudate	16 13 14	1301	6.4
	Right Caudate	21 -10 24	16	2.99
	Right Caudate	15 -5 17	32	2.66
	Right Putamen / Nucleus Accumbens	14 5 -15	4	1.93

The whole-brain spatial extent of the change in striatal [^{11}C]DASB BP_{ND} over time was also visualised by creating parametric delta images (i.e. subtracting pre-transplant from post-transplant) in $MPRAGE_{REG}$ space for each individual patient who underwent transplant (Figure 3.18) (Figure 3.19).

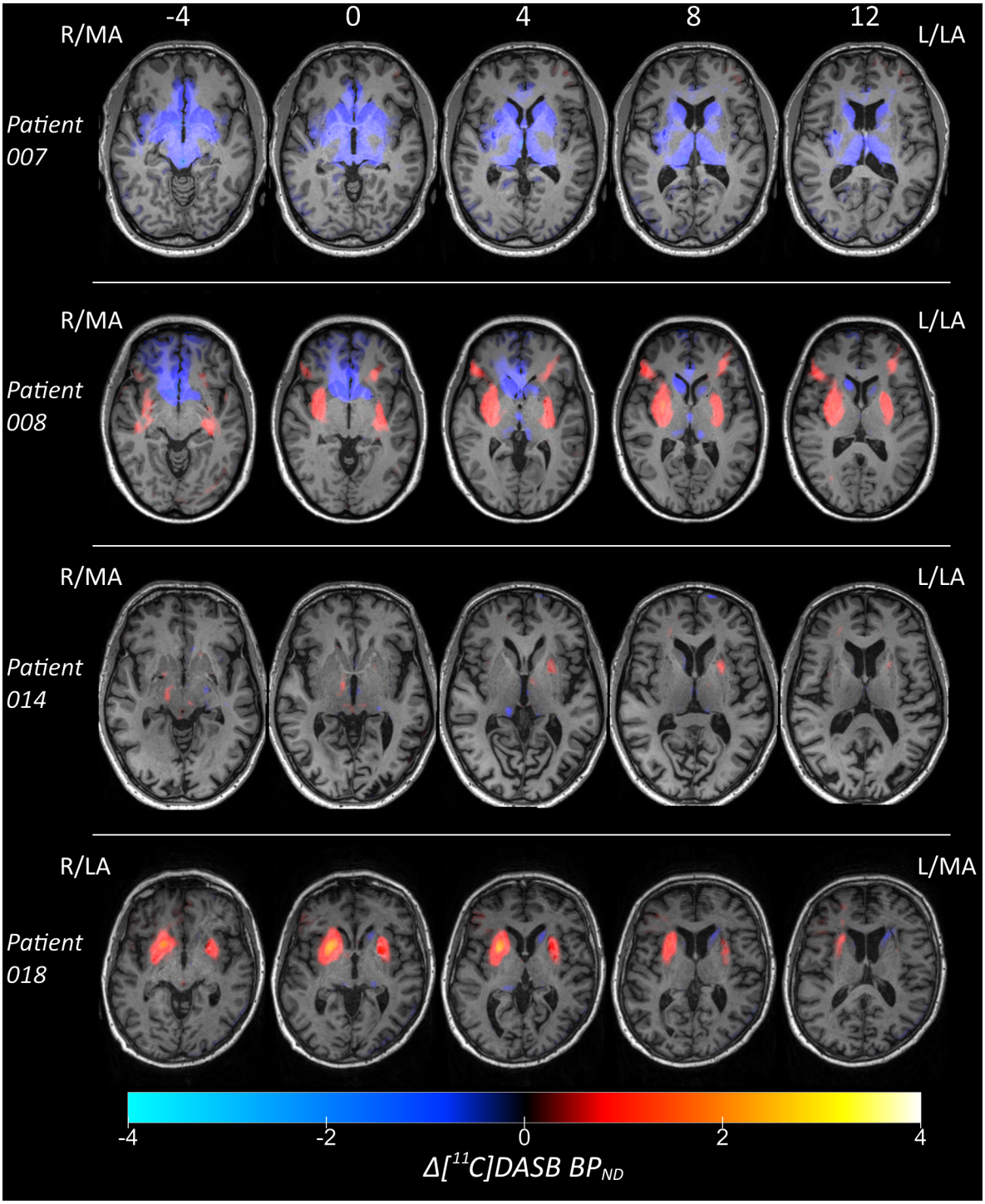


Figure 3.18: Post-operative [11C]DASB changes for patients 007, 008, 014 and 018. [11C]DASB BP_{ND} difference (Δ) images were derived by subtracting pre-transplant parametric images from post-transplant parametric images, overlaid onto post-transplant $MPRAGE_{REG}$ scans and displayed at 5 axial levels of the striatum. LA = least affected; MA = most affected.

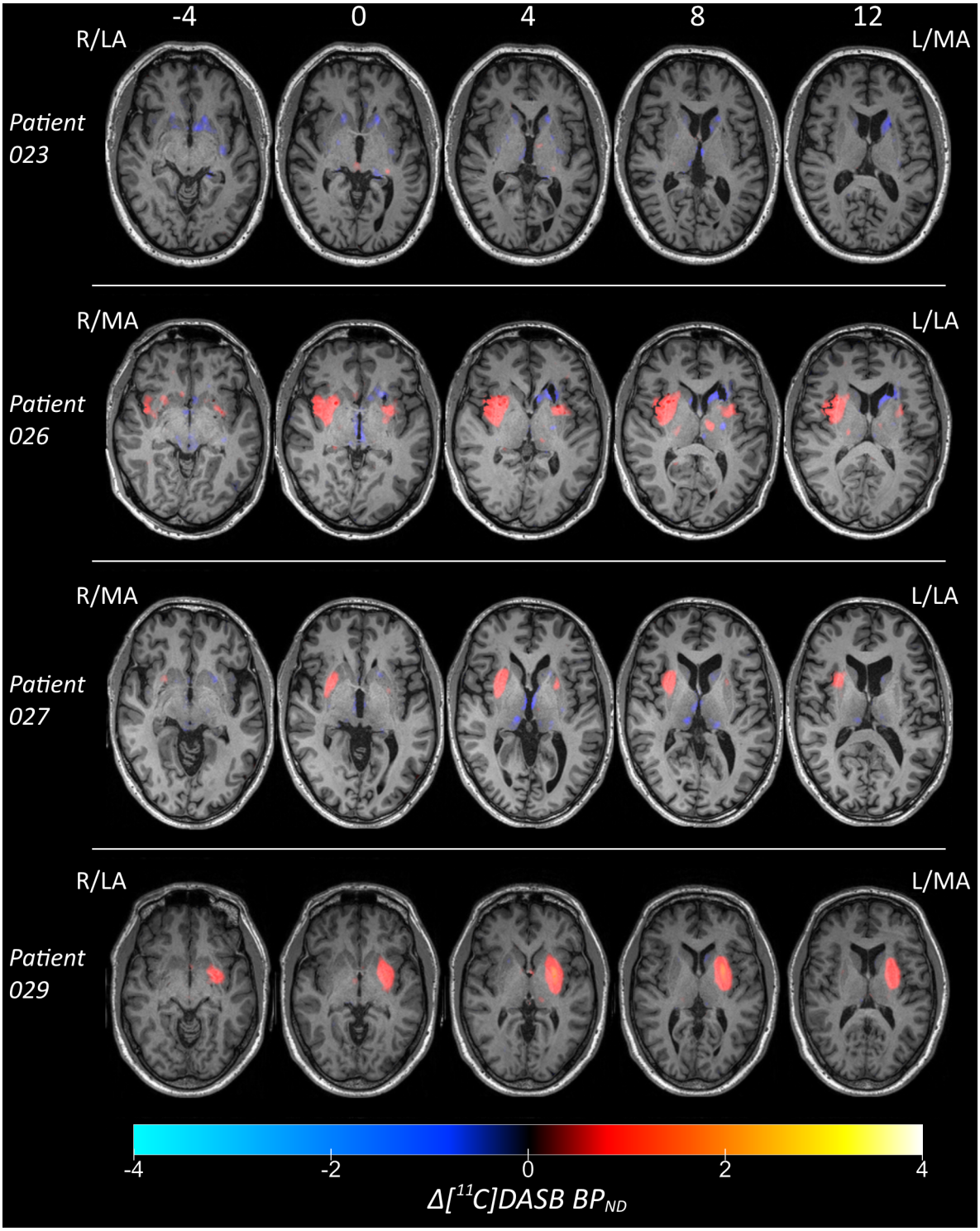


Figure 3.19: Post-operative [11C]DASB changes for patients 023, 026, 027 and 029. [11C]DASB BP_{ND} difference (Δ) images were derived by subtracting pre-transplant parametric images from post-transplant parametric images, overlaid onto post-transplant $MPRAGE_{REG}$ scans and displayed at 5 axial levels of the striatum. LA = least affected; MA = most affected.

3.2.5.4. Putamenal coverage

Data showing volume (mm^3) coverage of increased [^{11}C]DASB binding for the whole putamen as well as its anterior-posterior divisions is shown in Table 3.8. On average, the volume of the whole putamen that showed a positive change at post-transplant was 61.63 ±37.02% in the left and 65.09 ±39.35% in the right.

Non-parametric Friedman's test showed that there was no statistical difference between putamenal divisions when all divisions for both sides were included ($\chi^2(9) = 14.36$, $p = 0.110$). However, when left and right putamen were examined separately, there was a significant difference between putamenal divisions on the left ($\chi^2(4) = 11.58$, $p = 0.021$), but not the right ($\chi^2(4) = 5.06$, $p = 0.281$) (Figure 3.20). Post-hoc Dunn-Bonferroni tests showed that a pairwise difference was found between Divisions 3 and 5 ($p = 0.044$) after Bonferroni adjustment.

Plots of the anterior-posterior coverage profiles suggest high variation between individuals. Spearman's rho correlations support this observation, showing a range of both positive and negative coefficients between patient profiles with only patients 026 and 027 surpassing the threshold for a significant positive correlation (Benjamini-Hochberg corrected). Euclidean distance measures are also in line with this, showing low dissimilarity between patients 026 and 027 as well as lower dissimilarity between patients 007 and 023. However, there was generally high dissimilarity between all other patient pairs.

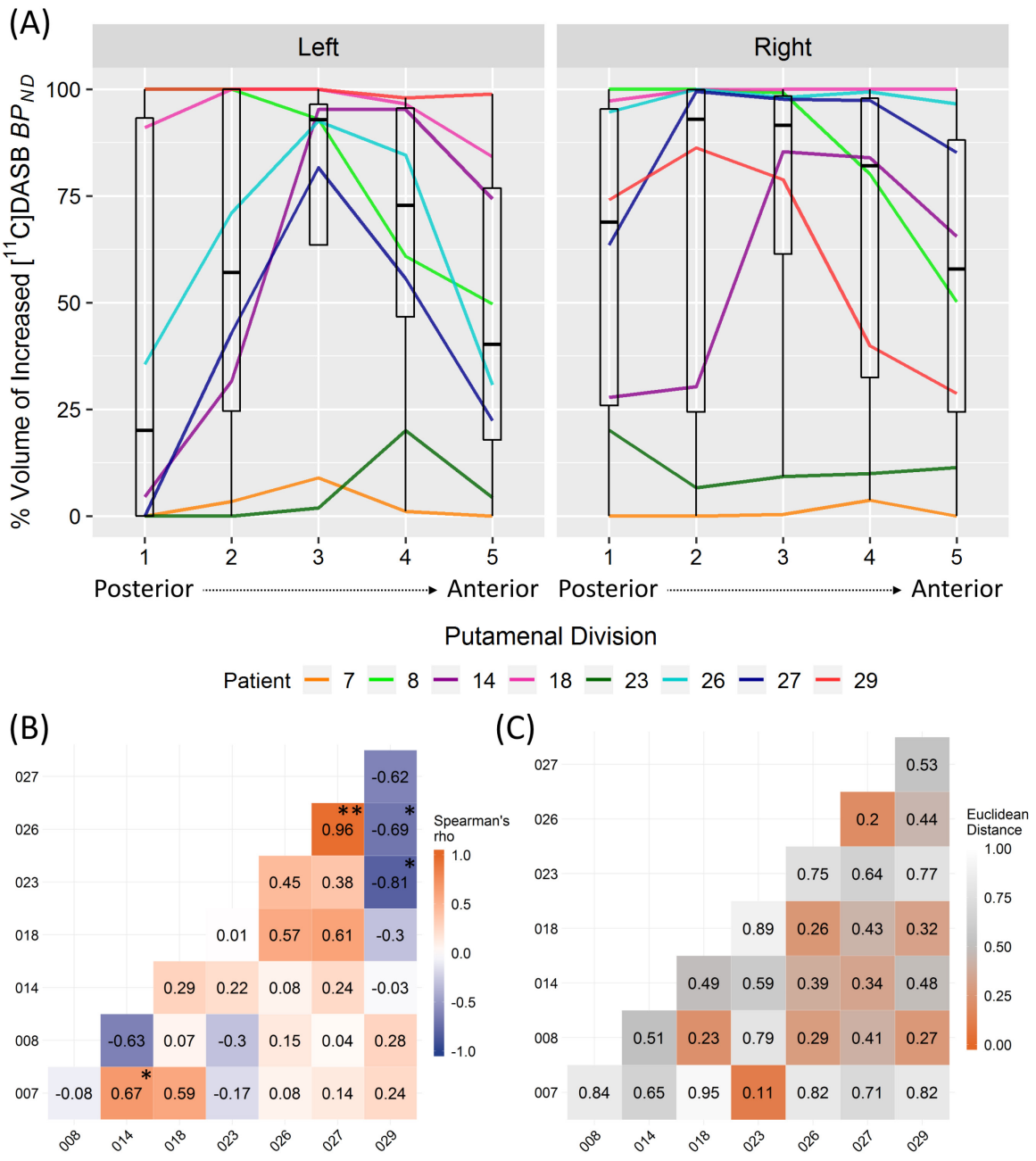


*Figure 3.20: Antero-posterior putamenal profiles for [11C]DASB. A | Antero-posterior spatial profiles generated for each participant showing the volume of each putamenal sub-region that exhibited a positive change in [11C]DASB BPND between pre-transplant and post-transplant time-points. Box and whisker plots represent the median and interquartile range. B | Spearman's rho correlation matrix showing correlations of antero-posterior spatial profiles (across both left and right putamen) between individual transplant patients. C | Double-scaled Euclidean distance matrix showing the similarity of antero-posterior spatial profiles (across both left and right putamen) between individual transplant patients. *p < 0.05, **Significant after Benjamini-Hochberg false discovery rate correction at threshold p < 0.05.*

Table 3.8: Putamenal volume showing post-operative increases in [^{11}C]DASB. Table showing the total volume (mm^3) and volume exhibiting positive voxel values in Δ[^{11}C]DASB BP_{ND} images for each putamenal sub-division along the antero-posterior axis for the left and right sides.

		Left Putamenal Division							Right Putamenal Division					
Patient	Volume (mm^3)	1	2	3	4	5	Whole		1	2	3	4	5	Whole
7	Positive	0	28	126	18	0	172		0	0	5	60	0	65
	Total	241	818	1413	1628	479	4579		247	741	1440	1614	484	4526
8	Positive	218	752	1325	1024	234	3553		218	762	1436	1317	241	3974
	Total	218	752	1424	1683	471	4548		218	762	1448	1645	480	4553
14	Positive	11	270	1364	1661	419	3725		73	276	1174	1344	370	3237
	Total	247	855	1433	1744	564	4843		263	910	1375	1601	565	4714
18	Positive	171	665	1284	1328	393	3841		211	683	1227	1408	481	4010
	Total	188	665	1284	1375	467	3979		217	684	1227	1408	481	4017
23	Positive	0	0	24	297	20	341		41	47	122	147	53	410
	Total	225	754	1250	1481	467	4177		204	713	1324	1477	468	4186
26	Positive	79	505	1279	1424	171	3458		212	820	1430	1644	555	4661
	Total	222	711	1383	1684	556	4556		224	820	1458	1654	575	4731
27	Positive	0	368	1264	1054	134	2820		165	790	1606	1857	489	4907
	Total	268	857	1549	1897	600	5171		260	794	1645	1908	574	5181
29	Positive	184	721	1316	1447	443	4111		143	595	1082	586	137	2543
	Total	184	721	1316	1477	448	4146		193	690	1374	1468	477	4202

3.3. Discussion

In this chapter, we assessed the dopaminergic and serotonergic outcomes of hfVM transplantation under the Transeuro protocol at 18 months using [^{18}F]FDOPA, [^{11}C]PE2I and [^{11}C]DASB PET. We found that putamenal dopamine synthesis and storage capacity was significantly increased in patients receiving hfVM transplantation as compared to those on optimal drug therapy whose dopaminergic dysfunction continued to worsen. This effect was also found when comparing putamenal AADC activity to that within the caudate nucleus in the same individuals, which appeared to sustain greater loss over the therapeutic as opposed to pre-transplant intervals, suggesting that in contrast to some previous reports (Lindvall *et al.*, 1990; Freed *et al.*, 1992; Spencer *et al.*, 1992; Peschanski *et al.*, 1994; Kordower *et al.*, 1995; Wenning *et al.*, 1997), at this early stage grafted hfVM cells are unable to re-innervate or induce sprouting and/or upregulation in the host neurons of non-targeted regions. The magnitude of this increase across the whole putamen was however only +6.8% from the pre-transplant time-point (-10.6% for non-transplanted PD), which falls a long way short of those reported in prior trials (see Appendix), and even of those values obtained in the Tampa (Olanow *et al.*, 2003) and Denver/New York (Freed *et al.*, 2001) randomised controlled trials whose outcomes were considered disappointing. Although we were not able to acquire data for healthy subjects, random-effects meta-analysis across [^{18}F]FDOPA studies using similar quantification methods estimates normal putamenal K_i values of 0.0113 [*95% CI*; 0.0103, 0.0123], thus putamenal AADC activity in our transplant group increased from 45% to 48% of normative levels while decreasing from 42% to 38% in non-transplanted PD controls.

We also found similar graft-related increases in putamenal DAT density in the transplanted patients (+13.7%) as compared to non-transplanted PD patients (-15.4%) as well as the caudate (-23.8%) within the same individuals. Furthermore, the magnitude of changes in DAT density across the scanning interval was positively related to the changes in [^{18}F]FDOPA influx over the same period. Because the slope describing this relationship was markedly different from the one characterising our PD control group, in which decreases in DAT density were relatively constant at widely varying changes in AADC activity, we believe it reflects the capability for surviving grafted neurons to express the dopamine

transporter and retain their dopaminergic phenotype within the host environment, without full subjection to the compensatory plasticity inherent within endogenous dopaminergic neurons (Tedroff *et al.*, 1999; Lee *et al.*, 2000; Ribeiro *et al.*, 2002; Adams *et al.*, 2005; Bruck *et al.*, 2006; Moore *et al.*, 2008; Nandhagopal *et al.*, 2009; Nandhagopal *et al.*, 2011; Pavese *et al.*, 2011).

Earlier studies have reported variable findings with respect to DAT expression. For instance, Cochen *et al.* (2003) employing a similar correlational analysis found no relationship between changes in [^{18}F]FDOPA uptake and [^{76}Br]FE-CBT binding in the putamina of six patients after transplantation with fewer donors (1-3 hfVM per putamen) and via three, as opposed to five, needle trajectories (Cochen *et al.*, 2003). This inconsistency in the literature is not easily reconcilable and may be due to a number of factors relating to the dissection, pre-treatment or viability of grafted tissue, as well as the surgical procedure and immunosuppressive regime. However, that [^{18}F]FDOPA uptake was increased by a greater magnitude in their patients suggests that at least it cannot be due to sub-optimal cell survival. Preclinical work in rodents shows that the expression of DAT appears to be developmentally protracted (Galineau *et al.*, 2004; Green *et al.*, 2019). Indeed, no significant increase in [^{76}Br]FE-CBT binding was found in the Paris cohort when including patients as early as 6 months post-transplant (Cochen *et al.*, 2003), and in one Lund case [^{18}F]FDOPA increased while [^{11}C]nomifensine binding decreased from 5 to 12 months (Hoffer *et al.*, 1992) despite post-mortem examination at 22 years demonstrating some, albeit light and patchy, DAT immunoreactivity (Kurowska *et al.*, 2011). Thus it seems conceivable that the correspondence between dopaminergic markers appears as a function of maturational stage. The propensity for young implanted neurons to conform to a PD-like profile including a down-regulation of DAT density (Tedroff *et al.*, 1999; Lee *et al.*, 2000; Ribeiro *et al.*, 2002; Adams *et al.*, 2005; Bruck *et al.*, 2006; Moore *et al.*, 2008; Nandhagopal *et al.*, 2009; Nandhagopal *et al.*, 2011; Pavese *et al.*, 2011), as suggested by some long-term imaging (Politis *et al.*, 2011) and post-mortem (Kordower *et al.*, 2008a; Kordower *et al.*, 2008b; Kurowska *et al.*, 2011) data, must also be considered as a potential factor underlying variations in DAT expression on surviving cells.

Interestingly, while we found no effect of the order in which transplantation was conducted between hemispheres, supporting preclinical work (Duan *et al.*, 1993), we did find a significant effect of Parkinsonian side for [^{11}C]PE2I BP_{ND}, in which the most depleted putamen showed a more pronounced response to treatment than did the least affected putamen. At this stage of illness, we would expect the host neurons of the least affected side to degenerate more rapidly (Nandhagopal *et al.*, 2009) (~40% difference within the pre-transplant interval), which might result in a more prominent negation of any elevations resulting from the graft, however the inclusion of the non-transplanted group in the statistical design means this is unlikely the sole cause. Only one study has previously drawn attention to this effect; Brundin *et al.* (2000) commented in their discussion of five bilaterally implanted patients that four exhibited a side bias in [^{18}F]FDOPA increases favouring the most affected putamen (Brundin *et al.*, 2000). This is surprising, given that upon review, the majority of imaging and post-mortem studies in which laterality data were reported (or are reported elsewhere) appear to be well in line with our findings (Freed *et al.*, 1992; Freeman *et al.*, 1995; Kordower *et al.*, 1996; Kordower *et al.*, 1998; Brundin *et al.*, 2000; Mendez *et al.*, 2005; Pogarell *et al.*, 2006), thus posing the question as to whether prior denervation influences subsequent graft function. If this is the case, we might expect pre-transplant dopaminergic PET values to be associated with graft-induced changes measured at post-transplant. Indeed, *post-hoc* analysis shows moderate negative correlations between pre-transplant [^{11}C]PE2I BP_{ND} and Δ[^{11}C]PE2I BP_{ND} (r = -0.475, p = 0.037, df = 13) in transplanted putamina after controlling for inter-scan interval.

It is important to note that although an analogous correlation was also found for [^{18}F]FDOPA K_i (r = -0.448, p = 0.047, df = 13), the effect of Parkinsonian side was not as pronounced for this measure. One possible explanation for this discordance may be related to the rather ubiquitous expression of the AADC enzyme across monoaminergic systems, including the serotonergic population (Zhu and Juorio, 1995; Ugrumov, 2009) which constitutes a relatively high proportion of cells within the striatum (Ginovart *et al.*, 2001; Ichise *et al.*, 2003; Kish *et al.*, 2005; Kish *et al.*, 2008; Miguelez *et al.*, 2014). In these neurons, AADC primarily facilitates the biosynthesis of serotonin from 5-hydroxytryptophan, but their potential to also take up and decarboxylate exogenous L-dopa to dopamine for vesicular packing and subsequent ectopic release has been demonstrated and is especially

notable under conditions of extensive nigrostriatal damage (Maeda *et al.*, 2005; Carta *et al.*, 2007; Navailles *et al.*, 2010). Indeed, several *in vivo* studies support the utility of [^{18}F]FDOPA for imaging non-dopaminergic systems in regions where neuronal composition is known (Brown *et al.*, 1999; Rakshi *et al.*, 1999; Moore *et al.*, 2003; Moore *et al.*, 2008; Pavese *et al.*, 2011; Pavese *et al.*, 2012). Thus as opposed to [^{11}C]PE2I BP_{ND}, which has consistently been demonstrated to be highly selective for the dopamine as compared to serotonin transporters (Emond *et al.*, 1997; Guilloteau *et al.*, 1998; Hall *et al.*, 1999; Halldin *et al.*, 2003), [^{18}F]FDOPA K_i values are influenced to some degree by serotonergic contributions to the overall signal. That some research reports symmetric raphe-striatal denervation in PD contrasting to the imbalance observed for the nigrostriatal system (Albin *et al.*, 2008), which is also apparent in our [^{11}C]DASB data, confounds the interpretation further, particularly with respect to lateralisation effects.

However, supporting evidence for an apparent disparity in graft behaviour with respect to neurodegenerative severity has been reported in an early study using [^{3}H]dopamine autoradiography and TH-immunocytochemistry in unilaterally lesioned 6-OHDA rats; no difference in cell survival or graft size was found between the intact and denerved striata following bilateral fVM implants, however the denerved side exhibited significantly larger TH+ cell bodies and the fiber outgrowth from the graft site was approximately 2-fold greater as compared to the non-denerved side (Doucet *et al.*, 1990). Similarly, in a human case with 18-month old grafts the extent of neuritic outgrowth was estimated to cover 53.5% of the most denerved posterior putamen but only 23.8% in the opposite more preserved side (Kordower *et al.*, 1996). Incidentally, if intrinsic denervation is inversely related to subsequent graft function, this might explain why our *in vivo* estimates of dopaminergic re-innervation are comparatively low, since our patients were recruited at a milder stage of illness than those entered into previous trials. Further preclinical work may be needed to elucidate the underlying mechanisms governing these host-graft interactions, although if they go beyond structural disposition then the current models that do not fully emulate the true disease process may only garner partial explanations.

With regards to our 2nd hypothesis, we found that intraputamenal grafting under the current protocol, despite avid awareness of the potential implications of "hot-spot" delivery (Ma *et*

al., 2002; Piccini *et al.*, 2005; Ma *et al.*, 2010) and considered modification of surgical procedure conforming to a more efficacious multi-micrograft approach (Nikkhah *et al.*, 1994; Maries *et al.*, 2006), including increasing the number of trajectories and deposit sites on needle withdrawal, was unsuccessful at providing homogenous re-innervation across the target nuclei. This was determined by voxel-wise comparison of parametric images, in which graft-related changes appeared localised to discrete clusters even at very lenient statistical thresholds, and by comparing the anterior-posterior putamenal profiles of "positive" imaging changes across the therapeutic interval for similarity between patients. Although at the time of writing we have not had access to cell data, our results are unlikely to be explained by differences in the cell volume, number of donors or cell viability, because for each putamen the tissue used for all needle passes was drawn from the same single composite batch, made up of 3-5 hfVMs. We also do not believe that this could be explained by PD-related local differences in the nuclear microenvironment because if this were the case we would expect patient profiles to be correlated. In contrast, profiles appeared sporadic with very little similarity between patients and in fact many pairs exhibited inverse re-innervation patterns. Similar irregularity between graft sites has previously been observed by TH+ immunostaining 18 months post-transplant (Kordower *et al.*, 1996; Kordower *et al.*, 1998). These findings are highly relevant for all future therapies involving invasive cell deposition since it implies that the surgical procedure may be sub-optimal and that it may require substantial revision. It remains entirely possible however, that grafted neurons may indeed have been evenly distributed and that our results are conflated by the continued neurodegeneration of endogenous neurons. This might be the case precisely because the extensive coverage calls for substantial division of the tissue samples, such that each individual deposit may contain lower cell numbers than those administered in previous trials. Thus on this matter it might be more informative to evaluate outcomes at a later time-point after embryonic neurons are given time to mature within the host. Additionally, the coverage profiles generated should be cautiously interpreted, as they are probably underestimated by virtue of our zero-point cut-off and likely biased by the smoothing applied as part of the image reconstruction protocol.

We also found evidence for an increase in serotonin transporter density within the transplanted putamina at eighteen months, consistent with previous long-term *in vivo*

(Politis *et al.*, 2010b; Politis *et al.*, 2011) and post-mortem (Mendez *et al.*, 2008) reports illustrating the presence of serotonergic neurons in the hfVM tissue and their subsequent growth within the host. Compared to our non-transplanted group, who showed virtually no decrease in [^{11}]DASB binding potential over 18 months, the transplanted patients showed a mean increase of ~26% from the pre-transplant time-point. Although not directly comparable, the magnitude of this increase appears to be substantially less than the +106-285% previously reported (Politis *et al.*, 2010b; Politis *et al.*, 2011), suggesting that the dissection technique employed for this trial successfully abated serotonergic contamination of the final tissue samples. However, imaging of those patients was conducted over 10 years after transplant and their selection was based on the appearance of GID, for which graft-derived serotonergic hyperinnervation was hypothesised. Regarding the latter, analyses reported in Chapter 5 of this thesis does not support a serotonergic basis for GID in our cohort and as such we discount selection bias as a potential differential factor. Continued cell maturation beyond 18 months does however remain possible.

Interestingly, we also found that as putamenal serotonin transporter increased, there was a substantial decrease in the non-transplanted caudate by ~40% across the therapeutic interval, while no significant change was found across the pre-transplant interval. Similarly, no changes in caudate values were found for the PD control group between baseline and 18-month follow-up (data not shown). We do not believe that this is due to misplacement of ROIs toward the ventricular space or image misregistration as the patterns exhibited comparatively little variation between subjects. Given that we did not acquire imaging measures for the PD control group at a third matched time-point, we are unable to discount the possibility that this decrease is due to the natural progression of illness. To our knowledge there are currently no longitudinal studies modelling the trajectories of serotonin markers within striatal sub-divisions, although imaging and *ex vivo* biochemical experiments suggest that it is comparatively slow and is preferential for the caudate (Kish *et al.*, 2008; Maillet *et al.*, 2016; Fazio *et al.*, 2020). Additionally, the lack of healthy control scans means that we are unable to formally compare progression slopes between tracers, thus it also remains possible that the magnitude of this decrease is equivalent across dopaminergic and serotonergic systems. These limitations highlight the importance and impact of trial design on the interpretability of novel results. There is some evidence from other fields of research

demonstrating down-regulation of serotonin transporter mRNA and neuronal death in regions adjacent to cortical contusion, however this has mainly been observed in models of blast-induced traumatic cortical tissue damage (Abe *et al.*, 2016; Kajstura *et al.*, 2018) and in humans sudden torque or impact injury has also been shown to significantly down-regulate caudatal dopamine transporters (Jenkins *et al.*, 2018). Moreover, in models of superficial stab injury, severed serotonergic neurons exhibit regrowth as early as 1 week following insult and are capable of traversing the stab rift (Jin *et al.*, 2016), thus even in the scenario where needle trajectories passing the caudate nucleus selectively damage serotonergic projections the effects may only be transient. Similarly, immune system response would be expected to impact upon multiple neurotransmitter systems (Miller *et al.*, 2013), and when reactive microglia and immunogenic markers were detected at post-mortem they were largely restricted to the graft sites (Kordower *et al.*, 1996; Mendez *et al.*, 2005; Kordower *et al.*, 2008a). Conversely, chronic administration of corticosteroids (e.g. prednisolone) can influence some aspects of serotonergic system function, including regulation of gene expression relating to tryptophan metabolism (Regan *et al.*, 2018), and may cause desensitisation of 5-HT_{1A} auto-receptors (Karten *et al.*, 1999; Fairchild *et al.*, 2003) and reductions in SERT density (Slotkin *et al.*, 1997; Reisinger *et al.*, 2019). Of our patients, only one withdrew from prednisolone treatment at six months and in this patient the decrease in caudate values was ~4%, contrasting to patients who remained on the anti-inflammatory for at least 15 months (range: -35.8% to -58.4%), hence offering one possible explanation for our results. If this is the case then our estimates of serotonergic growth within the putamen are likely to be underestimated. Further extended analysis of SERT-rich regions such as the raphe and hippocampus would help to exclude the possibility of acute trauma.

In summary, we confirm that hfVM-derived dopaminergic neurons can survive within the host putamen and add that these neurons are capable of expressing the dopamine transporter with some variability that is dependent on the dopaminergic state prior to transplant. Despite modifications to the Transeuro protocol in light of past findings, homogenous re-innervation across the anterior-posterior axis was not achieved and the fetal dissection techniques were unable to completely eliminate contamination by serotonergic neuroblasts. Further work evaluating the relationship between TH+ and SERT+ volume and cell numbers in the final tissue suspensions and post-transplant PET imaging measures

would be important to narrow the potential factors that may be responsible for inter-subject variability in outcomes. For future trials, we strongly advocate greater attention be placed on experimental design, particularly the inclusion of healthy controls and the matching of non-transplanted PD patients by disease duration given the dynamic nature of the disease process, which will undoubtedly promote clarity in the interpretation of neuroimaging data on the effects of cell transplant.

Chapter 4. Effects of Intraputamenal hfVM Transplants on the Motor Symptoms of Parkinson's Disease

In this chapter, the effects of intraputamenal hfVM tissue implantation on the cardinal motor symptoms of Parkinson's disease will be evaluated in 8 transplanted individuals as compared to 16 patients who remained on optimal drug therapy over a period of 60 months. The relationship between changes in dopaminergic and serotonergic neuroimaging measures in the posterior putamen and the longitudinal progression of bradykinesia, rigidity, tremor and axial symptoms will also be assessed in order to characterise the effects of graft composition and the regional coverage of graft survival on motor severity.

The aims of the current chapter are:

- To compare the progression of bradykinesia, rigidity, tremor and axial symptoms in patients in receipt of hfVM grafts against patients on optimal drug therapy over a period of 60 months
- To evaluate the relationship between graft-related changes in dopaminergic and serotonergic PET measures and changes in bradykinesia, rigidity, tremor and axial symptoms at 18 months following transplant
- To evaluate the impact of spatially homogenous cell survival on changes in the cardinal motor features

The hypotheses of the current chapter are:

- Patients receiving hfVM transplants will exhibit significant improvement in motor symptoms as compared to patients on optimal drug therapy over 60 months.
- Graft-related changes in posterior putamenal dopaminergic PET measures will be predictive of changes in bradykinesia and rigidity symptoms
- Graft coverage of the putamenal motor region will moderate the effect of hfVM transplant on motor recovery

We note here that the longitudinal observational arm of the Transeuro trial is at the time of writing still ongoing, and as such the results reported here should be treated as preliminary.

4.1. Statistical analysis

4.1.1. Linear mixed effects models

Linear mixed effects regression models were used to assess whether receipt of hfVM transplants was predictive of the evolution of each of the cardinal motor symptoms, as compared to Parkinson's disease individuals who were on best currently available drug therapy. "Off-state" UPDRS-III scores, collected as part of the observational sub-study of Transeuro (Figure 2.1) were obtained and sub-scores for the cardinal symptoms (bradykinesia, rigidity, tremor, axial) were calculated for the most and least affected sides where applicable (Table 2.2). "Off-state" peg board and tap test scores were also obtained for use as dependent variables. For the control group (n = 16), data were included within a range of 0-60 months starting from the time of the baseline PET scans, amounting to a mean of 9.31 ±2.39 visits. For the transplant group (n = 8), data were included within a range of 0-60 months beginning from the observational assessment immediately prior to the first transplant surgery, resulting in a mean of 6.75 ±1.75 visits. The use of linear mixed effects models allowed us to account for non-independence in repeated measurements for each individual, for missing data and the irregular intervals between observational visits. Thus, random intercepts for each individual were included to permit variation in symptom severity at 0 months based on their correlated set of repeated measurements. Random slopes for modelling differences in the rate of progression over time for each individual were desirable, however, attempts to fit random slopes consistently resulted in convergence failure and singularity (overfitting).

In the base additive model, *time* (months) was included as a continuous fixed effect and *group* (transplant, control) and *Parkinsonian side* (most affected, least affected) were included as categorical fixed effects, apart from when axial symptoms was used as the dependent variable. In the second model, an additional term was included for the interaction between *group* and *time*, which was of primary interest. In the third model, an additional three terms were included, in order to test whether *Parkinsonian side* * *group* and *Parkinsonian side* * *time* interactions contributed to the explained variance, and whether the interaction between *group* and *time* was moderated by *Parkinsonian side*. Models were estimated with restricted maximum likelihood using the lme4 package (Bates *et al.*, 2015) in R version 3.6.2 (R Core

Team, 2019). *t*/*F*-statistics to test for the significance of fixed effects in each model and for nested model comparisons were computed using the Kenward-Roger method for the approximation to degrees of freedom using packages "lmerTest" (Kuznetsova *et al.*, 2017) and "pbkrtest" (Halekoh and Hojsgaard, 2014) respectively, as it has recently been shown to be less anti-conservative than the likelihood ratio and other competing methods, especially at lower sample sizes (Halekoh and Hojsgaard, 2014; Kuznetsova *et al.*, 2017; Luke, 2017). In the case of significant interactions, post-hoc analyses for comparison of estimated marginal means and estimated slopes were conducted as appropriate using the "emmeans" package (Lenth, 2018). Intra-class correlation coefficients were also computed for each model using package "sjstats" (Lüdecke, 2020), to ascertain the variance explained by the inclusion of random effects. The "effects" package (Fox and Weisberg, 2019) was used to derive model predictions and "ggplot2" package (Wickham, 2016) for graphical representation.

Normal distribution of the residuals was assessed graphically using normal QQ, density plots and Shapiro-Wilk test, heteroscedasticity by plotting residuals against fitted values, multicollinearity by fixed effects correlation matrices and variance inflation factors and outliers and highly influential data points were detected using normal QQ plots as well as by Mahalanobis distance using the "car" (Fox and Weisberg, 2019) and "psych" packages (Revelle, 2019).

4.1.2. Multiple Regression

A series of multiple linear regression analyses were conducted to examine how the effect of transplant on posterior putamenal dopaminergic and serotonergic innervation impacted upon Parkinsonian symptoms. Changes in the severity of tremor, bradykinesia, rigidity and axial symptoms, as defined by the difference in UPDRS-III subscores between post-transplant and pre-transplant imaging time-points (Table 2.2), were included as dependent variables in separate models. For bradykinesia, rigidity and tremor, changes in severity were calculated for both the most and least affected sides. There were no significant correlations between most and least affected sides for change in tremor (r = 0.423, p = 0.297, n = 8), bradykinesia (r = 0.155, p = 0.714, n = 8) or rigidity (r = 0.434, p = 0.282, n = 8) sub-scores.

The posterior putamen was analysed here as this sub-region has previously been shown to be involved in motor function, while anterior portions of the putamen show greater

involvement with associative or limbic functions (Haber *et al.*, 2000). Δ[^{11}C]PE2I BP_{ND} and Δ[^{11}C]DASB BP_{ND} [*post-transplant - pre-transplant*] in the posterior putamen were therefore included as continuous predictors. *Parkinsonian side* was included as a categorical predictor, except when regressions concerned the prediction of axial symptoms, where bilateral Δ[^{11}C]PE2I BP_{ND} and Δ[^{11}C]DASB BP_{ND} were used instead.

Δ[^{18}F]FDOPA K_i was strongly correlated with Δ[^{11}C]PE2I BP_{ND} (r = 0.878, p =0.004, n = 8) and as such, due to concerns over variance inflation by multicollinearity, only Δ[^{11}C]PE2I BP_{ND} was included as a predictor representing dopaminergic innervation. Δ[^{11}C]PE2I BP_{ND} was selected over Δ[^{18}F]FDOPA K_i as the latter may not solely reflect dopaminergic function; [^{18}F]FDOPA can enter serotonergic neurons within which the aromatic amino acid decarboxylase enzyme is known to be present. Thus [^{18}F]FDOPA K_i may also in part reflect serotonergic function.

Posterior putamenal [^{11}C]PE2I BP_{ND} and [^{11}C]DASB BP_{ND} % coverage, as measured in Chapter 3, were also considered for inclusion as predictors. However, % coverage was also correlated with Δ[^{11}C]PE2I BP_{ND} (r = 0.813, p = 0.014, n = 8) and Δ[^{11}C]DASB BP_{ND} (r = 0.749, p = 0.032, n = 8) in this sub-region, therefore they were not included as separate variables in the same models as Δ[^{11}C]PE2I BP_{ND} and Δ[^{11}C]DASB BP_{ND} for reasons of multicollinearity. Separate models for % coverage were considered, however, without jointly including information on the absolute magnitude of change within the region of interest, and because % coverage is bounded at 0-100, this would not be informative. Therefore, to incorporate information on coverage, an *efficiency index* was derived consisting of the linear combination of the two variables for each tracer. That is, the mean of Δ[^{11}C]PE2I BP_{ND} and [^{11}C]PE2I BP_{ND} % coverage for each patient was calculated after [^{11}C]PE2I BP_{ND} % coverage was re-scaled to the same group range as Δ[^{11}C]PE2I BP_{ND}. Re-scaling was performed in order to maintain equal weight of each variable to the *efficiency index*. The same method was used to derive an *efficiency index* for [^{11}C]DASB BP_{ND}. *Efficiency indices* were entered into separate regression models and Akaike information criterion and likelihood ratio tests for non-nested models (Vuong, 1989) conducted using the "nonnest2" package (Merkle and You, 2020) to compare these model fits to those in which % coverage was not linearly incorporated. Root mean square error and standardised coefficients for each individual model were derived using

"caret" (Kuhn, 2020) and "lm.beta" (Behrendt, 2014) packages. Model estimates or marginal effects and plots were generated using "ggeffects" (Lüdecke, 2018) and "ggplot2" (Wickham, 2016).

Normal distribution of the residuals was assessed graphically using normal QQ, density plots and Shapiro-Wilk test, heteroscedasticity by plotting residuals against fitted values and Breusch-Pagan test, multicollinearity by variance inflation factors, independence of observations by the Durbin-Watson statistic and outliers and highly influential data points were detected using normal QQ plots as well as Mahalanobis distance using the "car"(Fox and Weisberg, 2019) and "psych" packages (Revelle, 2019).

4.2. Results

4.2.1. Progression of the cardinal motor symptoms in transplanted patients

Visual inspection of residual and normal QQ plots did not reveal substantial deviation from normal distribution or significant heteroscedasticity for models including bradykinesia as the dependent variable. However, models including axial and rigidity symptoms as the dependent variables produced moderately leptokurtic residual distributions, with Shapiro-Wilk test confirming departure from normality ($p < 0.001$, $p = 0.003$ respectively) and Mahalanobis distance identifying two multivariate outliers for the former DV. Data were therefore transformed using the Box-Cox procedure (Axial, $\lambda = 0.33$; Rigidity, $\lambda = 0.61$), which substantially reduced kurtosis and enabled conformation to a normal distribution, with no outliers remaining. For models involving tremor as the dependent variable, residual distributions showed positive skew (Shapiro-Wilk, $p = 0.002$) and non-constant variance, which was improved substantially by applying a Tukey power transformation ($\lambda = 0.5$). Because of the presence of some zero values in the dependent variables, transformations were applied after addition of a non-zero constant of 1.

The three-way *time* * *group* * *Parkinsonian side* interaction term introduced structural multicollinearity in all complete models in which it was included. No significant improvements to model fits were gained by its inclusion as compared to when it was removed (Kenward-Roger, $p > 0.05$). Due to concerns that this multicollinearity may mask effects from lower order terms it was dropped from model 3 for bradykinesia, rigidity and tremor analyses.

Results of all linear mixed effects analyses for the prediction of UPDRS-III motor sub-scores are reported in Table 4.1 and graphically presented in Figure 4.1. For bradykinesia, there was no significant improvement to the prediction of the outcome variable when including the *time* * *group* interaction term to the additive model. However, the full model in which *Parkinsonian side* was allowed to interact with the other fixed effects resulted in a significantly better fit ($p = 0.01$). There was a significant interaction between *time* and *Parkinsonian side* ($p < 0.01$), in which the least affected side showed a greater degree of

progression of 0.041 ±0.012 points per month as compared to the most affected side (Estimated slope = -0.001 ±0.012), irrespective of *group*. There were no interactions detected between *time* and *group* or between *group* and *Parkinsonian side*.

For rigidity, the inclusion of an interaction term between *time* and *group* resulted in a significantly improved model fit ($p < 0.01$). For this model, there was a significant difference in the progression of rigidity between groups, in which the transplant group exhibited a greater decrease in rigidity severity by -0.019 ±0.006 points per month (Box-Cox transformed, $\lambda = 0.61$), as compared to the control group (Estimated slope = -0.001 ±0.003), irrespective of *Parkinsonian side*. The model fit was not improved by the addition of 2-way interaction terms involving *Parkinsonian side*.

For tremor, a significant improvement in explained variance was achieved by including the *time* * *group* interaction term in the model ($p < 0.001$). For this model, tremor severity in the transplant group decreased by -0.019 ±0.002 points per month (Tukey power transformed, $\lambda = 0.5$) while the control group also exhibited a decreasing trend but to a lesser magnitude (Estimated slope = -0.006 ±0.003), across levels of *Parkinsonian side*. Inclusion of 2-way interaction terms involving *Parkinsonian side* did not increase the predictive ability of the model.

The prediction of axial symptoms by *time* and *group* was not improved by allowing their interaction. In the additive model, there was a significant main effect of *time*, in which there was an overall deterioration in axial severity by 0.012 ±0.003 points per month (Box-Cox transformed, $\lambda = 0.33$) across both groups ($p < 0.001$). There was no significant main effect of *group* on symptom severity.

Linear mixed models were also performed with peg board and tap test scores as the dependent variables. Models for the prediction of peg board scores exhibited positive skew and leptokurticity in the distribution of residuals, with Shapiro-Wilk test confirming departure from normality ($p < 0.001$). Applying Box-Cox transformation ($\lambda = -0.57$) substantially improved the distribution by eliminating skew and reducing leptokurticity, although Shapiro-Wilk remained significant ($p < 0.01$). Mahalanobis distance identified one extreme value from a transplant patient at the post-transplant time-point and as such was

subsequently removed. For models including tap test scores as the dependent variable, visual inspection of residual and normal QQ plots did not reveal substantial deviation from normal distribution or significant heteroscedasticity and no outliers were identified.

The prediction of peg board scores was significantly improved by permitting *time* and *group* to interact ($p < 0.05$), and then subsequently when including interaction terms with *Parkinsonian side* ($p < 0.001$) (Table 4.2) (Figure 4.2). Estimates derived from the full model show that completion time increases at a greater rate for the control group (Estimated slope = 0.0004 ±0.0001) in comparison to the transplant group (Estimated slope = 0.00003 ±0.00014) (Box-Cox transformed, $\lambda = -0.57$), across levels of *Parkinsonian side*. A *group* * *Parkinsonian side* interaction was also detected, with post-hoc Tukey-adjusted pairwise comparisons indicating that the most affected side was significantly slower than the least affected side for the control group ($\Delta Mean_{EM} = 0.023$, *95% CI* [0.017, 0.029], $p < 0.001$) across the 60 month period. No interaction was detected between *time* and *Parkinsonian side*.

Similarly, the prediction of tap test scores was significantly improved by addition of a *time* * *group* interaction ($p < 0.05$) and subsequently by *time* * *Parkinsonian side* and *group* * *Parkinsonian side* interactions ($p < 0.01$) (Table 4.2) (Figure 4.2). The transplant group exhibited improvement in the number of taps achieved over 30 seconds by 0.18 ±0.06 per month as compared to the control group who remained relatively stable at an estimated 0.0003 ±0.036, averaged over *Parkinsonian side*. The most affected side improved at a greater rate (Estimated slope = 0.15 ±0.047) than the least affected side (Estimated slope = 0.03 ±0.047), irrespective of *group*. Averaged over the 60 month period, the control group achieved fewer taps on the most affected side as compared to the least affected side ($\Delta Mean_{EM} = -8.29$, *95% CI* [-11.15, -5.43], $p < 0.001$) while no such difference was detected for the transplant group ($\Delta Mean_{EM} = -2.8$, *95% CI* [-7.31, 1.72], $p = 0.34$).

Table 4.1: Progression of clinical symptoms following transplant. Results of the linear mixed effects analysis, including random and fixed effects for the prediction of "off-state" UPDRS-III bradykinesia, rigidity, tremor and axial sub-scores by time (months), group (transplant, control) and Parkinsonian side (most affected, least affected).

		Random Effects (SD)			Fixed Effects					Model comparison		
Dependent Variable	Model	Patient	Residual	ICC	B	SE_B	df	t	p	F	df	p
UPDRS-III Bradykinesia	Additive Model	2.487	2.475	0.502						-	-	-
	Intercept				6.226	0.681	27.519	9.149	<0.001			
	Time				0.027	0.008	349.189	3.268	0.001			
	Group				0.422	1.116	22.161	0.378	0.709			
	Side				2.384	0.257	344.009	9.261	<0.001			
	Model 2	2.513	2.472	0.508						1.558	1, 348.228	0.213
	Intercept				6.099	0.694	28.586	8.792	<0.001			
	Time				0.032	0.009	348.008	3.471	<0.001			
	Group				0.924	1.197	28.077	0.773	0.446			
	Side				2.384	0.257	343.009	9.275	<0.001			
	Time * Group				-0.024	0.019	348.228	1.248	0.213			
	Model 3	2.515	2.446	0.514						4.711	2, 341.009	0.010
	Intercept				5.478	0.722	33.422	7.588	<0.001			
	Time				0.053	0.012	343.943	4.465	<0.001			
	Group				1.372	1.228	31.070	1.117	0.272			
	Side				3.626	0.478	341.009	7.582	<0.001			
	Time * Group				-0.024	0.019	346.095	1.265	0.207			
	Time * Side				-0.042	0.015	341.009	2.760	0.006			
	Group * Side				-0.892	0.562	341.009	1.589	0.113			

UPDRS-III Rigidity	Additive Model	1.033	0.859	0.591						-	-	-
	Intercept				2.376	0.276	25.867	8.621	<0.001			
	Time				-0.005	0.003	347.793	1.758	0.079			
	Group				-0.448	0.459	22.115	0.977	0.339			
	Side				0.483	0.089	344.005	5.411	<0.001			
	Model 2	1.054	0.849	0.606						7.481	1, 346.675	0.007
	Intercept				2.280	0.282	26.434	8.079	<0.001			
	Time				-0.001	0.003	346.547	0.239	0.811			
	Group				-0.069	0.487	26.113	0.143	0.887			
	Side				0.483	0.088	343.005	5.468	<0.001			
	Time * Group				-0.018	0.007	346.675	2.735	0.007			
	Model 3	1.054	0.848	0.607						1.965	2, 341.005	0.142
	Intercept				2.170	0.291	29.744	7.465	<0.001			
	Time				0.004	0.004	343.101	1.047	0.296			
	Group				-0.099	0.497	28.195	0.200	0.843			
	Side				0.702	0.166	341.005	4.241	<0.001			
	Time * Group				-0.018	0.007	344.636	2.744	0.006			
	Time * Side				-0.010	0.005	341.005	1.923	0.055			
	Group * Side				0.059	0.195	341.005	0.305	0.760			
UPDRS-III Tremor	Additive Model	0.588	0.442	0.639						-	-	-
	Intercept				1.891	0.155	25.172	12.199	<0.001			
	Time				-0.009	0.001	347.168	6.521	<0.001			

	Group				0.341	0.259	22.095	1.313	0.203			
	Side				0.331	0.046	344.003	7.199	<0.001			
	Model 2	0.595	0.433	0.654						14.487	1, 346.045	<0.001
	Intercept				1.823	0.158	25.611	11.574	<0.001			
	Time				-0.006	0.002	345.947	3.995	<0.001			
	Group				0.609	0.272	25.356	2.239	0.034			
	Side				0.331	0.045	343.003	7.345	<0.001			
	Time * Group				-0.013	0.003	346.045	3.806	<0.001			
	Model 3	0.595	0.432	0.655						1.899	2, 341.003	0.151
	Intercept				1.777	0.162	28.281	11.001	<0.001			
	Time				-0.004	0.002	342.742	1.942	0.053			
	Group				0.578	0.277	27.040	2.088	0.046			
	Side				0.424	0.085	341.003	5.014	<0.001			
	Time * Group				-0.013	0.003	344.013	3.817	<0.001			
	Time * Side				-0.005	0.003	341.003	1.773	0.077			
	Group * Side				0.064	0.099	341.003	0.644	0.520			
UPDRS-III Axial	Additive Model	0.853	0.607	0.664						-	-	-
	Intercept				1.985	0.229	25.669	8.654	<0.001			
	Time				0.012	0.003	162.557	4.137	<0.001			
	Group				-0.069	0.383	22.165	0.180	0.859			
	Model 2	0.839	0.605	0.658						2.481	1, 161.687	0.117
	Intercept				2.041	0.229	26.996	8.913	<0.001			
	Time				0.009	0.003	161.566	2.873	0.005			

	Group				-0.289	0.402	28.485	0.718	0.479			
	Time * Group				0.010	0.007	161.687	1.575	0.117			

B = unstandardized regression coefficient
df = Kenward-Roger approximated degrees of freedom
SD = standard deviation
ICC = intra-class correlation coefficient
SE_B = standard error of the coefficient

Table 4.2: Progression of objective measures of clinical severity following transplant. Results of the linear mixed effects analysis, including random and fixed effects for the prediction of "off-state" peg board and tap test scores by time (months), group (transplant, control) and Parkinsonian side (most affected, least affected).

		Random Effects (SD)			Fixed Effects					Model comparison		
Dependent Variable	Model	Patient	Residual	ICC	B	SE_B	df	t	p	F	df	p
Peg Board	Additive Model	0.034	0.021	0.716						-	-	-
	Intercept				1.46	0.009	24.163	165.91	<0.001			
	Time				0.0003	0.000	338.329	4.24	<0.001			
	Group				0.001	0.015	22.182	0.09	0.932			
	Side				0.018	0.002	336.071	7.90	<0.001			
	Model 2	0.034	0.021	0.724						4.226	1, 337.375	0.041
	Intercept				1.459	0.009	24.516	162.56	<0.001			
	Time				0.0003	0.000	337.167	4.73	<0.001			
	Group				0.009	0.016	24.613	0.55	0.587			
	Side				0.018	0.002	335.069	7.93	<0.001			
	Time * Group				-0.0003	0.0001	337.375	2.06	0.041			
	Model 3	0.035	0.021	0.734						7.414	2, 333.125	<0.001
	Intercept				1.454	0.009	26.248	158.621	<0.001			
	Time				0.0005	0.0001	334.270	4.473	<0.001			
	Group				0.018	0.016	25.803	1.144	0.263			
	Side				0.027	0.004	333.065	6.479	<0.001			
	Time * Group				-0.0004	0.0002	335.267	2.143	0.033			
	Time * Side				-0.0002	0.0001	333.098	1.198	0.232			
	Group * Side				-0.018	0.005	333.132	3.751	<0.001			

Tap Test	Additive Model	25.777	9.536	0.880						-	-	-
	Intercept				79.374	6.533	22.750	12.151	<0.001			
	Time				0.042	0.032	336.790	1.340	0.181			
	Group				-4.908	11.227	22.053	0.437	0.666			
	Side				-6.713	1.002	336.001	6.697	<0.001			
	Model 2	25.660	9.470	0.880						5.883	1, 335.743	0.016
	Intercept				80.323	6.515	22.909	12.329	<0.001			
	Time				0.0002	0.036	335.801	0.006	0.995			
	Group				-8.583	11.279	22.867	0.761	0.455			
	Side				-6.713	0.995	335.001	6.743	<0.001			
	Time * Group				0.180	0.074	335.743	2.426	0.016			
	Model 3	25.665	9.365	0.883						4.777	2, 333.001	0.009
	Intercept				82.491	6.559	23.541	12.576	<0.001			
	Time				-0.060	0.046	333.462	1.289	0.198			
	Group				-11.329	11.330	23.279	1.000	0.328			
	Side				-11.050	1.837	333.001	6.014	<0.001			
	Time * Group				0.180	0.073	333.723	2.452	0.015			
	Time * Side				0.120	0.059	333.001	2.028	0.043			
	Group * Side				5.492	2.185	333.001	2.513	0.012			

B = unstandardized regression coefficient

df = Kenward-Roger approximated degrees of freedom

ICC = intra-class correlation coefficient

SD = standard deviation

SE_B = standard error of the coefficient

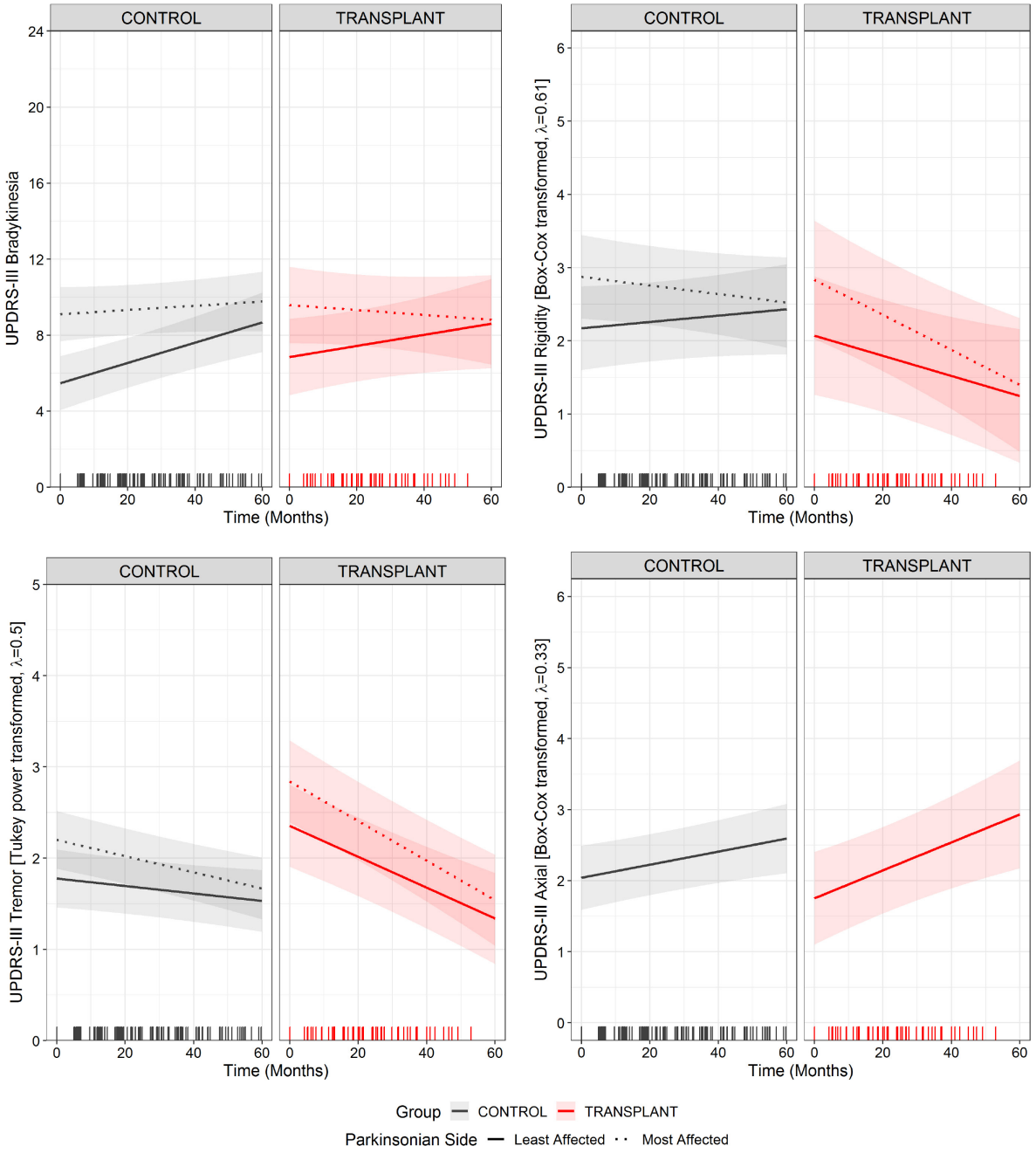


Figure 4.1: Mixed model plots showing progression of clinical symptoms following transplant. Plots illustrating fixed effects estimates of the complete linear mixed model analyses for the prediction of "off-state" UPDRS-III bradykinesia, rigidity, tremor and axial symptoms by time and group (transplant, control), as well as by Parkinsonian side (most affected, least affected) for all sub-scores apart from axial severity. Shaded ribbons represent 95% confidence intervals about the prediction lines and rug plots at the base of each graph represent the density of observations across time.

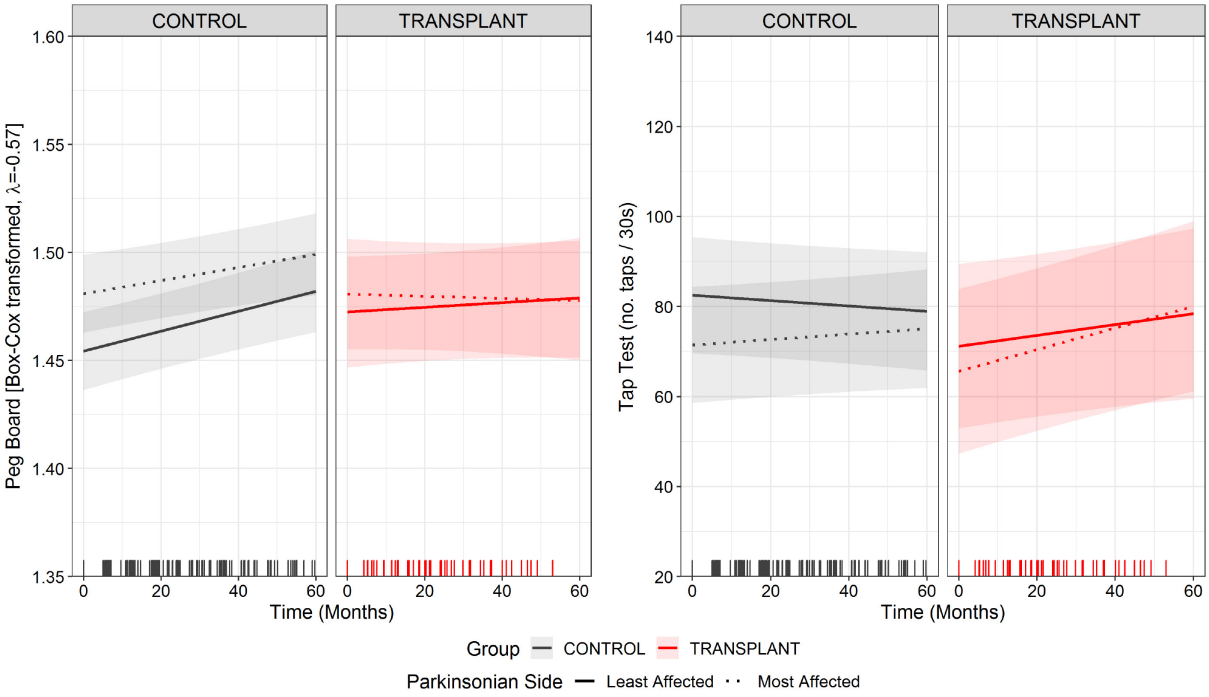


Figure 4.2: Mixed model plots showing progression of objective measures of clinical severity following transplant. Plots illustrating fixed effects estimates of the complete linear mixed model analyses for the prediction of "off-state" peg board and tap test scores by time, group (transplant, control) and Parkinsonian side (most affected, least affected). Shaded ribbons represent 95% confidence intervals about the prediction lines and rug plots at the base of each graph represent the density of observations across time.

4.2.2. Effect of dopaminergic and serotonergic re-innervation on the cardinal motor symptoms of transplanted patients

A series of multiple linear regression analyses were conducted to examine whether "off-state" Δbradykinesia, Δrigidity, Δtremor and Δaxial symptoms in transplanted patients could be predicted by posterior putamenal Δ[^{11}C]PE2I BP_{ND} and Δ[^{11}C]DASB BP_{ND}, as well as *Parkinsonian side*, and whether the linear addition of regional coverage for each of the PET measures significantly improved upon the model fits. Assumptions for most multiple linear regressions were satisfied, including those of multicollinearity, multivariate outliers, normality of residuals, homoscedasticity and independence of observations. Only the analysis predicting Δbradykinesia from Δ[^{11}C]PE2I BP_{ND}, Δ[^{11}C]DASB BP_{ND} and *Parkinsonian side* produced slightly leptokurtic and positively skewed residuals and non-normality confirmed by Shapiro-Wilk test ($p < 0.05$). On inspection of normal QQ plots one outlier was detected and upon removal improved the distribution. However, given that the departure from normality was marginal, this datum was retained and results of the complete dataset were reported in the first instance.

Results showed that ΔUPDRS-III bradykinesia was significantly explained by both Δ[^{11}C]PE2I BP_{ND} and Δ[^{11}C]DASB BP_{ND} in the posterior putamen, accounting for 60% of the variance (Table 4.3). The linear incorporation of % coverage made a slight improvement to the model, explaining an extra 10% variance and a moderate decrease in the Akaike information criterion values (Figure 4.3), although Vuong test showed only a trend towards significance ($Z = 1.293$, $p = 0.098$). Equations were:

Predictors: Parkinsonian side, Δ[^{11}C]PE2I BP_{ND} and Δ[^{11}C]DASB BP_{ND}*:*

$$\Delta UPDRS - III\ Bradykinesia = 1.149 - 1.460x_1 - 3.569x_2 + 2.187x_3 + \epsilon$$

Predictors: Parkinsonian side, [^{11}C]PE2I and [^{11}C]DASB *efficiency indices:*

$$\Delta UPDRS - III\ Bradykinesia = 0.244 - 1.179x_1 - 2.506x_2 + 1.945x_3 + \epsilon$$

, where x_1 denotes Parkinsonian side (dummy coded: least affected side = 0, most affected side = 1), x_2 denotes [^{11}C]PE2I measures and x_3 denotes [^{11}C]DASB measures (ΔBP_{ND} or *efficiency index* respectively), suggesting that while increasing posterior putamenal [^{11}C]PE2I

values has a beneficial impact on bradykinesia, the opposite is true for posterior putamenal [^{11}C]DASB, with greater increases in the latter resulting in increased bradykinesia symptom severity (Figure 4.3). Removal of the outlier described above resulted in lower prediction error and greater explained variance for both the ΔBP_{ND} ($F(3, 12) = 16.46$, $R^2 = 0.82$, $RMSE = 1.28$, $AIC = 59.98$, $p < 0.001$) and *efficiency index* ($F(3, 12) = 12.8$, $R^2 = 0.78$, $RMSE = 1.42$, $AIC = 62.99$, $p < 0.001$) models (Vuong test; $Z = 0.9$, $p = 0.82$), while there was minimal impact upon estimated coefficients.

Table 4.3: Relationship between changes in dopaminergic and serotonergic imaging measures and clinical progression following transplant. Model fits and parameter estimates of serial multiple linear regression analyses, including the prediction of "off-state" Δbradykinesia, Δrigidity, Δtremor and Δaxial symptoms in transplanted patients by changes in posterior putamenal dopamine (Δ[^{11}C]PE2I BP_{ND}) and serotonin (Δ[^{11}C]DASB BP_{ND}) transporter levels, or by graft-related re-innervation efficiency indices for both tracers, and Parkinsonian side (most affected, least affected).

	Model Fit						Estimated Coefficients				
Model	F(3, 12)	p	R^2	$R^2_{Adjusted}$	RMSE	AIC	B	SE_B	β	t(12)	p
ΔUPDRS-III Bradykinesia	6.076	0.009	0.603	0.504	2.139	79.739					
Intercept							1.149	0.882	0.000	1.302	0.217
Parkinsonian Side							-1.460	1.395	-0.215	1.047	0.316
Δ[^{11}C]PE2I BP_{ND}							-3.569	1.175	-0.722	3.037	0.010
Δ[^{11}C]DASB BP_{ND}							2.187	0.599	0.805	3.655	0.003
ΔUPDRS-III Bradykinesia	9.156	0.002	0.696	0.619	1.872	75.472					
Intercept							0.244	0.969	0.000	0.252	0.805
Parkinsonian Side							-1.179	1.303	-0.174	0.905	0.383
[^{11}C]PE2I Efficiency Index							-2.506	0.940	-0.522	2.665	0.021
[^{11}C]DASB Efficiency Index							1.945	0.429	0.754	4.535	<0.001
Model	F(3, 12)	p	R^2	$R^2_{Adjusted}$	RMSE	AIC	B	SE_B	β	t(12)	p
ΔUPDRS-III Rigidity	0.128	0.942	0.031	-0.211	1.748	73.273					
Intercept							-0.500	0.720	0.000	0.694	0.501
Parkinsonian Side							-0.628	1.139	-0.177	0.551	0.592
Δ[^{11}C]PE2I BP_{ND}							0.005	0.960	0.002	0.005	0.996
Δ[^{11}C]DASB BP_{ND}							-0.001	0.489	-0.001	0.002	0.999
ΔUPDRS-III Rigidity	0.255	0.856	0.060	-0.175	1.721	72.786					

Intercept							-0.794	0.891	0.000	0.892	0.390
Parkinsonian Side							-0.804	1.198	-0.227	0.672	0.515
[^{11}C]PE2I Efficiency Index							0.077	0.865	0.031	0.089	0.930
[^{11}C]DASB Efficiency Index							0.225	0.394	0.166	0.570	0.580
Model	F(3, 12)	p	R^2	$R^2_{Adjusted}$	RMSE	AIC	B	SE_B	β	t(12)	p
ΔUPDRS-III Tremor	3.701	0.043	0.481	0.351	1.675	71.915					
Intercept							-0.841	0.691	0.000	1.218	0.247
Parkinsonian Side							-0.173	1.092	-0.037	0.159	0.877
Δ[^{11}C]PE2I BP_{ND}							-0.761	0.921	-0.226	0.830	0.423
Δ[^{11}C]DASB BP_{ND}							-0.976	0.469	-0.525	2.083	0.059
ΔUPDRS-III Tremor	8.967	0.002	0.692	0.614	1.291	63.577					
Intercept							0.863	0.668	0.000	1.292	0.221
Parkinsonian Side							0.549	0.898	0.118	0.611	0.552
[^{11}C]PE2I Efficiency Index							-1.786	0.648	-0.544	-2.754	0.017
[^{11}C]DASB Efficiency Index							-0.979	0.296	-0.555	-3.314	0.006
Model	F(2, 5)	p	R^2	$R^2_{Adjusted}$	RMSE	AIC	B	SE_B	β	t(5)	p
ΔUPDRS-III Axial	0.063	0.939	0.025	-0.366	4.373	54.312					
Intercept							-0.739	2.581	0.000	0.286	0.786
Δ[^{11}C]PE2I BP_{ND}							-1.573	4.491	-0.176	0.350	0.740
Δ[^{11}C]DASB BP_{ND}							0.472	2.138	0.111	0.221	0.834
ΔUPDRS-III Axial											
Intercept	0.320	0.740	0.113	-0.241	4.169	53.548					

[^{11}C]PE2I Efficiency Index							1.122	3.775	0.000	0.297	0.778
[^{11}C]DASB Efficiency Index							-4.160	5.233	-0.347	-0.795	0.463
							0.231	1.901	0.053	0.121	0.908

AIC = Akaike information criterion

B = unstandardized regression coefficient

β = standardized coefficient

R^2 = coefficient of determination

$R^2_{Adjusted}$ = coefficient of determination adjusted for number of predictors

RMSE = root mean square error

SE_B = standard error of the coefficient

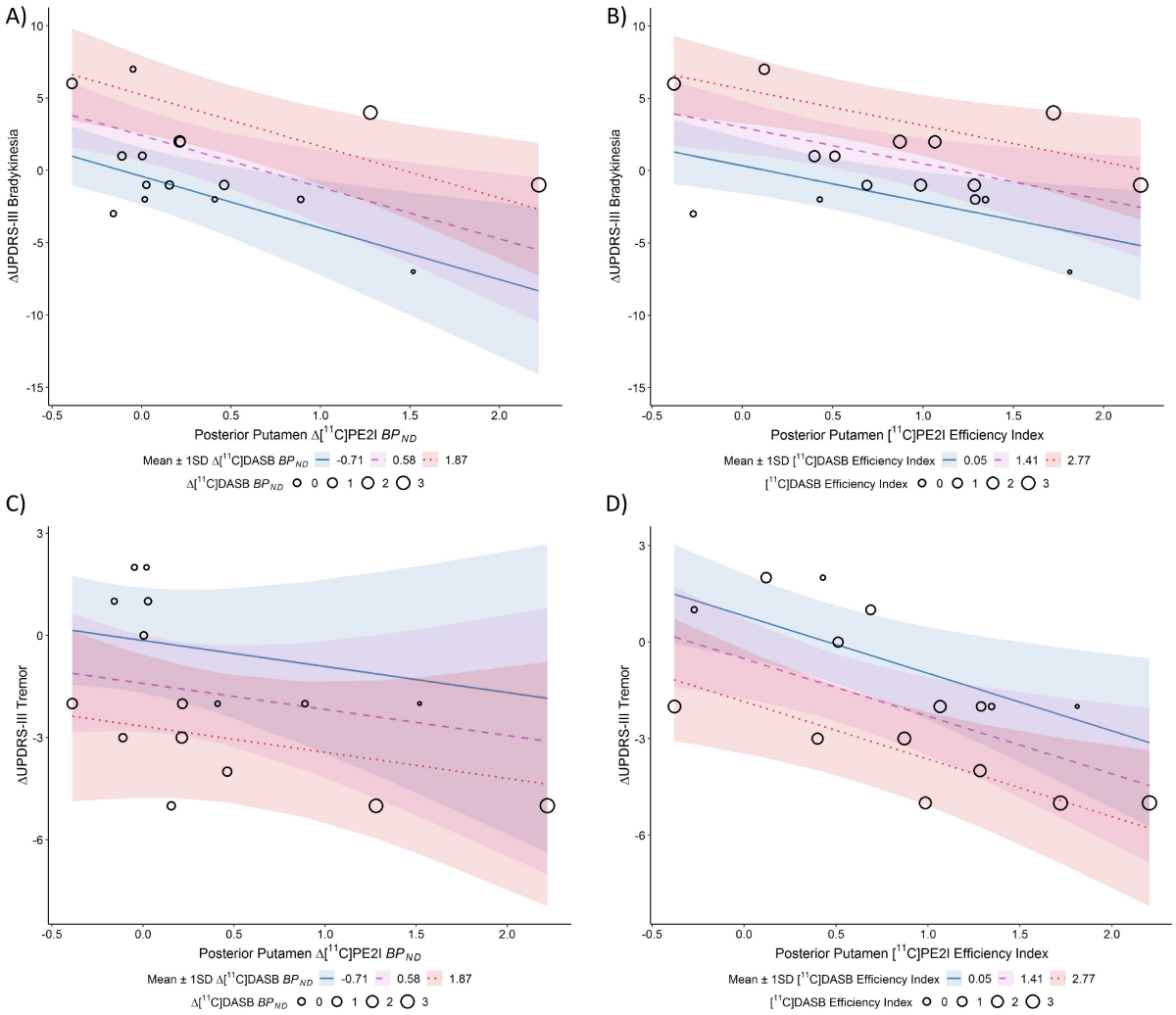


Figure 4.3: Plots illustrating multiple regression results for the prediction of post-operative clinical change by dopaminergic and serotonergic PET measures. Scatterplots illustrating results of the multiple regression analyses, including ΔUPDRS-III bradykinesia (A, B) and ΔUPDRS-III tremor (C, D) as dependent variables and posterior putamenal Δ[11C]PE2I BPND and Δ[11C]DASB BPND (A, C) or [11C]PE2I and [11C]DASB efficiency indices (B, D) as predictors, while Parkinsonian side was held constant. Hollow points represent raw data with point size corresponding to the magnitude of Δ[11C]DASB BPND or [11C]DASB efficiency index. Multiple best fit lines represent predictions at the mean ±1SD values of Δ[11C]DASB BPND or [11C]DASB efficiency index, with 95% confidence intervals illustrated by the shaded area about each line.

ΔUPDRS-III tremor was also significantly explained by both Δ[^{11}C]PE2I BP_{ND} and Δ[^{11}C]DASB BP_{ND} in the posterior putamen, accounting for 48% of the variance, though only Δ[^{11}C]DASB BP_{ND} made a near significant explanatory contribution (Table 4.3). The linear incorporation of % coverage made a significant improvement to the model, explaining an extra 21% variance with a large decrease in the Akaike information criterion values (Figure 4.3) (Vuong test; $Z = 2.764$, $p = 0.003$). Equations were:

Predictors: Parkinsonian side, Δ[^{11}C]PE2I BP_{ND} and Δ[^{11}C]DASB BP_{ND}*:*

$$\Delta UPDRS - III\ Tremor\ =\ -0.841\ -\ 0.173x_1 -\ 0.761x_2 -\ 0.976x_3 + \epsilon$$

Predictors: Parkinsonian side, [^{11}C]PE2I and [^{11}C]DASB *efficiency indices:*

$$\Delta UPDRS - III\ Tremor\ =\ 0.863\ +\ 0.549x_1 -\ 1.786x_2 -\ 0.979x_3 + \epsilon$$

However, as opposed to bradykinesia, analysis suggests that increases in both [^{11}C]PE2I and [^{11}C]DASB measures in the posterior putamen contribute to reduction of tremor symptoms. For both bradykinesia and tremor, *Parkinsonian side* made no significant explanatory contributions to the model predictions.

Using these predictors, multiple linear regression was not able to explain changes in UPDRS-III rigidity or axial symptoms. Including age and disease duration at the time of transplant as continuous predictors did not explain any extra variance in the existing models. Similarly, pre-transplant [^{11}C]PE2I BP_{ND} in the ventral striatum did not make any significant explanatory contributions.

4.3. Discussion

In this chapter, we found that as compared to patients remaining on optimal drug therapy, transplanted patients exhibited significant improvements in rigidity and tremor over the 60 month study period, whereas we were unable to detect any changes in the progressive decline of axial symptoms. Bradykinesia as measured using the UPDRS-III also did not change in the transplant group, however small but significant differences were observed when considering performance on objective measurements of upper limb movement speed and dexterity. Specifically, time to complete the 9-hole peg board was stable over the five year period for transplanted patients while the controls worsened, and the number of alternating taps completed within 30 seconds increased for the transplant group while the performance for controls did not change.

Bradykinesia is the cardinal feature of Parkinson's disease most consistently linked to nigrostriatal dopaminergic deficit (Seibyl *et al.*, 1995; Vingerhoets *et al.*, 1997; Rinne *et al.*, 1999; Benamer *et al.*, 2000; Pal *et al.*, 2001; Ribeiro *et al.*, 2002; Pirker, 2003; Pavese *et al.*, 2006; Bohnen *et al.*, 2007; Isaias *et al.*, 2007; Spiegel *et al.*, 2007; Verstappen *et al.*, 2007; Martin *et al.*, 2008; Nandhagopal *et al.*, 2009; Okamura *et al.*, 2010; Rossi *et al.*, 2010; Helmich *et al.*, 2011; Maillet *et al.*, 2016; Li *et al.*, 2018; Martin-Bastida *et al.*, 2019) and has reportedly incurred significant alleviation in prior hfVM trials (Lindvall *et al.*, 1990; Madrazo *et al.*, 1991; Freed *et al.*, 1992; Hoffer *et al.*, 1992; Lindvall *et al.*, 1992; Spencer *et al.*, 1992; Widner *et al.*, 1992; Lindvall *et al.*, 1994; Peschanski *et al.*, 1994; Defer *et al.*, 1996; Kopyov *et al.*, 1996; Kopyov *et al.*, 1997; López-Lozano *et al.*, 1997; Wenning *et al.*, 1997; Brundin *et al.*, 2000; Freed *et al.*, 2001; Mendez *et al.*, 2005), thus it is somewhat surprising that transplantation under the current Transeuro protocol appeared to have no effect on its severity. It should be noted however, that many longitudinal studies of non-transplanted PD patients have failed to find correlations between longitudinal changes in bradykinesia severity and dopaminergic decline (Antonini *et al.*, 1997; Morrish *et al.*, 1998; Marek *et al.*, 2001; Nurmi *et al.*, 2001; Pirker *et al.*, 2002; Nurmi *et al.*, 2003; Pirker, 2003; Colloby *et al.*, 2005; Bruck *et al.*, 2006; Bruck *et al.*, 2009; Nandhagopal *et al.*, 2009; Simuni *et al.*, 2018), indicating either insensitive or erroneous measurement or the involvement of other mechanisms in its pathophysiology. Here, we found that the degree of serotonergic re-innervation ([^{11}C]DASB) dampened the potential

effect of dopaminergic neuron replacement, in that greater increases in serotonin transporter density predicted lower symptomatic relief by graft-derived increases in dopamine transporter density ([^{11}C]PE2I). In Chapter 3, we presented evidence that serotonergic neurons were indeed grafted within the putamen of our patients, thus providing a likely explanation for the apparent lack of improvement as measured using the UPDRS-III. To our knowledge only one study in humans has explicitly reported correlative findings on bradykinesia with respect to serotonergic function, finding a non-significant but positive trend (r = 0.303, p = 0.16) for greater severity at higher raphe 5-HT$_{1A}$ receptor binding potential, measured using [^{11}C]WAY 100635 PET (Doder *et al.*, 2003). Currently there are no reports in humans investigating the combinatorial effects of dopaminergic and serotonergic decline in PD patients on bradykinetic symptoms, thus it is yet to be seen whether our results represent a specific phenomenon related to the introduction of allogeneic tissue into a denervated environment, or if it is a generalised clinicopathologic characteristic of the disease.

The mechanisms underlying this antagonistic effect are not possible to elucidate using the current methods. It has been proposed that the release of dopamine may be mediated by the 5-HT$_{2C}$ receptor sub-type that is expressed on GABAergic projection and interneurons at the cell body and terminal fields of the nigrostriatal system (Eberle-Wang *et al.*, 1997; Clemett *et al.*, 2000). Microdialysis experiments in rodents have demonstrated concentration-dependent increases in striatal dopamine efflux following intrastriatal infusion of selective 5-HT$_{2C}$ antagonists while conversely showing decreased basal dopamine levels after systemic administration of selective 5-HT$_{2C}$ agonists (Alex *et al.*, 2005; Burke *et al.*, 2014). In unilateral 6-OHDA rats, localised 5-HT$_{2C}$ receptor blockade elicited motoric benefits only when antagonists were infused into the lesioned as opposed to non-lesioned nigral region, while their systemic administration potentiated the anti-Parkinsonian effect of co-administered D$_2$ receptor agonist quinpirole (Fox *et al.*, 1998). 5-HT$_{2C}$ receptors may thus provide a means by which aberrantly grafted embryonic serotonergic neurons can attenuate dopamine release. However, despite a large body of biochemical and electrophysiological evidence the interaction between serotonergic and dopaminergic systems remains complex and only partially understood, with several 5-HT receptor sub-types facilitating rather than inhibiting

dopaminergic function in a region-specific state-dependent manner (Fox *et al.*, 2009; De Deurwaerdere and Di Giovanni, 2017).

In contrast, the alleviation of tremor symptoms in our patients was predicted by concurrent hfVM-derived increases in both dopamine and serotonin transporter density. The pathophysiology of tremor is comparatively less well understood but a small number of studies have identified serotonergic dysfunction as a key component. Of relevance, recent large-scale [^{123}I]FP-CIT SPECT studies of the PPMI cohort have demonstrated greater degeneration of the serotonergic raphe-striatal system in patients with tremor-dominant as compared to akinetic or mixed phenotypes, the degree of which was inversely correlated with resting tremor constancy and amplitude (Qamhawi *et al.*, 2015; Pasquini *et al.*, 2018; Pasquini *et al.*, 2019a). Similarly, Doder *et al.* (2003) found that rest tremor was negatively related with 5-HT$_{1A}$ receptor availability in the raphe complex using [^{11}C]WAY 100635 PET (Doder *et al.*, 2003), while Loane *et al.* (2013) reported a similar relationship between the severity of kinetic/postural tremor in tremulous patients and serotonin transporter density in the caudate, putamen and raphe, as measured using [^{11}C]DASB (Loane *et al.*, 2013). Correlations with *in vivo* measures of dopaminergic function are consistently absent (Seibyl *et al.*, 1995; Rinne *et al.*, 1999; Pirker, 2003; Ottaviani *et al.*, 2006; Spiegel *et al.*, 2007; Martin *et al.*, 2008; Rossi *et al.*, 2010; Li *et al.*, 2018; Martin-Bastida *et al.*, 2019), but the complete lack of dopaminergic involvement has been contended. Equivalent [^{123}I]FP-CIT declines were noted between akinetic-rigid and tremor-dominant phenotypes when patients were carefully matched on several measures of disease severity (Eggers *et al.*, 2011), while between drug-naïve groups matched by hypokinesia, those with additional tremor exhibited significantly greater dopaminergic deterioration (Isaias *et al.*, 2007). Moreover, tremor in a large portion of patients is to some degree responsive to dopaminomimetics (Sethi, 2008). To date, only one study has attempted to assess the impact of both dopaminergic and serotonergic decline on tremor severity. Using the non-specific binding characteristics of [^{123}I]FP-CIT and *a priori* knowledge of regional cell populations, Pasquini *et al.* (2018) recently demonstrated that resting tremor amplitude and constancy at ~4.5 years post-diagnosis was predicted by the raphe/putamen binding ratio and not raphe serotonin transporter density alone (Pasquini *et al.*, 2018). Thus our findings pertaining to a role for both dopaminergic and serotonergic re-innervation in reducing the severity of tremor appear to be supported by the current

literature. Given that the interpretation of results reported by Pasquini *et al.* (2018) remains somewhat confounded by the presence of serotonergic neurons within the putamen (Ginovart *et al.*, 2001; Ichise *et al.*, 2003; Kish *et al.*, 2008) and the generation of indices from values derived from distinct regions which likely possess differential neuronal profiles and interactions (De Deurwaerdere and Di Giovanni, 2017), our findings also serve to extend current knowledge on the generation of Parkinson's disease tremor.

Very few groups have reported outcomes for both bradykinesia and tremor as a result of hfVM transplantation. Interestingly, while significant improvements for bradykinesia had been reported in cohorts from New Haven (Spencer *et al.*, 1992), Denver/New York (Freed *et al.*, 2001; Nakamura *et al.*, 2001) and Lund (Lindvall *et al.*, 1992), no changes were noted for tremor. Oppositely, while the Tampa randomised controlled trial (Olanow *et al.*, 2003) reported no improvement in bradykinesia, there was a near-significant decrease in the severity of tremor ($p = 0.068$). Unfortunately the only autopsy (Mendez *et al.*, 2008; Kordower *et al.*, 2017) and long-term imaging (Politis *et al.*, 2010b; Politis *et al.*, 2011) cases for which serotoninergic re-innervation was examined do not detail clinical outcomes under formal evaluation. To our knowledge, only one group across the hfVM literature has previously conducted correlative analyses between the response of separable motor symptoms and putamenal dysfunction to surgery (Freed *et al.*, 2001; Nakamura *et al.*, 2001), finding an association between [^{18}F]FDOPA PET and bradykinesia but not tremor (Nakamura *et al.*, 2001). Our novel multi-tracer findings are suggestive of a counter-effective role of serotonergic re-innervation between tremor and bradykinesia, providing a possible physiological basis for the disparate clinical patterns previously reported (Lindvall *et al.*, 1992; Spencer *et al.*, 1992; Freed *et al.*, 2001; Nakamura *et al.*, 2001; Olanow *et al.*, 2003). We advocate that future cell-based restorative strategies focussed on purifying samples in favour of maximal dopaminergic content proceed cautiously with respect to patient selection, as our models imply that while akinetic predominant individuals may derive substantial benefit from concentrated dopaminergic grafts, this may not be as much the case for tremulous patients.

In line with our findings, a large number of studies have reported substantial alleviation of rigidity following transplant (Lindvall *et al.*, 1990; Madrazo *et al.*, 1991; Lindvall *et al.*, 1992;

Widner *et al.*, 1992; Lindvall *et al.*, 1994; López-Lozano *et al.*, 1997; Wenning *et al.*, 1997; Brundin *et al.*, 2000; Freed *et al.*, 2001). However, only in the Denver/New York trial (Freed *et al.*, 2001) was symptom severity assessed against *in vivo* PET markers, finding no relationship between improvements in UPDRS-III "off-state" rigidity scores and peri-operative changes in [^{18}F]FDOPA uptake ratio (Nakamura *et al.*, 2001). We add here that the significant amelioration experienced by our patients cannot be explained by changes in neither posterior putamenal dopamine transporter nor serotonin transporter density. Rigidity has been linked with dopaminergic dysfunction in PD patients, albeit to a lesser degree than bradykinesia (Vingerhoets *et al.*, 1997; Rinne *et al.*, 1999; Pal *et al.*, 2001; Pirker, 2003; Pavese *et al.*, 2006; Spiegel *et al.*, 2007; Rossi *et al.*, 2010; Martin-Bastida *et al.*, 2019), yet it remains amongst the more complex and poorly understood of Parkinsonian features, not least because the vast majority of researchers tend to combine both sub-scores on the basis of their co-association with dopaminergic deficit. However, the clinical features of rigidity do not readily fit with the classic cortico-basal ganglia-thalamo-cortical model of disease (Rodriguez-Oroz *et al.*, 2009) (Figure 1.5). Moreover, rigidity has been distinguished from bradykinesia and tremor by its association with hyperactivity and increased GABA concentrations in the primary motor cortex (Yu *et al.*, 2007; van Nuland *et al.*, 2020), while the clinical benefit derived from apomorphine appears to be mediated by inhibition of motor-evoked potentials in this region (Pierantozzi *et al.*, 2001). That rigidity appears to have a dopaminergic component but with distinct cortical activation patterns indicates that the anti-rigidity effects of hfVM transplant may be conditional upon the normal functioning of inhibitory regions across the wider motor network, including for instance the inferior frontal gyrus which has recently been implicated in the manifestation of LID (Cerasa *et al.*, 2015a). Additionally, the expression of rigidity may be modulated by grafting into the more rostral associative/limbic sub-regions of the putamen, which are postulated to influence downstream sensorimotor basal ganglia output via ascendant spiralling striato-nigro-striatal pathways (Haber *et al.*, 2000). Indeed, examination of this domain is required to provide a more complete picture of the neural correlates underlying graft-derived symptomatic changes and as such stands as a limitation of the current work. The difficulty with which rigidity is assessed is also cause for consideration; across all UPDRS-III items it exhibits the lowest inter-rater reliability (de Deus Fonticoba *et al.*, 2019) and is not video-recordable,

meaning that it cannot be retrospectively reviewed, is not easily taught and is more susceptible to subjectivity. While this may not necessarily discount the validity of our mixed model results, given the relative magnitude of data included and as the same variability may afflict both groups, this source of error may be appreciable for our smaller sample multiple regression analysis.

The axial sub-score of the UPDRS-III indicated no change in the progression of symptoms relating to dysarthrophonia, gait disturbance, balance impairment and hypomimia in patients who underwent transplantation as compared to those who did not. The current literature appears divided in this regard, with some group and case studies reporting alleviation (Madrazo *et al.*, 1991; Hoffer *et al.*, 1992; Widner *et al.*, 1992; Kopyov *et al.*, 1996; Kopyov *et al.*, 1997; López-Lozano *et al.*, 1997; Freed *et al.*, 2001) while others find no effect (Hoffer *et al.*, 1992; Spencer *et al.*, 1992; Defer *et al.*, 1996; Kudoh *et al.*, 1999; Olanow *et al.*, 2003; Kordower *et al.*, 2017). Moreover, in one study patients receiving high volume grafts exhibited greater improvements in sit-stand-walk time than those implanted with low tissue volume (Kopyov *et al.*, 1997). In contrast, our data indicate no relationship between the degree of dopaminergic (or serotonergic) re-innervation and changes in axial severity. Indeed, amelioration of axial symptoms might not be expected from intraputamenal dopaminergic hfVM grafts, particularly postural instability and gait disturbance which comprise the major part of this sub-score, as they generally do not respond well to dopamine pharmacotherapy (Rascol *et al.*, 2003) and have been strongly linked to pathological alterations of the pedunculopontine nucleus (Karachi *et al.*, 2010; Craig *et al.*, 2020), the subsequent cholinergic deafferentation of the thalamus and in some studies dysregulation of cortical cholinergic neurotransmission (Bohnen *et al.*, 2009; Bohnen *et al.*, 2013; Muller *et al.*, 2013; Bohnen *et al.*, 2014; Bohnen *et al.*, 2019). Recent analyses of [^{123}I]FP-CIT PPMI data has however indicated that lower binding in the caudate at baseline predicted greater gait disturbance and postural instability at 4-6 years follow-up (Pasquini *et al.*, 2019b; Craig *et al.*, 2020). In a dual-case study in which patients received both putamen and caudate implants, Hoffer *et al.* (1992) reported that the individual exhibiting post-operative caudate [^{18}F]FDOPA K_i^{Occ} increases of ~126% underwent substantial improvement to walking disability, unlike their other patient whose deterioration was associated with more modest caudatal increases (~20%) (Hoffer *et al.*, 1992). Similarly, no improvements in

sit-stand-walk time were noted for the Paris cohort, who despite receiving caudate grafts exhibited no [^{18}F]FDOPA K_i^{Occ} changes in this region but did show substantial increases in the putamen (Defer *et al.*, 1996). However, axial effects have also been reported in patients without caudate implants (Kopyov *et al.*, 1997) while conversely patients solely undergoing caudate transplantation (Kudoh *et al.*, 1999), with [^{18}F]FDOPA-derived confirmation of good cell survival (Spencer *et al.*, 1992), have shown no significant axial benefit. Thus the pathophysiological and graft-induced mechanistic basis for changes to axial symptoms remains unclear.

That we found mild but detectable improvements on the 9-hole peg board and 30 second tap test further raises pertinent and appreciable issues surrounding the UPDRS-III as the currently accepted gold-standard clinimetric for assessing disease severity in general research and in clinical trials. Both objective tests are generally believed to sensitively measure bradykinesia, particularly the peg board, given its weighting towards the assessment of fine and dextrous hand movements which are reportedly more sensitive to speed and amplitude impairment in PD patients as compared to the gross movements captured by UPDRS-III items such as fist clenching, pronation-supination, foot tapping and stamping (Agostino *et al.*, 2003). These tests arguably confer greater reliability (Haaxma *et al.*, 2008), given that they are insensitive to inter-rater and intra-rater bias that can be particularly impactful in small sample, longitudinal and multi-centre scenarios. There is also a tendency for clinicians and researchers to focus on movement amplitude over speed and interruptions when evaluating the extent of bradykinesia (Heldman *et al.*, 2011) and as such it is possible that the discordance between outcome measures might reflect graft-derived improvements in the latter two constructs. Similarly, that quantitative testing involves measurement of only the upper extremities might suggest that the effects of the graft on bradykinesia were less impactful on the lower limbs. However, the performance on these tasks is also influenced by other symptoms such as kinetic and re-emergent tremor, which as separate entities remained untested in the current work. Although kinematic/robotic/wearable technology is still in its infancy and cannot substitute expert evaluation, it may offer an unbiased mode of quantification capable of decomposing motoric elements consistently and on a scale beyond the restrictions of Likert-style ratings (Heldman *et al.*, 2011; Ruzicka *et al.*, 2016; Gaprielian *et al.*, 2019; Linn-Evans *et al.*, 2020). The current

results highlight that such methods may be useful in future multi-centre trials, particularly for the assessment of bradykinesia, gait disturbance and rigidity for which inter-reliability is poorest (de Deus Fonticoba *et al.*, 2019).

Lastly, we found that the prediction of graft-derived changes in tremor severity was substantially improved by incorporating information on the extent of posterior putamenal coverage into our regression model. A similar effect was also found for bradykinesia but this did not reach significance. These results demonstrate that the spatial homogeneity of graft-induced re-innervation, whether affected by deposition strategy or subsequent cell survival and function, is an important adjunctive factor to the overall magnitude of dopaminergic/serotonergic change for optimising the potential clinical efficacy associated with cell replacement therapy. Anatomical and physiological data consistently demonstrate somatotopic organisation of the motor territory of the putamen, with lower limb, upper limb and orofacial zones roughly represented along a dorsal to ventral gradient (Obeso *et al.*, 2008). As UPDRS-III tremor and bradykinesia scores were amalgamated from measures of both upper and lower extremities, it stands to reason that penalising the overall regional increase by an estimate of graft coverage would yield an index more reflective of the clinical situation. A major drawback of the current method however is that we cannot be certain as to whether symptomatic changes across different parts of the body directly correspond to patches of good/poor graft viability within their proposed zonal representation. Moreover, we are unable to discern the relative importance of each variable to the clinical outcome. The use of somatotopic atlases (Choi *et al.*, 2012) in future work would overcome these limitations but would require either substantially larger sample sizes or the use of quantitative motor assessment methods to circumvent the introduction of measurement error associated with the UPDRS-III that would be especially magnified when using only single items on a 0 to 4 scale. Such information may be crucial for discounting the possibility of aberrant function by the diffusion of dopamine from engrafted to neighbouring non-innervated and hypersensitised regions (Stromberg *et al.*, 2000).

In summary, we found that intraputamenal grafting of hfVM tissue altered the natural progression of tremor and rigidity, as well as some measures of bradykinesia, as compared to patients treated under standard dopamine replacement therapy, although clinical changes

were modest with respect to past trial outcomes. The post-operative elevation in dopamine transporter density was associated with improvements in tremor and bradykinesia, while the extent of serotonergic re-innervation appeared to have opposing effects on each of these symptoms, with greater increases related to worse bradykinesia and improved tremor outcome, thus offering a mechanistic basis for the selection of patients in future trials of cell therapeutics. Furthermore, the current analysis highlights the clinical importance of promoting consistent and homogenous graft function by either improvements to surgical technique or the facilitation of cell survival within the host. In contrast, *in vivo* PET biomarkers were unable to explain the improvements in rigidity or the lack of improvement in axial symptoms, which may be due to the involvement of regions external to the motor putamen, alternative neurotransmitter systems, or the sensitivity of the UPDRS-III to measurement error. Indeed, although expert evaluation cannot be replaced, future trials may benefit significantly from the implementation of quantitative motor assessment methodology to reduce the potential for inter-rater measurement error that is particularly disruptive in multi-centre, small sample and longitudinal designs. Such technology would facilitate the interpretation of and maximise the information gained from measurements derived from expensive neuroimaging techniques.

Chapter 5. Graft-induced Dyskinesia and the Relationship with Dopaminergic and Serotonergic Re-innervation

In this chapter, the effects of intraputamenal hfVM tissue implantation on the possible emergence of "off-state" graft-induced dyskinesias (GID) in Parkinson's disease patients will be examined. Few studies in past open-label and randomised controlled trial cohorts have so far investigated the origin of this potentially debilitating graft-related side effect, yet those that have propose three main theories.

Initially, upon the results of the Denver/New York trial, it was postulated that the intervention resulted in a "dopamine overdose" effect; that continued fiber outgrowth from the graft sites leads to dopamine hyperinnervation and excessive dopaminergic signalling (Freed *et al.*, 2001; Ma *et al.*, 2002), particularly within the movement-promoting direct basal ganglia pathway (Richardson *et al.*, 2011). However, increases in [^{18}F]FDOPA uptake in these patients were not especially high and a large number of patients from other trials exhibiting greater re-innervation, including those reaching normal levels, did not develop GID (see Appendix). These changes were not correlated with GID severity (Hagell *et al.*, 2002; Olanow *et al.*, 2003; Olanow *et al.*, 2009a) and in the Tampa cohort were comparable between patients who did versus did not acquire this complication (Olanow *et al.*, 2003; Olanow *et al.*, 2009a). Moreover, no association has been found with amphetamine-induced [^{11}C]raclopride displacement, suggesting that excessive dopamine release is unlikely to be the cause (Piccini *et al.*, 1999; Piccini *et al.*, 2005). Extending this hypothesis, Ma *et al.* (2002) identified local hotspots of [^{18}F]FDOPA uptake in the left ventrorostral putamen wherein transplanted GID patients showed significantly greater increases post-transplant than transplanted patients who did not have GID (Ma *et al.*, 2002). Similar findings related to patchy and uneven striatal dopaminergic function have been found in a transplanted 6-OHDA rat model whereby the magnitude of the difference in TH+ fiber density between the rostral and caudal aspects of the head of the striatum correlated with phenomenologically atypical amphetamine-induced dyskinesias (Carlsson *et al.*, 2006). Another study demonstrated GID development in rats grafted at a single striatal site but not in those receiving the same cell

volume distributed across the whole nucleus (Maries *et al.*, 2006). Despite this, there are no further studies to Ma *et al.* (2002) that attempt to replicate these findings in humans.

Currently within cell therapeutic research the most prominent hypothesis of GID implicates impure graft composition, and more specifically the presence of serotonergic cells within the dissected tissue sample, in the subsequent aberrant imbalance of putamenal serotonergic to dopaminergic neuronal populations. The basis for this hypothesis comes from observations made in three long-term GID case studies from the Lund series who at up to 16 years following transplant displayed large elevations of 140-230% in [^{11}C]DASB binding to [^{18}F]FDOPA influx ratios, as compared to healthy controls (Politis *et al.*, 2010b; Politis *et al.*, 2011). It is known that serotonergic neurons can take up excess dopamine from the synaptic cleft, store and release it as a false transmitter, but without expressing the necessary autoreceptor machinery to self-modulate their activity (Maeda *et al.*, 2005; Carlsson *et al.*, 2006; Carta *et al.*, 2007; Carta *et al.*, 2010; Politis *et al.*, 2014; Lee *et al.*, 2015; Smith *et al.*, 2015; Roussakis *et al.*, 2016). Artificially inhibiting serotonergic neuronal firing by administration of the 5-HT$_{1A}$ agonist buspirone has been shown to be effective in dampening the clinical expression of GID (Politis *et al.*, 2010b; Politis *et al.*, 2011), however, buspirone does not act specifically on grafted neurons and its clinical effect may equally be attributed to the attenuation of endogenous cells. Moreover, it has been shown that buspirone also holds pharmacological properties for the dopamine system and exerts antagonistic effects on presynaptic D$_2$-autoreceptors (McMillen *et al.*, 1983; Eison and Temple, 1986). These *in vivo* human reports are not supported by preclinical (Lane *et al.*, 2009b; Garcia *et al.*, 2012; Shin *et al.*, 2012) or post-mortem work (Mendez *et al.*, 2008; Kordower *et al.*, 2017) and crucially, they do not quantify the imaging outcomes of transplanted individuals who did not develop GID, severely limiting the interpretability and conclusiveness of their findings.

The aims of the current chapter are:

- To evaluate whether graft-related changes in individual PET measures of dopaminergic innervation in the anterior and posterior putamenal divisions are related to emergence of GID
- To evaluate the effect of putamenal serotonergic to dopaminergic imbalance on the emergence of GID

On the weight of evidence thus far, the hypotheses of the current chapter are:

- Patients with GID will show greater imbalance of dopaminergic re-innervation across the anterior-posterior putamenal axis with a possible anterior-ward weighting
- Patients with GID will show no difference in putamenal serotonergic to dopaminergic ratios as compared to patients who do not develop GID

5.1. Statistical analysis

The presence of graft-induced dyskinesia in 8 bilaterally transplanted patients was detected at post-transplant by means of a score of >0 on any item of the abnormal involuntary movement scale (AIMS) in the practically-defined off-medicated state.

Putamenal imbalance indices for [^{11}C]PE2I BP_{ND} and [^{18}F]FDOPA K_i were derived using the equation:

$$Imbalance\ Index\ = \frac{(Anterior\ -\ Posterior)}{(Anterior\ +\ Posterior)}$$

A series of Welch one-tailed independent sample *t*-tests were used to evaluate whether mean imbalance indices were significantly elevated in transplanted patients who developed graft-induced dyskinesia (GID+) as compared to those who did not (GID-). Tests were conducted at the post-transplant time-point and using difference measures representing the change over time [*post-transplant - pre-transplant*]. Identical analyses were also conducted using absolute [^{11}C]PE2I BP_{ND} and [^{18}F]FDOPA K_i values for the anterior and posterior putamen separately (see Image processing).

Using Welch one-tailed independent sample *t*-tests we also investigated whether PET-derived mean serotonergic to dopaminergic ratios ([^{11}C]DASB BP_{ND} / [^{18}F]FDOPA K_i and [^{11}C]DASB BP_{ND} / [^{11}C]PE2I BP_{ND}) were significantly greater in transplanted GID+ as compared GID- patients. Tests were conducted for the post-transplant time-point and using difference measures [*post-transplant - pre-transplant*] for the posterior and anterior putamen separately.

Retrospective exploratory analysis of clinical and demographic data was also carried out to evaluate whether the subsequent development of GID could be explained by age, disease duration, gender, "off-state" UPDRS-III, "off-state" H&Y, LEDD, LEDD-L-dopa dosage, ACE-R total score, "off-state" and "on-state" total AIMS scores at the pre-transplant time-point. Differences in pre-transplant [^{11}C]PE2I BP_{ND}, [^{18}F]FDOPA K_i, [^{11}C]DASB BP_{ND}, imbalance indices and ratios were also examined. For gender, Fisher's exact test was used to compare GID+ against GID-. For all other comparisons two-tailed Welch independent samples *t*-tests were used.

5.2. Results

5.2.1. Clinical and demographic analysis

Out of eight patients who received bilateral hfVM transplants, three developed graft-induced dyskinesia at the post-transplant time-point ("off-state" AIMS = 6.33 ±3.21). Clinical and demographic data at the pre-transplant time-point are presented in Table 5.1, with no significant differences detected between the groups.

5.2.2. Analysis of absolute PET values and imbalance indices

Welch's *t*-tests indicated a significant effect of group on the change in [^{11}C]PE2I BP_{ND} values in the anterior putamen between the post-transplant and pre-transplant time-points ($t(4.76) = 2.32$, $p = 0.035$, uncorrected), whereby the GID+ group increased over time (Δ[^{11}C]PE2I BP_{ND} = 0.395 ±0.229) while the GID- group exhibited a small decrease (Δ[^{11}C]PE2I BP_{ND} = -0.011 ±0.256). [^{18}F]FDOPA K_i also increased in the anterior putamen in the GID+ group (Δ[^{18}F]FDOPA K_i = 0.0013 ±0.0016) as compared to GID- patients who showed a decline over the interval (Δ[^{18}F]FDOPA K_i = -0.0006 ±0.0008), but this difference did not reach threshold ($t(2.59) = 1.95$, $p = 0.081$, uncorrected). At the post-transplant time-point, there was a trend towards higher anterior putamenal [^{18}F]FDOPA K_i for the GID+ group ([^{18}F]FDOPA K_i = 0.0072 ±0.0018) as compared to the GID- group ([^{18}F]FDOPA K_i = 0.0051 ±0.0011) but similarly this did not reach significance ($t(2.89) = 1.81$, $p = 0.086$, uncorrected). There were no significant differences found between groups at the pre-transplant time-point, in the posterior putamen or for the imbalance indices (Figure 5.1) (Table 5.1).

5.2.3. Serotonergic to dopaminergic ratio analysis

Welch's *t*-tests showed no significant differences between GID+ and GID- groups for [^{11}C]DASB BP_{ND} / [^{18}F]FDOPA K_i or [^{11}C]DASB BP_{ND} / [^{11}C]PE2I BP_{ND} ratios at pre-transplant or post-transplant time-points, or when the pre- to post-transplant change in ratio values were considered, in either the posterior or anterior putamen, at an uncorrected *p*-threshold of 0.05 (Figure 5.2).

Table 5.1: Pre-transplant demographic and clinical measures for the GID+ and GID- groups.

	GID+	GID-	t	p
Gender (m:f)	2:1	4:1	-	1.00
Age (years)	56.70±9.98	54.44±8.39	0.33	0.76
Disease duration (years)	7.32±2.57	7.65±2.41	0.18	0.86
"Off-state" UPDRS-III:				
Total	41.0±7.55	37.6±16.2	0.40	0.70
Bradykinesia	17.67±3.06	15.60±6.69	0.59	0.57
Rigidity	7.67±3.79	7.40±4.72	0.09	0.93
Tremor	9.0±4.36	9.6±4.28	0.19	0.86
Axial	6.67±4.73	5.00±4.74	0.48	0.65
"Off-state" Peg Board	50.83±48.90	24.30±5.57	0.94	0.45
"Off-state" Tap Test	60.67±25.26	72.50±15.11	0.74	0.52
"Off-state" H&Y	2±0	2.2±0.45	6.00 [a]	0.44
"Off-State" AIMS	0	0	-	-
"On-State" AIMS	0	2.8±3.35	1.87	0.13
LEDD	837.83±511.06	952.10±290.94	0.35	0.75
LEDD-L-dopa	634.50±577.84	624.10±272.73	0.03	0.98
ACE-R	98.67±0.58	98.60±1.14	0.11	0.92
PET				
[^{18}F]FDOPA K_i				
Anterior	0.0059±0.0005	0.0057±0.0010	0.39	0.71
Posterior	0.0038±0.0008	0.0032±0.0009	0.98	0.37
Imbalance Index	0.22±0.07	0.29±0.09	1.19	0.29
[^{11}C]PE2I BP_{ND}				
Anterior	1.88±0.31	1.84±0.90	0.09	0.94
Posterior	1.08±0.39	0.94±0.41	0.48	0.65
Imbalance Index	0.28±0.09	0.31±0.04	0.56	0.62
[^{11}C]DASB BP_{ND}				
Anterior	2.16±0.30	1.93±0.40	0.88	0.41
Posterior	1.98±0.32	1.75±0.29	1.01	0.37
Imbalance Index	0.04±0.02	0.05±0.04	0.14	0.89
[^{11}C]DASB BP_{ND} : [^{18}F]FDOPA K_i				
Anterior	367.90±79.69	341.60±58.51	0.50	0.65
Posterior	552.58±221.98	591.57±204.09	0.25	0.82
[^{11}C]DASB BP_{ND} : [^{11}C]PE2I BP_{ND}				
Anterior	1.18±0.35	1.23±0.52	0.16	0.88
Posterior	2.05±0.99	2.13±0.84	0.10	0.92

ACE-R = Addenbrooke's cognitive exam revised; AIMS = abnormal involuntary movement scale; GID+ = patients with graft-induced dyskinesia; GID- = patients without graft-induced dyskinesia; H&Y = Hoehn & Yahr scale; LEDD = levodopa-equivalent daily dosage; LEDD-L-dopa = levodopa-

equivalent daily dosage (levodopa only); PET = positron emission tomography; UPDRS-III = unified Parkinson's disease rating scale part-III

[a]Denotes Mann-Whitney U-statistic

H&Y was assessed using non-parametric Mann-Whitney U test

Gender was assessed using Fisher's Exact test

All other tests between groups were conducted using Welch two-tailed independent sample t-tests

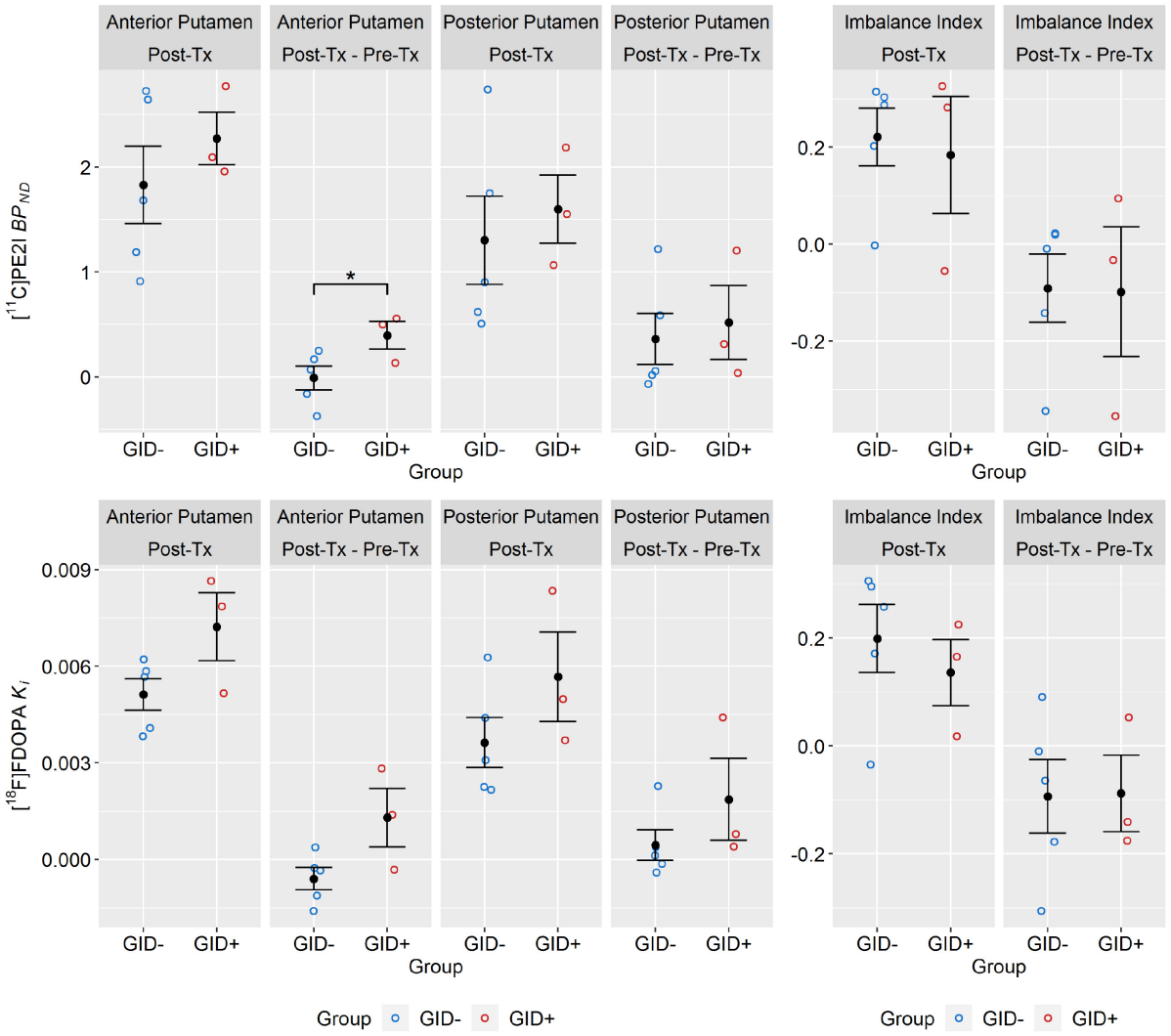


*Figure 5.1: Regional differences in dopaminergic measures between patients with and without graft-induced dyskinesia. Strip plots illustrating differences in [¹¹C]PE2I BP_{ND} and [¹⁸F]FDOPA K_i values in the anterior and posterior putamen between transplanted patients who exhibited graft-induced dyskinesia at post-transplant (GID+) and those who did not (GID-). Groups were compared at the post-transplant time-point as well as on difference measures [post-transplant - pre-transplant]. Anteroposterior imbalance indices [(anterior - posterior) / (anterior + posterior)] were also compared between groups; higher indices indicate greater PET values in the anterior relative to posterior putamen. Hollow data points represent individual patient values and error bars represent the mean ±standard error. *Denotes $p < 0.05$ uncorrected. Tx = transplant.*

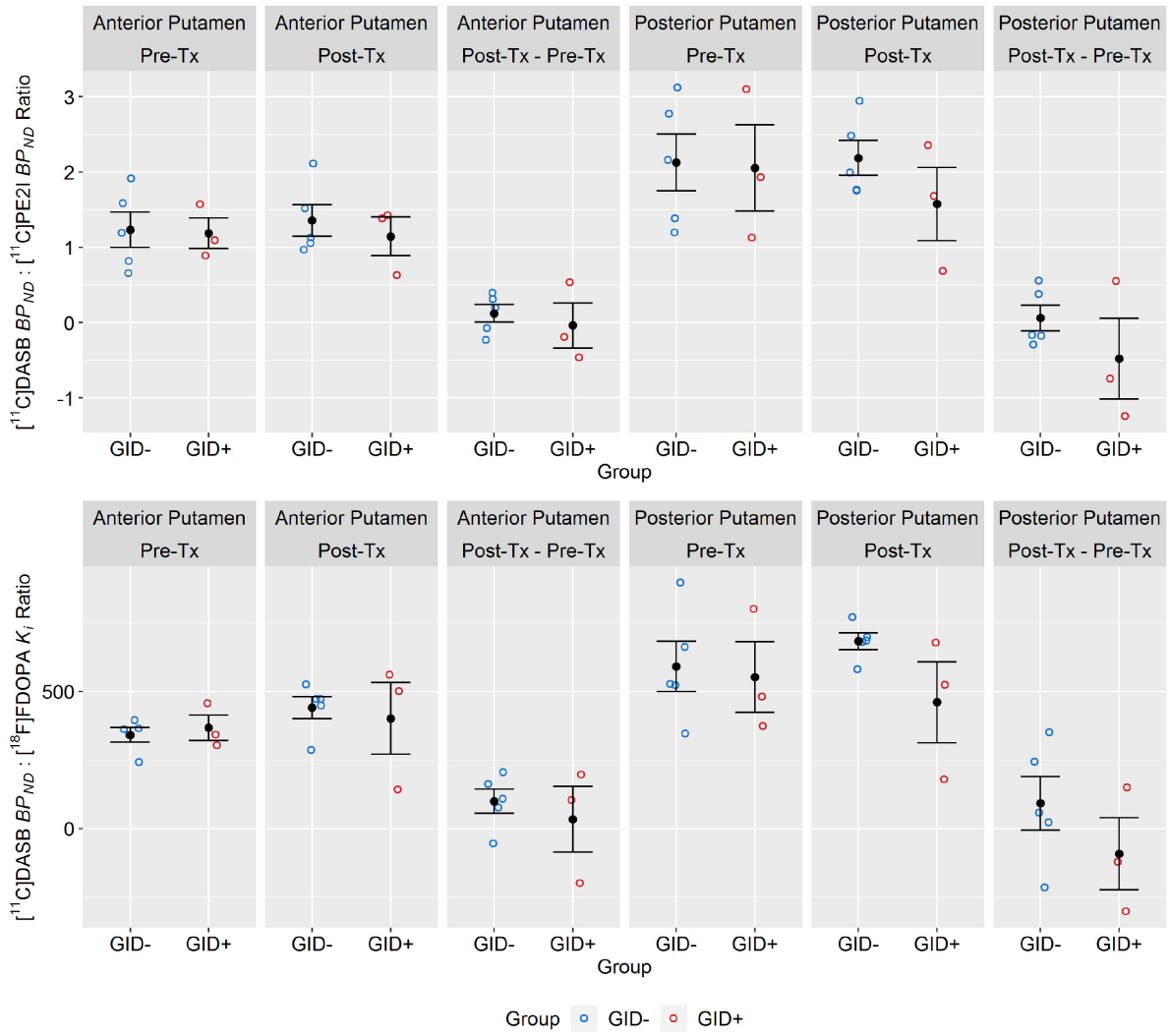


*Figure 5.2: Regional differences in dopaminergic to serotonergic ratio between patients with and without graft-induced dyskinesia. Strip plots illustrating differences in [¹¹C]DASB BP_{ND} / [¹⁸F]FDOPA K_i and [¹¹C]DASB BP_{ND} / [¹¹C]PE2I BP_{ND} ratios in the anterior and posterior putamen between transplanted patients who exhibited graft-induced dyskinesia at the post-transplant time-point (GID+) and those who did not (GID-). Group ratio comparisons were conducted at the pre-transplant and post-transplant time-points as well as on the difference values [post-transplant - pre-transplant]. Hollow data points represent individual values and error bars represent the mean ±standard error. *Denotes $p < 0.05$ uncorrected. Tx = transplant.*

5.2.4. Case Report: Patient 18

We report here a single case from the GID+ group above for whom we had the ability to clinically evaluate at a number of time-points following surgery and moreover derive lateralised ratings for the severity of dyskinesia. Alongside our neuroimaging acquisitions the data she has given may provide further information on the underlying mechanism of GID.

Patient 18 was diagnosed with idiopathic Parkinson's disease in 2010 at 62 years of age with an akinetic-rigid predominant form, but also displaying resting tremor, that was most pronounced on the right side of the body. At initial enrolment to the Transeuro observational study in 2011 she had not yet been treated with pharmacological therapy and only in 2012 was started on monoamine oxidase-B inhibitors (Rasagiline 1mg/od) and extended release dopamine agonists (Ropinirole 4mg/od) with good clinical response (Figure 5.3). Her rate of disease progression was relatively slow and was reflected by only a minor titration in ropinirole regime from 6mg/od to 10mg/od by the time of surgery (LEDD increase from 180 to 300). During this time she had never experienced dyskinesia and had never taken L-dopa. Daily off-time increased slightly from five years after diagnosis with off-periods reportedly unpredictable and having moderate impact on daily activities, which was alleviated satisfactorily by a mild increase in dopamine agonists, such that at the observational assessment immediately prior to surgery the patient was "on" during the entire waking day. Some early morning foot cramping (dystonia) was also reported.

In February 2016 patient 18 underwent bilateral intraputamenal transplantation of hfVM tissue derived from donors aged 6-8 weeks post-conception via five trajectories per side. Surgery was conducted on the right side first (no. donors = 4, TH+/Total = 5.4%, SERT+/Total = 10.6%, viability = 86%), followed by the left side one month later (no. donors = 3, TH+/Total = 6.6%, SERT+/Total = 11.5%, viability = 88.5%). One day prior to the first transplant she was started on a 12-month immunosuppressive regime consisting of ciclosporin (150mg/bd), azathioprine (150mg/od) and prednisolone (40mg/od), the latter being tapered down by 5mg per week until she was taking 5mg/od, as per protocol. Three months following the first procedure she experienced reactivation of herpes zoster, which was treated with aciclovir,

gabapentin and co-codamol and prompting a reduction of ciclosporin to 100mg/bd and complete withdrawal of azathioprine.

Following an initial transient decline in motor function within the first 2 months following surgery, patient 18 exhibited mild-moderate improvements in overall motor score that was mostly related to alleviation of tremor and rigidity. There was also a noticeable improvement to her posture and gait including arm swing, stride length, heel strike and walking speed that was appreciated by the patient. At 3-4 months post-surgery the patient began to exhibit very mild abnormal involuntary movements of the right foot that were atypical, discontinuous during assessment and presented as a combination of choreiform movement with dystonic posturing. The patient was not aware of these movements at first but became increasingly aware in the ensuing months as their prominence increased and by 18 months became persistent throughout the entire waking day. By 24 months, mild on-off motor fluctuations were reported but they were not impactful and bradykinesia had increased in severity, starting from 12 months post-transplant. From this point, there was a reversal of asymmetrical motor presentation whereby the right side, which was greater in severity prior to transplant, became the least affected side. Throughout the study period dyskinesia remained on the right side of the body and preferentially to the lower extremity. Dyskinesia scores in the "on-state" increased in parallel but were likely graft-induced given their phenomenological similarity and the fact that the patient had only added 2mg/day extended release dopamine agonists to her regime by 24 months (LEDD = 340) and was still not taking L-dopa.

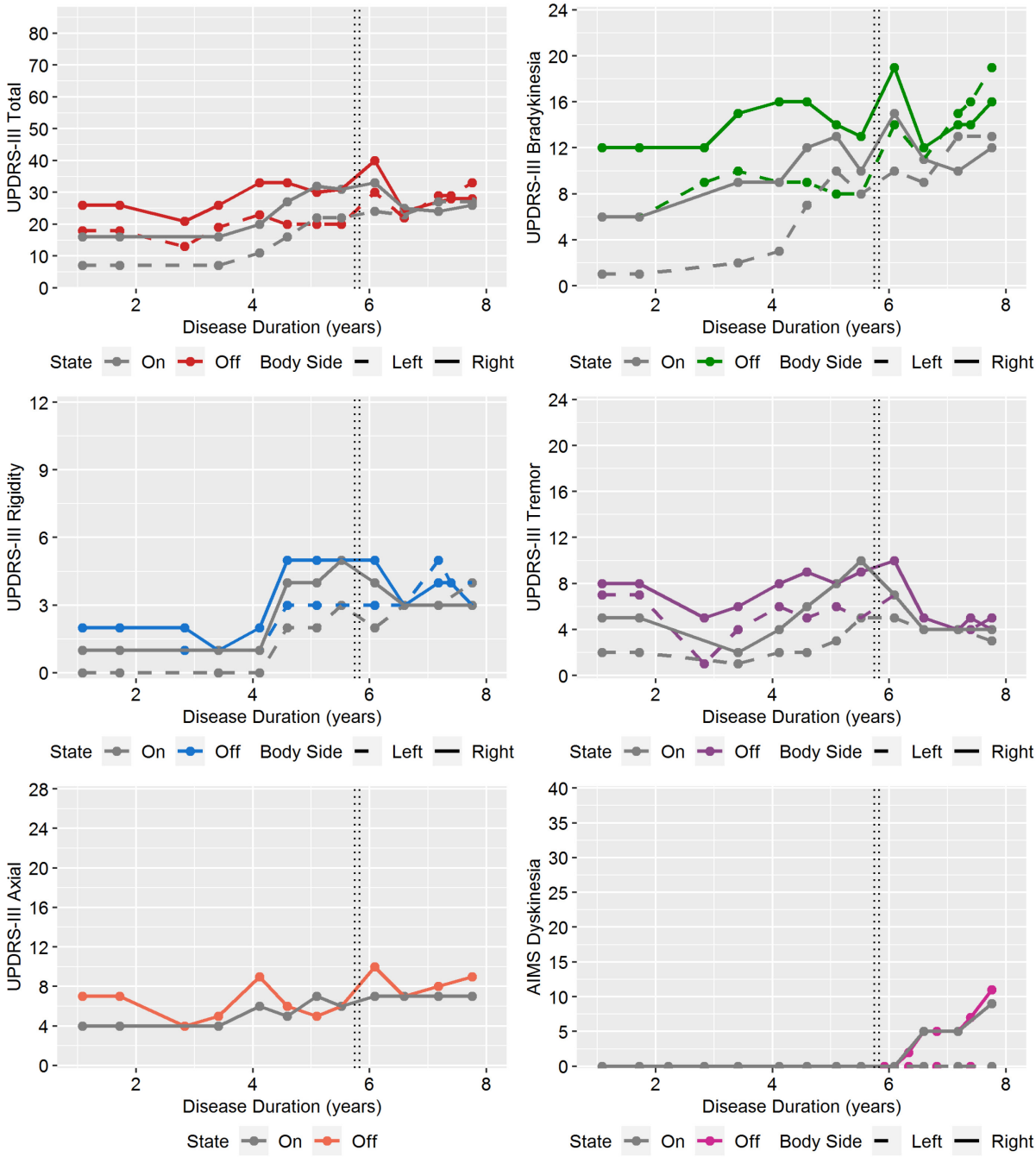


Figure 5.3: UPDRS-III motor and AIMS dyskinesia rating scores for patient 18 throughout the disease course, starting from enrolment into the Transeuro program. The right (solid line) and left (dashed line) body sides are presented where appropriate and both "off-state" (coloured line) and "on-state" (grey line) scores are plotted. The height of each graph represents the maximum possible score for that particular scale. Vertical dotted lines indicate the times of the 1st and 2nd transplant. Prior to transplant, patient 18 displayed a predominantly bradykinetic-rigid form but also exhibited resting tremor with asymmetry favouring greater severity on the right side.

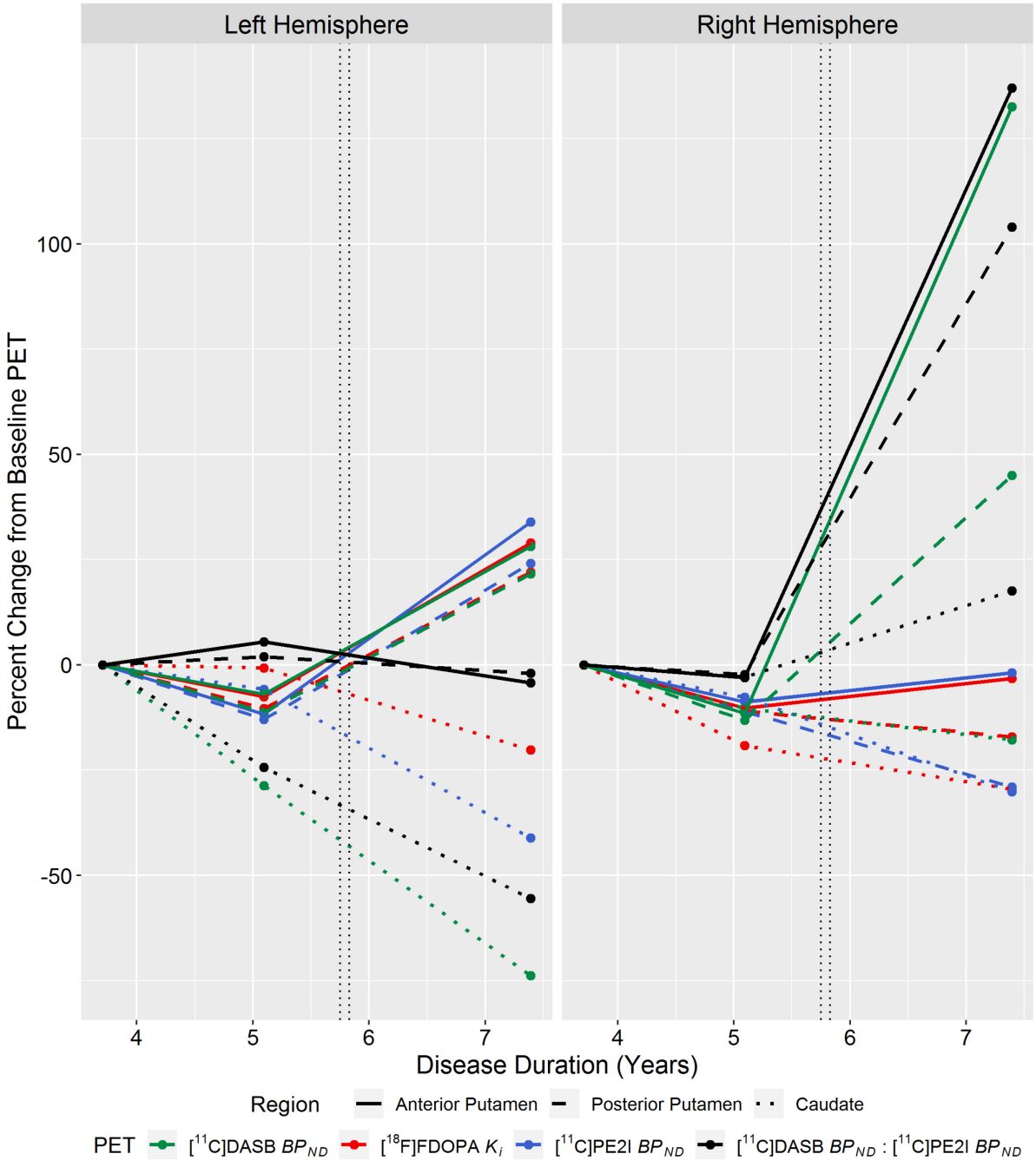


Figure 5.4: Longitudinal dopaminergic and serotonergic changes in patient 18. Progression of [18F]FDOPA K_i (AADC activity), [11C]PE2I BP_{ND} (DAT density), [11C]DASB BP_{ND} (SERT density) and [11C]DASB BP_{ND} : [11C]PE2I BP_{ND} (SERT:DAT ratio) for the anterior putamen, posterior putamen and caudate in patient 18. PET values at pre-transplant and post-transplant time-points were normalised to baseline and presented as percentages to illustrate relative changes between PET measures.

PET values obtained at baseline and pre-transplant confirmed progressive decreases in AADC activity, DAT and SERT density in both the left and right putamen and caudate (Figure 5.4). Between pre-transplant and post-transplant time-points, values for all three

tracers continued to decrease in the caudate, however in the left anterior and posterior putamen, both [^{18}F]FDOPA K_i and [^{11}C]PE2I BP_{ND} increased by ~25% over values obtained 3.5 years previously. [^{11}C]DASB BP_{ND} also increased by a similar degree which was reflected in a stable [^{11}C]PE2I BP_{ND} to [^{11}C]DASB BP_{ND} ratio over time. These changes occurred in the hemisphere contralateral to the body side wherein "off-state" dyskinesias emerged and which was more affected at baseline but subsequently became the least affected side post-transplant.

For the right putamen, ipsilateral to the side that developed GID, there was a slight increase in [^{18}F]FDOPA K_i and [^{11}C]PE2I BP_{ND} in the anterior division as compared to pre-transplant, such that post-transplant values were similar to those shown at baseline, while values in the posterior putamen continued to decline. In contrast, there were large increases in [^{11}C]DASB BP_{ND} of ~130% in the anterior and ~45% in the posterior putamenal regions, resulting in substantially elevated [^{11}C]PE2I BP_{ND} to [^{11}C]DASB BP_{ND} ratios of between ~100-140%. Similar changes were also seen for the ratio between [^{11}C]DASB BP_{ND} and [^{18}F]FDOPA K_i.

The reversal in clinical asymmetry was concordant with the degree to which re-innervation was achieved between the left and right sides but not entirely with absolute putamenal values, which became more symmetrical post-transplant yet retaining greater values in the right over the left (Left/Right [^{18}F]FDOPA K_i: Pre = 0.00446/0.00658; Post = 0.00616/0.00667) (Left/Right [^{11}C]PE2I BP_{ND}: Pre = 1.418/2.308; Post = 2.102/2.215).

5.3. Discussion

In the current chapter, we examined whether dopaminergic and serotonergic re-innervation resulting from bilateral intraputamenal hfVM grafts could explain the induction of graft-induced dyskinesias in a small sample of Parkinson's disease patients. We found that patients with GID displayed greater post-surgical elevations in dopamine transporter density, and to a marginal extent dopamine synthesis and storage capacity, in the anterior putamenal division, but not in the posterior putamen. These findings are in line with an earlier report in a similarly small cohort from the Denver/New York trial (Ma *et al.*, 2002) in which voxel-wise analysis identified a hot-spot within the left ventrorostral putamen reflecting greater AADC activity in five GID+ patients as compared to 5 out of 12 GID- patients who derived the best clinical benefit. It should be noted that the groups presented here also did not differ in the degree of clinical benefit achieved (GID+ = -18.8 ±23.0%; GID- = -11.2 ±21.2%, p = 0.66). We extend these findings by showing that the resultant imbalance across the anterior-posterior putamenal axis was not different between the groups, suggesting that GID does not necessarily emerge as a consequence of relative over-engraftment but rather when cell placement and survival encompasses the anterior domain.

Transplantation procedures restricted to the post-commissural putamen have however produced inconsistent outcomes in this regard; the Canadian series reported no incidence of GID (Mendez *et al.*, 2002; Mendez *et al.*, 2005; Mendez *et al.*, 2008) while 57% of patients from the Tampa randomised trial developed this complication (Olanow *et al.*, 2003; Olanow *et al.*, 2009a). Yet it is interesting to note that in one of these Tampa patients, post-mortem immunohistochemical observations revealed a virtually complete TH+ re-innervation pattern with morphologically healthy and well-integrated neurons extending into the pre-commissural putamen despite this area not receiving any graft deposits (Kordower *et al.*, 2017). Whether this level of outgrowth could underlie the GID seen in other post-commissurally engrafted patients (Olanow *et al.*, 2003) is unknown. Conversely, the autopsy reports from Mendez *et al.* (2005, 2008) of five Halifax patients explicitly documented to have not developed "off-state" dyskinesia are unclear with respect to sub-regional cell survival (Mendez *et al.*, 2005; Mendez *et al.*, 2008). It is non-trivial to draw conclusions from the results of all other clinical trials on the basis of the reported deposit locations, as it is clear

that even when large volumes are grafted, cell survival appears relatively sporadic (Figure 3.7, Figure 3.13, Figure 3.20).

Our results might be considered in contrast to those obtained pre-clinically using LID-induced 6-OHDA rat models. Carlsson *et al.* (2006) reported that animals injected within the caudal aspect of the head of the striatum subsequently developed more severe GID than those grafted within the rostral portion, consistently drawing correlations between GID severity and the rostrocaudal difference in TH+ fiber density (Carlsson *et al.*, 2006). While the rat striatal complex appears to conform to similar topographic functional arrangement (Voorn *et al.*, 2004; Mailly *et al.*, 2013) to those of primates (Haber and McFarland, 1999; Haber, 2003, 2014), proceeding from sensorimotor to associative to limbic domains along a dorsolateral to ventromedial axis, recent work comparing cortico-striatal terminal fields between species suggests a more substantial encroachment of limbic circuits towards the anatomically-defined caudal striatum in the rat that is seen to a lesser extent in macaques (Heilbronner *et al.*, 2016). Thus, striatal division schemes are likely not correspondent in terms of functional anatomy. Our use of the anterior commissure as an anatomical marker largely segregates sensorimotor from associative and limbic domains (Haber and McFarland, 1999; Haber, 2003, 2014), but this is also topographically incomplete and our analysis could be refined by applying histological, functional or structural neuroimaging probabilistic connectivity atlases to our data. Indeed, that rostral re-innervation yields dissimilar clinical outcomes between preclinical and *in vivo* neuroimaging studies raises the possibility of a more intricate zonal susceptibility pattern that is yet to be elucidated with regards to GID in humans. In rats, the ventrolateral striatum appears to be particularly relevant (Winkler *et al.*, 2002) and only in this region do hot-spot grafts (but not multi-site micrografts) induce massive upregulation of ΔFosB-like transcription factors, markers of neuronal plasticity, that are correlated with the degree of stereotypy (Maries *et al.*, 2006). If such dynamic structures exist in the human striatum then it is conceivable that hfVM grafts placed within their vicinity may invoke GID and in a dose-dependent manner (Hagell *et al.*, 2002; Lane *et al.*, 2009b).

It should be noted, and indeed it is widely acknowledged, that preclinical models do not fully emulate true GID; as opposed to these effects being observed in the "off-state" and

even after long-term cessation of L-dopa in humans (Politis *et al.*, 2010b; Politis *et al.*, 2011; Kefalopoulou *et al.*, 2014), in rats these atypical behaviours are only observed following administration of L-dopa or amphetamine. Moreover, work with 6-OHDA rats suggests that priming with L-dopa and induction of pre-graft LID is required in order for transplants to induce GID (Lane *et al.*, 2009b; Garcia *et al.*, 2011). The development of GID in patient 18 strongly suggests that this is not necessary in humans, as aside from L-dopa challenge as per protocol, she had never taken L-dopa nor had any signs of drug-induced dyskinesia prior to transplant. To our knowledge, all previously transplanted patients have had a long-standing history L-dopa therapy and as such, discussions over whether L-dopa-induced post-synaptic sensitisation is indeed a pre-requisite condition have largely remained unresolved (Steece-Collier *et al.*, 2009). The observations we report here are supported by prior clinical trial studies showing that in conflict with animal models, there is no correlation between pre-graft LID and post-graft GID (Hagell *et al.*, 2002; Olanow *et al.*, 2009a) and no association with L-dopa dose (Olanow *et al.*, 2009a).

With respect to L-dopa-induced dyskinesias, studies reporting sub-regional dopaminergic imaging outcomes are scarce and most focus their observations on the entire putamen (de la Fuente-Fernández *et al.*, 2001; Pavese *et al.*, 2006; Politis *et al.*, 2014; Eusebi *et al.*, 2018). It has been found that DAT density, as measured using [^{18}F]FP-CIT SPECT, appears to be lower in both the anterior and posterior putamen at initial evaluation in patients who would later develop LID as compared to those followed up for an equivalent mean period of time (Hong *et al.*, 2014). This effect persists even after retrospectively assessed LID- patients were propensity matched by age of onset, gender, time to commence L-dopa therapy and UPDRS-III score at initial evaluation (Yoo *et al.*, 2018). An earlier [^{11}C]raclopride PET study found evidence for greater synaptic dopamine fluctuations in the central putamen in dyskinetic patients as compared to stable responders one hour following L-dopa (de la Fuente-Fernandez *et al.*, 2004). However, this is not concordant with findings of decreased [^{18}F]FDOPA-derived dopamine turnover (Lohle *et al.*, 2016) and an aberrant dissociation between cerebral bloodflow and metabolic rate measured with $H_2{}^{15}O$ and [^{18}F]FDG PET respectively (Jourdain *et al.*, 2016), in the posterior but not anterior putamen in LID+ patients.

Although substantial overlap exists, animal tracing, functional and structural connectivity studies demonstrate the anterior putamen resides within the associative and limbic basal ganglia circuitries (Haber and McFarland, 1999; Haber, 2003; Lehericy *et al.*, 2004; Choi *et al.*, 2012; Haber, 2014; Tziortzi *et al.*, 2014). One preclinical study in MPTP-induced Parkinsonian primates whom had received chronic L-dopa treatment demonstrated that metabolic activity, as measured using [^{3}H]2-deoxyglucose autoradiography, was significantly lower in the associative and limbic divisions of the GPe in dyskinetic as compared to non-dyskinetic animals, but not in the sensorimotor territory. Similarly, the thalamic sub-nucleus involved in the associative basal ganglia loop (mediodorsal), but not the sensorimotor output nuclei (ventral anterior/lateral), also showed significant depression of metabolic activity (Guigoni *et al.*, 2005). No analysis was conducted on the putamen (Guigoni *et al.*, 2005). Further work from the Bezard lab using high-pressure liquid chromatography indicated significant elevations in dopamine and its metabolite 3,4-dihydroxyphenylacetic acid in the hippocampus, amygdala and prefrontal cortex, but not the motor cortex or posterior putamen, while the anterior putamen was untested (Engeln *et al.*, 2015). fMRI studies in humans have shown that the pre-supplementary motor area responds to the administration of L-dopa during no-go trials in the pre-dyskinetic period as an increase in BOLD activity that predicts the severity of the subsequent dyskinetic episode with ~70% variance explained, while increased activity in the anterior putamen held no significant predictive value (Herz *et al.*, 2014). Under the same experimental conditions, effective connectivity between the putamen and primary motor cortex appears to increase, while modulation of striato-cortical feedback coupling measures from putamen to pre-supplementary and primary motor cortices by exogenous L-dopa improved prior model predictions of subsequent LID severity to ~93% variance explained, including significant contributions from both connections (Herz *et al.*, 2015). Similar results have also been seen using fMRI functional connectivity techniques in the resting state (Herz *et al.*, 2016). Others have found that the inferior frontal gyrus exhibits hyperactivity during "off" and hypoactivity during "on" states in dyskinetic patients, opposite to that which is seen in those without (Cerasa *et al.*, 2015b). Similar inversion patterns were also observed for its connectivity to the motor cortex (negative) and mid-putamen (positive) during the "on" state, and repetitive transcranial magnetic stimulation of this area helped ameliorate symptoms of dyskinesia

induced by supramaximal L-dopa dosing (Cerasa *et al.*, 2015a). Recently, whole-brain diffusion-based structural connectomic analyses pointed to a similar region set (inferior frontal gyrus, thalamus, putamen) as having significantly increased nodal efficiency, a graph theoretical parameter describing the single-node connectivity pattern with the rest of the brain, in dyskinetic as compared to non-dyskinetic patients (Wang *et al.*, 2019). Thus it is possible that disruption to the integrative faculties of the limbic and associative sub-cortex in grafted individuals might affect downstream sensorimotor processes including motor execution (Joel and Weiner, 1994; Haber, 2003; Aoki *et al.*, 2019), in a similar manner to that which is postulated for those with LID.

In the current chapter, we failed to find any evidence that GID was caused by aberrant graft-induced elevations in serotonergic as compared to dopaminergic re-innervation. We overtly recognise that our analysis is severely hampered by small samples, however, it offers a major improvement over previous studies in human transplanted subjects on which the serotonergic hypothesis was based (Politis *et al.*, 2010b; Politis *et al.*, 2011). First, the multi-tracer PET imaging data were collected prior to transplant, allowing us to establish whether individuals had previously exhibited elevated ratios and to calculate the change in this measure as a result of therapeutic intervention. Second, our post-transplant data were collected at comparatively regular intervals following transplant, with the majority scanned within 18 months of the first procedure and only 1 subject scanned at approximately 3 years following transplant. Third, and perhaps most important, is that the same scanning protocol was conducted on transplanted individuals who at the post-transplant time-point had not developed graft-induced dyskinesia.

Serotonergic neurons can take up and convert L-dopa, store and release dopamine in an activity–dependent manner, but the absence of D_2-autoreceptor-mediated feedback renders them susceptible to non-physiologic dopamine release (Maeda *et al.*, 2005; Carlsson *et al.*, 2007; Carta *et al.*, 2007; Carta *et al.*, 2010). This mechanism appears valid under circumstances of excess synaptic dopamine that overwhelms the re-uptake and storage capacity of the surviving dopaminergic population, such as in the case of acute exogenous L-dopa provision. A critical characteristic of GID is that it appears in the "off-state" and even after long-term drug cessation, which negates the possible influence of trace plasma dopamine. If

grafted dopaminergic neurons remain healthy and express the necessary re-uptake machinery then presumably there would be no "fuel for the fire" and even large increases in the serotonergic population may be inconsequential. This is supported by preclinical studies, in which GID in 6-OHDA rats was evoked when grafts contained dopamine neurons only or, to a lesser degree, when transplants included a mixture of dopamine + serotonin neurons (Carlsson *et al.*, 2007; Garcia *et al.*, 2012; Shin *et al.*, 2012), but not when grafting was conducted purely with serotonin cells (Carlsson *et al.*, 2007; Shin *et al.*, 2012). Of the few post-mortem studies conducted in humans only two have reported on serotonergic innervation with explicit documentation of the presence of GID. In one patient from the Tampa randomised trial, for whom DBS was indicated to reduce GID severity, immunohistochemistry found more than 300, 000 TH+ cells per side, but very few serotonergic cells within the graft (counts not reported) (Kordower *et al.*, 2017). Conversely, in five Halifax patients who remained free of GID, the post-commissural graft sites displayed ample TrypOH+ staining (Mendez *et al.*, 2008). An interesting clinical-imaging observation of our case report is that although huge increases in SERT/DAT ratio were noted in one side of the brain, her GID appeared and remained on the ipsilateral body side. In a Lund series patient who developed GID from a unilateral transplant, abnormal movements appeared only on the contralateral body side (Li *et al.*, 2016), in line with the classic inverse dopamine-clinical asymmetry observed in Parkinson's disease. Collectively, these data oppose the hypothesis that aberrant serotonergic grafting is associated with GID.

Serotonin neurons may still modulate dyskinesia. Indeed, inhibition of serotonergic activity by selective 5-HT_{1A} and 5-HT_{1B} agonists 8-OH-DPAT and CP94253 significantly reduced GID, but that their associated efficacy was abolished when injecting 5,7-dihydroxytryptamine into the medial forebrain bundle would implicate the involvement of endogenous rather than graft-derived serotonergic terminals (Lane *et al.*, 2009a; Shin *et al.*, 2012). Interestingly, such lesions did not affect GID expression or the anti-GID effect of buspirone, while selective D_2 antagonism by eticlopride (Shin *et al.*, 2012) or raclopride (Lane *et al.*, 2009a) exerted effective GID suppression, suggesting that the prior pharmacodynamic observations made in long-term patients (Politis *et al.*, 2010b; Politis *et al.*, 2011) were probably due to drug-actions on D_2 receptors. Increasing serotonergic activity by inducing excessive neurotransmitter release (fenfluramine) or by blocking SERT sites (fluvoxamine)

can significantly worsen GID but *only* when the dopamine neuron population is also manipulated e.g. by either DAT inhibition (GBR-12909) or stimulating release (amphetamine) (Lane *et al.*, 2006; Shin *et al.*, 2012), suggesting that serotonergic neurons only modulate GID when dopaminergic neurons become dysfunctional.

Since "off-state" dyskinesia rarely occurs in non-grafted individuals (and if they do they are not as severe and are phenomenologically dissimilar), this phenomenon may be specific to the growth of embryonic cells within the diseased host environment. We have seen in Chapter 3 that transplanted dopamine neurons also express the dopamine transporter, however, we cannot say whether this is to a "healthy" level or if it is retained without subversion to the compensatory regulatory processes characteristic of host dopaminergic neurons aimed at increasing synaptic dopamine concentrations (Lee *et al.*, 2000; Nandhagopal *et al.*, 2009; Nandhagopal *et al.*, 2011). Indeed, in some studies graft-induced increases in DAT expression was seen to be limited (Hoffer *et al.*, 1992; Cochen *et al.*, 2003). It remains possible that host immunological reactions may compromise cellular function (Soderstrom *et al.*, 2008); in trials utilising no, short or mild suppression regimes, incidence of GID was relatively high (Freed *et al.*, 2001; Olanow *et al.*, 2003), and in a Lund subset withdrawal coincided with worsening of GID severity without detriment to cell survival (Piccini *et al.*, 2005). Similarly, patient 18 began exhibiting GID very soon after partial withdrawal at only three months while [^{18}F]FDOPA remained elevated at 18 months. However, preclinical trials indicate that induced neuroinflammation in and around graft sites is insufficient for generating GID (Lane *et al.*, 2008), and in the Tampa autopsy case neuroinflammatory biomarkers were noted as unremarkable (Kordower *et al.*, 2017). Moreover, our preliminary diffusion tensor imaging findings of mean diffusivity and fractional anisotropy as surrogates for increased oedema or surgical trauma indicate no putamenal differences between groups (data not shown). Still, future trials may benefit from *in vivo* monitoring of neuroinflammatory processes including microglial (e.g. ^{11}C-(*R*)-PK11195) and astroglial (e.g. [^{11}C]BU99008) activation.

Aside from our low sample size, an important limitation is the procurement of AIMS dyskinesia rating scores that only provides bilateral measurements, as opposed to other scales such as the CDRS, which does allow lateralised scoring. Clearly, on the basis of our

case report for whom we had the benefit of clinical assessment and access to video recordings, this may prove to be an important loss of information that we suggest future trials with potential for asymmetrical therapeutic application rectify. It has also been found previously that the graft-related effects on cortical cerebral bloodflow and motor scores only become detectable up to a year subsequent to the significant changes in putamenal dopaminergic function observed at 6.5 months (Piccini *et al.*, 2000). As such our follow-up time-point was similar, however it could be argued that our PET data might also be reflective of prospective clinical expression in addition to that which is seen at the same time-point. We therefore ascertained whether any of our patients developed GID further to the post-transplant time-point. From our five GID- patients, none developed this complication within 30 months, but one began to exhibit signs approximately 3.5 years following surgery. However, re-allocating this patient to the GID+ group made no difference to any of our results.

These findings have major implications on the future of cell-based therapeutics. Graft-induced complications such as dyskinesias represent a major limitation to the potential beneficial effect of cell therapy; in some cases they can be so severe and refractory to conventional pharmaceutical lines of treatment as to warrant further surgical intervention, which have also proven inconsistent in this regard and are not without their own risks. It is acknowledged that owing to a vast array of difficulties in procuring an adequate volume of viable hfVM tissue for each surgery, reviewed by Barker *et al.* (2019), that this particular cellular intervention will not proceed to the clinic (Barker and Transeuro Consortium, 2019). The movement towards stem cell lines quells many of these issues. However, it is also currently believed by many that relief of serotonergic cells from implanted tissue greatly reduces the risk of developing graft-induced dyskinesia. Given our data, we cautiously suggest that graft-related serotonergic hyperinnervation does not cause GID, at least at an early stage post-transplant, and that it may be sub-served by sub-region-specific over-engraftment. However, owing to our low sample size these conclusions remain tentative. Further preclinical studies evaluating graft placement within focal areas of the putamenal homolog are needed to ascertain whether limbic or associative regions are sensitive to producing this side effect. Collaborative pooling of existing imaging data in humans would

also be hugely beneficial for testing this hypothesis, as well as for more general re-appraisal in light of the potential for analogous risk factors of other cell interventions.

Chapter 6. General Discussion: Summary of Findings

Parkinson's disease is the second most common neurodegenerative disease characterised by the presence of α-synuclein-immunopositive intraneuronal proteinaceous inclusions (Lewy pathology) and the progressive loss of neuromelanin-laden dopaminergic cells of the substantia nigra pars compacta, resulting in striatal denervation and emergence of cardinal motor features including bradykinesia, rigidity, tremor and postural instability. Dopaminomimetic agents provide effective symptomatic relief in the early stages of illness, yet due to the inherently progressive nature of the disease and the induction of debilitating side effects their efficacy is eventually lost. Cellular strategies involving intrastriatal transplantation of human fetal ventral mesencephalic (hfVM) tissue began 30 years ago when a number of multidisciplinary teams across the globe reported on the potential clinical gains that could be achieved by inducing a more physiologically relevant manner of dopaminergic function. However, the outcomes of two NIH-funded double-blind randomised controlled trials were at best disappointing and furthermore reported the emergence of novel "off-state" graft-induced dyskinesia that upon retrospective review appeared to have also occurred in many patients transplanted under prior open-label efforts. Both post-mortem and *in vivo* neuroimaging studies have been insightful for providing potential explanations for such outcomes, highlighting several factors including inadequate graft viability, the lack of dopamine transporter expression, dopamine overdose, "hot-spot" or "patchy" re-innervation, serotonergic presence within the tissue suspensions and pre-operative patient characteristics as amongst the most important for influencing clinical efficacy. The extensive optimisations of all aspects of therapeutic delivery in the currently ongoing Transeuro trial were made upon these data, yet the scope of objective *in vivo* information retrieved from previous trials is appreciably limited, primarily constituting [^{18}F]FDOPA PET with relatively few small-sample or case studies using alternative imaging techniques at varying and unmatched time-points post-graft. Thus an extensive longitudinal neuroimaging battery including PET biomarkers probing both dopamine ([^{11}C]PE2I) and serotonin ([^{11}C]DASB) transporter expression in addition to dopamine synthesis and storage

capacity ([18F]FDOPA) was conceived, in an effort to advance our understanding of the neural mechanisms underlying graft-induced symptomatic modification.

The current thesis presents the *in vivo* PET imaging findings for eight patients who were transplanted bilaterally across the length of the anterior-posterior putamenal axis. In Chapter 3, we found that transplanted patients exhibited significant but modest graft-induced elevations in putamenal dopamine synthesis and storage capacity and dopamine transporter density at 18 months post-surgery, as compared to sixteen patients who remained on optimal dopamine pharmacotherapy and who continued to decline on both measures. A similar interaction was also seen when comparing putamenal and caudatal values, the latter continuing to decline for both measures and indicating that at this early stage hfVM transplants are unable to re-innervate or induce sprouting of host neurons in non-engrafted regions. The degree of cell survival was positively related to DAT expression, as measured using [18F]FDOPA and [11C]PE2I respectively, and this association was markedly different to that seen in the PD control group, reflecting the potential for grafted neurons to express the dopamine transporter and retain auto-regulatory function within the host environment, without full subjection to the compensatory plasticity inherent within endogenous dopaminergic neurons. Our findings relating to a greater magnitude of change in dopamine transporter density, but not AADC activity, following intervention in the putamen contralateral to the side on which symptoms were most severe prior to transplant raises the possibility that in line with early preclinical work, the degree of pre-operative intrinsic denervation may influence specific aspects of embryonic cell development. Given that our patients were in a milder stage of disease than those recruited for previous trials this might explain why imaging outcomes in the current study were comparably mild. We used a novel method for evaluating the consistency of cell deposition and/or cell survival across the putamen, finding that despite carefully considered modifications to the cell delivery protocol, the effort to induce homogenous re-innervation was unsuccessful. Given that the patterns of increased/decreased PET signal were wildly different between subjects, we posit that this is less likely a result of cell preparation or host-graft interaction and more so an issue related to surgical technique. Lastly, we provide evidence for a significant but comparatively low increase in serotonin transporter density within the grafted putamen at an early stage post-transplant, highlighting both an improvement to fetal dissection

methodology and the difficulty in completely eliminating serotonergic contamination. These cells may however continue to mature beyond this point and our estimates may be confounded by a potential serotonin modulating effect of corticosteroids.

The purpose of Chapter 4 was to establish whether hfVM transplantation under the Transeuro protocol had a significant impact on clinical symptomatology over a 60-month period as compared to patients on optimal drug therapy and whether changes in these measures were related to graft-induced dopaminergic and/or serotonergic re-innervation. We found that measures of tremor and rigidity, as measured using the UPDRS-III sub-scales, were significantly improved in the transplant group, while there was no change in bradykinesia or axial symptoms. Post-operative increases in both dopamine and serotonin transporter density in the motor domain of the putamen predicted improvement of tremor, whereas increased serotonin transporter density was detrimental to the potential for dopamine-derived alleviation of bradykinesia, offering a mechanistic basis for the interpretation of the clinical outcome in the current as well as previous trials that also stands as an important addition to the general clinicopathologic understanding of PD symptomatology across the wider literature. In contrast, we found that neither post-operative dopaminergic nor serotonergic changes were able to explain the significant improvement in rigidity. Given that rigidity has consistently been shown to have strong dopaminergic component, we posit that regions other than the posterior putamen, including cortical inhibitory hubs or more rostral associative/limbic putamenal territories may modulate clinical presentation. However, we also believe that the difficulty in assessing rigidity consistently across a multi-centre study such as this may impact our correlative findings. Such issues with the UPDRS-III are highlighted in their discordance with objective measures of bradykinesia, including the 9-hole peg board and 30 second tap test, for which significantly improved performance was indicated for the transplant as compared to the PD control group. In line with the current literature implicating cholinergic involvement in the disruption of gait, posture and balance, we did not find any significant modification to UPDRS-III axial sub-score with respect to PD control, and the change in severity was not explained by dopaminergic and serotonergic biomarkers. Finally, we established that the achievement of homogenous re-innervation of the target nucleus may have a significant

impact upon clinical efficacy and may be important in maximising the potential clinical benefit derived from cell transplantation strategies.

In Chapter 5, we investigated the role of dopaminergic and serotonergic re-innervation in the emergence of graft-induced dyskinesias in our group of eight transplanted patients. At the time of post-operative PET acquisition, three of these patients had developed detectable GID. We found that patients with GID displayed greater post-surgical elevations in dopamine transporter density and to a marginal extent dopamine synthesis and storage capacity, in the anterior putamenal division, but not in the posterior putamen, as compared to those who did not develop GID. Moreover, the derivation of imbalance indices between anterior and posterior sub-regions allowed us to discount the possibility that GID may be associated with relative over-engraftment, and rather that it appears when engraftment encompasses the associative/limbic domains. Conversely, we found no evidence supporting a role of graft-induced serotonergic hyperinnervation on the generation of GID, as postulated by the only other serotonergic imaging study conducted in transplanted patients. However, we note here that this work does not discredit the possibility of the involvement of host serotonergic cells. Given the influence of these aforementioned studies on the field of cell therapy, these findings have huge impact, as they suggest that GID remains a possible outcome even when serotonergic neurons are entirely abated from the cell preparations. There were no clinical or imaging measures at pre-transplant that were able to distinguish between patients who would from those who would not later develop GID. Indeed, the close evaluation of our case study provides contradictory evidence to the current opinion on the risk to develop GID following surgery, demonstrating that prior hypersensitisation by L-dopa, and relatedly the development of LID, are not strong pre-requisite conditions in humans.

Chapter 7. Limitations and Future Directions

The interpretation of our results and the methods by which we can analyse our data are severely limited by our small sample size. Initially, the Transeuro trial endeavoured to recruit 40 patients, randomised 1:1 to either transplant or control groups. However, the trial itself underwent severe delays brought upon by numerous factors including the consistent lack of substantial fetal tissue at any one time, limiting the number of patients that could be transplanted. Future trials are expected be relieved of this problem given that stem-cell-derived neurons should be readily and consistently available (Barker and Transeuro Consortium, 2019).

A knock-on effect of this was that on the basis of PET-based transplant exclusion criteria, PET imaging had to be repeated a second time prior to transplant, instead of at 18 months and 36 months following transplant, limiting our ability to more comprehensively track the development of grafted neurons over time and assess the neural correlates of long-term clinical recovery. Relatedly, we were unable scan PD control patients at a third time-point, meaning that we cannot discern whether some effects of the therapeutic process observed for our transplant group were due to the natural progression of the disease. As well as repeated measurements, this issue could also be resolved by ensuring that patients between groups are matched on measures of disease severity or duration at the time of scanning.

We have discussed in Chapter 3 the possible influence of corticosteroids on serotonergic function and specifically the serotonin transporter. If indeed this is the case, then it would follow that putamenal serotonergic values may also be attenuated and as such our data may underestimate the degree of serotonergic re-innervation. This could have implications on the estimates and interpretations of our clinical correlative analyses. Future trials using radioligands specific for the serotonergic system should ensure ample withdrawal periods from such medications prior to acquisition.

A major limitation of the current work is the lack of scans acquired for matched healthy control subjects. Healthy values would be useful for establishing a normative level of dopaminergic and serotonergic function against which to compare our patient data. Most

importantly, this would allow the derivation of standardised measures for the PD patients, which would in turn permit direct between-tracer comparisons regarding the relative rates of change, both as a result of surgery and as a function of natural disease progression. Indeed, Parkinson's disease is highly dynamic and neurotransmitter systems progress at different rates between different regions (Kish *et al.*, 2008; Nandhagopal *et al.*, 2009; Maillet *et al.*, 2016; Fazio *et al.*, 2020) (Kish *et al.*, 2008; Maillet *et al.*, 2016; Fazio *et al.*, 2020). The ability to account for this would significantly improve interpretability.

The method with which we derived an index of putamenal coverage is limited in a number of ways. First, because we employed a zero-point cut-off, the index may underestimate the degree of coverage in areas where endogenous neurodegeneration supersedes graft-induced re-innervation. It is also insensitive to large signal fluctuations where both the peaks and troughs remain above threshold. Indeed, such fluctuations may also be considered reflective of inhomogeneity. Moreover, profiles and coverage indices were generated from data that had been smoothed as part of the scanner reconstruction process. As opposed to the majority of analyses, in this particular case it may be more informative to evaluate images prior to smoothing.

As we did not have access to cell data, we were not able to directly evaluate the relationship between cell preparations (i.e. TH+ or SERT+ volume and cell numbers) and post-operative changes in PET data. This would be an important addition to the current work and would narrow the potential factors that may be responsible for inter-subject variability in outcomes.

The method by which we assessed the effect of posterior putamenal coverage on change in clinical symptoms does not permit understanding of the relative importance of this variable against the overall magnitude of re-innervation. The use of somatotopic atlases (Choi *et al.*, 2012) would in theory override the relevance of this index, by permitting assessment of smaller more localised parcels and their relationship with measures of motor ability from correspondent parts of the body. We did not enact this in the current work as we were concerned that reducing the UPDRS-III to single-item scores would greatly heighten the variability of measurements. Thus if this is to be done in future trials, in which heterogeneity of cell deposition will likely remain problematic, it is suggested that kinematic, robotic or

wearable technology (Heldman *et al.*, 2011; Ruzicka *et al.*, 2016; Gaprielian *et al.*, 2019; Linn-Evans *et al.*, 2020) be employed in conjunction with the standard rating scales.

Another limitation to the current work is that we did not consider extra-putamenal regions when assessing the impact of hfVM grafts on clinical presentation. Indeed, there is mounting evidence that both associative/limbic divisions of the basal ganglia and inhibitory neocortical nodes may moderate sensorimotor processes (Joel and Weiner, 1994; Haber, 2003; Guigoni *et al.*, 2005; Yu *et al.*, 2007; Cerasa *et al.*, 2015a; Aoki *et al.*, 2019; Wang *et al.*, 2019; van Nuland *et al.*, 2020). In addition, previous work using $H_2{}^{15}O$ PET has demonstrated that resurgence of cortical activity is delayed with respect to detectable increases in putamenal dopaminergic function (Piccini *et al.*, 2000). The inclusion of functional MRI data in accordance with movement paradigms would enrich the interpretation of the current results with regard to both symptoms that do not appear to have a dopaminergic or serotonergic substrate such as rigidity, as well as to those that do i.e. tremor and bradykinesia.

It is possible that host immunological reactions may compromise cellular function (Soderstrom *et al.*, 2008); in trials utilising no, short or mild suppression regimes, symptomatic improvement was negligible and the incidence of GID was relatively high (Freed *et al.*, 2001; Olanow *et al.*, 2003). While rodent studies indicate that neuroinflammation in and around graft sites is insufficient for generating GID (Lane *et al.*, 2008), it may be advisable to consider evaluating the immunogenic response *in vivo* through the use of additional radioligands such as [^{11}C](*R*)-PK11195 and [^{11}C]BU99008. Moreover, cortical injury or more specifically the presence of oedema may be assessed using diffusion-weighted imaging measures of the apparent diffusion coefficient.

Bibliography

Abbott RD, Petrovitch H, White LR, Masaki KH, Tanner CM, Curb JD, *et al.* Frequency of bowel movements and the future risk of Parkinson's disease. *Neurology* 2001; 57: 456-62.

Abe K, Shimada R, Okada Y, Kibayashi K. Traumatic brain injury decreases serotonin transporter expression in the rat cerebrum. *Neurol Res* 2016; 38: 358-63.

Abeyawardhane DL, Fernandez RD, Murgas CJ, Heitger DR, Forney AK, Crozier MK, *et al.* Iron Redox Chemistry Promotes Antiparallel Oligomerization of alpha-Synuclein. *J Am Chem Soc* 2018; 140: 5028-32.

Abi-Dargham A, Gandelman MS, DeErausquin GA, Zea-Ponce Y, Zoghbi SS, Baldwin RM, *et al.* SPECT imaging of dopamine transporters in human brain with iodine-123-fluoroalkyl analogs of beta-CIT. *J Nucl Med* 1996; 37: 1129-33.

Adams-Carr KL, Bestwick JP, Shribman S, Lees A, Schrag A, Noyce AJ. Constipation preceding Parkinson's disease: a systematic review and meta-analysis. *J Neurol Neurosurg Psychiatry* 2016; 87: 710-6.

Adams JR, van Netten H, Schulzer M, Mak E, McKenzie J, Strongosky A, *et al.* PET in LRRK2 mutations: comparison to sporadic Parkinson's disease and evidence for presymptomatic compensation. *Brain* 2005; 128: 2777-85.

Adler CH, Beach TG, Hentz JG, Shill HA, Caviness JN, Driver-Dunckley E, *et al.* Low clinical diagnostic accuracy of early vs advanced Parkinson disease: clinicopathologic study. *Neurology* 2014; 83: 406-12.

Agostino R, Curra A, Giovannelli M, Modugno N, Manfredi M, Berardelli A. Impairment of individual finger movements in Parkinson's disease. *Mov Disord* 2003; 18: 560-5.

Ahlskog JE, Muenter MD. Frequency of levodopa-related dyskinesias and motor fluctuations as estimated from the cumulative literature. *Mov Disord* 2001; 16: 448-58.

Ahn BH, Rhim H, Kim SY, Sung YM, Lee MY, Choi JY, *et al.* alpha-Synuclein interacts with phospholipase D isozymes and inhibits pervanadate-induced phospholipase D activation in human embryonic kidney-293 cells. *J Biol Chem* 2002; 277: 12334-42.

Ahn TB, Langston JW, Aachi VR, Dickson DW. Relationship of neighboring tissue and gliosis to α-synuclein pathology in a fetal transplant for Parkinson's disease. *American journal of neurodegenerative disease* 2012; 1: 49-59.

Albin RL, Koeppe RA, Bohnen NI, Wernette K, Kilbourn MA, Frey KA. Spared caudal brainstem SERT binding in early Parkinson's disease. *J Cereb Blood Flow Metab* 2008; 28: 441-4.

Albin RL, Young AB, Penney JB. The functional anatomy of basal ganglia disorders. *Trends Neurosci* 1989; 12: 366-75.

Alegre-Abarrategui J, Brimblecombe KR, Roberts RF, Velentza-Almpani E, Tilley BS, Bengoa-Vergniory N, *et al.* Selective vulnerability in alpha-synucleinopathies. *Acta Neuropathol* 2019; 138: 681-704.

Alessio A, Kinahan P. PET image reconstruction. In: Henkin RE, editor. Nuclear Medicine. 2nd ed. Philadelphia: Mosby Elsevier; 2006.

Alex KD, Yavanian GJ, McFarlane HG, Pluto CP, Pehek EA. Modulation of dopamine release by striatal 5-HT2C receptors. *Synapse* 2005; 55: 242-51.

Alexander GE, Crutcher MD. Functional architecture of basal ganglia circuits: neural substrates of parallel processing. *Trends Neurosci* 1990; 13: 266-71.

Alexander GE, DeLong MR, Strick PL. Parallel organization of functionally segregated circuits linking basal ganglia and cortex. *Annu Rev Neurosci* 1986; 9: 357-81.

Allen NE, Schwarzel AK, Canning CG. Recurrent falls in Parkinson's disease: a systematic review. *Parkinsons Dis* 2013; 2013: 906274.

Allyson Jones C, Wayne Martin WR, Wieler M, King-Jesso P, Voaklander DC. Incidence and mortality of Parkinson's disease in older Canadians. *Parkinsonism Relat Disord* 2012; 18: 327-31.

Alonso A, Rodriguez LA, Logroscino G, Hernan MA. Use of antidepressants and the risk of Parkinson's disease: a prospective study. *J Neurol Neurosurg Psychiatry* 2009; 80: 671-4.

Aloyo VJ, Ruffin JS, Pazdalski PS, Kirifides AL, Harvey JA. [3H]WIN 35,428 binding in the caudate nucleus of the rabbit: evidence for a single site on the dopamine transporter. *J Pharmacol Exp Ther* 1995; 273: 435-44.

Andica C, Kamagata K, Hatano T, Okuzumi A, Saito A, Nakazawa M, *et al.* Neurite orientation dispersion and density imaging of the nigrostriatal pathway in Parkinson's disease: Retrograde degeneration observed by tract-profile analysis. *Parkinsonism Relat Disord* 2018; 51: 55-60.

Antonini A, Barone P, Marconi R, Morgante L, Zappulla S, Pontieri FE, *et al.* The progression of non-motor symptoms in Parkinson's disease and their contribution to motor disability and quality of life. *J Neurol* 2012; 259: 2621-31.

Antonini A, Moresco RM, Gobbo C, De Notaris R, Panzacchi A, Barone P, *et al.* The status of dopamine nerve terminals in Parkinson's disease and essential tremor: a PET study with the tracer [11-C]FE-CIT. *Neurol Sci* 2001; 22: 47-8.

Antonini A, Poewe W, Chaudhuri KR, Jech R, Pickut B, Pirtosek Z, *et al.* Levodopa-carbidopa intestinal gel in advanced Parkinson's: Final results of the GLORIA registry. *Parkinsonism Relat Disord* 2017; 45: 13-20.

Antonini A, Schwarz J, Oertel WH, Beer HF, Madeja UD, Leenders KL. [11C]raclopride and positron emission tomography in previously untreated patients with Parkinson's disease: Influence of L-dopa and lisuride therapy on striatal dopamine D2-receptors. *Neurology* 1994; 44: 1325-9.

Antonini A, Schwarz J, Oertel WH, Pogarell O, Leenders KL. Long-term changes of striatal dopamine D2 receptors in patients with Parkinson's disease: a study with positron emission tomography and [11C]raclopride. *Mov Disord* 1997; 12: 33-8.

Antonini A, Vontobel P, Psylla M, Gunther I, Maguire PR, Missimer J, *et al.* Complementary Positron Emission Tomographic Studies of the Striatal Dopaminergic System in Parkinsons-Disease. *Arch Neurol* 1995; 52: 1183-90.

Aoki S, Smith JB, Li H, Yan X, Igarashi M, Coulon P, *et al.* An open cortico-basal ganglia loop allows limbic control over motor output via the nigrothalamic pathway. *eLife* 2019; 8.

Appel-Cresswell S, Vilarino-Guell C, Encarnacion M, Sherman H, Yu I, Shah B, *et al.* Alpha-synuclein p.H50Q, a novel pathogenic mutation for Parkinson's disease. *Mov Disord* 2013; 28: 811-3.

Appel L, Jonasson M, Danfors T, Nyholm D, Askmark H, Lubberink M, *et al.* Use of C-11-PE2I PET in Differential Diagnosis of Parkinsonian Disorders. *J Nucl Med* 2015; 56: 234-42.

Ashburner J. A fast diffeomorphic image registration algorithm. *Neuroimage* 2007; 38: 95-113.

Ashburner J, Ridgway GR. Symmetric diffeomorphic modeling of longitudinal structural MRI. *Front Neurosci* 2012; 6: 197.

Ashour R, Jankovic J. Joint and skeletal deformities in Parkinson's disease, multiple system atrophy, and progressive supranuclear palsy. *Mov Disord* 2006; 21: 1856-63.

Aviles-Olmos I, Kefalopoulou Z, Tripoliti E, Candelario J, Akram H, Martinez-Torres I, *et al.* Long-term outcome of subthalamic nucleus deep brain stimulation for Parkinson's disease using an MRI-guided and MRI-verified approach. *J Neurol Neurosurg Psychiatry* 2014; 85: 1419-25.

Baba M, Nakajo S, Tu PH, Tomita T, Nakaya K, Lee VM, *et al.* Aggregation of alpha-synuclein in Lewy bodies of sporadic Parkinson's disease and dementia with Lewy bodies. *The American journal of pathology* 1998; 152: 879-84.

Barbosa P, Lees AJ, Magee C, Djamshidian A, Warner TT. A Retrospective Evaluation of the Frequency of Impulsive Compulsive Behaviors in Parkinson's Disease Patients Treated with Continuous Waking Day Apomorphine Pumps. *Mov Disord Clin Pract* 2017; 4: 323-8.

Barker RA, Transeuro Consortium. Designing stem-cell-based dopamine cell replacement trials for Parkinson's disease. *Nat Med* 2019; 25: 1045-53.

Bastide MF, Meissner WG, Picconi B, Fasano S, Fernagut PO, Feyder M, *et al.* Pathophysiology of L-dopa-induced motor and non-motor complications in Parkinson's disease. *Prog Neurobiol* 2015; 132: 96-168.

Bates D, Machler M, Bolker BM, Walker SC. Fitting Linear Mixed-Effects Models Using lme4. *J Stat Softw* 2015; 67: 1-48.

Beach TG, Adler CH, Sue LI, Peirce JB, Bachalakuri J, Dalsing-Hernandez JE, *et al.* Reduced striatal tyrosine hydroxylase in incidental Lewy body disease. *Acta Neuropathol* 2008; 115: 445-51.

Beaurain M, Salabert AS, Ribeiro MJ, Arlicot N, Damier P, Le Jeune F, *et al.* Innovative Molecular Imaging for Clinical Research, Therapeutic Stratification, and Nosography in Neuroscience. *Frontiers in medicine* 2019; 6: 268.

Behrendt S. lm.beta: Add Standardized Regression Coefficients to lm-Objects. R package version 1.5-1. 2014. Available from: https://CRAN.R-project.org/package=lm.beta.

Benamer HT, Patterson J, Wyper DJ, Hadley DM, Macphee GJ, Grosset DG. Correlation of Parkinson's disease severity and duration with 123I-FP-CIT SPECT striatal uptake. *Mov Disord* 2000; 15: 692-8.

Bengoa-Vergniory N, Roberts RF, Wade-Martins R, Alegre-Abarrategui J. Alpha-synuclein oligomers: a new hope. *Acta Neuropathol* 2017; 134: 819-38.

Berg D, Postuma RB, Adler CH, Bloem BR, Chan P, Dubois B, *et al.* MDS research criteria for prodromal Parkinson's disease. *Mov Disord* 2015; 30: 1600-11.

Berg D, Postuma RB, Bloem B, Chan P, Dubois B, Gasser T, *et al.* Time to redefine PD? Introductory statement of the MDS Task Force on the definition of Parkinson's disease. *Mov Disord* 2014; 29: 454-62.

Bernheimer H, Birkmayer W, Hornykiewicz O, Jellinger K, Seitelberger F. Brain dopamine and the syndromes of Parkinson and Huntington. Clinical, morphological and neurochemical correlations. *J Neurol Sci* 1973; 20: 415-55.

Beucke JC, Plotkin M, Winter C, Endrass T, Amthauer H, Juckel G, *et al.* Midbrain serotonin transporters in de novo and L-DOPA-treated patients with early Parkinson's disease--a [123 I]-ADAM SPECT study. *Eur J Neurol* 2011; 18: 750-5.

Bezard E, Dovero S, Prunier C, Ravenscroft P, Chalon S, Guilloteau D, *et al.* Relationship between the appearance of symptoms and the level of nigrostriatal degeneration in a progressive 1-methyl-4-phenyl-1,2,3,6-tetrahydropyridine-lesioned macaque model of Parkinson's disease. *J Neurosci* 2001; 21: 6853-61.

Bjornestad A, Forsaa EB, Pedersen KF, Tysnes OB, Larsen JP, Alves G. Risk and course of motor complications in a population-based incident Parkinson's disease cohort. *Parkinsonism Relat Disord* 2016; 22: 48-53.

Blazejewska AI, Schwarz ST, Pitiot A, Stephenson MC, Lowe J, Bajaj N, *et al.* Visualization of nigrosome 1 and its loss in PD: pathoanatomical correlation and in vivo 7 T MRI. *Neurology* 2013; 81: 534-40.

Block ML, Zecca L, Hong JS. Microglia-mediated neurotoxicity: uncovering the molecular mechanisms. *Nat Rev Neurosci* 2007; 8: 57-69.

Bloem BR, Hausdorff JM, Visser JE, Giladi N. Falls and freezing of gait in Parkinson's disease: a review of two interconnected, episodic phenomena. *Mov Disord* 2004; 19: 871-84.

Blüml S, Kopyov O, Jacques S, Ross BD. Activation of Neurotransplants in Humans. *Exp Neurol* 1999; 158: 121-5.

Bodner CR, Dobson CM, Bax A. Multiple tight phospholipid-binding modes of alpha-synuclein revealed by solution NMR spectroscopy. *J Mol Biol* 2009; 390: 775-90.

Bohnen NI, Albin RL, Koeppe RA, Wernette KA, Kilbourn MR, Minoshima S, *et al.* Positron emission tomography of monoaminergic vesicular binding in aging and Parkinson disease. *J Cereb Blood Flow Metab* 2006; 26: 1198-212.

Bohnen NI, Frey KA, Studenski S, Kotagal V, Koeppe RA, Constantine GM, *et al.* Extra-nigral pathological conditions are common in Parkinson's disease with freezing of gait: an in vivo positron emission tomography study. *Mov Disord* 2014; 29: 1118-24.

Bohnen NI, Frey KA, Studenski S, Kotagal V, Koeppe RA, Scott PJ, *et al.* Gait speed in Parkinson disease correlates with cholinergic degeneration. *Neurology* 2013; 81: 1611-6.

Bohnen NI, Kanel P, Zhou Z, Koeppe RA, Frey KA, Dauer WT, *et al.* Cholinergic system changes of falls and freezing of gait in Parkinson's disease. *Ann Neurol* 2019; 85: 538-49.

Bohnen NI, Kuwabara H, Constantine GM, Mathis CA, Moore RY. Grooved pegboard test as a biomarker of nigrostriatal denervation in Parkinson's disease. *Neurosci Lett* 2007; 424: 185-9.

Bohnen NI, Müller ML, Koeppe RA, Studenski SA, Kilbourn MA, Frey KA, *et al.* History of falls in Parkinson disease is associated with reduced cholinergic activity. *Neurology* 2009; 73: 1670-6.

Boileau I, Guttman M, Rusjan P, Adams JR, Houle S, Tong J, *et al.* Decreased binding of the D3 dopamine receptor-preferring ligand [11C]-(+)-PHNO in drug-naive Parkinson's disease. *Brain* 2009; 132: 1366-75.

Booij J, Tissingh G, Boer GJ, Speelman JD, Stoof JC, Janssen AG, *et al.* [123I]FP-CIT SPECT shows a pronounced decline of striatal dopamine transporter labelling in early and advanced Parkinson's disease. *J Neurol Neurosurg Psychiatry* 1997; 62: 133-40.

Braak H, Del Tredici K. Potential Pathways of Abnormal Tau and alpha-Synuclein Dissemination in Sporadic Alzheimer's and Parkinson's Diseases. *Cold Spring Harb Perspect Biol* 2016; 8.

Braak H, Del Tredici K, Rüb U, de Vos RA, Jansen Steur EN, Braak E. Staging of brain pathology related to sporadic Parkinson's disease. *Neurobiol Aging* 2003a; 24: 197-211.

Braak H, Ghebremedhin E, Rub U, Bratzke H, Del Tredici K. Stages in the development of Parkinson's disease-related pathology. *Cell Tissue Res* 2004; 318: 121-34.

Braak H, Rub U, Gai WP, Del Tredici K. Idiopathic Parkinson's disease: possible routes by which vulnerable neuronal types may be subject to neuroinvasion by an unknown pathogen. *J Neural Transm (Vienna)* 2003b; 110: 517-36.

Braak H, Sandmann-Keil D, Gai W, Braak E. Extensive axonal Lewy neurites in Parkinson's disease: a novel pathological feature revealed by alpha-synuclein immunocytochemistry. *Neurosci Lett* 1999; 265: 67-9.

Brooks DJ, Ibanez V, Sawle GV, Playford ED, Quinn N, Mathias CJ, *et al.* Striatal D2 receptor status in patients with Parkinson's disease, striatonigral degeneration, and progressive supranuclear palsy, measured with 11C-raclopride and positron emission tomography. *Ann Neurol* 1992; 31: 184-92.

Brooks DJ, Ibanez V, Sawle GV, Quinn N, Lees AJ, Mathias CJ, *et al.* Differing patterns of striatal 18F-dopa uptake in Parkinson's disease, multiple system atrophy, and progressive supranuclear palsy. *Ann Neurol* 1990; 28: 547-55.

Broussolle E, Dentresangle C, Landais P, Garcia-Larrea L, Pollak P, Croisile B, *et al.* The relation of putamen and caudate nucleus 18F-Dopa uptake to motor and cognitive performances in Parkinson's disease. *J Neurol Sci* 1999; 166: 141-51.

Brown WD, Taylor MD, Roberts AD, Oakes TR, Schueller MJ, Holden JE, *et al.* FluoroDOPA PET shows the nondopaminergic as well as dopaminergic destinations of levodopa. *Neurology* 1999; 53: 1212-8.

Bruck A, Aalto S, Nurmi E, Vahlberg T, Bergman J, Rinne JO. Striatal subregional 6-[18F]fluoro-L-dopa uptake in early Parkinson's disease: a two-year follow-up study. *Mov Disord* 2006; 21: 958-63.

Bruck A, Aalto S, Rauhala E, Bergman J, Marttila R, Rinne JO. A follow-up study on 6-[18F]fluoro-L-dopa uptake in early Parkinson's disease shows nonlinear progression in the putamen. *Mov Disord* 2009; 24: 1009-15.

Brundin P, Li JY, Holton JL, Lindvall O, Revesz T. Research in motion: the enigma of Parkinson's disease pathology spread. *Nat Rev Neurosci* 2008; 9: 741-5.

Brundin P, Melki R. Prying into the Prion Hypothesis for Parkinson's Disease. *J Neurosci* 2017; 37: 9808-18.

Brundin P, Pogarell O, Hagell P, Piccini P, Widner H, Schrag A, *et al.* Bilateral caudate and putamen grafts of embryonic mesencephalic tissue treated with lazaroids in Parkinson's disease. *Brain* 2000; 123 (Pt 7): 1380-90.

Buell AK, Galvagnion C, Gaspar R, Sparr E, Vendruscolo M, Knowles TP, *et al.* Solution conditions determine the relative importance of nucleation and growth processes in alpha-synuclein aggregation. *Proc Natl Acad Sci U S A* 2014; 111: 7671-6.

Buhusi CV, Meck WH. What makes us tick? Functional and neural mechanisms of interval timing. *Nat Rev Neurosci* 2005; 6: 755-65.

Burke MV, Nocjar C, Sonneborn AJ, McCreary AC, Pehek EA. Striatal serotonin 2C receptors decrease nigrostriatal dopamine release by increasing GABA-A receptor tone in the substantia nigra. *J Neurochem* 2014; 131: 432-43.

Burke RE, O'Malley K. Axon degeneration in Parkinson's disease. *Exp Neurol* 2013; 246: 72-83.

Burre J, Sharma M, Sudhof TC. alpha-Synuclein assembles into higher-order multimers upon membrane binding to promote SNARE complex formation. *Proc Natl Acad Sci U S A* 2014; 111: E4274-83.

Burre J, Sharma M, Sudhof TC. Cell Biology and Pathophysiology of alpha-Synuclein. *Cold Spring Harb Perspect Med* 2018; 8.

Burré J, Sharma M, Tsetsenis T, Buchman V, Etherton MR, Südhof TC. Alpha-synuclein promotes SNARE-complex assembly in vivo and in vitro. *Science* 2010; 329: 1663-7.

Buter TC, van den Hout A, Matthews FE, Larsen JP, Brayne C, Aarsland D. Dementia and survival in Parkinson disease: a 12-year population study. *Neurology* 2008; 70: 1017-22.

Cabello CR, Thune JJ, Pakkenberg H, Pakkenberg B. Ageing of substantia nigra in humans: cell loss may be compensated by hypertrophy. *Neuropathol Appl Neurobiol* 2002; 28: 283-91.

Calo L, Wegrzynowicz M, Santivanez-Perez J, Grazia Spillantini M. Synaptic failure and alpha-synuclein. *Mov Disord* 2016; 31: 169-77.

Caminiti SP, Presotto L, Baroncini D, Garibotto V, Moresco RM, Gianolli L, *et al.* Axonal damage and loss of connectivity in nigrostriatal and mesolimbic dopamine pathways in early Parkinson's disease. *NeuroImage Clinical* 2017; 14: 734-40.

Carlsson T, Carta M, Winkler C, Bjorklund A, Kirik D. Serotonin neuron transplants exacerbate L-DOPA-induced dyskinesias in a rat model of Parkinson's disease. *J Neurosci* 2007; 27: 8011-22.

Carlsson T, Winkler C, Lundblad M, Cenci MA, Bjorklund A, Kirik D. Graft placement and uneven pattern of reinnervation in the striatum is important for development of graft-induced dyskinesia. *Neurobiol Dis* 2006; 21: 657-68.

Carpenter MB, Peter P. Nigrostriatal and nigrothalamic fibers in the rhesus monkey. *J Comp Neurol* 1972; 144: 93-115.

Carta M, Carlsson T, Kirik D, Bjorklund A. Dopamine released from 5-HT terminals is the cause of L-DOPA-induced dyskinesia in Parkinsonian rats. *Brain* 2007; 130: 1819-33.

Carta M, Carlsson T, Munoz A, Kirik D, Bjorklund A. Role of serotonin neurons in the induction of levodopa- and graft-induced dyskinesias in Parkinson's disease. *Mov Disord* 2010; 25 Suppl 1: S174-9.

Caslake R, Moore JN, Gordon JC, Harris CE, Counsell C. Changes in diagnosis with follow-up in an incident cohort of patients with parkinsonism. *J Neurol Neurosurg Psychiatry* 2008; 79: 1202-7.

Castrioto A, Lozano AM, Poon YY, Lang AE, Fallis M, Moro E. Ten-year outcome of subthalamic stimulation in Parkinson disease: a blinded evaluation. *Arch Neurol* 2011; 68: 1550-6.

Caughey B, Lansbury PT. Protofibrils, pores, fibrils, and neurodegeneration: separating the responsible protein aggregates from the innocent bystanders. *Annu Rev Neurosci* 2003; 26: 267-98.

Cerasa A, Donzuso G, Morelli M, Mangone G, Salsone M, Passamonti L, *et al.* The motor inhibition system in Parkinson's disease with levodopa-induced dyskinesias. *Mov Disord* 2015a; 30: 1912-20.

Cerasa A, Koch G, Donzuso G, Mangone G, Morelli M, Brusa L, *et al.* A network centred on the inferior frontal cortex is critically involved in levodopa-induced dyskinesias. *Brain* 2015b; 138: 414-27.

Chandra S, Chen X, Rizo J, Jahn R, Sudhof TC. A broken alpha -helix in folded alpha -Synuclein. *J Biol Chem* 2003; 278: 15313-8.

Chapuis S, Ouchchane L, Metz O, Gerbaud L, Durif F. Impact of the motor complications of Parkinson's disease on the quality of life. *Mov Disord* 2005; 20: 224-30.

Chen H, Zhao YF, Chen YX, Li YM. Exploring the Roles of Post-Translational Modifications in the Pathogenesis of Parkinson's Disease Using Synthetic and Semisynthetic Modified alpha-Synuclein. *ACS Chem Neurosci* 2019; 10: 910-21.

Cheng HC, Ulane CM, Burke RE. Clinical progression in Parkinson disease and the neurobiology of axons. *Ann Neurol* 2010; 67: 715-25.

Cherry SR, Dahlbom M. PET: Physics, Instrumentation, and Scanners. In: Phelps ME, editor. PET. 1st ed. New York, NY: Springer-Verlag; 2006.

Choi EY, Yeo BT, Buckner RL. The organization of the human striatum estimated by intrinsic functional connectivity. *J Neurophysiol* 2012; 108: 2242-63.

Chondrogiorgi M, Tatsioni A, Reichmann H, Konitsiotis S. Dopamine agonist monotherapy in Parkinson's disease and potential risk factors for dyskinesia: a meta-analysis of levodopa-controlled trials. *Eur J Neurol* 2014; 21: 433-40.

Chu Y, Kordower JH. Age-associated increases of alpha-synuclein in monkeys and humans are associated with nigrostriatal dopamine depletion: Is this the target for Parkinson's disease? *Neurobiol Dis* 2007; 25: 134-49.

Chu Y, Kordower JH. The prion hypothesis of Parkinson's disease. *Curr Neurol Neurosci Rep* 2015; 15: 28.

Chu Y, Morfini GA, Langhamer LB, He Y, Brady ST, Kordower JH. Alterations in axonal transport motor proteins in sporadic and experimental Parkinson's disease. *Brain* 2012; 135: 2058-73.

Cilia R, Akpalu A, Sarfo FS, Cham M, Amboni M, Cereda E, *et al.* The modern pre-levodopa era of Parkinson's disease: insights into motor complications from sub-Saharan Africa. *Brain* 2014; 137: 2731-42.

Cisbani G, Maxan A, Kordower JH, Planel E, Freeman TB, Cicchetti F. Presence of tau pathology within foetal neural allografts in patients with Huntington's and Parkinson's disease. *Brain* 2017; 140: 2982-92.

Clemett DA, Punhani T, Duxon MS, Blackburn TP, Fone KC. Immunohistochemical localisation of the 5-HT2C receptor protein in the rat CNS. *Neuropharmacology* 2000; 39: 123-32.

Cochen V, Ribeiro MJ, Nguyen JP, Gurruchaga JM, Villafane G, Loc'h C, *et al.* Transplantation in Parkinson's disease: PET changes correlate with the amount of grafted tissue. *Mov Disord* 2003; 18: 928-32.

Colloby SJ, Williams ED, Burn DJ, Lloyd JJ, McKeith IG, O'Brien JT. Progression of dopaminergic degeneration in dementia with Lewy bodies and Parkinson's disease with and without dementia assessed using 123I-FP-CIT SPECT. *Eur J Nucl Med Mol Imaging* 2005; 32: 1176-85.

Connolly BS, Lang AE. Pharmacological treatment of Parkinson disease: a review. *JAMA* 2014; 311: 1670-83.

Cox J, Witten IB. Striatal circuits for reward learning and decision-making. *Nat Rev Neurosci* 2019; 20: 482-94.

Craig CE, Jenkinson NJ, Brittain JS, Grothe MJ, Rochester L, Silverdale M, *et al.* Pedunculopontine Nucleus Microstructure Predicts Postural and Gait Symptoms in Parkinson's Disease. *Mov Disord* 2020; 35: 1199-207.

Cropley VL, Fujita M, Bara-Jimenez W, Brown AK, Zhang XY, Sangare J, *et al.* Pre- and post-synaptic dopamine imaging and its relation with frontostriatal cognitive function in Parkinson disease: PET studies with [11C]NNC 112 and [18F]FDOPA. *Psychiatry Res* 2008; 163: 171-82.

Damier P, Hirsch EC, Agid Y, Graybiel AM. The substantia nigra of the human brain. I. Nigrosomes and the nigral matrix, a compartmental organization based on calbindin D(28K) immunohistochemistry. *Brain* 1999a; 122 (Pt 8): 1421-36.

Damier P, Hirsch EC, Agid Y, Graybiel AM. The substantia nigra of the human brain. II. Patterns of loss of dopamine-containing neurons in Parkinson's disease. *Brain* 1999b; 122 (Pt 8): 1437-48.

Danzer KM, Haasen D, Karow AR, Moussaud S, Habeck M, Giese A, *et al.* Different species of alpha-synuclein oligomers induce calcium influx and seeding. *J Neurosci* 2007; 27: 9220-32.

Darweesh SK, Verlinden VJ, Stricker BH, Hofman A, Koudstaal PJ, Ikram MA. Trajectories of prediagnostic functioning in Parkinson's disease. *Brain* 2017; 140: 429-41.

Davidson WS, Jonas A, Clayton DF, George JM. Stabilization of alpha-synuclein secondary structure upon binding to synthetic membranes. *J Biol Chem* 1998; 273: 9443-9.

De Deurwaerdere P, Di Giovanni G. Serotonergic modulation of the activity of mesencephalic dopaminergic systems: Therapeutic implications. *Prog Neurobiol* 2017; 151: 175-236.

de Deus Fonticoba T, Santos Garcia D, Macias Arribi M. Inter-rater variability in motor function assessment in Parkinson's disease between experts in movement disorders and nurses specialising in PD management. *Neurologia* 2019; 34: 520-6.

de la Fuente-Fernández R, Lu JQ, Sossi V, Jivan S, Schulzer M, Holden JE*, et al.* Biochemical variations in the synaptic level of dopamine precede motor fluctuations in Parkinson's disease: PET evidence of increased dopamine turnover. *Ann Neurol* 2001; 49: 298-303.

de la Fuente-Fernandez R, Schulzer M, Kuramoto L, Cragg J, Ramachandiran N, Au WL*, et al.* Age-specific progression of nigrostriatal dysfunction in Parkinson's disease. *Ann Neurol* 2011; 69: 803-10.

de la Fuente-Fernandez R, Sossi V, Huang Z, Furtado S, Lu JQ, Calne DB*, et al.* Levodopa-induced changes in synaptic dopamine levels increase with progression of Parkinson's disease: implications for dyskinesias. *Brain* 2004; 127: 2747-54.

de Lau LM, Schipper CM, Hofman A, Koudstaal PJ, Breteler MM. Prognosis of Parkinson disease: risk of dementia and mortality: the Rotterdam Study. *Arch Neurol* 2005; 62: 1265-9.

de Lau LML, Breteler MMB. Epidemiology of Parkinson's disease. *The Lancet Neurology* 2006; 5: 525-35.

Defer GL, Geny C, Ricolfi F, Fenelon G, Monfort JC, Remy P*, et al.* Long-term outcome of unilaterally transplanted parkinsonian patients. I. Clinical approach. *Brain* 1996; 119 (Pt 1): 41-50.

Delgado MR, Schotter A, Ozbay EY, Phelps EA. Understanding overbidding: using the neural circuitry of reward to design economic auctions. *Science* 2008; 321: 1849-52.

DeLong MR. Primate models of movement disorders of basal ganglia origin. *Trends Neurosci* 1990; 13: 281-5.

DeLorenzo C, Kumar JS, Zanderigo F, Mann JJ, Parsey RV. Modeling considerations for in vivo quantification of the dopamine transporter using [(11)C]PE2I and positron emission tomography. *J Cereb Blood Flow Metab* 2009; 29: 1332-45.

Deng YP, Lei WL, Reiner A. Differential perikaryal localization in rats of D1 and D2 dopamine receptors on striatal projection neuron types identified by retrograde labeling. *J Chem Neuroanat* 2006; 32: 101-16.

Dentresangle C, Veyre L, Le Bars D, Pierre C, Lavenne F, Pollak P*, et al.* Striatal D2 dopamine receptor status in Parkinson's disease: an [18F]dopa and [11C]raclopride PET study. *Mov Disord* 1999; 14: 1025-30.

Desplats P, Lee HJ, Bae EJ, Patrick C, Rockenstein E, Crews L, *et al.* Inclusion formation and neuronal cell death through neuron-to-neuron transmission of alpha-synuclein. *Proc Natl Acad Sci U S A* 2009; 106: 13010-5.

Dettmer U, Ramalingam N, von Saucken VE, Kim TE, Newman AJ, Terry-Kantor E, *et al.* Loss of native alpha-synuclein multimerization by strategically mutating its amphipathic helix causes abnormal vesicle interactions in neuronal cells. *Hum Mol Genet* 2017; 26: 3466-81.

Deuschl G, Follett KA, Luo P, Rau J, Weaver FM, Paschen S, *et al.* Comparing two randomized deep brain stimulation trials for Parkinson's disease. *J Neurosurg* 2019: 1-9.

Dexter DT, Jenner P, Schapira AH, Marsden CD. Alterations in levels of iron, ferritin, and other trace metals in neurodegenerative diseases affecting the basal ganglia. The Royal Kings and Queens Parkinson's Disease Research Group. *Ann Neurol* 1991; 32 Suppl: S94-100.

Dhawan V, Ma Y, Pillai V, Spetsieris P, Chaly T, Belakhlef A, *et al.* Comparative analysis of striatal FDOPA uptake in Parkinson's disease: ratio method versus graphical approach. *J Nucl Med* 2002; 43: 1324-30.

Dickson DW. Parkinson's Disease and Parkinsonism: Neuropathology. *Cold Spring Harb Perspect Med* 2012; 2.

Dickson DW, Fujishiro H, DelleDonne A, Menke J, Ahmed Z, Klos KJ, *et al.* Evidence that incidental Lewy body disease is pre-symptomatic Parkinson's disease. *Acta Neuropathol* 2008; 115: 437-44.

Dijkstra AA, Voorn P, Berendse HW, Groenewegen HJ, Netherlands Brain B, Rozemuller AJ, *et al.* Stage-dependent nigral neuronal loss in incidental Lewy body and Parkinson's disease. *Mov Disord* 2014; 29: 1244-51.

Dirkx MF, den Ouden H, Aarts E, Timmer M, Bloem BR, Toni I, *et al.* The Cerebral Network of Parkinson's Tremor: An Effective Connectivity fMRI Study. *J Neurosci* 2016; 36: 5362-72.

Dirkx MF, den Ouden HE, Aarts E, Timmer MH, Bloem BR, Toni I, *et al.* Dopamine controls Parkinson's tremor by inhibiting the cerebellar thalamus. *Brain* 2017; 140: 721-34.

Dissanayaka NN, Sellbach A, Matheson S, O'Sullivan JD, Silburn PA, Byrne GJ, *et al.* Anxiety disorders in Parkinson's disease: prevalence and risk factors. *Mov Disord* 2010; 25: 838-45.

Doder M, Rabiner EA, Turjanski N, Lees AJ, Brooks DJ. Tremor in Parkinson's disease and serotonergic dysfunction: an 11C-WAY 100635 PET study. *Neurology* 2003; 60: 601-5.

Doherty KM, Silveira-Moriyama L, Parkkinen L, Healy DG, Farrell M, Mencacci NE, *et al.* Parkin disease: a clinicopathologic entity? *JAMA neurology* 2013; 70: 571-9.

Doherty KM, van de Warrenburg BP, Peralta MC, Silveira-Moriyama L, Azulay J-P, Gershanik OS, *et al.* Postural deformities in Parkinson's disease. *The Lancet Neurology* 2011; 10: 538-49.

Dorsey ER, Bloem BR. The Parkinson Pandemic-A Call to Action. *JAMA neurology* 2018; 75: 9-10.

Dorsey ER, Constantinescu R, Thompson JP, Biglan KM, Holloway RG, Kieburtz K, *et al.* Projected number of people with Parkinson disease in the most populous nations, 2005 through 2030. *Neurology* 2007; 68: 384-6.

Dorsey ER, Elbaz A, Nichols E, Abd-Allah F, Abdelalim A, Adsuar JC, *et al.* Global, regional, and national burden of Parkinson's disease, 1990–2016: a systematic analysis for the Global Burden of Disease Study 2016. *The Lancet Neurology* 2018; 17: 939-53.

Doucet G, Brundin P, Descarries L, Bjorklund A. Effect of Prior Dopamine Denervation on Survival and Fiber Outgrowth from Intrastriatal Fetal Mesencephalic Grafts. *Eur J Neurosci* 1990; 2: 279-90.

Doyon J, Bellec P, Amsel R, Penhune V, Monchi O, Carrier J, *et al.* Contributions of the basal ganglia and functionally related brain structures to motor learning. *Behav Brain Res* 2009; 199: 61-75.

Duan WM, Widner H, Bjorklund A, Brundin P. Sequential intrastriatal grafting of allogeneic embryonic dopamine-rich neuronal tissue in adult rats: will the second graft be rejected? *Neuroscience* 1993; 57: 261-74.

Eberle-Wang K, Mikeladze Z, Uryu K, Chesselet MF. Pattern of expression of the serotonin2C receptor messenger RNA in the basal ganglia of adult rats. *J Comp Neurol* 1997; 384: 233-47.

Ecker D, Unrath A, Kassubek J, Sabolek M. Dopamine Agonists and their risk to induce psychotic episodes in Parkinson's disease: a case-control study. *BMC Neurol* 2009; 9: 23.

Eggers C, Kahraman D, Fink GR, Schmidt M, Timmermann L. Akinetic-rigid and tremor-dominant Parkinson's disease patients show different patterns of FP-CIT single photon emission computed tomography. *Mov Disord* 2011; 26: 416-23.

Eison AS, Temple DL, Jr. Buspirone: review of its pharmacology and current perspectives on its mechanism of action. *Am J Med* 1986; 80: 1-9.

Emamzadeh FN. Alpha-synuclein structure, functions, and interactions. *J Res Med Sci* 2016; 21: 29.

Emmanouilidou E, Melachroinou K, Roumeliotis T, Garbis SD, Ntzouni M, Margaritis LH, *et al.* Cell-produced alpha-synuclein is secreted in a calcium-dependent manner by exosomes and impacts neuronal survival. *J Neurosci* 2010; 30: 6838-51.

Emond P, Garreau L, Chalon S, Boazi M, Caillet M, Bricard J, *et al.* Synthesis and ligand binding of nortropane derivatives: N-substituted 2beta-carbomethoxy-3beta-(4'-iodophenyl)nortropane and N-(3-iodoprop-(2E)-enyl)-2beta-carbomethoxy-3beta-(3',4'-disubstituted phenyl)nortropane. New high-affinity and selective compounds for the dopamine transporter. *J Med Chem* 1997; 40: 1366-72.

Endres CJ, Hammoud DA, Pomper MG. Reference tissue modeling with parameter coupling: application to a study of SERT binding in HIV. *Phys Med Biol* 2011; 56: 2499-513.

Engelhardt E, Gomes MDM. Lewy and his inclusion bodies: Discovery and rejection. *Dementia & neuropsychologia* 2017; 11: 198-201.

Engeln M, De Deurwaerdere P, Li Q, Bezard E, Fernagut PO. Widespread Monoaminergic Dysregulation of Both Motor and Non-Motor Circuits in Parkinsonism and Dyskinesia. *Cereb Cortex* 2015; 25: 2783-92.

Eshuis SA, Maguire RP, Leenders KL, Jonkman S, Jager PL. Comparison of FP-CIT SPECT with F-DOPA PET in patients with de novo and advanced Parkinson's disease. *Eur J Nucl Med Mol Imaging* 2006; 33: 200-9.

Eusebi P, Romoli M, Paoletti FP, Tambasco N, Calabresi P, Parnetti L. Risk factors of levodopa-induced dyskinesia in Parkinson's disease: results from the PPMI cohort. *NPJ Parkinson's disease* 2018; 4: 33.

Factor SA, Weiner W. Parkinson's Disease: Diagnosis and Clinical Management. 2nd Ed ed. New York: Demos Medical Publishing; 2008.

Faghihi R, Zeinali-Rafsanjani B, Mosleh-Shirazi MA, Saeedi-Moghadam M, Lotfi M, Jalli R, *et al.* Magnetic Resonance Spectroscopy and its Clinical Applications: A Review. *J Med Imaging Radiat Sci* 2017; 48: 233-53.

Fahn S, Oakes D, Shoulson I, Kieburtz K, Rudolph A, Lang A, *et al.* Levodopa and the progression of Parkinson's disease. *N Engl J Med* 2004; 351: 2498-508.

Fairchild G, Leitch MM, Ingram CD. Acute and chronic effects of corticosterone on 5-HT1A receptor-mediated autoinhibition in the rat dorsal raphe nucleus. *Neuropharmacology* 2003; 45: 925-34.

Fasano A, Romito LM, Daniele A, Piano C, Zinno M, Bentivoglio AR, *et al.* Motor and cognitive outcome in patients with Parkinson's disease 8 years after subthalamic implants. *Brain* 2010; 133: 2664-76.

Faucheux BA, Martin ME, Beaumont C, Hauw JJ, Agid Y, Hirsch EC. Neuromelanin associated redox-active iron is increased in the substantia nigra of patients with Parkinson's disease. *J Neurochem* 2003; 86: 1142-8.

Fazio P, Ferreira D, Svenningsson P, Halldin C, Farde L, Westman E, *et al.* High-resolution PET imaging reveals subtle impairment of the serotonin transporter in an early non-depressed Parkinson's disease cohort. *Eur J Nucl Med Mol Imaging* 2020.

Fazio P, Svenningsson P, Cselenyi Z, Halldin C, Farde L, Varrone A. Nigrostriatal dopamine transporter availability in early Parkinson's disease. *Mov Disord* 2018; 33: 592-9.

Fazio P, Svenningsson P, Forsberg A, Jonsson EG, Amini N, Nakao R, *et al.* Quantitative Analysis of (1)(8)F-(E)-N-(3-Iodoprop-2-Enyl)-2beta-Carbofluoroethoxy-3beta-(4'-Methyl-Phenyl) Nortropane Binding to the Dopamine Transporter in Parkinson Disease. *J Nucl Med* 2015; 56: 714-20.

Fearnley JM, Lees AJ. Ageing and Parkinson's disease: substantia nigra regional selectivity. *Brain* 1991; 114 (Pt 5): 2283-301.

Fereshtehnejad SM, Yao C, Pelletier A, Montplaisir JY, Gagnon JF, Postuma RB. Evolution of prodromal Parkinson's disease and dementia with Lewy bodies: a prospective study. *Brain* 2019; 142: 2051-67.

Ferguson LW, Rajput AH, Rajput A. Early-onset vs. Late-onset Parkinson's disease: A Clinical-pathological Study. *Can J Neurol Sci* 2016; 43: 113-9.

Fernandez HH, Lapane KL. Predictors of mortality among nursing home residents with a diagnosis of Parkinson's disease. *Med Sci Monit* 2002; 8: Cr241-6.

Fernandez HH, Standaert DG, Hauser RA, Lang AE, Fung VS, Klostermann F, *et al.* Levodopa-carbidopa intestinal gel in advanced Parkinson's disease: final 12-month, open-label results. *Mov Disord* 2015; 30: 500-9.

Ferreira JJ, Lees A, Rocha J-F, Poewe W, Rascol O, Soares-da-Silva P. Opicapone as an adjunct to levodopa in patients with Parkinson's disease and end-of-dose motor fluctuations: a randomised, double-blind, controlled trial. *The Lancet Neurology* 2016; 15: 154-65.

Firnau G, Sood S, Chirakal R, Nahmias C, Garnett ES. Cerebral metabolism of 6-[18F]fluoro-L-3,4-dihydroxyphenylalanine in the primate. *J Neurochem* 1987; 48: 1077-82.

Fisher SK, Novak JE, Agranoff BW. Inositol and higher inositol phosphates in neural tissues: homeostasis, metabolism and functional significance. *J Neurochem* 2002; 82: 736-54.

Flagmeier P, Meisl G, Vendruscolo M, Knowles TP, Dobson CM, Buell AK, *et al.* Mutations associated with familial Parkinson's disease alter the initiation and amplification steps of alpha-synuclein aggregation. *Proc Natl Acad Sci U S A* 2016; 113: 10328-33.

Folkerth RD, Durso R. Survival and proliferation of nonneural tissues, with obstruction of cerebral ventricles, in a parkinsonian patient treated with fetal allografts. *Neurology* 1996; 46: 1219-25.

Follett J, Darlow B, Wong MB, Goodwin J, Pountney DL. Potassium depolarization and raised calcium induces alpha-synuclein aggregates. *Neurotox Res* 2013; 23: 378-92.

Follett KA, Weaver FM, Stern M, Hur K, Harris CL, Luo P, *et al.* Pallidal versus subthalamic deep-brain stimulation for Parkinson's disease. *N Engl J Med* 2010; 362: 2077-91.

Forno LS. Neuropathology of Parkinson's Disease. *J Neuropathol Exp Neurol* 1996; 55: 259-72.

Fox J, Weisberg S. An {R} Companion to Applied Regression, Third Edition. 2019. Available from: https://socialsciences.mcmaster.ca/jfox/Books/Companion/.

Fox SH, Chuang R, Brotchie JM. Serotonin and Parkinson's disease: On movement, mood, and madness. *Mov Disord* 2009; 24: 1255-66.

Fox SH, Katzenschlager R, Lim SY, Barton B, de Bie RMA, Seppi K, *et al.* International Parkinson and movement disorder society evidence-based medicine review: Update on treatments for the motor symptoms of Parkinson's disease. *Mov Disord* 2018; 33: 1248-66.

Fox SH, Katzenschlager R, Lim SY, Ravina B, Seppi K, Coelho M, *et al.* The Movement Disorder Society Evidence-Based Medicine Review Update: Treatments for the motor symptoms of Parkinson's disease. *Mov Disord* 2011; 26 Suppl 3: S2-41.

Fox SH, Moser B, Brotchie JM. Behavioral effects of 5-HT2C receptor antagonism in the substantia nigra zona reticulata of the 6-hydroxydopamine-lesioned rat model of Parkinson's disease. *Exp Neurol* 1998; 151: 35-49.

Frankle WG, Huang YY, Hwang DR, Talbot PS, Slifstein M, Van Heertum R, *et al.* Comparative evaluation of serotonin transporter radioligands C-11-DASB and C-11-McN 5652 in healthy humans. *J Nucl Med* 2004; 45: 682-94.

Frankle WG, Slifstein M, Gunn RN, Huang Y, Hwang DR, Darr EA, *et al.* Estimation of serotonin transporter parameters with 11C-DASB in healthy humans: reproducibility and comparison of methods. *J Nucl Med* 2006; 47: 815-26.

Fratiglioni L, Qiu C. Prevention of common neurodegenerative disorders in the elderly. *Exp Gerontol* 2009; 44: 46-50.

Freed CR, Breeze RE, Rosenberg NL, Schneck SA, Kriek E, Qi JX, *et al.* Survival of implanted fetal dopamine cells and neurologic improvement 12 to 46 months after transplantation for Parkinson's disease. *N Engl J Med* 1992; 327: 1549-55.

Freed CR, Greene PE, Breeze RE, Tsai WY, DuMouchel W, Kao R, *et al.* Transplantation of embryonic dopamine neurons for severe Parkinson's disease. *N Engl J Med* 2001; 344: 710-9.

Freeman TB, Olanow CW, Hauser RA, Nauert GM, Smith DA, Borlongan CV, *et al.* Bilateral fetal nigral transplantation into the postcommissural putamen in Parkinson's disease. *Ann Neurol* 1995; 38: 379-88.

Fusco G, De Simone A, Gopinath T, Vostrikov V, Vendruscolo M, Dobson CM, *et al.* Direct observation of the three regions in alpha-synuclein that determine its membrane-bound behaviour. *Nature communications* 2014; 5: 3827.

Fusco G, Pape T, Stephens AD, Mahou P, Costa AR, Kaminski CF, *et al.* Structural basis of synaptic vesicle assembly promoted by alpha-synuclein. *Nature communications* 2016; 7: 12563.

Gaenslen A, Swid I, Liepelt-Scarfone I, Godau J, Berg D. The patients' perception of prodromal symptoms before the initial diagnosis of Parkinson's disease. *Mov Disord* 2011; 26: 653-8.

Galineau L, Kodas E, Guilloteau D, Vilar MP, Chalon S. Ontogeny of the dopamine and serotonin transporters in the rat brain: an autoradiographic study. *Neurosci Lett* 2004; 363: 266-71.

Gallagher CL, Christian BT, Holden JE, Dejesus OT, Nickles RJ, Buyan-Dent L, *et al.* A within-subject comparison of 6-[18F]fluoro-m-tyrosine and 6-[18F]fluoro-L-dopa in Parkinson's disease. *Mov Disord* 2011a; 26: 2032-8.

Gallagher CL, Oakes TR, Johnson SC, Chung MK, Holden JE, Bendlin BB, *et al.* Rate of 6-[18F]fluorodopa uptake decline in striatal subregions in Parkinson's disease. *Mov Disord* 2011b; 26: 614-20.

Gallagher DA, Lees AJ, Schrag A. What are the most important nonmotor symptoms in patients with Parkinson's disease and are we missing them? *Mov Disord* 2010; 25: 2493-500.

Gaprielian P, Scott SH, Lowrey C, Reid S, Pari G, Levy R. Integrated robotics platform with haptic control differentiates subjects with Parkinson's disease from controls and quantifies the motor effects of levodopa. *J Neuroeng Rehabil* 2019; 16: 124.

Garcia J, Carlsson T, Dobrossy M, Nikkhah G, Winkler C. Extent of pre-operative L-DOPA-induced dyskinesia predicts the severity of graft-induced dyskinesia after fetal dopamine cell transplantation. *Exp Neurol* 2011; 232: 270-9.

Garcia J, Carlsson T, Dobrossy M, Nikkhah G, Winkler C. Impact of dopamine versus serotonin cell transplantation for the development of graft-induced dyskinesia in a rat Parkinson model. *Brain Res* 2012; 1470: 119-29.

George JM. The synucleins. *Genome Biol* 2002; 3: Reviews3002.

Gerfen CR, Engber TM, Mahan LC, Susel Z, Chase TN, Monsma FJ, Jr., *et al.* D1 and D2 dopamine receptor-regulated gene expression of striatonigral and striatopallidal neurons. *Science* 1990; 250: 1429-32.

Gerfen CR, Surmeier DJ. Modulation of striatal projection systems by dopamine. *Annu Rev Neurosci* 2011; 34: 441-66.

German DC, Manaye KF, Sonsalla PK, Brooks BA. Midbrain dopaminergic cell loss in Parkinson's disease and MPTP-induced parkinsonism: sparing of calbindin-D28k-containing cells. *Ann N Y Acad Sci* 1992; 648: 42-62.

Gertz HJ, Siegers A, Kuchinke J. Stability of cell size and nucleolar size in Lewy body containing neurons of substantia nigra in Parkinson's disease. *Brain Res* 1994; 637: 339-41.

Ghaemi M, Hilker R, Rudolf J, Sobesky J, Heiss WD. Differentiating multiple system atrophy from Parkinson's disease: contribution of striatal and midbrain MRI volumetry and multi-tracer PET imaging. *J Neurol Neurosurg Psychiatry* 2002; 73: 517-23.

Giasson BI, Murray IV, Trojanowski JQ, Lee VM. A hydrophobic stretch of 12 amino acid residues in the middle of alpha-synuclein is essential for filament assembly. *J Biol Chem* 2001; 276: 2380-6.

Gibb WR, Lees AJ. The relevance of the Lewy body to the pathogenesis of idiopathic Parkinson's disease. *Journal of neurology, neurosurgery, and psychiatry* 1988; 51: 745-52.

Gibb WR, Lees AJ. Anatomy, pigmentation, ventral and dorsal subpopulations of the substantia nigra, and differential cell death in Parkinson's disease. *J Neurol Neurosurg Psychiatry* 1991; 54: 388-96.

Gibb WRG, Scott T, Lees AJ. Neuronal Inclusions of Parkinsons-Disease. *Mov Disord* 1991; 6: 2-11.

Giguere N, Burke Nanni S, Trudeau LE. On Cell Loss and Selective Vulnerability of Neuronal Populations in Parkinson's Disease. *Front Neurol* 2018; 9: 455.

Giladi N, Shabtai H, Rozenberg E, Shabtai E. Gait festination in Parkinson's disease. *Parkinsonism Relat Disord* 2001; 7: 135-8.

Ginovart N, Wilson AA, Meyer JH, Hussey D, Houle S. Positron emission tomography quantification of [(11)C]-DASB binding to the human serotonin transporter: modeling strategies. *J Cereb Blood Flow Metab* 2001; 21: 1342-53.

Goedert M, Spillantini MG, Del Tredici K, Braak H. 100 years of Lewy pathology. *Nat Rev Neurol* 2013; 9: 13-24.

Goerg GM. LambertW: An R package for Lambert W x F Random Variables. R package version 0.6.4. 2016. Available from:

Goetz CG, Stebbins GT, 3rd, Klawans HL, Koller WC, Grossman RG, Bakay RA, *et al.* United Parkinson Foundation Neurotransplantation Registry on adrenal medullary transplants: presurgical, and 1- and 2-year follow-up. *Neurology* 1991; 41: 1719-22.

Goetz CG, Tilley BC, Shaftman SR, Stebbins GT, Fahn S, Martinez-Martin P, *et al.* Movement Disorder Society-sponsored revision of the Unified Parkinson's Disease Rating Scale (MDS-UPDRS): scale presentation and clinimetric testing results. *Mov Disord* 2008a; 23: 2129-70.

Goetz CG, Wuu J, McDermott MP, Adler CH, Fahn S, Freed CR, *et al.* Placebo response in Parkinson's disease: comparisons among 11 trials covering medical and surgical interventions. *Mov Disord* 2008b; 23: 690-9.

Gómez-Tortosa E, Newell K, Irizarry MC, Sanders JL, Hyman BT. alpha-Synuclein immunoreactivity in dementia with Lewy bodies: morphological staging and comparison with ubiquitin immunostaining. *Acta Neuropathol* 2000; 99: 352-7.

Green AL, Eid A, Zhan L, Zarbl H, Guo GL, Richardson JR. Epigenetic Regulation of the Ontogenic Expression of the Dopamine Transporter. *Frontiers in genetics* 2019; 10: 1099.

Greene PE, Fahn S, Tsai WY, Breeze RE, Eidelberg D, Winfield H, *et al.* Severe spontaneous dyskinesias: A disabling complication of embryonic dopaminergic tissue implants in a subset of transplanted patients with advanced Parkinson's disease. *Mov Disord* 1999; 14: 904.

Greffard S, Verny M, Bonnet AM, Beinis JY, Gallinari C, Meaume S, *et al.* Motor score of the Unified Parkinson Disease Rating Scale as a good predictor of Lewy body-associated neuronal loss in the substantia nigra. *Arch Neurol* 2006; 63: 584-8.

Groiss SJ, Wojtecki L, Sudmeyer M, Schnitzler A. Deep brain stimulation in Parkinson's disease. *Ther Adv Neurol Disord* 2009; 2: 20-8.

Grosch J, Winkler J, Kohl Z. Early Degeneration of Both Dopaminergic and Serotonergic Axons - A Common Mechanism in Parkinson's Disease. *Front Cell Neurosci* 2016; 10: 293.

Gross RE, Watts RL, Hauser RA, Bakay RAE, Reichmann H, von Kummer R, *et al.* Intrastriatal transplantation of microcarrier-bound human retinal pigment epithelial cells versus sham surgery in patients with advanced Parkinson's disease: a double-blind, randomised, controlled trial. *The Lancet Neurology* 2011; 10: 509-19.

Guigoni C, Li Q, Aubert I, Dovero S, Bioulac BH, Bloch B, *et al.* Involvement of sensorimotor, limbic, and associative basal ganglia domains in L-3,4-dihydroxyphenylalanine-induced dyskinesia. *J Neurosci* 2005; 25: 2102-7.

Guilloteau D, Emond P, Baulieu JL, Garreau L, Frangin Y, Pourcelot L, *et al.* Exploration of the dopamine transporter: in vitro and in vivo characterization of a high-affinity and high-specificity iodinated tropane derivative (E)-N-(3-iodoprop-2-enyl)-2beta-carbomethoxy-3beta-(4'-m ethylph enyl)nortropane (PE2I). *Nucl Med Biol* 1998; 25: 331-7.

Gunn R, Coello C, Searle G. Molecular Imaging And Kinetic Analysis Toolbox (MIAKAT) - A Quantitative Software Package for the Analysis of PET Neuroimaging Data. *The Journal of Nuclear Medicine* 2016; 57: 1928.

Gunn RN, Lammertsma AA, Hume SP, Cunningham VJ. Parametric imaging of ligand-receptor binding in PET using a simplified reference region model. *Neuroimage* 1997; 6: 279-87.

Gunn RN, Murthy V, Catafau AM, Searle G, Bullich S, Slifstein M, *et al.* Translational characterization of [11C]GSK931145, a PET ligand for the glycine transporter type 1. *Synapse* 2011; 65: 1319-32.

Gunnery SD, Habermann B, Saint-Hilaire M, Thomas CA, Tickle-Degnen L. The Relationship between the Experience of Hypomimia and Social Wellbeing in People with Parkinson's Disease and their Care Partners. *J Parkinsons Dis* 2016; 6: 625-30.

Gunther I, Hall H, Halldin C, Swahn CG, Farde L, Sedvall G. [125I] beta-CIT-FE and [125I] beta-CIT-FP are superior to [125I] beta-CIT for dopamine transporter visualization: autoradiographic evaluation in the human brain. *Nucl Med Biol* 1997; 24: 629-34.

Gustafsson H, Nordström A, Nordström P. Depression and subsequent risk of Parkinson disease: A nationwide cohort study. *Neurology* 2015; 84: 2422-9.

Guttman M, Boileau I, Warsh J, Saint-Cyr JA, Ginovart N, McCluskey T, *et al.* Brain serotonin transporter binding in non-depressed patients with Parkinson's disease. *Eur J Neurol* 2007; 14: 523-8.

Guttman M, Burkholder J, Kish SJ, Hussey D, Wilson A, DaSilva J, *et al.* [11C]RTI-32 PET studies of the dopamine transporter in early dopa-naive Parkinson's disease: implications for the symptomatic threshold. *Neurology* 1997; 48: 1578-83.

Guy WA. Abnormal Involuntary Movement Scale (AIMS). In: Guy WA, editor. ECDEU Assessment Manaul for psychopharmacology, Revised 1976. Washington, DC: United States Department of Health, Education and Welfare; 1976. p. 534-7.

Haaxma CA, Bloem BR, Borm GF, Horstink MW. Comparison of a timed motor test battery to the Unified Parkinson's Disease Rating Scale-III in Parkinson's disease. *Mov Disord* 2008; 23: 1707-17.

Haber SN. The primate basal ganglia: parallel and integrative networks. *J Chem Neuroanat* 2003; 26: 317-30.

Haber SN. The place of dopamine in the cortico-basal ganglia circuit. *Neuroscience* 2014; 282: 248-57.

Haber SN, Fudge JL, McFarland NR. Striatonigrostriatal pathways in primates form an ascending spiral from the shell to the dorsolateral striatum. *J Neurosci* 2000; 20: 2369-82.

Haber SN, McFarland NR. The concept of the ventral striatum in nonhuman primates. *Ann N Y Acad Sci* 1999; 877: 33-48.

Haehner A, Boesveldt S, Berendse HW, Mackay-Sim A, Fleischmann J, Silburn PA, *et al.* Prevalence of smell loss in Parkinson's disease--a multicenter study. *Parkinsonism Relat Disord* 2009; 15: 490-4.

Hagell P, Cenci MA. Dyskinesias and dopamine cell replacement in Parkinson's disease: a clinical perspective. *Brain Res Bull* 2005; 68: 4-15.

Hagell P, Crabb L, Pogarell O, Schrag A, Widner H, Brooks DJ, *et al.* Health-related quality of life following bilateral intrastriatal transplantation in Parkinson's disease. *Mov Disord* 2000; 15: 224-9.

Hagell P, Piccini P, Bjorklund A, Brundin P, Rehncrona S, Widner H, *et al.* Dyskinesias following neural transplantation in Parkinson's disease. *Nat Neurosci* 2002; 5: 627-8.

Hagell P, Schrag A, Piccini P, Jahanshahi M, Brown R, Rehncrona S, *et al.* Sequential bilateral transplantation in Parkinson's disease: effects of the second graft. *Brain* 1999; 122 (Pt 6): 1121-32.

Halekoh U, Hojsgaard S. Kenward-Roger Approximation and Parametric Bootstrap Methods for Tests in Linear Mixed Models - The R Package pbkrtest. *J Stat Softw* 2014; 59: 1-32.

Hall H, Halldin C, Guilloteau D, Chalon S, Emond P, Besnard J, *et al.* Visualization of the dopamine transporter in the human brain postmortem with the new selective ligand [125I]PE2I. *Neuroimage* 1999; 9: 108-16.

Halldin C, Erixon-Lindroth N, Pauli S, Chou YH, Okubo Y, Karlsson P, *et al.* [(11)C]PE2I: a highly selective radioligand for PET examination of the dopamine transporter in monkey and human brain. *Eur J Nucl Med Mol Imaging* 2003; 30: 1220-30.

Hallett PJ, Cooper O, Sadi D, Robertson H, Mendez I, Isacson O. Long-term health of dopaminergic neuron transplants in Parkinson's disease patients. *Cell reports* 2014; 7: 1755-61.

Halliday GM, McRitchie DA, Cartwright H, Pamphlett R, Hely MA, Morris JG. Midbrain neuropathology in idiopathic Parkinson's disease and diffuse Lewy body disease. *J Clin Neurosci* 1996; 3: 52-60.

Han S, Oh M, Oh JS, Lee SJ, Oh SJ, Chung SJ, *et al.* Subregional Pattern of Striatal Dopamine Transporter Loss on 18F FP-CIT Positron Emission Tomography in Patients With Pure Akinesia With Gait Freezing. *JAMA neurology* 2016; 73: 1477-84.

Hansen C, Angot E, Bergstrom AL, Steiner JA, Pieri L, Paul G, *et al.* alpha-Synuclein propagates from mouse brain to grafted dopaminergic neurons and seeds aggregation in cultured human cells. *J Clin Invest* 2011; 121: 715-25.

Hare DJ, Double KL. Iron and dopamine: a toxic couple. *Brain* 2016; 139: 1026-35.

Harnack D, Kupsch A. The impact of subthalamic deep brain stimulation on nigral neuroprotection-myth or reality? *Neuromodulation* 2010; 13: 160-7.

Harrell Jr FE. Hmisc: Harrell Miscellaneous. R package version 4.0-3. 2017. Available from: https://CRAN.R-project.org/package=Hmisc.

Hauser RA, Freeman TB, Snow BJ, Nauert M, Gauger L, Kordower JH, *et al.* Long-term evaluation of bilateral fetal nigral transplantation in Parkinson disease. *Arch Neurol* 1999; 56: 179-87.

Hauser RA, Hsu A, Kell S, Espay AJ, Sethi K, Stacy M, *et al.* Extended-release carbidopa-levodopa (IPX066) compared with immediate-release carbidopa-levodopa in patients with Parkinson's disease and motor fluctuations: a phase 3 randomised, double-blind trial. *The Lancet Neurology* 2013; 12: 346-56.

Hauser RA, Rascol O, Korczyn AD, Jon Stoessl A, Watts RL, Poewe W, *et al.* Ten-year follow-up of Parkinson's disease patients randomized to initial therapy with ropinirole or levodopa. *Mov Disord* 2007; 22: 2409-17.

Hawkes C. Olfaction in neurodegenerative disorder. *Mov Disord* 2003; 18: 364-72.

Hawkes CH, Del Tredici K, Braak H. Parkinson's disease: a dual-hit hypothesis. *Neuropathol Appl Neurobiol* 2007; 33: 599-614.

Hechtner MC, Vogt T, Zollner Y, Schroder S, Sauer JB, Binder H, *et al.* Quality of life in Parkinson's disease patients with motor fluctuations and dyskinesias in five European countries. *Parkinsonism Relat Disord* 2014; 20: 969-74.

Heilbronner SR, Rodriguez-Romaguera J, Quirk GJ, Groenewegen HJ, Haber SN. Circuit-Based Corticostriatal Homologies Between Rat and Primate. *Biol Psychiatry* 2016; 80: 509-21.

Heiss WD, Hilker R. The sensitivity of 18-fluorodopa positron emission tomography and magnetic resonance imaging in Parkinson's disease. *Eur J Neurol* 2004; 11: 5-12.

Heldman DA, Giuffrida JP, Chen R, Payne M, Mazzella F, Duker AP, *et al.* The modified bradykinesia rating scale for Parkinson's disease: reliability and comparison with kinematic measures. *Mov Disord* 2011; 26: 1859-63.

Helmich RC, Hallett M, Deuschl G, Toni I, Bloem BR. Cerebral causes and consequences of parkinsonian resting tremor: a tale of two circuits? *Brain* 2012; 135: 3206-26.

Helmich RC, Janssen MJ, Oyen WJ, Bloem BR, Toni I. Pallidal dysfunction drives a cerebellothalamic circuit into Parkinson tremor. *Ann Neurol* 2011; 69: 269-81.

Hely MA, Morris JG, Reid WG, Trafficante R. Sydney Multicenter Study of Parkinson's disease: non-L-dopa-responsive problems dominate at 15 years. *Mov Disord* 2005; 20: 190-9.

Hely MA, Reid WG, Adena MA, Halliday GM, Morris JG. The Sydney multicenter study of Parkinson's disease: the inevitability of dementia at 20 years. *Mov Disord* 2008; 23: 837-44.

Herrera A, Munoz P, Steinbusch HWM, Segura-Aguilar J. Are Dopamine Oxidation Metabolites Involved in the Loss of Dopaminergic Neurons in the Nigrostriatal System in Parkinson's Disease? *ACS Chem Neurosci* 2017; 8: 702-11.

Herrington TM, Cheng JJ, Eskandar EN. Mechanisms of deep brain stimulation. *J Neurophysiol* 2016; 115: 19-38.

Herz DM, Haagensen BN, Christensen MS, Madsen KH, Rowe JB, Lokkegaard A, *et al.* The acute brain response to levodopa heralds dyskinesias in Parkinson disease. *Ann Neurol* 2014; 75: 829-36.

Herz DM, Haagensen BN, Christensen MS, Madsen KH, Rowe JB, Lokkegaard A, *et al.* Abnormal dopaminergic modulation of striato-cortical networks underlies levodopa-induced dyskinesias in humans. *Brain* 2015; 138: 1658-66.

Herz DM, Haagensen BN, Nielsen SH, Madsen KH, Lokkegaard A, Siebner HR. Resting-state connectivity predicts levodopa-induced dyskinesias in Parkinson's disease. *Mov Disord* 2016; 31: 521-9.

Hikosaka O, Nakamura K, Sakai K, Nakahara H. Central mechanisms of motor skill learning. *Curr Opin Neurobiol* 2002; 12: 217-22.

Hilker R, Portman AT, Voges J, Staal MJ, Burghaus L, van Laar T, *et al.* Disease progression continues in patients with advanced Parkinson's disease and effective subthalamic nucleus stimulation. *J Neurol Neurosurg Psychiatry* 2005a; 76: 1217-21.

Hilker R, Schweitzer K, Coburger S, Ghaemi M, Weisenbach S, Jacobs AH, *et al.* Nonlinear progression of Parkinson disease as determined by serial positron emission tomographic imaging of striatal fluorodopa F 18 activity. *Arch Neurol* 2005b; 62: 378-82.

Hilker R, Voges J, Ghaemi M, Lehrke R, Rudolf J, Koulousakis A, *et al.* Deep brain stimulation of the subthalamic nucleus does not increase the striatal dopamine concentration in parkinsonian humans. *Mov Disord* 2003; 18: 41-8.

Hiorth YH, Larsen JP, Lode K, Pedersen KF. Natural history of falls in a population-based cohort of patients with Parkinson's disease: an 8-year prospective study. *Parkinsonism Relat Disord* 2014; 20: 1059-64.

Hirvonen J, Johansson J, Teras M, Oikonen V, Lumme V, Virsu P, *et al.* Measurement of striatal and extrastriatal dopamine transporter binding with high-resolution PET and [11C]PE2I: quantitative modeling and test-retest reproducibility. *J Cereb Blood Flow Metab* 2008; 28: 1059-69.

Hlavnicka J, Cmejla R, Tykalova T, Sonka K, Ruzicka E, Rusz J. Automated analysis of connected speech reveals early biomarkers of Parkinson's disease in patients with rapid eye movement sleep behaviour disorder. *Sci Rep* 2017; 7: 12.

Hoehn MM, Yahr MD. Parkinsonism: onset, progression and mortality. *Neurology* 1967; 17: 427-42.

Hoffer BJ, Leenders KL, Young D, Gerhardt G, Zerbe GO, Bygdeman M, *et al.* Eighteen-month course of two patients with grafts of fetal dopamine neurons for severe Parkinson's disease. *Exp Neurol* 1992; 118: 243-52.

Holloway RG, Shoulson I, Fahn S, Kieburtz K, Lang A, Marek K, *et al.* Pramipexole vs levodopa as initial treatment for Parkinson disease: a 4-year randomized controlled trial. *Arch Neurol* 2004; 61: 1044-53.

Hong JY, Oh JS, Lee I, Sunwoo MK, Ham JH, Lee JE, *et al.* Presynaptic dopamine depletion predicts levodopa-induced dyskinesia in de novo Parkinson disease. *Neurology* 2014; 82: 1597-604.

Hornykiewicz O. Biochemical aspects of Parkinson's disease. *Neurology* 1998; 51: S2-9.

Houle S, Ginovart N, Hussey D, Meyer JH, Wilson AA. Imaging the serotonin transporter with positron emission tomography: initial human studies with [11C]DAPP and [11C]DASB. *Eur J Nucl Med* 2000; 27: 1719-22.

Hsiao IT, Weng YH, Hsieh CJ, Lin WY, Wey SP, Kung MP, *et al.* Correlation of Parkinson disease severity and 18F-DTBZ positron emission tomography. *JAMA neurology* 2014; 71: 758-66.

Huang C, Tang C, Feigin A, Lesser M, Ma Y, Pourfar M, *et al.* Changes in network activity with the progression of Parkinson's disease. *Brain* 2007; 130: 1834-46.

Huang Y, Hwang DR, Narendran R, Sudo Y, Chatterjee R, Bae SA, *et al.* Comparative evaluation in nonhuman primates of five PET radiotracers for imaging the serotonin transporters: [11C]McN 5652, [11C]ADAM, [11C]DASB, [11C]DAPA, and [11C]AFM. *J Cereb Blood Flow Metab* 2002; 22: 1377-98.

Hughes AJ, Daniel SE, Kilford L, Lees AJ. Accuracy of clinical diagnosis of idiopathic Parkinson's disease: a clinico-pathological study of 100 cases. *J Neurol Neurosurg Psychiatry* 1992; 55: 181-4.

Hunn BH, Cragg SJ, Bolam JP, Spillantini MG, Wade-Martins R. Impaired intracellular trafficking defines early Parkinson's disease. *Trends Neurosci* 2015; 38: 178-88.

Ichise M, Kim YJ, Ballinger JR, Vines D, Erami SS, Tanaka F, *et al.* SPECT imaging of pre- and postsynaptic dopaminergic alterations in L-dopa-untreated PD. *Neurology* 1999; 52: 1206-14.

Ichise M, Liow JS, Lu JQ, Takano A, Model K, Toyama H, *et al.* Linearized reference tissue parametric imaging methods: application to [11C]DASB positron emission tomography studies of the serotonin transporter in human brain. *J Cereb Blood Flow Metab* 2003; 23: 1096-112.

Innis RB, Cunningham VJ, Delforge J, Fujita M, Gjedde A, Gunn RN, *et al.* Consensus nomenclature for in vivo imaging of reversibly binding radioligands. *J Cereb Blood Flow Metab* 2007; 27: 1533-9.

Iranzo A, Fernandez-Arcos A, Tolosa E, Serradell M, Molinuevo JL, Valldeoriola F, *et al.* Neurodegenerative disorder risk in idiopathic REM sleep behavior disorder: study in 174 patients. *PLoS One* 2014; 9: e89741.

Isacson O, Bjorklund LM, Schumacher JM. Toward full restoration of synaptic and terminal function of the dopaminergic system in Parkinson's disease by stem cells. *Ann Neurol* 2003; 53 Suppl 3: S135-46; discussion S46-8.

Isaias IU, Benti R, Cilia R, Canesi M, Marotta G, Gerundini P, *et al.* [123I]FP-CIT striatal binding in early Parkinson's disease patients with tremor vs. akinetic-rigid onset. *Neuroreport* 2007; 18: 1499-502.

Isaias IU, Marzegan A, Pezzoli G, Marotta G, Canesi M, Biella GE, *et al.* A role for locus coeruleus in Parkinson tremor. *Front Hum Neurosci* 2011; 5: 179.

Ishibashi K, Ishii K, Oda K, Kawasaki K, Mizusawa H, Ishiwata K. Regional analysis of age-related decline in dopamine transporters and dopamine D2-like receptors in human striatum. *Synapse* 2009; 63: 282-90.

Ishikawa T, Dhawan V, Kazumata K, Chaly T, Mandel F, Neumeyer J, *et al.* Comparative nigrostriatal dopaminergic imaging with iodine-123-beta CIT-FP/SPECT and fluorine-18-FDOPA/PET. *J Nucl Med* 1996; 37: 1760-5.

Jacques DB, Kopyov OV, Eagle KS, Carter T, Lieberman A. Outcomes and complications of fetal tissue transplantation in Parkinson's disease. *Stereotact Funct Neurosurg* 1999; 72: 219-24.

Jahanshahi M, Obeso I, Rothwell JC, Obeso JA. A fronto-striato-subthalamic-pallidal network for goal-directed and habitual inhibition. *Nat Rev Neurosci* 2015; 16: 719-32.

Jakobson Mo S, Linder J, Forsgren L, Holmberg H, Larsson A, Riklund K. Pre- and postsynaptic dopamine SPECT in idiopathic Parkinsonian diseases: a follow-up study. *BioMed research international* 2013; 2013: 143532.

Jankovic J. Parkinson's disease: clinical features and diagnosis. *J Neurol Neurosurg Psychiatry* 2008; 79: 368-76.

Jellinger KA. A critical evaluation of current staging of alpha-synuclein pathology in Lewy body disorders. *Biochim Biophys Acta* 2009; 1792: 730-40.

Jellinger KA. Neuropathology of sporadic Parkinson's disease: evaluation and changes of concepts. *Mov Disord* 2012; 27: 8-30.

Jenkins PO, De Simoni S, Bourke NJ, Fleminger J, Scott G, Towey DJ, *et al.* Dopaminergic abnormalities following traumatic brain injury. *Brain* 2018; 141: 797-810.

Jenkinson M, Beckmann CF, Behrens TE, Woolrich MW, Smith SM. Fsl. *Neuroimage* 2012; 62: 782-90.

Jenner P. Molecular mechanisms of L-DOPA-induced dyskinesia. *Nat Rev Neurosci* 2008; 9: 665-77.

Jenner P, Katzenschlager R. Apomorphine - pharmacological properties and clinical trials in Parkinson's disease. *Parkinsonism Relat Disord* 2016; 33 Suppl 1: S13-S21.

Jin X, Costa RM. Shaping action sequences in basal ganglia circuits. *Curr Opin Neurobiol* 2015; 33: 188-96.

Jin Y, Dougherty SE, Wood K, Sun L, Cudmore RH, Abdalla A, *et al.* Regrowth of Serotonin Axons in the Adult Mouse Brain Following Injury. *Neuron* 2016; 91: 748-62.

Joel D, Weiner I. The organization of the basal ganglia-thalamocortical circuits: open interconnected rather than closed segregated. *Neuroscience* 1994; 63: 363-79.

Jonasson SB, Nilsson MH, Lexell J, Carlsson G. Experiences of fear of falling in persons with Parkinson's disease - a qualitative study. *BMC Geriatr* 2018; 18: 44.

Jourdain VA, Tang CC, Holtbernd F, Dresel C, Choi YY, Ma Y, *et al.* Flow-metabolism dissociation in the pathogenesis of levodopa-induced dyskinesia. *JCI insight* 2016; 1: e86615.

Jucaite A, Odano I, Olsson H, Pauli S, Halldin C, Farde L. Quantitative analyses of regional [11C]PE2I binding to the dopamine transporter in the human brain: a PET study. *Eur J Nucl Med Mol Imaging* 2006; 33: 657-68.

Kaasinen V, Ruottinen HM, Någren K, Lehikoinen P, Oikonen V, Rinne JO. Upregulation of putaminal dopamine D2 receptors in early Parkinson's disease: a comparative PET study with [11C] raclopride and [11C]N-methylspiperone. *J Nucl Med* 2000; 41: 65-70.

Kader M, Iwarsson S, Odin P, Nilsson MH. Fall-related activity avoidance in relation to a history of falls or near falls, fear of falling and disease severity in people with Parkinson's disease. *BMC Neurol* 2016; 16: 84.

Kajstura TJ, Dougherty SE, Linden DJ. Serotonin axons in the neocortex of the adult female mouse regrow after traumatic brain injury. *J Neurosci Res* 2018; 96: 512-26.

Kalaitzakis ME, Graeber MB, Gentleman SM, Pearce RK. The dorsal motor nucleus of the vagus is not an obligatory trigger site of Parkinson's disease: a critical analysis of alpha-synuclein staging. *Neuropathol Appl Neurobiol* 2008; 34: 284-95.

Kalia LV, Kalia SK, McLean PJ, Lozano AM, Lang AE. alpha-Synuclein oligomers and clinical implications for Parkinson disease. *Ann Neurol* 2013; 73: 155-69.

Kalia LV, Lang AE, Hazrati LN, Fujioka S, Wszolek ZK, Dickson DW, *et al.* Clinical correlations with Lewy body pathology in LRRK2-related Parkinson disease. *JAMA neurology* 2015; 72: 100-5.

Kanazawa T, Uchihara T, Takahashi A, Nakamura A, Orimo S, Mizusawa H. Three-layered structure shared between Lewy bodies and lewy neurites-three-dimensional reconstruction of triple-labeled sections. *Brain Pathol* 2008; 18: 415-22.

Karachi C, Grabli D, Bernard FA, Tande D, Wattiez N, Belaid H, *et al.* Cholinergic mesencephalic neurons are involved in gait and postural disorders in Parkinson disease. *J Clin Invest* 2010; 120: 2745-54.

Karten YJ, Nair SM, van Essen L, Sibug R, Joels M. Long-term exposure to high corticosterone levels attenuates serotonin responses in rat hippocampal CA1 neurons. *Proc Natl Acad Sci U S A* 1999; 96: 13456-61.

Kassambara A. ggpubr: 'ggplot2' Based Publication Ready Plots. R package version 0.2.4. 2019. Available from: https://CRAN.R-project.org/package=ggpubr.

Katzenschlager R, Poewe W, Rascol O, Trenkwalder C, Deuschl G, Chaudhuri KR, *et al.* Apomorphine subcutaneous infusion in patients with Parkinson's disease with persistent motor fluctuations (TOLEDO): a multicentre, double-blind, randomised, placebo-controlled trial. *The Lancet Neurology* 2018; 17: 749-59.

Kefalopoulou Z, Politis M, Piccini P, Mencacci N, Bhatia K, Jahanshahi M, *et al.* Long-term clinical outcome of fetal cell transplantation for Parkinson disease: two case reports. *JAMA neurology* 2014; 71: 83-7.

Kerenyi L, Ricaurte GA, Schretlen DJ, McCann U, Varga J, Mathews WB, *et al.* Positron emission tomography of striatal serotonin transporters in Parkinson disease. *Arch Neurol* 2003; 60: 1223-9.

Kieburtz K, Wunderle KB. Parkinson's disease: evidence for environmental risk factors. *Mov Disord* 2013; 28: 8-13.

Kim HJ, Mason S, Foltynie T, Winder-Rhodes S, Barker RA, Williams-Gray CH. Motor complications in Parkinson's disease: 13-year follow-up of the CamPaIGN cohort. *Mov Disord* 2020; 35: 185-90.

Kim YJ, Ichise M, Ballinger JR, Vines D, Erami SS, Tatschida T, *et al.* Combination of dopamine transporter and D2 receptor SPECT in the diagnostic evaluation of PD, MSA, and PSP. *Mov Disord* 2002; 17: 303-12.

Kish SJ, Furukawa Y, Chang LJ, Tong J, Ginovart N, Wilson A, *et al.* Regional distribution of serotonin transporter protein in postmortem human brain: is the cerebellum a SERT-free brain region? *Nucl Med Biol* 2005; 32: 123-8.

Kish SJ, Shannak K, Hornykiewicz O. Uneven Pattern of Dopamine Loss in the Striatum of Patients with Idiopathic Parkinsons-Disease - Pathophysiologic and Clinical Implications. *N Engl J Med* 1988; 318: 876-80.

Kish SJ, Tong J, Hornykiewicz O, Rajput A, Chang LJ, Guttman M, *et al.* Preferential loss of serotonin markers in caudate versus putamen in Parkinson's disease. *Brain* 2008; 131: 120-31.

Kleiner-Fisman G, Herzog J, Fisman DN, Tamma F, Lyons KE, Pahwa R, *et al.* Subthalamic nucleus deep brain stimulation: summary and meta-analysis of outcomes. *Mov Disord* 2006; 21 Suppl 14: S290-304.

Komsta L, Novomestky F. moments: Moments, cumulants, skewness, kurtosis and related tests. R package version 0.14. 2015. Available from: https://CRAN.R-project.org/package=moments.

Kong M, Ba M, Ren C, Yu L, Dong S, Yu G, *et al.* An updated meta-analysis of amantadine for treating dyskinesia in Parkinson's disease. *Oncotarget* 2017; 8: 57316-26.

Kopyov OV, Jacques Ds, Lieberman A, Duma CM, Rogers RL. Clinical study of fetal mesencephalic intracerebral transplants for the treatment of Parkinson's disease. *Cell Transplant* 1996; 5: 327-37.

Kopyov OV, Jacques DS, Lieberman A, Duma CM, Rogers RL. Outcome following intrastriatal fetal mesencephalic grafts for Parkinson's patients is directly related to the volume of grafted tissue. *Exp Neurol* 1997; 146: 536-45.

Kordower JH, Brundin P. Lewy body pathology in long-term fetal nigral transplants: is Parkinson's disease transmitted from one neural system to another? *Neuropsychopharmacology* 2009; 34: 254.

Kordower JH, Chu Y, Hauser RA, Freeman TB, Olanow CW. Lewy body-like pathology in long-term embryonic nigral transplants in Parkinson's disease. *Nat Med* 2008a; 14: 504-6.

Kordower JH, Chu Y, Hauser RA, Olanow CW, Freeman TB. Transplanted dopaminergic neurons develop PD pathologic changes: a second case report. *Mov Disord* 2008b; 23: 2303-6.

Kordower JH, Freeman TB, Chen EY, Mufson EJ, Sanberg PR, Hauser RA, *et al.* Fetal nigral grafts survive and mediate clinical benefit in a patient with Parkinson's disease. *Mov Disord* 1998; 13: 383-93.

Kordower JH, Freeman TB, Snow BJ, Vingerhoets FJG, Mufson EJ, Sanberg PR, *et al.* Neuropathological Evidence of Graft Survival and Striatal Reinnervation after the Transplantation of Fetal Mesencephalic Tissue in a Patient with Parkinson's Disease. *N Engl J Med* 1995; 332: 1118-24.

Kordower JH, Goetz CG, Chu Y, Halliday GM, Nicholson DA, Musial TF, *et al.* Robust graft survival and normalized dopaminergic innervation do not obligate recovery in a Parkinson disease patient. *Ann Neurol* 2017; 81: 46-57.

Kordower JH, Olanow CW, Dodiya HB, Chu Y, Beach TG, Adler CH, *et al.* Disease duration and the integrity of the nigrostriatal system in Parkinson's disease. *Brain* 2013; 136: 2419-31.

Kordower JH, Rosenstein JM, Collier TJ, Burke MA, Chen EY, Li JM, *et al.* Functional fetal nigral grafts in a patient with Parkinson's disease: chemoanatomic, ultrastructural, and metabolic studies. *The Journal of comparative neurology* 1996; 370: 203-30.

Kordower JH, Styren S, Clarke M, DeKosky ST, Olanow CW, Freeman TB. Fetal grafting for Parkinson's disease: expression of immune markers in two patients with functional fetal nigral implants. *Cell Transplant* 1997; 6: 213-9.

Kotagal V. Is PIGD a legitimate motor subtype in Parkinson disease? *Annals of clinical and translational neurology* 2016; 3: 473-7.

Kravitz AV, Freeze BS, Parker PR, Kay K, Thwin MT, Deisseroth K, *et al.* Regulation of parkinsonian motor behaviours by optogenetic control of basal ganglia circuitry. *Nature* 2010; 466: 622-6.

Kreitzer AC, Malenka RC. Striatal plasticity and basal ganglia circuit function. *Neuron* 2008; 60: 543-54.

Krüger R, Kuhn W, Müller T, Woitalla D, Graeber M, Kösel S, *et al.* Ala30Pro mutation in the gene encoding alpha-synuclein in Parkinson's disease. *Nat Genet* 1998; 18: 106-8.

Kudoh C, Detta A, Meyer C, Byrne P, Hitchcock E. Bilateral intracaudate cografting of fetal ventral mesencephalon and striatum in advanced Parkinson's disease. *Transplant Proc* 1999; 31: 3397-402.

Kuhn M. caret: Classification and Regression Training. R package version 6.0-85. 2020. Available from: https://CRAN.R-project.org/package=caret.

Kurowska Z, Englund E, Widner H, Lindvall O, Li JY, Brundin P. Signs of degeneration in 12-22-year old grafts of mesencephalic dopamine neurons in patients with Parkinson's disease. *J Parkinsons Dis* 2011; 1: 83-92.

Kuwabara H, Cumming P, Reith J, Leger G, Diksic M, Evans AC, *et al.* Human striatal L-dopa decarboxylase activity estimated in vivo using 6-[18F]fluoro-dopa and positron emission tomography: error analysis and application to normal subjects. *J Cereb Blood Flow Metab* 1993; 13: 43-56.

Kuznetsova A, Brockhoff PB, Christensen RHB. lmerTest Package: Tests in Linear Mixed Effects Models. *J Stat Softw* 2017; 82: 1-26.

Laguna Goya R, Busch R, Mathur R, Coles AJ, Barker RA. Human fetal neural precursor cells can up-regulate MHC class I and class II expression and elicit CD4 and CD8 T cell proliferation. *Neurobiol Dis* 2011; 41: 407-14.

Lammertsma AA, Hume SP. Simplified reference tissue model for PET receptor studies. *Neuroimage* 1996; 4: 153-8.

Lane EL, Brundin P, Cenci MA. Amphetamine-induced abnormal movements occur independently of both transplant- and host-derived serotonin innervation following neural grafting in a rat model of Parkinson's disease. *Neurobiol Dis* 2009a; 35: 42-51.

Lane EL, Soulet D, Vercammen L, Cenci MA, Brundin P. Neuroinflammation in the generation of post-transplantation dyskinesia in Parkinson's disease. *Neurobiol Dis* 2008; 32: 220-8.

Lane EL, Vercammen L, Cenci MA, Brundin P. Priming for L-DOPA-induced abnormal involuntary movements increases the severity of amphetamine-induced dyskinesia in grafted rats. *Exp Neurol* 2009b; 219: 355-8.

Lane EL, Winkler C, Brundin P, Cenci MA. The impact of graft size on the development of dyskinesia following intrastriatal grafting of embryonic dopamine neurons in the rat. *Neurobiol Dis* 2006; 22: 334-45.

Lashuel HA, Overk CR, Oueslati A, Masliah E. The many faces of alpha-synuclein: from structure and toxicity to therapeutic target. *Nat Rev Neurosci* 2013; 14: 38-48.

Latt MD, Lord SR, Morris JG, Fung VS. Clinical and physiological assessments for elucidating falls risk in Parkinson's disease. *Mov Disord* 2009; 24: 1280-9.

Leak RK, Frosch MP, Beach TG, Halliday GM. Alpha-synuclein: prion or prion-like? *Acta Neuropathol* 2019; 138: 509-14.

Lee CS, Samii A, Sossi V, Ruth TJ, Schulzer M, Holden JE, *et al.* In vivo positron emission tomographic evidence for compensatory changes in presynaptic dopaminergic nerve terminals in Parkinson's disease. *Ann Neurol* 2000; 47: 493-503.

Lee CS, Schulzer M, de la Fuente-Fernández R, Mak E, Kuramoto L, Sossi V, *et al.* Lack of regional selectivity during the progression of Parkinson disease: implications for pathogenesis. *Arch Neurol* 2004; 61: 1920-5.

Lee HJ, Bae EJ, Lee SJ. Extracellular alpha--synuclein-a novel and crucial factor in Lewy body diseases. *Nat Rev Neurol* 2014; 10: 92-8.

Lee JW, Song YS, Kim H, Ku BD, Lee WW. Alteration of Tremor Dominant and Postural Instability Gait Difficulty Subtypes During the Progression of Parkinson's Disease: Analysis of the PPMI Cohort. *Front Neurol* 2019a; 10: 471.

Lee JY, Lao-Kaim NP, Pasquini J, Deuschl G, Pavese N, Piccini P. Pallidal dopaminergic denervation and rest tremor in early Parkinson's disease: PPMI cohort analysis. *Parkinsonism Relat Disord* 2018; 51: 101-4.

Lee JY, Seo S, Lee JS, Kim HJ, Kim YK, Jeon BS. Putaminal serotonergic innervation: monitoring dyskinesia risk in Parkinson disease. *Neurology* 2015; 85: 853-60.

Lee JY, Yoon EJ, Kim YK, Shin CW, Nam H, Jeong JM, *et al.* Nonmotor and Dopamine Transporter Change in REM Sleep Behavior Disorder by Olfactory Impairment. *J Mov Disord* 2019b; 12: 103-12.

Leentjens AF, Dujardin K, Marsh L, Martinez-Martin P, Richard IH, Starkstein SE. Symptomatology and markers of anxiety disorders in Parkinson's disease: a cross-sectional study. *Mov Disord* 2011; 26: 484-92.

Lees AJ, Ferreira J, Rascol O, Poewe W, Rocha JF, McCrory M, *et al.* Opicapone as Adjunct to Levodopa Therapy in Patients With Parkinson Disease and Motor Fluctuations: A Randomized Clinical Trial. *JAMA neurology* 2017; 74: 197-206.

Lees AJ, Katzenschlager R, Head J, Ben-Shlomo Y. Ten-year follow-up of three different initial treatments in de-novo PD: a randomized trial. *Neurology* 2001; 57: 1687-94.

Lehericy S, Ducros M, Van de Moortele PF, Francois C, Thivard L, Poupon C, *et al.* Diffusion tensor fiber tracking shows distinct corticostriatal circuits in humans. *Ann Neurol* 2004; 55: 522-9.

Lenth RV. emmeans: Estimated Marginal Means, aka Least-Squares Means. R package version 1.2.3. 2018. Available from: https://CRAN.R-project.org/package=emmeans.

Lerner A, Bagic A. Olfactory pathogenesis of idiopathic Parkinson disease revisited. *Mov Disord* 2008; 23: 1076-84.

Lesage S, Anheim M, Letournel F, Bousset L, Honore A, Rozas N, *et al.* G51D alpha-synuclein mutation causes a novel parkinsonian-pyramidal syndrome. *Ann Neurol* 2013; 73: 459-71.

Letanneux A, Danna J, Velay JL, Viallet F, Pinto S. From micrographia to Parkinson's disease dysgraphia. *Mov Disord* 2014; 29: 1467-75.

Leverenz JB, Umar I, Wang Q, Montine TJ, McMillan PJ, Tsuang DW, *et al.* Proteomic identification of novel proteins in cortical lewy bodies. *Brain Pathol* 2007; 17: 139-45.

Levy G, Tang MX, Louis ED, Côté LJ, Alfaro B, Mejia H, *et al.* The association of incident dementia with mortality in PD. *Neurology* 2002; 59: 1708-13.

Li JY, Englund E, Holton JL, Soulet D, Hagell P, Lees AJ, *et al.* Lewy bodies in grafted neurons in subjects with Parkinson's disease suggest host-to-graft disease propagation. *Nat Med* 2008; 14: 501-3.

Li JY, Englund E, Widner H, Rehncrona S, Bjorklund A, Lindvall O, *et al.* Characterization of Lewy body pathology in 12- and 16-year-old intrastriatal mesencephalic grafts surviving in a patient with Parkinson's disease. *Mov Disord* 2010; 25: 1091-6.

Li Q, Ma L, Innis RB, Seneca N, Ichise M, Huang H, *et al.* Pharmacological and genetic characterization of two selective serotonin transporter ligands: 2-[2-(dimethylaminomethylphenylthio)]-5-fluoromethylphenylamine (AFM) and 3-amino-4-[2-(dimethylaminomethyl-phenylthio)]benzonitrile (DASB). *J Pharmacol Exp Ther* 2004; 308: 481-6.

Li W, Englund E, Widner H, Mattsson B, van Westen D, Latt J, *et al.* Extensive graft-derived dopaminergic innervation is maintained 24 years after transplantation in the degenerating parkinsonian brain. *Proc Natl Acad Sci U S A* 2016; 113: 6544-9.

Li W, Lao-Kaim NP, Roussakis AA, Martin-Bastida A, Valle-Guzman N, Paul G, *et al.* (11) C-PE2I and (18) F-Dopa PET for assessing progression rate in Parkinson's: A longitudinal study. *Mov Disord* 2018; 33: 117-27.

Lidstone SC, Schulzer M, Dinelle K, Mak E, Sossi V, Ruth TJ, *et al.* Effects of expectation on placebo-induced dopamine release in Parkinson disease. *Arch Gen Psychiatry* 2010; 67: 857-65.

Lieberman A, Olanow CW, Sethi K, Swanson P, Waters CH, Fahn S, *et al.* A multicenter trial of ropinirole as adjunct treatment for Parkinson's disease. Ropinirole Study Group. *Neurology* 1998; 51: 1057-62.

Lima VA, do Nascimento LA, Eliezer D, Follmer C. Role of Parkinson's Disease-Linked Mutations and N-Terminal Acetylation on the Oligomerization of alpha-Synuclein Induced by 3,4-Dihydroxyphenylacetaldehyde. *ACS Chem Neurosci* 2019; 10: 690-703.

Lin SC, Lin KJ, Hsiao IT, Hsieh CJ, Lin WY, Lu CS, *et al.* In vivo detection of monoaminergic degeneration in early Parkinson disease by (18)F-9-fluoropropyl-(+)-dihydrotetrabenzazine PET. *J Nucl Med* 2014; 55: 73-9.

Lindvall O, Brundin P, Widner H, Rehncrona S, Gustavii B, Frackowiak R, *et al.* Grafts of fetal dopamine neurons survive and improve motor function in Parkinson's disease. *Science* 1990; 247: 574-7.

Lindvall O, Sawle G, Widner H, Rothwell JC, Björklund A, Brooks D, *et al.* Evidence for long-term survival and function of dopaminergic grafts in progressive Parkinson's disease. *Ann Neurol* 1994; 35: 172-80.

Lindvall O, Widner H, Rehncrona S, Brundin P, Odin P, Gustavii B, *et al.* Transplantation of fetal dopamine neurons in Parkinson's disease: one-year clinical and neurophysiological observations in two patients with putaminal implants. *Ann Neurol* 1992; 31: 155-65.

Linn-Evans ME, Petrucci MN, Amundsen Huffmaster SL, Chung JW, Tuite PJ, Howell MJ, *et al.* REM sleep without atonia is associated with increased rigidity in patients with mild to moderate Parkinson's disease. *Clin Neurophysiol* 2020; 131: 2008-16.

Lloyd KG, Davidson L, Hornykiewicz O. The neurochemistry of Parkinson's disease: effect of L-dopa therapy. *J Pharmacol Exp Ther* 1975; 195: 453-64.

Lloyd KG, Hornykiewicz O. Occurrence and distribution of aromatic L-amino acid (L-DOPA) decarboxylase in the human brain. *J Neurochem* 1972; 19: 1549-59.

Loane C, Wu K, Bain P, Brooks DJ, Piccini P, Politis M. Serotonergic loss in motor circuitries correlates with severity of action-postural tremor in PD. *Neurology* 2013; 80: 1850-5.

Logan J, Fowler JS, Volkow ND, Wang GJ, Ding YS, Alexoff DL. Distribution volume ratios without blood sampling from graphical analysis of PET data. *J Cereb Blood Flow Metab* 1996; 16: 834-40.

Lohle M, Mende J, Wolz M, Beuthien-Baumann B, Oehme L, van den Hoff J, *et al.* Putaminal dopamine turnover in de novo Parkinson disease predicts later motor complications. *Neurology* 2016; 86: 231-40.

Lohr KM, Bernstein AI, Stout KA, Dunn AR, Lazo CR, Alter SP, *et al.* Increased vesicular monoamine transporter enhances dopamine release and opposes Parkinson disease-related neurodegeneration in vivo. *Proc Natl Acad Sci U S A* 2014; 111: 9977-82.

Lokkegaard A, Werdelin LM, Regeur L, Karlsborg M, Jensen SR, Brodsgaard E, *et al.* Dopamine transporter imaging and the effects of deep brain stimulation in patients with Parkinson's disease. *Eur J Nucl Med Mol Imaging* 2007; 34: 508-16.

Loonen AJ, Ivanova SA. Circuits regulating pleasure and happiness: the evolution of reward-seeking and misery-fleeing behavioral mechanisms in vertebrates. *Front Neurosci* 2015; 9: 394.

López-Lozano JJ, Bravo G, Abascal J. Grafting of perfused adrenal medullary tissue into the caudate nucleus of patients with Parkinson's disease. Clinica Puerta de Hierro Neural Transplantation Group. *J Neurosurg* 1991; 75: 234-43.

Lopez-Lozano JJ, Bravo G, Brera B, Millan I, Dargallo J, Salmean J, *et al.* Long-term improvement in patients with severe Parkinson's disease after implantation of fetal ventral mesencephalic tissue in a cavity of the caudate nucleus: 5-year follow up in 10 patients. Clinica Puerta de Hierro Neural Transplantation Group. *J Neurosurg* 1997; 86: 931-42.

López-Lozano JJ, Bravo G, Brera B, Millán I, Dargallo J, Salmeán J, *et al.* Long-term improvement in patients with severe Parkinson's disease after implantation of fetal ventral mesencephalic tissue in a cavity of the caudate nucleus: 5-year follow up in 10 patients. Clinica Puerta de Hierro Neural Transplantation Group. *J Neurosurg* 1997; 86: 931-42.

Lüdecke D. ggeffects: Tidy Data Frames of Marginal Effects from Regression Models. *Journal of Open Source Software* 2018; 3: 772.

Lüdecke D. _sjstats: Statistical Functions for Regression Models (Version 0.17.9)_. 2020.

Luk KC, Kehm V, Carroll J, Zhang B, O'Brien P, Trojanowski JQ, *et al.* Pathological α-synuclein transmission initiates Parkinson-like neurodegeneration in nontransgenic mice. *Science* 2012; 338: 949-53.

Luke SG. Evaluating significance in linear mixed-effects models in R. *Behav Res Methods* 2017; 49: 1494-502.

Lynd-Balta E, Haber SN. The organization of midbrain projections to the striatum in the primate: sensorimotor-related striatum versus ventral striatum. *Neuroscience* 1994; 59: 625-40.

Ma J, Gao J, Wang J, Xie A. Prion-Like Mechanisms in Parkinson's Disease. *Front Neurosci* 2019; 13: 552.

Ma SY, Röyttä M, Rinne JO, Collan Y, Rinne UK. Correlation between neuromorphometry in the substantia nigra and clinical features in Parkinson's disease using disector counts. *J Neurol Sci* 1997; 151: 83-7.

Ma Y, Feigin A, Dhawan V, Fukuda M, Shi Q, Greene P, *et al.* Dyskinesia after fetal cell transplantation for parkinsonism: a PET study. *Ann Neurol* 2002; 52: 628-34.

Ma Y, Peng S, Dhawan V, Eidelberg D. Dopamine cell transplantation in Parkinson's disease: challenge and perspective. *Br Med Bull* 2011; 100: 173-89.

Ma Y, Tang C, Chaly T, Greene P, Breeze R, Fahn S, *et al.* Dopamine cell implantation in Parkinson's disease: long-term clinical and (18)F-FDOPA PET outcomes. *J Nucl Med* 2010; 51: 7-15.

Macht M, Kaussner Y, Moller JC, Stiasny-Kolster K, Eggert KM, Kruger HP, *et al.* Predictors of freezing in Parkinson's disease: a survey of 6,620 patients. *Mov Disord* 2007; 22: 953-6.

Mackay AV, Davies P, Dewar AJ, Yates CM. Regional distribution of enzymes associated with neurotransmission by monoamines, acetylcholine and GABA in the human brain. *J Neurochem* 1978; 30: 827-39.

Macleod AD, Taylor KS, Counsell CE. Mortality in Parkinson's disease: a systematic review and meta-analysis. *Mov Disord* 2014; 29: 1615-22.

Madrazo I, Franco-Bourland R, Aguilera M, Ostrosky-Solis F, Madrazo M, Cuevas C, *et al.* Autologous adrenal medullary, fetal mesencephalic, and fetal adrenal brain transplantation in Parkinson's disease: a long-term postoperative follow-up. *J Neural Transplant Plast* 1991; 2: 157-64.

Maeda T, Nagata K, Yoshida Y, Kannari K. Serotonergic hyperinnervation into the dopaminergic denervated striatum compensates for dopamine conversion from exogenously administered L-DOPA. *Brain Res* 2005; 1046: 230-3.

Magrinelli F, Picelli A, Tocco P, Federico A, Roncari L, Smania N, *et al.* Pathophysiology of Motor Dysfunction in Parkinson's Disease as the Rationale for Drug Treatment and Rehabilitation. *Parkinsons Dis* 2016; 2016: 9832839.

Mahul-Mellier AL, Burtscher J, Maharjan N, Weerens L, Croisier M, Kuttler F, *et al.* The process of Lewy body formation, rather than simply alpha-synuclein fibrillization, is one of the major drivers of neurodegeneration. *Proc Natl Acad Sci U S A* 2020; 117: 4971-82.

Maillet A, Krack P, Lhommee E, Metereau E, Klinger H, Favre E, *et al.* The prominent role of serotonergic degeneration in apathy, anxiety and depression in de novo Parkinson's disease. *Brain* 2016; 139: 2486-502.

Mailly P, Aliane V, Groenewegen HJ, Haber SN, Deniau JM. The rat prefrontostriatal system analyzed in 3D: evidence for multiple interacting functional units. *J Neurosci* 2013; 33: 5718-27.

Marchand WR. Cortico-basal ganglia circuitry: a review of key research and implications for functional connectivity studies of mood and anxiety disorders. *Brain Struct Funct* 2010; 215: 73-96.

Marek K, Innis R, van Dyck C, Fussell B, Early M, Eberly S, *et al.* [123I]beta-CIT SPECT imaging assessment of the rate of Parkinson's disease progression. *Neurology* 2001; 57: 2089-94.

Maries E, Kordower JH, Chu YP, Collier TJ, Sortwell CE, Olaru E, *et al.* Focal not widespread grafts induce novel dyskinetic behavior in parkinsonian rats. *Neurobiol Dis* 2006; 21: 165-80.

Markesbery WR, Jicha GA, Liu H, Schmitt FA. Lewy body pathology in normal elderly subjects. *J Neuropathol Exp Neurol* 2009; 68: 816-22.

Marklund U, Alekseenko Z, Andersson E, Falci S, Westgren M, Perlmann T, *et al.* Detailed expression analysis of regulatory genes in the early developing human neural tube. *Stem Cells Dev* 2014; 23: 5-15.

Maroteaux L, Campanelli JT, Scheller RH. Synuclein: a neuron-specific protein localized to the nucleus and presynaptic nerve terminal. *J Neurosci* 1988; 8: 2804-15.

Marras C, Lang A. Parkinson's disease subtypes: lost in translation? *J Neurol Neurosurg Psychiatry* 2013; 84: 409-15.

Martin-Bastida A, Lao-Kaim NP, Loane C, Politis M, Roussakis AA, Valle-Guzman N, *et al.* Motor associations of iron accumulation in deep grey matter nuclei in Parkinson's disease: a cross-sectional study of iron-related magnetic resonance imaging susceptibility. *Eur J Neurol* 2017; 24: 357-65.

Martin-Bastida A, Lao-Kaim NP, Roussakis AA, Searle GE, Xing Y, Gunn RN, *et al.* Relationship between neuromelanin and dopamine terminals within the Parkinson's nigrostriatal system. *Brain* 2019; 142: 2023-36.

Martin WR, Wieler M, Stoessl AJ, Schulzer M. Dihydrotetrabenazine positron emission tomography imaging in early, untreated Parkinson's disease. *Ann Neurol* 2008; 63: 388-94.

Masuda-Suzukake M, Nonaka T, Hosokawa M, Kubo M, Shimozawa A, Akiyama H, *et al.* Pathological alpha-synuclein propagates through neural networks. *Acta neuropathologica communications* 2014; 2: 88.

Masuda-Suzukake M, Nonaka T, Hosokawa M, Oikawa T, Arai T, Akiyama H, *et al.* Prion-like spreading of pathological alpha-synuclein in brain. *Brain* 2013; 136: 1128-38.

Mazziotta JC, Toga AW, Evans A, Fox P, Lancaster J. A probabilistic atlas of the human brain: theory and rationale for its development. The International Consortium for Brain Mapping (ICBM). *Neuroimage* 1995; 2: 89-101.

McColgan P, Evans JR, Breen DP, Mason SL, Barker RA, Williams-Gray CH. Addenbrooke's Cognitive Examination-Revised for mild cognitive impairment in Parkinson's disease. *Mov Disord* 2012; 27: 1173-7.

McGregor MM, Nelson AB. Circuit Mechanisms of Parkinson's Disease. *Neuron* 2019; 101: 1042-56.

McLaren FH, Svendsen CN, Van der Meide P, Joly E. Analysis of neural stem cells by flow cytometry: cellular differentiation modifies patterns of MHC expression. *J Neuroimmunol* 2001; 112: 35-46.

McLennan JE, Nakano K, Tyler HR, Schwab RS. Micrographia in Parkinson's disease. *J Neurol Sci* 1972; 15: 141-52.

McMillen BA, Matthews RT, Sanghera MK, Shepard PD, German DC. Dopamine receptor antagonism by the novel antianxiety drug, buspirone. *J Neurosci* 1983; 3: 733-8.

Meade RM, Fairlie DP, Mason JM. Alpha-synuclein structure and Parkinson's disease - lessons and emerging principles. *Mol Neurodegener* 2019; 14: 29.

Meikle SR, Badawi RD. Quantitative Techniques in PET. In: Bailey DL, Townsend DW, Valk PE, N. MM, editors. Positron Emission Tomography. 1st ed. London: Springer; 2005.

Melton LJ, 3rd, Leibson CL, Achenbach SJ, Bower JH, Maraganore DM, Oberg AL, *et al.* Fracture risk after the diagnosis of Parkinson's disease: Influence of concomitant dementia. *Mov Disord* 2006; 21: 1361-7.

Mendez I, Dagher A, Hong M, Gaudet P, Weerasinghe S, McAlister V, *et al.* Simultaneous intrastriatal and intranigral fetal dopaminergic grafts in patients with Parkinson disease: a pilot study. Report of three cases. *J Neurosurg* 2002; 96: 589-96.

Mendez I, Dagher A, Hong M, Hebb A, Gaudet P, Law A, *et al.* Enhancement of survival of stored dopaminergic cells and promotion of graft survival by exposure of human fetal nigral tissue to glial cell line--derived neurotrophic factor in patients with Parkinson's disease. Report of two cases and technical considerations. *J Neurosurg* 2000; 92: 863-9.

Mendez I, Sanchez-Pernaute R, Cooper O, Vinuela A, Ferrari D, Bjorklund L, *et al.* Cell type analysis of functional fetal dopamine cell suspension transplants in the striatum and substantia nigra of patients with Parkinson's disease. *Brain* 2005; 128: 1498-510.

Mendez I, Vinuela A, Astradsson A, Mukhida K, Hallett P, Robertson H, *et al.* Dopamine neurons implanted into people with Parkinson's disease survive without pathology for 14 years. *Nat Med* 2008; 14: 507-9.

Merkle E, You D. nonnest2: Tests of Non-Nested Models. R package version 0.5-3. 2020. Available from: https://CRAN.R-project.org/package=nonnest2.

Meyer JH, Wilson AA, Sagrati S, Hussey D, Carella A, Potter WZ, *et al.* Serotonin transporter occupancy of five selective serotonin Reuptake inhibitors at different doses: An [C-11]DASB positron emission tomography study. *Am J Psychiatry* 2004; 161: 826-35.

Mezey E, Dehejia AM, Harta G, Tresser N, Suchy SF, Nussbaum RL, *et al.* Alpha synuclein is present in Lewy bodies in sporadic Parkinson's disease. *Mol Psychiatry* 1998; 3: 493-9.

Michel V, Yuan Z, Ramsubir S, Bakovic M. Choline transport for phospholipid synthesis. *Exp Biol Med (Maywood)* 2006; 231: 490-504.

Middleton ER, Rhoades E. Effects of curvature and composition on alpha-synuclein binding to lipid vesicles. *Biophys J* 2010; 99: 2279-88.

Miguelez C, Morera-Herreras T, Torrecilla M, Ruiz-Ortega JA, Ugedo L. Interaction between the 5-HT system and the basal ganglia: functional implication and therapeutic perspective in Parkinson's disease. *Frontiers in neural circuits* 2014; 8: 21.

Milber JM, Noorigian JV, Morley JF, Petrovitch H, White L, Ross GW, *et al.* Lewy pathology is not the first sign of degeneration in vulnerable neurons in Parkinson disease. *Neurology* 2012; 79: 2307-14.

Miller AH, Haroon E, Raison CL, Felger JC. Cytokine targets in the brain: impact on neurotransmitters and neurocircuits. *Depress Anxiety* 2013; 30: 297-306.

Minguez-Castellanos A, Escamilla-Sevilla F, Hotton GR, Toledo-Aral JJ, Ortega-Moreno A, Mendez-Ferrer S, *et al.* Carotid body autotransplantation in Parkinson disease: a clinical and positron emission tomography study. *J Neurol Neurosurg Psychiatry* 2007; 78: 825-31.

Mioshi E, Dawson K, Mitchell J, Arnold R, Hodges JR. The Addenbrooke's Cognitive Examination Revised (ACE-R): a brief cognitive test battery for dementia screening. *Int J Geriatr Psychiatry* 2006; 21: 1078-85.

Mizuno Y, Abe T, Hasegawa K, Kuno S, Kondo T, Yamamoto M, *et al.* Ropinirole is effective on motor function when used as an adjunct to levodopa in Parkinson's disease: STRONG study. *Mov Disord* 2007; 22: 1860-5.

Mizuno Y, Nomoto M, Hasegawa K, Hattori N, Kondo T, Murata M, *et al.* Rotigotine vs ropinirole in advanced stage Parkinson's disease: a double-blind study. *Parkinsonism Relat Disord* 2014; 20: 1388-93.

Molina H, Quiñones R, Alvarez L, Ortega I, Muńoz JL, González C, *et al.* Stereotactic Transplantation of Foetal Ventral Mesencephalic Cells: Cuban Experience from Five Patients with Idiopathic Parkinson's Disease. *J Neural Transplant Plast* 1992a; 3: 338-9.

Molina H, Quiñones R, Alvarez L, Suárez C, Ortega I, Muñoz JL, *et al.* Transplantation of Human Fetal Mesencephalic Tissue in Caudate Nucleus as a Treatment for Parkinson's Disease. Long-Term Follow-Up. *J Neural Transplant Plast* 1992b; 3: 323-4.

Moore RY, Whone AL, Brooks DJ. Extrastriatal monoamine neuron function in Parkinson's disease: an 18F-dopa PET study. *Neurobiol Dis* 2008; 29: 381-90.

Moore RY, Whone AL, McGowan S, Brooks DJ. Monoamine neuron innervation of the normal human brain: an 18F-DOPA PET study. *Brain Res* 2003; 982: 137-45.

Morrish PK, Rakshi JS, Bailey DL, Sawle GV, Brooks DJ. Measuring the rate of progression and estimating the preclinical period of Parkinson's disease with [18F]dopa PET. *J Neurol Neurosurg Psychiatry* 1998; 64: 314-9.

Morrish PK, Sawle GV, Brooks DJ. Regional changes in [18F]dopa metabolism in the striatum in Parkinson's disease. *Brain* 1996; 119 (Pt 6): 2097-103.

Mosharov EV, Larsen KE, Kanter E, Phillips KA, Wilson K, Schmitz Y, *et al.* Interplay between cytosolic dopamine, calcium, and alpha-synuclein causes selective death of substantia nigra neurons. *Neuron* 2009; 62: 218-29.

Muller ML, Albin RL, Kotagal V, Koeppe RA, Scott PJ, Frey KA, *et al.* Thalamic cholinergic innervation and postural sensory integration function in Parkinson's disease. *Brain* 2013; 136: 3282-9.

Muller T. Catechol-O-methyltransferase inhibitors in Parkinson's disease. *Drugs* 2015; 75: 157-74.

Nakamura T, Dhawan V, Chaly T, Fukuda M, Ma Y, Breeze R, *et al.* Blinded positron emission tomography study of dopamine cell implantation for Parkinson's disease. *Ann Neurol* 2001; 50: 181-7.

Nandhagopal R, Kuramoto L, Schulzer M, Mak E, Cragg J, Lee CS, *et al.* Longitudinal progression of sporadic Parkinson's disease: a multi-tracer positron emission tomography study. *Brain* 2009; 132: 2970-9.

Nandhagopal R, Kuramoto L, Schulzer M, Mak E, Cragg J, McKenzie J, *et al.* Longitudinal evolution of compensatory changes in striatal dopamine processing in Parkinson's disease. *Brain* 2011; 134: 3290-8.

Navailles S, Bioulac B, Gross C, De Deurwaerdere P. Serotonergic neurons mediate ectopic release of dopamine induced by L-DOPA in a rat model of Parkinson's disease. *Neurobiol Dis* 2010; 38: 136-43.

Neumeyer JL, Wang S, Gao Y, Milius RA, Kula NS, Campbell A, *et al.* N-omega-fluoroalkyl analogs of (1R)-2 beta-carbomethoxy-3 beta-(4-iodophenyl)-tropane (beta-CIT): radiotracers for positron emission tomography and single photon emission computed tomography imaging of dopamine transporters. *J Med Chem* 1994; 37: 1558-61.

Nikkhah G, Cunningham MG, Jodicke A, Knappe U, Bjorklund A. Improved graft survival and striatal reinnervation by microtransplantation of fetal nigral cell suspensions in the rat Parkinson model. *Brain Res* 1994; 633: 133-43.

Nimura T, Yamaguchi K, Ando T, Shibuya S, Oikawa T, Nakagawa A, *et al.* Attenuation of fluctuating striatal synaptic dopamine levels in patients with Parkinson disease in response to subthalamic nucleus stimulation: a positron emission tomography study. *J Neurosurg* 2005; 103: 968-73.

Nomoto M, Mizuno Y, Kondo T, Hasegawa K, Murata M, Takeuchi M, *et al.* Transdermal rotigotine in advanced Parkinson's disease: a randomized, double-blind, placebo-controlled trial. *J Neurol* 2014; 261: 1887-93.

Noyce AJ, Bestwick JP, Silveira-Moriyama L, Hawkes CH, Giovannoni G, Lees AJ, *et al.* Meta-analysis of early nonmotor features and risk factors for Parkinson disease. *Ann Neurol* 2012; 72: 893-901.

Nurmi E, Bergman J, Eskola O, Solin O, Vahlberg T, Sonninen P, *et al.* Progression of dopaminergic hypofunction in striatal subregions in Parkinson's disease using [18F]CFT PET. *Synapse* 2003; 48: 109-15.

Nurmi E, Ruottinen HM, Bergman J, Haaparanta M, Solin O, Sonninen P, *et al.* Rate of progression in Parkinson's disease: a 6-[18F]fluoro-L-dopa PET study. *Mov Disord* 2001; 16: 608-15.

Nyberg P, Nordberg A, Wester P, Winblad B. Dopaminergic deficiency is more pronounced in putamen than in nucleus caudatus in Parkinson's disease. *Neurochem Pathol* 1983; 1: 193-202.

Nyholm D, Karlsson E, Lundberg M, Askmark H. Large differences in levodopa dose requirement in Parkinson's disease: men use higher doses than women. *Eur J Neurol* 2010; 17: 260-6.

Obeso JA, Rodriguez-Oroz MC, Benitez-Temino B, Blesa FJ, Guridi J, Marin C, *et al.* Functional organization of the basal ganglia: Therapeutic implications for Parkinson's disease. *Mov Disord* 2008; 23: S548-S59.

Obeso JA, Rodríguez-Oroz MC, Rodríguez M, Lanciego JL, Artieda J, Gonzalo N, *et al.* Pathophysiology of the basal ganglia in Parkinson's disease. *Trends Neurosci* 2000; 23: S8-19.

Odano I, Varrone A, Hosoya T, Sakaguchi K, Gulyas B, Padmanabhan P, *et al.* Simplified estimation of binding parameters based on image-derived reference tissue models for dopamine transporter bindings in non-human primates using [(18)F]FE-PE2I and PET. *Am J Nucl Med Mol Imaging* 2017; 7: 246-54.

Odano I, Varrone A, Savic I, Ciumas C, Karlsson P, Jucaite A, *et al.* Quantitative PET analyses of regional [11C]PE2I binding to the dopamine transporter--application to juvenile myoclonic epilepsy. *Neuroimage* 2012; 59: 3582-93.

Oertel W, Eggert K, Pahwa R, Tanner CM, Hauser RA, Trenkwalder C, *et al.* Randomized, placebo-controlled trial of ADS-5102 (amantadine) extended-release capsules for levodopa-induced dyskinesia in Parkinson's disease (EASE LID 3). *Mov Disord* 2017; 32: 1701-9.

Oertel WH, Wolters E, Sampaio C, Gimenez-Roldan S, Bergamasco B, Dujardin M, *et al.* Pergolide versus levodopa monotherapy in early Parkinson's disease patients: The PELMOPET study. *Mov Disord* 2006; 21: 343-53.

Oh M, Kim JS, Kim JY, Shin KH, Park SH, Kim HO, *et al.* Subregional patterns of preferential striatal dopamine transporter loss differ in Parkinson disease, progressive supranuclear palsy, and multiple-system atrophy. *J Nucl Med* 2012; 53: 399-406.

Okamura N, Villemagne VL, Drago J, Pejoska S, Dhamija RK, Mulligan RS, *et al.* In vivo measurement of vesicular monoamine transporter type 2 density in Parkinson disease with (18)F-AV-133. *J Nucl Med* 2010; 51: 223-8.

Olanow CW, Goetz CG, Kordower JH, Stoessl AJ, Sossi V, Brin MF, *et al.* A double-blind controlled trial of bilateral fetal nigral transplantation in Parkinson's disease. *Ann Neurol* 2003; 54: 403-14.

Olanow CW, Gracies JM, Goetz CG, Stoessl AJ, Freeman T, Kordower JH, *et al.* Clinical pattern and risk factors for dyskinesias following fetal nigral transplantation in Parkinson's disease: a double blind video-based analysis. *Mov Disord* 2009a; 24: 336-43.

Olanow CW, Kieburtz K, Odin P, Espay AJ, Standaert DG, Fernandez HH, *et al.* Continuous intrajejunal infusion of levodopa-carbidopa intestinal gel for patients with advanced Parkinson's disease: a randomised, controlled, double-blind, double-dummy study. *The Lancet Neurology* 2014; 13: 141-9.

Olanow CW, Kieburtz K, Rascol O, Poewe W, Schapira AH, Emre M, *et al.* Factors predictive of the development of Levodopa-induced dyskinesia and wearing-off in Parkinson's disease. *Mov Disord* 2013; 28: 1064-71.

Olanow CW, Koller W, Goetz CG, Stebbins GT, Cahill DW, Gauger LL, *et al.* Autologous transplantation of adrenal medulla in Parkinson's disease. 18-month results. *Arch Neurol* 1990; 47: 1286-9.

Olanow CW, Obeso JA, Stocchi F. Continuous dopamine-receptor treatment of Parkinson's disease: scientific rationale and clinical implications. *The Lancet Neurology* 2006; 5: 677-87.

Olanow CW, Perl DP, DeMartino GN, McNaught KSP. Lewy-body formation is an aggresome-related process: a hypothesis. *The Lancet Neurology* 2004; 3: 496-503.

Olanow CW, Prusiner SB. Is Parkinson's disease a prion disorder? *Proc Natl Acad Sci U S A* 2009; 106: 12571-2.

Olanow CW, Rascol O, Hauser R, Feigin PD, Jankovic J, Lang A, *et al.* A Double-Blind, Delayed-Start Trial of Rasagiline in Parkinson's Disease. *N Engl J Med* 2009b; 361: 1268-78.

Ory-Magne F, Corvol JC, Azulay JP, Bonnet AM, Brefel-Courbon C, Damier P, *et al.* Withdrawing amantadine in dyskinetic patients with Parkinson disease: the AMANDYSK trial. *Neurology* 2014; 82: 300-7.

Otsuka M, Ichiya Y, Kuwabara Y, Hosokawa S, Sasaki M, Yoshida T, *et al.* Differences in the reduced 18F-Dopa uptakes of the caudate and the putamen in Parkinson's disease: correlations with the three main symptoms. *J Neurol Sci* 1996; 136: 169-73.

Ottaviani S, Tinazzi M, Pasquin I, Nothdurfter W, Tomelleri G, Fincati E, *et al.* Comparative analysis of visual and semi-quantitative assessment of striatal [123I]FP-CIT-SPET binding in Parkinson's disease. *Neurol Sci* 2006; 27: 397-401.

Ouchi Y, Kanno T, Okada H, Yoshikawa E, Futatsubashi M, Nobezawa S, *et al.* Presynaptic and postsynaptic dopaminergic binding densities in the nigrostriatal and mesocortical systems in early Parkinson's disease: a double-tracer positron emission tomography study. *Ann Neurol* 1999; 46: 723-31.

Pacelli C, Giguere N, Bourque MJ, Levesque M, Slack RS, Trudeau LE. Elevated Mitochondrial Bioenergetics and Axonal Arborization Size Are Key Contributors to the Vulnerability of Dopamine Neurons. *Curr Biol* 2015; 25: 2349-60.

Pagano G, Niccolini F, Fusar-Poli P, Politis M. Serotonin transporter in Parkinson's disease: A meta-analysis of positron emission tomography studies. *Ann Neurol* 2017; 81: 171-80.

Pahwa R, Tanner CM, Hauser RA, Sethi K, Isaacson S, Truong D, *et al.* Amantadine extended release for levodopa-induced dyskinesia in Parkinson's disease (EASED Study). *Mov Disord* 2015; 30: 788-95.

Pal G, Ouyang B, Verhagen L, Serrano G, Shill HA, Adler CH, *et al.* Probing the striatal dopamine system for a putative neuroprotective effect of deep brain stimulation in Parkinson's disease. *Mov Disord* 2018; 33: 652-4.

Pal GD, Ouyang B, Serrano G, Shill HA, Goetz C, Stebbins G, *et al.* Comparison of neuropathology in Parkinson's disease subjects with and without deep brain stimulation. *Mov Disord* 2017; 32: 274-7.

Pal PK, Lee CS, Samii A, Schulzer M, Stoessl AJ, Mak EK, *et al.* Alternating two finger tapping with contralateral activation is an objective measure of clinical severity in Parkinson's disease and correlates with PET. *Parkinsonism Relat Disord* 2001; 7: 305-9.

Pandey S, Kumar H. Assessment of striatal & postural deformities in patients with Parkinson's disease. *Indian J Med Res* 2016; 144: 682-8.

Parent A, Hazrati LN. Functional anatomy of the basal ganglia. I. The cortico-basal ganglia-thalamo-cortical loop. *Brain Res Brain Res Rev* 1995; 20: 91-127.

Parkinson's Disease Collaborators. Global, regional, and national burden of Parkinson's disease, 1990-2016: a systematic analysis for the Global Burden of Disease Study 2016. *Lancet Neurol* 2018; 17: 939-53.

Parkinson J. An essay on the shaking palsy. 1817. *J Neuropsychiatry Clin Neurosci* 2002; 14: 223-36; discussion 2.

Parkinson Study Group. Pramipexole vs levodopa as initial treatment for Parkinson disease: A randomized controlled trial. Parkinson Study Group. *JAMA* 2000; 284: 1931-8.

Parkinson Study Group. Dopamine transporter brain imaging to assess the effects of pramipexole vs levodopa on Parkinson disease progression. *JAMA* 2002; 287: 1653-61.

Parkinson Study Group. A randomized placebo-controlled trial of rasagiline in levodopa-treated patients with Parkinson disease and motor fluctuations: the PRESTO study. *Arch Neurol* 2005; 62: 241-8.

Parkinson Study Group CALM Cohort Investigators. Long-term effect of initiating pramipexole vs levodopa in early Parkinson disease. *Arch Neurol* 2009; 66: 563-70.

Parkkinen L, O'Sullivan SS, Collins C, Petrie A, Holton JL, Revesz T, *et al.* Disentangling the relationship between lewy bodies and nigral neuronal loss in Parkinson's disease. *J Parkinsons Dis* 2011; 1: 277-86.

Parkkinen L, Pirttila T, Alafuzoff I. Applicability of current staging/categorization of alpha-synuclein pathology and their clinical relevance. *Acta Neuropathol* 2008; 115: 399-407.

Parmar M, Grealish S, Henchcliffe C. The future of stem cell therapies for Parkinson disease. *Nat Rev Neurosci* 2020; 21: 103-15.

Parsey RV, Kent JM, Oquendo MA, Richards MC, Pratap M, Cooper TB, *et al.* Acute occupancy of brain serotonin transporter by sertraline as measured by [11C]DASB and positron emission tomography. *Biol Psychiatry* 2006; 59: 821-8.

Pasanen P, Myllykangas L, Siitonen M, Raunio A, Kaakkola S, Lyytinen J, *et al.* Novel alpha-synuclein mutation A53E associated with atypical multiple system atrophy and Parkinson's disease-type pathology. *Neurobiol Aging* 2014; 35: 2180 e1-5.

Pasquini J, Ceravolo R, Brooks DJ, Bonuccelli U, Pavese N. Progressive loss of raphe nuclei serotonin transporter in early Parkinson's disease: A longitudinal (123)I-FP-CIT SPECT study. *Parkinsonism Relat Disord* 2019a; 77: 170-75.

Pasquini J, Ceravolo R, Qamhawi Z, Lee JY, Deuschl G, Brooks DJ, *et al.* Progression of tremor in early stages of Parkinson's disease: a clinical and neuroimaging study. *Brain* 2018; 141: 811-21.

Pasquini J, Durcan R, Wiblin L, Gersel Stokholm M, Rochester L, Brooks DJ, *et al.* Clinical implications of early caudate dysfunction in Parkinson's disease. *J Neurol Neurosurg Psychiatry* 2019b; 90: 1098-104.

Pasupathy A, Miller EK. Different time courses of learning-related activity in the prefrontal cortex and striatum. *Nature* 2005; 433: 873-6.

Patel A, Simon S, I ME, Amalchandran J, A SJ, S T. Dopamine Transporter maging with Tc-99m TRODAT-1 SPECT in Parkinson's isease and its orrelation with linical isease everity. *Asia Ocean J Nucl Med Biol* 2019; 7: 22-8.

Patlak CS, Blasberg RG. Graphical evaluation of blood-to-brain transfer constants from multiple-time uptake data. Generalizations. *J Cereb Blood Flow Metab* 1985; 5: 584-90.

Paulus W, Jellinger K. The neuropathologic basis of different clinical subgroups of Parkinson's disease. *J Neuropathol Exp Neurol* 1991; 50: 743-55.

Pavese N, Evans AH, Tai YF, Hotton G, Brooks DJ, Lees AJ, *et al.* Clinical correlates of levodopa-induced dopamine release in Parkinson disease: a PET study. *Neurology* 2006; 67: 1612-7.

Pavese N, Rivero-Bosch M, Lewis SJ, Whone AL, Brooks DJ. Progression of monoaminergic dysfunction in Parkinson's disease: a longitudinal 18F-dopa PET study. *Neuroimage* 2011; 56: 1463-8.

Pavese N, Simpson BS, Metta V, Ramlackhansingh A, Chaudhuri KR, Brooks DJ. [18F]FDOPA uptake in the raphe nuclei complex reflects serotonin transporter availability. A combined [18F]FDOPA and [11C]DASB PET study in Parkinson's disease. *Neuroimage* 2012; 59: 1080-4.

Payer DE, Guttman M, Kish SJ, Tong J, Adams JR, Rusjan P, *et al.* D3 dopamine receptor-preferring [11C]PHNO PET imaging in Parkinson patients with dyskinesia. *Neurology* 2016; 86: 224-30.

PD MED Collaborative Group. Long-term effectiveness of dopamine agonists and monoamine oxidase B inhibitors compared with levodopa as initial treatment for Parkinson's disease (PD MED): a large, open-label, pragmatic randomised trial. *The Lancet* 2014; 384: 1196-205.

Peelaerts W, Bousset L, Van der Perren A, Moskalyuk A, Pulizzi R, Giugliano M, *et al.* alpha-Synuclein strains cause distinct synucleinopathies after local and systemic administration. *Nature* 2015; 522: 340-4.

Perrin RJ, Woods WS, Clayton DF, George JM. Interaction of human alpha-Synuclein and Parkinson's disease variants with phospholipids. Structural analysis using site-directed mutagenesis. *J Biol Chem* 2000; 275: 34393-8.

Peschanski M, Defer G, N'Guyen JP, Ricolfi F, Monfort JC, Remy P, *et al.* Bilateral motor improvement and alteration of L-dopa effect in two patients with Parkinson's disease following intrastriatal transplantation of foetal ventral mesencephalon. *Brain* 1994; 117 (Pt 3): 487-99.

Pezzoli G, Cereda E. Exposure to pesticides or solvents and risk of Parkinson disease. *Neurology* 2013; 80: 2035-41.

Piccini P, Brooks DJ, Björklund A, Gunn RN, Grasby PM, Rimoldi O, *et al.* Dopamine release from nigral transplants visualized in vivo in a Parkinson's patient. *Nat Neurosci* 1999; 2: 1137-40.

Piccini P, Lindvall O, Björklund A, Brundin P, Hagell P, Ceravolo R, *et al.* Delayed recovery of movement-related cortical function in Parkinson's disease after striatal dopaminergic grafts. *Ann Neurol* 2000; 48: 689-95.

Piccini P, Pavese N, Brooks DJ. Endogenous dopamine release after pharmacological challenges in Parkinson's disease. *Ann Neurol* 2003; 53: 647-53.

Piccini P, Pavese N, Hagell P, Reimer J, Bjorklund A, Oertel WH, *et al.* Factors affecting the clinical outcome after neural transplantation in Parkinson's disease. *Brain* 2005; 128: 2977-86.

Picconi B, Hernández LF, Obeso JA, Calabresi P. Motor complications in Parkinson's disease: Striatal molecular and electrophysiological mechanisms of dyskinesias. *Mov Disord* 2018; 33: 867-76.

Pierantozzi M, Palmieri MG, Marciani MG, Bernardi G, Giacomini P, Stanzione P. Effect of apomorphine on cortical inhibition in Parkinson's disease patients: a transcranial magnetic stimulation study. *Exp Brain Res* 2001; 141: 52-62.

Pinborg LH, Videbaek C, Svarer C, Yndgaard S, Paulson OB, Knudsen GM. Quantification of [(123)I]PE2I binding to dopamine transporters with SPET. *Eur J Nucl Med Mol Imaging* 2002; 29: 623-31.

Pirc K, Ulrih NP. alpha-Synuclein interactions with phospholipid model membranes: Key roles for electrostatic interactions and lipid-bilayer structure. *Biochim Biophys Acta* 2015; 1848: 2002-12.

Pirker W. Correlation of dopamine transporter imaging with parkinsonian motor handicap: how close is it? *Mov Disord* 2003; 18 Suppl 7: S43-51.

Pirker W, Djamshidian S, Asenbaum S, Gerschlager W, Tribl G, Hoffmann M, *et al.* Progression of dopaminergic degeneration in Parkinson's disease and atypical parkinsonism: a longitudinal beta-CIT SPECT study. *Mov Disord* 2002; 17: 45-53.

Pirker W, Holler I, Gerschlager W, Asenbaum S, Zettinig G, Brucke T. Measuring the rate of progression of Parkinson's disease over a 5-year period with beta-CIT SPECT. *Mov Disord* 2003; 18: 1266-72.

Plotkin M, Amthauer H, Klaffke S, Kuhn A, Ludemann L, Arnold G, *et al.* Combined 123I-FP-CIT and 123I-IBZM SPECT for the diagnosis of parkinsonian syndromes: study on 72 patients. *J Neural Transm (Vienna)* 2005; 112: 677-92.

Poewe WH, Rascol O, Quinn N, Tolosa E, Oertel WH, Martignoni E, *et al.* Efficacy of pramipexole and transdermal rotigotine in advanced Parkinson's disease: a double-blind, double-dummy, randomised controlled trial. *The Lancet Neurology* 2007; 6: 513-20.

Pogarell O, Koch W, Gildehaus FJ, Kupsch A, Lindvall O, Oertel WH, *et al.* Long-term assessment of striatal dopamine transporters in Parkinsonian patients with intrastriatal embryonic mesencephalic grafts. *Eur J Nucl Med Mol Imaging* 2006; 33: 407-11.

Politis M, Oertel WH, Wu K, Quinn NP, Pogarell O, Brooks DJ, *et al.* Graft-induced dyskinesias in Parkinson's disease: High striatal serotonin/dopamine transporter ratio. *Mov Disord* 2011; 26: 1997-2003.

Politis M, Sauerbier A, Loane C, Pavese N, Martin A, Corcoran B, *et al.* Sustained striatal dopamine levels following intestinal levodopa infusions in Parkinson's disease patients. *Mov Disord* 2017; 32: 235-40.

Politis M, Wu K, Loane C, Brooks DJ, Kiferle L, Turkheimer FE, *et al.* Serotonergic mechanisms responsible for levodopa-induced dyskinesias in Parkinson's disease patients. *J Clin Invest* 2014; 124: 1340-9.

Politis M, Wu K, Loane C, Kiferle L, Molloy S, Brooks DJ, *et al.* Staging of serotonergic dysfunction in Parkinson's disease: an in vivo 11C-DASB PET study. *Neurobiol Dis* 2010a; 40: 216-21.

Politis M, Wu K, Loane C, Quinn NP, Brooks DJ, Oertel WH, *et al.* Serotonin neuron loss and nonmotor symptoms continue in Parkinson's patients treated with dopamine grafts. *Sci Transl Med* 2012; 4: 128ra41.

Politis M, Wu K, Loane C, Quinn NP, Brooks DJ, Rehncrona S, *et al.* Serotonergic neurons mediate dyskinesia side effects in Parkinson's patients with neural transplants. *Sci Transl Med* 2010b; 2: 38ra46.

Polymeropoulos MH, Lavedan C, Leroy E, Ide SE, Dehejia A, Dutra A, *et al.* Mutation in the alpha-synuclein gene identified in families with Parkinson's disease. *Science* 1997; 276: 2045-7.

Ponsen MM, Stoffers D, Twisk JW, Wolters E, Berendse HW. Hyposmia and executive dysfunction as predictors of future Parkinson's disease: a prospective study. *Mov Disord* 2009; 24: 1060-5.

Postuma RB, Aarsland D, Barone P, Burn DJ, Hawkes CH, Oertel W, *et al.* Identifying prodromal Parkinson's disease: pre-motor disorders in Parkinson's disease. *Mov Disord* 2012a; 27: 617-26.

Postuma RB, Berg D. Advances in markers of prodromal Parkinson disease. *Nat Rev Neurol* 2016; 12: 622-34.

Postuma RB, Berg D, Stern M, Poewe W, Olanow CW, Oertel W, *et al.* MDS clinical diagnostic criteria for Parkinson's disease. *Mov Disord* 2015a; 30: 1591-9.

Postuma RB, Gagnon JF, Bertrand JA, Génier Marchand D, Montplaisir JY. Parkinson risk in idiopathic REM sleep behavior disorder: preparing for neuroprotective trials. *Neurology* 2015b; 84: 1104-13.

Postuma RB, Iranzo A, Hogl B, Arnulf I, Ferini-Strambi L, Manni R, *et al.* Risk factors for neurodegeneration in idiopathic rapid eye movement sleep behavior disorder: a multicenter study. *Ann Neurol* 2015c; 77: 830-9.

Postuma RB, Lang AE, Gagnon JF, Pelletier A, Montplaisir JY. How does parkinsonism start? Prodromal parkinsonism motor changes in idiopathic REM sleep behaviour disorder. *Brain* 2012b; 135: 1860-70.

Poulopoulos M, Levy OA, Alcalay RN. The neuropathology of genetic Parkinson's disease. *Mov Disord* 2012; 27: 831-42.

Pringsheim T, Jette N, Frolkis A, Steeves TD. The prevalence of Parkinson's disease: a systematic review and meta-analysis. *Mov Disord* 2014; 29: 1583-90.

Prunier C, Payoux P, Guilloteau D, Chalon S, Giraudeau B, Majorel C, *et al.* Quantification of dopamine transporter by 123I-PE2I SPECT and the noninvasive Logan graphical method in Parkinson's disease. *J Nucl Med* 2003; 44: 663-70.

Qamhawi Z, Towey D, Shah B, Pagano G, Seibyl J, Marek K, *et al.* Clinical correlates of raphe serotonergic dysfunction in early Parkinson's disease. *Brain* 2015; 138: 2964-73.

R Core Team. R: A language and environment for statistical computing. Vienna, Austria. 2019. Available from: https://www.R-project.org/.

Rahman MK, Nagatsu T, Nagatsu I, Iizuka R, Narabayashi H. Aromatic L-amino acid decarboxylase activity in brains from normal human subjects and from patients with extrapyramidal diseases. *Biomedical Research* 1981; 2: 560-6.

Rahman S, Griffin HJ, Quinn NP, Jahanshahi M. On the nature of fear of falling in Parkinson's disease. *Behav Neurol* 2011; 24: 219-28.

Rajput AH, Sitte HH, Rajput A, Fenton ME, Pifl C, Hornykiewicz O. Globus pallidus dopamine and Parkinson motor subtypes: clinical and brain biochemical correlation. *Neurology* 2008; 70: 1403-10.

Rakshi JS, Pavese N, Uema T, Ito K, Morrish PK, Bailey DL, *et al.* A comparison of the progression of early Parkinson's disease in patients started on ropinirole or L-dopa: an 18F-dopa PET study. *J Neural Transm (Vienna)* 2002; 109: 1433-43.

Rakshi JS, Uema T, Ito K, Bailey DL, Morrish PK, Ashburner J, *et al.* Frontal, midbrain and striatal dopaminergic function in early and advanced Parkinson's disease A 3D [(18)F]dopa-PET study. *Brain* 1999; 122 (Pt 9): 1637-50.

Ranjan P, Kumar A. Perturbation in Long-Range Contacts Modulates the Kinetics of Amyloid Formation in alpha-Synuclein Familial Mutants. *ACS Chem Neurosci* 2017; 8: 2235-46.

Rascol O, Brooks DJ, Korczyn AD, De Deyn PP, Clarke CE, Lang AE. A Five-Year Study of the Incidence of Dyskinesia in Patients with Early Parkinson's Disease Who Were Treated with Ropinirole or Levodopa. 2000; 342: 1484-91.

Rascol O, Brooks DJ, Korczyn AD, De Deyn PP, Clarke CE, Lang AE, *et al.* Development of dyskinesias in a 5-year trial of ropinirole and L-dopa. *Mov Disord* 2006; 21: 1844-50.

Rascol O, Brooks DJ, Melamed E, Oertel W, Poewe W, Stocchi F, *et al.* Rasagiline as an adjunct to levodopa in patients with Parkinson's disease and motor fluctuations (LARGO, Lasting effect in Adjunct therapy with Rasagiline Given Once daily, study): a randomised, double-blind, parallel-group trial. *The Lancet* 2005; 365: 947-54.

Rascol O, Payoux P, Ory F, Ferreira JJ, Brefel-Courbon C, Montastruc JL. Limitations of current Parkinson's disease therapy. *Ann Neurol* 2003; 53 Suppl 3: S3-12; discussion S-5.

Rcom-H'cheo-Gauthier AN, Davis A, Meedeniya ACB, Pountney DL. Alpha-synuclein aggregates are excluded from calbindin-D28k-positive neurons in dementia with Lewy bodies and a unilateral rotenone mouse model. *Mol Cell Neurosci* 2016; 77: 65-75.

Recasens A, Dehay B. Alpha-synuclein spreading in Parkinson's disease. *Front Neuroanat* 2014; 8: 159.

Regan T, Gill AC, Clohisey SM, Barnett MW, Pariante CM, Harrison NA, *et al.* Effects of anti-inflammatory drugs on the expression of tryptophan-metabolism genes by human macrophages. *J Leukoc Biol* 2018; 103: 681-92.

Reijnders JS, Ehrt U, Weber WE, Aarsland D, Leentjens AF. A systematic review of prevalence studies of depression in Parkinson's disease. *Mov Disord* 2008; 23: 183-9; quiz 313.

Reisinger SN, Wanek T, Langer O, Pollak DD. PET imaging of the mouse brain reveals a dynamic regulation of SERT density in a chronic stress model. *Translational psychiatry* 2019; 9: 80.

Remy P, Samson Y, Hantraye P, Fontaine A, Defer G, Mangin JF, *et al.* Clinical correlates of [18F]fluorodopa uptake in five grafted parkinsonian patients. *Ann Neurol* 1995; 38: 580-8.

Revelle W. psych: Procedures for Personality and Psychological Research. 2019. Available from: https://CRAN.R-project.org/package=psych.

Ribeiro MJ, Vidailhet M, Loc'h C, Dupel C, Nguyen JP, Ponchant M, *et al.* Dopaminergic function and dopamine transporter binding assessed with positron emission tomography in Parkinson disease. *Arch Neurol* 2002; 59: 580-6.

Richardson RM, Freed CR, Shimamoto SA, Starr PA. Pallidal neuronal discharge in Parkinson's disease following intraputamenal fetal mesencephalic allograft. *J Neurol Neurosurg Psychiatry* 2011; 82: 266-71.

Rinne JO, Laihinen A, Någren K, Bergman J, Solin O, Haaparanta M, *et al.* PET demonstrates different behaviour of striatal dopamine D-1 and D-2 receptors in early Parkinson's disease. *J Neurosci Res* 1990; 27: 494-9.

Rinne JO, Laihinen A, Ruottinen H, Ruotsalainen U, Någren K, Lehikoinen P, *et al.* Increased density of dopamine D2 receptors in the putamen, but not in the caudate nucleus in early Parkinson's disease: a PET study with [11C]raclopride. *J Neurol Sci* 1995; 132: 156-61.

Rinne JO, Rummukainen J, Paljärvi L, Rinne UK. Dementia in Parkinson's disease is related to neuronal loss in the medial substantia nigra. *Ann Neurol* 1989; 26: 47-50.

Rinne JO, Ruottinen H, Bergman J, Haaparanta M, Sonninen P, Solin O. Usefulness of a dopamine transporter PET ligand [(18)F]beta-CFT in assessing disability in Parkinson's disease. *J Neurol Neurosurg Psychiatry* 1999; 67: 737-41.

Rinne UK, Bracco F, Chouza C, Dupont E, Gershanik O, Marti Masso JF, *et al.* Early treatment of Parkinson's disease with cabergoline delays the onset of motor complications. Results of a double-blind levodopa controlled trial. The PKDS009 Study Group. *Drugs* 1998; 55 Suppl 1: 23-30.

Rizzo G, Copetti M, Arcuti S, Martino D, Fontana A, Logroscino G. Accuracy of clinical diagnosis of Parkinson disease: A systematic review and meta-analysis. *Neurology* 2016; 86: 566-76.

Roberts RF, Wade-Martins R, Alegre-Abarrategui J. Direct visualization of alpha-synuclein oligomers reveals previously undetected pathology in Parkinson's disease brain. *Brain* 2015; 138: 1642-57.

Rocha MSG, Bassetti EM, Oliveira MO, Kuark RGB, Estevam NM, Brucki SMD. Addenbrooke's Cognitive Examination-Revised is accurate for detecting dementia in Parkinson's disease patients with low educational level. *Dementia & neuropsychologia* 2014; 8: 20-5.

Rodriguez-Oroz MC, Jahanshahi M, Krack P, Litvan I, Macias R, Bezard E, *et al.* Initial clinical manifestations of Parkinson's disease: features and pathophysiological mechanisms. *The Lancet Neurology* 2009; 8: 1128-39.

Rosenblum S, Samuel M, Zlotnik S, Erikh I, Schlesinger I. Handwriting as an objective tool for Parkinson's disease diagnosis. *J Neurol* 2013; 260: 2357-61.

Ross BD, Hoang TQ, Blüml S, Dubowitz D, Kopyov OV, Jacques DB, *et al.* In vivo magnetic resonance spectroscopy of human fetal neural transplants. *NMR Biomed* 1999; 12: 221-36.

Ross GW, Petrovitch H, Abbott RD, Tanner CM, Popper J, Masaki K, *et al.* Association of olfactory dysfunction with risk for future Parkinson's disease. *Ann Neurol* 2008; 63: 167-73.

Rossi A, Berger K, Chen H, Leslie D, Mailman RB, Huang X. Projection of the prevalence of Parkinson's disease in the coming decades: Revisited. *Mov Disord* 2018; 33: 156-9.

Rossi C, Frosini D, Volterrani D, De Feo P, Unti E, Nicoletti V, *et al.* Differences in nigro-striatal impairment in clinical variants of early Parkinson's disease: evidence from a FP-CIT SPECT study. *Eur J Neurol* 2010; 17: 626-30.

Roussakis AA, Politis M, Towey D, Piccini P. Serotonin-to-dopamine transporter ratios in Parkinson disease: Relevance for dyskinesias. *Neurology* 2016; 86: 1152-8.

Rudow G, O'Brien R, Savonenko AV, Resnick SM, Zonderman AB, Pletnikova O, *et al.* Morphometry of the human substantia nigra in ageing and Parkinson's disease. *Acta Neuropathol* 2008; 115: 461-70.

Ruzicka E, Krupicka R, Zarubova K, Rusz J, Jech R, Szabo Z. Tests of manual dexterity and speed in Parkinson's disease: Not all measure the same. *Parkinsonism Relat Disord* 2016; 28: 118-23.

Sakamoto M, Uchihara T, Hayashi M, Nakamura A, Kikuchi E, Mizutani T, *et al.* Heterogeneity of nigral and cortical Lewy bodies differentiated by amplified triple-labeling for alpha-synuclein, ubiquitin, and thiazin red. *Exp Neurol* 2002; 177: 88-94.

Santaniello S, McCarthy MM, Montgomery EB, Jr., Gale JT, Kopell N, Sarma SV. Therapeutic mechanisms of high-frequency stimulation in Parkinson's disease and neural restoration via loop-based reinforcement. *Proc Natl Acad Sci U S A* 2015; 112: E586-95.

Sasaki T, Ito H, Kimura Y, Arakawa R, Takano H, Seki C, *et al.* Quantification of Dopamine Transporter in Human Brain Using PET with F-18-FE-PE2I. *J Nucl Med* 2012; 53: 1065-73.

Savica R, Grossardt BR, Bower JH, Ahlskog JE, Rocca WA. Time Trends in the Incidence of Parkinson Disease. *JAMA neurology* 2016; 73: 981-9.

Sawada H, Oeda T, Kuno S, Nomoto M, Yamamoto K, Yamamoto M, *et al.* Amantadine for dyskinesias in Parkinson's disease: a randomized controlled trial. *PLoS One* 2010; 5: e15298.

Sawle GV, Bloomfield PM, Björklund A, Brooks DJ, Brundin P, Leenders KL, *et al.* Transplantation of fetal dopamine neurons in Parkinson's disease: PET [18F]6-L-fluorodopa studies in two patients with putaminal implants. *Ann Neurol* 1992; 31: 166-73.

Sawle GV, Playford ED, Brooks DJ, Quinn N, Frackowiak RS. Asymmetrical pre-synaptic and post-synpatic changes in the striatal dopamine projection in dopa naïve parkinsonism. Diagnostic implications of the D2 receptor status. *Brain* 1993; 116 (Pt 4): 853-67.

Schenck CH, Boeve BF, Mahowald MW. Delayed emergence of a parkinsonian disorder or dementia in 81% of older men initially diagnosed with idiopathic rapid eye movement sleep behavior disorder: a 16-year update on a previously reported series. *Sleep Med* 2013; 14: 744-8.

Scherman D, Desnos C, Darchen F, Pollak P, Javoy-Agid F, Agid Y. Striatal dopamine deficiency in Parkinson's disease: role of aging. *Ann Neurol* 1989; 26: 551-7.

Schillaci O, Chiaravalloti A, Pierantozzi M, Di Pietro B, Koch G, Bruni C, *et al.* Different patterns of nigrostriatal degeneration in tremor type versus the akinetic-rigid and mixed types of Parkinson's disease at the early stages: molecular imaging with 123I-FP-CIT SPECT. *Int J Mol Med* 2011; 28: 881-6.

Schrag A, Horsfall L, Walters K, Noyce A, Petersen I. Prediagnostic presentations of Parkinson's disease in primary care: a case-control study. *The Lancet Neurology* 2015; 14: 57-64.

Schrag A, Sheikh S, Quinn NP, Lees AJ, Selai C, Mathias C, *et al.* A comparison of depression, anxiety, and health status in patients with progressive supranuclear palsy and multiple system atrophy. *Mov Disord* 2010; 25: 1077-81.

Schuepbach WM, Rau J, Knudsen K, Volkmann J, Krack P, Timmermann L, *et al.* Neurostimulation for Parkinson's disease with early motor complications. *N Engl J Med* 2013; 368: 610-22.

Schuepbach WMM, Tonder L, Schnitzler A, Krack P, Rau J, Hartmann A, *et al.* Quality of life predicts outcome of deep brain stimulation in early Parkinson disease. *Neurology* 2019; 92: e1109-e20.

Schulz-Schaeffer WJ. Is Cell Death Primary or Secondary in the Pathophysiology of Idiopathic Parkinson's Disease? *Biomolecules* 2015; 5: 1467-79.

Schwarz J, Storch A, Koch W, Pogarell O, Radau PE, Tatsch K. Loss of dopamine transporter binding in Parkinson's disease follows a single exponential rather than linear decline. *J Nucl Med* 2004; 45: 1694-7.

Schwarz ST, Afzal M, Morgan PS, Bajaj N, Gowland PA, Auer DP. The 'swallow tail' appearance of the healthy nigrosome - a new accurate test of Parkinson's disease: a case-control and retrospective cross-sectional MRI study at 3T. *PLoS One* 2014; 9: e93814.

Schwarz ST, Mougin O, Xing Y, Blazejewska A, Bajaj N, Auer DP, *et al.* Parkinson's disease related signal change in the nigrosomes 1-5 and the substantia nigra using T2* weighted 7T MRI. *NeuroImage Clinical* 2018; 19: 683-9.

Scott D, Roy S. alpha-Synuclein inhibits intersynaptic vesicle mobility and maintains recycling-pool homeostasis. *J Neurosci* 2012; 32: 10129-35.

Scott NW, Macleod AD, Counsell CE. Motor complications in an incident Parkinson's disease cohort. *Eur J Neurol* 2016; 23: 304-12.

Segura-Aguilar J. On the Role of Aminochrome in Mitochondrial Dysfunction and Endoplasmic Reticulum Stress in Parkinson's Disease. *Front Neurosci* 2019; 13: 271.

Seibyl JP, Marek KL, Quinlan D, Sheff K, Zoghbi S, Zea-Ponce Y, *et al.* Decreased single-photon emission computed tomographic [123I]beta-CIT striatal uptake correlates with symptom severity in Parkinson's disease. *Ann Neurol* 1995; 38: 589-98.

Seki C, Ito H, Ichimiya T, Arakawa R, Ikoma Y, Shidahara M, *et al.* Quantitative analysis of dopamine transporters in human brain using [11C]PE2I and positron emission tomography: evaluation of reference tissue models. *Ann Nucl Med* 2010; 24: 249-60.

Seppi K, Schocke MF, Donnemiller E, Esterhammer R, Kremser C, Scherfler C, *et al.* Comparison of diffusion-weighted imaging and [123I]IBZM-SPECT for the differentiation of patients with the Parkinson variant of multiple system atrophy from those with Parkinson's disease. *Mov Disord* 2004; 19: 1438-45.

Serpell LC, Berriman J, Jakes R, Goedert M, Crowther RA. Fiber diffraction of synthetic alpha-synuclein filaments shows amyloid-like cross-beta conformation. *Proc Natl Acad Sci U S A* 2000; 97: 4897-902.

Sethi K. Levodopa unresponsive symptoms in Parkinson disease. *Mov Disord* 2008; 23 Suppl 3: S521-33.

Shahmoradian SH, Lewis AJ, Genoud C, Hench J, Moors TE, Navarro PP, *et al.* Lewy pathology in Parkinson's disease consists of crowded organelles and lipid membranes. *Nat Neurosci* 2019; 22: 1099-109.

Shen CC, Tsai SJ, Perng CL, Kuo BI, Yang AC. Risk of Parkinson disease after depression: a nationwide population-based study. *Neurology* 2013; 81: 1538-44.

Shen X, Wong-Yu IS, Mak MK. Effects of Exercise on Falls, Balance, and Gait Ability in Parkinson's Disease: A Meta-analysis. *Neurorehabil Neural Repair* 2016; 30: 512-27.

Shin E, Garcia J, Winkler C, Bjorklund A, Carta M. Serotonergic and dopaminergic mechanisms in graft-induced dyskinesia in a rat model of Parkinson's disease. *Neurobiol Dis* 2012; 47: 393-406.

Shingai Y, Tateno A, Arakawa R, Sakayori T, Kim W, Suzuki H, *et al.* Age-related decline in dopamine transporter in human brain using PET with a new radioligand [(1)(8)F]FE-PE2I. *Ann Nucl Med* 2014; 28: 220-6.

Shinotoh H, Inoue O, Hirayama K, Aotsuka A, Asahina M, Suhara T, *et al.* Dopamine D1 receptors in Parkinson's disease and striatonigral degeneration: a positron emission tomography study. *J Neurol Neurosurg Psychiatry* 1993; 56: 467-72.

Siderowf A, Jennings D, Eberly S, Oakes D, Hawkins KA, Ascherio A, *et al.* Impaired olfaction and other prodromal features in the Parkinson At-Risk Syndrome Study. *Mov Disord* 2012; 27: 406-12.

Simonet C, Schrag A, Lees AJ, Noyce AJ. The motor prodromes of parkinson's disease: from bedside observation to large-scale application. *J Neurol* 2019.

Simuni T, Siderowf A, Lasch S, Coffey CS, Caspell-Garcia C, Jennings D, *et al.* Longitudinal Change of Clinical and Biological Measures in Early Parkinson's Disease: Parkinson's Progression Markers Initiative Cohort. *Mov Disord* 2018; 33: 771-82.

Singleton AB, Farrer M, Johnson J, Singleton A, Hague S, Kachergus J, *et al.* alpha-Synuclein locus triplication causes Parkinson's disease. *Science* 2003; 302: 841.

Singmann H, Bolker B, Westfall J, Aust F. afex: Analysis of Factorial Experiments. R package version 0.18-0. 2017. Available from: https://CRAN.R-project.org/package=afex.

Sixel-Döring F, Trautmann E, Mollenhauer B, Trenkwalder C. Associated factors for REM sleep behavior disorder in Parkinson disease. *Neurology* 2011; 77: 1048-54.

Skamris T, Marasini C, Madsen KL, Fodera V, Vestergaard B. Early Stage Alpha-Synuclein Amyloid Fibrils are Reservoirs of Membrane-Binding Species. *Sci Rep* 2019; 9: 1733.

Slotkin TA, McCook EC, Ritchie JC, Carroll BJ, Seidler FJ. Serotonin transporter expression in rat brain regions and blood platelets: aging and glucocorticoid effects. *Biol Psychiatry* 1997; 41: 172-83.

Smith R, Wu K, Hart T, Loane C, Brooks DJ, Bjorklund A, *et al.* The role of pallidal serotonergic function in Parkinson's disease dyskinesias: a positron emission tomography study. *Neurobiol Aging* 2015; 36: 1736-42.

Snow BJ, Tooyama I, McGeer EG, Yamada T, Calne DB, Takahashi H, *et al.* Human positron emission tomographic [18F]fluorodopa studies correlate with dopamine cell counts and levels. *Ann Neurol* 1993; 34: 324-30.

Soderstrom KE, Meredith G, Freeman TB, McGuire SO, Collier TJ, Sortwell CE, *et al.* The synaptic impact of the host immune response in a parkinsonian allograft rat model: Influence on graft-derived aberrant behaviors. *Neurobiol Dis* 2008; 32: 229-42.

Sofic E, Riederer P, Heinsen H, Beckmann H, Reynolds GP, Hebenstreit G, *et al.* Increased iron (III) and total iron content in post mortem substantia nigra of parkinsonian brain. *J Neural Transm* 1988; 74: 199-205.

Solodkin A, Hlustik P, Noll DC, Small SL. Lateralization of motor circuits and handedness during finger movements. *Eur J Neurol* 2001; 8: 425-34.

Spencer DD, Robbins RJ, Naftolin F, Marek KL, Vollmer T, Leranth C, *et al.* Unilateral transplantation of human fetal mesencephalic tissue into the caudate nucleus of patients with Parkinson's disease. *N Engl J Med* 1992; 327: 1541-8.

Spiegel J, Hellwig D, Samnick S, Jost W, Mollers MO, Fassbender K, *et al.* Striatal FP-CIT uptake differs in the subtypes of early Parkinson's disease. *J Neural Transm (Vienna)* 2007; 114: 331-5.

Spiegel J, Mollers MO, Jost WH, Fuss G, Samnick S, Dillmann U, *et al.* FP-CIT and MIBG scintigraphy in early Parkinson's disease. *Mov Disord* 2005; 20: 552-61.

Spillantini MG, Crowther RA, Jakes R, Hasegawa M, Goedert M. alpha-Synuclein in filamentous inclusions of Lewy bodies from Parkinson's disease and dementia with lewy bodies. *Proc Natl Acad Sci U S A* 1998; 95: 6469-73.

Spillantini MG, Schmidt ML, Lee VMY, Trojanowski JQ, Jakes R, Goedert M. α-Synuclein in Lewy bodies. *Nature* 1997; 388: 839-40.

St George RJ, Nutt JG, Burchiel KJ, Horak FB. A meta-regression of the long-term effects of deep brain stimulation on balance and gait in PD. *Neurology* 2010; 75: 1292-9.

Staffen W, Mair A, Unterrainer J, Trinka E, Ladurner G. Measuring the progression of idiopathic Parkinson's disease with [123I] beta-CIT SPECT. *J Neural Transm (Vienna)* 2000; 107: 543-52.

Steece-Collier K, Soderstrom KE, Collier TJ, Sortwell CE, Maries-Lad E. Effect of levodopa priming on dopamine neuron transplant efficacy and induction of abnormal involuntary movements in parkinsonian rats. *J Comp Neurol* 2009; 515: 15-30.

Stephens AD, Zacharopoulou M, Kaminski Schierle GS. The Cellular Environment Affects Monomeric alpha-Synuclein Structure. *Trends Biochem Sci* 2019; 44: 453-66.

Stocchi F, Hsu A, Khanna S, Ellenbogen A, Mahler A, Liang G, *et al.* Comparison of IPX066 with carbidopa-levodopa plus entacapone in advanced PD patients. *Parkinsonism Relat Disord* 2014; 20: 1335-40.

Stocchi F, Rascol O, Kieburtz K, Poewe W, Jankovic J, Tolosa E, *et al.* Initiating levodopa/carbidopa therapy with and without entacapone in early Parkinson disease: the STRIDE-PD study. *Ann Neurol* 2010; 68: 18-27.

Stocchi F, Vacca L, Ruggieri S, Olanow CW. Intermittent vs continuous levodopa administration in patients with advanced Parkinson disease: a clinical and pharmacokinetic study. *Arch Neurol* 2005; 62: 905-10.

Stowe R, Ives N, Clarke CE, Deane K, van H, Wheatley K, *et al.* Evaluation of the efficacy and safety of adjuvant treatment to levodopa therapy in Parkinson s disease patients with motor complications. *Cochrane Database Syst Rev* 2010: CD007166.

Strafella AP, Sadikot AF, Dagher A. Subthalamic deep brain stimulation does not induce striatal dopamine release in Parkinson's disease. *Neuroreport* 2003; 14: 1287-9.

Strecker K, Wegner F, Hesse S, Becker GA, Patt M, Meyer PM, *et al.* Preserved serotonin transporter binding in de novo Parkinson's disease: negative correlation with the dopamine transporter. *J Neurol* 2011; 258: 19-26.

Stromberg I, Kehr J, Andbjer B, Fuxe K. Fetal ventral mesencephalic grafts functionally reduce the dopamine D2 receptor supersensitivity in partially dopamine reinnervated host striatum. *Exp Neurol* 2000; 164: 154-65.

Sulzer D. Multiple hit hypotheses for dopamine neuron loss in Parkinson's disease. *Trends Neurosci* 2007; 30: 244-50.

Sulzer D, Bogulavsky J, Larsen KE, Behr G, Karatekin E, Kleinman MH, *et al.* Neuromelanin biosynthesis is driven by excess cytosolic catecholamines not accumulated by synaptic vesicles. *Proc Natl Acad Sci U S A* 2000; 97: 11869-74.

Sulzer D, Zecca L. Intraneuronal dopamine-quinone synthesis: a review. *Neurotox Res* 2000; 1: 181-95.

Sung C, Lee JH, Oh JS, Oh M, Lee SJ, Oh SJ, *et al.* Longitudinal Decline of Striatal Subregional [(18)F]FP-CIT Uptake in Parkinson's Disease. *Nucl Med Mol Imaging* 2017; 51: 304-13.

Surmeier DJ, Ding J, Day M, Wang Z, Shen W. D1 and D2 dopamine-receptor modulation of striatal glutamatergic signaling in striatal medium spiny neurons. *Trends Neurosci* 2007; 30: 228-35.

Surmeier DJ, Obeso JA, Halliday GM. Parkinson's Disease Is Not Simply a Prion Disorder. *J Neurosci* 2017a; 37: 9799-807.

Surmeier DJ, Schumacker PT, Guzman JD, Ilijic E, Yang B, Zampese E. Calcium and Parkinson's disease. *Biochem Biophys Res Commun* 2017b; 483: 1013-9.

Szabo J. Organization of the ascending striatal afferents in monkeys. *J Comp Neurol* 1980; 189: 307-21.

Szabo Z, McCann UD, Wilson AA, Scheffel U, Owonikoko T, Mathews WB, *et al.* Comparison of (+)-C-11-McN5652 and C-11-DASB as serotonin transporter radioligands under various experimental conditions. *J Nucl Med* 2002; 43: 678-92.

Tagliaferro P, Burke RE. Retrograde Axonal Degeneration in Parkinson Disease. *J Parkinsons Dis* 2016; 6: 1-15.

Tanaka M, Kim YM, Lee G, Junn E, Iwatsubo T, Mouradian MM. Aggresomes formed by alpha-synuclein and synphilin-1 are cytoprotective. *J Biol Chem* 2004; 279: 4625-31.

Tanner CM, Goldman SM. Epidemiology of Parkinson's disease. *Neurol Clin* 1996; 14: 317-35.

Tarutani A, Suzuki G, Shimozawa A, Nonaka T, Akiyama H, Hisanaga S, *et al.* The Effect of Fragmented Pathogenic alpha-Synuclein Seeds on Prion-like Propagation. *J Biol Chem* 2016; 291: 18675-88.

Tedroff J, Ekesbo A, Rydin E, Långström B, Hagberg G. Regulation of dopaminergic activity in early Parkinson's disease. *Ann Neurol* 1999; 46: 359-65.

Tedroff J, Pedersen M, Aquilonius SM, Hartvig P, Jacobsson G, Långström B. Levodopa-induced changes in synaptic dopamine in patients with Parkinson's disease as measured by [11C]raclopride displacement and PET. *Neurology* 1996; 46: 1430-6.

Thenganatt MA, Jankovic J. Parkinson disease subtypes. *JAMA neurology* 2014; 71: 499-504.

Thobois S, Fraix V, Savasta M, Costes N, Pollak P, Mertens P, *et al.* Chronic subthalamic nucleus stimulation and striatal D2 dopamine receptors in Parkinson's disease--A [(11)C]-raclopride PET study. *J Neurol* 2003; 250: 1219-23.

Tinazzi M, Gandolfi M, Ceravolo R, Capecci M, Andrenelli E, Ceravolo MG, *et al.* Postural Abnormalities in Parkinson's Disease: An Epidemiological and Clinical Multicenter Study. *Mov Disord Clin Pract* 2019; 6: 576-85.

Tomlinson CL, Stowe R, Patel S, Rick C, Gray R, Clarke CE. Systematic review of levodopa dose equivalency reporting in Parkinson's disease. *Mov Disord* 2010; 25: 2649-53.

Tompkins MM, Hill WD. Contribution of somal Lewy bodies to neuronal death. *Brain Res* 1997; 775: 24-9.

Tritsch NX, Sabatini BL. Dopaminergic modulation of synaptic transmission in cortex and striatum. *Neuron* 2012; 76: 33-50.

Turjanski N, Lees AJ, Brooks DJ. In vivo studies on striatal dopamine D1 and D2 site binding in L-dopa-treated Parkinson's disease patients with and without dyskinesias. *Neurology* 1997; 49: 717-23.

Turkheimer FE, Selvaraj S, Hinz R, Murthy V, Bhagwagar Z, Grasby P, *et al.* Quantification of ligand PET studies using a reference region with a displaceable fraction: application to occupancy studies with [(11)C]-DASB as an example. *J Cereb Blood Flow Metab* 2012; 32: 70-80.

Turkheimer FE, Veronese M, Dunn J. Experimental design and practical data analysis in positron emission tomography. 1st ed. London: CreateSpace Independent Publishing Platform; 2014.

Tuttle MD, Comellas G, Nieuwkoop AJ, Covell DJ, Berthold DA, Kloepper KD, *et al.* Solid-state NMR structure of a pathogenic fibril of full-length human alpha-synuclein. *Nat Struct Mol Biol* 2016; 23: 409-15.

Tziortzi AC, Haber SN, Searle GE, Tsoumpas C, Long CJ, Shotbolt P, *et al.* Connectivity-based functional analysis of dopamine release in the striatum using diffusion-weighted MRI and positron emission tomography. *Cereb Cortex* 2014; 24: 1165-77.

Tziortzi AC, Searle GE, Tzimopoulou S, Salinas C, Beaver JD, Jenkinson M, *et al.* Imaging dopamine receptors in humans with [11C]-(+)-PHNO: dissection of D3 signal and anatomy. *Neuroimage* 2011; 54: 264-77.

Ugrumov MV. Non-dopaminergic neurons partly expressing dopaminergic phenotype: distribution in the brain, development and functional significance. *J Chem Neuroanat* 2009; 38: 241-56.

Ulla M, Bonny JM, Ouchchane L, Rieu I, Claise B, Durif F. Is R2* a new MRI biomarker for the progression of Parkinson's disease? A longitudinal follow-up. *PLoS One* 2013; 8: e57904.

Usman S, Patil A. Radiation detector deadtime and pile up: A review of the status of science. *Nucl Eng Technol* 2018; 50: 1006-16.

Vaghi MM, Vertes PE, Kitzbichler MG, Apergis-Schoute AM, van der Flier FE, Fineberg NA, *et al.* Specific Frontostriatal Circuits for Impaired Cognitive Flexibility and Goal-Directed Planning in Obsessive-Compulsive Disorder: Evidence From Resting-State Functional Connectivity. *Biol Psychiatry* 2017; 81: 708-17.

Van Den Eeden SK, Tanner CM, Bernstein AL, Fross RD, Leimpeter A, Bloch DA, *et al.* Incidence of Parkinson's disease: variation by age, gender, and race/ethnicity. *Am J Epidemiol* 2003; 157: 1015-22.

Van Laere K, Clerinx K, D'Hondt E, de Groot T, Vandenberghe W. Combined striatal binding and cerebral influx analysis of dynamic 11C-raclopride PET improves early differentiation between multiple-system atrophy and Parkinson disease. *J Nucl Med* 2010; 51: 588-95.

van Nuland AJM, den Ouden HEM, Zach H, Dirkx MFM, van Asten JJA, Scheenen TWJ, *et al.* GABAergic changes in the thalamocortical circuit in Parkinson's disease. *Hum Brain Mapp* 2020; 41: 1017-29.

Venables WN, Ripley BD. Modern Applied Statistics with S. Fourth Edition. 2002. Available from: http://www.stats.ox.ac.uk/pub/MASS4.

Verel I, Visser GW, van Dongen GA. The promise of immuno-PET in radioimmunotherapy. *J Nucl Med* 2005; 46 Suppl 1: 164S-71S.

Verhagen Metman L, Del Dotto P, van den Munckhof P, Fang J, Mouradian MM, Chase TN. Amantadine as treatment for dyskinesias and motor fluctuations in Parkinson's disease. *Neurology* 1998; 50: 1323-6.

Verschuur CVM, Suwijn SR, Boel JA, Post B, Bloem BR, van Hilten JJ, *et al.* Randomized Delayed-Start Trial of Levodopa in Parkinson's Disease. *N Engl J Med* 2019; 380: 315-24.

Verstappen CC, Bloem BR, Haaxma CA, Oyen WJ, Horstink MW. Diagnostic value of asymmetric striatal D2 receptor upregulation in Parkinson's disease: an [123I]IBZM and [123I]FP-CIT SPECT study. *Eur J Nucl Med Mol Imaging* 2007; 34: 502-7.

Vingerhoets FJG, Schulzer M, Caine DB, Snow BJ. Which clinical sign of Parkinson's disease best reflects the nigrostriatal lesion? *Ann Neurol* 1997; 41: 58-64.

Visanji NP, Brooks PL, Hazrati LN, Lang AE. The prion hypothesis in Parkinson's disease: Braak to the future. *Acta neuropathologica communications* 2013; 1: 2.

Volpicelli-Daley LA, Luk KC, Patel TP, Tanik SA, Riddle DM, Stieber A, *et al.* Exogenous alpha-synuclein fibrils induce Lewy body pathology leading to synaptic dysfunction and neuron death. *Neuron* 2011; 72: 57-71.

Voon V, Napier TC, Frank MJ, Sgambato-Faure V, Grace AA, Rodriguez-Oroz M, *et al.* Impulse control disorders and levodopa-induced dyskinesias in Parkinson's disease: an update. *The Lancet Neurology* 2017; 16: 238-50.

Voorn P, Vanderschuren LJ, Groenewegen HJ, Robbins TW, Pennartz CM. Putting a spin on the dorsal-ventral divide of the striatum. *Trends Neurosci* 2004; 27: 468-74.

Vuong QH. Likelihood Ratio Tests for Model Selection and Non-Nested Hypotheses. *Econometrica* 1989; 57: 307-33.

Wakabayashi K, Hayashi S, Kakita A, Yamada M, Toyoshima Y, Yoshimoto M, *et al.* Accumulation of alpha-synuclein/NACP is a cytopathological feature common to Lewy body disease and multiple system atrophy. *Acta Neuropathol* 1998; 96: 445-52.

Wakabayashi K, Tanji K, Mori F, Takahashi H. The Lewy body in Parkinson's disease: molecules implicated in the formation and degradation of alpha-synuclein aggregates. *Neuropathology* 2007; 27: 494-506.

Wakabayashi K, Tanji K, Odagiri S, Miki Y, Mori F, Takahashi H. The Lewy body in Parkinson's disease and related neurodegenerative disorders. *Mol Neurobiol* 2013; 47: 495-508.

Wang J, Zuo CT, Jiang YP, Guan YH, Chen ZP, Xiang JD, *et al.* 18F-FP-CIT PET imaging and SPM analysis of dopamine transporters in Parkinson's disease in various Hoehn & Yahr stages. *J Neurol* 2007; 254: 185-90.

Wang JY, Zhuang QQ, Zhu LB, Zhu H, Li T, Li R, *et al.* Meta-analysis of brain iron levels of Parkinson's disease patients determined by postmortem and MRI measurements. *Sci Rep* 2016; 6: 36669.

Wang L, Das U, Scott DA, Tang Y, McLean PJ, Roy S. alpha-synuclein multimers cluster synaptic vesicles and attenuate recycling. *Curr Biol* 2014; 24: 2319-26.

Wang L, Wang M, Si Q, Yuan Y, Ma K, Gan C, *et al.* Altered brain structural topological properties in Parkinson's disease with levodopa-induced dyskinesias. *Parkinsonism Relat Disord* 2019; 67: 36-41.

Wanneveich M, Moisan F, Jacqmin-Gadda H, Elbaz A, Joly P. Projections of prevalence, lifetime risk, and life expectancy of Parkinson's disease (2010-2030) in France. *Mov Disord* 2018; 33: 1449-55.

Weaver FM, Follett K, Stern M, Hur K, Harris C, Marks WJ, Jr., *et al.* Bilateral deep brain stimulation vs best medical therapy for patients with advanced Parkinson disease: a randomized controlled trial. *JAMA* 2009; 301: 63-73.

Weintraub D, Nirenberg MJ. Impulse control and related disorders in Parkinson's disease. *Neurodegener Dis* 2013; 11: 63-71.

Wenning GK, Odin P, Morrish P, Rehncrona S, Widner H, Brundin P, *et al.* Short- and long-term survival and function of unilateral intrastriatal dopaminergic grafts in Parkinson's disease. *Ann Neurol* 1997; 42: 95-107.

Wertheimer J, Gottuso AY, Nuno M, Walton C, Duboille A, Tuchman M, *et al.* The impact of STN deep brain stimulation on speech in individuals with Parkinson's disease: the patient's perspective. *Parkinsonism Relat Disord* 2014; 20: 1065-70.

Whone AL, Watts RL, Stoessl AJ, Davis M, Reske S, Nahmias C, *et al.* Slower progression of Parkinson's disease with ropinirole versus levodopa: The REAL-PET study. *Ann Neurol* 2003; 54: 93-101.

Wickham H. ggplot2: Elegant Graphics for Data Analysis. 2016. Available from: https://ggplot2.tidyverse.org.

Wickham H, François R, Henry L, Müller K. dplyr: A Grammar of Data Manipulation. R package version 0.8.4. 2020. Available from: https://CRAN.R-project.org/package=dplyr.

Wickham H, Henry L. tidyr: Tidy Messy Data. R package version 1.0.2. 2020. Available from: https://CRAN.R-project.org/package=tidyr.

Widner H, Tetrud J, Rehncrona S, Snow B, Brundin P, Gustavii B, *et al.* Bilateral fetal mesencephalic grafting in two patients with parkinsonism induced by 1-methyl-4-phenyl-1,2,3,6-tetrahydropyridine (MPTP). *N Engl J Med* 1992; 327: 1556-63.

Wieler M, Gee M, Martin WR. Longitudinal midbrain changes in early Parkinson's disease: iron content estimated from R2*/MRI. *Parkinsonism Relat Disord* 2015; 21: 179-83.

Wile DJ, Agarwal PA, Schulzer M, Mak E, Dinelle K, Shahinfard E, *et al.* Serotonin and dopamine transporter PET changes in the premotor phase of LRRK2 parkinsonism: cross-sectional studies. *The Lancet Neurology* 2017; 16: 351-9.

Williams A, Gill S, Varma T, Jenkinson C, Quinn N, Mitchell R, *et al.* Deep brain stimulation plus best medical therapy versus best medical therapy alone for advanced Parkinson's disease (PD SURG trial): a randomised, open-label trial. *The Lancet Neurology* 2010; 9: 581-91.

Wilson AA, Ginovart N, Hussey D, Meyer J, Houle S. In vitro and in vivo characterisation of [11C]-DASB: a probe for in vivo measurements of the serotonin transporter by positron emission tomography. *Nucl Med Biol* 2002; 29: 509-15.

Wilson AA, Ginovart N, Schmidt M, Meyer JH, Threlkeld PG, Houle S. Novel radiotracers for imaging the serotonin transporter by positron emission tomography: synthesis, radiosynthesis, and in vitro and ex vivo evaluation of (11)C-labeled 2-(phenylthio)araalkylamines. *J Med Chem* 2000; 43: 3103-10.

Wilson H, Dervenoulas G, Pagano G, Koros C, Yousaf T, Picillo M, *et al.* Serotonergic pathology and disease burden in the premotor and motor phase of A53T α-synuclein parkinsonism: a cross-sectional study. *The Lancet Neurology* 2019; 18: 748-59.

Winkler C, Kirik D, Bjorklund A, Cenci MA. L-DOPA-induced dyskinesia in the intrastriatal 6-hydroxydopamine model of parkinson's disease: relation to motor and cellular parameters of nigrostriatal function. *Neurobiol Dis* 2002; 10: 165-86.

Winner B, Jappelli R, Maji SK, Desplats PA, Boyer L, Aigner S, *et al.* In vivo demonstration that alpha-synuclein oligomers are toxic. *Proc Natl Acad Sci U S A* 2011; 108: 4194-9.

Wright Willis A, Evanoff BA, Lian M, Criswell SR, Racette BA. Geographic and ethnic variation in Parkinson disease: a population-based study of US Medicare beneficiaries. *Neuroepidemiology* 2010; 34: 143-51.

Wu K, Politis M, Piccini P. Parkinson disease and impulse control disorders: a review of clinical features, pathophysiology and management. *Postgrad Med J* 2009; 85: 590-6.

Wu Y, Carson RE. Noise reduction in the simplified reference tissue model for neuroreceptor functional imaging. *J Cereb Blood Flow Metab* 2002; 22: 1440-52.

Yin HH, Knowlton BJ. The role of the basal ganglia in habit formation. *Nat Rev Neurosci* 2006; 7: 464-76.

Yoo HS, Chung SJ, Chung SJ, Moon H, Oh JS, Kim JS, *et al.* Presynaptic dopamine depletion determines the timing of levodopa-induced dyskinesia onset in Parkinson's disease. *Eur J Nucl Med Mol Imaging* 2018; 45: 423-31.

Yu H, Sternad D, Corcos DM, Vaillancourt DE. Role of hyperactive cerebellum and motor cortex in Parkinson's disease. *Neuroimage* 2007; 35: 222-33.

Zarranz JJ, Alegre J, Gómez-Esteban JC, Lezcano E, Ros R, Ampuero I, *et al.* The new mutation, E46K, of alpha-synuclein causes Parkinson and Lewy body dementia. *Ann Neurol* 2004; 55: 164-73.

Zecca L, Casella L, Albertini A, Bellei C, Zucca FA, Engelen M, *et al.* Neuromelanin can protect against iron-mediated oxidative damage in system modeling iron overload of brain aging and Parkinson's disease. *J Neurochem* 2008; 106: 1866-75.

Zecca L, Zucca FA, Wilms H, Sulzer D. Neuromelanin of the substantia nigra: a neuronal black hole with protective and toxic characteristics. *Trends Neurosci* 2003; 26: 578-80.

Zhang J, Li X, Li JD. The Roles of Post-translational Modifications on alpha-Synuclein in the Pathogenesis of Parkinson's Diseases. *Front Neurosci* 2019; 13: 381.

Zhu MY, Juorio AV. Aromatic L-amino acid decarboxylase: biological characterization and functional role. *Gen Pharmacol* 1995; 26: 681-96.

Zibetti M, Merola A, Rizzi L, Ricchi V, Angrisano S, Azzaro C, *et al.* Beyond nine years of continuous subthalamic nucleus deep brain stimulation in Parkinson's disease. *Mov Disord* 2011; 26: 2327-34.

Ziebell M, Andersen BB, Thomsen G, Pinborg LH, Karlsborg M, Hasselbalch SG, *et al.* Predictive value of dopamine transporter SPECT imaging with [(1)(2)(3)I]PE2I in patients with subtle parkinsonian symptoms. *Eur J Nucl Med Mol Imaging* 2012; 39: 242-50.

Ziebell M, Holm-Hansen S, Thomsen G, Wagner A, Jensen P, Pinborg LH, *et al.* Serotonin transporters in dopamine transporter imaging: a head-to-head comparison of dopamine transporter SPECT radioligands 123I-FP-CIT and 123I-PE2I. *J Nucl Med* 2010; 51: 1885-91.

Zucca FA, Segura-Aguilar J, Ferrari E, Munoz P, Paris I, Sulzer D, *et al.* Interactions of iron, dopamine and neuromelanin pathways in brain aging and Parkinson's disease. *Prog Neurobiol* 2017; 155: 96-119.

Appendix

Table summarising clinical and imaging findings in all original accessible research articles published regarding the effect of intrastriatal fetal ventral mesencephalic allotransplants in Parkinson's disease. Conflicting information for each clinical and experimental measure between some studies may be due to differing evaluation methods. Group-wise statistics are reported in favour of case study values unless they were not conducted (Case profiles are reported when group-wise statistics are unavailable). Statistical tests and their significance level are denoted as $^{NS}p > 0.1$, $^{TR}p < 0.1$, $^{*}p < 0.05$, $^{†}p < 0.01$, $^{‡}p < 0.001$; if no symbols are presented alongside results then no formal statistical tests were conducted. Studies were only included if they were original articles; abstracts were not included.

Author	Group / Patients [max FU]	Cardinal motor	Other	Imaging
China				
(Folkerth and Durso, 1996)	**1 Tx:** lPut + rCau (2 ¦ ?); 16w (GA) [15m]	*Pt also had infusion of dissociated diencephalic/mesodiencephalic cells from 1 5-6w GA embryo into CSF* Worsening within 6w After 6w improved speech, swallowing, gait, facial expression Improvements persisted	6m-14m improved response to L-dopa, Time ON ↑, minimal freezing but with increased daily L-dopa Improvements persisted	**[^{18}F]FDOPA:** "an area of uptake just lateral and posterior to the left caudate nucleus…in the posterior portion of the left putamen, and on the left side of the pons. There was no specific uptake of FD in the ventricles"
Cuba				
(Molina *et al.*, 1992b)	**30 Tx:** Cau (? ¦ ?); 6-12w [52m]	**UPDRS (OFF ǀ ON) [36m]:** ↓~52% ǀ ↓~77% 3-36m < BL (†)	Time OFF [42m]: ↓96% Frequency OFF [post-op]: ↓71% Daily L-dopa [42m]: ↓59%	
(Molina *et al.*,	**5 Tx:**	**UPDRS (OFF ǀ ON) [3m]:**	Time OFF [3m]: ↓78%	

1992a)	rPut + rCau (? ¦ ?); 8-13w (CA) [3m]	↓45%* ¦ ↓~25%* Reduction of pre-surgical differences between OFF and ON states	Frequency OFF [3m]: ↓66% Time ON-DYS-: ↑187% Daily L-dopa [3m]: ↓59% Shorter ON latency [3m]: ↓67% Longer duration ON [3m]: ↑215%	
Denver				
(Freed *et al.*, 1992)	**7 Tx:** Pt1-2: rPut + rCau (1 ¦ 10-14); 6-8w (CA) Pt3-5, 7: bPut (1 ¦ 10-14); 6-8w (CA) Pt6: bPut (2 ¦ 10-14); 6-8w (CA) [46m]	**In all Tx (n=7):** H&Y ON [post-op]: ↓33%† UPDRS ON Motor [3m -- 6m -- 12m]: ↑~6% -- ↓~24% -- ↓~22% **In bPut Tx (n=5):** Facial Expression: ↓63%* Postural Control: ↓70%* Gait: ↓45%* Body bradykinesia: ↓58%* **In Pt1 [9m -- 40m]:** Walking speed OFF: ↓~62% -- ↑~85% Walking speed ON: ↑~11% -- ↑~37% 40m > 15m (†)	**In all Tx (n=7):** Daily L-dopa [post-op]: ↓39%† ↑ dyskinesia post-op UPDRS ADL [3m -- 6m -- 12m]: OFF: ↓~23%NS -- ↓~36%NS -- ↓~36%* ON: ↓~41%† -- ↓~59%† -- ↓~55%† **In Pt3:** ↓ dyskinesia and off-episode severity	**[18F]FDOPA K_3^{Plasma}:** Pt1 [9m→33m]: aPut (l/r): ↓2%/↓7% mPut (l/r): ↑2%/↑2% pPut (l/r): ↑21%/↑52% Cau (l/r): ↑5%/↓1% Pt3 [9m]: Put (l/r): 0%/↓25% Cau (l/r): ↓43%/↑22%
Denver/NY (RCT)	33 Tx: lPut (2 ¦ 2), rPut (2 ¦ 2); 7-8w (CA)			
(Freed *et al.*, 2001)	**19 Tx:** 10 ≤ 60y age 9 > 60y age **20 Sham:** 11 ≤ 60y age	**UPDRS OFF Total [12m]:** Tx (↓15%) = Sham (~0%) (NS) Young Tx (↓28%) < Young Sham (↓~4%) (*) Old Tx (↑~1%) = Old Sham (↓~1%) (NS)	**Schwab & England OFF [12m]:** Tx (↑~24%) > Sham (↓~2%) (†) Young Tx (↑~30%) > Young Sham (~0%) (†) Old Tx (↑~9%) = Old Sham (↓~5%) (NS)	**[18F]FDOPA $Ratio^{Occ}$ [12m]:** 16/19 Tx and 1/20 Sham judged by blinded rater to have received Tx Tx ↑40%‡ in Put ΔYoung Tx = ΔOld Tx in Put (NS) Sham ↓2%NS in Put

	9 > 60y age 14/20 received open-label Tx after 12m 1 Tx (>60y age) died at 7m by unrelated cause [12m, blind] [36m, blind + open-label]	**UPDRS OFF Total [36m]:** Tx ↓28%**†** Young Tx ↓38%**‡** Old Tx ↓14%^{NS} **UPDRS OFF Motor [12m]:** Tx ↓18%***** Young Tx ↓34%**†** *Rigidity and bradykinesia showed improvement but not tremor*	**Schwab & England ON [12m]:** No difference between groups (^{NS}) **Daily L-dopa [12m]: no change** **Dyskinesia Clinical Evaluation:** 5/33 Tx (blind + open-label) developed dystonia/dyskinesia by 36m that persisted despite reduced dopaminergic medication	ΔTx > ΔSham in Put (**‡**)
(Nakamura *et al.*, 2001)	**19 Tx:** 10 ≤ 60y age 9 > 60y age **20 Sham:** 11 ≤ 60y age 9 > 60y age [12m]	**UPDRS OFF Motor [12m]:** Young Tx: ↓31.3%**†** Old Tx: ↓6.6%^{NS} Young Sham: ↑0.2%^{NS} Old Sham: ↓1.4%^{NS}		**[^{18}F]FDOPA Ratio^{Occ} [12m]:** Young Tx: Put ↑35.1%*****; Cau ↑0.3%^{NS} Old Tx: Put ↑46%**†**; Cau ↓2.1%^{NS} Young Sham: Put ↓6.5%*****; Cau ↓2.6%^{NS} Old Sham: Put ↑3.4%^{NS}; Cau ↑1.2%^{NS} ΔTx > ΔSham in Put (**†**) ΔTx = ΔSham in Cau (^{NS}) **[^{18}F]FDOPA Ratio^{Occ} SPM:** Tx 12m > BL in bilateral posterior Put [-28 -2 2; 30 -8 2] (**‡**) Young Sham 12m < BL in rostral Put [20 8 -8] (**‡**) ΔTx > ΔSham in bilateral posterior Put [-28 -2 2; 32 -6 0] (**†**) **Correlations:** ΔUPDRS with Δ[^{18}F]FDOPA Put in all PD (r=0.56*****) ΔUPDRS with Δ[^{18}F]FDOPA Put in

				young PD (r=0.58†) ΔBradykinesia with Δ[^{18}F]FDOPA Put in young PD (r=0.53*) ΔRigidity & ΔTremor with Δ[^{18}F]FDOPA Put in young PD (^{NS}) ΔUPDRS with Δ[^{18}F]FDOPA Put in old PD (r=0.01^{NS})
(Ma *et al.*, 2002)	**17 Tx ≤ 60y age:** 9 blind 8 open-label 5 OFF-DYS+ 12 OFF-DYS- 5 OFF-DYS^{R}- (best clinical responders of 12 OFF-DYS- group) [1y, n=17] [2y, n=13]	**UPDRS OFF Motor [BL]:** OFF-DYS+ < OFF-DYS- (-26%) (*) **UPDRS OFF Motor [12m]:** ΔOFF-DYS+ (↓53.9%) > ΔOFF-DYS- (↓10.8%) (†) **UPDRS OFF Motor [24m]:** ΔOFF-DYS+ (↓63.6%) > ΔOFF-DYS- (↓13.6%) (†)	**Pre-surgery:** All patients had significant LID **Post-surgery:** 3 OFF-DYS+ primarily of head & neck 2 OFF-DYS+ primarily of UE 3 OFF-DYS+ required further pallidal DBS	**[^{18}F]FDOPA Ratio^{Occ} in bPut [BL]:** OFF-DYS+ = OFF-DYS- (^{NS}) **[^{18}F]FDOPA Ratio^{Occ} in bPut [12m]:** ΔOFF-DYS+ (↑55.8%†) > ΔOFF-DYS- (↑25.9%*) (*) **[^{18}F]FDOPA Ratio^{Occ} in bPut [24m]:** ΔOFF-DYS+ (↑73.5%†) > ΔOFF-DYS- (↑26.8%^{NS}) (†) **[^{18}F]FDOPA Ratio^{Occ} [across timepoints]:** OFF-DYS+ > OFF-DYS- in lPut (‡) OFF-DYS+ = OFF-DYS- in rPut, lCau, rCau (^{NS}) **[^{18}F]FDOPA Ratio^{Occ} SPM [post-op]:** OFF-DYS+ > OFF-DYS- (‡) in: left posterodorsal Put [-32 -2 6] OFF-DYS+ = OFF-DYS^{R}- (^{NS}) at this locus left anteroventral Put [-28 2 -8] OFF-DYS+ > OFF-DYS^{R}- (*) at this locus

(Ma *et al.*, 2010)	**33 Tx:** 19 blind 14 open-label 18 ≤ 60y age 15 > 60y age 15 male 18 female [1y, n=33] [2y, n=29] [4y, n=15]	**UPDRS OFF Total:** 1-way repeated ANOVA (BL, 1y, 2y) (‡, n=33): Tx: ↓15.1% [1y] (*) Tx: ↓30.8% [2y] (‡) 1-way repeated ANOVA (BL, 1y, 2y, 4y) (‡, n=15): Tx: ↓20.9% [1y] (NS) Tx: ↓42.7% [2y] (†) Tx: ↓24.9% [4y] (*) ΔUPDRS was independent of BL disease duration and disease severity 3-way repeated ANOVA (time, age, gender) (n=33) for BL→1y: Main effect of time (†) Age*Time interaction (*): Young Tx: ↓23.1% Old Tx: ↓5.3% Gender*Time interaction (*): Male Tx: ↓25.8% Female Tx: ↓6% 3-way repeated ANOVA (time, age, gender) (n=33) for BL→2y: Main effect of time (‡) Age*Time interaction (TR): Young Tx: ↓44.6% Old Tx: ↓16.8% Gender*Time interaction (NS): Male Tx: ↓32.6%		**[18]F]FDOPA Ratio^{Occ}:** 1-way repeated ANOVA (BL, 1y, 2y) in bPut (‡, n=33): Tx: ↑28.7%‡ [1y], ↑38.1%‡ [2y] 1-way repeated ANOVA (BL, 1y, 2y, 4y) in bPut (‡, n=15): Tx: ↑25.7%* [1y], ↑31.6%† [2y], ↑45.7%‡ [4y] 1-way repeated ANOVA in bCau (NS) 3-way Repeated ANOVA (time, age, gender) in bPut for BL→1y & BL→2y: Main effect of time (‡) No Age*Time interaction (p>0.19) No Gender*Time interaction (p>0.19) **Correlations, ΔUPDRS with:** [18F]FDOPA in bPut across BL, 1y & 2y (r=-0.3*, n=33) [18F]FDOPA in bPut across BL, 1y, 2y & 4y (r=-0.31*, n=15) **[18F]FDOPA Ratio^{Occ} SPM:** 1-way repeated ANOVA (BL, 1y, 2y, 4y) (‡, n=33): 1y, 2y & 4y > BL in posterior bPut (‡) 2y > 1y in posterior bPut (†) 1y, 2y & 4y < BL in bCau & ventrorostral bPut (‡) 4y < 1y in bCau & ventrorostral bPut (‡) 4y < 2y in bCau & ventrorostral bPut

		Female Tx: ↓29.3%		(†) **Voxelwise correlations:** BL [^{18}F]FDOPA with ΔUPDRS at 1y in ventrorostral Put [-26 8 -10, r=0.54*] [14 18 -4, r=0.59†] BL [^{18}F]FDOPA with ΔUPDRS at 2y in ventrorostral Put [14 18 -4, r=0.46*]
(Richardson *et al.*, 2011)	**1 Tx OFF-DYS+ in OFF-state** [10y] **13 non-Tx PD in OFF-state** **1 non-Tx OFF-DYS- PD in ON-state**	**UPRDS OFF Motor:** Tx: ↓60% [12m] Tx: ↓60% [24m] Tx: ↓53% [48m]	**Tx OFF-DYS+:** Buccofacial dystonia (50% of the time) Prominent dyskinesia (50% of the time) Walking-induced dystonic posturing of left leg and arm	**[^{18}F]FDOPA Ratio^{Occ}:** Tx maintained uptake in putamen [9y] **Single Cell Recording in GPi [10y for Tx]:** ***At rest:*** Mean discharge rate: OFF > ON (‡); OFF > Tx (‡); Tx > ON (†) Burst Index: OFF < ON (‡); OFF < Tx (*); Tx = ON (^{NS}) Proportion of spikes in burst: OFF < ON (‡); OFF < Tx (†); Tx = ON (^{NS}) L-statistic (Burst discharge irregularity): OFF < ON (‡); OFF < Tx (‡); Tx = ON (^{NS}) % units with significant oscillations: OFF (55%); Tx (20%); ON (42%) (^{NS}) % units with 2-10Hz oscillations:

				OFF (29%); Tx (30%); ON (0%) (NS) % units with 11-35Hz oscillations: OFF (3%); Tx (0%); ON (5%) (NS) % units with >35Hz oscillations: OFF (9%); Tx (10%); ON (37%) (NS) ***During movement:*** ΔDischarge rate: Tx: ↓63%*, marked ↓ in 3/4 OFF: ↑17%†, ↓>10% in 3/23 ON: ↑8%TR, ↓ in 1/7 No changes noted in GPe at rest
Halifax	Pt1: plPut (3 ¦ 4), prPut (3 ¦ 4); 6-9w (GA) Pt2: plPut (3 ¦ 4), prPut (4 ¦ 4); 6-9w (GA) Pt3-5: plPut + lSN (3 ¦ 4 + 1), prPut + rSN (3 ¦ 4 + 1); 6-9w (GA) Pt6: plPut (2 ¦ 4), prPut (3 ¦ 4); 6-9w (GA) Pt7: plPut + lSN (3 ¦ 1 + 1), prPut + rSN (4 ¦ 6 + 1); 6-9w (GA) Pt8: plPut (3 ¦ 4), prPut (4 ¦ 4); 6-10w (GA) Pt9: plPut (2-3 ¦ 3); 6-10w (GA) Pt10: plPut (4 ¦ 4), prPut (3 ¦ 4); 6-10w (GA)			
(Mendez *et al.*, 2000)	**2 Tx:** Pt1-2 [15m]	**UPDRS Total (OFF ǀ ON):** ↓32%* ǀ ↓28%* **H&Y (OFF ǀ ON):** ↓8% ǀ 0%	**Time OFF:** ↓50% **S&E (OFF ǀ ON):** ↓7% ǀ 0% **Daily L-dopa:** ↓50% in Pt1, 0% change in Pt2	**[18F]FDOPA K_i^{Cer} [12m]:** bPut: ↑107%* pbPut: ↑150%* bCau: ↑37%TR
(Mendez *et al.*, 2002)	**3 Tx:** Pt3-5 [13m]	**UPDRS Total (OFF ǀ ON) [last timepoint]:** ↓37%* ǀ ↓33%TR **H&Y (OFF ǀ ON) [last timepoint]:**	**S&E (OFF ǀ ON) [last timepoint]:** ↑33%* ǀ ↑~9%NS **Daily L-dopa:** ↓37%	**[18F]FDOPA K_i^{Cer} [12m]:** Put (l/r): ↑9%/↑70% SN (l/r): ↑38%/↑66%

		↓24%* | ↓14%* **P-S^{NUM} (OFF | ON):** lUE: ↑48%^{TR} | ↑~3%^{NS} rUE: ↑45%^{TR} | ↓~3%^{NS}		
(Mendez *et al.*, 2005)	**2 Tx:** Pt6-7 [52m]	**Pt6 [3y]:** UPDRS Motor (OFF | ON): ↓54% | ↓47% UPDRS Total (OFF | ON): ↓31% | ↓25% P-S^{NUM} (OFF | ON): lUE ↑64% | ↑47% rUE ↑53% | ↑26% **Pt7 [3y]:** UPDRS Motor (OFF | ON): ↓48% | ↓22% UPDRS Total (OFF | ON): ↓46% | ↓28% P-S^{NUM} (OFF | ON): lUE ↑187% | 0% rUE ↑40% | ↓27%	**Pt6 [3y]:** ON-DYS+: ↓34% Time OFF: ↓50% Never had OFF-DYS+ Daily L-dopa unchanged **Pt7 [3y]:** ON-DYS+: ↓91% Time OFF: ↓50% Daily L-dopa ↓30%	**[^{18}F]FDOPA K$_i^{Cer}$:** Pt6 [28m]: Put (l/r): ↑98%/↑306% 65%/88% of normal Pt7 [36m]: Put (l/r): ↓45%/↑222% 24%/64% of normal SN (l/r): ↑22%/↑90%
(Mendez *et al.*, 2008)	**5 Tx:** Pt6-10 [14y]	**Pt8 [21m]:** UPDRS Motor (OFF | ON): ↑39% | ↑75% UPDRS Total (OFF | ON): ↑38% | ↑67% **Pt10 [21m]:** UPDRS Motor (OFF | ON): ↓2% | ↑6%	**Pt8 [21m]:** Dyskinesia (OFF | ON): 0% | ↑25% **Pt10 [21m]:** Dyskinesia (OFF | ON): 0% | ↑11%	**[^{18}F]FDOPA K$_i^{Cer}$:** Pt8 [12m]: lPut (l/r): ↓3%/↑18% Pt10 [12m]: lPut (l/r): ↓29%/↑185%

		UPDRS Total (OFF ׀ ON): ↓13% ׀ ↑3%		
Los Angeles	*(see individual studies)*			
(Kopyov *et al.*, 1996)	**22 Tx:** 9 uStr (1-2 ¦ ?); 6-10w (GA) 3 bStr (1-2 ¦ ?); 6-10w (GA) 10 bPut (2-4 ¦ ?); 6-10w (GA) [24m]	**Repeated ANOVA (BL, 6m, 12m, 18m, 24m), Dunnett's post-hoc pairwise contrasts [2y]:** UPDRS OFF (‡): ↓~60% [2y] (*) UPDRS ON (‡): ↓~80% [2y] (*) H&Y OFF (‡): ↓40% [2y] (*) H&Y ON (‡): ↓47% [2y] (*) P-S^{NUM}: OFF lUE (†): ↑~60% [2y] (^{NS}) ON lUE (†): ↑~39% [2y] (*) OFF rUE (†): ↑~30% [2y] (^{NS}) ON rUE (‡): ↑~33% [2y] (*) FDex^{NUM}: OFF lUE (*): ↑~38% [2y] (^{NS}) ON lUE (^{NS}): ↑~9% [2y] (^{NS}) OFF rUE (†): ↑~22% [2y] (^{NS}) ON rUE (*): ↑~11% [2y] (^{NS}) Foot tapping (no./min): OFF lLE (†): ↑~40% [2y] (^{NS}) ON lLE (‡): ↑~36% [2y] (*) OFF rLE (*): ↑~23% [2y] (^{NS}) ON rLE (‡): ↑~29% [2y] (*) S-S-W^{TIME}: OFF (‡): ↓~50% [2y] (*) ON (‡): ↓~40% [2y] (*)	**Repeated ANOVA (BL, 6m, 12m, 18m, 24m), Dunnett's post-hoc pairwise contrasts [2y]:** Daily L-dopa (‡): ↓54% [2y] (*) ADL OFF (‡): ↓~53% [2y] (*) ADL ON (‡): ↓~40% [2y] (*) AIMS (‡): ↓~51% [2y] (*) Dyskinesia severity (‡): ↓~33% [2y] (*) Dyskinesia duration (‡): ↓~30% [2y] (*)	

(Kopyov *et al.*, 1997)	**13 Tx:** 6 Low Tissue Volume: pmlPut + pmrPut (2 ¦ 4 + 4); 7.7w (GA) 7 High Tissue Volume: pmlPut + pmrPut (3.1 ¦ 4 + 4); 7.3w (GA) [6m] **5 HC**	**2-way repeated ANOVA (time, group) – interaction: Scheffe group comparison [6m]:** UPDRS OFF (✝): High < Low (-34%) UPDRS ON (✝): High < Low (-31%) H&Y OFF (*): High < Low (-24%) H&Y ON (*): High = Low P-S^{NUM}: OFF lUE (*): High = Low ON lUE (✝): High > Low (+21%) OFF rUE (*): High > Low (+29%) ON rUE (✝): High > Low (+7%) FDex^{NUM}: OFF lUE (✝): High > Low (+23%) ON lUE (✝): High > Low (+5%) OFF rUE (✝): High > Low (+12%) ON rUE (*): High > Low (+1%) Foot tapping (no./min): OFF lLE (^{NS}): High = Low ON lLE (^{NS}): High = Low OFF rLE (^{NS}): High = Low ON rLE (^{NS}): High = Low S-S-W^{TIME}: OFF (*): High < Low (-30%) ON (^{NS}): High = Low	**2-way repeated ANOVA (time, group) – interaction: Scheffe group comparison [6m]:** Daily L-dopa (^{NS}): High = Low ADL OFF (*): High < Low (-18%) ADL ON (‡): High < Low (-47%) AIMS (*): High < Low (-62%) Dyskinesia severity (^{NS}): High < Low (-42%) Dyskinesia duration (^{NS}): High < Low (-50%) Time OFF (✝): High < Low (-66%)	
(Blüml *et al.*, 1999)	**2 Tx with good clinical outcome:** lPut + rPut (3 ¦ 4 + 4);	**Pt1:** UPDRS Motor [12m -- 24m]: ↓68% -- ↓65%	**Pt1:** ADL [12m -- 24m]: ↑29% -- ↑29%	**fMRI wrist-forearm lever task:** **Pt1 [3y] (α<0.01):** OFF rUE: Task-related activity in left

	6-10w (GA) [3y]	**Pt2:** UPDRS Motor [12m -- 24m]: ↓54% -- ↓54%	Daily L-dopa: ↓100% **Pt2:** ADL [12m -- 24m]: ↓79% -- ↓82% Daily L-dopa: ↓44%	grafted region (4/5 runs) OFF lUE: No task-related activity in BG (0/3 runs) **Pt2 [2.5y] (α<0.01):** OFF lUE: Task-related activity in rBG (2/2 runs) and in left peristriatal region (1/2 runs) ON lUE: No task-related activity in BG (0/1 runs) OFF rUE: No task-related activity in BG (0/2 runs) ON rUE: No task-related activity in BG (0/1 runs)
(Jacques *et al.*, 1999)	**60 Tx:** pmlPut + pmrPut (? ¦ 4 + 4); 6-10w (GA) [12m]	UPDRS ↓44.5% [12m] (*) (n=45)	Daily L-dopa ↓17.8% (n=60) 1 Tx increased dyskinesia at post-op, not alleviated by L-dopa adjustment but GPi pallidotomy effective	
(Ross *et al.*, 1999)	**24 Tx:** lPut + rPut (? ¦ 4 + 4); 6-10w (GA) **9 non-Tx PD:** 5 cross-over to Tx at 12m: lPut + rPut (? ¦ 4 + 4); 6-10w (GA) [12m]			**Graft volume (cm^3) determined by hyperintensity on T_2-weighted MRI** ≤2cm^3 (≤40% ^{1}H-MRS VOI) (26 Put) 2-3cm^3 (40-60% ^{1}H-MRS VOI) (9 Put) ≥3cm^3 (≥60% ^{1}H-MRS VOI) (8 Put) **^{1}H-MRS (VOI=5.12cm^3) in Put (α<0.05) [12m]:** non-Tx PD = HC on all measures ≥3cm^3 grafted Put (n=8): NAA/Cr: Tx < non-Tx PD (-19%)

	13 HC			Cho/Cr: Tx > non-Tx PD (+26%) mI/Cr: Tx = non-Tx PD NAA: Tx = non-Tx PD Cr: Tx = non-Tx PD Cho: Tx > non-Tx PD (+43%) mI: Tx > non-Tx PD (+60%) Glx: Tx = non-Tx PD In 5 Tx who had pre- & post- MRS: ↑ mI/Cr **In vitro ^{1}H-MRS of fetal neural tissue:** NAA <0.4mM (<5% of *in vivo* values)
Lund	Pt1: amlPut + lCau (4 ¦ 2 + 1); 8-10w (GA) Pt2: amrPut + rCau (4 ¦ 2 + 1); 8-10w (GA) Pt3: lPut (4 ¦ 3); 8-9w (GA) Pt4: rPut (4 ¦ 3); 6-7w (CA) Pt5: lPut + lCau (3-4 ¦ 3 + 1), rPut + rCau (3-4 ¦ 3 + 1); 6-8w (CA) Pt6: lPut (3-4 ¦ 3), rPut + rCau (3-4 ¦ 3 + 1); 6-8w (CA) Pt7: lPut (5 ¦ 5); 6-8w (CA) Pt8: lPut + lCau (5 ¦ 4 + 2); 6-8w (CA) Pt9: lPut (4 ¦ 5); 6-8w (CA) Pt10: rPut + rCau (7 ¦ 5 + 2); 6-8w (CA) Pt12: lPut + lCau (4 ¦ 5 + 2), rPut + rCau (3 ¦ 5 + 2); 5-7w (CA) Pt13: lPut + lCau (4 ¦ 5 + 2), rPut + rCau (5 ¦ 5 + 2); 5-7w (CA) Pt14: lPut + lCau (4 ¦ 5 + 2), rPut + rCau (4 ¦ 5 + 2); 5-7w (CA) Pt15: lPut + lCau (4 ¦ 5 + 2), rPut + rCau (4 ¦ 5 + 2); 5-7w (CA) Pt16: lPut + lCau (3 ¦ 5 + 2), rPut + rCau (4 ¦ 5 + 2); 5-7w (CA) Pt17: lPut (?¦ ?), rPut (? ¦ ?); 5-9w (CA) Pt18: rPut (? ¦ ?); 5-9w (CA)			
(Lindvall *et al.*,	**1 Tx:**	OFF Rigidity (lUE/rUE) [5m]:	Time OFF [5m]: ↓~50%	**[^{18}F]FDOPA K_i^{Occ} [5m]:**

1990)	Pt3 [5m]	↓~88%/↓~66% OFF P-S^{TIME}: (lUE/rUE) [5m]: ↓~33%/↓~54% lUE = rUE [3-5m] OFF = ON [3-5m] ON P-S^{TIME}: 1-5m = BL OFF UE EMG Time [5m]: ↓*	Frequency OFF [5m]: ↓~62%	Put (l/r): ↑133%/↑19% Cau (l/r): ↑1%/↑33% lPut = rPut
(Hoffer *et al.*, 1992)	**2 Tx:** Pt1-2 [82w]	**Pt1:** OFF P-S^{TIME} ↓ from 12w (*) [2w -- 12w -- 82w]: lUE ↑~18% -- ↓~3% -- ↓~15% rUE ↑~19% -- ↓~15% -- ↓~30% lUE = rUE [19w to 82w] (^{NS}) Negative correlation with months (*) ON P-S^{TIME}: ↓~24% [post-op] No correlation with months (^{NS}) OFF walking disability (80w): ↓~57%* **Pt2:** P-S^{TIME} [post-op]: OFF ↓15%*, ON ↓22%* Trend over time for OFF walking disability conforms to a quadratic regression curve; Initial worsening in first 9w	**Pt1:** No change in duration ON phase (^{NS})	**Motor readiness potential amplitude (0.5s before voluntary movement)** **EEG at C3′/C4′:** ↑ peaks at 4-7m for Pt1 & Pt2 Pt1 ↑ at 15m & 18m (†) ΔlPut > ΔrPut (+50%) Pt2 14m-18m = BL (^{NS}) **[^{18}F]FDOPA K_i^{Occ}:** Pt1 [6m → 13m]: Put (l/r): ↑33%/↓21% Cau (l/r): ↑126%/↓26% Pt2 [5m → 12m]: Put (l/r): ↓22%/↑27% Cau (l/r): ↑20%/↓7% **[^{11}C]nomifensine Ratio^{Occ}:** Pt2 [5m → 12m]: Put (l/r): ↓8%/↓21% Cau (l/r): ↓3%/↓30%

		Improvement peaking at 35w Decline back to BL by 60w Could not complete tasks at 61w-80w OFF walking no. steps/7m [2w -- 35w -- 60w] (R^2 = 0.58): ↑~39% -- ↑~3% -- ↑~18% OFF walking steps/s [2w -- 35w -- 60w] (R^2 = 0.97): ↓~10% -- ↑~22% -- ↑~6%		
(Lindvall *et al.*, 1992)	**2 Tx:** Pt3-4 [14m]	**Pt3 [8m -- 13m]:** OFF Rigidity: lUE: ↓~85% -- ↓~65% rUE: ↓~90% -- ↓~66% OFF P-S^{TIME}: lUE: ↓~40% -- ↓~33% rUE: ↓~54% -- ↓~63% lUE = rUE [8m & 13m] OFF = ON [8m & 13m] OFF UE EMG Time sustained ↓ [8m & 13m] OFF FDex^{TIME} [5m -- 8m -- 13m]: lUE: ↓~9% -- ↓~13% -- ↓~9% rUE: ↓~28% -- ↓~32% -- ↓~28% **Pt4 [3m -- 7m -- 12m]:** OFF Rigidity: lUE: ↑~20% -- ↓~40% -- ~0% rUE: ↑~33% -- ↓~22% -- ↓~13%	**Pt3 [8m -- 13m]:** Time OFF: ↓~49% -- ↓~58% Frequency OFF: ↓~58% -- ↓~65% Duration ON Phase [5w-13m]: ↑52% **Pt4 [3m -- 7m -- 12m]:** Time OFF: ↑~14% -- ↓~51% -- ↓~46% Frequency OFF: ↑~21% -- ↓~43% -- ↓~27% Duration ON Phase [9w-12m]: ↑41%	

		OFF P-S^{TIME}: lUE: ↑~18% -- ↓~29% -- ↓~39% rUE: ↑~59% -- ↑~12% -- ↑~6% lUE = rUE [7m & 12m] OFF > ON [7m & 12m] OFF UE EMG Time: ↓ [7m] 12m = BL OFF FDex^{TIME}: lUE: ↓~7% -- ↑~15% -- ↓~7% rUE: ↑~12% -- ↑~28% -- ↑~24%		
(Sawle *et al.*, 1992)	**2 Tx:** Pt3-4 [14m]			**[^{18}F]FDOPA K_i^{Occ}:** Pt3 [5m -- 8m -- 13m]: lPut: ↑~8% -- ↑~42% -- ↑~36% rPut: ↓~31% -- ↓~35% -- ↓~55% lCau: ↓~27% -- ↓~31% -- ↓~47% rCau: ↓~13% -- ↓~35% -- ↓~30% Pt4 [7m -- 12m]: lPut: ↓~18% -- ↓~55% rPut: ↑~67% -- ↑~79% lCau: ↓~12% -- ↓~37% rCau: ↓~43% -- ↓~25%
(Widner *et al.*, 1992)	**2 Tx:** Pt5-6 [24m]	**Pt5 [4-6m -- 10-13m -- 22-24m]:** OFF Rigidity: Left: ↓~28% -- ↓~38% -- ↓~92% Right: ↓~25% -- ↓~35% -- ↓~91% OFF P-S^{NUM}: lUE: ↓5% -- ↑140% -- ↑580%	**Pt5 [4-6m -- 10-13m -- 22-24m]:** OFF S&E: ↓11% -- ↑43% -- ↑96% ON AIMS: ↓8% -- ↓35% -- ↓94% **Pt6 [6m -- 12m -- 22m]:** OFF S&E: ↑25% -- ↑72% -- ↑119%	**[^{18}F]FDOPA K_i^{Occ}:** Pt5 [5m -- 13m -- 24m]: lStr: ↑~30% -- ↑~74% -- ↑~67% rStr: ↓~4% -- ↑~60% -- ↑~79% Pt6 [6m -- 12m -- 22m]: lStr: ↓~12% -- ↑~48% -- ↑~48%

		rUE: ↓31% -- ↑107% -- ↑169% OFF UPDRS Total: ↓8% -- ↓25% -- ↓47% OFF Movement Velocity: lUE: ↑~20% -- ↑~60% -- ↑~400% rUE: ↑~50% -- ↑~133% -- ↑~400% OFF Walking (s): ↓27% -- ↓25% -- ↓60% **Pt6 [6m -- 12m -- 22m]:** OFF Rigidity: Left: ↓~62% -- ↓~94% -- ↓~94% Right: ↓~44% -- ↓~80% -- ↓~90% OFF P-S^{TIME}: lUE: ↑14% -- ↓33% -- ↓38% rUE: ↑2% -- ↓35% -- ↓36% OFF UPDRS Total: ↓31% -- ↓49% -- ↓53% OFF Movement Velocity: lUE: ↑~71% -- ↑~500% -- ↑~457% rUE: ↑~214% -- ↑~571% -- ↑~571% OFF Walking (s): ↓39% -- ↓55% -- ↓57%	ON AIMS: ↓53% -- ↓54% -- ↓40%	rStr: ↑~59% -- ↑~165% -- ↑~194%
(Lindvall *et al.*, 1994)	**2 Tx:** Pt3-4 [36m]	**Pt3 [34-36m]:** OFF Rigidity (lUE/rUE): ↓~50%/↓~83% OFF P-S^{TIME} (lUE/rUE): ↓~29%/↓~68% lUE > rUE (+43%)	**Pt3:** Time OFF [34m]: ↓~50% Duration ON Phase [1-3y]: ↑90% **Pt4:** Time OFF ↓~100% from 33m Cessation of L-dopa at 32m	**[^{18}F]FDOPA K_i^{Occ}:** Pt3 [34m]: Put (l/r): ↑~42%/↓~66% Cau (l/r): ↓~47%/↓~67% Pt4 [36m]: Put (l/r):↓~50%/↑~183%

		OFF UE EMG Time: Sustained ↓ at 34m **Pt4 [36m]:** OFF Rigidity (lUE/rUE): ↓~100%/↓~80% OFF P-S^{TIME} (lUE/rUE): ↓~80%/↓~47% lUE > rUE (+22%) OFF UE EMG Time: lUE & rUE ↓	Fluctuations [36m]: ↓~100% Duration ON Phase [1-3y]: ↑95%	Cau (l/r):↓~22%/↓~28%
(Wenning *et al.*, 1997)	**6 Tx:** Pt3-4, 7-10 [72m]	**UPDRS OFF Motor [1y -- 2y -- 4y -- 6y]:** Pt3: ↓49% -- ↓47% -- ↓21% -- ND Pt4: ↓6% -- ↓54% -- ↓68% -- ↓38% Pt7: ↓20% -- ↓37% -- ND -- ND Pt8: ↑23% -- ↑35% -- ND -- ND Pt9: ↓23% -- ND -- ND -- ND Pt10: ↓28% -- ND -- ND -- ND **OFF Rigidity, P-S^{TIME} & EMG Time:** ↓iUE, ↓↓cUE Continued clinical improvement from 1st to 2nd post-op year across all Pts	**Time OFF [1y -- 2y -- 4y -- 6y]:** Pt3: ↓60% -- ↓54% -- ↓44% -- ND Pt4: ↓53% -- ↓71% -- ↓100% -- ↓100% Pt7: ↓17% -- ↓60% -- ND -- ND Pt8: ↑25% -- ↑10% -- ND -- ND Pt9: ↓55% -- ND -- ND -- ND Pt10: ↓43% -- ND -- ND -- ND **Duration ON phase [1y -- 2y -- 4y -- 6y]:** Pt3: ↑56% -- ↑68% -- ↑86% -- ND Pt4: ↑45% -- ↑95% -- ↑120% -- ↑76% Pt7: ↑31% -- ↑31% -- ND -- ND Pt8: ↑59% -- ↑39% -- ND -- ND Pt9: ↑27% -- ND -- ND -- ND Pt10: ↑51% -- ND -- ND -- ND **Time ON-DYS+ [1y -- 2y -- 4y -- 6y]:**	**[^{18}F]FDOPA K_i^{Occ}:** Pt3 [53m]: Put (l/r): ↑~94%/↓~40% Cau (l/r): ↓~19%/↑~14% Pt4 [72m]: Put (l/r): ↓~37%/↑~257% Cau (l/r): ↓~19%/↓~46% Pt7 [9m]: Put (l/r): ↑~76%/↓~1% Cau (l/r): ↑~30%/↑~14% Pt8 [9m -- 18m]: lPut ↑~93% -- ↑~33% rPut ↓~34% -- ↓~31% lCau ↑~14% -- ↑~9% rCau ↓~17% -- ↓~62% Pt9 [10m]: Put (l/r): ↑~46%/↓~27% Cau (l/r): ↓~60%/↓~50% Pt10 [9m]:

			Pt3: 0% -- 0→2 -- 0% -- ND Pt4: 0% -- 0% -- 0% -- 0% Pt7: ↓28% -- ↓69% -- ND -- ND Pt8: ↑5% -- ↑57% -- ND -- ND Pt9: ↑128% -- ND -- ND -- ND Pt10: ↑21% -- ND -- ND -- ND **Daily ʟ-dopa [End of FU]:** Pt3: 0% Pt4: ↓100% Pt7: ↓33% Pt8: ↑18% Pt9: ↓11% Pt10: ↓15%	Put (l/r): ↓~18%/↑~71% Cau (l/r): ↑~30%/↓~4%
(Hagell *et al.*, 1999)	**5 Tx:** Pt3, 7-10 [72m]	**UPRDS OFF Motor [pre Tx2 -- Tx2+13-24m]:** Pt3: ↓~2% -- ↓~23% Pt7: ↓~24% -- ↓~36% Pt8: ↑~7% -- ↑~47% Pt9: ↓~30% -- ↓~15% Pt10: ↓~39% -- ↓~44% OFF P-S^{TIME}: Minimal change following 2nd graft in both lUE & rUE	**Time OFF [pre Tx2 -- Tx2+13-24m]:** Pt3: ↓43% -- ↓42% Pt7: ↓57% -- ↓100% Pt8: ↓26% -- ↓30% Pt9: ↓68% -- ↑53% Pt10: ↓55% -- ND **Duration ON phase [pre Tx2 -- Tx2+13-24m]:** Pt3: ↑86% -- ↑71% Pt7: ↑26% -- ↑121% Pt8: ↑48% -- ↓14% Pt9: ↑29% -- ↑116% Pt10: ↑46% -- ↑110% **Time ON-DYS+ [pre Tx2 --**	**[^{18}F]FDOPA K_i^{Occ}:** Pt3 [65m -- 72m] – Tx2 at 55m: lPut: ↑~73% -- ↑~53% rPut: ↓~24% -- ↑~6% lCau: ↓~49% -- ↓~32% rCau: ↓~15% -- ↓~33% Pt7 [30m] – Tx2 at 18m: Put (l/r): ↑~78%/↑~77% Cau (l/r): ↑~5%/↑~10% Pt8 [36m] – Tx2 at 23m: Put (l/r): ↑~39%/↑~15% Cau (l/r): ↑~14%/↓~16% Pt9 [23m] – Tx2 at 11m: Put (l/r): ↑~14%/↑~35% Cau (l/r): ↓~68%/↓~53%

			Tx2+13-24m]: Pt3: 0% -- 0→1.4 Pt7: ↓54% -- ↓100% Pt8: ↑61% -- ↓84% Pt9: ↑187% -- ↓86% Pt10: ↑3% -- ND **Daily L-dopa [At Tx2 → End of FU]:** Pt3: ↑14% Pt7: ↓100% Pt8: ↓40% Pt9: ↓21% Pt10: ↓65% Pt10: OFF-DYS+ 9m after 1st Tx	Pt10 [24m] – Tx2 at 10m: Put (l/r): ↑~103%/↑~71% Cau (l/r): ↓~19%/↑~1%
(Piccini *et al.*, 1999)	**1 Tx:** Pt4 [10y] **5 HC**	UPRDS OFF Motor [10y]: ↓~46%	Time OFF [10y]: ↓~100% Daily L-dopa [32m -- 10y]: ↓100% -- ↓67%	**[18F]FDOPA K_i^{Occ} [10y]:** Put (l/r): ↓~70%/↑~307% **[11C]Raclopride BP^{Cer} (Tx [10y] vs. HC)** lPut Tx > HC (+43.7%) rPut Tx < HC (-4%) lCau Tx > HC (+22%) rCau Tx > HC (+14%) Methamphetamine challenge: Meth-ΔlPut Tx < HC (-81%) Meth-ΔrPut Tx > HC (+13%) Meth-ΔlCau Tx < HC (-34%) Meth-ΔrCau Tx < HC (-39%)
(Brundin *et al.*,	**5 Tx:**	**At 2nd post-op year:**	**At 2nd post-op year:**	**[18F]FDOPA K_i:**

2000)	Pt12-16 [24m]	OFF P-S^{TIME} (lUE/rUE): Pt12: ↓77%/↓31% Pt13: ↓50%/↓30% Pt14: ↓49%/↓13% Pt15: ↓18%/↓20% Pt16: ↓31%/↓22% OFF Rigidity (lUE/rUE): Pt12: ↓75%/↓66% Pt13: ↓100%/↓100% Pt14: ↓50%/↓100% Pt15: 0%/0% Pt16: ↓100%/↓59% UPRDS OFF Motor: Pt12: ↓37% Pt13: ↓53% Pt14: ↓58% Pt15: ↑13% Pt16: ↓42% **Motor improvement from 3-5m**	Time OFF: Pt12: ↑44% Pt13: ↓100% Pt14: ↓30% Pt15: ↓52% Pt16: ↓60% Duration ON phase: Pt12: ↑54% Pt13: ND Pt14: ↑59% Pt15: ↓38% Pt16: ↓9% Time ON-DYS+: Pt12: ↓19% Pt13: ↑890% Pt14: ↓30% Pt15: ↓93% Pt16: ↓28% Daily L-dopa: Pt12: ↓40% Pt13: ↓100% Pt14: ↓41% Pt15: ↓56% Pt16: ↓33%	Pt12 [~9m -- ~21m]: lPut: ↑~74% -- ↑~78% rPut: ↑~27% -- ↑~23% lCau: ↑~34% -- ↑~41% rCau: ↑~30% -- ↑~25% Pt13 [~9m -- ~23m]: lPut: ↑~100% -- ↑~103% rPut: ↑~37% -- ↑~50% lCau: ↑~25% -- ↑~33% rCau: ↑~35% -- ↑~34% Pt14 [~8m -- ~21m]: lPut: ↑~18% -- ↑~25% rPut: ↑~100% -- ↑~84% lCau: ↑~4% -- ↑~9% rCau: ↑~28% -- ↑~33% Pt15 [~6m -- ~14m]: lPut: ↑~74% -- ↑~97% rPut: ↑~21% -- ↑~29% lCau: ↑~30% -- ↑~39% rCau: ↑~16% -- ↑~24% Pt16 [~10m]: Put (l/r): ↑~33%/↑~103% Cau (l/r): ↑~4%/↑~10% **lPut 49% & rPut 47% of normal values [10-23m]**
(Hagell *et al.*, 2000)	**5 Tx**: Pt12-16 [24m]		**NHP [18-24m]:** Lack of energy ↓75%^{NS} Poor sleep ↓56%^{NS}	

			Pain ↓63%^{NS} Physical immobility ↓59%* Social isolation ↓20%^{NS} Emotional reactions ↓75%^{NS} Distress ↓68%^{TR}	
(Piccini *et al.*, 2000)	**4 Tx:** lPut + lCau (3-5 ¦ 5 + 2), rPut + rCau (3-5 ¦ 5 + 2); 5-7w (CA) [18.3m]	**UPDRS OFF Motor:** ↓25%^{NS} [6.5m] ↓50%‡ [18.3m] **Joystick RT:** ↓10%^{TR} [6.5m] ↓19%* [18.3m]	**Daily L-dopa intake:** ↓60% [18.3m]	**[^{18}F]FDOPA K_i^{Occ} [6.5m -- 18.3m]:** Put: ↑77%‡ -- ↑79%‡ Cau: ↑27%‡ -- ↑29%‡ **$H_2{}^{15}O$ PET – Left Handed Joystick Movement vs. Rest SPM** rCBF at 6.5m = BL (^{NS}) rCBF at 18.3m > BL (‡): bilateral rostral SMA [-1 1 54] right dlPFC [30 36 32]
(Hagell *et al.*, 2002)	**14 Tx Mixed Tx target:** Put (6.3±2.8 ¦ ?), Cau (1.1±1 ¦ ?); 5-9w [mean 39.8m]	**At max. post-op OFF dyskinesia:** UPDRS OFF Motor: ↓36%†	**At max. post-op OFF dyskinesia:** Time OFF: ↓33%^{TR} Time ON-DYS+: ↓30%^{NS} LEDD: ↓39%‡ OFF hyperkinesia: 0 → 4 (‡) OFF dystonia: 0.5 → 2.8 (*) ON hyperkinesia: 10 → 6 (^{NS}) ON dystonia: 5 → 2 (^{NS}) **Correlations**: Max. post-op OFF CDRS with: Post-op peak ON CDRS (r=0.634*) Pre-op peak ON CDRS	**Correlations:** Pre-op Put [^{18}F]FDOPA K_i with: Max. post-op OFF CDRS (r=-0.549^{TR}) Max. post-op OFF hyperkinesia (-0.554^{TR}) Max. post-op OFF dystonia (-0.356^{NS}) Post-op Put [^{18}F]FDOPA K_i with: Max. post-op OFF CDRS (r=-0.132^{NS}) Put Δ[^{18}F]FDOPA K_i with: Max. post-op OFF CDRS (r=-0.267^{NS})

			(r=0.266^{NS}) Pre-op OFF CDRS (r=0.426^{NS}) ΔUPDRS OFF Motor (r=0.003^{NS}) Put donor no. (r=0.562*) Put no. tracts (r=0.492^{TR})	
(Piccini *et al.*, 2005)	**9 Tx** Pt4, 7, 12-18 [2y] **6 non-Tx PD** **16 HC ([^{18}F]FDOPA)**	**Clinical (n=6, bilateral Tx) [1y -- 2y]:** UPDRS OFF Motor: ↓51% -- ↓42% **Effect of Immunosuppression (n=6) [pre-withdrawal -- post-withdrawal]:** UPDRS OFF Motor: ↓46% -- ↓47% Post-withdrawal = Pre-withdrawal (^{NS}) **[^{11}C]Raclopride Group (n=8) [PET Time]:** UPDRS OFF Motor: ↓47%	**Clinical (n=6, bilateral Tx) [1y -- 2y]:** Time OFF: ↓47% -- ↓15% LEDD: ↓41% -- ↓49% CDRS OFF: 0 → 0.8 → 2 **Effect of Immunosuppression (n=6) [pre-withdrawal -- post-withdrawal]:** CDRS OFF: 0 → 0.8 → 4.3 Post-withdrawal > Pre-withdrawal (*) **[^{11}C]Raclopride Group (n=8) [PET Time]:** Time OFF: ↓60% LEDD: ↓46% CDRS OFF: 0 → 3.5	**[^{18}F]FDOPA K_i^{Occ}:** SPM (n=6, bilateral Tx Pts) (α<0.01): 1y > BL in rPut [22 0 2, k=104] & lPut [-22 -6 -2, k=535] 2y > 1y in rPut [28 2 2, k=153] 1y < BL in rSN [14 -18 -16] & median raphe [4 -24 -16] SPM Tx vs. HC in vStr (n=8) (α<0.01): Tx = HC for GOO=5 (n=3) at BL, 1y, 2y Tx < HC for GOO=4 (n=2) at 1y, 2y Tx < HC for GOO=1-3 (n=3) at BL, 1y, 2y Effect of Immunosuppression (n=6) [pre-withdrawal -- post-withdrawal]: K_i^{Occ} ↑64% -- ↑131% Post-withdrawal > Pre-withdrawal (*) **[^{11}C]Raclopride BP^{Cer} (n=8, 14 Put):** Methamphetamine challenge: Meth-ΔPut -9.55% **Correlations (n=8, 14 Put):**

				Meth-ΔBP^{Cer} with K_i^{Occ} (r=0.7†) For similar level of K_i^{Occ}, Tx show trend for lower Meth-ΔBP^{Cer} than non-Tx cCDRS OFF with: BP^{Cer} in Put, aPut, pPut (^{NS}) Meth-ΔBP^{Cer} in Put, aPut, pPut (^{NS})
(Pogarell *et al.*, 2006)	**2 Tx** Pt12-13 [8y]	**Pt12 [6m -- 1y -- 3y -- 6y -- 8y]:** UPRDS OFF Motor: ↓28% -- ↓39% -- ↓42% -- ↓45% -- ↓58% **Pt13 [2y -- 3y -- 8y]:** UPRDS OFF Motor: ↓53% -- ↓78% -- ↓55%	**Pt12 [6m -- 1y -- 3y -- 6y -- 8y]:** UPDRS-II OFF ADL: ↓40% -- ↓51% -- ↓58% -- ↓47% -- ↓60% OFF-DYS+: + -- ++ -- +++ -- +++ -- +++ Daily L-dopa: ↓7% -- ↓33% -- ↓53% -- ↓100% -- ↓100% **Pt13 [2y -- 3y -- 8y]:** UPDRS-II OFF ADL: ↓43% -- ↓61% -- ↓35% OFF-DYS+: ++ -- ++ -- ++ Daily L-dopa: ↓100% -- ↓100% -- ↓100% Amantadine 200mg used from 3y	**[^{123}I]IPT Ratio^{Occ}:** Pt12 [6m -- 1y -- 3y -- 6y -- 8y]: lStr: ↑65% -- ↑81% -- ↑109% -- ↑169% -- ↑170% rStr: ↑35% -- ↑42% -- ↑79% -- ↑102% -- ↑175% Pt13 [2y -- 3y -- 8y]: lStr: ↑17% -- ↑15% -- ↓3% rStr: ↑35% -- ↑40% -- ↑44%
(Politis *et al.*, 2010b)	**2 Tx OFF-DYS+:** Pt7 [16y], 15 [13y] **12 non-Tx PD in advanced stage ([^{11}C]DASB)**	**UPDRS OFF Motor:** Pt7 [1y -- 2y -- 3y -- 4y -- 9y -- 16y]: ↓~20% -- ↓~35% -- ↓~47% -- ↓~50% -- ↓~53% -- ↓~67% Pt15 [1y -- 2y -- 3y -- 7y -- 13y]: ↑~17% -- ↓~4% -- ↓~30% -- ↓~52% --	**Tx vs. non-Tx PD:** Duration illness: Pt7 > non-Tx (+108%) [16y] Pt15 > non-Tx (+100%) [13y] LEDD: Pt7 < non-Tx (-100%) [16y]	**[^{18}F]FDOPA K_i^{Occ} bPut:** Pt7 [1y -- 2y -- 4y -- 9y]: ↑~33% -- ↑~73% -- ↑~122% -- ↑~133% Pt15 [1y -- 2y -- 3y -- 7y]: ↑~45% -- ↑~63% -- ↑~97% -- ↑~150% **[^{11}C]Raclopride BP^{Cer}:**

	12 HC ([11C]DASB) **6 HC ([11C]Raclopride BP^{Cer})** **16 HC ([18F]FDOPA)**	↓~70% **Tx vs. non-Tx PD:** UPDRS OFF Motor: Pt7 < non-Tx (-71%) [16y] Pt15 < non-Tx (-84%) [13y] UPDRS OFF Total: Pt7 < non-Tx (-52%) [16y] Pt15 < non-Tx (-78%) [13y]	Pt15 < non-Tx (-100%) [13y] **Amantadine has minimal effect on OFF-DYS+** **Buspirone (5-HT_{1A} agonist) administered 3x5mg at 30min intervals:** AIMS OFF (Buspirone vs. Placebo): Pt7 ↓~60% at 90-240 minutes Pt15 ↓~60% at 90-240 minutes	Methamphetamine challenge: Pt7 [9y]: Meth-ΔbPut -~23% Pt15 [7y]: Meth-ΔbPut -~21% HC: Meth-ΔbPut -~23.5% **[11C]DASB BP_{ND}^{Cer}:** Pt7 [16y]: bPut Tx > HC (+172%) bPut Tx > non-Tx PD (+285%) bCau Tx < HC (-29.4%) bCau Tx > non-Tx PD (+~17%) Pt15 [13y]: bPut Tx > HC (+77%) bPut Tx > non-Tx PD (+150%) bCau Tx > HC (+123%) bCau Tx > non-Tx PD (+252%) **[11C]DASB / [18F]FDOPA Ratio:** Pt7: bPut Tx > HC (+230%) Pt15: bPut Tx > HC (+146%)
(Politis *et al.*, 2011)	**1 Tx:** Pt13 [14y] **12 non-Tx PD in advanced stage ([11C]DASB)** **12 HC ([11C]DASB)** **16 HC ([18F]FDOPA)**	**UPDRS OFF Motor [1y -- 2y -- 3y -- 6y -- 14y]:** ↓~49% -- ↓~53% -- ↓~53% -- ↓~51% -- ↓~49%	Continuous OFF-DYS+ starting at 12m Daily L-dopa [18m]: ↓100% No OFF periods GPi DBS at 8y transiently alleviated OFF-DYS+ **Buspirone (5-HT_{1A} agonist) administered 3x5mg at 30min intervals:**	**[18F]FDOPA K_i^{Occ} [1y -- 2y -- 3y -- 6y -- 14y]:** lPut: ↑~66% -- ↑~71% -- ↑~77% -- ↑~100% -- ↑97~% rPut: ↑~27% -- ↑~36% -- ↑~47% -- ↑~61% -- ↑~54% **[123I]IPT $Ratio^{Occ}$ [2y -- 3y -- 8y]:** lStr: ↑17% -- ↑15% -- ↓3% rStr: ↑35% -- ↑40% -- ↑44% **[123I]FP-CIT $Ratio^{Occ}$ [14y]:**

			AIMS OFF (Buspirone vs. Placebo): ↓~64% at 90-240 minutes	rStr: "normal" lPut: "significantly reduced" lCau: "slightly reduced" **[^{11}C]Raclopride BP^{Cer} [5y]:** Methamphetamine challenge: Tx: Meth-ΔlPut -15% Tx: Meth-ΔrPut -23% HC: normal range -19.6 to -27.2% **[^{11}C]DASB BP$_{ND}^{Cer}$ [14y]:** lPut > HC (+34%) & > non-Tx PD (+90%) rPut > HC (+57%) & > non-Tx PD (+122%) lCau > HC (+34%) & > non-Tx PD (+112%) rCau > HC (+21%) & > non-Tx PD (+91%) **[^{11}C]DASB / [^{18}F]FDOPA Ratio:** lPut Tx > HC (+152%) rPut Tx > HC (+128%) **[^{11}C]DASB / [^{123}I]FP-CIT Ratio:** lPut Tx > HC (+102%) rPut Tx > HC (+63%)
(Politis *et al.*, 2012)	**3 Tx** Pt7 [16y], 13 [14y], 15 [13y] **12 non-Tx PD in**	**[Last PET timepoint]:** UPDRS OFF Total: Tx < non-Tx (-57%) (‡) UPDRS OFF Motor: Tx < non-Tx (-70%) (‡)	**[Last PET timepoint]:** LEDD: Tx < non-Tx (-100%) PDQ39: Tx < non-Tx (-64%) (‡)	**[^{18}F]FDOPA K$_i^{Occ}$ [last timepoint]:** Non-Tx < HC in: amygdala‡, aCC†, BG‡, hypothalamus*, insula†, LC*, pCC‡, PFC‡, RN†, Thalamus* Tx < HC in: amygdala†

	advanced stage ([11C]DASB) **12 non-Tx PD in advanced stage ([18F]FDOPA)** **12 HC**		Duration of illness: Tx > non-Tx (+252%) Nonmotor symptoms: Tx < non-Tx (-37%) BDI: Tx > HC (+143) (†) Non-Tx > HC (+209%) (†) Tx < non-Tx (-21%)	Non-Tx < Tx in: BG‡, insula†, pCC†, PFC‡ **[11C]Raclopride BP^{Cer}:** Methamphetamine challenge: Tx: Meth-ΔBG -8% HC: normal range -6 to -13% **[11C]DASB BP_{ND}^{Cer} [last timepoint]:** Non-Tx < HC in: amygdala*, aCC†, raphe‡, hypothalamus‡, insula‡, pCC‡, PFC‡, Thalamus‡, mid-pons‡ Tx < HC in: amygdala‡, aCC‡, raphe‡, hypothalamus‡, insula‡, pCC‡, PFC‡, Thalamus‡, mid-pons‡ Tx < non-Tx in: amygdala*, raphe†, hypothalamus*, insula*, pCC†, PFC‡
(Kefalopoulou *et al.*, 2014)	**2 Tx:** Pt7 [18y], 15 [15y]	**Pt7 [18y]:** UPDRS OFF Motor: ↓41% **Pt15 [15y]:** UPDRS OFF Motor: ↓22%	**Pt7 [18y]:** UPDRS-II ADL = 11 UPDRS-IV.A dyskinesia = 3 UPDRS-IV.B fluctuations = 0 LEDD: ↓100% AIMS OFF = 16 ; moderate OFF-DYS+ improved slightly by amantadine (300mg) + buspirone (15mg) No falls or freezing **Pt15 [15y]:** UPDRS-II ADL = 15 UPDRS-IV.A dyskinesia = 7	

			UPDRS-IV.B fluctuations = 2 LEDD: ↓100% AIMS OFF = 11 ; mild-moderate OFF-DYS+ slightly improved by amantadine 300mg No falls or freezing	
Mexico				
(Madrazo *et al.*, 1991)	**1 Tx:** Cau (? ¦ ?); ? [25m]	**UPDRS Motor (OFF ǀ ON) [25m]:** ↓~66% ǀ ↓~78% ↓ Rigidity, bradykinesia, postural imbalance, gait disturbance and facial expression at 5m ↓ Tremor at 25m		
New Haven				
(Spencer *et al.*, 1992)	**4 Tx:** rCau (1 ¦ 2-4); 7-11w (GA) **3 non-Tx PD:** Cross-over to Tx at 12m [18m] **12 HC ([^{18}F]FDOPA)**	**ON Medication [18m]:** UPDRS Motor: ↓17%^{NS} Bradykinesia: ↓25%* Gait: ↓3%^{NS} Rigidity: ↑4%^{NS} Tremor: ↓37%^{NS} Finger taps (lUE/rUE): ↑400%^{NS}/↑174%^{TR} Fist clenches (lUE/rUE): ↑193%^{NS}/↑38%^{NS} P-S^{NUM} (lUE/rUE): ↑128%^{TR}/↑105%^{NS} Foot taps (lLE/rLE): ↑95%^{TR}/↑172%* Walking (no. steps/15m): ↓43%^{NS}	**ON Medication [18m]:** UPDRS ADL: ↓52%* S&E: ↑54%* ΔTx = Δnon-Tx [12m] for above measures (^{NS}) Daily L-dopa Tx < non-Tx (*) Non-Tx ↑✝ [12m]	**[^{18}F]FDOPA K_3 [6m] in Pt3** Increase to normal range in bCau Cau (l/r): ↑170%/↑100% bPut remained below normal range (*)

		ΔTx = Δnon-Tx [12m] for above measures (NS)		
Paris	Pt1: rPut (2 ¦ 3); 6-8w (GA) Pt2: lPut + lCau (3 ¦ 3 + 1); 6-9w (GA) Pt3: rPut + rCau (3 ¦ 3 + 1); 6-9w (CA) Pt4: rPut + rCau (1 ¦ 3 + 1); 6-9w (CA) Pt5: rPut + rCau (2 ¦ 3 + 1); 6-9w (CA) Pt6: lPut (1 ¦ 3); 6-9w (CA) Pt7: lPut (2 ¦ 3), rPut (1 ¦ 3); 6-9w (CA) Pt8: lPut (1 ¦ 3), rPut (2 ¦ 3); 6-9w (CA) Pt9: lPut (2 ¦ 3), rPut (3 ¦ 3); 6-9w (CA) Pt10: rPut (2 ¦ 3); 6-9w (CA) Pt11: lPut (3 ¦ 3), rPut (3 ¦ 3); 6-9w (CA)			
(Peschanski *et al.*, 1994)	**2 Tx:** Pt1-2 [17m]	**Pt1 [3m -- 7m -- 13m -- 17m]:** OFF FDexTIME: lUE: ↓~18% -- ↓~44% -- ↓~33% -- ↓~33% post-op < pre-op (*****) rUE: ↓~16% -- ↓~21% -- ↓~32% -- ↓~37% post-op < pre-op (**†**) ON FDexTIME: lUE: ↓~12% -- ↓~20% -- ↓~20% -- ↓~20% post-op < pre-op (**†**) rUE: ↓~13% -- ↓~13% -- ↓~13% -- ↓~13% post-op < pre-op (*****)	**Pt1 [3m -- 6m -- 14m -- 15m]:** Duration ON: ↑~5% -- ↑~44% -- ↑~35% -- ↑~45% Time ON-DYS+: ↑~150% -- ↓~100% -- ↓~100% -- ↓~100% Daily L-dopa [12m]: ↓19% **Pt2 [3m -- 7m -- 9m]:** Duration ON: ↑~138% -- ↑~106% -- ↑~75% Time ON-DYS+: ↓~41% -- ↓~88% -- ↓~100%	**[18F]FDOPA K_i^{Occ}:** Pt1 [3m -- 6m -- 12m]: lPut: ↓~17% -- ↓~12% -- ↓~17% rPut: ↑~3700% -- ↑~2150% -- ↑~6200% Pt2 [3m -- 7m]: lPut: ↑~242% -- ↑~350% rPut**:** ↑~3% -- ↑~17%

		OFF P-S^{TIME}: lUE: ↓~10% -- ↓~28% -- ↓~28% -- ↓~35% post-op < pre-op (*****) rUE: ↓~8% -- ↓~16% -- ↓~24% -- ↓~30% post-op < pre-op (**†**) ON P-S^{TIME}: lUE: 0% -- ↑~4% -- ↓~4% -- ↑~4% post-op = pre-op (^{NS}) rUE: ↑~4% -- 0% -- ↓~13% -- ↓~4% post-op = pre-op (^{TR}) **Pt2 [3m -- 8m -- 9m]:** OFF FDex^{TIME}: lUE: ↓~35% -- ↓~35% -- ↓~23% post-op < pre-op (*****) rUE: ↓~29% -- ↓~48% -- ↓~38% post-op < pre-op (**†**) ON FDex^{TIME}: lUE: ↓~24% -- ↓~51% -- ↓~41% post-op < pre-op (*****) rUE: ↓~37% -- ↓~53% -- ↓~42% post-op < pre-op (**†**) OFF P-S^{TIME}: lUE: ↓~32% -- ↓~42% -- ↓~55% post-op = pre-op (^{NS}) rUE: ↓~27% -- ↓~42% -- ↓~49% post-op = pre-op (^{NS})		

		ON P-S^{TIME}: lUE: 0% -- ↓~21% -- ↓~29% post-op = pre-op (^{TR}) rUE: ↑~8% -- ↓~23% -- ↓~31% post-op = pre-op (^{NS})		
(Remy *et al.*, 1995)	**5 Tx:** Pt1-5 [24m]	Clinical scores corresponding to timepoint at which [^{18}F]FDOPA K_i^{Occ} in grafted putamen was highest (equating to ↑96%): OFF cUE FDex^{TIME}: ↓27% Clinical scores corresponding to timepoint at which [^{18}F]FDOPA K_i^{Occ} in ungrafted putamen was highest (equating to ↓5%): OFF cUE FDex^{TIME}: ↓11%	Clinical scores corresponding to timepoint at which [^{18}F]FDOPA K_i^{Occ} in grafted putamen was highest (equating to ↑96%): Daily ON Time: ↑117%	**[^{18}F]FDOPA K_i^{Occ} [mean 3-24m]:** Grafted Put: ↑48%* Ungrafted Put: ↓1%^{NS} Grafted Cau: ↓8%^{NS} Ungrafted Cau: ↓12%^{NS} **Correlations (all scans pooled):** [^{18}F]FDOPA K_i^{Occ} in grafted putamen with: Daily ON Time (r=0.673) Daily OFF Time (r=-0.585) OFF FDex^{TIME} in cUE (r=-0.544) Regression trend for cUE FDex^{TIME}: When Put K_i^{Occ} = 0.002, OFF > ON (+105%) When Put K_i^{Occ} = 0.006, OFF = ON
(Defer *et al.*, 1996)	**5 Tx:** Pt1-5 [36m]	**Timed tests (OFF ǀ ON) [mean 2-31m]:** P-S^{TIME}: ↓26%† ǀ ↓12%* FDex^{TIME}: ↓39%† ǀ ↓22%† Hand-Arm (time): ↓32%† ǀ ↓8%^{NS} S-S-W^{TIME}: ↓13%^{NS} ǀ ↓5%^{NS}	Daily L-dopa: ↓1% [1y], ↑12% [last timepoint] All Tx had ON-DYS+ & fluctuations pre-op **Asymmetrical dyskinesia noted in 3/5 pts post-op, dominating on body side contralateral to grafted striatum**	**[^{18}F]FDOPA K_i^{Occ}:** Grafted Put: ↑61% [1y] 1y = BL in ungrafted Put & bCau

(Cochen *et al.*, 2003)	**6 Tx:** Pt6-11 [24m] **10 HC ([^{18}F]FDOPA)** **10 HC ([^{76}Br]-FE-CBT)**	UPDRS-III OFF Motor [6-24m]: ↓12%^{NS} **Correlations:** **No. of donors with:** ΔUPDRS-III OFF Motor (τ = -0.8*)	Daily L-dopa [6-24m]: ↓16%^{NS} No pts showed OFF-DYS+ [6-24m] **Correlations:** **No. of donors with:** ΔDaily L-dopa (τ = -0.93†)	**[^{18}F]FDOPA K_i^{Occ} in grafted Put:** ↑30%*; 42% of HC **[^{76}Br]-FE-CBT BP^{Occ} in grafted Put:** ↑8%^{NS} **Correlations:** ΔK_i^{Occ} with no. donors (τ = -0.47*) K_i^{Occ} with BP^{Occ} in grafted Put (r=0.76†) ΔK_i^{Occ} with ΔBP^{Occ} in grafted Put (r=0.14^{NS})
Spain				
(López-Lozano *et al.*, 1997)	**10 Tx:** uCau (1 ¦ 1); 6-8w (GA) [5y]	**[Time of first significant change (α<0.01) -- Time peak clinical improvement (α<0.01) -- 60m (α<0.01)]:** **OFF:** UPDRS Total: 5-7m -- 36m ↓46% -- ↓34% UPDRS Motor: 5-7m -- 36m ↓49% -- ↓39% Rigidity: 2-3m -- 18-24m ↓61% -- ↓54% Facies: 2-3m -- 18m ↓54% -- ↓36% Postural stability: 5-7m -- 30m ↓57% -- ↓36% Rising from sitting: 5m -- 15m ↓66% -- ↓54% Speech: 7m -- 30-36m ↓50% -- ↓45% Bradykinesia: 7m -- 18m ↓35% --	**[Time of first significant change (α<0.01) -- Time peak clinical improvement (α<0.01) -- 60m (α<0.01)]:** Time ON: 5-7m -- 48m ↑92% -- ↑85% Time ON-DYS+: 5m -- 18m ↓82% -- ↓46%	

		↓25% Gait: 7-9m -- 30-36m ↓45% -- ↓33% **ON:** UPDRS Total: 5-7m -- 36m ↓45% -- ↓40% UPDRS Motor: 5-7m -- 36m ↓50% -- ↓43% Rigidity: 5m -- 27m ↓49% -- ↓49% Facies: 5m -- 18m ↓59% -- ↓39% Postural stability: NS -- NS -- NS Rising from sitting: ND Speech: 7m -- 18m ↓54% -- ↓30% Bradykinesia: 9-12m -- 30m ↓40% -- ↓37% Gait: 7-9m -- 18-36m ↓58% -- ↓49% OFF Tremor [60m]: ↓33-83% Beginning between 9-33m post-op ON Tremor [24m]: 4/5 Pts asymptomatic Daily L-dopa [60m]: ↓64%		
Tampa (open-label)	Pt1-4, 6: plPut (3-4 ¦ 6-8), prPut (3-4 ¦ 6-8); 6.5-9w (CA) Pt5: plPut (3 ¦ 6-8), prPut (4 ¦ 6-8); 6.5-9w (CA)			
(Freeman *et al.*, 1995)	**4 Tx:** Pt1-4 [6m]	**(OFF ǀ ON) [6m]:** UPDRS Motor: ↓20%NS ǀ ↓20%NS H&Y: ↓15%NS ǀ ↓13%NS	**(OFF ǀ ON) [6m]:** UPDRS ADL: ↓38%* ǀ ↓19%NS S&E: ↑41%* ǀ 0%NS Time OFF: ↓65%*	**[18F]FDOPA K_i^{Plasma} [6m]:** Put (l/r): ↑33%TR/↑53%* Cau (l/r): ↑9%NS/↑1%NS

			Time ON-DYS+: ↓91%* Freezing ↓ Daily L-dopa ↓	
(Kordower *et al.*, 1995)	**1 Tx:** Pt1 [18m]	**At 15m:** UPDRS OFF Total: ↓37%	Post-op fluctuations, dyskinesia & dystonia virtually disappeared **At 15m:** Time OFF: ↓100% Time ON-DYS+: ↓100%	**[^{18}F]FDOPA K_i^{Plasma} [6m -- 12m]:** lPut: ↑28% -- ↑61%† rPut: ↑48% -- ↑103%* lCau: ↓1% -- ↑1%^{NS} rCau: ↑10% -- ↑39%†
(Kordower *et al.*, 1998)	**1 Tx:** Pt5 [19m]	**OFF [6m -- 12m]:** UPDRS Motor: ↓27% -- ↓26% **ON [6m -- 12m]:** UPDRS Motor: ↓8% -- ↑59%	**OFF [6m -- 12m]:** UPDRS ADL: ↓23% -- ↓16% **ON [6m -- 12m]:** UPDRS ADL: ↑47% -- ↑95% Time OFF: ↓62% -- ↓62% Time ON-DYS-: ↑45% -- ↑45% Daily L-dopa: 0% -- ↑45%	**[^{18}F]FDOPA K_i^{Plasma} [6m -- 12m]:** lPut: ↑5% -- ↑29%* rPut: ↑108% -- ↑152%‡ lCau: ↓28% -- ↓13%^{NS} rCau: ↑2% -- ↑18%^{NS}
(Hauser *et al.*, 1999)	**6 Tx:** Pt1-6 [24m]	**(OFF ǀ ON) [20.5m]:** UPDRS Motor: ↓30%* ǀ ↑11%^{NS} P-S^{TIME}: ↓33%† ǀ ↑2%^{NS}	**(OFF ǀ ON) [20.5m]:** UPDRS ADL: ↓35%* ǀ ↑3%^{NS} S&E: ↑25%^{NS} ǀ ↓3%^{NS} Time OFF: ↓43%^{NS} Time DYS+: ↓53%^{NS} Time ON-DYS-: ↑174%* Daily L-dopa: ↓16%^{NS}	**[^{18}F]FDOPA K_i^{Plasma} [6m -- 12m]:** bPut: ↑48%‡ -- ↑61%‡ bCau: ↑9%^{NS} -- ↑1%^{NS} ↑ in 11/12 Put **Correlations:** Δ[^{18}F]FDOPA K_i^{Plasma} with: ΔUPDRS OFF Total (r=-0.8†) ΔTime ON-DYS+ (r=-0.74*) ΔTime OFF (r=-0.73*) ΔTime ON-DYS- (r=0.59*)
Tampa (RCT)	23 Tx			

	11 1-donor: plPut (1 ¦ 8), prPut (1 ¦ 8); 6-9w (CA) 12 4-donor: plPut (4 ¦ 8), prPut (4 ¦ 8); 6-9w (CA)			
(Olanow *et al.*, 2003)	**23 Tx:** 11 1/1 donor 6 ≤ UPDRS 49 12 4/4 donor 6 ≤ UPDRS 49 **11 Placebo** 6 ≤ UPDRS 49 [24m] 5 Tx died at 15-53m post-op by unrelated cause	**1-way ANCOVA BL adjusted (DV = Δ at 24m, IV = Group; Placebo, 1-donor, 4-donor), Tukey-Kramer pairwise contrasts:** OFF Assessments: UPDRS Motor (NS): Placebo (↑16%) vs. 4-donor (↓1%) (TR) Tremor (TR): Placebo (↑) vs. 4-donor (↓) (TR) Rigidity (NS), Bradykinesia (NS), Postural instability (NS) ON Assessments: Postural instability (*): Placebo (↑) vs. 4-donor (↑↑) (*) UPDRS Motor (NS), Tremor (NS), Rigidity (NS), Bradykinesia (NS) In mild PD (UPDRS OFF Motor ≤49): UPDRS OFF Motor (†): Placebo (↑~47%) vs. 1-donor (↑~25%) (TR) Placebo (↑~47%) vs. 4-donor (↓~7%) (†) 1-donor (↑~25%) vs. 4-donor (↓~7%) (NS) In severe PD (UPDRS OFF Motor	**1-way ANCOVA BL adjusted (DV = Δ at 24m, IV = Group; Placebo, 1-donor, 4-donor), Tukey-Kramer pairwise contrasts:** OFF Assessments: UPDRS ADL (NS) ON Assessments: UPDRS ADL (NS) Time ON-DYS- (NS) Time OFF (NS) Time ON-DYS+ (NS) LEDD (NS) OFF-DYS+ [24m]: 13/23 Tx & 0/11 placebo Disabling in 3/13, surgical intervention *(see Olanow 2009 for more complete analysis)*	**1-way ANCOVA BL adjusted (DV = Δ[18F]FDOPA Ratio^{Occ} at 24m, IV = Group; Placebo, 1-donor, 4-donor), Tukey-Kramer pairwise contrasts:** lPut (‡): Placebo (↓) vs. 1-donor (↑) (†) Placebo (↓) vs. 4-donor (↑) (‡) 1-donor (↑) vs. 4-donor (↑↑) (TR) rPut (‡): Placebo (↑) vs. 1-donor (↑↑) (*) Placebo (↑) vs. 4-donor (↑↑) (‡) 1-donor (↑) vs. 4-donor (↑↑) (NS) lCau (NS): Placebo (↓) vs. 4-donor (↑) (TR) rCau (NS): No correlation with OFF M-AIMS (NS)

		≥49): UPDRS OFF Motor (NS) No treatment effect in young Tx (≤60y) (NS)		
(Olanow *et al.*, 2009a)	**23 Tx** 11 1/1 donor 7 OFF-DYS+ 4 OFF-DYS- 12 4/4 donor 6 OFF-DYS+ 6 OFF-DYS- **11 Placebo** [24m]	**At baseline (OFF-DYS+ vs. OFF-DYS-):** No difference for UPDRS OFF/ON **Δ at 24m (OFF-DYS+ vs. OFF-DYS-):** No difference for UPDRS OFF/ON **Δ at 6m (OFF-DYS+ vs. OFF-DYS-):** UPDRS OFF Motor: OFF-DYS+ (↓~22%) vs. OFF-DYS- (↓~5%) (*)	**1-way ANCOVA BL adjusted (DV = ΔM-AIMS at 24m, IV = Group; Placebo, 1-donor, 4-donor), Tukey-Kramer pairwise contrasts:** ON M-AIMS (NS): Placebo (↑~42%) vs. 1-donor (↑~62%) (NS) Placebo (↑~42%) vs. 4-donor (↑~15%) (NS) 1-donor (↑~62%) vs. 4-donor (↑~15%) (NS) 33/34 PD [BL]; 34/34 PD [3-24m] OFF M-AIMS (*): Placebo (0→0) vs. 1-donor (0→3.2) (*) Placebo (0→0) vs. 4-donor (0→2.7) (†) 1-donor (0→3.2) vs. 4-donor (0→2.7) (NS) 0/34 PD [BL]; 13/34 PD [3-24m] Onset latency = 5.1±3.3m Scores remain constant after	**[18F]FDOPA Ratio^{Occ} [BL] (OFF-DYS+ vs. OFF-DYS-):** No difference for lPut, rPut, lCau, rCau (NS) **Δ[18F]FDOPA Ratio^{Occ} [24m] (OFF-DYS+ vs. OFF-DYS-):** No difference for lPut, rPut, lCau, rCau (NS) **Correlations:** No correlation with OFF M-AIMS at BL, 24m or Δ24m (NS)

			12m LEs most affected in 12/13 Side dominance in 10/13 **At baseline (OFF-DYS+ vs. OFF-DYS-):** LEDD: OFF-DYS+ < OFF-DYS- (-38%) (‡) Time ON-DYS+: OFF-DYS+ > OFF-DYS- (+157%) (TR) No difference for Time OFF, ON M-AIMS, Age, Gender (NS) **Δ at 24m (OFF-DYS+ vs. OFF-DYS-):** No difference for LEDD, Time ON-DYS+, Time OFF, ON M-AIMS, Age, Gender (NS) **Correlations:** No correlation for OFF M-AIMS with ON M-AIMS, UPDRS Motoror LEDD at BL, 24m or Δ24m (NS)	
(Kordower *et al.*, 2017)	**1 Tx:** OFF-DYS+ [16y] **1 non-Tx PD** **1 HC**	At BL: Aged 47y, good response to L-dopa, peak dose dyskinesia, H&Y OFF = 4 **UPDRS-III Motor [3m -- 15m -- 24m -- 31m]:** OFF: ↓29% -- ↑15% -- ↑17% -- ↓2%	Freezing and falls ↑ OFF-DYS+ mainly LE DBS in bilateral STN at 8y Improved peak dose dyskinesia Improved motor function	**[18F]FDOPA Ratio^{Occ} [1y -- 2y]:** lPut: ↑143% -- ↑157% rPut: ↑220% -- ↑220% lCau: ↑44% -- ↑25% rCau: ↑114% -- ↑86%

		ON: ↑19% -- 0% -- ↑54% -- ↑54%	Wheelchair bound Required help with ADL Cognitive impairment Severe hypophonia and dysphagia	
UK				
(Kudoh *et al.*, 1999)	**19 Tx:** A) 7 fetal mesencephalon + striatum: lCau + rCau (1 ¦ 1 + 1); 18-20w (GA) B) 12 fetal mesencephalon (3 lost to FU): lCau + rCau (1 ¦ 1 + 1); 17-19w (GA) [18m]	**ΔGroup A vs. ΔGroup B [18m]:** UPDRS OFF Motor: A (↓59%*) = B (↓30%^{NS}) (^{NS}) H&Y OFF: A (↓50%*) = B (↓25%^{NS}) (^{NS}) OFF P-S^{TIME}: lUE: A (↓51%*) > B (↓35%^{NS}) (*) rUE: A (↓65%*) > B (↓20%^{NS}) (*) OFF Hand-Arm movement (Time): lUE: A (↓45%*) = B (↓30%^{NS}) (^{NS}) rUE: A (↓64%*) > B (↓37%^{NS}) (*) OFF FDex^{TIME}: lUE: A (↓56%*) > B (↓33%^{NS}) (*) rUE: A (↓53%*) = B (↓5%^{NS}) (^{NS}) OFF S-S-W^{TIME}: A (↓65%*) > B (↑12%^{NS}) (*) ON P-S^{TIME}: lUE: A > B (*) rUE: A > B (*) *No other significant differences between groups when ON medication*	**ΔGroup A vs. ΔGroup B [18m]:** UPDRS OFF ADL: A (↓53%*) = B (↓17%^{NS}) (^{NS}) S&E OFF: A (↑111%*) = B (↑50%^{NS}) (^{NS}) Daily L-dopa: A (↓56%*) > B (↓10%^{NS}) (*) Time ON: A (↑25%*) > B (↓14%^{NS}) (*) ON-DYS+: Severity: A (↓75%^{NS}) > B (0%^{NS}) (*) Duration: A (↓67%*) > B (0%^{NS}) (*)	
Transplantation details are of the form: *Region* (*no. donors ¦ no. tracts*); *fetal age* (CA/GA)				

↑/↓ denotes increase/decrease from baseline (pre-operative values) unless otherwise stated
~ = denotes approximate values derived from graphical data representation
a = anterior; b = bilateral; c = contralateral; d = dorsal; i = ipsilateral; l = left; m = middle; p = posterior; r = right; u = unilateral; v = ventral
^{1}H-MRS – proton magnetic resonance spectroscopy; αS = α-synuclein; ADL = activities of daily living; AIMS [0-42] = abnormal involuntary movement scale; BDI = Beck's depression inventory; BG = basal ganglia; BL = baseline; CA = post-conceptual age; Cau = Caudate; Cb = Calbindin; CC = cingulate cortex; CDRS = clinical dyskinesia rating scale; Cer = cerebellar reference; Cho = choline; Cr = creatine + phosphocreatine; DBS = deep brain stimulation; dlPFC = dorsolateral prefrontal cortex; DYS = with dyskinesia; FDex = Finger dexterity (time to complete ^{TIME} or no. completed within unit time ^{NUM}); fMRI = functional magnetic resonance imaging; FU = follow-up; GA = gestational age; GFAP = glial fibrillary acidic protein; GID = graft-induced dyskinesia; Girk2 = G-protein-coupled inward rectifying current potassium channel type 2 (In HC, Girk2+ neurons restricted to ventral midbrain); Glx = glutamine + glutamate; GOO = global ordered outcome; GPi = globus pallidus pars interna; H&Y = Hoehn and Yahr Scale; HC = healthy controls; HRQoL = Health related quality of life; Iba1 = ionized calcium-binding adaptor molecule 1; m = month; ns = not significant; LB = Lewy body; LC = locus coeruleus; LE = lower extremity; LEDD – L-dopa equivalent daily dose; LID = L-dopa-induced dyskinesia; M-AIMS [0-28] = modified abnormal involuntary movement scale; mI = myoinositol; MRI = magnetic resonance imaging; NAA = N-acetylaspartate; ND = not done; NHP = Nottingham Health Profile; NM = neuromelanin; Occ = occipital reference; OFF = off medication state; ON = on medication state; PDQ39 = 39-item Parkinson's disease questionnaire; P-S = pronations-supinations (time to complete ^{TIME} or no. completed within unit time ^{NUM}); Pt = patient; Put = putamen; RN = red nucleus; S&E = Schwab & England; SMA = supplementary motor area; SN = substantia nigra; S-S-W^{TIME} = Time to complete Sit-Stand-Walk over unit distance; STN = subthalamic nucleus; Str = striatum; TH = tyrosine hydroxylase; TrypOH = tryptophan hydroxylase; Tx = transplant; Ub = ubiquitin; UE = upper extremity; UPDRS = unified parkinson's disease rating scale; UPDRS-II ADL [0-52] = unified parkinson's disease rating scale part II – activities of daily living; y = year;